Post-installed fastening solution for strengthening of RC frames with seismic bracing – A displacement based approach

Von der Fakultät Bau- und Umweltingenieurwissenschaften der Universität Stuttgart
zur Erlangung der Würde eines Doktor-Ingenieurs (Dr.-Ing.)
genehmigte Abhandlung

Vorgelegt von
Erik Johannes Stehle
aus Schwäbisch Gmünd

Hauptberichter: Prof. Dr.-Ing. Akanshu Sharma
Mitberichter: Prof. Dr.-Ing. habil. Joško Ožbolt
                       Prof. Dr. Emad Gad

Tag der mündlichen Prüfung: 21. November 2023

Institut für Werkstoffe im Bauwesen der Universität Stuttgart

2024

Outline

Author: Erik Johannes Stehle (Schwäbisch Gmünd, Germany)

Title (English):   Post-installed fastening solution for strengthening of RC frames with seismic bracing – A displacement based approach

Title (German):   Befestigungslösung für die nachträgliche Befestigung von Stahlaussteifungen an Stahlbeton-Rahmentragwerke zur Ertüchtigung gegen seismische Beanspruchungen – Ein Verschiebungs-basierter Ansatz

Institution: University of Stuttgart

                            Faculty of Civil and Environmental Engineering

                            Institute of Construction Materials (IWB)

Declaration of originality

I declare that I have written this thesis independently and have not used any sources or auxiliary materials other than those indicated. All segments of the work that have been taken verbatim or in substance from publications or other statements are marked as such.

Eigenständigkeitserklärung

Ich erkläre, dass ich die vorliegende Arbeit selbständig verfasst und keine anderen als die angegebenen Quellen und Hilfsmittel benutzt habe. Alle Stellen der Arbeit, die wörtlich oder sinngemäß aus Veröffentlichungen oder aus anderweitigen Äußerungen entnommen wurden, sind als solche gekennzeichnet.

Stuttgart, January 2024

Erik Johannes Stehle

Abstract (English)

Steel bracing is a popular solution for strengthening of reinforced concrete (RC) frame structures against seismic hazards. The new structural brace elements can be directly connected to the existing frame structure by means of post-installed anchors. Such a connection offers a low invasive, economical, and practical solution. However, there are also certain challenges which arise when using post-installed anchors.

Different types of post-installed anchors exhibit different displacement and hysteretic behavior. Since the displacement (and hysteretic) behavior of the anchorage has a marked influence on the performance of a strengthening solution, it is important to understand the actual behavior of the anchors and to take their behavior into account in the design of a strengthening solution. Therefore, it is required to assess the suitability of different types of anchors for such structural applications. This is associated with an adequate procedure for the assessment of the hysteretic and displacement behavior of the same.

When post-installed anchors are used to form the connection between the steel bracing and the RC frame, they might be subjected to geometric restrictions that negatively affect the performance of the anchors. For instance, the limited dimensions of the structural members, such as beams and columns, in which the anchors are installed in. Or the arrangement of anchors in a spatial corner configuration in case the steel braces are to be fastened to the corner of a RC frame.

These challenges call for a displacement based design solution for post-installed anchors, which accounts for the actual performance of the anchors and anchor connections in terms of the displacement and hysteretic behavior.

The first part of this thesis investigates the hysteretic and displacement behavior of tension loaded single anchors. For this purpose, a new displacement-based testing procedure is presented. An experimental program was carried out, in which five different types of post-installed anchors were tested following the new testing procedure and the current testing approaches for qualification of anchors against seismic actions. Based on the evaluation of the single anchor behavior, a hysteretic model was developed to simulate the behavior of anchors under pulsating tension load. The model includes the unloading and reloading behavior of the anchors, strength degradation in subsequent cycles at the same displacement level, and accounts for the residual displacements of the anchors after unloading.

The second part of this thesis deals with the behavior of anchor groups. Two focal points are investigated. One is the hysteretic behavior of anchors groups. For this purpose, an experimental program is carried using the displacement-controlled testing procedure previously applied to single anchors. Based on the experimental results the hysteretic model for single anchors is extended to anchor groups. Second is the

behavior of tension loaded anchor groups in narrow concrete members. Thus, anchor groups in the vicinity of two parallel close edges. The results of the experimental results highlight the need for a modified analytical design approach for anchor groups in narrow members to overcome the current over-conservatism.

In the third part of the thesis, the connection between steel bracing and RC frame corner is investigated. The experimental and numerical analysis of the spatial corner configuration highlights the feasibility of such a connection approach. Based on the results, an analytical and a displacement-based design solution for the connection is proposed. The displacement-based solution is based on the nonlinear spring modelling approach and allows the assessment of the complete connection.

Kurzfassung (Deutsch)

Die Aussteifung durch Stahlstreben ist eine effektive Lösung zur Verstärkung von Stahlbeton-Rahmentragwerken gegen seismische Beanspruchungen. Dabei können die neuen Aussteifungselemente mit Hilfe von Dübeln nachträglich montiert werden, wodurch eine direkte Verbindung zwischen dem neuen tragenden Bauteil und der bestehenden Konstruktion ermöglicht wird. Eine solche Verbindung bietet eine wenig invasive, wirtschaftliche und praktische Lösung. Allerdings gibt es auch einige Herausforderungen, die bei einer solchen Befestigungslösung auftreten.

Zum einen gilt es festzustellen, welche Arten von Dübeln sich für diese Anwendung eignen. Dafür werden adäquate Verfahren benötigt, mit denen, neben der Tragfähigkeit, insbesondere auch das Hysterese- und Verschiebungsverhalten der Dübel beurteilt werden können. Zum anderen ergeben sich aus der Geometrie und den Abmessungen des bestehenden Rahmentragwerks gewisse Einschränkungen, welche sich negativ auf die Leistungsfähigkeit der Dübel auswirken. Bauteile, wie Balken und Stützen, in welche die Dübel montiert werden, weisen meist begrenzte Abmessungen auf. Dies kann dazu führen, dass die Dübel sehr nah an den Bauteilrändern belastet werden, wodurch zum Beispiel die Tragfähigkeit gegen Betonausbruch deutlich abgemindert wird. Des Weiteren werden die Stahlstreben oft in den Ecken der Rahmentragwerke befestigt. Dadurch kommt es zu einer räumlichen Eckkonfiguration der Dübel, bei der sich die in den Ecken montierten Dübel gegenseitig beeinflussen können. Solche Eckkonfigurationen sind in den aktuellen Normen nicht geregelt.

Aus den genannten Herausforderungen ergibt sich die Notwendigkeit einer Bemessungslösung, die nicht nur die Tragfähigkeit der Dübel bzw. der Verbindung, sondern auch deren Hysterese- und Verschiebungsverhalten berücksichtigt.

Im ersten Teil dieser Arbeit wird das Hysterese- und Verschiebungsverhalten von zugbelasteten Einzeldübeln untersucht. Zu diesem Zweck wurden Versuche mit fünf Arten von Dübeln durchgeführt, welche durch schwingende Zugbelastung beansprucht wurden. Dabei wurden zwei Belastungsprotokolle für schwingende Zugbelastung untersucht. Zum einen das Belastungsprotokoll, welches aktuell zur Beurteilung der Dübel-Tragfähigkeit bei seismischer Beanspruchung verwendet wird. Zum anderen ein neues wegkontrolliertes Belastungsprotokoll, welches in dieser Arbeit vorgestellt wird. Basierend auf den Ergebnissen der Versuche wurde ein Modell entwickelt, mit dem das hysteretische Verhalten von Dübeln bei schwingender Zugbelastung simuliert werden kann. Das Modell berücksichtigt das Entlastungs- und Wiederbelastungsverhalten der Dübel, den Tragfähigkeitsverlust in aufeinanderfolgenden Zyklen bei gleichem Verschiebungsniveau und die bleibenden Verschiebungen der Dübel, wenn diese nicht zurück in das Bohrloch gedrückt werden.

Der zweite Teil dieser Arbeit beschäftigt sich mit dem Verhalten von Gruppenbefestigungen. Dabei wurden zwei Schwerpunkte gesetzt. Der Erste ist das hysteretische Verhalten von Gruppenbefestigungen. Zu diesem Zweck wurde ein Versuchsprogramm durchgeführt, bei dem das zuvor für Einzeldübel angewandte wegkontrollierte Prüfverfahren verwendet wurde. Basierend auf den Versuchsergebnissen wird das für Einzeldübel entwickelte Hysteresemodell für Gruppenbefestigungen erweitert. Ferner wird das Verhalten zugbelasteter Gruppenbefestigungen in schmalen Betonbauteilen untersucht. Dafür wurden Versuche an Gruppenbefestigungen in der Nähe von zwei parallelen, nahen Bauteilrändern durchgeführt. Die Ergebnisse der experimentellen Untersuchungen zeigen, dass der aktuelle Bemessungsansatz für zugbeanspruchte Gruppenbefestigungen in schmalen Bauteilen zu konservativen Vorhersagen der Tragfähigkeit führt. Daher werden modifizierte Bemessungsansätze vorgeschlagen.

Im dritten Teil der Arbeit wird die Verbindung zwischen einer Stahlstrebe und einer Stahlbeton-Rahmenecke untersucht, welche mit Hilfe von Dübeln realisiert wird. Die experimentellen und numerischen Untersuchungen der räumlichen Eckkonfiguration unterstreichen die Brauchbarkeit einer solchen direkten Verbindung. Auf der Grundlage der Ergebnisse wurden Bemessungslösungen erarbeitet, welche zum einen die Abschätzung der Tragfähigkeit einer solchen Eckkonfiguration erlauben, und zum anderen eine realitätsnahe Beurteilung des Tragverhaltens der gesamten Verbindung bei Betonversagen ermöglichen. Letztere Bemessungslösung wurde basierend auf dem nichtlineare Federmodellansatz entwickelt.

Acknowledgements

Table of contents

XIV

Symbols and abbreviations

Latin uppercase letters

$A_{c,N}^0$	Projected area of tension loaded single anchor
$A_{c,N}^i$	Tributary area of an individual anchor within a tension loaded anchor group
$A_{c,N}$	Projected area of a tension loaded anchor group considering anchor spacing and close edges
ADRS	Acceleration-displacement response spectra
BRB	Buckling Restrained Brace
CV	Coefficient of variation
DCR	Demand capacity ratio
E	Young's modulus
FE	Finite element
FEM	Finite Element Method
FFHRS	Fully Fastened Haunch Retrofit Solution
G_F	Fracture energy
I	Second moment of area
L_H	Length of gusset plate-to-beam interface
L_V	Length of the gusset plate-to-column interface
LVDT	Linear Variable Differential Transformer
M	Moment
N	Normal force
N_c, V_c, N_b, V_b	Interface forces according to the Uniform Force Method
N_{Ed}	Design tension load
N_{eq}	Maximum load at which cyclic loading is performed in the C1.1 tests
N_i	Load corresponding to the maximum displacement s_i of a particular cycle
N_{max}	Maximum load at which cyclic loading is performed in the C2.3 tests
$N_{max,i}$	Maximum tension load in cycle "i"

$N_{max,j}$	Maximum tension load in a particular displacement level "j" in the displacement-controlled cyclic tests
N_{min}	Minimum tension in tests for pulsating tension load
N_R	Capacity of an anchor group under tension load
N_{Rd}	Design capacity under tension load
$N_{Rk,c}^0$	Characteristic tension resistance of an unrestricted single anchor in case of concrete cone failure
$N_{Rk,c}$	Characteristic tension resistance of an anchor group or single anchor due to concrete cone failure
$N_{Rm,c}^0$	Mean tension resistance of an unrestricted single anchor in case of concrete cone failure
$N_{Rm,c}$	Mean tension resistance of an anchor group or single anchor due to concrete cone failure
N_u	Ultimate tension load
$N_{u,m}$	Mean ultimate tension load of a test series
$N_{u,m,cyc,cr}$	Mean ultimate tension load in cyclic tests in cracked concrete
$N_{u,m,cyc,ucr}$	Mean ultimate tension load in cyclic tests in uncracked concrete
$N_{u,m,ref,cr}$	Mean ultimate tension load in monotonic reference tests in cracked concrete
$N_{u,m,ref,ucr}$	Mean ultimate tension load in monotonic reference tests in uncracked concrete
$N_{sj,n}$	Load corresponding to the targeted maximum displacement amplitude of a particular displacement level "j" in the nth cycle of the displacement level
N_{w1}, N_{w2}	Load levels in the crack cycling tests C2.5
P_{first}	Load corresponding to the first peak in the load-displacement curve of a corner configuration
P_{tot}	Calculated capacity of a corner configuration
P_u	Ultimate load of a corner configuration
RC	Reinforced concrete
$R_{k,eq}^0$	Basic seismic resistance of an anchor group
$R_{k,eq}$	Characteristic seismic resistance of an anchor group

SDOF	Single-degree-of-freedom
S_S, S_1	Response acceleration parameters
T_B, T_C, T_D	Values for time period defining the acceleration response spectrum according to EN 1998-1
UFM	Uniform Force Method
V	Shear force
V_{Ed}	Design shear load
V_{eq}	Maximum load at which cyclic loading is performed in the C1.2 tests
V_R	Capacity of an anchor group under shear load
V_{Rd}	Design capacity under shear load
$V_{Rm,c}$	Mean shear resistance of an anchor group or single anchor in case of concrete edge failure
V_u	Ultimate shear load
$V_{u,m}$	Mean ultimate shear load of a test series
W	Section modulus

Latin lowercase letters

a_{gR}	Reference peak ground acceleration
a_w	Weld size
c_1	Actual edge distance in the 1-direction
c_2	Actual edge distance in the 2-direction
$c_{cr,N}$	Critical edge distance for which a single anchor or anchor group under tension load can develop the full capacity in case of concrete cone failure without the negative influence of close edges
d	Diameter of anchor rod
e_1	Load eccentricity in the 1-direction
e_2	Load eccentricity in the 2-direction
f_c	Concrete compressive strength
f_{ck}	Characteristic cylinder concrete compressive strength
$f_{cc,150}$	Mean cube concrete compressive strength at the time of testing measured on concrete cubes with a side length of 150 mm

f_{cm}	Mean cylinder concrete compressive strength at the time of testing
f_{ctm}	Tensile strength of concrete
f_t	Tensile strength
f_u	Steel ultimate tensile strength
f_{uk}	Characteristic steel ultimate tensile strength
f_y	Steel yield strength
f_{yk}	Characteristic steel yield strength
h_b	Beam height
h_{cc}	Depth of the concrete cone breakout body
h_{ef}	Effective embedment depth
$k_{50\%Nu}$	Secant stiffness at 50% of the ultimate tension load in the ascending branch of the load-displacement curve
$k_{50\%Vu}$	Secant stiffness at 50% of the ultimate shear load in the ascending branch of the load-displacement curve
k_{cyc}	Idealized unloading and reloading stiffness
$k_{cyl/cube}$	Conversion factor from cube concrete compressive strength to cylinder concrete compressive strength
k_N	Stiffness of a tension loaded anchor group
k_{Nu}	Secant stiffness at ultimate load of a tension loaded single anchor or anchor group
k_{RL}	Reloading stiffness
k_{UL}	Unloading stiffness
k_V	Stiffness of a shear loaded anchor group
k_{Vu}	Secant stiffness at ultimate load of a shear loaded single anchor or anchor group
k_{α}, k_{β}	Parameter required for idealization of unloading and reloading behavior of an anchor
q	Behavior factor
s_1	Actual anchor spacing in the 1-direction
s_2	Actual anchor spacing in the 2-direction
$s_{50\%Nu}$	Displacement corresponding to 50% of the ultimate tension load in the ascending branch of the load-displacement curve

$s_{80\%Nu}$	Displacement corresponding to 80% of the ultimate tension load in the post-peak range of the load-displacement curve
$s_{cr,N}$	Critical anchor spacing for which two adjacent anchors can develop the full capacity in case of concrete cone failure
s_i	Maximum displacement in cycle "i"
s_j	Targeted displacement amplitude of a displacement level in the displacement-controlled cyclic tests
s_{max}	Maximum displacement at which cycling is performed in the displacement-controlled pulsating tension load tests
$s_{max,i}$	Displacement corresponding to the maximum tension load $N_{max,i}$ in cycle "i"
$s_{max,j}$	Displacement corresponding to the maximum tension load $N_{max,j}$ in a particular displacement level "j" in the displacement-controlled cyclic tests
$s_{Res,i}$	Residual displacement of an anchor after unloading to almost zero load in cycle "i"
s_u	Displacement corresponding to the ultimate load
t_g	Thickness of the gusset plate
w	Width of a narrow RC member
w_w	Whitmore width

Greek symbols

α	Parameter used to define the idealized unloading and reloading behavior of an anchor
α_i	Load angle of internal forces of the two groups forming the anchor bracket
α_{eq}	Factor to consider the negative influence of seismic actions and cracking in the base material
α_{gap}	Factor to consider a reduction of the shear resistance due to inertia effects resulting from the annular gap between the anchor and the baseplate Load angle of internal forces of the two groups forming the anchor bracket
β	Parameter used to define the idealized unloading and reloading behavior of an anchor

γ_{ov}	Overstrength factor according to EN 1998-1
δ_{ij}	Kronecker delta
Δs	Displacement step
Δw	Crack width
ε	Strain
η	Strength reduction factor
θ	Angle at which the load is applied on the corner configuration
λ	Parameter used to define the hysteretic behavior in the three parameter model
ν	Poisson's ratio
σ	Stress
τ	Bond stress
$\psi_{II,Approach2}$	Modification factor to consider the conservatism of the CC method in case of tension loaded anchors located close to two parallel close edges based on the ratio c_2/h_{ef}
$\psi_{II,N}$	Modification factor introduced by Anderson et al. (2017) to consider the conservatism of the CC method in case of tension loaded anchors located close to two parallel close edges based on the ratio s_2/c_2
$\psi_{s,N}$	Reduction factor to consider the negative effect caused by a disturbance of the rotationally symmetric stress field in the concrete due to close edges
$\psi_{ec,N}$	Reduction factor to consider eccentricity of loading in case of tension loaded anchor groups
$\psi_{re,N}$	Reduction factor to consider densely distributed reinforcement
$\psi_{M,N}$	Factor to consider the beneficial effect of compression forces on the concrete cone breakout capacity when an anchor group is loaded by bending moments
$\psi_{w,N}$	Modification factor to consider the conservatism of the CC method in case of tension loaded anchors located close to two parallel close edges based on the width of the narrow RC member
ω	Parameter used to define the idealized unloading and reloading behavior of an anchor

1 Introduction

1.1 Motivation

Earthquakes are natural disasters with a massive destructive impact, which is particularly evident from the losses they cause. This becomes apparent with regard to two aspects through which the losses can be quantified. On the one hand the human losses and on the other hand the economic losses (Desramaut et al., 2013). During an earthquake, not only do many people lose their lives, but many also lose their homes, can no longer support themselves with basic human needs, and are seriously injured. In the 30 years before 2004, there have been around 660 seismic events which were responsible for approximately 560000 fatalities, and an additional 82 million who suffered directly from the seismic event or its aftermath (Guha-Sapir et al., 2004). Wallemacq et al. (2018) report that from 1998 to 2017, 56% of all fatalities caused by natural disasters were a consequence of earthquakes. They found that earthquakes cause significantly more casualties than other natural disasters such as storms, extreme weather events, floods, droughts, landslides, wildfires, or volcanic activity. Besides the human losses, economic consequences such as unemployment, damaged or destroyed properties, closing of stores, companies, and factories because of destroyed or damaged premises, and the costs associated with the reconstruction and repair of buildings or infrastructure, have a significant impact on society (Desramaut et al., 2013).

While in ancient times, earthquakes were believed to be the result of divine will or supernatural forces (Reitherman, 2012), nowadays it is known that most earthquakes occur as a result of abrupt fracture processes due to the movements of the tectonic plates, which form the outer, solid geological layer of the earth, the lithosphere. The plates move horizontally against each other, which is why most seismic activity occurs at their boundaries. Thereby, a distinction is made between divergent boundaries where plates drift apart from each other, convergent boundaries where two plates move towards each other, with one plate being forced under the other, and transform boundaries where two plates move past each other without destroying or generating new lithosphere. At these boundaries, major faults, that are fractures in the ground or rock, occur due to the plate movement. At faults, rock fragments can either move away from each other, with one rock fragment sliding downward, they can slide horizontally past each other, or they can slide on top of each other. Due to the resulting friction between the rocks, very high stresses build up. Once a sudden fracture of the rocks occurs, an enormous amount of energy is released. This energy is partly dissipated by

frictional heat. However, part of it is released in the form of seismic waves, which are perceived as earthquakes at the surface of the earth. The resulting shaking of the ground eventually causes the buildings to resonate as well, which leads to the high demands imposed on a structure during an earthquake. Ultimately, the load imposed on a structure is part of the energy released during the fracture of the rock. If a building is not able to absorb or convert this energy, it will suffer severe damage or even collapse. Besides tectonic quakes there are also other types like volcanic quakes, or artificial quakes caused by detonations or explosions.

The fatal consequences of seismic events are often due to the fact that many of the buildings in seismic zones are prone to seismic loading and therefore collapse during an earthquake. Wallemacq et al. (2018) compared the 2010 Haiti earthquake to the 2010 New Zealand earthquake. In the 2010 Haiti earthquake an estimated 160,000 died (Kolbe et al., 2010) during the earthquake, while, as far as the number of fatalities is concerned, a similar earthquake in New Zealand in 2010 had a significantly less severe outcome (Wallemacq et al., 2018). Wallemacq et al. (2018) concluded that the striking difference in terms of impact is due in large part to the fact that New Zealand has strict rules for the design of buildings to withstand earthquake loads. If a building collapses, it is often because it was designed before the introduction of modern seismic codes, where for example the reinforcing details for reinforced concrete (RC) structures were not adequate for the demands imposed on the structure during an earthquake. On the other hand, there are countries that due to socio-economic constraints, still have a large volume of earthquake deficient buildings.

The necessity for the development of design recommendation for buildings against seismic actions was made particularly clear by severe earthquakes at the beginning of the twentieth century, such as the San Francisco earthquake in 1906 and the earthquake in Messina, Italy in 1908. While the former earthquake in 1906 did not yet lead to a change of building design for seismic impacts (Housner, 1984; Fajfar, 2018), it was particularly the devasting earthquake in Messina, which resulted in the early design recommendations against seismic loading (Housner, 1984). As a result, the equivalent static approach was introduced, where buildings were designed against horizontal loads equal to a certain percentage of the building weight (Housner, 1984; Fajfar, 2018). The value for this seismic coefficient varied across countries. However, typically a value of around 10% of the building weight was considered (Fajfar, 2018). According to Housner (1984), the first indirect attempts to consider both the stiffness and the mass of a structure, thus relating the seismic demands to the dynamic characteristics of a building, were made in 1943 in Los Angeles, where design criteria were modified accordingly (e.g., seismic demand was related to the actual height of the building and load patterns were introduced which considered that the lateral loads are not uniformly distributed over the height of the structure). It was the development of computers and the Finite Element Method (FEM) which finally made way for the development of response spectra and the dynamic analysis of structures and hence to

modern seismic design. According to Fajfar (2018), the development of modern seismic codes started in 1978 with the introduction of ATC 3-06 in the United States, involving seismic maps and force reduction factors (R-factors). Furthermore, the significant development of modern seismic codes was promoted by the capacity design approach, where the design of structures is based on a certain failure mechanism or rather the sequence of failure mechanisms of various structural elements. This design approach gained the attention of a wider audience through the work of Paulay and Priestley (1992). In simple terms, this approach is based on the idea that certain structural members are designed in such a way that the loads they can resist while remaining in the elastic range are higher than those resisted by adjacent structural members which are designed to dissipate energy during a seismic event. In this context, the work of Park and Paulay (1975) should be mentioned, which, through their work on thoughtful detailing in reinforced concrete structural members, lay down the basis for implementation of the capacity design approach. Today in earthquake engineering the concept of performance based design is becoming increasingly popular and has already been incorporated in standards and guidelines such as ASCE/SEI 41, SEAOC or FEMA 356, whereby deformations in the structure and the real structural behavior during a seismic event are directly considered (Stehle and Sharma, 2020). However, such a design approach requires models, which adequately reflect the nonlinear behavior of the individual structural components.

While the consideration of nonlinearity in the design of structural members and the overall load-displacement behavior of a structure has already gained a wide acceptance in the (earthquake) engineering community, the design of anchorage relies heavily on the strength of the anchors, while only little attention is paid to their displacement behavior (Sharma, 2019). When designing an anchorage, all possible failure modes are considered. The possible failure modes depend primarily on the type of loading. When subjected to tension loads, the European standard EN 1992-4 assumes that an anchorage may fail due to concrete cone failure, steel failure, pull-out failure, splitting failure, blow-out failure or a mixed concrete cone and pull-out failure in case of bonded anchors. When subjected to shear loads, an anchorage may fail due to steel failure, concrete edge failure, or pry-out failure (EN 1992-4). For each possible failure mode, the resistance of the anchorage is determined. The resulting minimum resistance determines the design of the anchorage. Simultaneous tension and shear loading is dealt with via interaction equations, whereby it is distinguished between steel failure modes and other failure modes (EN 1992-4).

When an anchorage is designed to resist seismic actions, EN 1992-4 provides two main design options. The first option considers no ductility requirements for the anchors. The anchorage is designed in such a way that in remains in the elastic range while the attached elements or the baseplate yields. The second design option accounts for the ductility of the anchors. Thus, the anchors are expected to yield before

the yielding of the attached elements or the baseplate. The latter option, however, is solely allowed for the tension load component and for steel failure of the anchors.

Neither option accounts for the actual displacement (deformation) behavior of the anchors. In case of seismic retrofitting, where anchors are used to form the connection between the existing structure and the new structural element, the effectiveness of the strengthening solution may very well depend strongly on the displacement behavior of the anchors and thus the performance (in terms of displacements) of the anchors should be considered for a safe and reliable design (Sharma, 2019).

1.2   Context of the research

Earthquakes in the past decades have shown the vulnerability of reinforced concrete (RC) structures to seismic actions. Watanabe (1997) provides a report about the damage in RC buildings after the Hyougoken-Nanbu earthquake in 1995. His evaluation of the structural damage shows that particularly RC buildings designed before the introduction of modern seismic design provision in 1981 in Japan were severely damaged or even collapsed during the earthquake, whereby unfavorable failure mechanisms such as soft story mechanism were observed.

In Kam et al. (2011), the building damage caused by the 22 February 2011 earthquake in Christchurch, New Zealand is reported with a particular focus on RC structures. According to the authors, mainly the more recently designed buildings which were designed following the capacity design approach exhibited a desired structural behavior, characterized by the plastic response of certain structural elements such as beams. In contrast, the authors note that pre-1970 RC buildings showed a particular vulnerability against earthquakes, which was mainly evident from a brittle behavior after exceeding the elastic capacity characterized by typical undesirable failure modes such as joint shear failure, beam lap-splice failure, wall shear and flexural failure or coupling-beams shear failure.

Ricci et al. (2011) present an evaluation of the damage to RC buildings during the earthquake close to L'Aquila, Italy in 2009. It was found by the authors that the observed structural damage occurred mainly in structural elements such as columns, walls, and beam-column joints, which were designed before the introduction of modern seismic codes with an emphasis on the force capacity and where brittle failure of the structural members has not been given adequate consideration. According to Ricci et al. (2011), collapse was mainly observed in case of irregular buildings.

A numerical study conducted by Liel et al. (2011) investigated the behavior of RC frame structures with two to 12 stories, which were designed according to seismic regulations of 1967 that were in place before the introduction of modern seismic codes. According to Liel et al. (2011), the results of the numerical simulation indicate that the probability of failure in case of RC frame structures designed before the introduction of modern seismic codes is notably higher compared to RC frame structures designed according

to modern seismic codes. From the results the authors conclude that the capacity design approach introduced in modern seismic codes provides an effective tool to a safer and more reliable design against seismic actions, which can reduce the risk of undesirable failure mechanisms.

Correspondingly, Sadjadi et al. (2007) performed numerical simulations on a 5-story RC frame structure. The authors designed the frames either according to the modern seismic codes in Canada as ductile or nominally ductile, or by only considering the gravity loads. In the analysis both nonlinear time history analysis and pushover analysis was used, and the analytical models were compared to experimental results to show their suitability. The authors concluded that when the RC frames were designed according to modern seismic codes, the structures were able to withstand substantial lateral loads. "Both ductile and nominally ductile structures were able to withstand the loading of major earthquakes without severe damage. Although the ductile structure was designed for half of the value of the design lateral load of the nominally ductile structure, the incorporation of good detailing and also the implementation of a capacity based design enabled the structure to perform well during major earthquakes" (Sadjadi et al., 2007, p. 2379).

The examples in the literature highlight that it is not so much the new buildings constructed according to modern seismic codes that pose a risk. It is mainly older buildings, where brittle failure can occur, that pose a risk during an earthquake. The structural deficiencies associated with these older structures require strengthening against seismic actions such that their seismic performance in future earthquakes is improved. Often seismic strengthening implies that additional structural elements are added to the older (existing) building. Typically, this includes steel bracings or reinforced concrete structural members like shear walls. The addition of structural members to the existing RC frame changes its global behavior, generally resulting in improved global strength and stiffness of the entire structure. However, the addition of new structural members is only efficient if the connection between the existing structure and the new structural element can reliably transfer the high seismic forces. In case of steel bracings, typical connection approaches include bolted-through connections, steel jackets, or pre-cast hooks, or more elaborate approaches such as an additional steel frame which is in turn connected to the RC frame.

The motivation for this work is to investigate a low invasive and practical connection solution, where post-installed anchors are used to attach steel bracings to the RC frame structures. In this context, the concrete cone failure mode is of particular interest as the breakout capacity of an anchor, in contrast to other failure modes such as pull-out failure or steel failure, is significantly influenced by neighboring anchors in a group or close edges (Eligehausen et al., 2006; Bokor, 2021), which will typically be the case in narrow members such as beams and columns of a RC frame. Furthermore, no rules currently exist for the design of an anchor group where the anchors are installed in orthogonal members (such as beam and column) using an L-shaped anchor group,

which is the most practical solution for making corner connections required for steel bracing. Therefore, concrete breakout failure is deemed the dominant and crucial failure mode for post-installed anchors used in the above discussed applications. Moreover, the quasi-brittle load-displacement behavior, generally associated with concrete cone failure demands a detailed understanding of the inherent behavior of such a connection, particularly under seismic loading.

1.3   Organization of the work

Following a brief overview on the seismic retrofitting of RC structures with seismic bracing in Chapter 2, the seismic qualification and design of anchors in Chapter 3 and discussing the objectives and methodology in Chapter 4, the work performed in the context of this thesis is structured as follows:

1. Part I: Single anchor level

    a. Experimental investigations on the behavior of single anchors under pulsating tension loads (Chapter 5)

    b. Development of hysteretic model for tension loaded single anchors (Chapter 6)

    c. Recommendations for testing and assessment of post-installed anchors under seismic action (Chapter 7)

2. Part II: Anchor group level

    a. Experimental investigations on anchor groups subjected to displacement-controlled static and cyclic tension load (Chapter 8)

    b. Experimental and numerical investigations on anchor groups in narrow concrete members (Chapters 9 and 10)

    c. Development of modified design approaches for anchor groups in narrow concrete members (Chapter 11)

    d. Application of the hysteretic model to anchor groups (Chapter 12)

3. Part III: Subassembly level

    a. Experimental and numerical investigations on the geometrical influence of a corner configuration (Chapters 13 and 14)

    b. Development of an analytical design concept for corner configurations (Chapter 15)

    c. Extension of the nonlinear spring modelling approach to spatial corner configurations (Chapter 16)

    d. Case study on the design of connections between steel bracing and RC frame structure in the context of a performance based analysis (Chapter 16)

2 An overview of seismic retrofitting of RC structures

2.1 The concept of performance based seismic design

When it comes to the design of new buildings or the strengthening of already existing structures against earthquake hazards, the concept of performance based structural design is becoming increasingly popular in earthquake engineering (Stehle and Sharma, 2020). Its popularity is also evident as it has been incorporated in standards and guidelines like ASCE/SEI 41, SEAOC and FEMA 356, or in guidelines for the testing of RC structural elements under seismic actions such as ACI 374.2R-13. The basic idea of this design concept is to establish a target performance of a building during and after the event of an earthquake. Simply put, the performance expresses how much damage to a building may be caused by an earthquake and thus provides an indication on whether and when a building is ready for re-use after a seismic event. The strengthening solution or the design of a new building is then chosen accordingly to ensure that the targeted performance is achieved. Typically, standards and guidelines define the performance through predefined levels or objectives, which are discussed in Section 2.1.1.

To assess whether the targeted performance can be achieved, the structural behavior (in terms of strength, deformation, etc.) is compared with the expected seismic demand. Besides using acceleration time-histories based on ground motion records in the context of a dynamic analysis, acceleration response spectra offer a less elaborate option, which is commonly used to represent seismic hazards. Therefore, acceleration response spectra are briefly discussed in Section 2.1.2.

Finally, the evaluation of building performance is discussed in Section 2.1.3.

2.1.1 Performance levels

In most codes, the performance of a building is classified by means of performance levels or performance objectives, whereby the designation of the individual levels may vary between different codes. Commonly, four major performance levels can be encountered that are operational, immediate occupancy, life safety and collapse prevention (e.g., FEMA 356). Like in FEMA 356, each performance level is typically related to a certain story-drift ratio (hence a certain deformation of the structure generally described by the roof displacement) and is further specified by the level of damage in the members as shown in Figure 2.1. In the following, the four major performance levels are briefly described based on the definitions in FEMA 356.

After an earthquake, a building is operational when the demands have not exceeded the elastic range of the overall structure during the seismic event. Thus, the building is lightly damaged, and the deformations that occurred during the earthquake do not remain permanent (FEMA 356). At this performance level, the strength and stiffness of the structure after an earthquake is basically the same as before. According to FEMA 356, at the Immediate Occupancy level, some structural damage, characterized by minor cracks and limited yielding at some locations, is possible. However, "the basic vertical- and lateral-force-resisting systems of the building retain nearly all of their pre-earthquake strength and stiffness. The risk of life-threatening injury as a result of structural damage is very low" (FEMA 356, p. 1-12) and therefore, the structure can be re-used basically directly after the seismic event. In the Life Safety damage state, FEMA 356 expects that some deformation that occurred during the earthquake will remain after the event and structural elements such as beams and columns are expected to be severely damaged with cracking occurring in the joint region. Nevertheless, it is expected that the building has enough residual capacity to ensure that the building will not collapse. In general, injuries caused by the building damage in the course of the seismic event are possible, with the probability of fatal injuries remaining rather low (FEMA 356). According to FEMA 356, the fourth performance level, Collapse Prevention, is characterized by severe structural damage and cracking in the structural members, where the building has just enough residual capacity after the earthquake not to fail. As a result of the severe damage in the structural members, FEMA 356 states that particularly the stiffness and strength of the structure against lateral loads is significantly reduced, which is why the resistance against any aftershock cannot be relied upon. As can be seen in Figure 2.1, the performance level Collapse Prevention is associated with significant lateral deformations of the structure, which in large parts are not recoverable. It is evident that at this level, it is not safe to re-use or re-enter the building (FEMA 356).

As can be seen, the performance based design approach directly considers the nonlinear behavior of the structure with regards to the deformation of the structure and the real structural behavior during an earthquake. For a meaningful utilization of this approach, it is required that some structural members are able to behave in a ductile manner so that forces and moments can be redistributed before the entire structure fails. It becomes evident that a reliable prediction of the performance is only possible if the nonlinear behavior of the complete structure and its individual members is adequately considered. This requires the development of models that precisely describe the load-displacement behavior or moment-rotation behavior of the individual components and take into consideration the different modes of failure.
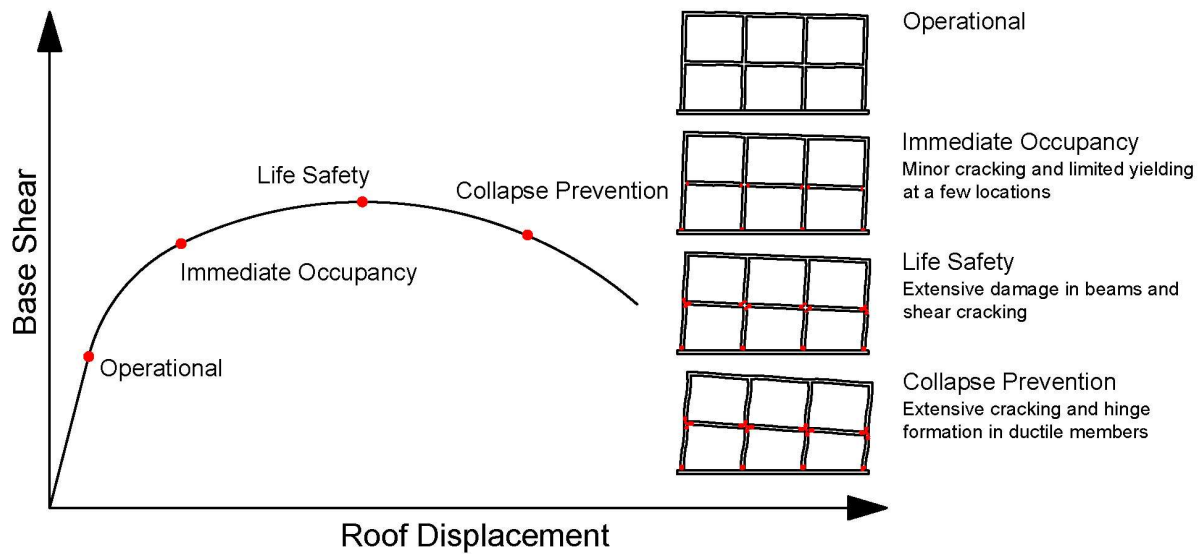
Figure 2.1. Definition of the major performance levels. Reproduced based on Sharma (2017).

2.1.2   Seismic hazard

In general, standards and guidelines, such as FEMA 356, EN 1998-1, ATC-40 or ASCE 7, describe the seismic demand due to ground shaking by acceleration response spectra or acceleration time-histories. Thereby the magnitude of the impact is based on the location of the building, the site-specific geological characteristics, and a hazard level defined by the value of the return period which is selected upon the importance of the building.

The most common description of seismic demands due to ground motions for the design of buildings against earthquakes, are acceleration response spectra, which plots the peak acceleration response of a single degree of freedom system with varying time period. The general shape of an idealized acceleration response spectrum for spectral response acceleration versus structural period is shown in Figure 2.2. However, it should be mentioned that the equations used to develop the response spectrum vary upon standards and guidelines and depend on the country-specific geological and seismic conditions. In EN 1998-1, the horizontal elastic response spectrum is defined by four equations. The main parameter which defines the response spectrum is the site-specific reference peak ground acceleration, a_{gR}. The reference peak ground acceleration for a specific location is determined from spectral response acceleration contour maps which define the seismic zones within a country. In the German national annex for EN 1998-1, DIN EN 1998-1/NA the seismic zone map is valid for earthquakes with a reference return period of 475 years (which is equivalent with a 10% chance of exceedance in 50 years) and 5% viscous damping ratio. The reference peak ground acceleration is then adjusted using different factors. In EN

1998-1, the actual ground conditions of the site under consideration are accounted for by the soil factor, which depends on the ground type, and which is defined by the average shear wave velocity and the stratigraphic profile. Furthermore, the time periods T_B, T_C, and T_D are defined based on the ground type. A so-called importance factor considers the consequences related to the failure of different types of buildings. Lifeline facilities such as hospitals or fire stations are more important for the protection of the general public and their failure is considered more critical than for example the failure of residential buildings. The importance factor should be chosen according to the category of the building by adjusting the return period to a smaller or higher value (EN 1998-1). Since the basic seismic zone map is based on the assumption of 5% viscous damping ratio for the structure, a damping correction factor is introduced to consider higher or lower viscous damping ratios of the structure.
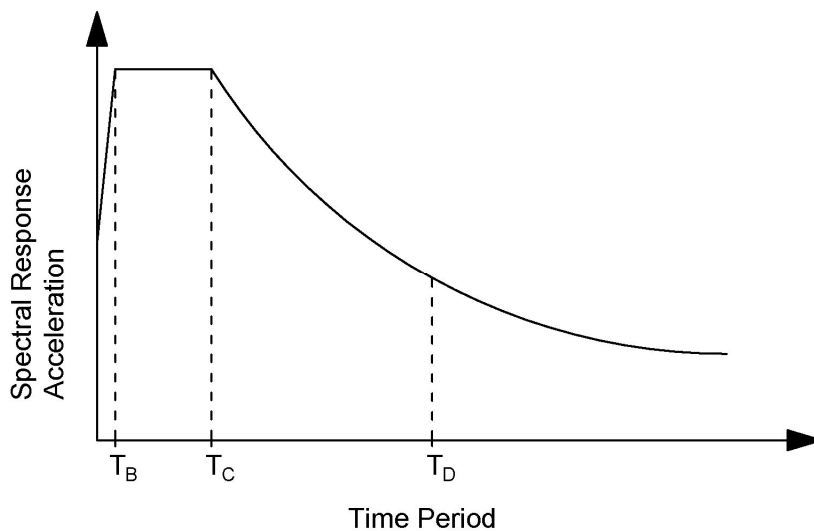
Figure 2.2. Typical shape of the idealized acceleration response spectrum. Redrawn on basis of EN 1998-1.

It is worth mentioning that, in contrast to EN 1998-1, the shape of the response spectrum according to FEMA 356 and ASCE 7 is characterized by two response acceleration parameters S_S and S_1 for short-period (0.2 second) and long-period (1 second) response, respectively. As in the European standard, the response acceleration parameters are determined using spectral response acceleration contour maps of 5% damping response spectrum. Furthermore, in FEMA 356, the general shape of the acceleration response spectrum is defined by three equations instead of four. Nevertheless, the development of the response spectra basically follows the same procedures.

2.1.3 Evaluation of building performance – Analysis procedures

For the design of new buildings against seismic actions or the retrofit of existing structures standards and guidelines such as FEMA 356, EN 1998-1, or ATC-40,

provide different ways to analyze a structure. Commonly, this includes procedures using linear static analysis, nonlinear static analysis, and nonlinear dynamic analysis, whereby the complexity of the procedures increases from linear static to nonlinear dynamic.

In case of a linear static analysis, the nonlinear behavior of the structure and its individual members is not directly modelled, and a linear-elastic behavior is assumed. The beneficial effect that can result from nonlinear deformations of the structure (e.g., the dissipation of energy when ductile structural members undergo deformations in the nonlinear range) are addressed in other ways. In EN 1998-1, for example, the seismic demand represented by the elastic response spectrum is reduced by a so-called behavior factor q. The reduced response spectrum is generally called design spectrum. To determine the level of reduction, EN 1998-1 distinguishes between the materials used in the construction of the building (e.g., reinforced concrete, steel, timber, masonry) and the force resisting system against seismic loading (e.g., frame structure, wall system, etc.). A detailed analysis of the nonlinear behavior of individual structural members is not performed.

Due to its simplicity, the linear static analysis has the major drawback that it relies heavily on the assumptions that were made for the ductility of the structure. During a severe earthquake, it is very likely that a structure will be subjected to loads greater than the linear-elastic capacity of the structure. In this case, the increasing nonlinear demand will lead to damage in the structure, whereby the extent of the structural damage depends on the previously assumed ductility. It becomes evident that if the actual ductility of the structure deviates significantly from the assumed ductility, the design according to the linear static procedure might be unsafe and may lead to severe damage in the structure or even the total collapse. In addition, the applicability of this approach is limited to regular structures in plan and elevation (EN 1998-1) with no irregularities such as in-plane and out-of-plane discontinuities, severe weak story irregularity, severe torsional strength irregularity, and irregular distributions of mass and stiffness (FEMA 356).

Nonlinear procedures offer a more detailed analysis, directly considering the nonlinear behavior of the individual structural members through detailed modelling. In this way the engineer becomes aware of damage development in the structural members and gains a better understanding of the structural system by directly accounting for effects like the redistribution of forces with increasing horizontal demands. The nonlinear static analysis or pushover analysis is probably the most popular analysis procedure when it comes to performance based design as it combines accuracy with relatively easy application and acceptable computational costs. The main benefit in comparison with linear procedures is that it does not rely on assumptions regarding the nonlinear behavior of the structure and the ductility characteristics.

Following FEMA 356, the nonlinear static analysis is based on the numerical model of the structure, whereby, the structural components are modelled individually, and their nonlinear behavior is directly accounted for. Generally, the nonlinear behavior of the structural components is determined based on experimental results on individual structural members or theoretical analysis and expressed in terms of the load-deformation behavior (FEMA 356). The idealization of the load-deformation behavior is in general realized by means of so-called backbone curves or envelope curves. Thereby, the idealized behavior of the structural components considers the descending branch in the post-peak range, stiffness degradation and potential residual strength of the structural components (FEMA 356). In particular, potential plastic hinge zones (e.g., at the ends of columns and beams and the joint regions in case of RC frames) should be carefully modelled. Since the global stiffness of the structure and thus its load-deformation behavior is calculated based on the (modeled) behavior of the individual components, a change in the behavior at the local component level also leads to a change in the behavior at the global level.

Once the numerical model of the structure is created, the lateral loads are applied over the height of the structure following prescribed patterns, e.g., uniform distribution, triangular shaped load patterns, or load patterns based on the mass of the individual stories or the fundamental mode. In a step-by-step procedure the lateral loads, or displacements while maintaining the load pattern, are statically increased so that the complete load-displacement curve of the structure is obtained, the so-called capacity curve or pushover curve. Note that also gravity loads should be incorporated in the model (ATC-40, FEMA 356). This curve is generally represented by base shear versus roof displacement (e.g., FEMA 356). Therefore, the base shear (total applied lateral force) and the roof displacement (displacement at control node on the roof of the structure) are recorded at every load step.

So far, the seismic demand on the structure represented by the acceleration response spectrum and the capacity of the structure against seismic actions have been determined. To assess the performance of a structure commonly the coefficient method as described in FEMA 356 and the capacity spectrum method as described in ATC-40 are used (FEMA 440). A detailed discussion of these two methods is presented in FEMA 440, where both methods are evaluated, and limitations are shown. Exemplarily, the assessment of the performance of a structure according to the capacity spectrum method (ATC-40) will briefly be discussed in the following.

As shown above, the seismic demand is commonly plotted in the spectral response acceleration versus structural period format (see Figure 2.2), while the capacity is plotted in the base shear versus roof displacement format (see Figure 2.1). Therefore, a direct comparison of the demand and capacity is not possible. To allow the comparison, in case of the capacity spectrum method, both the acceleration response spectrum and the capacity curve are plotted in the acceleration-displacement response spectra (ADRS) format (ATC-40, FEMA 440). Therefore, the spectral response

acceleration versus structural period format and the base shear versus roof displacement format are transformed using the dynamic properties of the structure, such as the modal mass coefficient and first mode participation factor (ATC-40, FEMA 440). After the transformation, the capacity and the demand curve can be directly compared. The point where the demand and the capacity curve intersect is called the performance point. It identifies the maximum nonlinear displacement to be expected for the investigated structure under the investigated seismic demand (ATC-40).

However, as noted in ATC-40 and FEMA 440, an iterative process is required to determine the performance point. When the structure is subjected to cyclic loading in the nonlinear range, the actual equivalent damping of the structure may be higher than the 5% viscous damping assumed for the acceleration response spectrum (ATC-40). Thus, in ATC-40, the demand spectrum is reduced depending on the equivalent damping of the structure related to the tentative performance point in the previous iteration. Although more elaborate than the linear static procedure, this approach allows a more accurate and reliable estimation of the reduction of the seismic demand resulting from nonlinear deformations of the structure.

An example on how the nonlinear static analysis is applied in the context of performance based design is given in Figure 2.3. The figure shows the capacity spectrum and the demand spectrum in the acceleration-displacement response spectrum format. Assuming the performance level for the investigated building is set as Collapse Prevention as indicated by the red dot on the capacity curve. As can be seen, for the initial demand spectrum for 5% viscous damping, the performance requirement is not met. However, from the graph it is apparent that the structure will undergo nonlinear deformations during the investigated seismic demand. The nonlinear response of the structure results in additional damping and the demand is reduced. A comparison between the reduced demand spectrum and the capacity spectrum shows that the performance requirement is met.

Since the demand side, represented by the response spectra, is defined by standards and guidelines based on the seismic and geotechnical site conditions, it is evident that the result of a nonlinear static analysis depends heavily on how accurately the structure could be developed into a numerical model. As already mentioned above, it is therefore crucial for the application of the performance based design approach, to consider the nonlinear behavior through precise models, which simulate the load-displacement behavior or moment-rotation behavior of the individual members and account for the different possible failure modes.
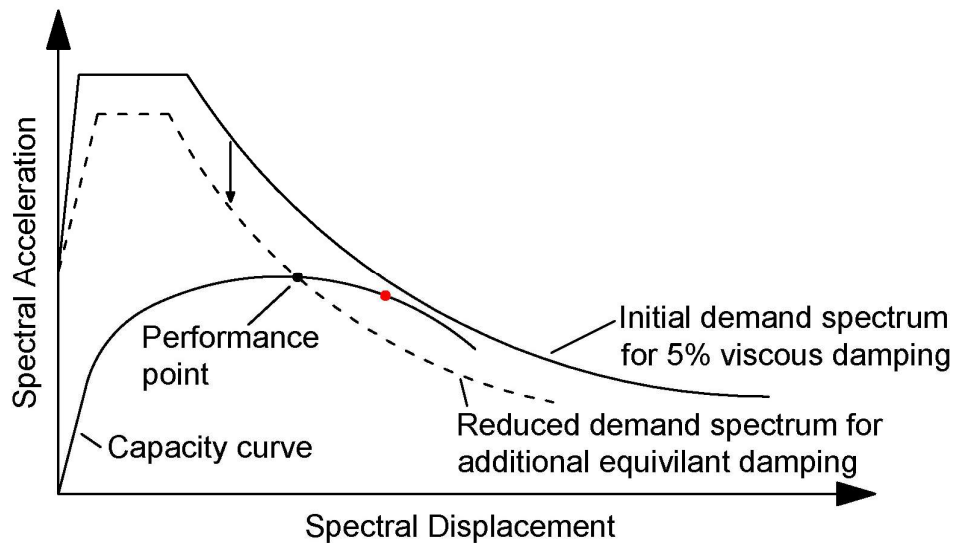
Figure 2.3. Schematic representation of the capacity spectrum method. Reproduced based on Sharma (2020).

Finally, it should be mentioned that there are some limitations of the nonlinear static procedure. First, this procedure is only applicable if higher mode effects have a negligible influence and second, it does not accurately consider that the dynamic characteristics of a structure depend on its stiffness, which likely decreases due to seismic actions (FEMA 356). Advanced nonlinear static analysis methods such as the modal pushover analysis or the adaptive pushover analysis may be used for better accuracy with slightly more computational efforts. However, a detailed discussion of these methods is out-of-scope of this thesis.

Dynamic analysis offers probably the most accurate but equally the most (computationally) costly procedure for evaluating the building performance. In FEMA 356, dynamic analysis considers the seismic demand by acceleration time-histories using ground motion records which are adjusted to the site conditions, whereby linear or nonlinear behavior of the structure may be assumed in dynamic analysis. In combination with accurate numerical models, which in addition to the aforementioned characteristics, consider the hysteretic behavior of the individual structural members (FEMA 356), the nonlinear dynamic (time-history) analysis procedure provides the most accurate solutions with relatively low uncertainties. At the same time the computational costs increase. It is therefore the responsibility of the engineer to balance effectiveness and accuracy, which is why the nonlinear static (pushover) analysis is in many cases the appropriate choice.

Although dynamic approaches are able to provide an accurate assessment of the building performance, it should be mentioned, though, that there are two areas of weakness inherent to this approach, which can have a significant influence on its accuracy. The first weak link are the models for the behavior of the individual elements, which results from a lack of data on the realistic structural and hysteretic behavior. It is

therefore of paramount importance to assess the structural behavior of individual members by performing seismic qualification tests on these members. Only with the information gained from such cyclic tests, it is possible to develop the accurate numerical models, required for a safe design. The second weak link refers to the high variability of ground motion records. FEMA 356 therefore recommends subjecting the structure to several ground motion records. Only then can the critical parameters for design be determined and the structural behavior be accurately predicted.

2.2   Strengthening of RC frames with seismic bracing

As discussed in Section 1.2, RC frame structures designed before the introduction of modern seismic codes are known to be vulnerable against seismic loading. These structures bare the potential risk of severe damage or even total collapse in the event of future earthquakes. This problem has been recognized, and a number of retrofitting techniques have been developed in the past decades, which can be roughly grouped into local and global strengthening approaches (Moehle, 2000).

Local strengthening approaches target to enhance the strength or performance of individual structural members. In case of RC structures, this includes for example local strengthening of beams, columns, or beam-column joints. By locally improving the strength of weak structural members, the failure of the overall structure can be delayed, allowing an increase in the displacement of the structure (FEMA 356; Moehle, 2000). Typical local strengthening approaches include steel jacketing, concrete jacketing, fiber-reinforced polymer (FRP) wrapping (Gkournelos et al., 2021), or steel haunches (Genesio, 2012; Sharma, 2013). With the exception of steel haunches, in general, local strengthening approaches do not alter the global structural system and the load transfer mechanism of the structure.

In case of global strengthening approaches, the addition of structural elements alters the global structural system (Moehle, 2000) and in turn, the load transfer mechanism or the global behavior of the structure. Additional shear walls, infills with masonry or concrete blocks, and steel bracings generally result in increased strength and stiffness of the structure (Sugano, 1996). Other techniques such as base isolators result in an increased time period of the structure (Reddy et al., 2019).

Badoux and Jirsa (1990) highlight several advantages of using steel bracing to strengthen RC frames over other global strengthening solutions such as the rather fast installation, the associated rapid reoccupation of the building, and minimal interference with the internal space and accessibility. In addition, the authors argue that steel bracing of the structure does not come with a significant mass increase, which is why an enhancement of the foundations is generally not an issue and thus provides an economic advantage. Although the focus of Badoux and Jirsa (1990) was rather on exterior steel bracings, those advantages over other global strengthening solutions such as shear walls is also deemed valid for internal steel bracings. With respect to

the structural advantages, steel bracing significantly improves the lateral strength and stiffness of a structure as shown in various studies (Bush et al., 1991; Maheri and Sahebi, 1997; Youssef et al., 2007; TahamouliRoudsari et al., 2017). Equally important, steel bracing offers a highly flexible strengthening solution that can be adapted to various structural problems by choosing the appropriate bracing configuration and brace sections. This enables the designer to find the most suitable force path in the complete structure. Due to their advantages over other strengthening solutions, steel bracing has been used in practice for the rehabilitation RC frame structures as shown in Usami et al. (1988) and Ohishi et al. (1988).

2.2.1   General characteristics of braced frames

Figure 2.4 exemplarily shows the basic idea of this strengthening approach and its application in the context of performance based design. Assuming the target performance level for the investigated RC frame structure is Immediate Occupancy (red dot). To comply with the requirements of the target performance level, the nonlinear displacement of the structure that can occur during the investigated seismic demand must not exceed the target displacement corresponding to the performance level. As can be seen, the existing structure does not meet this requirement. Through seismic bracing of the RC frame structure, the strength and stiffness of the whole structure is increased, and the target performance level can be achieved. The capability of seismic bracing to improve the strength and stiffness of RC frame structures has been demonstrated in experimental and numerical studies (Bush et al., 1991; Pincheira and Jirsa, 1995; Youssef et al., 2007).
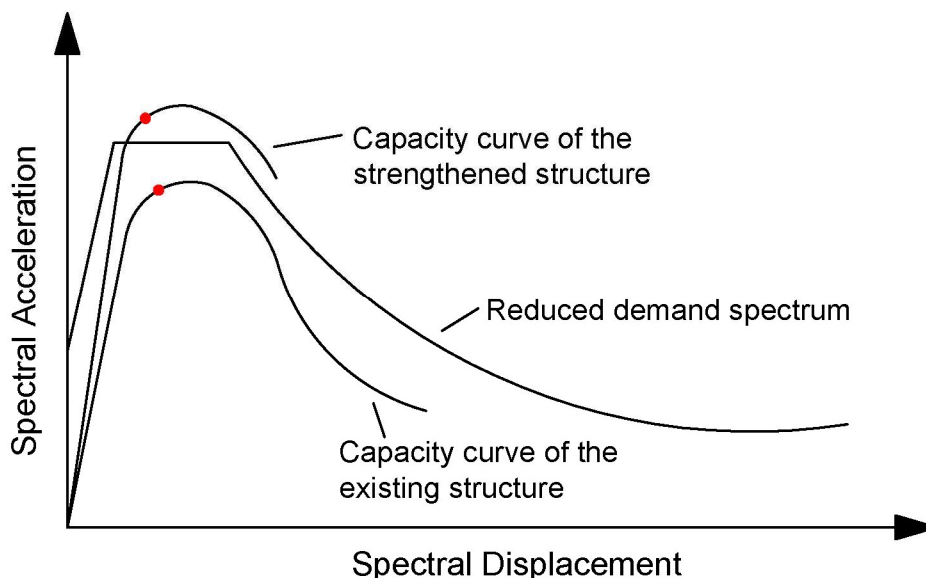
Figure 2.4. Principle of seismic bracing: Improving global strength and stiffness characteristics. Reproduced based on Sharma (2020).

Youssef et al. (2007) conducted experiments on a bare moment resisting frame and a steel braced frame. Thereby, they measured the strains in the reinforcements of both frames. Compared to the strains measured in the bare frame, the authors report that the strains in the both the transverse column reinforcement and the top longitudinal beam reinforcement reduced significantly when the RC frame was strengthened, indicating reduced bending and shear stresses in the members. By retrofitting RC frames with steel bracing, the load transfer mechanism is altered from a moment resisting frame to a predominantly truss mechanism. As a result, the axial demands on the RC frame members increase, while the bending moments decrease. Typically, the axial capacity and stiffness of RC frame members is higher than their flexural capacity and stiffness, which is why the change of load transfer mechanism improves the strength and stiffness of the complete RC frame structure. The increased axial demands on the RC structural members can, however, require an additional local strengthening of the same as highlighted in Pincheira and Jirsa (1995).

In the following a brief overview is given on typical bracing configurations (Section 2.2.1.1), commonly used structural steel sections (Section 2.2.1.2) and buckling restrained braces (BRBs) which are a technical development of the classic steel braces (Section 2.2.1.3).

2.2.1.1 Types of steel bracing configurations

Figure 2.5 shows different types of steel bracing configurations typically used to strengthen RC frame structures, such as single diagonal bracing, X-bracing, chevron bracing, knee-bracing, diamond-bracing, or eccentric-bracing, to name a few. The application of either of these configurations results in an increased strength and stiffness of RC frames. However, the degree to which both strength and stiffness increases might vary depending on the chosen configuration. As shown in TahamouliRoudsari et al. (2017), there are also certain differences when it comes to the seismic characteristics of strengthened RC frames, like energy dissipation, and ductility, or the damage development (e.g., cracking). In this section a brief overview is provided on the most commonly used configurations.
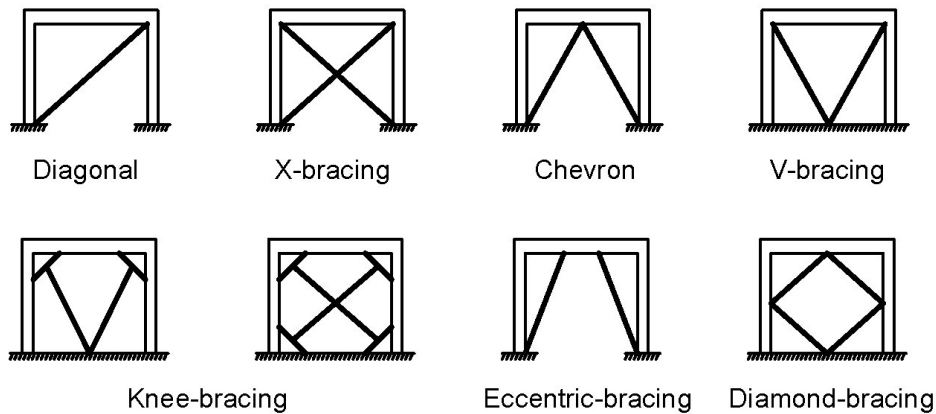
Figure 2.5. Typical types of steel bracing configurations.

Single diagonal bracing has been investigated experimentally by Maheri and Sahebi (1997). It was shown that the strengthening approach could markedly improve the strength of the tested RC frame. However, the enhancement of the capacity using diagonal bracing was not as pronounced compared to the tested X-braced frame in the same study. When subjected to seismic actions, the single diagonal brace is alternately loaded in tension and compression. When loaded in compression the steel braces are often prone to buckling which can significantly limit the efficiency of the strengthening. Therefore, single diagonal bracing is often used in combination with buckling restrained braces (BRB) in order to increase the energy dissipation and ductility of the structure as shown in Mazzolani et al. (2009) and Mahrenholtz et al. (2015). BRBs will be discussed in more detail in Section 2.2.1.3.

The behavior of X-bracings has been investigated experimentally by Maheri et al. (2003), Youssef et al. (2007) and TahamouliRoudsari et al. (2017). In all three studies the tested retrofitted frames showed an increased strength and stiffness compared to the bare frame. In terms of strength, X-bracing resulted in a superior behavior in comparison to chevron-bracing or knee-bracing tested in the same studies (Maheri et al., 2003; TahamouliRoudsari et al., 2017). The ductility of the X-braced RC frame, on the other hand, is less satisfactory. In the three experimental studies, it was observed that the ductility of the strengthened frame reduced compared to the bare frame. In Youssef et al. (2007) and TahamouliRoudsari et al. (2017), the energy dissipation capacity of the braced frames was evaluated. In the two studies it was found that when the complete nonlinear behavior is considered, the energy dissipation can be increased by using X-bracing. It should be noted, however, that in the beginning of loading, the energy dissipation of X-braced frames was rather poor. Youssef et al. (2007) attributes this observation to the significant increase in stiffness compared to the bare frame. The three studies report that reaching the ultimate capacity in the tests was generally accompanied by buckling of the braces in compression.

Chevron bracings have been investigated by Ozcelik et al. (2013) and TahamouliRoudsari et al. (2017). The results of the experiments showed an increased

strength and stiffness compared to the bare frame. Similar to X-bracings, the tested chevron braces exhibited a less favorable behavior in terms of ductility. In TahamouliRoudsari et al. (2017) chevron bracings showed notable pinching, which resulted in less energy dissipation compared to other types of steel bracing in the study. However, in Ozcelik et al. (2013) it was shown that when the braces buckled while the structure was still able to undergo large cyclic deformations without failure, the structure could dissipate a significant amount of energy compared to the bare frame. TahamouliRoudsari et al. (2017) report that the failure of the chevron braced frame is governed by severe damage in the upper beam where the steel braces are attached. Ozcelik et al. (2013) attribute similar observations of severe damage in the beam to buckling of the compression brace, which leads to an imbalance between the tension and compression forces transferred from the braces to the beam.

Maheri et al. (2003) and TahamouliRoudsari et al. (2017) report a significant increase in strength and stiffness of the strengthened RC frame with knee-bracing. In both studies, the ductility of the strengthened frame reduced in comparison to the reference bare frame. Nonetheless, the observed behavior in terms of ductility was better as for the tested X-braced frames.

In TahamouliRoudsari et al. (2017), eccentric-bracing of the tested RC frame resulted in an increased strength and stiffness, and even showed improved ductility compared to the bare frame. This is interesting insofar as in the previously discussed configurations, the observed ductility of the strengthened frames rather decreased compared to the bare frame. On the other hand, the authors observed more significant damage in the structure at the end of the test compared to other bracing configurations.

Diamond-bracing or double-K configuration have been investigated in Qu et al. (2015). It should be noted that in this study BRBs were applied instead of classic steel braces. The authors report that besides the increased strength and stiffness, the strengthened frame showed adequate ductility and satisfying hysteretic behavior. Diamond-bracings have the beneficial effect of reducing the brace buckling length compared to other configurations such as diagonal bracings or X-bracings as they do not span across the complete bay. As argued by the authors, there are two benefits over other bracing configurations such as diagonal bracing or X-bracing with respect to the connection of the steel braces. First, the point where the braces are connected to the beams is away from plastic hinge zones, which typically occur at the ends of the beams. Second, since the gusset plates are not located in the corner of the frames, they are not subjected to additional forces induced by bending of the beams and columns.

Comparison of the individual steel bracing configurations shows that the choice of configuration can have a marked influence on the performance of the retrofitted building in terms of strength, stiffness, ductility, and energy dissipation. Moreover, the choice of configuration can, to some extent, control the expected damage in the

structure. Overall, the comparison highlights the adaptability of steel bracing to the objectives of the strengthening.

2.2.1.2   Cross-sectional shapes

The analytical study in Badoux and Jirsa (1990) and the experimental studies in Bush et al. (1991) and Youssef et al. (2007) have shown that failure of the strengthened RC frame structure is often governed or initiated by buckling of the steel braces when loaded in compression. Along with buckling of the steel braces may come a negative impact on the effectiveness of the strengthening solution in terms of strength or the hysteretic behavior (and thus on the capacity to dissipate energy). In this context, the slenderness ratio of the chosen steel brace plays a key role as shown in Badoux and Jirsa (1990) and Ozcelik et al. (2013). Related to this is the need to identify suitable structural steel sections for seismic bracing. Typical structural steel sections that may be used for forming the bracing elements are shown in Figure 2.6.

| Angle | Double-Angle | Tee | Structural Pipe | Steel Plate |

| Channel | Double-Channel | Wide Flange | Structural Tube | Steel Bar |
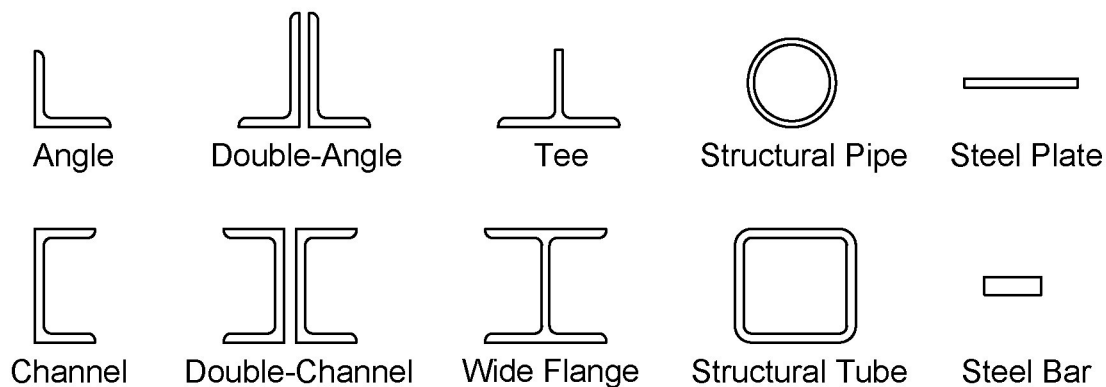
Figure 2.6. Typical cross-sectional shapes of structural steel used for the bracing of frame structures.

In order to determine the effectiveness of steel braces with respect to varying shapes and sizes, Black et al. (1980) conducted cyclic axial tests on 24 steel braces. The examined structural steel sections comprised wide flanges, double-angles, structural pipes, structural tubes, double-channels, and structural tees. Thereby, the thickness of the steel elements, the cross-sectional area, the shapes of the steel sections and the slenderness ratio was varied. In accordance with the analytical studies in Badoux and Jirsa (1990) and Ozcelik et al. (2013), the slenderness ratio was identified as the critical parameter influencing the hysteretic behavior. Black et al. (1980) compared the load-displacement curves and the hysteretic behavior of varying steel elements and found that braces with lower slenderness ratio performed more favorable with fuller hysteretic loops compared to slender braces, indicating a higher energy dissipation capacity for braces with low slenderness ratio. The authors observed that with increasing slenderness, the difference between the maximum tension and compression load which is achieved in one cycle increases. This particularly applies to the nonlinear part

of the load-displacement curve after the brace has buckled in compression. The influence of the cross-sectional shape on the hysteretic behavior of the tested structural steel sections, on the other hand, was found to be less pronounced. Nevertheless, by comparing the results for different cross-sectional shapes with equal slenderness-ratio and boundary conditions, Black et al. (1980) found that some shapes showed superior behavior over others. The authors associated the unfavorable behavior with certain geometrical characteristics which facilitate local buckling effects or torsional buckling. Thereby, round, and square tubes showed the most favorable hysteretic behavior, whereas steel braces composed of several sections, such as double-angles, have shown a less favorable behavior.

2.2.1.3   Buckling restrained braces

The discussion so far has demonstrated that buckling of the braces is one of the major parameters which influences the performance of steel braced RC frames. To overcome this shortcoming in the steel bracing strengthening scheme, systems were developed to limit buckling of the steel brace, so-called buckling restrained braces (BRBs). Della Corte et al. (2001) mention two major benefits of BRBs. The first benefit named by the authors is that, just like for classic steel braces, the stiffness of the strengthened frame is markedly higher than the stiffness of normal RC frames or moment resisting frames. The second benefit is that the ability of BRBs to dissipate energy is significantly more distinct compared to typical cross-sectional shapes of structural steel used for bracing RC frames. The additional damping as a result of the high level of energy dissipation leads to a reduced seismic demand.

The two effects are schematically shown in Figure 2.7. In the example the target performance, in this case Life Safety, cannot be achieved solely through increasing the strength and stiffness of the RC frame structure. Only by reducing the demand through additional damping of the BRBs it is possible to meet the desired performance level.
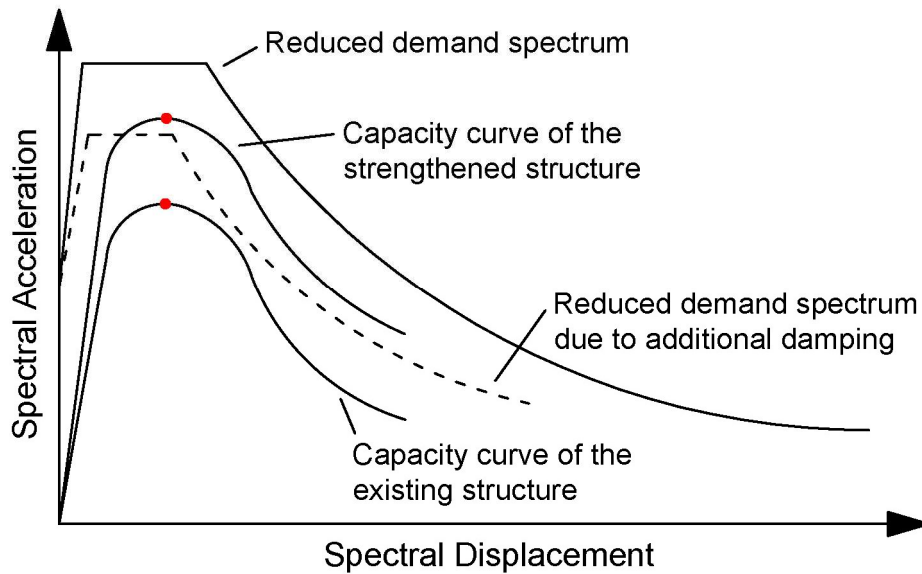
Figure 2.7. Principle of buckling restrained braces: Increased strength and stiffness and reduced seismic demand. Reproduced based on Sharma (2020).

A brief synopsis of the research activities on BRBs to date and the related design issues can be found in Della Corte et al. (2011). The review paper briefly summarizes the findings of the experimental investigations with respect to the required casing stiffness, the deformation capacity, the connections, and the influence of the unbonding layer. Typically, the restraining member of a BRB is either composed of concrete encased by a steel member or it is solely composed of steel parts. Figure 2.8 schematically depicts some of the cross-sectional shapes found in the literature for both steel-only and concrete encased BRBs.
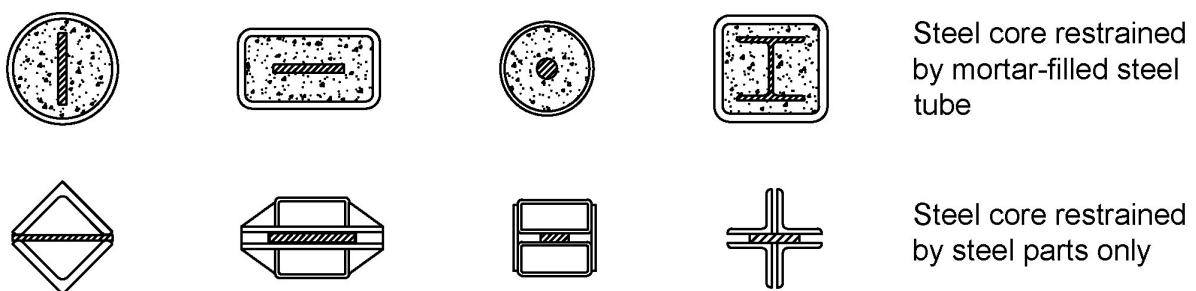
Figure 2.8. Typical examples of cross-sectional shapes used in BRBs. The top row shows BRBs where the restraining element comprises a steel tube which is filled with mortar. The bottom row shows BRBs where the restraining member is solely composed of steel elements.

The basic principles of BRBs are discussed by Watanabe et al. (1988). They argue that by restraining the steel braces from buckling in compression before it starts yielding, it is possible to design the yield strength of the brace according to the desired

strengthening objectives. In their experimental study, the BRBs comprised a core steel element encased by concrete which was in turn enclosed by a steel tube. They separated the concrete and steel tube from the frame structure, thus only the core steel element was connected to the frame. Friction between steel core and concrete was inhibited by means of an intermediate layer of foaming polystyrol and vinyl/mastic tape. Watanabe et al. (1988) performed tests on different specimens where the core steel of the BRBs had the same dimensions, while the dimensions of the casing was varied. The intension of the authors was to investigate the behavior of the specimen with equal yield strength of the core steel and varying Euler buckling load of the encasing element. It was observed that the tested specimen did not buckle when the buckling strength was higher than the yield strength. According to the authors, the specimens exhibited stable and full hysteretic loops with significant energy dissipation. In contrast, when the buckling load was lower than the yield force of the core steel, the authors report that the specimen buckled prior to yielding in compression which resulted in a rather poor hysteretic behavior.

On the component level, Palazzo et al. (2009) and Wu et al. (2014) have investigated the behavior of concrete-filled and only-steel encased BRBs, respectively. In Palazzo et al. (2009), cyclic axial tests on BRBs are performed. The tested BRBs comprised a round steel bar as the core element, which was encased by a mortar-filled steel tube. According to the authors, friction between core and casing was successfully inhibited by filling the gap between mortar and core steel with coating material. This was concluded from the rather small axial forces measured in the casing. The experimental results showed stable and full hysteretic loops in compression and in tension. According to the authors, the mortar displayed no sign of deterioration due to buckling of the core steel. A model was proposed to calculate the bending moment in the casing due to buckling of the core steel element, which allows a more accurate design of the casing system. The design and tests on a BRB only comprising steel members is described in Wu et al. (2014). The design considerations include global flexural buckling, strong-axis high-mode buckling and weak-axis high-mode buckling of the core steel element. No coating material was placed between the core steel plate and the restraining members. Nonetheless, the reported peak compression-to-tension load ratios in each cycle were below 1.24, which according to the authors indicate that the effect of friction between the core steel and the restraining members was rather limited. The tested specimens were able to develop stable and full hysteretic loops.

A RC column subassembly strengthened by a BRB was experimentally investigated by Yooprasertchai and Warnitchai (2008). In the experiment, the BRB was fixed to the subassembly by means of adhesive anchors. It was shown that, in comparison to the bare column, the strength, stiffness, and energy dissipation of the system could be significantly improved due to the BRB. Thereby it was observed that the amount of energy dissipated by the BRB was substantially higher than the amount of energy dissipated by the RC column. Finally, failure of the strengthened subassembly was

governed by severe damage and lap-splice failure in the RC column. The results show that for a successful implementation of the strengthening approach, the performance of the existing members must also be taken into account. The connection using adhesive anchors proved to be an efficient solution. According to the authors, the applied anchorage solution performed adequately.

Full-scale tests have been conducted by Tsai et al. (2008) on a steel frame structure strengthened by means of BRBs in chevron configuration. The authors describe the design considerations and the observations from the experiments. In the tests, the strengthened structure was subjected to a number of different scaled ground accelerations. It is reported that the strengthening solution could successfully comply with the targeted performance in terms of deformation of the structure even though the structures were subsequently loaded using varying scaled ground accelerations. However, buckling of the gusset plate was observed in the tests, which had to be fixed by means of additional stiffeners. This observation highlights that special consideration has to be put into the design of the connections to guarantee the effectiveness of the complete strengthening solution. The performance of the gusset plate is further assessed in the accompanying paper by Tsai and Hsiao (2008), where a modified design approach for the gusset plate was proposed. Furthermore, Tsai and Hsiao (2008) evaluated the performance of the strengthened structure. The results showed full hysteretic loops without pinching and a considerable energy dissipation capacity of the strengthened frame. As noted by the authors, particularly the BRBs participated in the energy dissipation of the complete structure. They concluded that only in case of severe seismic events the moment frame would come into play.

In Mahrenholtz et al. (2015), a full scale RC frame was strengthened by a BRB in single diagonal configuration. In this study, the BRB was attached to the primary RC structure via post-installed bonded expansion anchors, whereby the connection element comprised a L-shaped steel bracket with gusset plate as shown in Figure 2.9 (b). The test setup used in the experiments is schematically shown in Figure 2.9 (a). The stepwise increasing cyclic load was applied in displacement control in such a way that the BRB was alternately loaded in tension and compression until the complete structure failed. The study showed that the applied strengthening approach could increase the global strength and stiffness of the RC frame and led to a significant increase in the amount of dissipated energy in comparison to the bare RC frame. Equally important, the experimental observations showed that the used anchor system could provide sufficient strength, as it proved effective in transferring the loads from the BRB to the frame structure. However, the authors found that buckling of the transition segment of the BRB was likely caused by the irrecoverable anchor displacement which led to an offset of the gusset plate (see Figure 2.9 (c) and (d)). Eventually, the left column in Figure 2.9 (a) failed in shear at relatively high drift levels during the final loading phase, where the BRB was only loaded in tension. These tests

clearly highlighted that a good performance of anchors connecting the bracing system to the structure is essential for the bracing system to serve its intended function well.
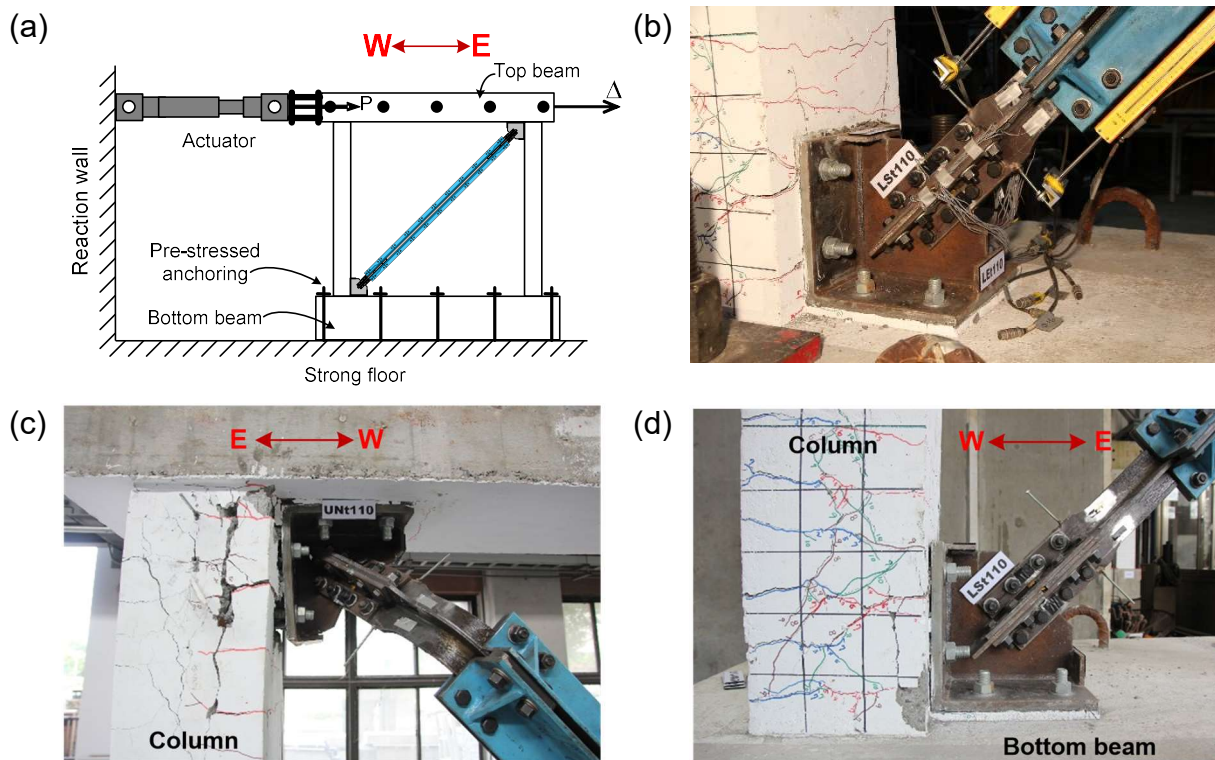
Figure 2.9. (a) Side view of the test setup used in Mahrenholtz et al. (2015), (b) lower anchor bracket and initial cracking of concrete close to the bracket, (c) buckling of the transition segment of the BRB of the upper and (d) lower connection. Source: Mahrenholtz et al. (2015).

2.2.2   Connection between steel bracing and RC frame

As a matter of fact, not only in the case of steel bracing, but for almost all retrofitting schemes, there must be some kind of connection between the new strengthening element and the existing structure. It is apparent that the efficiency of the strengthening is highly related to the performance of the connection itself and thus it requires a careful design. Besides, the choice of connection may have an influence on several other aspects which have to be taken into account, such as the invasiveness of the solution, its costs, its practicability regarding the installation, and architectural concerns.

In case of steel bracings, the brace is typically connected to a so-called gusset plate. The behavior of the gusset plate in such applications is relatively well understood. Therefore, to begin with, the design considerations for gusset plates are briefly discussed. However, it should be noted that most of the investigations were focused on the use in steel construction, where the gusset plate is directly welded to the steel frame. In concrete construction, however, the gusset plate is either fixed to an additional steel frame which is in turn connected to the RC frame or it is fixed to an

anchor bracket which is then fixed to the RC frame (see Figure 2.9). The first approach is generally referred to as an indirect connection since an additional steel frame is required, while the second approach is generally referred to as a direct connection since it connects the braces directly to the RC frame. Following the discussion on the gusset plate design, both indirect and direct approaches will be discussed.

2.2.2.1 Gusset plate design considerations

While in steel construction the gusset plate is directly welded to the steel column and beam, in RC structures this is not possible. Here the gusset plate is either welded to an anchor bracket which is then fastened to the RC elements or to an additional steel frame, which is somehow connected to the RC frame. Assuming that the performance and stress distribution in the gusset plate itself remains essentially the same, the design can be carried out according to the existing design principles of steel construction.

In Thornton (1984) and Lin et al. (2014) a detailed description of the gusset plate design can be found. Therein the recommended design checks include the welds at the gusset interfaces, yield strength at the Whitmore section, gusset plate buckling below the Whitmore section, block shear failure, von Mises yield criteria at the interfaces, tensile rupture at the interfaces and shear rupture at the interfaces.

The Whitmore section refers to an area at the attached end of the steel bracings. It is based on experimental studies of a Warren truss conducted by Whitmore (1952), where both a tension diagonal and a compression diagonal were attached to the lower chord by means of a gusset plate. Thereby the diagonals were fixed to the gusset plate by means of rivets. In an experimental study by Whitmore (1952), the general distribution of stress in the gusset plate was investigated. It was found that the location of the maximum tensile and compression stress is at the end of the tension and compression diagonal, respectively. Whitmore (1952) found that those maximum stresses can be reasonably well estimated from the maximum brace forces and the Whitmore section at the end of the respective diagonal. This section is defined by the thickness of the gusset plate and the Whitmore width, w_w, perpendicular to the diagonal. The definition of the Whitmore width is exemplarily shown in Figure 2.10 for a gusset plate used to connect a steel bracing to the corner of a RC frame. Typically, it is located at the bottom end of the connection between attached element and gusset plate. For the specimen tested by Whitmore (1952), this means that the Whitmore width is located parallel to the bottom row of rivets and runs through them as indicated in Figure 2.10.
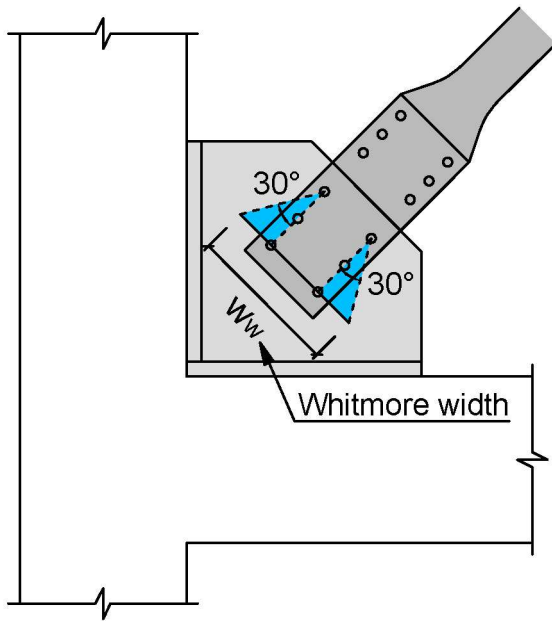
Figure 2.10. Determination of the Whitmore width.

In steel construction, a commonly accepted approach for the distribution of the brace forces on the gusset interfaces is the Uniform Force Method (UFM). A schematic depiction of the approach is shown in Figure 2.11. The UFM was introduced by Thornton (1984) for determination of the interfacial forces between the gusset plate and the beam and column surfaces in steel constructions and represents the lower bound theorem of limit analysis. Although commonly used in steel construction, the method can be applied to the described steel bracing connections in RC structures as well (Maheri and Hadjipour, 2003; Mahrenholtz et al. 2015).

Referring to Figure 2.11, the interface forces are calculated using following equations:

$$N_c = \text{P} \cdot \frac{e_c}{r}, \tag{2.1}$$

$$V_c = \text{P} \cdot \frac{\beta}{r}, \tag{2.2}$$

$$N_b = \text{P} \cdot \frac{e_b}{r}, \tag{2.3}$$

$$V_b = \text{P} \cdot \frac{\alpha}{r}. \tag{2.4}$$

$$r = \sqrt{(e_b + \beta)^2 + (e_c + \alpha)^2}$$
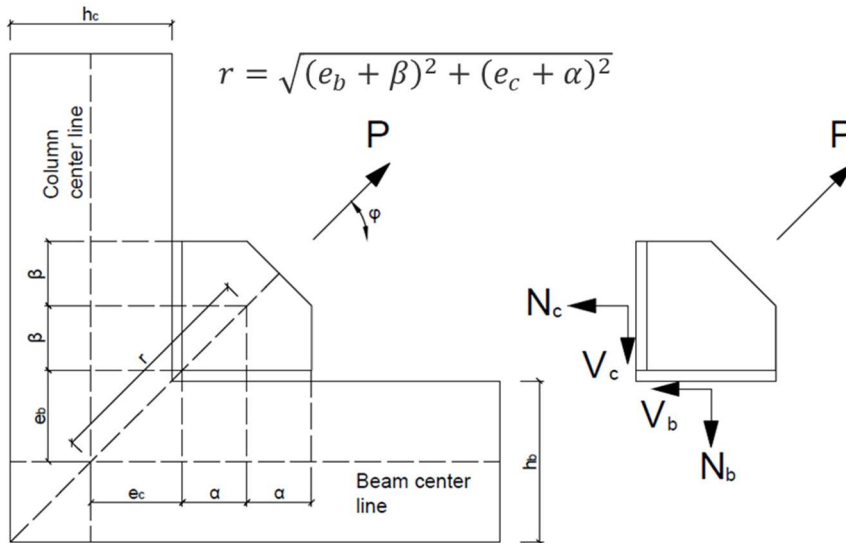
Figure 2.11. Uniform Force Method.

To design the gusset plate connection between steel bracing and RC frame in experimental studies, this method has already been successfully adopted as shown in Maheri and Hadjipour (2003) and Mahrenholtz et al. (2015). The design approach for the connection, which was used in the experimental study by Maheri and Hadjipour (2003), was further analyzed in a numerical parametric study conducted by Maheri and Yazdani (2016). In Maheri and Yazdani (2016), the design variables under investigation included the gusset plate size and the load angle. The numerical study showed that, in general, the horizontal interface forces (N_c and V_b in Figure 2.11) were larger than the vertical interface forces (N_b and V_c in Figure 2.11) when the load angle, φ, was low. The ratio between horizontal and vertical interface forces reversed as the load angle increased in value. While this result was not particularly surprising, the authors were able to show that the relation between the horizontal and vertical interface forces at varying load angles also depends on the dimensions of the gusset plate. For the investigated cases, the interface forces according to the UFM were in most cases higher than those determined in the numerical analysis. For load angels between 30° and 60° the authors calculated that the difference is a maximum of 20%. In conclusion, the study suggests that using the UFM provides a rather conservative design approach. An alternative approach to the UFM is the Generalized Uniform Force Method (GUFM) proposed by Muir (2008). The advantage of the GUFM is that it imposes less geometrical restrictions on the dimensions of the gusset plate. This leads to more practical configurations, while still realistic force distributions are achieved (Lin et al., 2014).

In real applications, the gusset plate is subjected to the so-called frame action effect. This essentially means that when the frame structure is subjected to reversed cyclic loading, the beams and columns bend, resulting in an opening and closing of the joint region. In the process, additional forces are imposed on the gusset plate which need

to be considered for a safe design. One way to obtain or account for the demand resulting from the frame action effect is the equivalent strut model proposed by Lee (2002). He investigated rib reinforcements for steel moment connections in a numerical study. It was shown that due to the frame action effect a strut forms in the ribs under closing moments. The starting and ending point of the strut was numerically determined as 0.6 times the length of the rib-to-beam and rib-to-column interface, respectively. It represents the location of the resulting force obtained from the stresses at the respective interface. In Lin et al. (2014) the equivalent strut model was applied for the design of a gusset plate connection, whereby the width of the strut was taken as 0.5 times the strut length L_g (see Figure 2.12). Lin et al. (2014) showed in a numerical investigation that the forces calculated from the equivalent strut model match reasonably well the values obtained in numerical analysis. It is worth mentioning that the same value for the strut width was also considered in Mahrenholtz et al. (2015). In Figure 2.12 the principles of the equivalent strut model are illustrated.
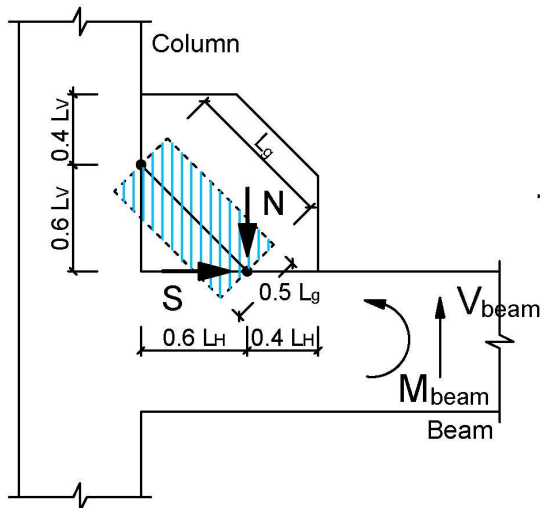
Figure 2.12. Schematic depiction of the equivalent strut model resulting from the frame action effect. Redrawn on basis of Lin et al. (2014).

To determine the maximum resulting forces S and N, Lin et al. (2014) use the maximum shear force V_{beam} in the beams considering that the plastic hinge in the beam is located close to the free end of the gusset plate. S and N are then calculated as (Lin et al., 2014):

$$S = \frac{h_b \cdot L_H \cdot V_{beam} \cdot (0.3L - 0.18L_H)}{4I_{beam}/t_g + h_b \cdot L_H \cdot (0.3h_b + 0.18L_V)} \tag{2.5}$$

$$N = \frac{L_V}{L_H} \cdot S \tag{2.6}$$

Where h_b is the height of the beam, I_{beam} is the second moment of area of the beam, and L is the clear span of the beam. L_V and L_H are the length of the gusset plate interfaces at the column and beam, respectively (see Figure 2.12).

2.2.2.2　Indirect connection approach

Examples for indirect connections are reported in Usami et al. (1988), Ohishi et al. (1988), Goel and Lee (1990), Bush et al. (1991), and Ishimura et al. (2012). In general, this method features an additional steel frame which is connected to the primary RC frame structure along its inner perimeter. In such an approach, the gusset plates can be directly welded to the additional steel frame. Figure 2.13 shows the schematic depiction of a chevron-braced frame with additional steel frame. As can be seen, the steel frame is attached to the primary structure using post-installed anchors along the complete perimeter. In Usami et al. (1988) and Ishimura et al. (2012), the connection detail between the steel frame and the RC frame featured adhesive anchors which are installed in the RC beams and columns. These anchors feature a head at the free side which is not driven into the concrete frame. Headed studs are also welded to the steel frame sections. The headed studs are then anchored in an intermediate layer of mortar which is subsequently poured in, thus realizing the connection between the steel and the RC frame. Generally, spiral reinforcement is provided to strengthen the connection (Usami et al., 1988). Alternatively, the steel frame may be fixed to the RC frame by adhesives or by means of a combination of adhesives and anchors (Ishimura et al., 2012). The steel bracing is then fixed to the steel frame using gusset plates as illustrated in Figure 2.13. One advantage of this connection approach is the beneficial effect it may have on the RC beams and columns. When the steel frame is properly encasing the RC members as shown in Goel and Lee (1990), it can function as a local strengthening. This is particularly helpful when the preliminary analysis of the existing structure identified weak members or when RC beams and columns were weakened due to a previous earthquake. Other than that, an additional steel frame is an expensive connection method for the steel bracing with several shortcomings. It becomes apparent that the installation of the additional steel frame is rather elaborate and time consuming, which also makes it susceptible to flaws associated with the construction process. As pointed out by Mahrenholtz et al. (2015), there is an absence of design guidelines, which is why post-installed anchors are installed along the complete height and length of the RC columns and beams as shown in Usami et al. (1988), Ohishi et al. (1988), and Ishimura et al. (2012). Thus, this solution is also deemed as rather invasive. Moreover, the weight of the complete structure may increase significantly due to the additional steel frame, which is why a strengthening of the foundation might be required as well. The drawbacks of this method outweigh the potential benefits of a local strengthening. Therefore, it is preferable to directly connect the steel bracing to the existing RC frame structure.
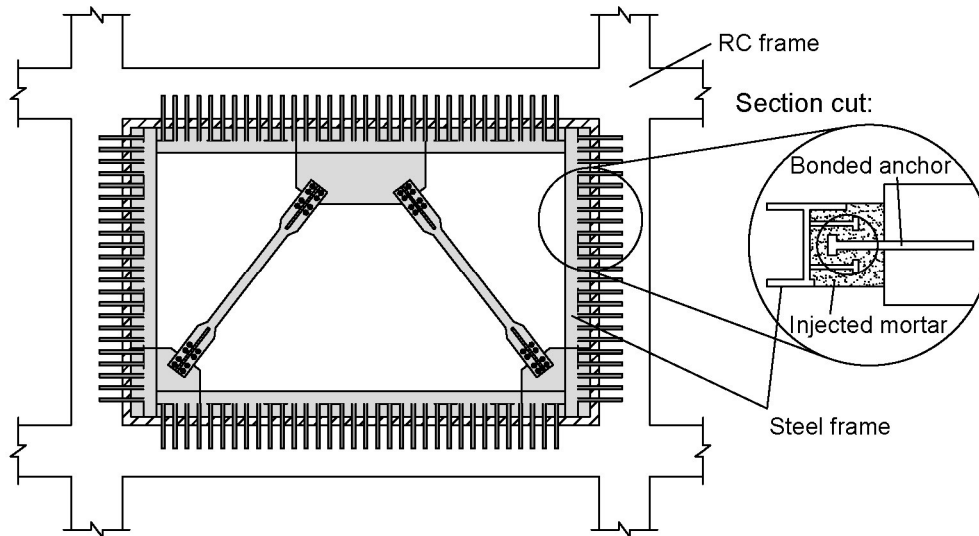
Figure 2.13. Schematic depiction of a steel bracing indirectly fixed to the primary RC frame structure by means of an additional steel frame. Based on Usami et al. (1988) and Ohishi et al. (1988).

2.2.2.3   Direct connection approach

In the direct connection approach, the additional steel frame is omitted, and the bracing system is directly attached to the RC frame structure via an anchor bracket-to-gusset plate connection. In comparison to the indirect approach, this results in a clear force path. Furthermore, such direct approaches are less expensive, more practical regarding the installation (low invasive), and at the same time they are capable to provide a connection between bracing and RC frame which is robust enough to guarantee the effectiveness of the strengthening solution. Several direct methods have been investigated in the past. Commonly, the anchor bracket is fixed to the RC frame by means of bolted-through connections, steel jackets, or pre-cast hooks as schematically depicted in Figure 2.14 (a) - (c). Pre-cast solutions were mostly investigated to assess the suitability of directly connected steel bracings in case of new structures. Obviously, these solutions are unsuitable for the retrofit of already existing structures. However, some of the findings also apply to post-installed solutions, which is why they will also be discussed where deemed helpful for a better understanding of the connection.

(a)   (b)   (c)   (d)
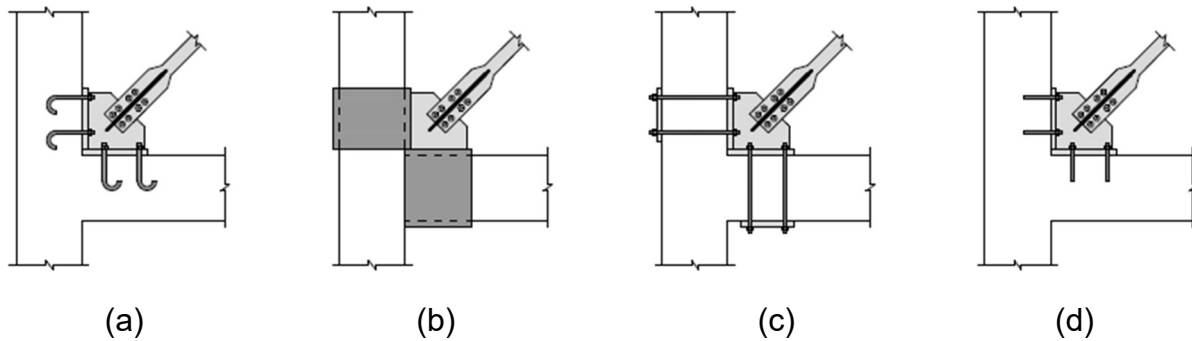
Figure 2.14. Schematic depiction of direct connection solutions using (a) pre-cast hooks, (b) steel jackets, (c) bolted-through connections, and (d) post-installed anchors.

On subassembly level, bolted-through connections were investigated by Maheri and Hadjipour (2003) and Li et al. (2013). In Maheri and Hadjipour (2003), the gusset plate is fixed to the RC members by straight bolts, which are fastened to the opposite side of the concrete members using a second steel plate as indicated in Figure 2.14 (c). The authors designed the complete connection in such a way that it would withstand the rupture of the brace element, whereby their design approach was based on current guidelines and standards for the design of brace-to-steel frame connections and baseplate-to-concrete connections. The experimental results clearly highlight the feasibility of the connection approach, where the final failure occurred in the steel brace as intended. However, in this approach, for the exterior frames, the steel plates are exposed to outside weather making them susceptible to corrosion. The post-tensioned bars require maintenance by regular inspection and re-tightening of the rods, since if the bolts get loose, the effectiveness of the force-transfer between the braces and the structure reduces significantly.

Li et al. (2013) investigated an alternative approach for bolted-through connections using ribbed anchor bars which were welded to the baseplates on both sides before casting. Although this approach is unsuitable for the use in retrofitting, it provides valuable insights into the behavior of such connections. The experimental campaign included subassembly tests with several loading schemes, where the loading direction (vertical, horizontal, combined loading) and the type of loading (monotonic and cyclic loading) were varied. The authors report that under monotonic loading, the best performance in terms of strength, initial stiffness, and ductility, was observed for the tension loaded connection. In the cyclic tests when the connection was alternately loaded in tension and compression, the compression behavior was superior as only small displacements were observed. Li et al. (2013) attribute this observation to the fact that the load is directly transferred from the baseplate to the concrete by contact pressure. A similar behavior was observed for the cyclic tests under inclined loading. Overall, the authors conclude from the hysteretic behavior of the connections in all tests that this kind of connection is not suitable to serve as an additional source of

energy dissipation for the structure. The failure mechanism in the vertical loading tests clearly showed the importance of considering the baseplate stiffness for the performance of the connection. It is reported that the baseplate deformed notably during the tests, which led to an uneven distribution of the forces among the anchors. Li et al. (2013) observed that when loaded in shear, the anchors were initially pressed against the concrete, which eventually resulted in concrete crushing around the anchors as the shear load increased. In consequence, the anchors started to bend and finally ruptured. It was observed that the connection slightly rotated during the experiments.

The feasibility and effectiveness of direct connection solutions has also been demonstrated in full-scale tests on RC frames. Maheri and Sahebi (1997) could show a marked improvement of the strength for the steel braced frames using direct connection approaches. Five different direct approaches were investigated by Massumi and Tasnimi (2008) in cyclic tests on single bay, single story frames strengthened using X-bracings. Two approaches featured bolted-through connections, whereby once the connection was fixed to both the beam and the column and the other time it was solely fixed to the column. In another two approaches the connection was fixed to the column by means of steel jackets. Thereby, in one test there was no additional layer between steel jacket and concrete, while in the other test the steel jacket was fixed to the column by means of adhesives. The fifth approach featured a pre-cast solution with anchors welded to the bracket, which were placed in the specimen before casting. The applied direct approaches were successful in so far as that in all tests, the strengthened frame exhibited an increase in strength and initial stiffness compared to the bare frame. However, differences between the approaches were observed. The authors report that in case of the bolted-thorough connection, which was only connected to the column, the strengthened frame showed more ductile behavior with high energy dissipation, whereas when the bolted-through connection was connected to both the beam and column the stiffness of the structure was markedly enhanced. When only connected to the column, the strength increase was somewhat less compared to when connected to both the column and beam. The steel jacket connection approach without adhesives led to pinched hysteretic loops of the strengthened frame and poor energy dissipation. The authors associate the observed unfavorable behavior with shifting of the jacket connection. The problem can be solved by fixing the steel jacket to the column by means of adhesives, which led to a preferable behavior of the strengthened frame with sufficient energy dissipation.

The experimental observations discussed so far clearly highlight that a direct connection between the steel bracing and the RC frame structure is a feasible and effective solution. For the retrofitting of RC structures, the previously discussed connection approaches are associated with some shortcomings though. Although the invasiveness of these solutions is significantly reduced in comparison to the indirect approach, in particular the bolted-through connection is still deemed rather invasive as

it requires drilling through the complete RC members. Also, the solutions suitable for retrofitting such as bolted-through connection and steel jacketing require an access from at least two sides. In case of retrofitting already existing buildings, the accessibility might not always be guaranteed and establishing it would entail elaborate construction work. These shortcomings can be overcome by using post-installed anchors to form the connection (Figure 2.14 (d)). Post-installed anchors offer a low invasive solution. The number of anchors and the embedment depth (thus the depth of the drill hole) can be adjusted to the given problem. Thus, only as many anchors as are actually needed must be installed. The installation of the anchors is carried out entirely in the bay where the bracing system is installed in, and no further access is required. Besides, when using post-installed anchors, the force path from the steel braces to the RC frame is relatively straight forward. On top, it offers an architecturally appealing solution compared to bolted-through connections or steel jackets. Nonetheless, there are also some challenges that arise when using post-installed anchors in such connections. These challenges will be discussed in the next section.

2.3   Challenges arising for direct connections using post-installed anchors

2.3.1   Hysteretic and displacement behavior of the anchors

Only few studies have been conducted on steel braced frames using post-installed anchors to form a direct connection between steel bracing and RC frame. As mentioned above, Yooprasertchai and Warnitchai (2008) conducted an experimental investigation on the behavior of a RC frame subassembly using a BRB to enhance the performance of the RC column. In their study, the subassembly featured only a small part of the top beam to which the BRB was attached using adhesive anchors. The results clearly showed the effectiveness of the solution in enhancing the seismic performance of the RC column. Besides, the authors reported that the anchors performed adequately without failure. Nonetheless, it should be noted that the used subassembly could not adequately simulate the stress condition and crack formation in the anchorage zone generally observed in RC frames. In Maheri and Sahebi (1997) and Qu et al. (2015) post-installed anchors were used to successfully fasten the steel bracings or BRBs to the RC frame in full-scale experimental tests. While these studies demonstrate the feasibility of the approach, the investigations mainly focus on the global behavior of the structure itself and not on the performance of the anchorage. Nonetheless, Maheri and Sahebi (1997) point out that the strength of the tested connection with post-installed anchors was somewhat lower compared to the connection with a pre-cast solution. The authors observed either concrete related or pull-out failure of the post-installed anchors.

As shown in Mahrenholtz et al. (2015), however, the performance of the anchors may very well have a significant influence on the performance of the strengthening solution.

As mentioned before, bonded expansion anchors were used to fasten the BRB to the RC frame (see Figure 2.9). The authors reported that as the load on the frame was increased during the course of the experiment, also the load on the anchorage increased and the anchors were steadily pulled out of the concrete. Since the anchors were not meant to take up any compression load and thus were not pushed back when the BRB was under compression (compression force is directly transferred from the baseplate to the concrete via contact pressure), the irrecoverable anchor displacements led to an offset of the gusset plate. Such geometric imperfections of the gusset plate can result in local buckling of the transition segment of the BRB and thus reduce its effectiveness as shown in Mazzolani et al. (2009).

Another example of how the performance of the chosen anchor system can affect the effectiveness of a strengthening solution is reported in Genesio (2012), Sharma (2013), and Sharma (2019). Although the study is not dealing with steel bracings per se, the results of the experiments with different types of post-installed anchors clearly showed that the displacement and hysteretic behavior of different types of anchors may significantly influence the performance of the complete strengthening solution. In Genesio (2012) and Sharma (2013), tests are reported on RC beam-column-joint subassemblies prone to brittle shear failure under seismic actions. To strengthen the joint and change the failure mode into a ductile beam failure, the so-called Fully Fastened Haunch Retrofit Solution (FFHRS) was applied. An analysis of the test results in terms of the influence of the anchorage on the performance of the attached strengthening solution was performed in Sharma (2019) and is presented hereafter. The FFHRS was fastened to the RC members by means of different types of post-installed anchors, namely expansion anchors, concrete screws, and bonded anchors. Thereby, for all types of anchors, the anchorage was designed for approximately the same resistance. It is worth mentioning that all anchors used in the experiments held an approval for the use under seismic actions. While in each test, the dimensions and properties of the concrete specimen and the haunch element were the same, the performance of the strengthened structure varied notably when different types of anchors were used. Depending on the type of anchor, the effectiveness of the strengthening solution changed with respect to the obtained increase in strength and the observed failure mode.

This example reveals the first two challenges when using post-installed anchors. First, for the use in structural applications, it is insufficient to design the anchorage solely for the resistance in terms of forces. A design solution is required which considers the complete load-displacement behavior of the anchorage. The first point inevitably leads to the second point. The varying performance of different types of post-installed anchors, requires qualification tests and assessment criteria, which are capable to determine the individual hysteretic and displacement characteristics that are required for a safe design (Sharma, 2019). Only then is it possible to identify the type of anchor that is best suited for a particular task. Moreover, it is required to understand the

hysteretic and displacement behavior of anchor groups and their individual anchors under seismic loading.

2.3.2 Geometrical restrictions

In case of steel braced RC frames, the braces are generally fastened to the RC members such as beams and columns. Several bracing configurations further require an installation in the corner of the frame (such as X-bracing or diagonal bracing). This imposes certain geometrical restrictions on the anchorage as illustrated in Figure 2.15. The limited dimensions of the beams and columns pose a challenge on the anchorage in such a way that it limits the capacity in case of concrete related failure modes, such as concrete cone breakout failure, due the parallel close edges (Figure 2.15 (a)). Since other failure modes, such as pull-out failure or steel failure are not affected by close edges or neighboring anchors, concrete related failure modes become the dominant failure mode for such connections. These failure modes are in turn associated with a rather brittle failure. Also, the limited depth of the beams and columns limits the maximum possible embedment depth as indicated in Figure 2.15 (b). Finally, by placing the connection in the corner of the frame, basically two perpendicular anchor groups are placed relatively close to each other. As indicated in Figure 2.15 (a), these two anchor groups share a common breakout body. Furthermore, the two anchor groups might have a mutual influence on each other. This spatial anchor configuration in the corner presents a particular challenge for practitioners as no design recommendations are available in current guidelines or standards for such configurations.

(a)   (b)
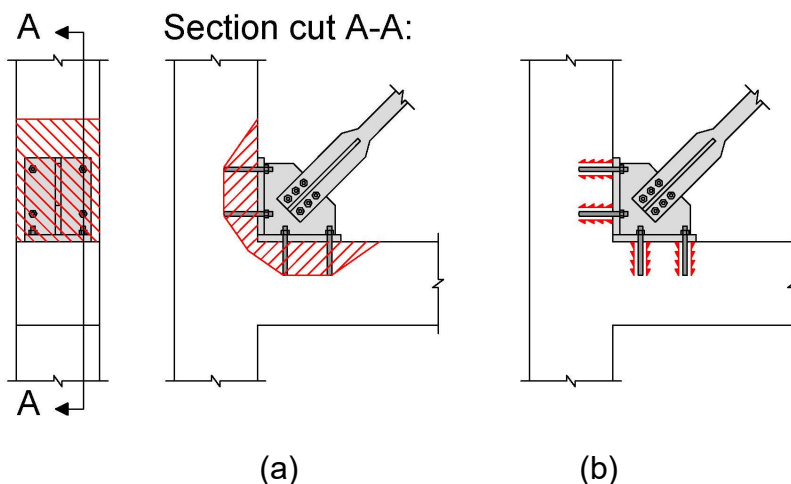
Figure 2.15. Challenges arising from the geometrical conditions of a corner configuration.

2.3.3 Cracking in the concrete members

Due to the relatively high demands during a seismic event, it is reasonable to assume a cracked condition of the RC members in which the anchors are installed in. Generally, post-installed anchors are only to be used in areas of the structure where no inelastic behavior is expected during an earthquake, which can be seen from the fact that specifically plastic hinges zones are currently not covered in the qualification of post-installed anchors under seismic actions according to EOTA TR 049 or in the design of anchors according to EN 1992-1. Thus, considering a RC member dominated by bending, the maximum expected crack width during a seismic event, just outside of a potential plastic hinge zone, can be related to the point where the reinforcement starts yielding (Hoehler, 2006; Nuti and Santini, 2008). Based on these assumptions, Hoehler (2006) and Nuti and Santini (2008) conducted analytical studies to determine the crack width at steel yield strain for various RC cross sections. Thereby, they calculated the crack width using empirical equations given in standards and literature. The parameters considered in the studies included the reinforcement ratio, number of reinforcing bars, diameter of reinforcement, yield strength, neutral axis depth, and concrete cover. According to their studies, it can be assumed that during a seismic event, a crack width of 0.8 mm can occur in the anchorage zone. This value was also adopted for cyclic qualification tests of post-installed anchors used in structural applications according to EOTA TR 049.

Since both the RC members (base material) and the connected elements (load) are set in motion by the earthquake, the cracks in the anchorage zone are cyclically closing and opening while at the same time the anchors are subjected to an alternation of loading and unloading. Thereby, Mahrenholtz and Eligehausen (2016) state that phasing between load and crack cycling depends strongly on the application itself. The two extreme cases are out-of-phase and in-phase (Mahrenholtz and Eligehausen, 2016). However, anchors might also exhibit a particular phase or phasing might even be random in nature.

In Mahrenholtz and Eligehausen (2016), tests on single anchor headed bolts were performed, investigating the influence of different phases between tension load and crack cycling on the anchor behavior. The investigated phases included crack cycling at constant load, in-phase crack and load cycling, out-of-phase crack and load cycling, and crack and load cycling at different frequencies. According to the authors, the typical failure mode in these experiments was concrete cone failure. The experiments were evaluated with respect to the displacement behavior of the anchors. It was found that crack cycling at constant tension load yields the least favorable behavior in comparison to out-of-phase or in-phase cycling, while out-of-phase cycling showed a superior displacement behavior with less anchor displacement after cycling compared to the other tests. As the anchor is simultaneously (re-) loaded while the cracks are closing, it was observed that the stiffness increases and the reloading branch becomes steeper due to the closing crack (Mahrenholtz and Eligehausen, 2016).

On the other hand, experiments conducted by Sharma et al. (2016) on two different types of undercut anchors with different embedment depth, which were exposed to crack cycling at constant load, in-phase crack and load cycling and out-of-phase crack and load cycling, showed that the displacement behavior depends on various parameters. Depending on the type of anchor, the authors report that either crack cycling at constant load or in-phase cycling yielded the least favorable behavior. However, in agreement with the results of Mahrenholtz and Eligehausen (2016), out-of-phase crack cycling showed the most favorable displacement behavior, regardless of the type of anchor. In addition, Sharma et al. (2016) conclude from the test results that crack cycling had basically no influence on the ultimate load of the tested undercut anchors in the residual pull-out tests resulting in concrete cone breakout.

Figure 2.16 shows the distribution of internal forces and the deformed shape of a braced frame which is loaded by a horizontal force in such a way that the steel brace is in tension. Thus, representing the case where the anchors are loaded during a seismic event. It can be seen that when the anchors are actually activated, the RC members adjacent to the corner joint, where the bracing is fastened to the RC frame, are in compression. Thus, the anchorage zone is compressed. Moreover, the negative bending moment in the corner results in the beam and column bending inwards. Consequently, in case of steel bracing, cracks open when there is practically no load on the anchor. Likewise, the cracks have mostly closed by the time the anchors are loaded again as shown in Mahrenholtz et al. (2015). Besides, as shown in Mahrenholtz et al. (2012) and Piccinin et al. (2013), it can be assumed that the compressive force acting in the anchorage zone when the anchors are loaded has a positive effect on their behavior (Mahrenholtz et al., 2015). These considerations indicate that in the case of steel bracing connections in the corner of RC frame structures, the behavior of the anchors is rather influenced by the cyclic displacement and force demands than by cyclic crack opening in the concrete members.

It should be noted however, that in other strengthening applications, the opposite behavior may occur. This is for example the case when post-installed anchors are used to attach haunch elements to the RC members (Sharma, 2013). Here, the haunch element is tensioned, and thus the anchors are loaded, when the RC beam and column are bending outwards. This means that when the anchors are activated, the anchorage zone is tensioned, and cracks are opening. In such an application, load and crack cycling of the anchors happens in-phase and the behavior is strongly influenced by the cyclic opening and closing of the cracks (Sharma, 2019).

| Bending moment | Axial force | Deformed shape |
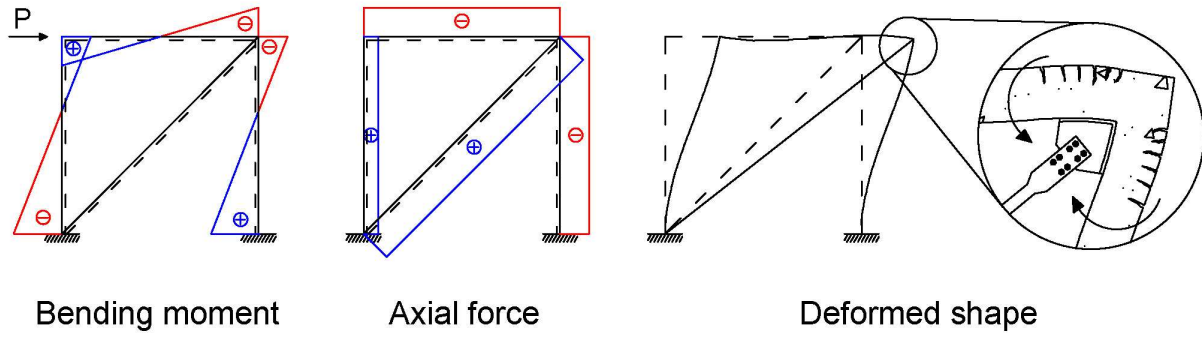
Figure 2.16. Internal forces and deformed shape of a horizontally loaded braced frame.

3 Seismic qualification and design of anchors – State of the art

3.1 Seismic qualification of anchors

To assess the performance of post-installed anchors under seismic actions, qualification tests are performed. In Europe, these qualification tests, the testing procedures, and the corresponding assessment criteria are specified in EOTA TR 049. Here, two performance categories, C1 and C2 are given for which the anchors can be qualified. Category C1 is generally only used for post-installed anchors whose intended use is to fasten non-structural elements to the RC structure, while category C2 may be used to assess the performance of anchors used in structural and non-structural applications (EN 1992-4). The tests which are performed to assess the anchor performance varies between the two categories and so do the assessment criteria. Since category C2 is also used for structural applications, the qualification tests are generally more demanding, and the assessment criteria are more rigorous than the ones in category C1. In this context it is worth mentioning that the current American qualification guidelines for post-installed anchors under seismic actions, ACI 355.2 and ACI 355.4, are comparable to category C1 in the European guideline. However, discussions are ongoing to upgrade them to make them comparable to category C2 in the next cycle of the guidelines.

EN 1992-4 specifies for which of the two categories an anchor must be qualified to be suitable for certain applications. Thereby, the decision is mainly based on the level of seismicity (ground acceleration) and the building performance class, both of which are defined in EN 1998-1. Additionally, in Germany, the categories are related to the expected damage in the structure defined by the maximum calculated crack width (DIN EN 1992-4/NA).

Both categories feature force-controlled pulsating tension load tests and alternating shear load tests. The main difference with respect to the testing procedures in the two categories is the maximum load for which the anchors are tested in the cycling phase, the maximum considered crack width, the number of load steps, the number of cycles applied in each load step, and whether the load is stepwise decreased (C1) or stepwise increased (C2). Besides, category C2 features additional qualification tests where the anchors are subjected to crack cycling (opening and closing of cracks) at constant tension load. As the test conditions in these crack cycling tests are generally deemed to be particularly severe, they are generally crucial for the seismic qualification of anchors in category C2 (Muciaccia, 2017; Muciaccia and Marchisella, 2017). The

maximum considered crack width in category C1 is Δw = 0.5 mm. In category C2, the maximum considered crack width is increased to Δw = 0.8 mm, to account for the possibility of anchors being located close to plastic hinge zones.

When post-installed anchors are used in nuclear power plants or nuclear facilities in Germany, the requirements for the use of anchors are significantly higher compared to the requirements assessed in EOTA TR 049. Therefore, the suitability of an anchor system for the use in nuclear power plants and nuclear facilities in Germany is assessed according to DIBt (2010) Guideline for Fastenings with Anchors in Nuclear Power Plants and Nuclear Facilities. Here, the maximum considered crack width is Δw = 1.5 mm.

The following provides an overview of the testing procedures and assessment criteria which are required for the qualification of anchors under seismic loading according to EOTA TR 049 and DIBt (2010). Note that parts of the following discussion have been published in Stehle and Sharma (2021a).

3.1.1 EOTA TR 049: Category C1

Category C1 includes tests under pulsating tension load (C1.1) and tests under alternating shear load (C1.2). The maximum considered crack width in category C1 is Δw = 0.5 mm. Thereby, Δw refers to the targeted crack opening after installation of the anchor, thus as a difference to the already existing hairline crack. A summary of the testing conditions is given in Table 3.1.

Table 3.1. Summary of the required test series in category C1 according to EOTA TR 049.

ID	Test type	Number of tests	Load	Crack width, Δw (mm)	Number of cycles
C1.1	Pulsating tension load	5	$N_{eq} = 0.5\,N_{u,m}$[1]	0.5	140
C1.2	Alternating shear load	5	$V_{eq} = 0.5\,V_{u,m}$[2]	0.5	140

(1) $N_{u,m}$ is the mean ultimate tension load obtained from reference tension tests in cracked concrete according to EAD 330232 or in case of bonded anchors from service condition tests according to EAD 330499.

(2) $V_{u,m}$ is the mean ultimate shear load measured in tests for characteristic resistance to steel failure under shear load in non-cracked concrete according to EAD 330232.

3.1.1.1 Test series C1.1 – Pulsating tension load

In C1.1, the anchors are tested for their performance under simulated tension load in cracked concrete with a crack width of Δw = 0.5 mm and away from the edge. The respective loading history is shown in Figure 3.1 (a). As can be seen the protocol comprises stepwise decreasing load with 10 cycles in the first load step, 30 cycles in the second load step and 100 cycles in the last load step. After completion of the

loading history, a residual pull-out test is performed where the anchor is loaded until failure. The maximum applied tension load during load cycling, N_{eq}, is calculated as 50% of the mean ultimate tension load obtained from reference tension tests in cracked concrete according to EAD 330232 or in case of bonded anchors from service condition tests according to EAD 330499. The loads to be applied in the subsequent two load levels, N_i and N_m, are 75% and 50% of N_{eq}, respectively.
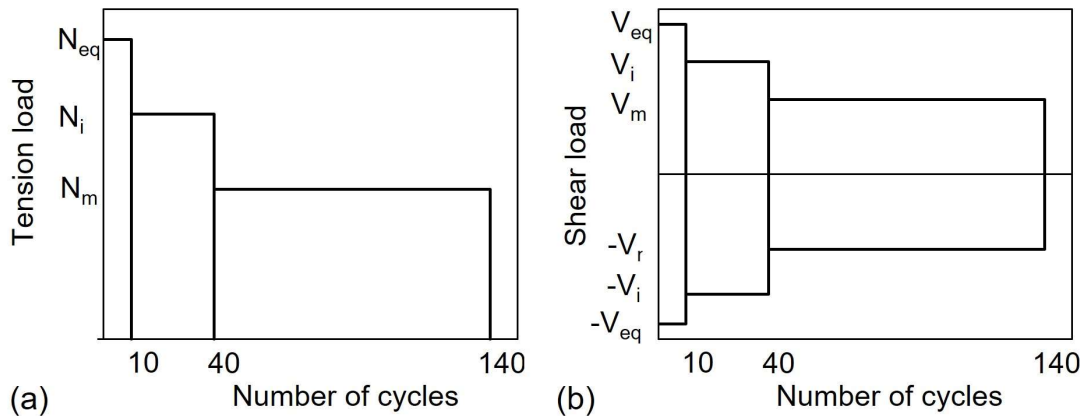
Figure 3.1. Schematic test procedure for (a) pulsating tension load tests in test series C1.1 and (b) alternating shear load tests in test series C1.2. Redrawn on basis of EOTA TR 049.

3.1.1.2   Test series C1.2 – Alternating shear load

Similar to C1.1, the tests in series C1.2 under alternating shear load are performed in a constant crack with a width of $\Delta w = 0.5$ mm and away from the edge. Again, the load is stepwise decreasing as can be seen in Figure 3.1 (b) and the number of cycles in the respective load steps is the same as in test series C1.1. After completion of the loading history the anchor is loaded in shear until failure in order to determine the residual ultimate load after cycling. The maximum applied shear load during the cycling phase, V_{eq}, is determined based on the tests for characteristic resistance to steel failure under shear load in non-cracked concrete according to EAD 330232 and is taken as 50% of the corresponding mean ultimate shear load. The shear loads for the two subsequent levels, V_i and V_m, are 75% and 50% of V_{eq}, respectively.

3.1.1.3   Assessment criteria for category C1

In both, tests under pulsating tension load and tests under alternating shear load, the anchor has to complete the above described cyclic loading history. Furthermore, the mean residual ultimate load in the respective test series shall be at least 160% of N_{eq} and V_{eq} in case of tension and shear tests, respectively. If these two requirements are met the seismic reduction factors $\alpha_{N,C1}$ for tension loading and $\alpha_{V,C1}$ for shear loading equal 1. Thus, the characteristic seismic resistance equals the characteristic resistance in cracked concrete as reported in the ETA for monotonic loading. If the

anchor is unable to meet one of the two requirements in one of the test series, the respective test series is repeated. Thereby the tests are conducted with a reduced maximum cyclic load, $N_{eq,red}$ or $V_{eq,red}$. Accordingly, the load values of the subsequent load levels are also reduced. If the anchor is able to fulfill the two requirements with the reduced cyclic load, the seismic reduction factors for tension and shear loading are calculated using following equations (EOTA TR 049):

$$\alpha_{N,C1} = \frac{N_{eq,red}}{N_{eq}}, \tag{3.1}$$

$$\alpha_{V,C1} = \frac{V_{eq,red}}{V_{eq}}. \tag{3.2}$$

The characteristic seismic resistance of an anchor for the individual failure modes is calculated by multiplying the seismic reduction factor by the respective characteristic resistance against monotonic loading.

3.1.2   EOTA TR 049: Category C2

Note that parts of this section have been published in Stehle and Sharma (2021a).

According to Mahrenholtz et al. (2017), the qualification tests in category C2 were developed in such a way that they would allow the assessment of the anchor performance at suitability level and at the serviceability level. The authors state that for suitability level, it must be demonstrated that an anchor functions well even under severe earthquakes (large crack width $\Delta w = 0.8$ mm and load cycling up to the characteristic load based on the corresponding reference tests) and that an anchor can reliably transfer loads even after a seismic event. At serviceability level, the performance of an anchor in terms of displacement is judged for more moderate conditions, that is medium crack width $\Delta w = 0.5$ mm and load cycling up to the design load based on the reference tests (Mahrenholtz et al., 2017).

In contrast to C1, category C2 includes monotonic reference tests for tension and shear load (C2.1 and C2.2, respectively), which are performed in cracked concrete with a crack width of $\Delta w = 0.8$ mm. The following cyclic tests include tests under pulsating tension load (C2.3), tests under alternating shear load (C2.4), and crack cycling tests at constant tension load (C2.5). The crack cycling tests were newly incorporated into the test program and, as mentioned above, the corresponding test conditions are generally deemed to be the most severe, which is why these tests are often pivotal to the qualification of the tension behavior of anchors (Muciaccia, 2017; Muciaccia and Marchisella, 2017). Moreover, in category C2, a larger crack width is considered. Here the anchors are tested in cracked concrete with a maximum crack width of $\Delta w = 0.8$ mm. Again, Δw refers to the targeted crack opening as a difference to the hairline crack after the anchor has been installed but before the test has started. As previously mentioned, the maximum crack width in category C2 is based on the stipulation given

in EOTA TR 049 and EN 1992-1, which limits the potential location of post-installed anchors to areas of the structure where no inelastic behavior is expected during an earthquake. In this context, several studies (Hoehler, 2006 and Nuti and Santini, 2008) have determined the maximum crack width which might occur in the anchorage zone during an earthquake as $\Delta w = 0.8$ mm. A summary of the testing conditions is given in Table 3.2.

Table 3.2. Summary of the required test series in category C2 according to EOTA TR 049.

ID	Test type	Number of tests	Load	Crack width, Δw (mm)	Number of cycles
C2.1	Reference tension test	5	Until failure	0.8	-
C2.2	Reference shear test	5	Until failure	0.8	-
C2.3	Pulsating tension load	5	$N_{max} = 0.75\ N_{u,m,C2.1}$	0.5 ($\leq 0.5\ N/N_{max}$) 0.8 ($> 0.5\ N/N_{max}$)	75
C2.4	Alternating shear load	5	$V_{max} = 0.85\ V_{u,m,C2.2}$	0.8	75
C2.5	Crack cycling	5	$N_{w1} = 0.4\ N_{u,m,C.21}$ $N_{w2} = 0.5\ N_{u,m,C.21}$	0.1 - 0.8	59

3.1.2.1   Test series C2.1 and C2.2 – Monotonic reference tests

In category C2, additional reference tests are performed in cracked concrete with a crack width of $\Delta w = 0.8$ mm. The main information which is determined from these reference tests is the mean ultimate load of the anchors in tension and shear, $N_{u,m,C2.1}$ and $V_{u,m,C2.1}$, respectively. These parameters are required to define the load levels in the cycling phase of the following test series, C2.3, C2.4 and C2.5.

3.1.2.2   Test series C2.3 – Pulsating tension load

Figure 3.2 shows the cyclic loading history for test series C2.3. It can be seen that the loading protocol for the cyclic phase differs from the procedure in category C1. The main differences are the number of load steps, the number of applied cycles per load step and a cyclic loading history which features stepwise increasing load steps instead of stepwise decreasing load steps. It is worth mentioning that the major benefit of stepwise increasing loading protocols is that the anchor stiffness can be assessed in the individual cycles in the complete cycling phase as pointed out by Silva (2001). In C2.3, more load steps are considered compared to C1.1. In total, the protocol comprises nine load steps. Starting at $0.2\ N_{max}$, the load is increased by $0.1\ N_{max}$ in every step. The maximum load level for which the anchor is cycled, is N_{max}, whereby N_{max} is defined as 75% of the mean ultimate load, $N_{u,m,C2.1}$, determined from the

reference tension tests in C2.1. After the anchor has undergone the complete loading history, a residual pull-out test is performed to determine the residual capacity of the anchor. Although more load steps are considered, the total number of cycles was reduced to 75 compared to the C1.1 procedure. Thereby, 25 cycles are applied in the first load step, 15 cycles in the second load step and five cycles in each subsequent load step. As outlined in Mahrenholtz et al. (2017), the number of cycles at different relative load levels was determined based on the calculated behavior of various single-degree-of-freedom (SDOF) systems representing typical nonstructural elements in buildings under seismic excitations. Note that in case of the protocol for alternating shear load in test series C2.4, the number of cycles per load level was determined in the same way.
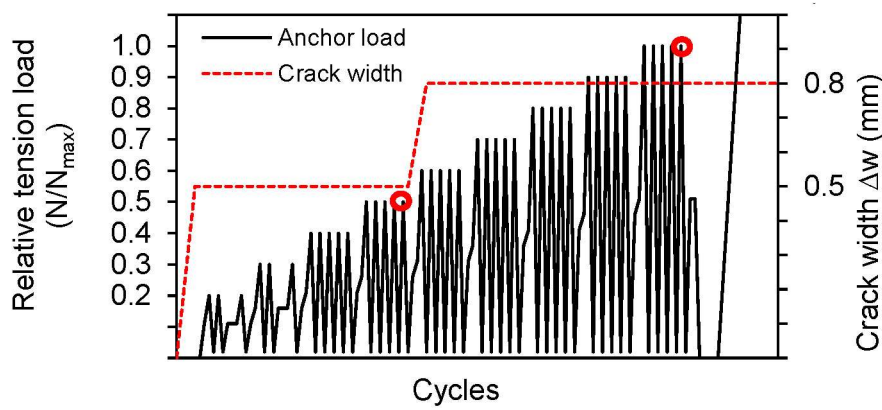
Figure 3.2. Schematic test procedure for pulsating tension load tests in test series C2.3. Redrawn on basis of EOTA TR 049.

During the cyclic phase, the serviceability level and the suitability level are assessed at different load levels. These points are marked by a red dot in Figure 3.2. As already mentioned, the characteristic capacity of an anchor is considered at suitability level. Here, the maximum load at which the anchor is cycled, N_{max}, represents the characteristic ultimate load of an anchor. It is calculated as 75% of the mean ultimate load obtained from the reference tension tests in C2.1. According to Mahrenholtz et al. (2017), this value is based on the corresponding 5% fractile, assuming a coefficient of variation of 15%. At serviceability level, the design ultimate load of an anchor is considered, which is determined as around 50% of the characteristic capacity, thus 0.5 N_{max} (Mahrenholtz et al., 2017). Besides the load levels, suitability level and serviceability level are characterized by the considered crack width. It can be seen in Figure 3.2 that the test starts at a crack width of $\Delta w = 0.5$ mm, which is maintained up to a load of 0.5 N_{max}. After completion of the cycles at 0.5 N_{max}, the test is paused, and the crack is widened to $\Delta w = 0.8$ mm, which is maintained for the remaining cyclic phase and the subsequent residual pull-out test. It is worth mentioning that it is allowed to perform the tests already starting at a crack width of $\Delta w = 0.8$ mm.

3.1.2.3 Test series C2.4 – Alternating shear load

Figure 3.3 shows the cyclic loading history used in test series C2.4. Like in test series C2.3, the protocol for alternating shear load tests is characterized by nine stepwise increasing load levels, whereby the anchors are loaded in the direction in which the crack extends. The first step considers a load of 0.2 V_{max}. In each subsequent step, the load is increased by 0.1 V_{max} with V_{max} being the maximum load applied in the cyclic phase. Similar to C2.3, the maximum shear load is considered as the characteristic ultimate load of the anchor based on the monotonic reference tests in C2.2. According to Mahrenholtz et al. (2017), this value is determined from the 5% fractile of the corresponding mean ultimate load obtained in the reference tests, assuming a coefficient of variation of 10%. Thus, V_{max} corresponds to 85% of the mean ultimate load obtained from the monotonic shear tests in C2.2. The first load step comprises 25 cycles, the second load step comprises 15 cycles, and each subsequent load step comprises five cycles. It can be seen that in contrast to the procedure in C2.3, the complete test is performed with a crack width of $\Delta w = 0.8$ mm. This approach simplifies the testing procedure considerably since the test must not be interrupted to increase the crack width. The difference from the C2.3 procedure can be explained by the fact that experimental shear tests on anchors in cracked concrete indicated that the crack width had only a minor effect on the behavior of the anchors (Mahrenholtz et al., 2016; Lee and Jung, 2021).
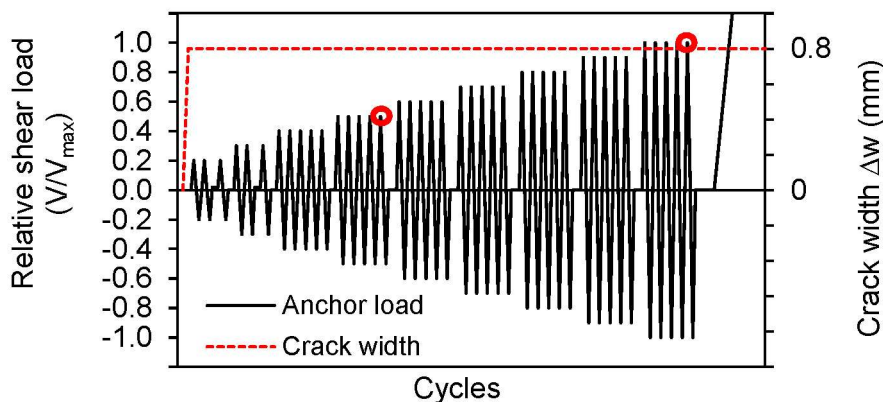
Figure 3.3. Schematic test procedure for alternating shear load tests in test series C2.4. Redrawn on basis of EOTA TR 049.

3.1.2.4 Test series C2.5 – Crack cycling at constant tension load

In contrast to category C1 or guidelines for qualification and testing of anchors under seismic actions such as ACI 355.2 and ACI 355.4, category C2 introduces a test series where the crack width is cycled at constant tension load. Again, a stepwise increasing approach was chosen for the development of the protocol. In each step, the crack is opened by 0.1 mm, starting at a crack width of $\Delta w = 0.1$ mm, and ending at a maximum crack width of $\Delta w = 0.8$ mm. Here, similar to C2.3, serviceability is checked after

completion of the crack cycles at a crack width of $\Delta w = 0.5$ mm and suitability is checked after completion of the crack cycles at $\Delta w = 0.8$ mm (Mahrenholtz et al., 2017). The red dots in Figure 3.4 indicate the corresponding points during the procedure. As can be seen in Figure 3.4, two load levels are considered. N_{w2} is calculated as 50% of the mean ultimate load obtained from the reference tension tests in C2.1. According to Mahrenholtz et al. (2017), this value is based on the characteristic ultimate load of an anchor, while taking the design material strength into account. N_{w1} is defined as 80% of the load level at suitability level. Thus, N_{w1} is calculated as 40% of the mean ultimate load obtained from the reference tension tests in C2.1. The difference between the constant load levels is based on experimental results conducted by Mahrenholtz and Eligehausen (2016). The results suggest that phasing, that is simultaneous crack and tension load cycling, is actually less demanding than crack cycling at constant tension load (see discussion above). Since in real applications, anchors are generally subjected to both load and crack cycling at the same time, the load at serviceability level was reduced to consider the more demanding test procedure (Mahrenholtz, 2013; Mahrenholtz et al., 2017). In the first step at 0.1 mm crack width, 20 cycles are performed, 10 cycles at 0.2 mm crack width, five cycles at a crack width of 0.3 mm - 0.7 mm, and four cycles in the last step at 0.8 mm crack width. In total, 59 crack cycles are performed. The number of crack cycles in each step was determined based on a numerical parametric study (Mahrenholtz et al., 2017).
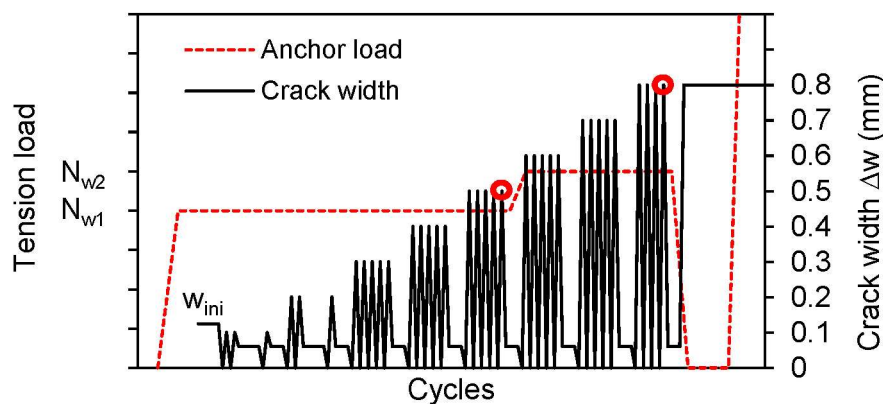
Figure 3.4. Schematic test procedure for crack cycling tests at constant tension load in test series C2.5. Redrawn on basis of EOTA TR 049.

3.1.2.5   Assessment criteria for category C2

In category C2, the anchor performance is assessed with respect to the capacity that can be achieved after a defined seismic action in the residual pull-out test and with respect to the displacement behavior at serviceability level. In addition to the α reduction factor already introduced in category C1, a second reduction factor, β, is introduced. Note that the loads in this section refer to those normalized depending on the failure mode.

For test series C2.1 and C2.2, the α reduction factors, $\alpha_{C2.1}$ and $\alpha_{C2.2}$, are determined based on the mean ultimate load of the anchors. The mean ultimate load in C2.1, must be at least 80% of the mean ultimate tension load obtained from the respective qualification tests for large crack width according to EAD 330232 or EAD 330499. The mean ultimate load in C2.2 must be at least 80% of the mean ultimate shear load obtained from the qualification tests in EAD 330232 to determine the characteristic resistance to steel failure. If the mean loads measured in test series C2.1 and C2.2 fall below the specified criteria, the reduction factors $\alpha_{C2.1}$ and $\alpha_{C2.2}$ are defined as the ratio between the obtained mean ultimate capacity in C2.1 or C2.2 and the targeted minimum capacity.

The definition of the α reduction factors in test series C2.3, C2.4, and C2.5 is more complex since the final reduction factor for one test series is determined from three individual assessment criteria. For each of these criteria a particular factor is determined. The first criterion concerns the performance of the anchors in the cycling phase. If an anchor fails under the specified cyclic demands, the test series is performed again, whereby the demands in terms of applied forces are reduced. In this case, the first reduction factor, α_A, is defined as the ratio between the reduced maximum load value during cycling and the initially considered maximum load value. The second criterion concerns the displacement of the anchors at serviceability level, after completion of the last cycle of the corresponding load or crack level. If the corresponding mean anchor displacement is larger than 7 mm, the anchors must be tested again for lower loads. In this case, the second reduction factor, α_B, is defined as the ratio between the reduced maximum load value during cycling and the initially considered maximum load value. The third criterion stipulates a minimum mean ultimate load which shall be achieved in the residual capacity tests. In test series C2.3 and C2.5 for cyclic tension, the mean ultimate load shall be at least 90% of the mean ultimate load obtained from the monotonic reference test series C2.1. In test series C2.4 for cyclic shear, the mean ultimate load shall be at least 95% of the mean ultimate shear load obtained in the monotonic reference test series C2.2. If the actual mean ultimate load of an anchor is below the stipulated minimum value, the third reduction factor, α_C, is defined as the ratio between the actual mean ultimate load and the targeted load value. Based on these three factors, the reduction factor for the individual test series can be calculated as (EOTA TR 049):

$$\alpha_{C2.3} = \min\left(\alpha_{C2.3,A}; \alpha_{C2.3,B}\right) \cdot \alpha_{C2.3,C}, \tag{3.3}$$

$$\alpha_{C2.4} = \min\left(\alpha_{C2.4,A}; \alpha_{C2.4,B}\right) \cdot \alpha_{C2.4,C}, \tag{3.4}$$

$$\alpha_{C2.5} = \min\left(\alpha_{C2.5,A}; \alpha_{C2.5,B}\right) \cdot \alpha_{C2.5,C}. \tag{3.5}$$

The final α reduction factors for tension loading, $α_{N,C2}$, and shear loading, $α_{V,C2}$, in category C2 are defined as (EOTA TR 049):

$$\alpha_{N,C2} = \alpha_{C2.1} \cdot \min(\alpha_{C2.3}; \alpha_{C2.5}), \tag{3.6}$$

$$\alpha_{V,C2} = \alpha_{C2.2} \cdot \alpha_{C2.4}. \tag{3.7}$$

The β reduction factors consider the scatter of ultimate loads in the monotonic reference tests and in the residual capacity tests after completion of the cyclic loading histories. In EOTA TR 049, the scatter is defined by means of the coefficient of variation (CV). In the tension tests, the CV shall not exceed 20% and in the shear tests, the CV shall not exceed 15%. Note that if the scatter of measured loads in any test series is very high (CV > 30%), the tested anchor cannot be approved for category C2. In the end, the final β reduction factor for tension loading, $β_{CV,N,C2}$, and shear loading, $β_{CV,V,C2}$, respectively are determined from the reduction factors of the individual test series (EOTA TR 049):

$$\beta_{CV,N,C2} = \min(\beta_{CV,C2.1}; \beta_{CV,C2.3}; \beta_{CV,C2.5}), \tag{3.8}$$

$$\beta_{CV,V,C2} = \min(\beta_{CV,C2.2}; \beta_{CV,C2.4}). \tag{3.9}$$

The characteristic tension and shear resistance of anchors which are fit for the use in category C2 are eventually calculated based on the two reduction factors.

Besides the discussed assessment criteria which define the characteristic resistance of an anchor, there are certain criteria which, if they are not fulfilled, result in the anchor not being fit for category C2. In general, these criteria are intended to guarantee a robust and reliable load-displacement behavior during a seismic event. In case of the tension tests, there are certain characteristics which are unacceptable if they occur before an anchor has achieved 70% of its final failure load. One such case is when the tested anchor is pulled out of the base material, while the tension load remains at a constant level and when the corresponding displacement during this instance exceeds 10% of the displacement measured at ultimate load. Another case is when the load falls to a local minimum, where the corresponding reduction exceeds 5% of the ultimate load. Additionally, the displacements at 50% of the mean ultimate load are assessed in the tension tests. The guideline stipulates that the corresponding scatter in terms of the coefficient of variation shall not exceed 40%. It should be noted that in case of the C2.3 and C2.5 tests, only the residual pull-out test is considered. This means that the displacement measured in the cyclic phase must be subtracted from the total measured displacement of the anchor. The intention behind limiting the scatter of the initial displacement is to ensure a uniform load distribution among the anchors in a

group, thus preventing a reduction of the failure load of anchor groups (Mahrenholtz, 2013). In case of the shear tests, an anchor cannot be approved for category C2, when pull-out or pull-through failure occurs. However, the tests may be performed again with the anchors being embedded deeper in the base material.

Finally, EOTA TR 049 stipulates the verification of the mean displacements at the end of serviceability and suitability level during the cycling phase of the tension and shear tests, respectively. These values are then reported in the corresponding assessment document. Although these values are not directly used to assess the anchor behavior under seismic actions, they do provide an estimation of the displacements that might be expected for different types of anchors during an earthquake.

3.1.3 DIBt Guideline for Fastenings with Anchors in Nuclear Power Plants and Nuclear Facilities

The DIBt (2010) guideline stipulates supplemental tests and criteria for which post-installed anchors shall be assessed when used for safety relevant applications in nuclear power plants or nuclear facilities in Germany. In this context, supplemental criteria means that an anchor must already be qualified for general use in concrete under predominantly static loads.

In the DIBt (2010) guideline, two crack widths are considered, w_1 and w_2. In general, the values $w_1 = 1.0$ mm and $w_2 = 1.5$ mm are regarded as adequate without further evaluation of the crack width in the anchorage zone. As can be seen, these values are markedly higher compared to the maximum crack width considered in EOTA TR 049.

The DIBt (2010) guideline distinguishes between different sets of test series, each of which is intended for specific situations or objectives. The first set of test series, in the following denoted as T1, is used to check the anchor performance at suitability level. The second set of test series, in the following denoted as T2, is used to determine the characteristic tension and shear resistance at serviceability level. The third set of test series, in the following denoted as T3, is used to determine the displacement of the anchors when subjected to cyclic tension and shear loads at serviceability level. A summary of the required test series and the test conditions is given in Table 3.3.

Table 3.3. Summary of the required test series in the DIBt (2010) guideline.

ID	Test type	Number of tests	Load	Crack width, Δw	Number of cycles
T1-1	Monotonic tension test	5	Until failure	w_2	-
T1-2	Cyclic tension load	5	$N_{max} = N_{Rk}$ (T2-1)$/\gamma_{Mc}$	w_2	15
T1-3	Crack cycling	5	$N_p = N_{Rk}$ (T2-1)$/\gamma_{Mc}$	$w_{max} = w_2$	10
T2-1	Monotonic tension load	5	Until failure	w_1	-
T2-2	Alternating shear load	5	$V_{max} = \pm V_{Rk}$ (w_1)$/\gamma_{Ms}$	w_1	15
T3-1	Crack cycling	5	$N_p = N_{Rk}$ (T2-1)$/\gamma_{Mc}$	$w_{max} = w_1$	5
T3-2	Cyclic tension load	5	$N_{max} = N_{Rk}$ (T2-1)$/\gamma_{Mc}$	w_1	10
T3-3	Alternating shear load	5	$V_{max} = \pm V_{Rk}$ (w_1)$/\gamma_{Ms}$	w_1	10

3.1.3.1　Suitability tests

As can be seen in Table 3.3, three test series are performed to check the anchor performance at suitability level. All three test series consider the maximum crack width w_2. In this first set of test series, the anchor performance is checked solely for anchors loaded in tension.

In the first test series, T1-1, monotonic tension tests in cracked concrete are performed. In these tests, anchors are tested in cracked concrete with a crack width of $\Delta w = w_2$. The anchors are loaded until failure.

In the second test series, T1-2, cyclic tension tests in cracked concrete are performed. Anchors are tested in cracked concrete with a crack width of $\Delta w = w_2$ and loaded according to the cyclic protocol shown in Figure 3.5. In total, 15 load cycles are performed. The load amplitude in all 15 cycles is given as N_{max}, which is calculated by dividing the normalized characteristic tension load determined in test series T2-1, N_{Rk}, by the partial safety factor for material resistance, γ_{Mc}. Note that the definition of N_{Rk} is given below. In contrast to the pulsating tension load tests in EOTA TR 049, the guideline stipulates that after each tension load amplitude, the anchor must be brought back to the position it had before the tension load was applied. This requires a special experimental setup which also allows to load the anchors in compression (Mahrenholtz and Eligehausen, 2015). After completion of the cyclic phase, a residual pull-out test is performed where the anchors are loaded until failure.
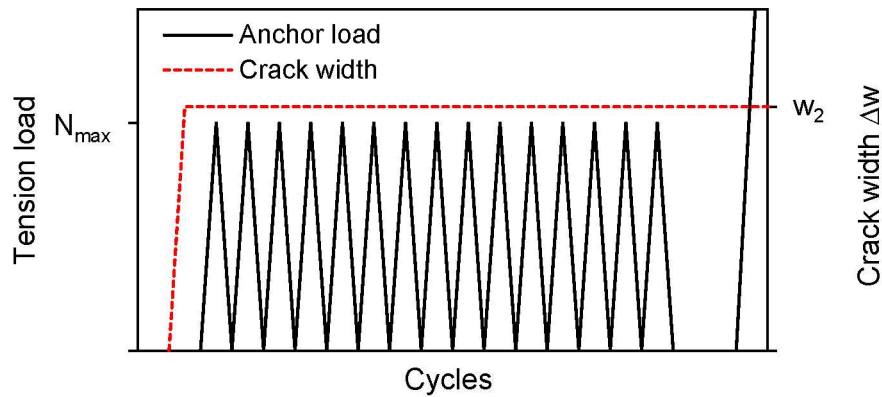
Figure 3.5. Schematic test procedure for cyclic tension tests for suitability level according to DIBt (2010).

The third test series features crack cycling tests at constant tension load. A schematic depiction of the testing procedure is given in Figure 3.6. After installation of the anchor, the crack is opened to w_2, which is also the upper value, w_{max}, for the crack amplitudes. Then the constant tension load, N_p, is applied, which is calculated by dividing the normalized characteristic tension capacity determined in test series T2-1, N_{Rk}, by the partial safety factor for material resistance, γ_{Mc}. The cycling phase features 10 crack cycles with a maximum amplitude of $w_{max} = w_2$ and a minimum amplitude of $w_{min} = w_2$ – 0.5 mm. If the crack width w_2 is smaller than 1.2 mm, the crack is completely closed after each crack opening by applying a compression force on the concrete specimen. The applied compression force is defined to generate pressure in the concrete specimen equal to 15% of the concrete compressive strength. After completion of the cyclic phase, the crack is again opened to w_{max}, and a residual pull-out test is performed.
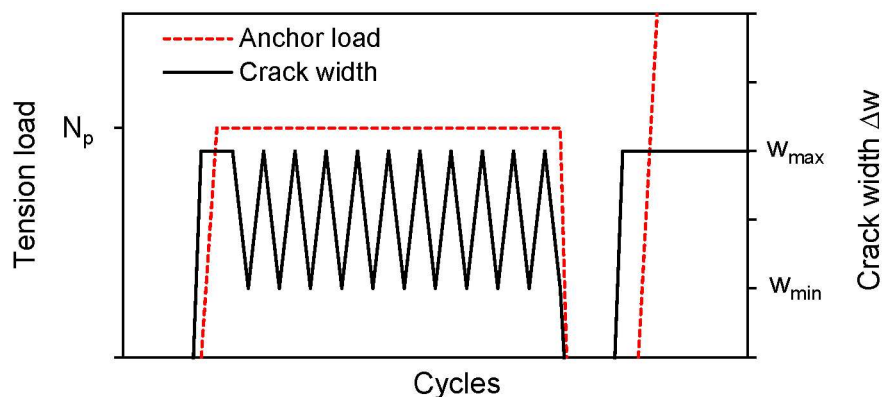
Figure 3.6. Schematic test procedure for crack cycling tests at constant tension load for suitability level according to DIBt (2010).

The assessment criteria in T1 consider both the load-displacement behavior and the residual capacity of an anchor. To assess the load-displacement behavior, the same

criteria are used in all three test series. Note that in case of cyclic tests, only the behavior in the residual pull-out test is considered. Thus, the displacement of anchors during cycling is neglected. The first criterion considers the scatter of displacements at 50% of the mean ultimate load of the anchors. Therefore, the corresponding coefficient of variation must be lower than 50%. If the CV is larger than 30%, the number of tests is increased to 10. The second criterion considers the scatter of ultimate loads. Here, the corresponding CV must be lower than 20%. If the CV is larger than 10%, additional tests shall be performed so that a total of 10 tests have been performed. Besides the criteria for scatter, the guideline stipulates a uniform load-displacement behavior.

With regard to the residual capacity of the anchors, the criteria slightly differ between the monotonic test series and the cyclic test series. In the monotonic T1-1 tests, the guideline stipulates that the mean ultimate load of the anchors shall be at least 80% of the mean ultimate load obtained in test series T2-1. In the cyclic tests T1-2 and T1-3, the mean residual ultimate load after the cyclic phase shall be at least 90% of the mean ultimate load obtained in test series T1-1 and not less than 70% of the mean ultimate load obtained in test series T2-1. If the requirements for the ultimate load cannot be met, the characteristic tension load of the anchor, $N_{Rk,p}$, is reduced accordingly. Finally, the cyclic loading history must be completed in the cyclic tests. If an anchor fails to fulfill this requirement, the tests are performed again with a reduced tension load during the cycling phase. This also results in a reduction of the characteristic tension load of the anchor.

3.1.3.2 Determination of the characteristic tension and shear resistance of anchors under service conditions

The characteristic resistance of an anchor is determined under service conditions. To this purpose, monotonic tension tests and alternating shear load tests in cracked concrete with a crack width of $\Delta w = w_1$ are performed (see Table 3.3).

The characteristic tensile resistance of an anchor is determined in test series T2-1, where the anchors are monotonically pulled out of the concrete while installed in cracked concrete with a crack width of $\Delta w = w_1$. In this test series, the scatter of displacements at 50% of the mean ultimate load in terms of the coefficient of variation shall not exceed 40%. Also, the scatter of ultimate loads in terms of the coefficient of variation shall not exceed 15%. The characteristic resistance in test series T2-1 is determined from the 5% fractile assuming a confidence level of 90%. If the assessment criteria in the suitability tests are not fulfilled, the characteristic pull-out resistance of an anchor which is used for the design of anchors in nuclear power plants and nuclear facilities, shall be reduced accordingly. The corresponding reduction factor is defined as the ratio between the obtained ultimate load and the required minimum load. The test series from set T1, which provides the most unfavorable values, is decisive. In any case, the ratio shall not be smaller than the value 0.7.

The characteristic shear resistance of an anchor is determined in test series T2-2. Here the anchors are subjected to alternating shear load with a crack width of $\Delta w = w_1$. The anchors are loaded in the direction parallel to the crack, following the cyclic protocol shown in Figure 3.7. In total, 15 load cycles are performed with a load amplitude of $\pm V_{max}$. The maximum considered load in the cyclic phase, V_{max}, is calculated by dividing the monotonic characteristic shear load obtained in tests with a crack width of $\Delta w = w_1$ by the partial safety factor for material resistance for steel, γ_{Ms}. Note that the guideline does not stipulate to perform monotonic reference shear tests with a crack width of $\Delta w = w_1$. Therefore, in the absence of reference tests, the results from qualification tests with a crack width of $\Delta w = 0.3$ mm may be used. After completion of the loading history, the anchor is loaded in shear until failure to determine the residual capacity. From the results in test series T2-2, the characteristic shear resistance, $V_{Rk,s}$, is calculated as the 5% fractile of the ultimate loads in the residual capacity tests assuming a confidence level of 90%. For test series T2-2, three assessment criteria are defined in the guideline, which result in a reduction of the characteristic resistance if they cannot be fulfilled. The first criterion stipulates the completion of the cyclic loading history. If the anchor fails before completion, the test is performed again with a reduced value for V_{max}. Accordingly, the characteristic resistance is reduced based on the ratio between the reduced load and the initial value for V_{max}. The second criterion stipulates that the mean ultimate load obtained in the residual capacity tests is at least 90% of the mean ultimate load obtained in monotonic shear tests with a crack width of w_1. Again, in the absence of reference tests, the results from qualification tests with a crack width of $\Delta w = 0.3$ mm may be used. If the second criterion cannot be met, the characteristic resistance is reduced based on the ratio between the obtained ultimate load and the required minimum load. The last criterion considers the scatter of ultimate loads. If the corresponding coefficient of variation is smaller than 10% no reduction is required. However, for a CV between 10% and 30%, the characteristic shear resistance shall be reduced using following reduction factor (DIBt, 2010):

$$\alpha_V = 1/\big(1 + 0.03 \cdot (CV(V_u) - 10)\big). \qquad (3.10)$$

It can be seen that the characteristic shear resistance is solely based on the alternating shear load tests under service conditions. Whereas the characteristic tension resistance of the anchors is determined from the monotonic reference tests under service conditions and, if necessary, reduced according to the results in the suitability tests.
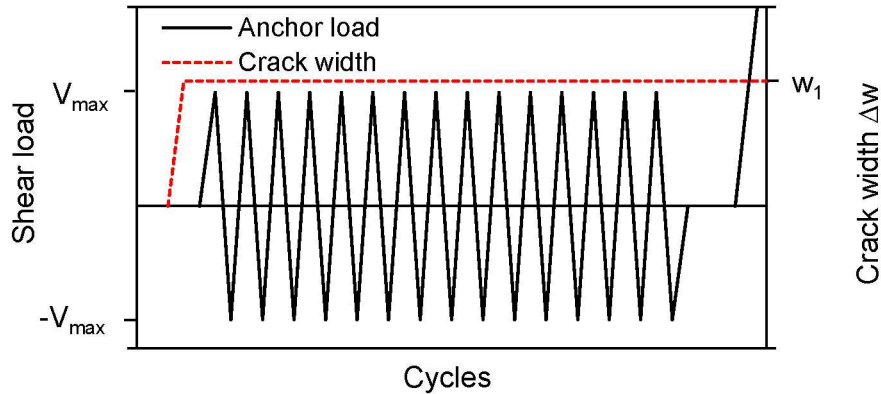
Figure 3.7. Schematic test procedure for alternating shear load tests for serviceability level according to DIBt (2010).

3.1.3.3 Assessment of displacement behavior of anchors

Three test series are performed to assess the displacement behavior of anchors under service conditions (see Table 3.3). The vertical displacement behavior is assessed by means of two test series, featuring one test series with cyclic tension load in cracked concrete with a crack width of $\Delta w = w_1$ and one test series with crack cycling at constant tension load. The third test series assess the horizontal displacement behavior by means of alternating shear load tests. The testing procedures essentially follow the procedures described above for the respective types of tests, whereby the residual capacity tests are not specifically prescribed. Also, the number of applied cycles and the applied crack width are varied (see Table 3.3). Note that the applied tension and shear loads are the same. Due to the similar structure of the loading protocols, a detailed description of the tests is omitted here. Reference is made to the DIBt (2010) guideline.

In the tension tests, the displacement is assessed after completion of all load or crack cycles with the anchor still being subjected to the corresponding tension load, N_{max} or N_p. The mean displacement value is calculated for both test series, T3-1 and T3-2, and the larger value is taken as the displacement of individual anchors at the corresponding load N_{max} or N_p. Likewise, the horizontal displacement under shear load is assessed after completion of the loading history at $\pm V_{max}$. The mean displacement in test series T3-3 is taken as the displacement of individual anchors. In all test series, the DIBt (2010) guideline stipulates a coefficient of variation of the anchor displacement not larger than 40%. For a CV larger than 30%, an additional five tests shall be performed. It is worth mentioning that the guideline stipulates an anchor deformation of maximum 3 mm in any direction for an anchor group to be considered as rigid.

3.2   Design of anchors

Taking a look at standards and guidelines, such as EN 1992-4, ACI 318, and fib Bulletin 58, one finds that the current design approaches for single anchors and anchor groups are intended to provide the resistance mainly in terms of forces. The displacement of anchors is still of rather secondary importance. In particular, the Concrete Capacity Design (CCD) Method for the calculation of the failure load for concrete breakout failure should be mentioned here, which was first introduced by Fuchs et al. (1995). As shown in Bokor et al. (2017), these design methods incorporated in the standards and guidelines are, however, subjected to several limitations. Among others, these include the allowed number of anchors and their arrangement within the anchor group (Bokor et al., 2018). For these cases, displacement-based design approaches have been developed in recent years. These displacement-based design solutions allow the designer to consider the stiffness of the baseplate, the behavior of the individual anchors of a group and the overall behavior of the group with respect to the displacement behavior. As a result, design solutions can be found for more sophisticated problems. The associated concepts that will be discussed in the following include the component model by Kuhlmann et al. (2014), the equivalent spring model introduced by Sharma (2013), and the more recently developed nonlinear spring modelling approach by Bokor (2021).

In the following, some of the force-based and displacement-based design approaches will be discussed. As the main emphasis of this work is on the concrete breakout capacity of anchors and anchor groups, in particular for tension loading, the following discussion is focused on the design of anchors against tension load.

3.2.1   Design according to current standards and guidelines

In current standards and guidelines, such as EN 1992-4, the capacity of anchor groups is evaluated for all possible failure modes. Accordingly, the capacity for each relevant failure mode is calculated and compared. The resulting minimum capacity is then employed as the capacity used for the design of the anchorage. Figure 3.8 shows the possible failure modes of headed studs and post-installed anchors under tension and shear load according to EN 1992-4. For anchors subjected to tension load, EN 1992-4 considers steel failure, concrete cone failure, pull-out failure, concrete splitting failure, concrete blow-out failure or a combined pull-out and concrete failure in case of bonded anchors. For tension loaded anchors and anchor groups, often concrete cone failure is the governing failure mode which results in the minimum capacity. For anchors subjected to shear load, EN 1992-4 considers steel failure (with or without lever arm), or concrete pry-out failure. In the case where anchors are located close to an edge and loaded in shear towards the free edge, also concrete edge failure can occur. Note that the maximum capacity for tension and shear load is verified individually.

When anchors are loaded simultaneously in tension and shear, for example in case of an inclined applied load, the design capacity under tension load, N_{Rd}, and the design

capacity under shear load, V_{Rd}, are determined and following requirement has to be fulfilled:

$$\left(\frac{N_{Ed}}{N_{Rd}}\right)^k + \left(\frac{V_{Ed}}{V_{Rd}}\right)^k \leq 1. \tag{3.11}$$

Where N_{Ed} and V_{Ed} are the design tension and shear load, respectively. In EN 1992-4, the exponent k is set to 2.0 when steel failure dominates the capacity under tension and shear load. In case of other failure modes, the exponent k is set to 1.5. Besides, the tension and shear load are not allowed to exceed the respective capacity of the anchors in tension or shear.
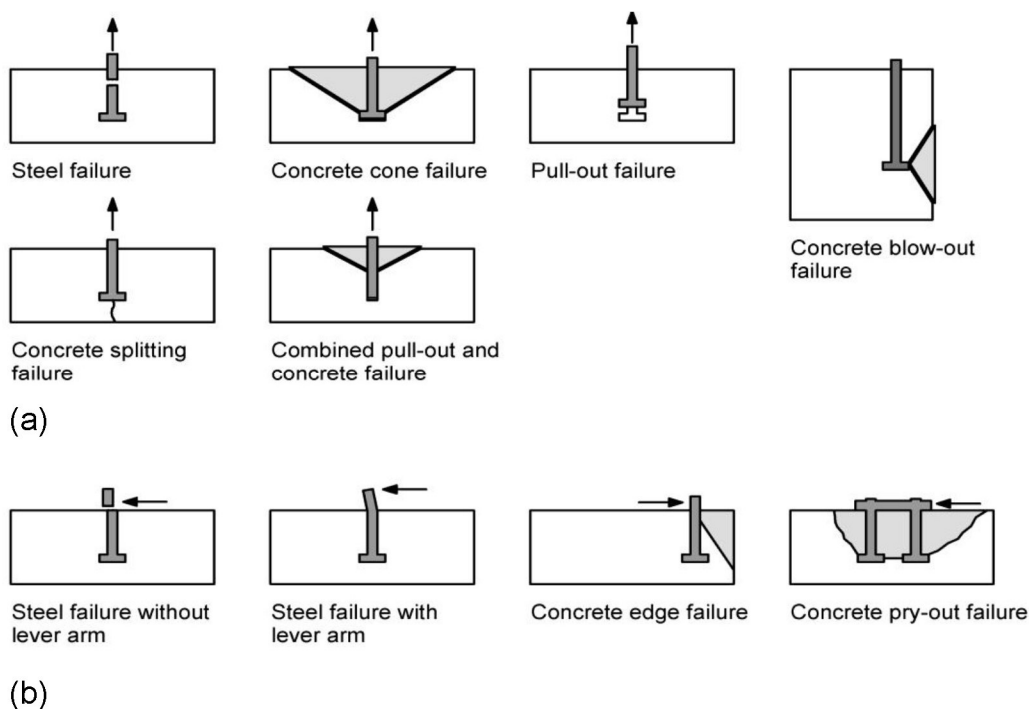
Figure 3.8. Failure modes under (a) tension and (b) shear load. Redrawn on the basis of EN 1992-4.

3.2.1.1   Concrete cone failure under tension load

Most guidelines and standards have adopted the CCD method (Fuchs et al., 1995) to determine the concrete breakout strength of anchor groups under tension loads. In this method, the conical breakout body of a single tension loaded anchor is idealized as a square pyramid with an angle of 35°. Thereby, the apex of the pyramid is the tip of the embedded end of the anchor while the base of the pyramid is the corresponding projected surface area. The breakout strength is further related to the effective embedment depth, h_{ef}, raised to the power of 1.5, thereby considering the size effect (Bažant, 1984; Eligehausen and Ožbolt, 1990; Ožbolt, 1995). The mean concrete cone

resistance of a single anchor in uncracked and unreinforced concrete, without the negative influence of close edges is calculated as:

$$N_{Rm,c}^0 = 1.33 \cdot k_1 \cdot \sqrt{f_{cm}} \cdot h_{ef}^{1.5}. \tag{3.12}$$

Where k_1 is an empirical factor provided in the technical assessment of an anchor. The factor k_1 takes the value $k_{cr,N}$ in case of cracked concrete and $k_{ucr,N}$ in case of uncracked concrete. According to EN 1992-4, indicative values for $k_{cr,N}$ and $k_{ucr,N}$, are 7.7 and 11.0, respectively, for post-installed anchors. The factor f_{cm} is the mean concrete cylinder compressive strength in N/mm². Note that Equation (3.12) determines the mean concrete cone resistance, where the factor 1.33 considers the ratio between the mean and characteristic value of the pre-factor k_1. For calculation of the characteristic resistance of a single anchor, $N_{Rk,c}^0$, the factor 1.33 is neglected and the mean compressive strength is replaced by the characteristic compressive strength of concrete.

When calculating the concrete cone failure load for centrically loaded anchor groups, the CCD method considers the potentially reduced capacity of the individual anchors within the group as their breakout bodies overlap if the spacing between the anchors is not sufficiently large (Eligehausen et al., 2006). This effect is indicated in Figure 3.9. It is accounted for by comparing the projected area of the idealized breakout body of the anchor group with the projected area of a single anchor with the same embedment depth. The ratio between the projected area of the group, $A_{c,N}$, and the reference projected area of the single anchor, $A_{c,N}^0 = 9h_{ef}^2$, determines the capacity of the anchor group for concrete cone failure in case of centrically loaded anchor groups in unreinforced concrete members without the negative effect of close edges:

$$N_{Rm,c} = N_{Rm,c}^0 \cdot \frac{A_{c,N}}{A_{c,N}^0}. \tag{3.13}$$

Thus, if the anchor spacing is smaller than the critical spacing $s_{cr,N} = 3h_{ef}$, the capacity of the anchor group is smaller than the capacity of a single anchor multiplied by the number of anchors in the group.
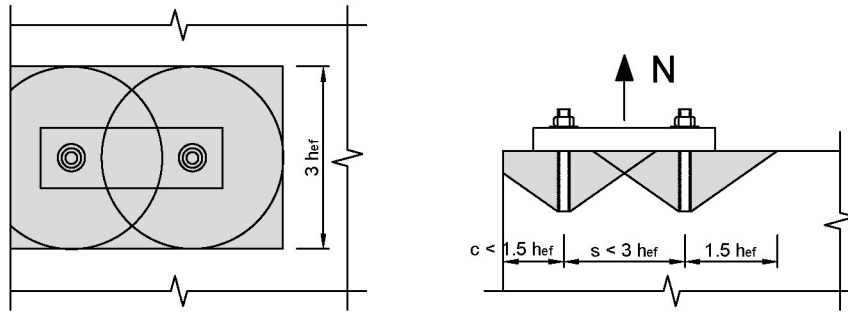
Figure 3.9. Projected surface area for a centrically loaded 2 x 1 anchor group placed close to one free edge.

If an anchor group is placed in the vicinity of one or more edges, the capacity of the group reduces. Thereby two effects are considered. First, the available concrete to resist the tension load is reduced due to the close edges. Similar to the consideration of closely spaced anchors within a group, this effect is accounted for by a reduced projected area of the group as indicated in Figure 3.9. Second, the reduction factor $\psi_{s,N}$ was introduced to consider a load reduction due to a disturbance of the rotationally symmetric stress field in the concrete, which results from the close edge:

$$\psi_{s,N} = 0.7 + 0.3 \cdot \frac{c}{c_{cr,N}} \leq 1. \tag{3.14}$$

Where c is the actual smallest distance to a free edge and $c_{cr,N} = 1.5 h_{ef}$ is the critical edge distance for which a reduction has to be considered. It should be noted however that this approach is mainly based on experimental data on single anchors and anchor groups placed close to one edge or placed in the corner of a concrete slab. For the case where an anchor group is placed close to two parallel edges and loaded in tension only limited experimental data is available to verify the design approach. A detailed discussion is found in Chapter 9.

If the tension load is applied with an eccentricity, e_N, with respect to the center of gravity of the anchor group, the negative influence on the group capacity is considered via the reduction factor $\psi_{ec,N}$, which is based on the work of Riemann (1985). For eccentricity in one direction, the reduction factor can be determined using following equation:

$$\psi_{ec,N} = \frac{1}{1 + 2 \cdot (e_N / s_{cr,N})} \leq 1. \tag{3.15}$$

If there is an eccentricity in two directions, the eccentricity factor is calculated for both directions separately and the product of these two factors is taken as the final reduction factor for eccentric loading.

Besides these two factors, EN 1992-4 considers two more influencing factors, $\psi_{re,N}$ and $\psi_{M,N}$. The first factor is the so-called shell spalling factor and is applied when anchors are installed at rather shallow embedment depths and reinforcement with rather small spacing is present in the anchorage zone. It is calculated using following equation:

$$\psi_{re,N} = 0.5 + \frac{h_{ef}}{200} \leq 1. \tag{3.16}$$

The factor $\psi_{M,N}$ is based on the work of Fichtner (2011) and considers a beneficial effect of compression stresses in the concrete generated by the contact between baseplate and concrete surface. When an anchorage is subjected to a bending moment, it is resisted by the anchorage through couple of the tension forces in the anchors and a resultant compression force between the concrete and the baseplate. If the compression force is sufficiently large, the formation of the breakout cone can be hindered, which results in an increased capacity. This effect is considered if the internal lever arm, z, between the resulting tension force of the anchors and the compression force is smaller than $1.5h_{ef}$. Moreover, the anchors must be installed away from the edge. Following equation is used to calculate the factor:

$$\psi_{M,N} = 2 - \frac{z}{1.5h_{ef}} \geq 1. \tag{3.17}$$

In conclusion, the mean concrete cone capacity of an anchor group according to the model given in EN 1992-4 can be calculated as follows:

$$N_{Rm,c} = N_{Rm,c}^0 \cdot \frac{A_{c,N}}{A_{c,N}^0} \cdot \psi_{s,N} \cdot \psi_{ec,N} \cdot \psi_{re,N} \cdot \psi_{M,N}. \tag{3.18}$$

3.2.1.2 Seismic loading

When designing anchors against seismic actions according to EN 1992-4, the code provides two main design options. These two design options are classified with respect to the requirements on the ductility of the anchors. The first option considers no ductility requirements for the anchors. Consequently, the anchors are not intended for participating in the energy dissipation and they will not enhance the global ductility. Muciaccia (2017) aptly refers to this design option as "protection of the fastener", since the anchors are designed in such a way that an elastic behavior of anchors during a seismic event can be assumed. According to EN 1992-4 this can be achieved through capacity design or elastic design of the anchors. In the capacity design approach, the anchorage must be robust enough to allow the formation of a plastic hinge in either the baseplate or the attached steel element. Effects such as overstrength, or the capacity of an attached element which is not intended to yield must also be considered. Note

that it is specifically highlighted in EN 1992-4 that when the plastic hinge is assumed in the baseplate, the resulting redistribution of forces among the individual anchors within the group has to be considered. In the elastic design approach, the anchors are designed for the maximum load which results from the linear static analysis (see Section 2.1.3) assuming design level demands (including seismic loads) and a linear-elastic behavior of both the structure and the anchorage. As emphasized by Muciaccia (2017), the consideration of overstrength and the premise of anchors remaining in the elastic range, results in loads well below the actual capacity. Thus, in case of the capacity design approach, he concludes that the loads which an anchor is allowed to take up is halved compared to the actual monotonic resistance of an anchor.

The second design option in EN 1992-4 accounts for the ductility of anchors. Thus, the anchors are expected to yield before the yielding of the baseplate or the attached element. However, the ductility of an anchor may only be considered in the longitudinal direction of an anchor and only when steel failure is the governing failure mode in tension. To ensure steel failure of the anchorage, EN 1992-4 requires that the characteristic seismic capacity for steel failure is smaller than 70% of the characteristic seismic capacity associated with concrete related failure modes, additionally considering the factor for sensitivity towards installation. Besides, it must be ensured that anchors provide adequate elongation capacity. According to EN 1992-4, this requirement is deemed satisfied when the stretch length of an anchor is larger than eight times its diameter. If an anchor features a threaded part or a similarly reduced section, either the stretch length of the reduced part must be long enough, or yielding of the unreduced section must be guaranteed by design. It should be noted that although the anchors are expected to yield, they are not considered in the energy dissipation of the overall structure unless this has been explicitly verified through analysis.

According to EN 1992-4, the characteristic seismic resistance of a single anchor or an anchor group is calculated as:

$$R_{k,eq} = R_{k,eq}^0 \cdot \alpha_{eq} \cdot \alpha_{gap}. \tag{3.19}$$

$R_{k,eq}^0$ is the basic seismic resistance of the anchorage for a certain failure mode. In case of concrete cone failure, it is determined from Equation (3.18) assuming cracked concrete, whereby the mean resistance of a single anchor, $N_{Rm,c}^0$, is replaced by the characteristic resistance of a single anchor, $N_{Rk,c}^0$. If the annular gap between the anchor and the baseplate is not closed (e.g., through filling with appropriate mortar), additional shear forces may act on the anchors due to the impact of the baseplate. To account for this negative effect, the reduction factor α_{gap} was introduced in EN 1992-4. Values for α_{gap} are given in EN 1992-4 or, if available, in the corresponding assessment documents of the anchors. The factor α_{eq} considers that during a severe

earthquake the anchors may be intersected by larger cracks and that not all anchors in a group are necessarily intersected by a crack. The latter point is of particular interest as it highlights the importance of the individual anchor behavior on the performance of an anchor group. Since cracking has a severe negative effect on the displacement and stiffness behavior of an anchor, anchors within a group will have a different stiffness depending on whether they are intersected by a crack or not. This in turn causes an uneven distribution of forces among the individual anchors, with some anchors taking higher forces and potentially failing prematurely (Mahrenholtz and Eligehausen, 2010). As a result, the overall capacity of the group will reduce even further compared to the case when all anchors are assumed in a crack (Okelo, 1996; Mahrenholtz, 2013). Values for α_{eq} are given in EN 1992-4 for the respective failure modes in tension and shear.

For the design of anchors under seismic actions, EN 1992-4 also indirectly considers the displacement behavior of the anchors. In this context, the code stipulates displacement limits at damage limitation state, $\delta_{N,req(DLS)}$ and $\delta_{V,req(DLS)}$ for tension and shear loads, respectively. Among others, these displacement limits are meant to ensure the proper performance and operational capability of the attached elements. However, these displacement limits are not further specified. Only an indicative value is given which limits the displacement arbitrarily to 3 mm, representing the displacement of an anchor for which the rigid baseplate assumption is deemed valid. If the actual displacement of an anchor, given in the corresponding technical assessment, is higher than the chosen limit value, the design resistance is reduced based on the ratio between the limit value and the actual displacement value.

In some design cases (e.g., for the second design option according to EN 1992-4) it might be required that the connection is able to develop a certain rotation. To verify whether the connection is able to meet the requirements, the rotation of a connection may be calculated using following equation:

$$\theta_p = \delta_{N,eq}/s_{max}. \tag{3.20}$$

Where $\delta_{N,eq}$ is the displacement of an anchor under seismic actions and s_{max} is the distance between the outermost row of anchors and the opposite edge of the baseplate.

3.2.2 Component method for steel-to-concrete connections

Based on similar approaches for steel-only connections, the component method has been developed by Kuhlmann et al. (2014). The essential idea is to decompose the nonlinear behavior of an anchor into basic components. Thereby, these components are defined by an idealized load-displacement behavior. Thus, besides the strength of an anchor, also its stiffness and displacement behavior are accounted for in the design. For a tension loaded single headed stud, embedded in concrete, the basic components

include steel failure, pull-out failure, and concrete failure (concrete cone failure). After the characteristics of the individual components have been determined, the complete behavior is assembled as indicated in Figure 3.10. As can be seen, the behavior of the individual components is characterized by springs. In order to obtain the overall behavior, these springs are then connected in series. The individual components and their corresponding spring characteristics are presented in the following.
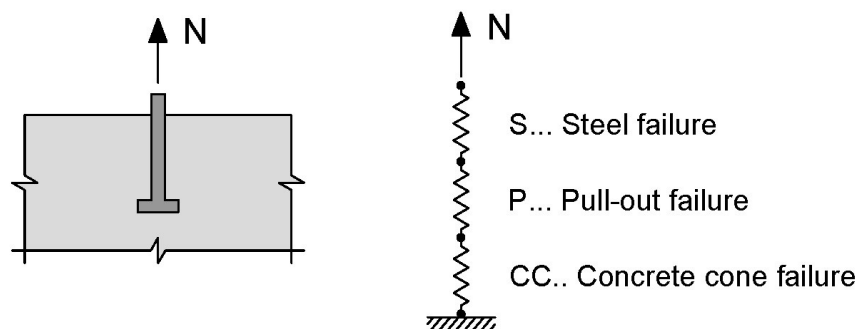
Figure 3.10. Schematic depiction of the idealization and assembly of the behavior of a tension loaded single headed stud. Redrawn on the basis of Kuhlmann et al. (2014).

The spring characteristics for the individual components are defined by means of load-displacement curves as shown in Figure 3.11. The first component, which considers the behavior of the steel shaft of the headed stud, is idealized through a bi-linearized load-displacement curve (see Figure 3.11 (a)). Since the stiffness value, k_{s2}, is set to zero, basically an elastic perfectly plastic behavior is assumed for the steel component. Thus, three values are required to define the curve, that is the design load at steel yielding, $N_{Rd,s}$, the corresponding displacement, $\delta_{Rd,sy}$, and the displacement corresponding to the point where the steel reaches its elongation capacity, $\delta(\varepsilon_{su})$. Note that for ϵ_{su}, the value 0.8% is recommended by Kuhlmann et al. (2014). The design load for steel yielding is calculated as follows:

$$N_{Rd,s} = A_{s,nom} \cdot \frac{f_{uk}}{\gamma_{Ms}} = \pi \cdot \left(\frac{d_{s,nom}^2}{4}\right) \cdot \frac{f_{uk}}{\gamma_{Ms}}.$$

(3.21)

Where $A_{s,nom}$ is the nominal cross section area of the steel shaft, f_{uk} is the characteristic ultimate strength of the steel, γ_{Ms} is the partial safety factor for steel, and $d_{s,nom}$ is the nominal diameter of the steel shaft. The corresponding displacement at steel yielding is calculated as:

$$\delta_{Rd,sy} = \frac{N_{Rd,s} \cdot L_h}{A_{s,nom} \cdot E_s}.$$

(3.22)

Where L_h is the length of the anchor shaft and E_s is Young's modulus of steel.

The component which considers concrete cone failure is shown in Figure 3.11 (c). As can be seen, no displacement is attributed to this component up to the point where the design concrete cone capacity is reached. This is due to the fact that up to this point, the displacement of the anchors comes mainly from the steel elongation and from local crushing of the concrete at the anchor head (Bokor, 2021). The former displacement is already considered in component S, and the latter is considered in component P. Upon reaching the concrete cone capacity, the descending branch is defined by the stiffness, $k_{c,de}$, which is calculated as follows:

$$k_{c,de} = \alpha_c \cdot \sqrt{f_{ck} \cdot h_{ef}} \cdot \psi_{A,N} \cdot \psi_{s,N} \cdot \psi_{re,N}. \tag{3.23}$$

The ψ-reduction factors are defined according to EN 1992-4, as shown in Section 3.2.1, where $\psi_{A,N}$ represents the ratio between the projected area of an anchor group and the projected area of a single anchor with equal embedment depth. Based on previous scientific work, the factor α_c was determined as α_c = -537. The design concrete cone capacity, $N_{Rd,c}$, is calculated according to EN 1992-4, following the principles stated in Section 3.2.1 and accounting for the corresponding material safety factor.

(a) Component S   (b) Component P   (c) Component CC
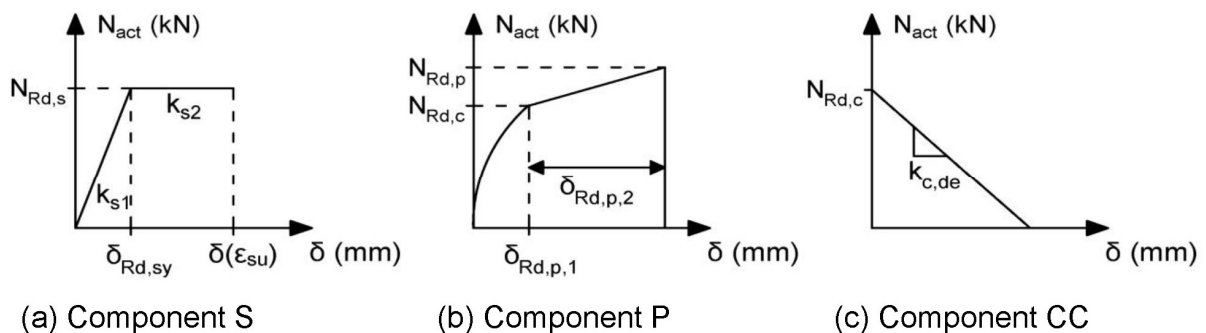
Figure 3.11. Idealization of the behavior of the components: (a) Steel failure, (b) pull-out failure, and (c) concrete cone failure. Redrawn on basis of Kuhlmann et al. (2014).

The last component considers the displacement resulting from the local crushing of the concrete around the anchor head due to increasing local stresses. The corresponding idealized load-displacement behavior is shown in Figure 3.11 (b). As can be seen, two phases can be distinguished. The first phase describes the behavior up to the point where the design concrete cone capacity is reached at the displacement $\delta_{Rd,p,1}$. The displacement at any point in the first phase can be calculated using the following equation:

$$\delta = k_p \cdot \left(\frac{N_{act}}{A_h \cdot f_{ck}}\right)^2. \tag{3.24}$$

Where A_h is the area on the head of the anchor and k_p is a factor introduced to consider the geometry of the headed stud and whether the headed stud is installed in cracked or uncracked concrete. After the design concrete cone capacity is reached, the second phase begins which is characterized by a markedly reduced stiffness. Nonetheless, the strength further increases up to the design failure load for pull-out failure, $N_{Rd,p}$, at the corresponding displacement $\delta_{Rd,p,2}$. The design failure load for pull-out failure is calculated as follows:

$$N_{Rd,p} = p_{uk} \cdot \frac{A_h}{\gamma_{Mc}}. \tag{3.25}$$

The factor p_{uk} is the characteristic ultimate bearing pressure at the anchor head. The displacement at any point in the second phase can be calculated using the following equation:

$$\delta = 2k_p \cdot \left(\frac{N_{act}}{A_h \cdot f_{ck}}\right)^2 - \delta_{Rd,p,1}. \tag{3.26}$$

3.2.3 Equivalent spring model

Sharma (2013) proposed an equivalent spring model to consider the nonlinear load-displacement behavior of an anchorage. The overall objective was to evaluate the performance of beam-column joints retrofitted with fully fastened haunch retrofit solution considering the nonlinear behavior of the individual structural elements by means of springs (see Figure 3.12 (b)). Thereby, besides the nonlinear behavior of the RC beam and columns and the corresponding potential failure modes, also the behavior of the steel haunch element and the nonlinear behavior of the post-installed anchors, which are used to form the connection between the haunch element and the RC members, are considered. The need to also model the behavior of the anchorage emerged from experimental observations that showed that the behavior of the anchors can have a significant impact on the effectiveness and behavior of the overall strengthening solution (see Section 2.3.1). To simplify the modeling approach, the anchors which attach the haunch element to one of the RC members are not modelled individually, but the complete anchor group is considered by means of a single spring which idealizes the behavior of the complete anchor group. Furthermore, the model only considers the tension behavior of the anchorage, which was deemed critical compared to the behavior of the anchors in shear.

In Sharma (2013), the behavior of the anchorage is idealized by means of a penta-linear format shown in Figure 3.12 (a). As noted by the author, this format is deemed adequate to describe the behavior of post-installed anchors, typically observed in experiments. Once defined, the characteristic points can be assigned to the respective spring in the finite element model. The ultimate capacity of the anchor group, N_u, is

determined on basis of the CCD Method (see Section 3.2.1). This load value is assigned to points B and C of the load-displacement curve. The load value for point A is taken as 80% of the ultimate load and for point D, 20% of the ultimate load are considered. It is well known that the displacement behavior of anchors may vary significantly with respect to the failure mode. This observation is accounted for by varying the distance between point B and C and between point C and D. Thus, in case of a ductile failure mode, the distance between the points is larger than in case of a rather brittle failure. The displacements of the characteristic points are defined by two stiffness values, $k_{50\%Nu}$ and k_{Nu}. The stiffness values were taken from the evaluation presented in Mahrenholtz (2011). The first value defines the initial stiffness of the ascending branch connecting the origin to point A. It is determined from tests on single anchors or from the technical assessment of an anchor and is defined by the stiffness corresponding to 50% of the ultimate load in the ascending branch of the load-displacement curve. The latter stiffness value is used to characterize the remaining points of the penta-linear curve. It is the secant stiffness corresponding to the ultimate load of an anchor. Note that by determining the stiffness values from the technical assessment or through testing, the individual displacement behavior of different types of anchors is directly accounted for in the model. While the displacement at point B is defined by the ratio N_u/k_{Nu}, the determination of the displacement values for point C and D vary depending on the failure mode by multiplying the ratio between the ultimate load and the secant stiffness at ultimate load by different values. At point E, the load drops to zero at the same displacement as Point D. The definition of the characteristic points for different failure modes is given in Sharma (2013). For concrete cone failure, the displacement of point C is calculated as $1.25\,N_u/k_{Nu}$ and the displacement of point D is calculated as $2\,N_u/k_{Nu}$.

Cracking in the base material is considered by a reduced ultimate capacity and by a reduced stiffness. In accordance with EN 1992-4, the ultimate capacity of an anchor group in cracked concrete is calculated as 70% of the capacity in uncracked concrete. Furthermore, the stiffness of an anchor reduces when intersected by a crack. Indicative values for the ratio between the stiffness in cracked concrete and the stiffness in uncracked concrete are given in Sharma (2013) for different failure modes.

(a)   (b)
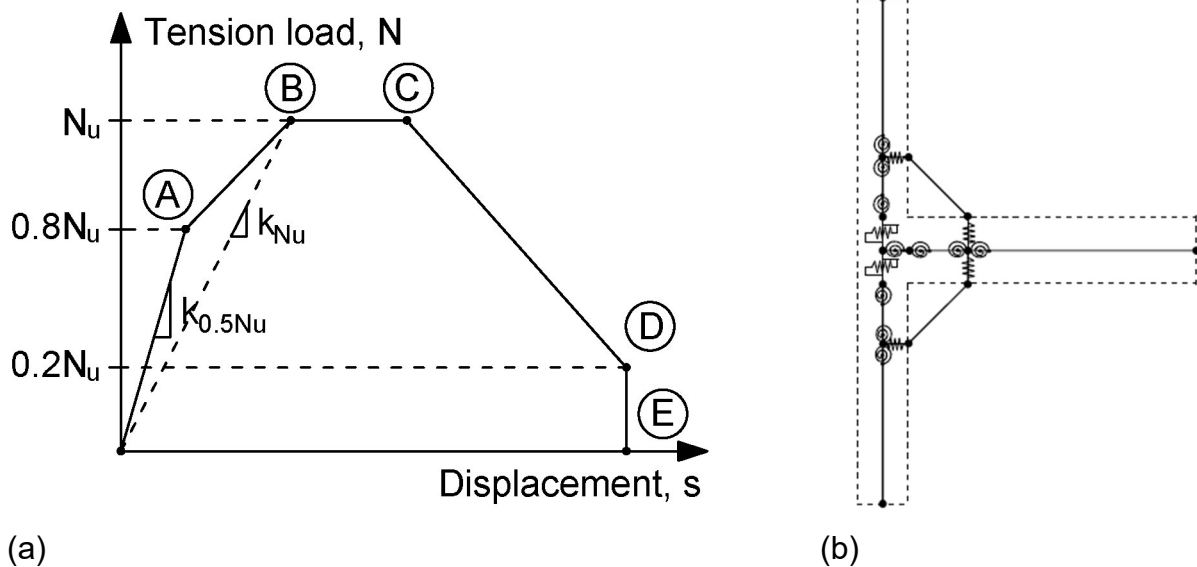
Figure 3.12. (a) Idealization of the behavior of the anchorage system. Redrawn on basis of Sharma (2013) and (b) idealized numerical model of a retrofitted beam-column joint using the equivalent spring model to consider the behavior of the anchorage. Source: Sharma (2013).

In case of anchor groups, Sharma (2013) proposes to determine the required stiffness values for the group from the values valid for single anchors. In case of concrete cone failure, the projected area approach of the CCD method is adopted. The stiffness of an anchor group failing due to concrete cone failure is therefore calculated as (Sharma, 2013):

$$k_{group} = \frac{A_{c,N}}{A_{c,N}^0} \cdot k_{individual}.$$

(3.27)

In case of failure modes other than concrete cone failure, the stiffness of the anchor group is determined by multiplying the stiffness of a single anchor by the number of anchors in the group (Sharma, 2013).

The modelling approach for anchors introduced as part of the equivalent spring model by Sharma (2013) has since been used by other researchers to describe the load-displacement behavior of anchors. In some cases, the basic model has been modified to extend the scope. In this context, the model introduced by Hofmann et al. (2015) should be mentioned, which extends the previous model in such a way that different crack widths can be accounted for. In Dwenger (2019) the model is altered from a penta-linear format to a hexa-linear format to improve the accuracy of the ascending branch of the load-displacement curve. Furthermore, the idealization proposed by Sharma (2013) forms the basis for the idealization of the individual anchor behavior within a group in the nonlinear spring model proposed by Bokor (2021), which will be discussed in the next section.

3.2.4 Nonlinear spring modelling for evaluation of anchor groups

The nonlinear spring modelling approach presented in Bokor (2021) is able to predict the load and the displacement behavior of tension loaded anchor groups failing due to concrete cone failure mode and the behavior of shear loaded anchor groups close to the edge, which fail due to concrete edge failure mode. Moreover, it is possible to simulate an inclined loading case regarding these two failure modes. The model was developed with the aim to overcome some limitations which are inherent to the current force-based design solution, such as:

- A narrow choice of possible or allowed anchor layouts in an anchor group

- Rather poor utilization of the actual anchorage capacity for some applications

- Required verification of rigid baseplate to ensure that the assumptions made in the CCD method regarding the distribution of forces are valid

The nonlinear spring modelling approach introduced by Bokor (2021) allows the load-displacement behavior of anchor groups to be studied without the expense of elaborate experiments. This is made possible through explicitly incorporating the deformation behavior of the essential elements of an anchor group in a finite element analysis. These essential elements were identified by Bokor (2021) as the individual anchors, the baseplate, and the concrete base material (or rather the contact between baseplate and concrete).

The basic modelling approach is schematically depicted in Figure 3.13 for a 3 x 1 tension loaded anchor group. As can be seen, springs are used to idealize the behavior of the anchors and the interaction between baseplate and concrete, while the baseplate itself is modelled via 2D finite shell or 3D finite solid elements. It is important to note that the springs are intended to carry either pure tension loads (anchors) or pure compression loads (contact elements). Therefore, Bokor (2021) uses the terms "tension-only spring" and "compression-only spring". This terminology is adopted in this work.

Figure 3.13 shows only the elements of a tension loaded anchor group. If an anchor group is loaded in shear, springs acting in the direction of the shear load are applied. Moreover, Bokor (2021) applies springs in the direction away from the loading direction to model what she calls "push-back" effect. To keep things simple, the focus of the following discussion is on tension loaded anchor groups. However, the modeling for groups subjected to shear loads essentially follows the procedure used for groups subjected to tension loads.

The basic idea of this method is that by taking into account the deformations of the baseplate and the stiffness of the individual anchors, a load distribution is obtained that agrees reasonably well with the experimental behavior. Additional effects such as the prying action, where compression forces are generated between the baseplate and the concrete due the deformations of the baseplate, are addresses by Bokor (2021)

through the compression-only contact elements. This is an important feature as these additional forces reduce the resistance of the anchor group as they pose additional demands on the anchors. Considering the anchor behavior beyond their linear-elastic range, including the descending branch of the load-displacement curve, allows forces on the individual anchors to be redistributed. In this way, for example, groups placed in the vicinity of concrete edges or loaded by an eccentrically applied load can be assessed without additional factors such as those required in the CCD method (Bokor, 2021). It is apparent that the key to this approach lies in the viable assumption of the properties of the tension-only springs for the anchors, which should ideally be determined from single anchor tests. The same applies to the springs representing the behavior of anchors under shear loads. As Bokor (2021) points out, the aforementioned approach requires to perform a step-by-step nonlinear static analysis in displacement control, where at each step the nonlinear equations are solved.
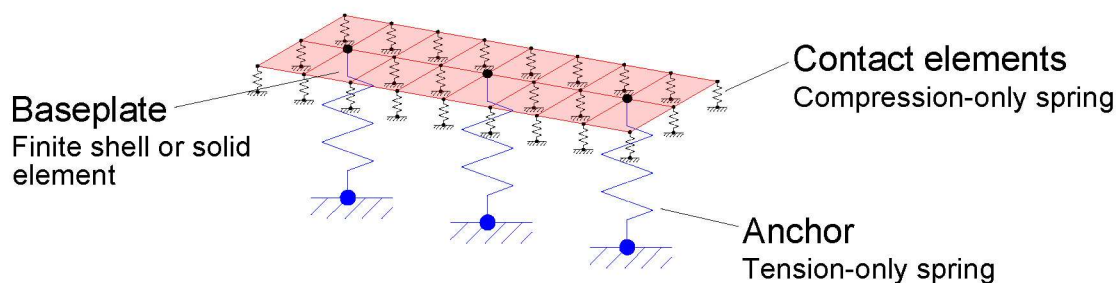
Figure 3.13. Schematic depiction of the spring model for a tension loaded anchor group and its basic components. Redrawn on the basis of Bokor (2021).

According to Bokor (2021), anchor groups for which the failure of the individual anchors is governed by steel failure or pull-out failure can be modelled using the idealized load-displacement behavior of a single anchor, as there is no mutual influence of the anchors for these failure modes. However, this is not possible in case of concrete cone failure, since the individual breakout cones of the anchors will overlap if the spacing between the anchors is not sufficiently large (Eligehausen et al., 2006). This effect results in a reduced capacity of the individual anchors. Similarly, the behavior of anchors failing due to concrete edge failure is influenced by nearby anchors if the spacing is not large enough to avoid any mutual influence. In such cases, it is required to modify the idealized load-displacement behavior determined from single anchor tests to be able to realistically reproduce the actual behavior of individual anchors within a group. The following describes how Bokor (2021) determines the spring characteristics of individual anchors within a tension loaded group for concrete cone failure.

First, tests on single anchors with an embedment depth corresponding to the embedment depth of the anchors in the spring model are performed. The obtained load-displacement curves in each test within the test series are idealized by means of a penta-linear format based on the equivalent spring model by Sharma (2013).

Indicative values for the idealization of the load-displacement curves are provided in Bokor (2021). However, the characteristic points may also be chosen in such a way to best fit the experimental curves. The characteristic points of the idealized curve (A – D in Figure 3.12) are specified by a load value and the corresponding secant stiffness (k_1 – k_4). Within one test series, the mean idealized load-displacement curve can thus be determined from the mean load values and mean secant stiffness values at each point. The corresponding displacements of each point are then calculated by dividing the load by the secant stiffness.

For modelling anchor groups where the anchor spacing is sufficiently large ($s \geq s_{cr,N} = 3h_{ef}$), the mean idealized curve can directly be assigned to each anchor spring. However, the anchor spacing in a group is typically smaller than the critical value. In this case the individual cones will overlap, and the individual anchors are unable to develop the full capacity of a single anchor (Eligehausen et al., 2006). Consequently, the spring characteristics obtained from the single anchor tests must be reduced accordingly. In Bokor (2021), this is done by a so-called tributary area approach similar to the projected area approach according to the CCD method (Fuchs et al., 1995). Thereby, the actual tributary areas of the individual anchors, $A_{c,N}^i$, within the group are compared to the projected area of an unrestricted single anchor according to the CCD method, $A_{c,N}^0 = 9h_{ef}^2$. The load value at each characteristic point is then reduced based on the ratio $A_{c,N}^i / A_{c,N}^0$ for all anchors of a group. The tributary area of each anchor is calculated based on the distance to the adjacent anchors, whereby half of the spacing is assigned to each anchor. Note that in accordance with the CCD method, the length of the tributary area is limited by $1.5h_{ef}$ in each direction. If the anchor group is placed in the vicinity of one or more edges, the tributary area is also limited by the edge distance. In this way, if a nonlinear analysis is performed, the negative effect of close edges is directly accounted for. Thus, no further reduction factors are required. The tributary area approach is solely applied to modify the load values of the individual anchors, while the secant stiffness values remain unaltered. This assumption is based on experimental observations which showed that the stiffness values of individual anchors within a group are essentially equal to the stiffness values of single anchors with the same embedment depth (Bokor, 2021).

The example in Figure 3.14 is from Bokor (2021) and shall be reproduced here since it illustrates the determination of the tributary areas in a simple but comprehensive way. The 3 x 1 anchor group is placed close to one edge as indicated in Figure 3.14 (a). As can be seen, the tributary areas of all anchors are not restricted in the direction parallel to the free edge. Thus, the total side length in this direction is $3h_{ef}$ for the tributary area of all anchors. For the side length in the second direction the following applies: Anchor A is placed close to one edge and one adjacent anchor. Therefore, the tributary area is limited by the distance to the edge and half the distance to the adjacent anchor, $A_{c,N}^A = (c_1 + 0.5s_1) \cdot 3h_{ef}$. Anchor B is limited by two adjacent anchors. Therefore, the

tributary area is limited by half the distance to the anchors A and C, respectively. In the example, this equals the spacing between the anchors, s_1. Therefore, $A_{c,N}^B = s_1 \cdot 3h_{ef}$. The tributary area of anchor C is only restricted by one adjacent anchor. Thus, $A_{c,N}^C = (0.5s_1 + 1.5h_{ef}) \cdot 3h_{ef}$. It is apparent that in case of the 3 x 1 anchor group in this example, the spring characteristics of each individual anchor vary. Figure 3.14 schematically shows how the spring characteristics are adjusted based on the ratio between the tributary areas and the projected area of a single anchor. As mentioned above, only the load values are changed, while the secant stiffness at each characteristic point remains the same.
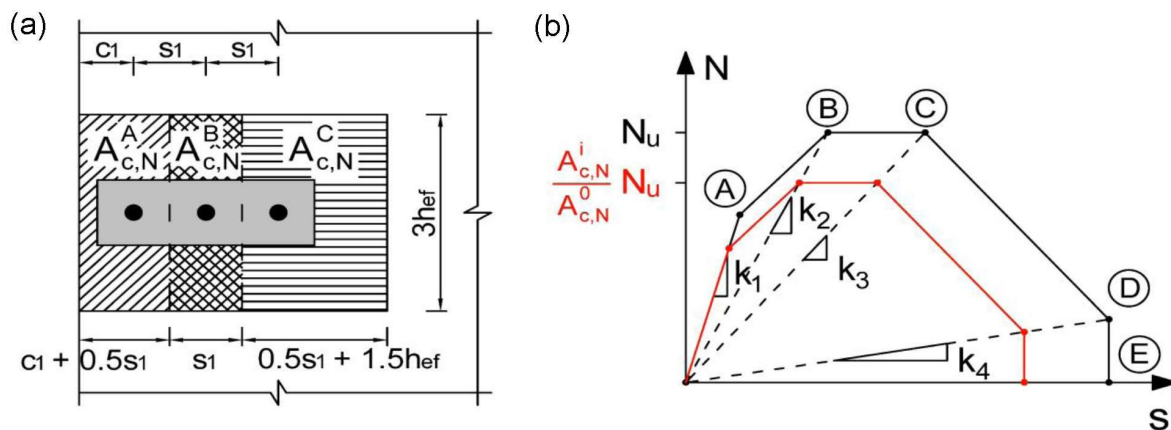
Figure 3.14. Concept of tributary area approach: (a) Partitioning into tributary areas and (b) modification of the idealized load-displacement behavior based on the tributary area of the individual anchors. Redrawn on the basis of Bokor (2021).

The behavior of the baseplate, which is used to connect the individual anchors, is directly accounted for by modelling the geometry using 2D finite shell or 3D solid elements to which the material properties are assigned (e.g., Young's modulus of steel, baseplate thickness). This means that the requirement of a sufficiently rigid baseplate as stipulated in EN 1992-4 is not relevant for the spring modelling approach, since the displacements and flexibility of the baseplate are directly considered in the analysis of the overall behavior (Bokor, 2021).

As indicated in Figure 3.13 the baseplate is bedded on compression-only springs. These springs are supposed to simulate the contact between the baseplate and the concrete surface in case where compression forces are directly transferred from the baseplate to the concrete. In Bokor (2021), the compression-only springs are determined based on the Winkler spring characteristics using a Young's modulus of 30000 N/mm².

4 Objectives and methodology

If post-installed anchors are to be used in structural applications for the purpose of fastening strengthening elements, such as steel bracings, to an already existing RC frame structure, the requirements and demands on such a connection are particularly high. On the one hand there are geometrical restriction arising from narrow concrete members or spatial anchor configurations in the corner of a frame structure. In particular for the latter case there are no design solutions available. On the other hand, the hysteretic and displacement behavior of anchors becomes increasingly important. In case of seismic loading, it is not necessarily the forces that can be resisted by the connection but rather its displacement behavior that is vital for the success of a strengthening solution. This is even more relevant in the modern seismic design philosophy because the structures are seldom, if at all, designed to withstand the seismic action elastically. In this context, the current force-based design solutions which are available in standards and guidelines are deemed unsuitable to guarantee the desired performance of a strengthening solution. Rather displacement-based design solutions, such as the nonlinear spring modelling approach, are required. Using such methods can help to better understand the behavior of the connection. Moreover, the results in terms of the load-displacement behavior, can directly be considered in the numerical analysis of the structure under seismic actions. However, the displacement-based design solutions discussed in Chapter 3 do not consider the hysteretic behavior of the anchors. Furthermore, in order to be able to consider the hysteretic behavior in the first place, it is essential to carry out suitable qualification tests to determine the varying seismic behavior for different types of post-installed anchors in the complete range of the load-displacement curve.

4.1 Assessment of anchor performance under seismic actions

In current guidelines for the assessment of post-installed anchors under seismic actions, such as EOTA TR 049, qualification of the anchors relies on force-based tests. The most relevant testing scheme for anchors used in general structural applications is provided in category C2 in EOTA TR 049. Here the anchors are subjected to load cycles up to their characteristic resistance. As a result, the range of the load-displacement curve that is covered by cyclic loading is rather limited. In case of non-structural applications, a limitation of cyclic loading up to the characteristic resistance is a perfectly viable approach. The forces that will act on the anchors are resulting from the oscillation of the connected non-structural element. The resulting inertial forces can be reasonably well estimated, and the anchors can be designed accordingly.

Therefore, it can be assumed that the qualification tests in category C2 indeed cover the relevant part of the load-displacement curve for non-structural applications. In case of structural applications, however, it is significantly more difficult to estimate the actual demands on the anchors during a seismic event. In particular when the connected elements are part of the load-transfer mechanism against the seismic actions.

In this context, Stehle and Sharma (2021a) pointed out that, for one thing, current force-based design approaches that are provided in standards such as EN 1998-1, acknowledge the beneficial effect of ductility and energy dissipation for certain structural elements by reducing the seismic demands on the structure. In doing so, the ductility and energy dissipation are assumed based on the force resisting system against the seismic loads (e.g., frame structure, wall system, etc.) and the building materials used in the construction of the building (e.g., reinforced concrete, steel, timber, masonry). This means that if the assumption is not correct and the estimated ductility and energy dissipation of the structural system is lower than expected, the actual seismic demands might be significantly higher than the demands which were assumed in the design of the structure. In this case, if post-installed anchors are used to fasten structural elements to the RC structure, they are in turn subjected to loads that might be significantly higher than the loads for which they were designed. For another, these design approaches do consider the ability of some systems to behave in a ductile manner, meaning the deformation of the structure in the nonlinear range and the formation of plastic hinges. However, they often ignore the increased deformation on the remaining structural elements or a redistribution of forces. Again, this might result in an underestimation of the actual demands on the anchors during a seismic event.

The mentioned issues concern rather specific applications such as the attachment of a steel bracing for seismic retrofitting, but in these cases, they can lead to significant damage if not considered. Thus, for such applications it might be advisable to perform supplementary qualification tests to assess the displacement and hysteretic behavior of the anchors in a wider range of the load-displacement curve. The simple pass/fail criteria given in the current seismic qualification approaches might not be suitable for such cases.

4.2 Hysteretic model for post-installed anchors

The examples in Chapter 2 have shown that the behavior of the anchors can have a significant influence on the performance of the overall strengthening solution. It is therefore inevitable to know the nonlinear behavior of the anchorage that forms such connections for seismic retrofitting. This becomes even more important with respect to the difficulties in predicting the seismic demands on structural elements as discussed above.

Modelling of the nonlinear seismic behavior of single anchors should be based on the assessment of the displacement and hysteretic behavior of different types of post-installed anchors determined from displacement-based qualification tests. Since the displacement behavior of different types of post-installed anchors varies, generally applicable hysteretic rules are required which can be used to idealize the hysteretic behavior of different types of anchors. These rules can then be implemented in nonlinear design approaches, such as the nonlinear spring model by Bokor (2021), to allow the assessment of anchor groups under seismic actions without excessive experimental studies of the same. Such an approach directly considers the varying performance of different types of post-installed anchors, which allows to identify the type of anchor that is best suited for a particular task.

For an implementation in such models, however, it is required to know how the behavior of individual anchors in a group differs from the behavior of single anchors in terms of the individual capacity, stiffness, and unloading and reloading behavior in case of cyclic loading.

4.3   Anchor groups installed in narrow concrete members

Geometrical restrictions imposed by the limited dimensions of the beams and columns in which the anchors are installed in, pose a challenge on the anchorage in such a way that it limits the capacity in case of concrete related failure modes such as concrete cone breakout failure of tension loaded anchor groups. That is particularly critical when anchors are used in structural strengthening applications against earthquakes, since such connections are already subjected to rather high demands. Moreover, the vicinity of two parallel close edges as in case of beams and columns, may also have a detrimental influence on the displacement behavior of the anchor groups.

It is evident that the design of such anchor groups in narrow members requires a detailed understanding of the load-displacement behavior, failure mechanism, and the capacity that may be achieved. Currently, the design of anchor groups with two parallel close edges is based on experimental works on anchor groups in the vicinity of one close edge or anchor groups which were placed in the corner of a slab (two perpendicular close edges). In these cases, the rotationally symmetric stress condition is disturbed (Eligehausen, 2006), resulting in an additional reduction of the anchor capacity. In the CCD method, this effect is considered via the reduction factor $\psi_{s,N}$ (Equation (3.14)). However, it is arguable whether this also applies to anchor groups with two parallel edges with equal edge distance on both sides. In Anderson et al. (2017) it was shown that current design approaches yield quite conservative results for anchor groups in narrow concrete members. Accordingly, current approaches would result in unrealistic and over-conservative designs for anchorages in narrow members since the capacity is already reduced by the geometrical restriction of the concrete members. In turn, this would limit the possible use of post-installed anchors in structural

applications. Due to the limited available data, it is worthwhile to carry out experimental and numerical investigations in order to verify the current design approaches or to modify them if necessary.

4.4   Corner configuration

Some types of steel bracing require the braces to be fastened in the corner of the RC frame. If a direct connection is to be formed, the braces are fixed to a connection element which is in turn fastened to the RC frame. Typically, the connection element comprises an anchor bracket, a gusset plate, and the anchors themselves. In principle, the anchor bracket represents two perpendicular groups of anchors which are placed in the corner of the frame. Since the distance of the anchors to the concrete joint is rather low, it is likely that these two groups share a common breakout body and might even have a mutual influence on each other.

In such a spatial anchor configuration, it is intuitive that the distribution of forces among the anchors is more complex than it is for two-dimensional configurations. Moreover, due to the inclined load resulting from the steel brace, the anchors are simultaneously subjected to tension and shear loads. The resulting load-bearing behavior of the connection is therefore quite complex, making it essential to understand the overall behavior of the connection and its individual elements for a safe design.

In current standards and guidelines, there are no design recommendations for such spatial anchor configurations. Therefore, an analytical design approach is required which allows for a simple and reliable way to evaluate the resistance of the post-installed anchors used in such a connection. The possible baseline for the development of such an analytical design approach could be the design concepts for two-dimensional anchor configurations like the CCD method. In this way, a certain continuity in the design approach for anchors as recommended in current standards and guidelines, such as EN 1992-4 is ensured.

As previously mentioned, modern design of structures against earthquake hazards applies a performance based design approach, which heavily relies on the displacement behavior of the structure and its individual members. In this design approach it is crucial to predict the behavior of the members as accurately as possible in order to determine the location and sequence of formation of possible plastic hinges and the sequence of failure of the individual members. This allows to account for a redistribution of forces within the structure. Consequently, the resistance of the members alone is insufficient in this design approach. The same applies to anchors if they are used to form the connection between structural members. Thus, a performance based design of structures also requires a performance based design for anchors or anchor connections as argued by Sharma (2019). In this context, the behavior of the connection element between steel bracing and RC frame should also be modelled when designing the strengthening solution against earthquakes. One way

to account for the behavior of the connection is to first model the connection using the nonlinear spring modelling approach by Bokor (2021), whereby the behavior of the individual anchors, the gusset plate and the anchor bracket are directly considered. An analysis of the spring model gives the overall load-displacement behavior of the connection, which can in turn be implemented in the global structural model of the strengthened building.

For both the analytical and displacement based design approach, a detailed investigation on the behavior of such connections is required by means of experimental and numerical methods.

4.5 Objectives of this work

The aim of this work is to investigate the possible use of post-installed anchors in structural strengthening applications against earthquake hazards. The focus lies on direct connections between steel bracings and RC frame structures in the corner of the frame. Before coming up with a design solution for the complete connection, the first step is to assess which anchor systems are eligible in the first place. For this purpose, new displacement-controlled testing schemes are required to determine the displacement and hysteretic behavior of single anchors. Once the hysteretic behavior of single anchors is known, it can be idealized for design purposes. In addition, cyclic tests on anchor groups are required to compare the hysteretic behavior of single anchors to the behavior of individual anchors within a group. In the second step the geometrical conditions are investigated. Thus, the influence of two parallel close edges on the breakout behavior of anchor groups and the geometrical influence related to a corner configuration. The objectives of this work can be summarized as follows:

1. Conceptualization and development of a new testing protocol for single anchors subjected to pulsating tension load for the assessment of the displacement and hysteretic behavior of anchors in a broader range of the load-displacement curve.

2. Development of hysteretic rules for the idealization of the hysteretic behavior of post-installed anchors.

3. Investigation on the hysteretic behavior of anchor groups and the individual anchors forming the group. Comparison between the behavior of individual anchors and single anchors with the aim to extend the hysteretic rules for anchors in a group and to allow the assessment of the hysteretic behavior of anchor groups within the framework of the nonlinear spring modelling approach by Bokor (2021).

4. Detailed investigation on the load-displacement behavior of tension loaded anchor groups in the vicinity of two parallel close edges.

5. Detailed investigation on corner configurations with respect to the overall load-displacement behavior, the failure mechanism, the behavior of the individual anchors, and the distribution of forces among the anchors.

6. Conceptualization and development of an analytical design approach for corner configurations.

7. Extension of the spring modelling approach to spatial anchor configuration such as the corner configuration for a possible application in performance based design approaches.

In order to achieve the objectives, an extensive experimental and numerical program has been conducted.

4.6   Research methodology

As can be seen from the objectives, there are primarily three levels for the given problem of using post-installed anchors to connect steel bracings to existing RC frame structures for seismic retrofitting. The first level can be identified as the "single anchor level". At this level, the focus is on the behavior of single anchors subjected to cyclic loading. Thus, on appropriate ways to test and assess anchors for the use in structural strengthening applications. And finally, to idealize their hysteretic behavior for implementation in the spring modeling approach or equivalent displacement based design solutions. For this purpose, tests on single anchors subjected to pulsating tension load have been performed in the first phase of the research work, whereby a new displacement-controlled testing protocol was applied. In total five different anchor system were investigated, and their hysteretic characteristics have been evaluated.

The second level can be identified as the "anchor group level". Here the behavior of anchor groups is investigated with respect to their cyclic behavior. In case of the nonlinear spring modeling approach (Bokor, 2021), the spring characteristics for the individual anchors within a group are determined from the load-displacement behavior obtained in single anchor tests. Thus, if the model is to be extended for cyclic loads, it is essential to investigate how the hysteretic and displacement behavior of individual anchors within a group change with respect to the behavior of single anchors. Besides the behavior of individual anchors, it is important to understand the overall behavior of anchors groups themselves. Thereby several questions arise such as how cyclic loading affects the behavior of anchor groups in comparison to monotonic loading, or what influence have two parallel close edges on the breakout behavior of anchor groups. For a safe design, these questions need to be answered. For this purpose, two experimental programs have been conducted in the second phase. In the first program, anchor groups have been installed far away from the edge and have been loaded to failure by applying both monotonic and cyclic tension load. Thereby, the same displacement-controlled testing protocol has been applied as in the single anchor tests. Several anchor configurations have thus been tested, which allowed a detailed

investigation on their behavior. The second program considered the behavior of anchor groups installed in narrow concrete members. Here the groups were loaded monotonically in tension since the focus lay on the investigation of the breakout behavior.

The third level can be identified as the "subassembly level". In this final level, the complete connection is investigated, which comprises the gusset plate, the anchor bracket, and the post-installed anchors. Here the focus is really on the geometrical influences on such a connection. To this purpose, the experimental program was developed in such way that global influences, like bending of the RC members that would arise in a real structure, are avoided. This approach allows to focus on the connection element itself and on the behavior of the individual anchors.

The applied research methodology allowed a step by step analysis of the whole connection and its individual elements. Each level builds on the previous one, and the insights gained from the previous level could be directly used to develop the subsequent experimental program. Along with the experiments, vast numerical investigations have been performed to supplement the experimental findings. The use of numerical methods usually pursued two goals. On the one hand, it was used to anticipate the behavior during an experiment allowing for a better planning of the same. On the other hand, based on the experimental results, the behavior of an anchorage could be further investigated.

The following structure of the work reflects the described research methodology. It is organized in three parts, which deal with the "single anchor level", the "anchor group level", and the "subassembly level"

Part I

Single anchor level

5 Behavior of single anchors under pulsating tension - displacement based approach

In order to allow the assessment of the hysteretic anchor behavior in a broader range of the load-displacement curve, a new displacement-controlled testing procedure for pulsating tension load was developed. In this new approach, the anchors undergo cyclic demands over the entire range of interest including the post-peak range of the load-displacement curve. In comparison, the force-controlled qualification test for pulsating tension load, currently stipulated for category C2 in EOTA TR 049, provides information on the cyclic behavior only up to a certain load level in the ascending branch of the load-displacement curve, which often lies within the linear branch of the curve. Therefore, although the current approach is able to segregate anchors that will behave very poorly under seismic loads, it is arguable whether cycling the load within the linear range of load-displacement curve can provide information required for assessment of seismic performance of anchors.

The current approach might be useful for cases where the seismic load can be anticipated well, which refers to the cases for some non-structural applications only, if any. Since the seismic design philosophy for structures relies significantly on ductility, estimation of seismic demands in terms of load becomes irrelevant. Therefore, for anchorages used in structural applications, and in particular for seismic strengthening applications, the seismic tension testing protocol stipulated in EOTA TR 049 cannot provide all the required information. The new approach presented in this chapter can be used to obtain such additional information that cannot be obtained from current qualification tests, but that is helpful in assessing the suitability of post-installed anchors used in structural strengthening application. It should be noted that this new approach is intended to augment the current approaches, not to replace it altogether.

In this chapter a displacement-controlled procedure for pulsating tension load is introduced and described. The new cyclic loading protocol is compared to the force-controlled protocol, C2.3 according to EOTA TR 049. For this purpose, tests on single anchors were performed in cracked and uncracked concrete. Additional monotonic single anchor reference tests were performed to allow a comparison between the cyclic and monotonic behavior. Thereby, various anchor systems were investigated in order to identify differences in their seismic response. The tested anchor systems comprise undercut anchors, expansion anchors, bonded anchors, concrete screws, and bonded expansion anchors. This chapter presents the detailed description of the experimental

program, the tested anchor systems, the test specimen, the experimental setup, the testing procedure, and the experimental results. The evaluation and discussion of the results is divided into two parts. In the first part, the derivable outputs that can be obtained from both protocols are discussed. In the second part, the results are evaluated with respect to the additional information that can be obtained from the displacement-controlled protocol.

It should be noted that parts of this chapter have been previously published in Stehle and Sharma (2019a), Stehle and Sharma (2019b) and Stehle and Sharma (2020).

5.1 Description of the new displacement-controlled testing approach

A schematic depiction of the displacement-controlled loading protocol is shown in Figure 5.1. As can be seen, the protocol is characterized by stepwise increasing cyclic loading in displacement control. Stepwise increasing the displacement, or the applied load as in the pulsating tension load test C2.3, has the beneficial effect that the stiffness of the anchor can be assessed in the individual cycles in the complete cycling phase as pointed out by Silva (2001). The test sequence proposed here is an adaptation of the test sequence recommended in ACI 374.1-05(19) and is intended to ensure that displacements are increased gradually in steps that are neither too large nor too small. In Figure 5.1, the relative displacement of 1 refers to the mean displacement at peak load as obtained from the reference static tension tests. As the cyclic loading in the new protocol covers the load-displacement curve over the entire range of interest, the new approach allows the evaluation of the anchor stiffness for the whole range instead of the initial range only as done in the current force-controlled approach. This allows for the characterization of stiffness degradation with increasing displacements of the anchors. In each displacement level three cycles are applied. Thus, compared to the force-controlled procedure according to EOTA TR 049, the number of load cycles is reduced. This is particularly true for the initial part of the load-displacement curve, where, in the force-controlled protocol, already 40 cycles are performed in the first two load levels. However, the new protocol is intended to augment the current testing procedures for cases where post-installed anchors are used to form the connection in structural (strengthening) applications. Therefore, the number of cycles is based on displacement-controlled testing procedures for RC structural members under simulated seismic loads, such as described in ACI 374.2R-13. In this context the reduced number of cycles in each displacement level is deemed adequate to assess the anchor performance. After completion of the cyclic loading phase, a residual pull-out test is performed similar to the procedure stipulated in the C2.3 protocol. However, it should be noted that the final pull-out test has a different purpose. While in C2.3 the pull-out test is intended to obtain the residual capacity of the anchor in the aftermath of seismic loading, the pull-out test in the new protocol is solely performed to obtain

the remaining (descending) part of the load-displacement curve. Consequently, since in the new approach, the entire range of interest of the load-displacement curve is already captured during the cyclic phase (including reaching the ultimate load), performing a residual capacity test is redundant. It is worth mentioning that the intention of the three displacement levels in the post-peak range is to gain additional information on the displacement and hysteretic behavior of the anchors after the ultimate load has been reached. Therefore, it is not necessarily required that an anchor withstands all cycles in the post-peak range. If an anchor fails before completion of the cyclic loading history, the information obtained from the completed cycles in the post-peak range covers the relevant information.

For the tests carried out in cracked concrete, before the tension load is applied, the crack is opened to the specified crack width for which the test is to be performed. In comparison to the C2.3 procedure, the crack width is not manually increased during the cyclic loading phase, but the entire test is carried out with the higher value of crack width as per C2.3. However, the crack shall not be restricted from further opening due to the applied tension load.

The new displacement-controlled testing approach is intended for design cases where the anchors are not forced back to zero displacement. This is for example the case when the anchors are solely taking up the tension loads while the compression loads are directly transferred from the baseplate to the RC members by means of contact pressure. Therefore, a lower bound, N_{min}, is introduced which limits the minimum tension load applied on the anchor (see Figure 5.1). Similarly, for practical reasons EOTA TR 049 stipulates a minimum load for the bottom of the tension load pulses in the force-controlled testing procedure in C2.3. In order to ensure a better comparability, the definition of N_{min} in the new protocol follows the definition in C2.3. Thus, N_{min} is taken as the higher of 2% of N_{max} and 200 N. Where N_{max} is defined according to EOTA TR 049.
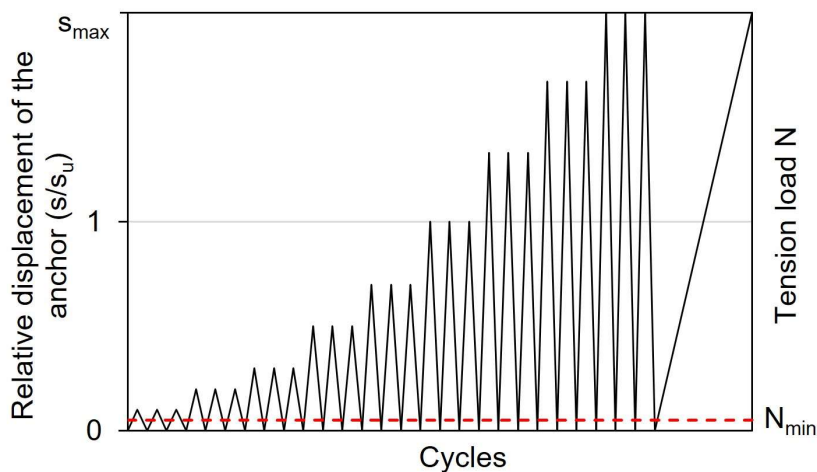
Figure 5.1. Schematic test procedure for the displacement-controlled protocol for pulsating tension load (Stehle and Sharma, 2020).

As can be seen from Figure 5.1, the cyclic loading phase comprises nine displacement levels. The determination of the corresponding displacement amplitudes is provided in Table 5.1. Basically, two displacement values, s_u and s_{max}, are required to define the displacement amplitudes. These displacement values are derived from monotonic reference tests in cracked concrete. The value s_u corresponds to the mean displacement at ultimate load obtained from the monotonic reference tests and defines the displacement amplitudes in the first six levels. The value s_{max} describes the behavior of an anchor in the post-peak range of the load-displacement curve. It is defined as the higher of either the mean displacement corresponding to the point where the load has dropped to 80% of the ultimate load in the post-peak range, $s_{80\%Nu}$, or twice the displacement value corresponding to the ultimate load, $2s_u$. The definition of s_{max} is rather similar to the approach followed in EAD 330087-01-0601 for the determination of the minimum slip value until which the cyclic tests are performed in case of post-installed rebar connections with mortar.

$$s_{max} = \max(s_{80\%Nu}; 2s_u).$$
(5.1)

Table 5.1. Definition of displacement amplitudes.

Displacement level	Displacement amplitude, s_j	Number of cycles
1	$s_1 = 0.1s_u$	3
2	$s_2 = 0.2s_u$	3
3	$s_3 = 0.3s_u$	3
4	$s_4 = 0.5s_u$	3
5	$s_5 = 0.7s_u$	3
6	$s_6 = s_u$	3
7	$s_7 = 2s_u/3 + s_{max}/3$	3
8	$s_8 = s_u/3 + 2s_{max}/3$	3
9	$s_9 = s_{max}$	3

The distinction made for s_{max} is based on the behavior in the post-peak range observed for different types of post-installed anchors. Some types of anchors, such as expansion anchors, may exhibit a rather gradual drop in the strength in the post-peak range. In this case $s_{80\%Nu}$ applies (see Figure 5.2 (a)). Other types of anchors, such as bonded anchors may exhibit a rather brittle failure. In this case, the load drops rather fast after the ultimate load has been reached and thus, $s_{80\%Nu}$ would only represent a scarce segment of the post-peak range. Therefore, in order to enable the investigation of a reasonable part of the post-peak range, $2s_u$ applies in this case.

(a)   (b)
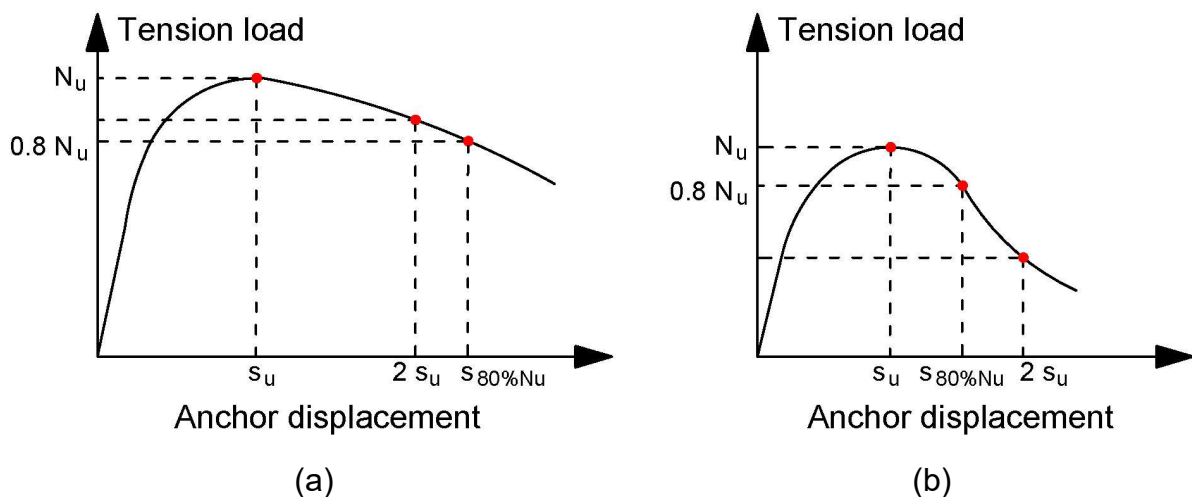
Figure 5.2. Schematic test procedure for the displacement-controlled protocol for pulsating tension load.

5.2 Experimental program

The experimental program is set out to compare the current force-controlled testing approach for pulsating tension load, C2.3, to the new displacement-controlled approach described in the previous section. Therefore, tests on single post-installed anchors were conducted in cracked and uncracked concrete following the two procedures. In order to determine the values that define the load and displacement levels of the respective cyclic protocols, monotonic reference tests were performed beforehand. All tests in cracked concrete were carried out with an initial crack width of 0.8 mm. Thus, the cracks were opened to 0.8 mm before the tension load was applied on the anchors. By doing so, the procedure deviates from the procedure commonly used for C2.3 tests, where the crack is first opened to 0.5 mm and then to 0.8 mm after a specified load level is reached. The applied procedure was adopted to ensure a better comparability of the two protocols and is an accepted but more conservative approach according to EOTA TR 049. As discussed above, in case of certain strengthening solutions such as steel bracing, the cracks close when the anchors are loaded. Thus, additional tests in uncracked concrete were performed. For each anchor system six test series were performed with three tests each. Consequently, a total of 90 tests were performed, 45 of which were conducted in uncracked concrete and 45 in cracked concrete. A summary of the test parameters and the experimental program is given in Table 5.1.

Five different anchor systems were investigated to assess and compare the hysteretic behavior of various types of anchors. A detailed description of the anchor systems used in the experiments is given in the next section. All tests were performed in normal strength concrete (C20/25) with an unconfined test setup according to EOTA TR 048. Note that also the bonded anchors were tested with an unconfined test setup to facilitate the comparison of the anchor systems and because concrete cone failure was the desired failure mode. To ensure no influence of close edges or neighboring anchors, the anchors were positioned in a way that the clear distance between the anchors and the edge and the clear distance between neighboring anchors was at least $4h_{ef}$. The concrete specimens which served as the anchorage material were cast from two concrete batches. However, it was made sure that all tests for one anchor system were performed in slabs of the same concrete batch. The nomenclature adopted for the identification of the individual test series is composed of three groups of letters. The first group identifies the tested anchor system (UC for undercut anchor, EA for expansion anchors, BA for bonded anchor, CS for concrete screw, and BEA for bonded expansion anchor. The second group identifies the type of loading (RF for monotonic reference test, ETAG for the C2.3 protocol, and DISP for the new displacement-controlled protocol). The third group indicates whether the tests were performed in uncracked (UCR) or cracked (CR) concrete.

Table 5.2. Summary of the experimental program.

Anchor system	Test ID	Loading protocol	h_{ef}[1] (mm)	Δw[2] (mm)	f_{cm}[3] (N/mm²)	Number of tests
Undercut anchor M12	UC-RF-UCR	Monotonic		0.0		3
	UC-RF-CR	Monotonic		0.8		3
	UC-ETAG-UCR	C2.3	80	0.0	21.9	3
	UC-ETAG-CR	C2.3		0.8		3
	UC-DISP-UCR	Displ.-controlled		0.0		3
	UC-DISP-CR	Displ.-controlled		0.8		3
Expansion anchor M16	EA-RF-UCR	Monotonic		0.0		3
	EA-RF-CR	Monotonic		0.8		3
	EA-ETAG-UCR	C2.3	80	0.0	21.9	3
	EA-ETAG-CR	C2.3		0.8		3
	EA-DISP-UCR	Displ.-controlled		0.0		3
	EA-DISP-CR	Displ.-controlled		0.8		3
Bonded anchor M16	BA-RF-UCR	Monotonic		0.0		3
	BA-RF-CR	Monotonic		0.8		3
	BA-ETAG-UCR	C2.3	80	0.0	21.9	3
	BA-ETAG-CR	C2.3		0.8		3
	BA-DISP-UCR	Displ.-controlled		0.0		3
	BA-DISP-CR	Displ.-controlled		0.8		3
Concrete screw M12	CS-RF-UCR	Monotonic		0.0		3
	CS-RF-CR	Monotonic		0.8		3
	CS-ETAG-UCR	C2.3	81	0.0	23.9	3
	CS-ETAG-CR	C2.3		0.8		3
	CS-DISP-UCR	Displ.-controlled		0.0		3
	CS-DISP-CR	Displ.-controlled		0.8		3
Bonded expansion anchor M16	BEA-RF-UCR	Monotonic		0.0		3
	BEA-RF-CR	Monotonic		0.8		3
	BEA-ETAG-UCR	C2.3	95	0.0	23.9	3
	BEA-ETAG-CR	C2.3		0.8		3
	BEA-DISP-UCR	Displ.-controlled		0.0		3
	BEA-DISP-CR	Displ.-controlled		0.8		3

(1) Effective embedment depth
(2) Crack width
(3) Mean cylinder concrete compressive strength at the time of testing

5.3   Description of the tested anchor systems and test specimen

5.3.1   Tested anchor systems

The tested anchors systems comprise undercut anchors (UC), expansion anchors (EA), bonded anchors (BA), concrete screws (CS), and bonded expansion anchors (BEA). All tested anchors were produced by the manufacturer fischer. Figure 5.3 shows samples of the anchors used in the experiments. Following is a brief description of the anchors used in the experimental program.

(a)   (b)   (c)   (d)   (e)

Figure 5.3. (a) Undercut anchor FZA, (b) expansion anchor FAZ II, (c) cartridge of the two-component system FIS EM Plus, (d) concrete screw ULTRACUT FBS II, and (e) bonded expansion anchor rod FHB II – A S.

5.3.1.1   Undercut anchor

The undercut anchor FZA which was used in the experiments is anchored in the base material by mechanical interlock. To generate the undercut hole in the concrete, a special universal drill bit, FZUB 18x80 is required. The FZA anchor is qualified for the seismic category C1 according to EOTA TR 049. The technical design details are provided in the corresponding technical assessment ETA-98/0004. Figure 5.3 (a) shows a typical FZA anchor.

The installation of the anchors was performed according to the manufacturer's installation instructions (ETA-98/0004). The hole was drilled with a hammer drill using a special universal drill bit. Once the required embedment depth was reached, the drill hole undercut was generated by rotating the operating drilling machine. Thereafter the

drill hole was cleaned using a vacuum cleaner. The undercut anchor was inserted into the borehole before the fixture was placed. Using a special setting tool, the expansion sleeve was hammered over a cone at the embedded end of the anchor to establish the mechanical interlock between anchor and the drill hole undercut.

5.3.1.2   Expansion anchor

The expansion anchor FAZ II, consisting of an expansion sleeve and a cone bolt, is anchored in the base material by torque-controlled expansion. It holds a qualification for seismic category C1 and C2 according to EOTA TR 049. Technical design details are provided in the corresponding technical assessment ETA-05/0069. A typical FAZ II anchor is shown in Figure 5.3 (b).

The installation of the anchors was performed according to the manufacturer's installation instructions (ETA-05/0069). The hole was drilled using a rotary hammer and a hardened metal drill bit. After the required depth of the bore hole has been reached, the hole was cleaned, and the anchor was installed by applying the required torque.

5.3.1.3   Bonded anchor

The bonded anchor system comprises the two-component injection system FIS EM Plus and a high-strength threaded rod. The threaded rods had a size of M16 and the strength class 8.8. The injection system FIS EM Plus is qualified for the seismic category C1 and C2. Technical design details are provided in the corresponding technical assessment ETA-17/0979. Figure 5.3 (c) shows a typical FIS EM Plus cartridge.

The installation of the anchors was performed according to the manufacturer's installation instructions (ETA-17/0979). The hole was drilled using a rotary hammer and a hardened metal drill bit. Once the desired depth of the bore hole has been achieved, the hole was cleaned. Therefore, the drill hole was blown out three times, using oil-free compressed air. Thereafter, a metal brush was used to roughen the inner surface of the drill hole, followed by the second cleaning of the drill hole by again blowing out the drill hole three times using oil-free compressed air. After the installation, a curing time of 24 hours was kept before testing the anchors.

5.3.1.4   Concrete screw

The concrete screw ULTRACUT FBS II is driven into the bore hole with its thread carving into the concrete, creating a mechanical interlock between the screw thread and the base material. It holds a qualification for seismic category C1 and C2. Technical design details are provided in the corresponding technical assessment ETA-15/0352. Figure 5.3 (d) shows a typical ULTRACUT FBS II anchor.

The installation process includes drilling of the hole using a hammer drill, cleaning of the drill hole, and applying the maximum mentioned torque moment according to the

technical assessment. The installation was performed according to the manufacturer's installation instructions (ETA-15/0352).

5.3.1.5 Bonded expansion anchor

The Highbond-Anchor FHB II is a torque controlled bonded expansion anchor comprising fischer FIS HB mortar and a special anchor rod FHB II - A S, which has cones at the embedded end of the rod. Those cones generate a mechanical interlock between the anchor rod and the surrounding mortar. Technical design details are provided in the corresponding technical assessment ETA-16/0637. A typical sample of the anchor rod is depicted in Figure 5.3 (e).

The installation of the anchors was performed according to the manufacturer's installation instructions (ETA-16/0637). The hole was drilled using a hammer drill. Thereafter the drill hole was cleaned by blowing out three times, using oil-free compressed air, then brushing the bore hole three times to roughen the concrete surface and then again blowing out the drill hole three times using oil-free compressed air.

5.3.2 Description of the test specimen

Two types of test specimen were used in the experiments. The first type is an unreinforced concrete slab with a side length of 1635 mm and a height of 300 mm. Only on the side faces, reinforcing bars with diameter of 6 mm were provided at the top and bottom of the slab for handling. These slabs were used for the tests in uncracked concrete. For the tests in cracked concrete, special slabs were used which were designed to facilitate the opening of the cracks. These slabs had a length of 1600 mm, a width of 800 mm and a height of 300 mm. As indicated in Figure 5.4, the slabs feature 2 mm thick I-shaped steel plates which serve as crack inducers, and which were placed in the formwork before casting. The crack inducers guarantee the formation of the cracks along a defined plane. Thus, the mutual distance of the anchors is also defined by the position of the crack inducers and was 400 mm. Furthermore, the slab has precast holes which are required for the crack opening by hammering in special steel wedges. It is worth noting that in applications in shallow beams or columns, typical flexural cracks would be tapered and not uniform along the embedment depth of the anchors as in these test specimens. Therefore, it is rather likely that the reduction of the anchor capacity in the tests in cracked concrete are at the upper end. Three tests could be performed on each side of the concrete specimen. The slabs were produced according to the state of the art in accordance with DIN EN 206. The composition of the aggregates was chosen such that a grading curve between the standard grading curves A16 and B16 according to DIN EN 206 was obtained. To determine the hardened concrete compressive strength at the time of testing, nine concrete cubes with a side length of 150 mm were used for each concrete batch. The measured mean concrete cube compressive strength was converted into

the mean concrete cylinder compressive strength using a conversion factor of $k_{cyl/cube}$ = 0.82. The conversion factor is based on DIN EN 206, Fingerloos et al. (2015), and Loch (2014). The mean concrete cylinder compressive strength for the respective test series is reported in Table 5.2.
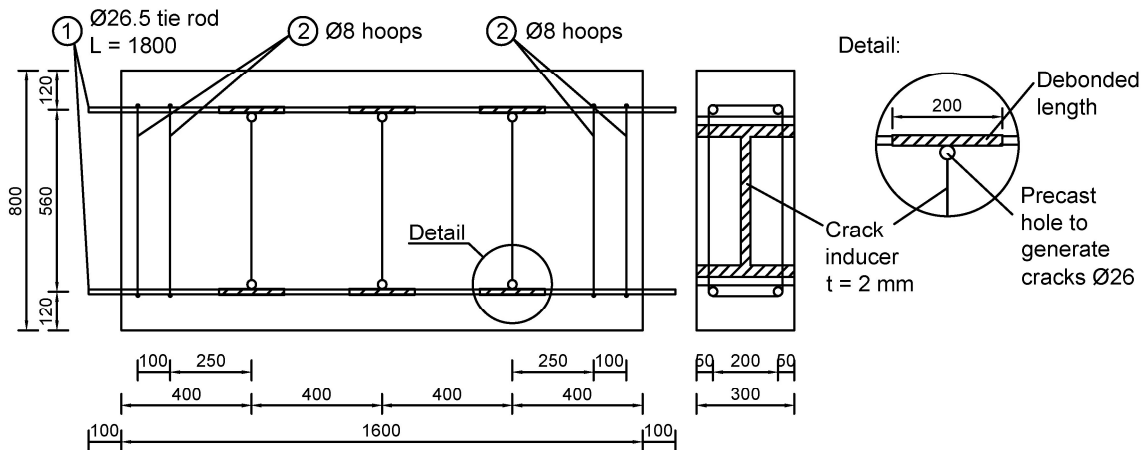
Figure 5.4. Specimen used for the tests in cracked concrete (Stehle and Sharma, 2020).

5.4   Description of the experimental setup and testing procedure

Figure 5.5 shows the experimental setup. An unconfined test setup was used in all tests to facilitate the desired concrete cone failure mode and to ensure the comparability of the tested anchor systems. To maintain the stipulated support distance to the anchors, the two I-beams were placed at a distance of at least $2h_{ef}$ from the anchors on both sides (EOTA TR 048). The test rig on which the servo-hydraulic cylinder is mounted, was placed on the two I-beams as shown in Figure 5.5 (a). The tension load was applied on the anchors via the 250 kN hydraulic cylinder and the axial load was measured continuously using a calibrated load cell with a measuring rang of 250 kN. The anchors were fastened to a steel fixture as shown in Figure 5.5 (c). The fixture was in turn connected to a hinge to nullify any possible moment load and thus to the servo-hydraulic cylinder. To measure (or control) the displacement of the anchors and the crack width, displacement transducers were utilized with a measuring range up to 75 mm. In the displacement-controlled tests, the displacement of the anchors was directly measured on top of the anchors using Linear Variable Differential Transformers (LVDT). To do so, the LVDT was mounted on a bridge-like stand, which was attached to the concrete slab (see Figure 5.5 (b)). In the force-controlled tests, a steel wire was used to indirectly connect the LVDT to the top of the anchors as shown in Figure 5.5 (c). In both cases the reference point for the displacement measurement was the surface of the concrete slab.

The experiments were performed in the testing laboratory of the Institute of Construction Materials at the University of Stuttgart. In case of the tests in cracked concrete, first the bore hole was drilled, as this increases the likelihood of the crack crossing the complete hole. Subsequently, steel sleeves were put into the precast holes in the specimen and wedges were hammered into the sleeves to open the hairline crack. After generating the hairline crack, the wedges were loosened, and the anchor was installed in the hairline crack. Following the installation of the anchor, the experimental setup was arranged, and the crack was opened to the specified crack width by again hammering the wedges into the sleeves. Thereby, the crack width was continuously measured on both sides of the anchor as indicated in Figure 5.5 (b). Thereafter, the anchor was either monotonically pulled out of the concrete, whereby the tension load was applied in such a way that the ultimate load was reached within one to three minutes, or the anchor was loaded following the cyclic loading protocols described above.
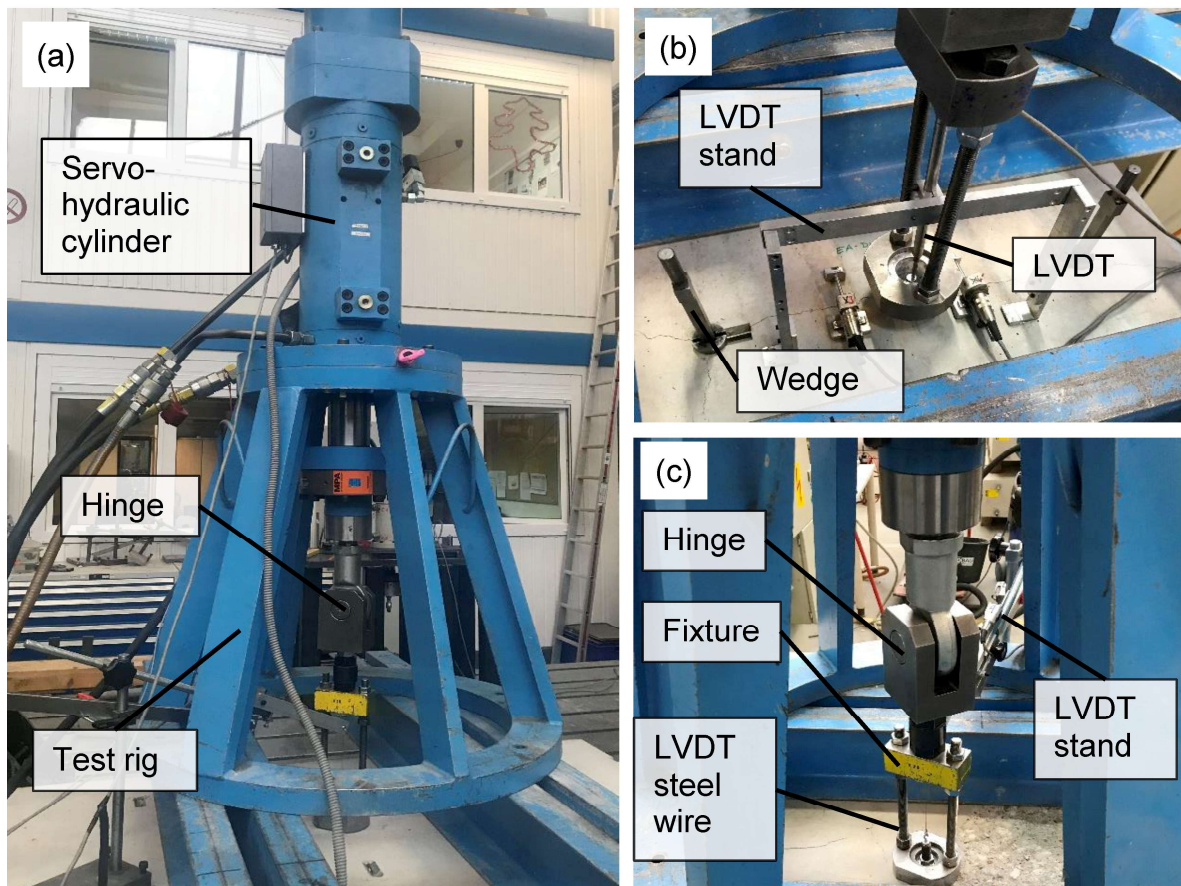
Figure 5.5. Experimental setup for pulsating tension load tests.

5.5   Experimental results

The experimental results are presented individually for the respective types of anchors with respect to the load-displacement behavior and the observed failure mode. A summary of the experimental results in terms of ultimate loads, mean displacements at ultimate load, and mean displacements at 50% of the ultimate load in the ascending branch of the load-displacement curve, alongside the scatter of the respective results in terms of the coefficient of variation (CV) is presented in Table 5.3. As intended, concrete cone failure was the most common failure mode observed in the experiments. Nonetheless, also other failure modes were observed, such as pull-through failure in case of expansion anchors, pull-out failure and combined pull-out and concrete cone failure in case of bonded anchors or concrete screws.

5.5.1   Undercut anchor

Regardless of the applied loading protocol or the condition of the concrete slab (cracked or uncracked), when loaded in tension until failure, all tested undercut anchors failed in concrete cone breakout. Typical failure modes observed in the experiments are shown in Figure 5.6. Thereby, the anchors exhibited relatively large displacements before failure. When loaded according to the force-controlled C2.3 protocol, all tested undercut anchors were able to complete the loading history. In contrast, when loaded according to the new displacement-controlled protocol, in most tests the anchors failed during the cyclic loading phase. Thereby, most anchors failed, or failure was initiated during the seventh displacement level (see s_7 in Table 5.1). Only in two tests in uncracked concrete the anchors could complete the cyclic loading history followed by residual monotonic loading until failure. The obtained load-displacement curves are shown in Figure 5.7 and Figure 5.8. Comparing the results summarized in Table 5.3 and the load-displacement curves, it can be seen that the envelope of the cyclic loops obtained from cyclic loading tests matches well with the results of monotonic reference tests.

Table 5.3. Summary of the experimental results (Sharma and Stehle, 2020).

Test series	Ultimate load, N_u in the respective test (kN)			$N_{u,m}$[1] (kN)	$CV(N_u)$ (%)	$s_{u,m}$[2] (mm)	$CV(s_u)$ (%)	$s_{50\%N_u,m}$[3] (mm)	$CV(s_{50\%N_u})$ (%)
	1	2	3						
UC-RF-UCR	55.0	51.6	49.5	52.0	5.4	4.54	9.6	0.49	30.8
UC-RF-CR	33.2	39.4	37.6	36.7	8.6	6.34	33.8	1.41	13.8
UC-ETAG-UCR	48.6	51.5	49.9	50.0	2.9	4.96	26.5	0.83	59.3
UC-ETAG-CR	45.5	42.1	38.0	41.9	6.2	6.14	10.0	0.90	29.7
UC-DISP-UCR	50.8	50.6	58.3	53.2	8.2	4.83	37.5	0.60	40.4
UC-DISP-CR	45.0	44.9	38.2	42.7	9.0	6.69	41.3	1.49	21.7
EA-RF-UCR	44.6	38.6	46.2	43.1	7.6	4.96	4.1	0.13	45.5
EA-RF-CR	29.2	29.4	35.7	31.4	9.6	9.60	31.0	1.60	13.5
EA-ETAG-UCR	41.8	44.5	42.1	42.8	2.8	6.72	24.4	0.55	101.8
EA-ETAG-CR	31.6	34.1	32.5	32.7	3.1	7.96	9.4	1.67	11.2
EA-DISP-UCR	47.9	47.8	52.1	49.3	4.1	6.32	2.0	0.18	16.1
EA-DISP-CR	38.7	31.7	36.7	35.7	8.3	7.50	16.3	1.34	9.2
BA-RF-UCR	54.1	57.9	61.2	57.7	5.0	0.97	70.2	0.07	22.4
BA-RF-CR	27.6	29.0	27.6	28.0	2.4	0.73	16.7	0.04	35.0
BA-ETAG-UCR	48.3	47.9	47.6	47.9	0.6	0.53	44.1	0.05	40.0
BA-ETAG-CR	30.1	25.9	28.0	28.0	6.2	0.91	16.7	0.15	30.6
BA-DISP-UCR	48.2	51.9	51.3	50.5	3.2	0.43	26.3	0.08	18.8
BA-DISP-CR	29.9	36.5	41.3	35.9	13.0	0.98	18.6	0.26	4.5
CS-RF-UCR	58.1	54.3	60.5	57.7	4.4	1.54	50.0	0.13	17.4
CS-RF-CR	34.5	26.9	34.5	32.0	11.2	2.72	13.8	0.59	18.6
CS-ETAG-UCR	57.0	54.7	55.3	55.7	1.7	1.23	18.9	0.25	42.9
CS-ETAG-CR	32.3	34.7	32.3	33.1	3.4	2.68	19.5	0.64	26.3
CS-DISP-UCR	58.6	61.2	56.2	58.7	3.5	1.38	18.8	0.36	20.9
CS-DISP-CR	32.8	35.3	32.3	33.5	3.9	2.61	2.8	0.78	12.0
BEA-RF-UCR	72.2	73.4	65.9	70.5	4.7	4.38	20.7	0.46	13.3
BEA-RF-CR	60.1	60.8	55.9	59.0	3.7	6.62	7.7	1.64	1.5
BEA-ETAG-UCR	69.4	57.9	69.1	65.4	8.2	4.09	15.2	0.48	3.5
BEA-ETAG-CR	58.5	51.7	55.7	55.3	5.0	6.57	3.5	1.62	11.2
BEA-DISP-UCR	67.8	72.0	69.6	69.8	2.5	4.37	15.3	0.58	4.5
BEA-DISP-CR	62.4	59.2	58.0	59.8	3.1	6.92	19.4	1.77	16.9

(1) Mean ultimate load

(2) Mean displacement at ultimate load

(3) Mean displacement at 50% of ultimate load in the ascending branch

Figure 5.6. Typical failure modes of undercut anchors in uncracked and cracked concrete.

5.5.2   Expansion anchor

In case of the tested expansion anchors the failure mode varied depending on whether the anchors were tested in uncracked or cracked concrete. In uncracked concrete almost all tested anchors (regardless of the loading protocol) failed in pull-through failure. Concrete cone failure was only observed once in test EA-ETAG-UCR-2 when loaded according to the C2.3 protocol. When tested in cracked concrete the failure mode changed to a concrete related failure. Thereby, the anchors already underwent large displacements before failure. In one test, EA-DISP-CR-1, the anchor failed due to pull-through failure when loaded according to the displacement-controlled protocol. One explanation for the variation in the observed failure modes might be that due to the intersecting crack, the concrete cone capacity is significantly reduced (Eligehausen et al., 2006), thus facilitating a breakout failure. Typical failure modes are shown in Figure 5.9.
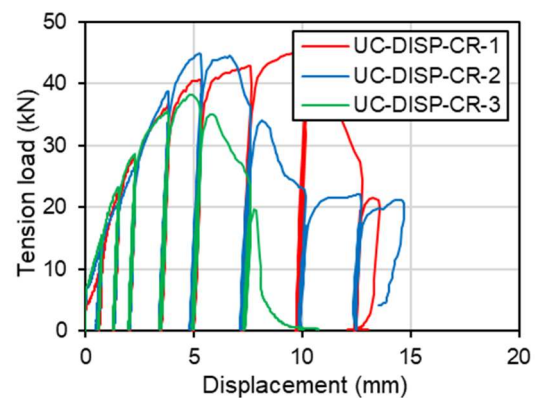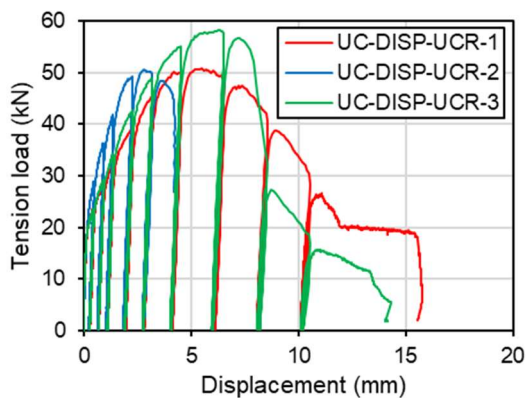
Figure 5.7. Load-displacement curves for undercut anchors under monotonic and cyclic loading according to C2.3 protocol and the displacement-controlled protocol in uncracked concrete.

Figure 5.8. Load-displacement curves for undercut anchors under monotonic and cyclic loading according to C2.3 protocol and the displacement-controlled protocol in cracked concrete.

Comparing the scatter of displacements at 50% of the load given in Table 5.3, it can be seen that the scatter is significantly larger in case of tests that were performed in uncracked concrete. Thus, in the case where the anchors failed largely due to pull-through failure. This observation indicates a rather unpredictable and erratic behavior when the anchors fail due to pull-through failure, while in case of concrete cone failure the behavior appears more stable as the scatter is notably smaller.

Figure 5.9. Typical failure modes of expansion anchors in uncracked and cracked concrete.

Figure 5.10 and Figure 5.11 show the load-displacement curves obtained in the experiments on expansion anchors. Compared to the behavior of undercut anchors, expansion anchors show a pronounced post-peak behavior. This behavior is attributable to the ability of expansion anchors to develop so-called follow-up expansion (Eligehausen et al., 2006). According to Eligehausen et al. (2006), such a behavior can occur due to the increasing anchor displacement, the expansion segment further widens and is pressed against the bore hole, thereby increasing the friction between the anchor and the concrete. In this way, the anchor can still retain a large part of its load-bearing capacity even at relatively large displacement levels. This rather ductile displacement behavior of the tested anchors is considered in the new displacement-controlled protocol by defining s_{max} as $s_{80\%Nu}$. The envelops of the cyclic load-displacement curves essentially follow the monotonic load-displacement curves. In the displacement-controlled cyclic tests, the obtained load-displacement curves show practically vertical unloading and reloading paths, almost throughout the complete range. This means that when the anchor is unloaded, the anchor itself keeps its displaced position, only slightly returning into its former position. In practical applications, when loading is actually reversed, at zero load, the baseplate would first have to overcome the complete anchor displacement before it touches the concrete and could thus transfer a compressive load to the concrete via contact pressure. Such a behavior could have an adverse effect on the performance of the strengthening solution. While, this phenomenon is also apparent in the cycling phase of the force-controlled procedure, it is limited to a rather small range in the initial phase. In the new protocol on the other hand, the unloading and reloading behavior is obtained in almost the complete range. In case of C2.3 tests, the cyclic loading history could be completed in all tests, while premature failure before completion of the cyclic loading history occurred twice when tested according to the new protocol.
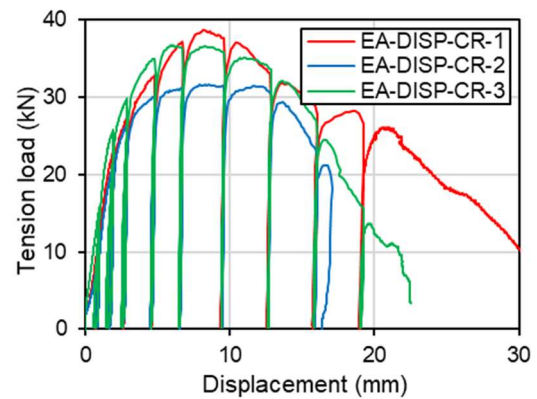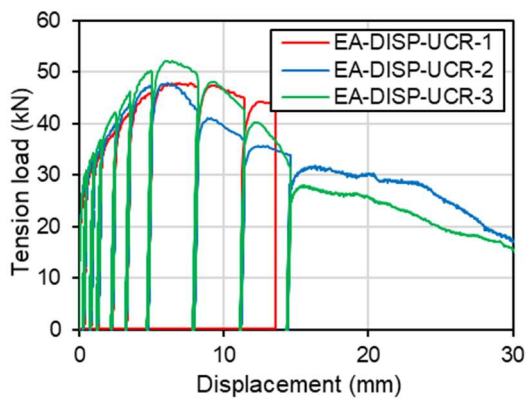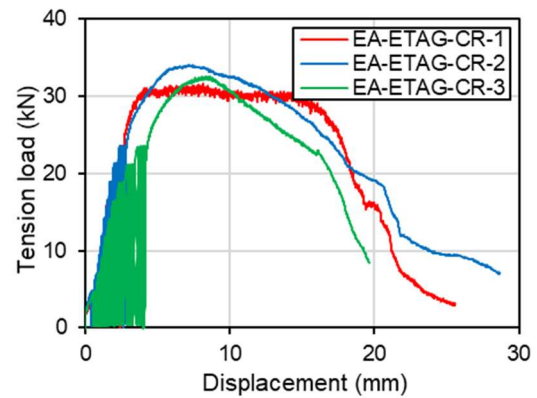
Figure 5.10. Load-displacement curves for expansion anchors under monotonic and cyclic loading according to C2.3 protocol and the displacement-controlled protocol in uncracked concrete.
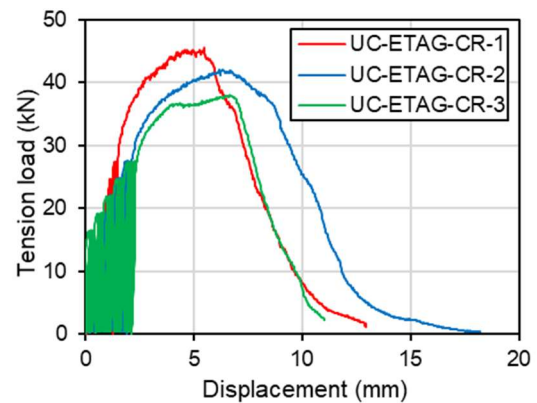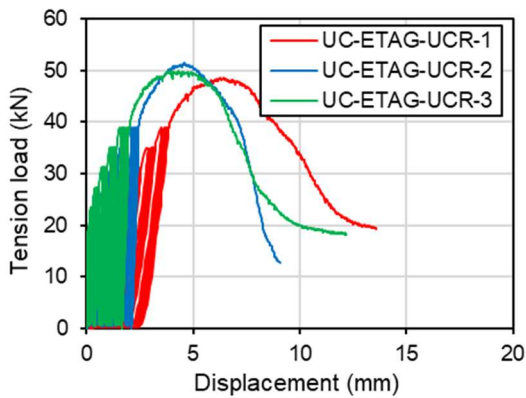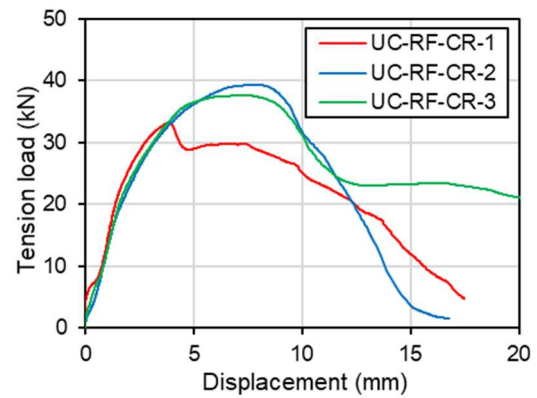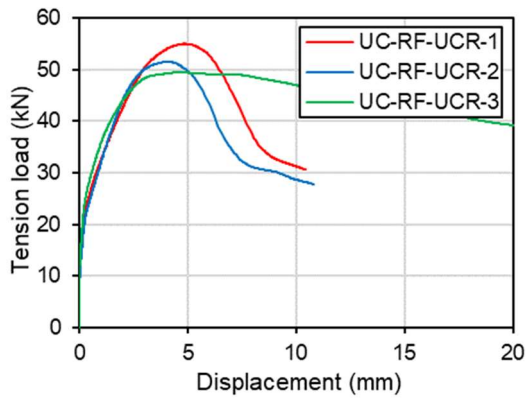
Figure 5.11. Load-displacement curves for expansion anchors under monotonic and cyclic loading according to C2.3 protocol and the displacement-controlled protocol in cracked concrete.

5.5.3 Bonded anchor

The tested bonded anchors either failed due to concrete cone failure or a mixed concrete cone and pull-out failure. Typical failure modes are shown in Figure 5.12. When comparing the mean displacements at ultimate load obtained from the monotonic reference tests in uncracked and cracked concrete in Table 5.3, it stands

out that the obtained mean displacement at ultimate load in uncracked concrete is larger than the corresponding values in cracked concrete. This is a rather atypical behavior as generally the displacement of an anchor in cracked concrete is larger than the displacement in uncracked concrete. In Figure 5.13 it can be seen that in case of monotonically loaded anchors in uncracked concrete the displacement behavior in one test deviates widely from the results in the remaining two tests. Since only three tests have been performed in one test series, the result of one test has a marked influence on the mean value, thus also explaining the large scatter in the results. Conducting additional tests would have notably weakened the influence of an individual test and put it into perspective. Nonetheless, the divergent test has also been considered for the definition of the displacement levels in the new protocol, which is why the demand on the anchors in the displacement-controlled cyclic tests was relatively high. Note that if only the first two reference tests are considered, the mean displacement at ultimate load in uncracked concrete would reduce to 0.57 mm.
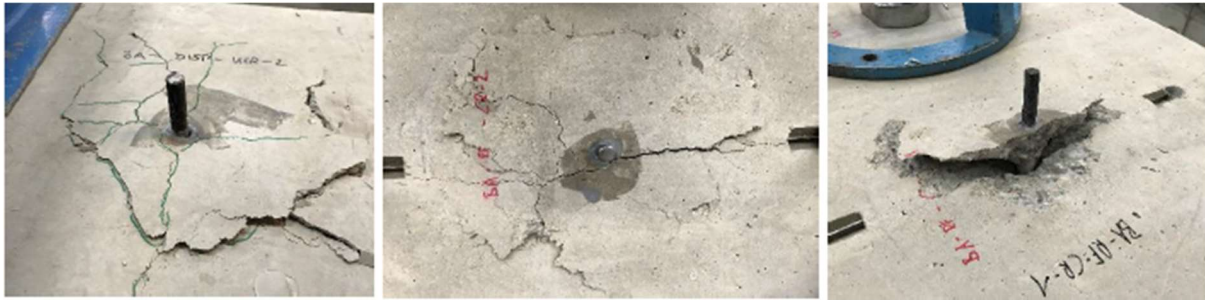
Figure 5.12. Typical failure modes of bonded anchors in uncracked and cracked concrete.

Compared to undercut anchors or expansion anchors, the actual displacement of bonded anchors is significantly smaller, which is also why bonded anchors are notably stiffer as will be discussed later. What becomes apparent from the curves obtained in the displacement-controlled cyclic tests, is that also the hysteretic behavior of the anchor is somewhat more pronounced compared to undercut anchors or expansion anchors. This also results in smaller residual displacements when unloading during one cycle. When loaded according to the new protocol, it was found that the tests in cracked concrete yielded higher ultimate loads than the corresponding reference tests or the C2.3 tests. Nonetheless, the envelope of the anchors under cyclic loading matches well with the behavior in the reference tests. Due to the relatively high demands in the displacement-controlled cyclic tests in uncracked concrete, in all three tests the anchors failed before completing the loading history. In two tests, BA-DISP-UCR-1 and BA-DISP-UCR-2, the anchors failed before reaching s_u.
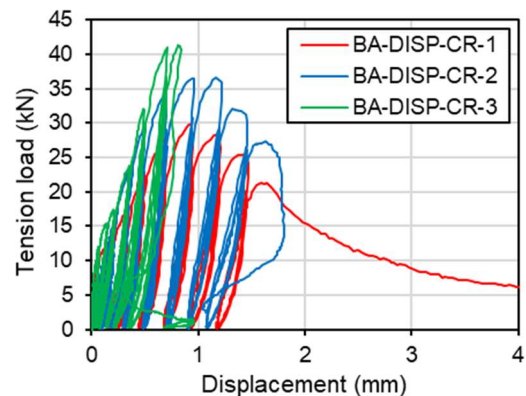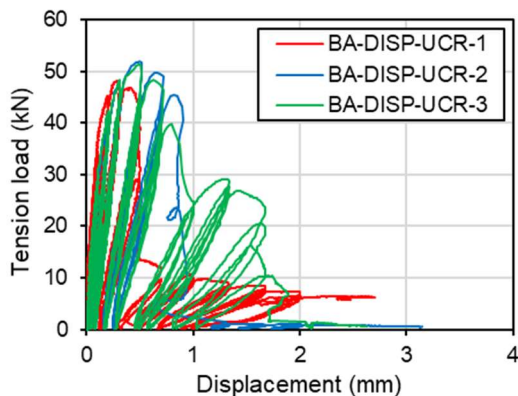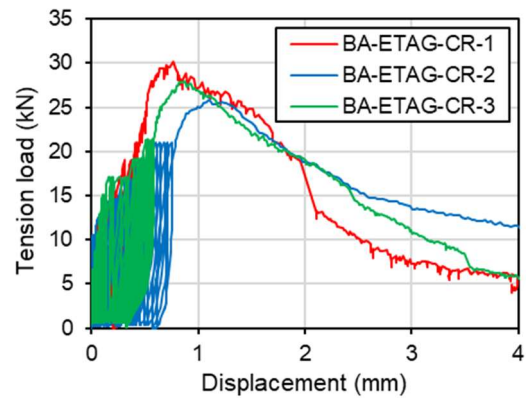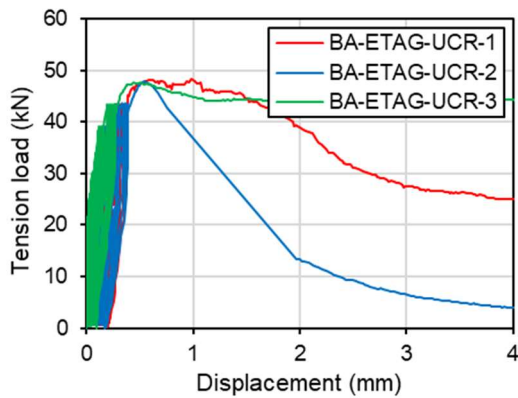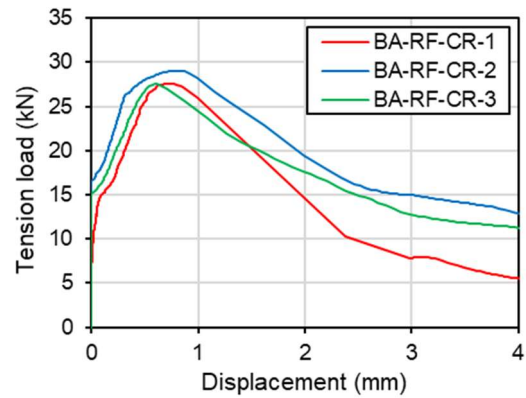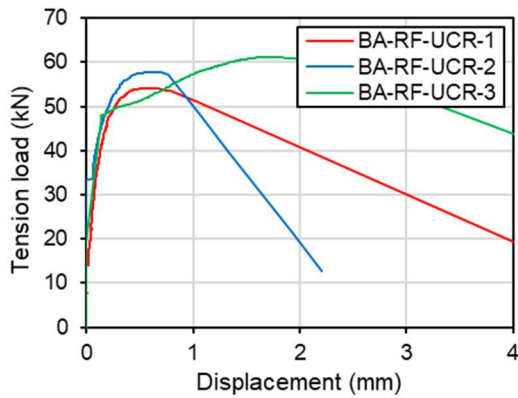
Figure 5.13. Load-displacement curves for bonded anchors under monotonic and cyclic loading according to C2.3 protocol and the displacement-controlled protocol in uncracked concrete.

Figure 5.14. Load-displacement curves for bonded anchors under monotonic and cyclic loading according to C2.3 protocol and the displacement-controlled protocol in cracked concrete.

5.5.4 Concrete screw

The failure modes observed for the tested concrete screws varied depending on whether the anchors were tested in cracked or uncracked concrete. In uncracked concrete the anchors failed either in concrete cone failure or in a mixed concrete cone and pull-out failure mode, whereby concrete cone failure was the dominant failure mode. In cracked concrete, the failure occurred mostly due to a mixed concrete cone

and pull-out failure. In few tests the anchors were also pulled out of the concrete. Typical failure modes are shown in Figure 5.15. Apparently, the presence of a crack has a significant influence on the anchor behavior. This is also evident from the reduced load capacity of the tested anchors in cracked concrete.

Figure 5.15. Typical failure modes of concrete screws in uncracked and cracked concrete.

Similar to bonded anchors, the hysteretic behavior of the tested concrete screws appears more pronounced compared to undercut anchors or expansion anchors. Also, the displacements at ultimate load are relatively small. As can be seen from the load-displacement curves shown in Figure 5.16 and Figure 5.17, the obtained envelopes of the cyclic curves match very well with the load-displacement curves obtained from the monotonic reference tests. The good agreement between the results obtained from the different loading protocols is also evident from the comparison of mean ultimate loads and corresponding displacements in Table 5.3. The cyclic loading protocols could be completed by almost all tested anchors. There was only one exception in test CS-DISP-UCR-1 where the anchor failed in the eighth displacement level.
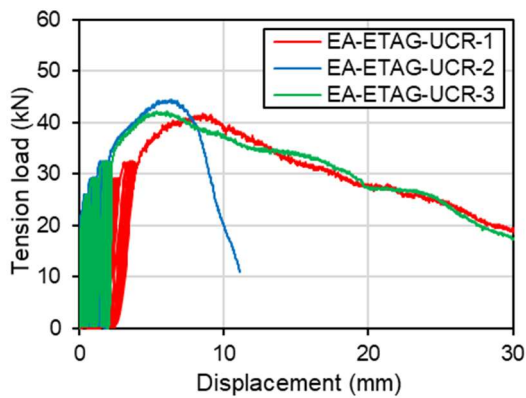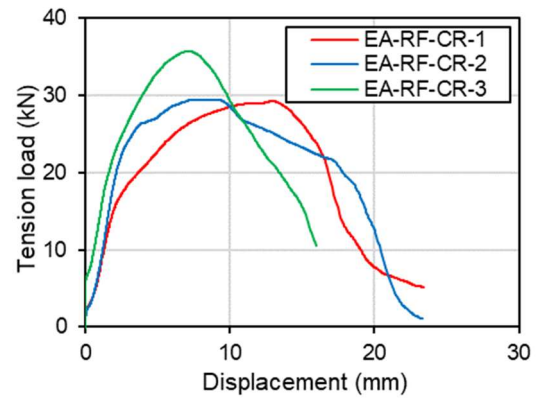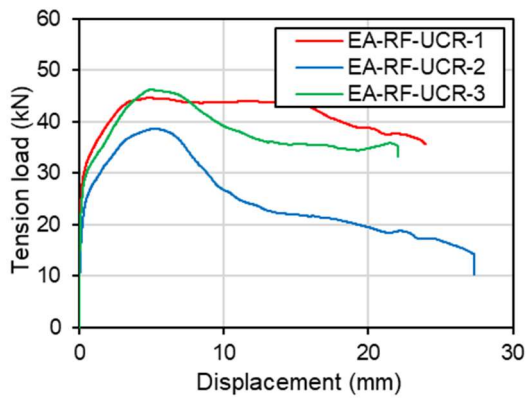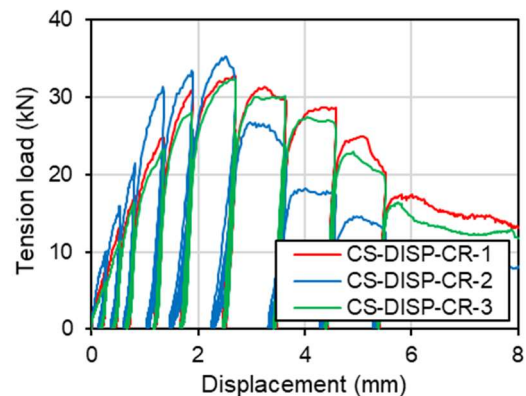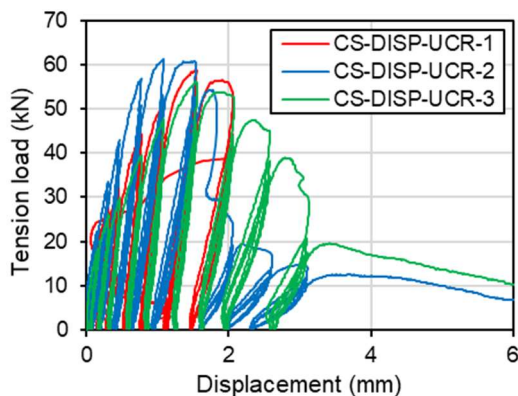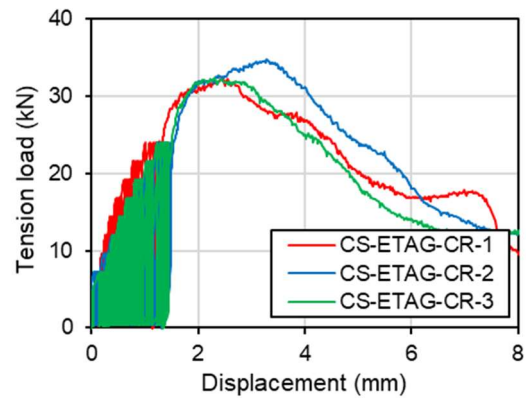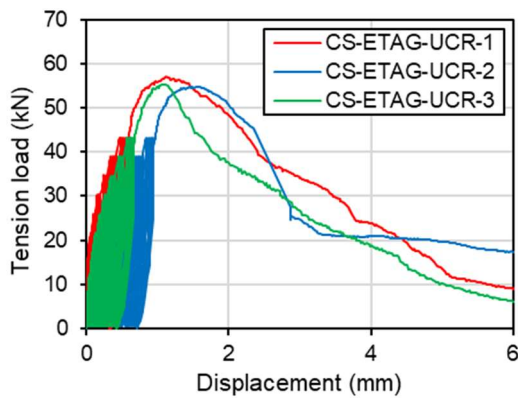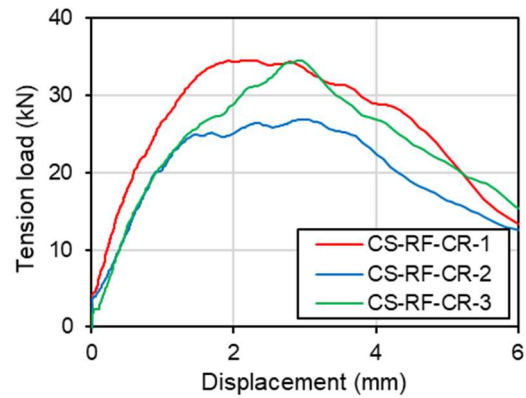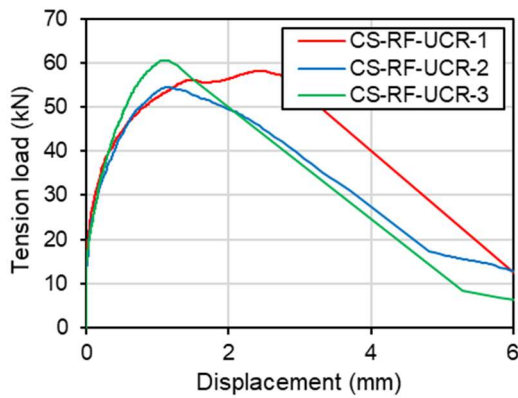
Figure 5.16. Load-displacement curves for concrete screws under monotonic and cyclic loading according to C2.3 protocol and the displacement-controlled protocol in uncracked concrete.

Figure 5.17. Load-displacement curves for concrete screws under monotonic and cyclic loading according to C2.3 protocol and the displacement-controlled protocol in cracked concrete.

5.5.5 Bonded expansion anchor

Typical failure modes observed in the tests on bonded expansion anchor are shown in Figure 5.18. In all tests the anchors were able to utilize the concrete strength failing either in concrete cone failure or in a mixed failure mode. No pull-out failure was observed. Compared to other tested anchor systems, bonded expansion anchors showed a superior performance in cracked concrete which is evident from the low

scatter in the test results and a rather small reduction of the ultimate load when the anchors were intersected by a crack.

Figure 5.18. Typical failure modes of bonded expansion anchors in uncracked and cracked concrete.

Bonded expansion anchors show a rather similar displacement and hysteretic behavior to the tested undercut anchors. However, the larger embedment depth of the bonded expansion anchors renders a direct comparison difficult. Nevertheless, the results obtained in the cyclic tests agree with the previous findings, where it was shown that the overall load-displacement curves obtained for different types of loading match quite well. This becomes evident from the load-displacement curves shown in Figure 5.19 and Figure 5.20, and from the results reported in Table 5.3. In all tests following the force-controlled procedure, C2.3, the anchors completed the loading history and failed in the subsequent residual capacity test. Failure during the loading phase in case of the new protocol occurred only once in test BEA-DISP-UCR-2. However, it should be noted that in the other two tests in uncracked concrete, the failure was already initiated before the last displacement level was reached.

5.6   Evaluation

The evaluation and discussion of the results is divided into two parts. First, the results are discussed with respect to the derivable outputs that can be obtained from both protocols. The second part addresses the additional information that can be obtained from the displacement-controlled protocol. The anchor behavior is assessed with respect to the strength degradation in subsequent displacement cycles in one level, the behavior during unloading and reloading, and the residual displacements during unloading.
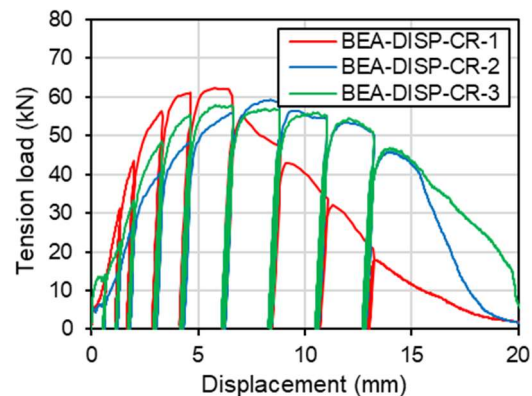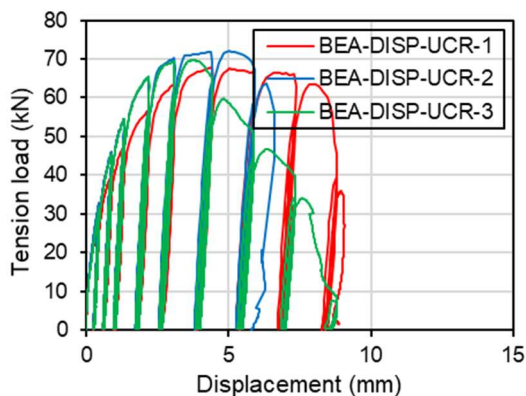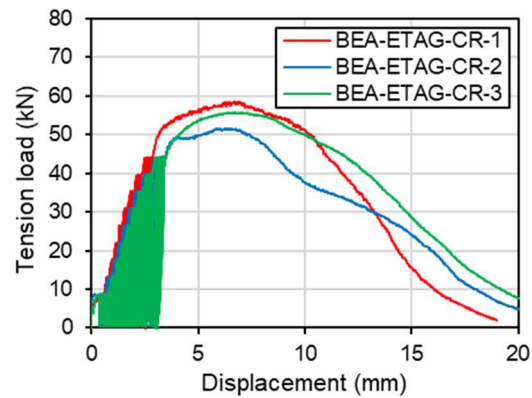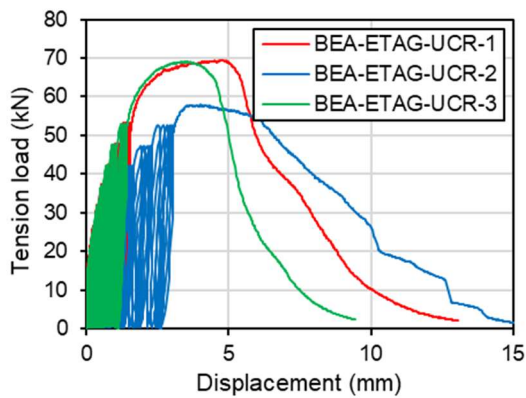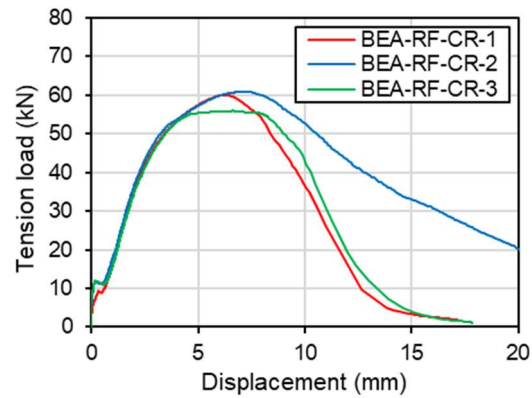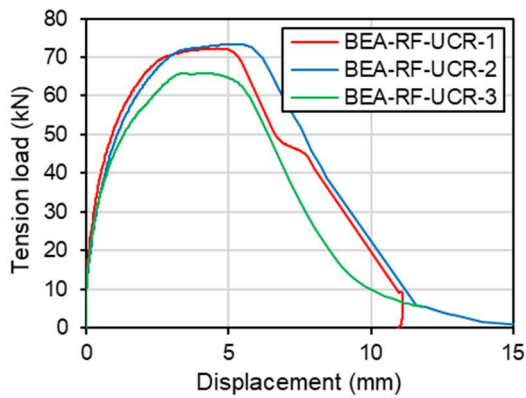
Figure 5.19. Load-displacement curves for bonded expansion anchors under monotonic and cyclic loading according to C2.3 protocol and the displacement-controlled protocol in uncracked concrete.

Figure 5.20. Load-displacement curves for bonded expansion anchors under monotonic and cyclic loading according to C2.3 protocol and the displacement-controlled protocol in cracked concrete.

5.6.1 Comparison of anchor characteristics obtainable in both protocols

As shown in the previous section, the obtained overall load-displacement behavior, such as the shape of the envelope curve, is rather similar for both protocols. Therefore, some information is derivable from both protocols. Accordingly, the results obtained by the two cyclic protocols will be compared with respect to the obtained mean ultimate loads, the displacements at ultimate load, the scatter of displacements at 50% of the

ultimate load in the ascending branch of the load-displacement curve, the secant stiffness values at ultimate load and at 50% of the ultimate load in the ascending branch of the load-displacement curve, and the shape of the load-displacement curves.

5.6.1.1   Ultimate load

Figure 5.21 compares the mean ultimate loads obtained from the monotonic and cyclic tests in uncracked and cracked concrete. The black markers indicate the results obtained in uncracked concrete and the red markers indicate the results obtained in cracked concrete. From Figure 5.21 and from the results provided in Table 5.3 it can be seen that the mean ultimate loads obtained from the two cyclic protocols and from the monotonic tests are in a good agreement and are approximately the same for respective tested anchor systems. Nonetheless, minor differences in the behavior of different types of anchors were observed. In uncracked concrete, mechanical anchors and concrete screws showed a slight reduction of the ultimate capacity when loaded according to the force-controlled protocol compared to the monotonic tests, while the capacity slightly increased when loaded according to the displacement-controlled protocol, however the actual values were within the accepted scatter of 15% for concrete related failure modes. In case of bonded anchors tested in uncracked concrete, the difference between the three loading schemes is rather small with respect to the ultimate loads. However, the monotonic tests yielded somewhat higher ultimate loads compared to the cyclic tests. In cracked concrete, both load cycling and displacement cycling had primarily a beneficial effect on the ultimate loads. In almost all cyclic tests, the obtained ultimate loads were either equal or slightly higher compared to the ultimate loads obtained from the reference tests. The only exception was observed for bonded expansion anchors in the force-controlled cyclic protocol, where the mean ultimate load was 94% of the mean ultimate load from the reference tests. In general, the ultimate loads obtained from the displacement-controlled protocol where slightly higher than those obtained from the force-controlled protocol. Nonetheless, the results obtained from both protocols are in a very good agreement.
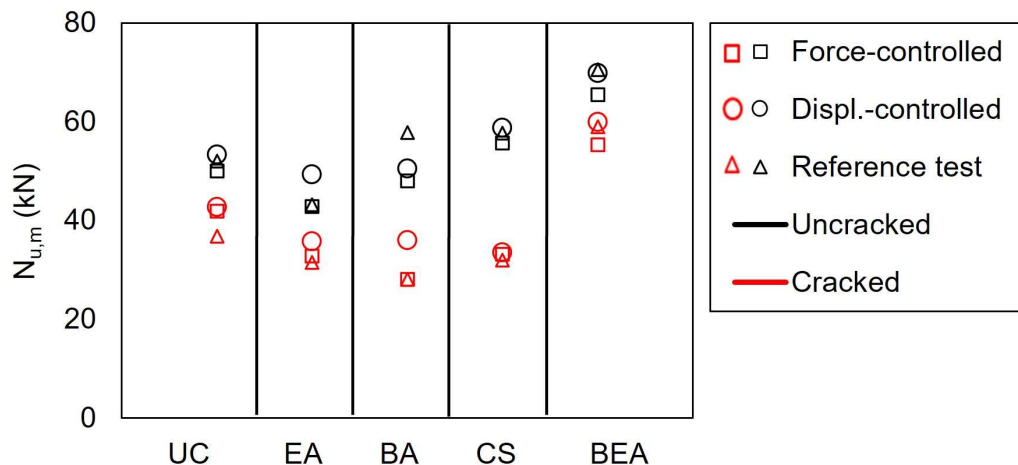
Figure 5.21. Mean ultimate loads obtained in the monotonic and cyclic tests in uncracked and cracked concrete.

Regarding the scatter of ultimate loads, all test series in uncracked concrete showed a scatter below the maximum allowed scatter in EOTA TR 049. The highest scatter was observed for undercut anchors when loaded in the displacement-controlled protocol. Here, the coefficient of variation was 8.2%. It should be noted that in general the scatter of ultimate loads was higher for the displacement-controlled protocol with the only exception being bonded expansion anchors. In cracked concrete, it was observed that the scatter is indeed higher than it is in uncracked concrete. However, it is below the maximum allowed scatter according to EOTA TR 049 (15%). In cracked concrete the largest scatter was observed for bonded anchors when loaded according to the displacement-controlled protocol. This observation reflects their inferior behavior (in terms of load-carrying capacity) in cracked concrete compared to other types of anchors. Again, the displacement-controlled protocol yielded larger values for the coefficient of variation than the force-controlled protocol with the only exception being bonded expansion anchors.

The findings support two conclusions. First, tension cycling appears to have basically no negative influence on the anchor load carrying capacities. Second, the comparison of the two cyclic protocols has shown that the obtained ultimate loads and the corresponding scatter are in good agreement. Nevertheless, it should be noted that due to the increased number of cycles in the force-controlled protocol, slightly more damage is induced than in the displacement-controlled protocol. This results in slightly lower ultimate loads in the force-controlled tests. In combination with observations from other studies conducted by Hoehler (2006), Mahrenholtz et al. (2016) and Ghobarah and Aziz (2004) on different types of anchors, where it was found that force-controlled tension load cycling has either no major effect or rather a beneficial effect on the anchor

load carrying capacity, it can be concluded that the displacement-controlled protocol provides basically the same information with respect to the ultimate loads as the force-controlled protocol C2.3 according to EOTA TR 049.

5.6.1.2 Displacement behavior

The mean displacements at ultimate load obtained from the tests in uncracked and cracked concrete are graphically presented in Figure 5.22. It is apparent that the values obtained from the two cyclic protocols are in a very good agreement. Furthermore, it can be seen that in almost all cases, the mean displacement at ultimate load is below the displacement limit of 7 mm stipulated by EOTA TR 049 after completion of the last cycle of the load level at $0.5N_{max}$. The only exception being the tested expansion anchors. However, at 50% of ultimate load the observed displacements were well below 7 mm in all test series. This observation raises the question how meaningful this criterion is. In general, the tested bonded anchors and concrete screws yielded the lowest displacements, while undercut anchors, expansion anchors and bonded expansion anchors exhibited rather large displacements upon reaching their ultimate capacity. Thereby, expansion anchors yielded the largest displacements.

The scatter of displacements was evaluated at the point where 50% of the mean ultimate load was reached for the first time (generally defined as initial stiffness of the anchors). This value provides a more general statement on the overall displacement behavior as it does not neglect the displacements during the cycling phase as stipulated in EOTA TR 049. In tests conducted in uncracked concrete, undercut anchors, expansion anchors and concrete screws showed a large scatter of displacements when loaded according to the force-controlled protocol. This is evident from the coefficient of variation, which is above 40% for the tested anchors (see Table 5.3). Such high values indicate a rather erratic anchor behavior. Especially the expansion anchors in uncracked concrete, which failed in pull-through failure, showed a particularly volatile behavior. When loaded according to the displacement-controlled protocol, the observed behavior of the tested anchors in uncracked concrete was significantly more stable, and the scatter in the displacement-controlled cyclic tests reduced in comparison to the scatter observed in the force-controlled cyclic tests. In cracked concrete, the coefficient of variation was below 40% in all cyclic tests, regardless of the loading protocol. In general, all anchors showed a more stable or an identical behavior when tested in cracked concrete while subjected to cyclic loading. Again, the displacement behavior in the displacement-controlled tests was generally more stable than in the force-controlled tests. This might be attributed to the increased number of load cycles in the force-controlled protocol, leading to slightly more damage in the base material.
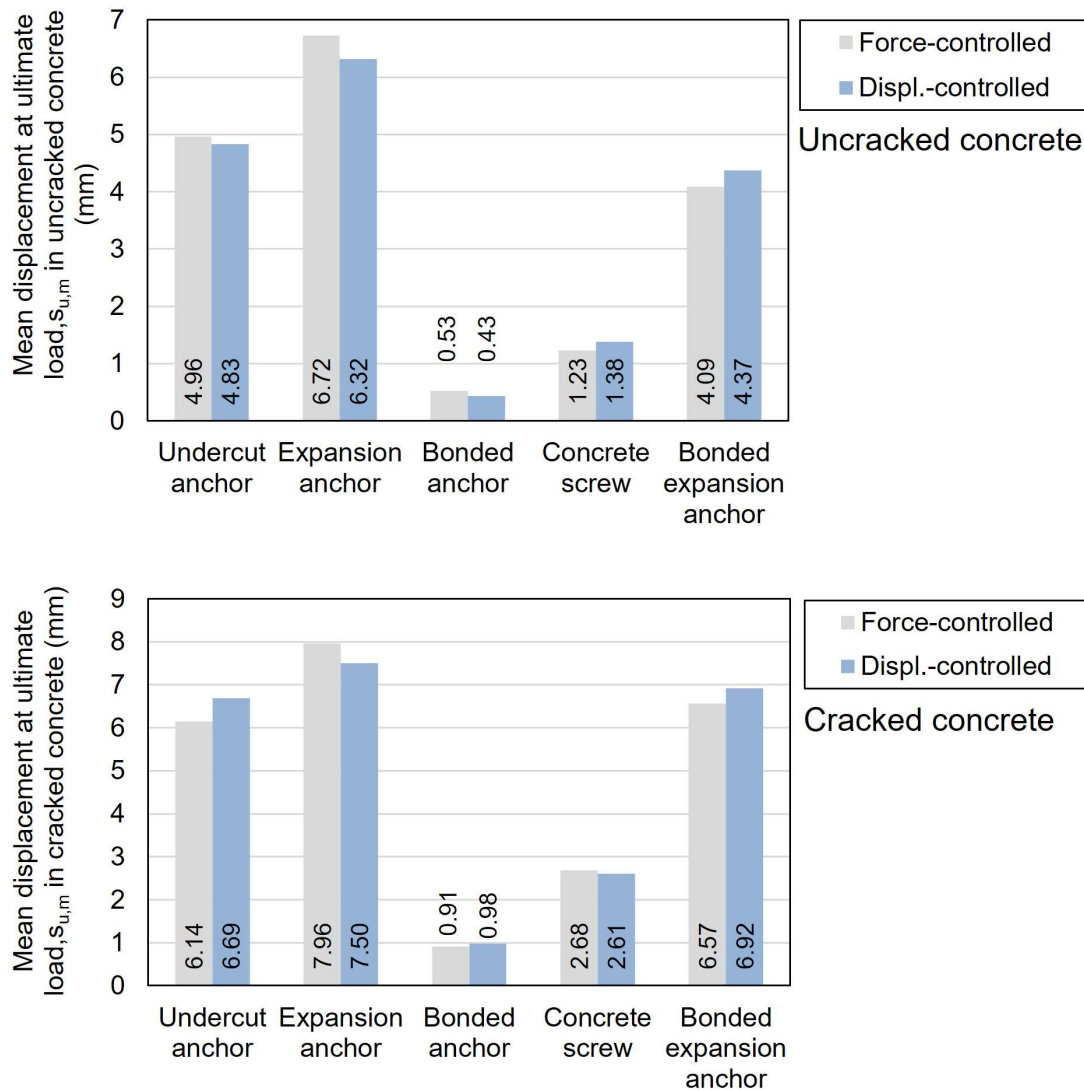
Figure 5.22. Mean displacements at ultimate load obtained in the cyclic tests in uncracked (top) and cracked (bottom) concrete.

5.6.1.3   Secant stiffness

Table 5.4 presents the mean secant stiffness values at ultimate load and at 50% of the ultimate load obtained in the cyclic test series. As can be seen, the secant stiffness values at ultimate load obtained from tests in uncracked concrete following the two cyclic loading protocols are generally in a good agreement. It becomes apparent that bonded anchors yield significantly higher stiffness values compared to other types of post-installed anchors. Furthermore, it can be seen that the mean secant stiffness at ultimate load is larger when the bonded anchors were loaded according to the displacement-controlled protocol. It should be noted that in particular one test showed a significantly higher stiffness while the other two performed tests resulted in stiffness values similar to the ones that were observed in the force-controlled tests. The same

applies to the secant stiffness values at ultimate load obtained from tests in cracked concrete.

Table 5.4. Stiffness values obtained in cyclic tests in cracked and uncracked concrete.

Anchor system	Uncracked / cracked concrete	Loading protocol	$k_{Nu,m}$[1] (kN/mm)	$k_{50\%Nu,m}$[2] (kN/mm)
Undercut anchor	Uncracked	C2.3	10.56	122.13
		Displ.-controlled	12.27	53.16
	Cracked	C2.3	6.90	25.64
		Displ.-controlled	6.94	14.87
Expansion anchor	Uncracked	C2.3	6.62	101.58
		Displ.-controlled	7.80	138.48
	Cracked	C2.3	4.15	9.90
		Displ.-controlled	4.87	13.44
Bonded anchor	Uncracked	C2.3	91.40	535.45
		Displ.-controlled	123.87	324.64
	Cracked	C2.3	31.64	105.98
		Displ.-controlled	37.85	68.73
Concrete screw	Uncracked	C2.3	46.36	133.13
		Displ.-controlled	43.77	86.24
	Cracked	C2.3	12.59	27.45
		Displ.-controlled	12.85	21.74
Bonded expansion anchor	Uncracked	C2.3	16.26	69.19
		Displ.-controlled	16.21	60.60
	Cracked	C2.3	8.41	17.26
		Displ.-controlled	8.89	17.44

(1) Mean secant stiffness at ultimate load
(2) Mean secant stiffness at 50% of the ultimate load

Regarding the secant stiffness at 50% of the ultimate load, it is apparent that the differences between the two cyclic protocols increase. This is particularly evident in case of undercut anchors and bonded anchors. Correspondingly, the overall scatter of the test results increases. This was already noted when discussing the displacements, where it was shown that the scatter of displacements at 50% of the ultimate load was relatively high in some test series. One reason for the discrepancy could be attributed to the relatively small displacements and possible measurement inaccuracies especially at very small displacement levels. Another reason for the divergent results obtained from the two cyclic protocols is that in tests following the displacement-controlled protocol the anchor displacements were measured directly on top of the anchor, whereas in tests following the force-controlled protocol, the anchor displacements were measured indirectly by means of a steel wire connecting the LVDT to the top of the anchor. The measurement approach using steel wires can lead to

deviations caused by friction between the steel wire and the winch, especially in case of small displacements. In this regard the test results are deemed less meaningful when it comes to assessing the consistency of the two protocols in terms of their secant stiffness values at 50% of the ultimate load.

5.6.1.4 Shape of the load-displacement curve and influence of loading history

It is found that the envelopes of the load-displacement curves obtained by loading the tested post-installed anchors according to the two cyclic protocols are well matched. Furthermore, they largely follow the load-displacement curve obtained from the reference static tests. This observation is in accordance with studies by Hoehler (2006) where it was found that regarding the ultimate capacity and the obtained load-displacement behavior, force-controlled cyclic tension tests yield almost the same information as can be obtained from monotonic reference tests in cracked concrete. Furthermore, the tested anchors showed no sensitivity to the cyclic loading protocols with respect to the observed failure modes. Essentially, the experimental results show that the same failure modes could be observed regardless of whether an anchor was loaded monotonically or loaded according to one of the two cyclic protocols. Thus, it can be concluded that the displacement-controlled protocol and the force-controlled protocol yield the same results with respect to the type of failure.

In case of the tests according to the force-controlled protocol, where cyclic loading is limited to a certain load level defined by 75% of the mean ultimate capacity of the respective reference tests, all tested anchors were able to complete the loading history. When loaded according to the displacement-controlled protocol the tested anchors were often unable to complete the loading history and not all displacement cycles were executed. This is attributable to the fact that in the displacement-controlled protocol the demands during the cycling phase are significantly higher than in the force-controlled protocol since the anchors are exposed to cyclic loading in the post-peak range of the load displacement curve. Furthermore, it should be noted that the new protocol is not intended to withstand all cycles in the post-peak range. Rather the additional information obtained in the post-peak range becomes relevant.

5.6.2 Additional information obtained from the displacement-controlled protocol

In this section, the additional information is discussed that is obtained from the displacement-controlled protocol, which allows the assessment of additional aspects regarding the anchor behavior when subjected to pulsating tension load. Furthermore, it is shown that different types of anchors, although having the same load capacity, might behave very differently with regards to their displacement and hysteretic behavior.

On the one hand such information might be used to assess the performance of a connection using post-installed anchors in structural (strengthening) applications, such

as steel bracing or post-installed haunch elements against earthquake hazards. On the other hand, this information can be used to develop numerical models which are able to realistically reflect the anchor behavior under cyclic tension loads. The information that will be discussed include:

- Strength degradation in subsequent cycles of a displacement level

- Stiffness degradation: Cycling throughout a broader range of the load-displacement curve allows to assess the stiffness degradation as the unloading and reloading stiffness changes with increasing displacement of the anchors

- Residual displacements at each cycle: The residual displacement of an anchor can be an indicator for its suitability in different applications

Especially in the case of seismic strengthening applications, post-installed anchors with large strength degradation, stiffness degradation or residual displacements might not be suitable

Note that expansion anchors will not be considered in the following evaluation. The reason for this is that pull-through failure occurred in all displacement-controlled cyclic tests in uncracked concrete and in one test in cracked concrete. Since this failure mode is considered as a product failure, those anchors are deemed unsuitable for the use in structural strengthening applications against seismic actions.

5.6.2.1   Strength degradation in subsequent cycles

When an anchor is cycled at the same displacement level, it can exhibit a reduction in strength in subsequent cycles. Thus, the load achieved in the first cycle of a particular displacement level might not be achieved in the subsequent cycles at the same displacement level as schematically illustrated in Figure 5.23. This is also a well-known phenomenon in reinforced concrete structural sub-assemblies (ACI 374.2R-13). In Figure 5.23, $N_{max,j}$ is the maximum obtained load at a certain displacement level j, which is generally obtained in the first cycle of the respective displacement level. The corresponding displacement is $s_{max,j}$. $N_{sj,n}$ is defined as the load corresponding to the targeted maximum displacement amplitude of a particular displacement level, s_j, in the nth cycle of the respective level. Thus, $N_{s3,2}$ designates the load corresponding to the maximum displacement in the second cycle of the third displacement level, s3. Note, since the displacement value s_j defines the upper limit of the individual displacement levels, it is the maximum displacement in all cycles of the same displacement level (see Table 5.1). In order to determine the strength degradation in subsequent cycles, the loads corresponding to the maximum displacement value s_j in one level are compared. In the elastic range of the load-displacement curve, generally the maximum obtained load in one cycle corresponds to the load obtained at the displacement value s_j. Thus, $s_{max,j} = s_j$. However, when an anchor enters the nonlinear range of the load-displacement curve, the maximum load in one cycle might be achieved before the

maximum displacement, s_j, of the respective displacement level is reached (see Figure 5.23). Thus, $s_{max,j} < s_j$. This is particularly true for the first cycle of a displacement level. This effect is attributable to the so-called "in-cycle strength degradation" where due to additional inelastic displacement a smaller resistance is developed. In general, in-cycle strength degradation is observed mainly in the first cycle of a particular displacement level. Thus, in subsequent cycles (second and third cycle) the displacement corresponding to the maximum load for that cycle generally coincides with the targeted maximum displacement of the respective displacement level. Note that the maximum load obtained in the second and third cycle may be significantly lower than the maximum load obtained in the first cycle at the given displacement level. It becomes apparent that in this case larger displacement would be needed to reach the maximum load in the second and third cycle compared to displacement corresponding to the maximum load in the first cycle (see Figure 5.23). Therefore, in the following, the loads obtained in the second and third cycle which correspond to the targeted displacement s_j of the respective displacement level are compared to the obtained load in the first cycle of the displacement level which correspond to the same displacement s_j.
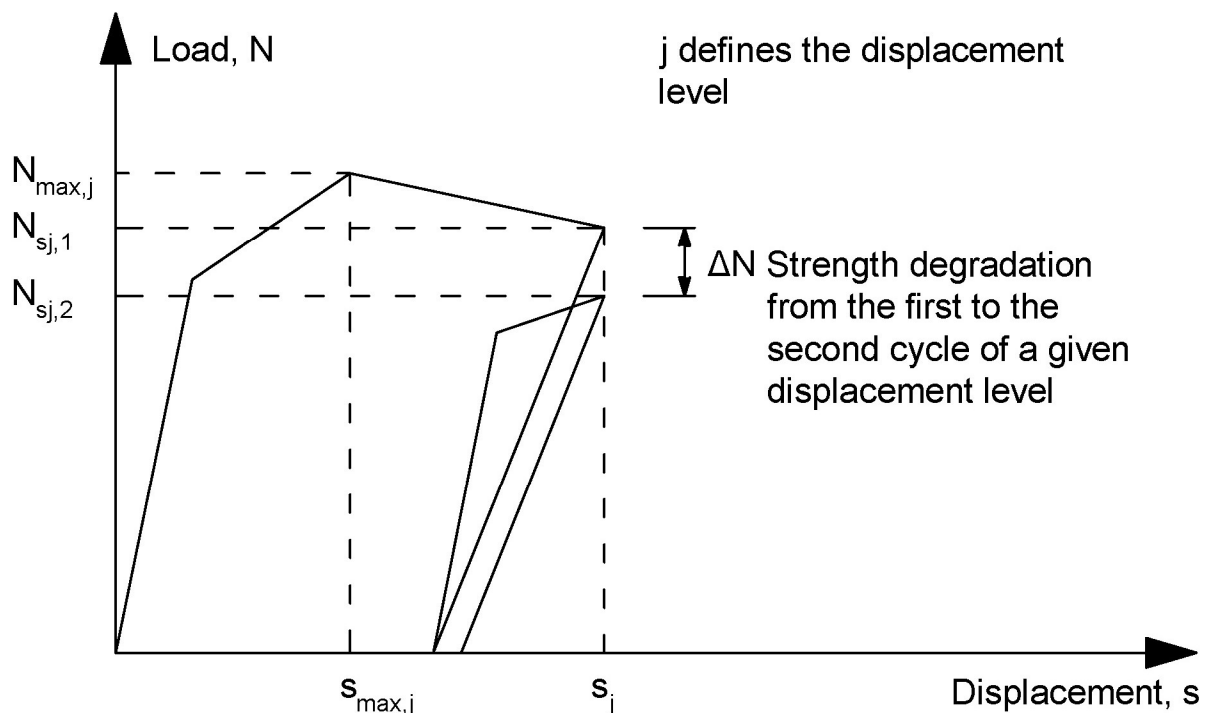
Figure 5.23. Definition of strength degradation in subsequent cycles of the same displacement level.

Figure 5.24 presents the results obtained from tests in uncracked concrete for different types of anchors. The upper graph in Figure 5.24 shows the average strength degradation in the second and third cycle with respect to the first cycle over all

displacement levels. The two bottom graphs show the strength degradation in the second and third cycle as a function of the ratio of the displacement s_j in the corresponding displacement level and the displacement s_u, corresponding to the ultimate load in the respective cyclic test. Thereby a ratio less than one on the horizontal axis represents the ascending branch of the load-displacement curve, and a ratio greater than one represents the descending branch. Linear regression curves for the individual types of anchors are used to illustrate the behavior of the anchors with increasing displacements. Bonded anchors show the most favorable behavior with regard to strength degradation in subsequent cycles. On an average, in the third cycle of a displacement level, bonded anchors were able to achieve 90% of the strength obtained in the first cycle of the respective displacement level. However, with increasing displacements (thus increasing damage in the base material), it was observed that the strength degradation in subsequent cycles increases more rapidly as compared to the other types of anchors tested. The strength degradation in subsequent cycles in case of undercut anchors and bonded expansion anchors is rather similar. This is despite the fact that undercut anchors failed in concrete cone failure while bonded expansion anchors failed in a combined pull-out and concrete failure mode. However, it should be noted that the depth of the concrete cone breakout body in case of combined failure was rather large. On an average, in the third cycle of a displacement level, the tested anchors were able to achieve around 85% of the strength obtained in the first cycle of the respective displacement level. With respect to the progressively increasing amount of strength degradation with increasing displacements, both types of anchors showed a more moderate progress than the bonded anchors. It can be seen that the level of degradation is quite constant with increasing displacements. The tested concrete screws demonstrate the least favorable behavior. On an average the strength in the third cycle decreased by around 20% in comparison to the strength obtained in the first cycle.
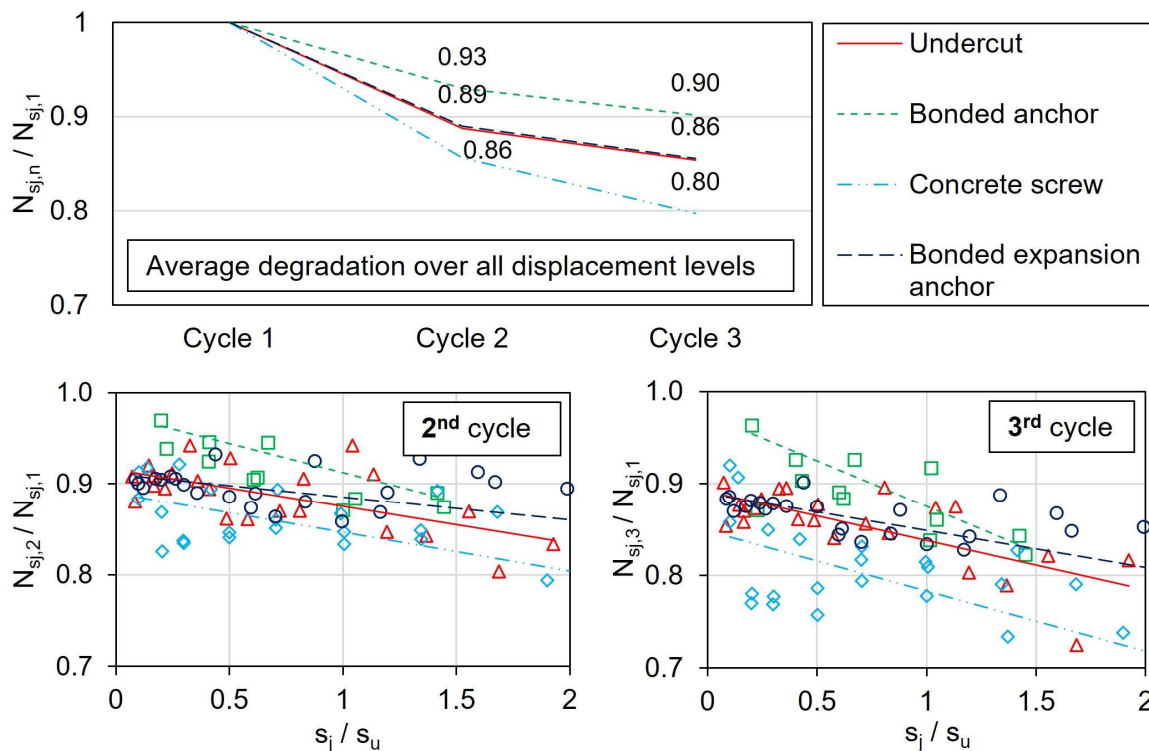
Figure 5.24. Strength degradation in second and third cycle in the displacement-controlled cyclic tests in uncracked concrete.

Figure 5.25 presents the results for the tests in cracked concrete. Three main observations emerge from these results. First, by neglecting the amount of strength degradation with increasing displacement level and only considering the average reduction in the second and third cycle with respect to the first cycle (upper graph in Figure 5.25), the observed degradation in case of undercut anchors, bonded anchors, and bonded expansion anchors is almost identical (around 13% reduction in the second cycle and around 18% reduction in the third cycle). For undercut anchors and bonded expansion anchors, the difference to uncracked concrete is relatively small, whereas in case of bonded anchors the amount of strength degradation per cycle increases notably. The average degradation in case of concrete screws is markedly more severe with a reduction of 22% in the second cycle and 31% in the third cycle. Second, in case of concrete screws, the strength degradation in subsequent cycles is almost constant at all displacement levels. Similarly, in case of undercut anchors and bonded expansion anchors, the amount of strength degradation remains relatively constant with increasing displacement. In accordance with the findings in uncracked concrete, bonded anchors showed the least favorable behavior with respect to progressively increasing strength degradation at larger displacements. Third, compared to undercut anchors or bonded anchors, the initial strength degradation at smaller displacement levels observed for bonded expansion anchors is notably higher. Whereas, especially in case of bonded anchors, the initial amount of degradation was rather low.
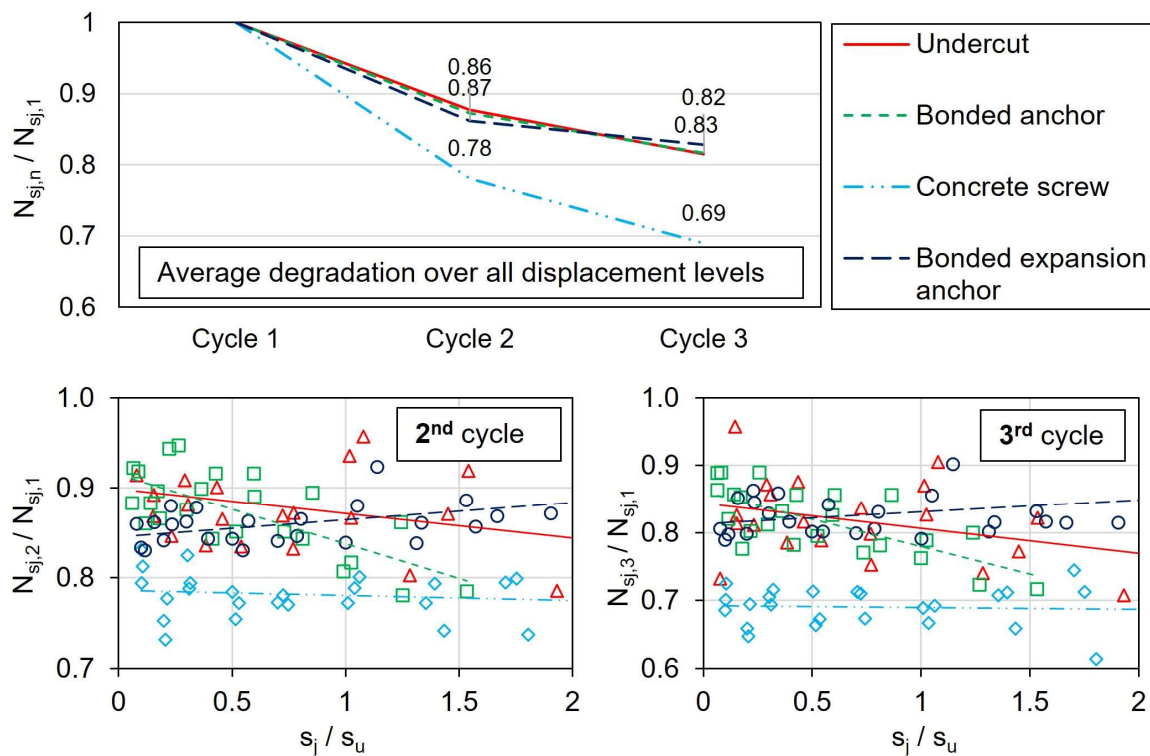
Figure 5.25. Strength degradation in second and third cycle in the displacement-controlled cyclic tests in cracked concrete.

Figure 5.26 compares the strength degradation in uncracked concrete for different failure modes. By comparing the behavior of anchors failing in concrete cone failure and combined pull-out and concrete failure, no major differences are apparent regarding the amount of strength degradation in subsequent cycles or the rate at which the strength degradation increases with increasing displacement levels. It should be noted that in this study, the transmission from concrete cone failure to a combined failure was defined by the ratio of the depth of the concrete breakout body, h_{cc}, and the effective embedment depth, h_{ef} following the classification in Mohyeddin et al. (2019). For a ratio $h_{cc} / h_{ef} < 0.85$, the failure was characterized as a combined failure (Mohyeddin et al., 2019). In case of the evaluated anchors in uncracked concrete, the range of values for the ratio h_{cc} / h_{ef} lies within 0.64-1.00, whereby only two anchors showed a value below 0.80.
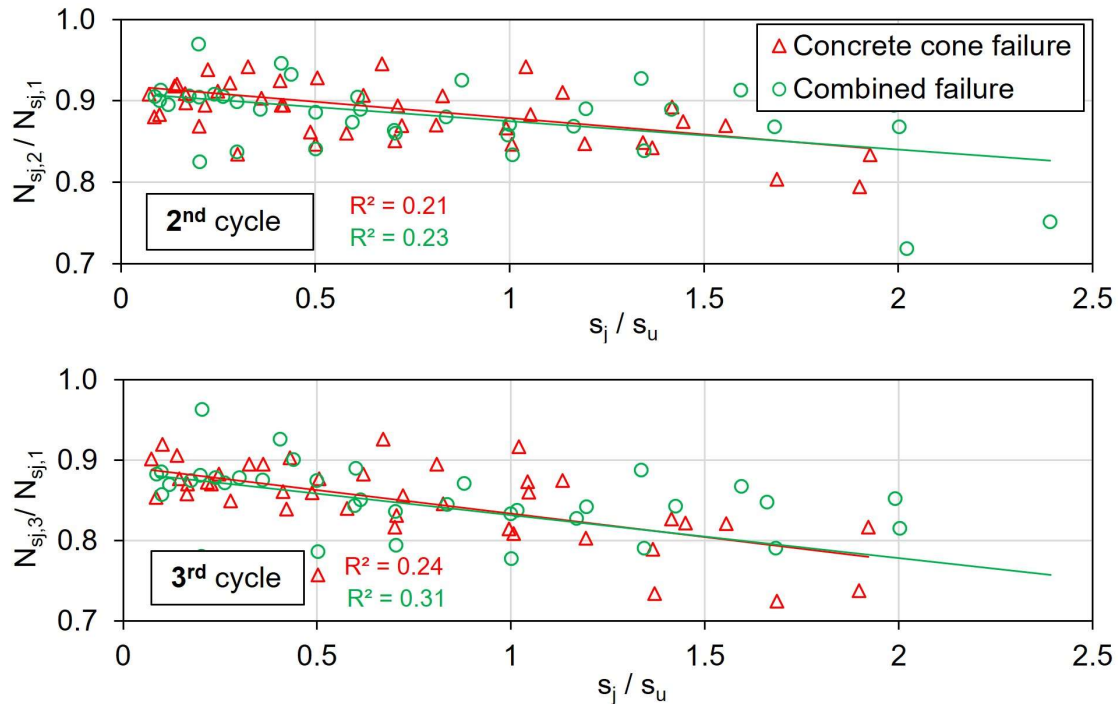
Figure 5.26. Strength degradation in second and third cycle in case of different failure modes in uncracked concrete.

In comparison to the results obtained in uncracked concrete, depending on the failure mode, the behavior in cracked concrete differed to some extent. It appears that as the failure mode turns from concrete cone failure to combined pull-out and concrete failure to pull-out failure, the amount of strength degradation increases. Note that pull-out failure occurred only for the tested concrete screws. At initial displacement levels, the differences between anchors failing due to concrete cone failure and combined failure are comparatively small, whereas the difference to anchors failing due to pull-out failure is more pronounced. This is particularly true for the strength degradation in the third cycle. In Figure 5.27 it can be seen that in case of a combined failure, the scatter in the third cycle at higher displacement levels is rather high. This may be related to the classification of the failure modes which was adopted from the classification of failure modes for concrete screws according to Mohyeddin et al. (2019). In their study, concrete cone failure is defined by a breakout body with a depth of 85% of the embedment depth or larger, combined failure is defined by a breakout body with a depth between 20% and 85% of the embedment depth, and for breakout bodies with a depth smaller than 20% of the embedment depth a failure mode is defined as pull-out failure. It becomes apparent that the range for which a failure is defined as combined failure is rather large.
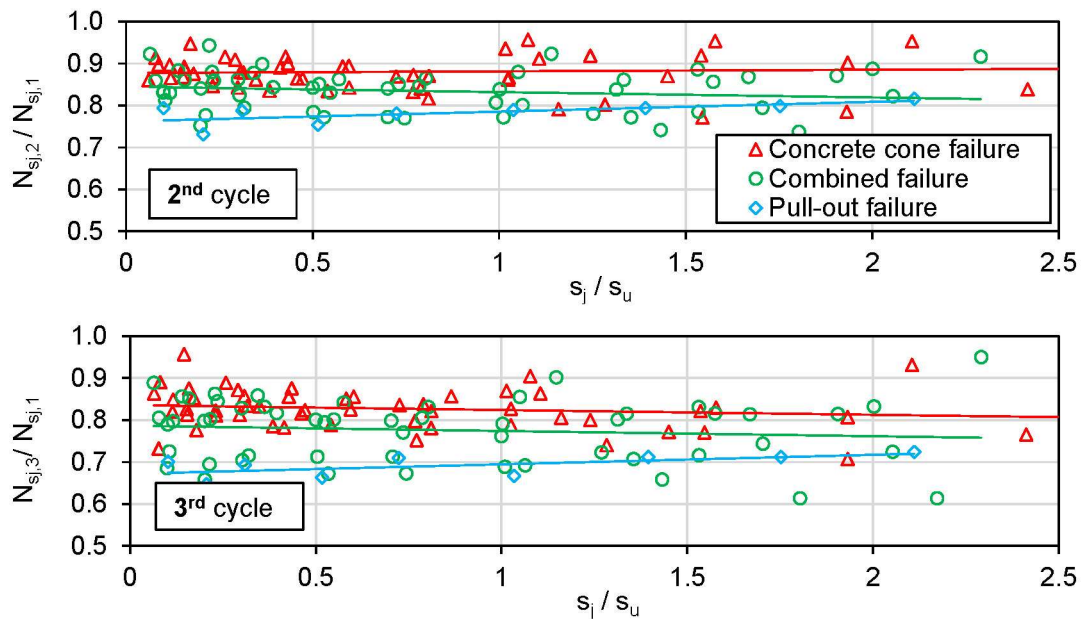
Figure 5.27. Strength degradation in second and third cycle in case of different failure modes in cracked concrete.

In order to investigate the behavior with decreasing cone depth in more detail, Figure 5.28 presents the strength degradation in the third cycle as a function of the ratio between the cone depth, h_{cc}, and the embedment depth h_{ef} for uncracked and cracked concrete, respectively. It can be seen that for tests in cracked concrete (bottom graph), indeed with decreasing ratio h_{cc} / h_{ef}, the strength degradation in subsequent cycles increases. However, up to a ratio of around 0.5-0.6, the average strength degradation appears to be rather constant, similar to the behavior in uncracked concrete (top graph in Figure 5.28). Thereafter, a sharp increase in the strength degradation is apparent. If the depth of the concrete cone is equated with the utilization of the concrete, the results suggest that the behavior is relatively constant up to a certain level of utilization. Thereby, in case of concrete cone failure, it seems that the average reduction in the third cycle is around 15% - 20% of the strength in the first cycle. As the failure mode transitions to a pull-out failure, the average reduction increases to around 30%.
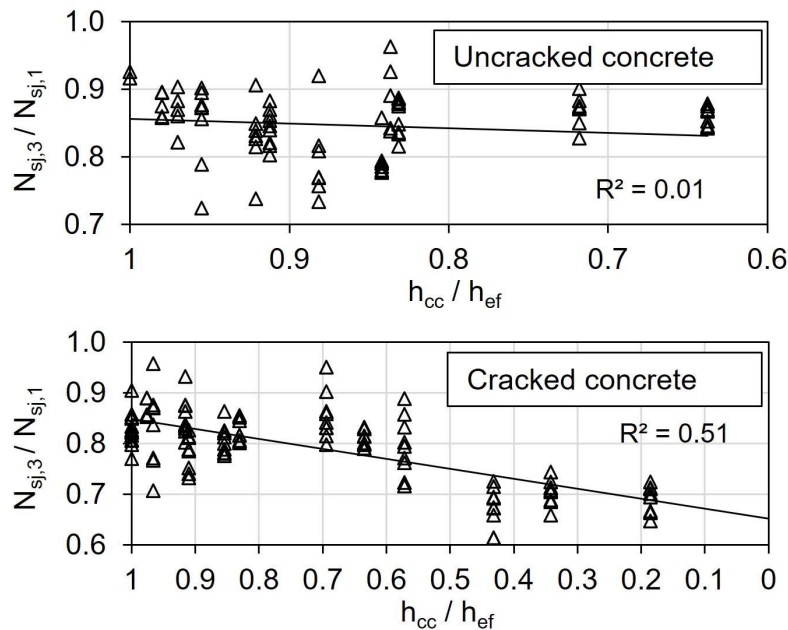
Figure 5.28. Strength degradation in the third cycle with respect to the first cycle of the respective displacement level as a function of the ratio between the cone depth and the effective embedment depth. The top graph shows the results obtained in uncracked concrete and the bottom graph shows the results obtained in cracked concrete.

5.6.2.2   Unloading and reloading stiffness

Under seismic excitation an anchor is subjected to repeated loading and unloading. Thereby, the unloading and reloading path of an anchor is defined by its unloading stiffness (k_{UL}) and reloading stiffness (k_{RL}). Depending on what type of anchor is used, these stiffness values and the alteration of the same with increasing anchor displacement may vary significantly. For an accurate numerical simulation of the hysteretic anchor behavior in a preferably wide range of the load-displacement curve, the information on these stiffness values is an essential factor. Therefore, the tested anchors are evaluated regarding the observed stiffness values and the progression of these values with increasing displacements. Figure 5.29 schematically depicts the unloading and reloading behavior of an anchor subjected to the displacement-controlled loading history. Note that in contrast to the evaluation of the strength degradation, where the focus was on the cycles in one displacement level, here the stiffness values are evaluated individually for each cycle i, without considering the displacement level per se. Therefore, s_i refers to the maximum displacement of a cycle, where N_i is the corresponding load. $N_{max,i}$ refers to the maximum load reached in one cycle, where $s_{max,i}$ is the corresponding displacement. As described above, in each cycle the anchors were loaded to a certain displacement, s_i. Then the anchors were again unloaded to almost zero load. As already mentioned, no compression force was

applied on the anchors, thus the anchors were not forced back to zero displacement. This generally resulted in residual displacements of the anchors, $s_{Res,i}$, after each cycle. In this study, unloading and reloading stiffness are defined according to the following equations and Figure 5.29.

$$k_{UL} = \frac{N_i}{(s_i - s_{Res,i})}, \tag{5.2}$$

$$k_{RL} = \frac{N_{max,i}}{(s_{max,i} - s_{Res,i-1})}. \tag{5.3}$$

Unloading of the anchors starts at the point where the maximum displacement, s_i, is reached and ends at the point where the force reaches its minimum with the corresponding displacement $s_{Res,i}$ in cycle i. Then reloading in the next cycle $i + 1$ starts. Thus, the point of residual displacement of the previous cycle i becomes the starting point for reloading in cycle $i + 1$. Reloading ends when the maximum load $N_{max,i+1}$, of cycle $i + 1$ is reached. The more general definition of parameters is also illustrated in Figure 5.29.
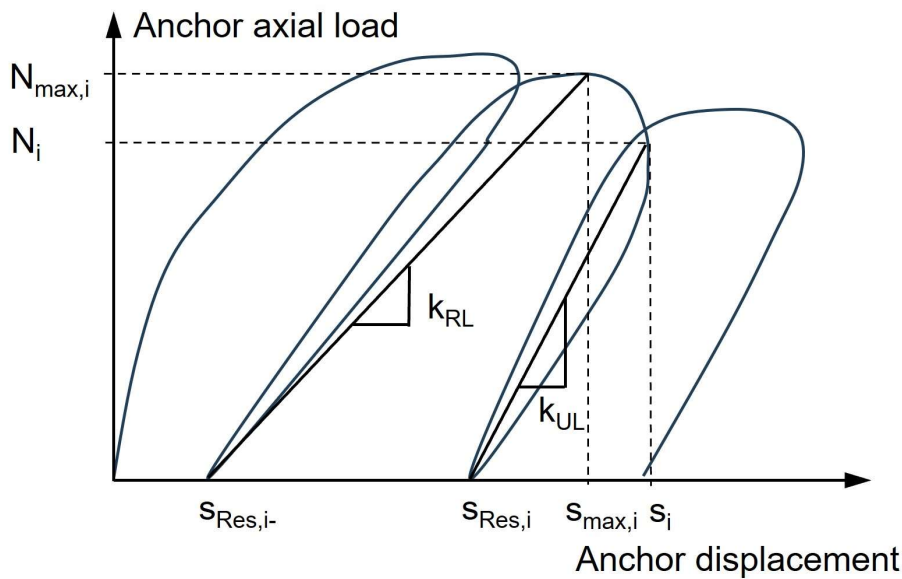
Figure 5.29. Definition of unloading and reloading stiffness and the corresponding parameters.

Figure 5.30 shows the unloading and reloading stiffness of anchors tested in uncracked concrete as a function of the ratio of the maximum displacement s_i in the corresponding cycle and the displacement s_u, corresponding to the ultimate load in the respective test. It can be seen that the stiffness may differ considerably depending on which type of anchor is used. Furthermore, within an individual anchor system the unloading and reloading stiffness varies depending on the displacement level.

In the case of the tested undercut anchors, the unloading stiffness is rather constant until reaching the ultimate capacity of the anchor at the corresponding displacement s_u. The unloading stiffness up to this point is slightly above 100 kN/mm, which is significantly higher than the initial stiffness of the undercut anchor in the corresponding tests. This means that the unloading branch is steeper than the initial loading path, which is also apparent from the load-displacement curves. From the load-displacement curves it can further be seen that the unloading path is almost vertical. This indicates that when the anchor is unloaded to a load slightly above zero, the anchor basically remains in its displaced position. The reloading stiffness shown in the right graphs in Figure 5.30 is assessed separately for the first cycle of a displacement level (dashed line; circles) and the second and third cycle (solid line; squares). The progression of the reloading stiffness with increasing displacement observed in the second and third cycle matches well with the behavior during unloading. While on the other hand the loading stiffness in the first cycle remains almost constant throughout the test. Thereby, the loading stiffness in the first cycle is about the same as the mean initial stiffness, $k_{50\%Nu,m}$, of corresponding tests. Reloading in the first cycle implies the transition from one displacement level to the next. As the unloading path is almost vertical it is apparent that the loading stiffness in the first cycle needs to be smaller compared to the reloading stiffness in the second and third cycle. A similar behavior was observed for bonded expansion anchors and concrete screws. However, in both cases, the initial unloading and reloading stiffness values were higher, and the stiffness degradation started already at smaller displacements. In case of the tested concrete screws, the difference in the loading stiffness for cycle one and the reloading stiffness for subsequent cycles is not as pronounced as in case of undercut anchors or bonded expansion anchors. The stiffness appears to decrease rather linearly with increasing displacements. In the case of bonded anchors, the unloading and reloading stiffness progress similarly in all cycles of the same displacement level. This indicates that the residual displacements are rather small in case of bonded anchors, since there is no large difference when the anchor is loaded to the next displacement level. The greatest difference between bonded anchors and the other tested types of anchors was that the unloading and reloading stiffness decrease rather strongly in the beginning while the degradation becomes more gradual with increasing displacements. As can be seen in Figure 5.30 (b), the unloading and reloading stiffness in the first displacement levels is relatively high. With increasing displacements, however, the stiffness decreases rapidly until reaching the displacement value $0.5s_u - s_u$, where the regression curves start to flatten.

In cracked concrete (see Figure 5.31), undercut anchors and bonded expansion anchors showed a similar behavior as in uncracked concrete. For both anchors systems, the stiffness was only slightly influenced by the presence of a crack. The stiffness reduction was particularly evident in the case of bonded anchors. Nonetheless, the general progression of the stiffness values with increasing

displacements matched well with the behavior in uncracked concrete. Only the behavior of concrete screws changed markedly when tested in cracked concrete. While in uncracked concrete the initial stiffness values at low displacement levels was rather high and decreased with increasing anchor displacement, in cracked concrete the initial stiffens values were notably smaller and kept almost constant throughout the test. In addition, the scatter of stiffness values at approximately the same displacement level was relatively large. Especially at higher levels, the results obtained from the individual tests deviated markedly. Finally, in cracked concrete, it was observed that the difference between the loading stiffness in the first cycle and the reloading stiffness in the second and third cycle increased. The results support the finding of a particular sensitivity of concrete screws to cracked concrete.

From the graphs in Figure 5.30 and Figure 5.31 it appears that the unloading stiffness and the reloading stiffness in the second and third cycle of a displacement level progress rather similarly. To further investigate this observation the ratio between the unloading and reloading stiffness in the second and third cycle of a displacement level is evaluated in Figure 5.32 for tests in uncracked concrete. The results are plotted as a function of the displacement ratio s_i / s_u. As expected, the unloading and reloading stiffness determined from single anchor tests correspond well for the shown types of post-installed anchors. The values are evenly distributed above and below a line corresponding to k_{UL} / k_{RL} = 1. For undercut anchors, bonded anchors and concrete screws, the average of the stiffness ratio is around 0.99-1.03 with a maximum coefficient of variation of 15% for concrete screws. The stiffness ratio is slightly higher in case of bonded expansion anchors with a value of 1.09. In general, however, the results indicate that assuming equal stiffness during unloading and reloading in one cycle is a reasonable simplification.

In cracked concrete, the average of the stiffness ratio k_{UL} / k_{RL} is somewhat larger than in uncracked concrete. Here the values range between 1.02 (bonded anchor) and 1.13 (bonded expansion anchor). Thus, the unloading behavior appears to be slightly stiffer than the reloading behavior. Nonetheless, the results are in good agreement and thus the simplified assumption is deemed reasonable for cracked concrete as well.
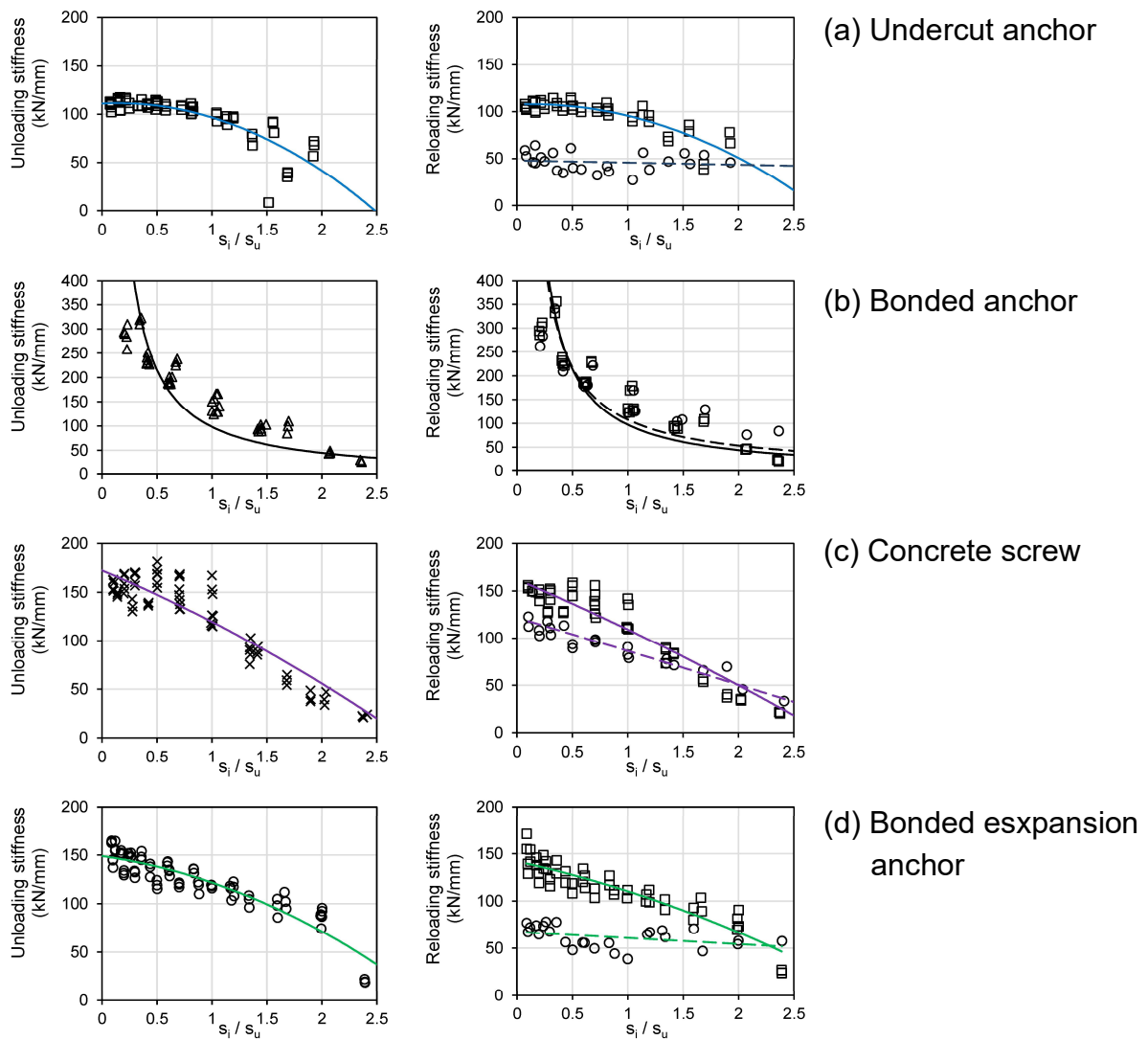
Legend for reloading stiffness in right graphs:

○   Loading stiffness in first cycle

□   Reloading stiffness in second and third cycle

– – –   Loading stiffness in first cycle

——   Reloading stiffness in second and third cycle

Figure 5.30. Unloading (left graphs) and reloading (right graphs) stiffness obtained from displacement-controlled cyclic tests in uncracked concrete.
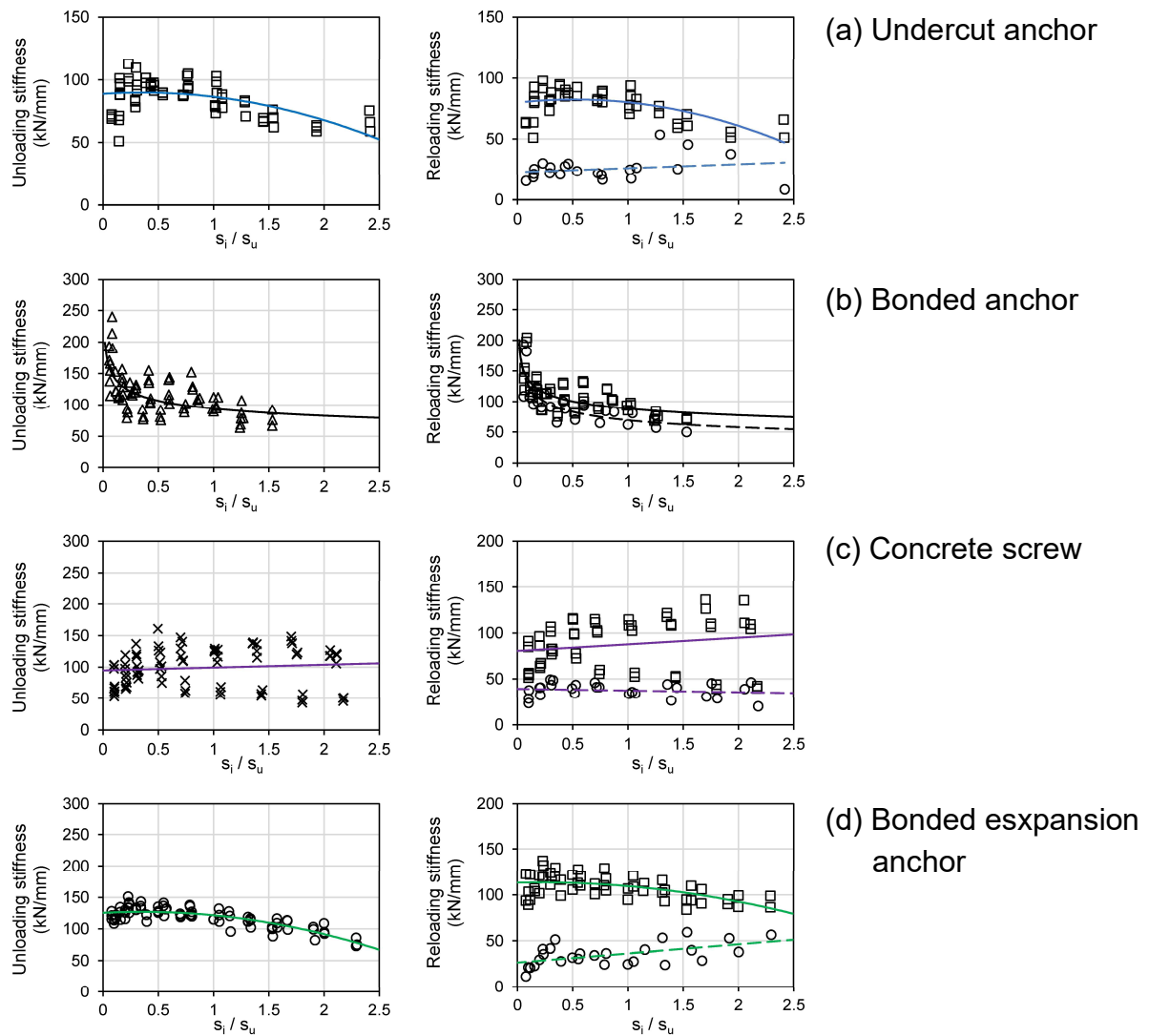
Legend for reloading stiffness in right graphs:

- ○   Loading stiffness in first cycle
- □   Reloading stiffness in second and third cycle
- – – –   Loading stiffness in first cycle
- ——   Reloading stiffness in second and third cycle

Figure 5.31. Unloading (left graphs) and reloading (right graphs) stiffness obtained from displacement-controlled cyclic tests in cracked concrete.
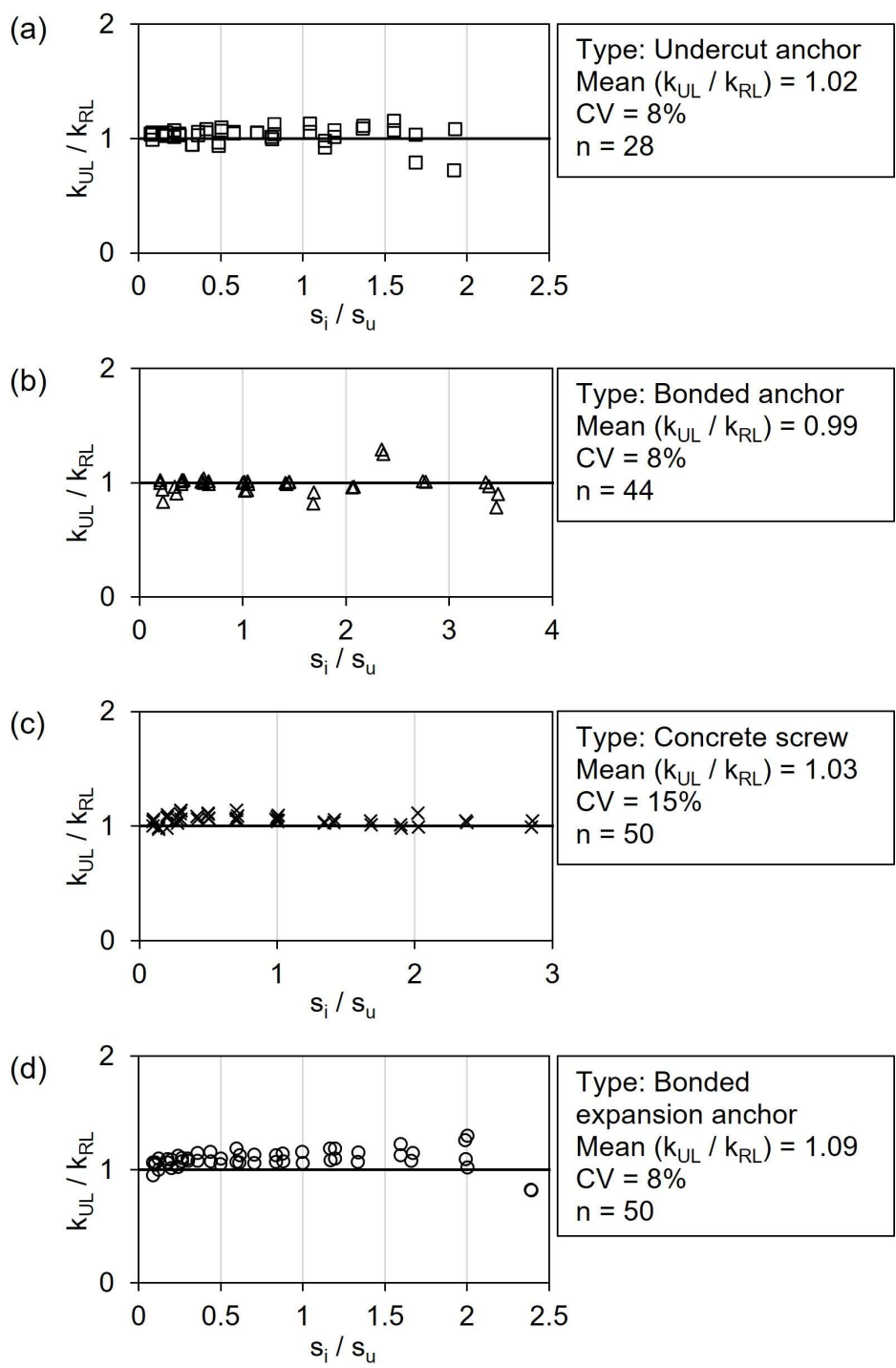
Figure 5.32. Comparison of the unloading stiffness k_{UL} and the reloading stiffness k_{RL} for the tested types of post-installed anchors in uncracked concrete: (a) Undercut anchor, (b) Bonded anchor, (c) Concrete screw, and (d) Bonded expansion anchor.

5.6.2.3   Residual displacements

Although in structural members, the residual displacements occur due to inelastic excursion in the system, for anchors, the residual displacements may occur even in the elastic part of the ascending branch of the curve since the anchor is only intended to take up tension forces, while the compression forces when loaded in the opposite direction, are directly transferred from the baseplate to the concrete surface. In this case, the anchor is not forced back into its original position. Residual displacements of anchors in a group may have a considerable negative effect on the connection as discussed in Chapter 2. Consequently, anchors that exhibit small residual displacements even under high loads or applied displacements are preferable. It has already been shown that the absolute displacement of an anchor at ultimate load differs significantly depending on which type of anchor is used. While the tested undercut anchors and bonded expansion anchors showed rather large displacements at ultimate load, the displacements of bonded anchors and concrete screws were comparatively small. The tested types of anchors behave accordingly with respect to the observed residual displacements at the end of unloading. This is shown in Figure 5.33 for anchors installed in uncracked and cracked concrete, respectively. It can be seen that undercut anchors and bonded expansion anchors exhibit relatively large residual displacements. At ultimate load, the residual displacements range from 4 mm to 6 mm in case of uncracked concrete and from 5 mm to 8 mm in case of cracked concrete. Thereby, especially undercut anchor tested in cracked concrete show a relatively large scatter. For concrete screws, the residual displacements at ultimate load were around 1.2 mm and 2 mm for uncracked and cracked concrete, respectively. As expected, the smallest residual displacements were observed in the tests on bonded anchors (around 0.7 mm in case of cracked concrete). It is worth mentioning that all tested anchors show linearly increasing residual displacements with respect to the relative anchor displacement.
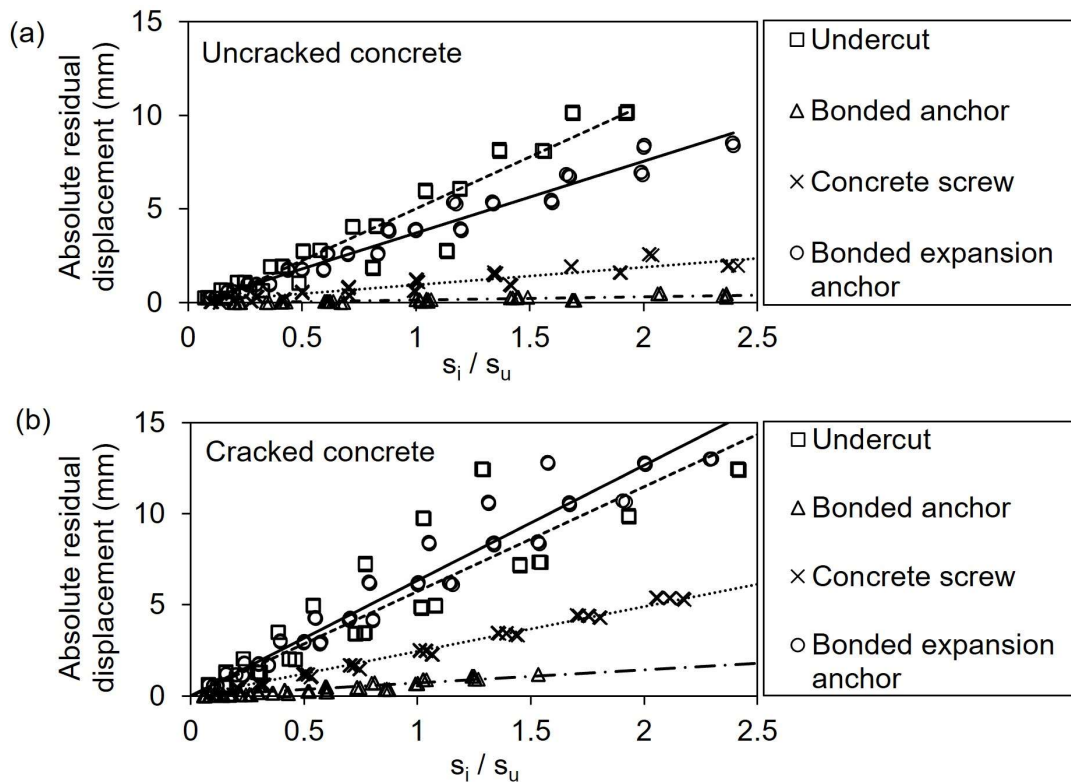
Figure 5.33. Absolute residual anchor displacement at the end of unloading (a) anchors installed in uncracked concrete and (b) anchors installed in cracked concrete with Δw = 0.8 mm.

5.7   Summary

The experimental results suggest that the two cyclic protocols basically provide similar overall behavior when it comes to the loads, displacements, secant stiffness values and failure modes. The main differences observed in the experiments have to do with the fact that the two protocols have a different emphasis on what is to be investigated. The emphasis of the force-controlled protocol C2.3 is to ensure the safety of a non-structural connection after a defined seismic event and therefore focuses on the residual capacity test. Accordingly, the cycling phase in the force-controlled protocol covers only a rather small part of the load-displacement curve, as seen from the experimental results. In this context, the load levels at which the anchors are actually cycled are deemed rather low. It is worth mentioning, that also the majority of the information required for assessing the anchor performance according to the guideline is obtained in the residual capacity test. The emphasis of the displacement-controlled protocol is set on the anchor behavior during the seismic event itself, whereby it is expected that the actual demand on the anchors may exceed the design forces. Therefore, the displacement and hysteretic behavior of the anchors is examined in a broader range of the load-displacement curve, also covering the post-peak range. In

this context the new displacement-controlled procedure can be used as an additional test for anchors that are intended for the use in structural applications, where primary structural elements, that is elements that are part of the load-transfer mechanism, are connected to the existing RC structure. In such applications, the information obtained in the current force-controlled procedures alone may not be sufficient for a safe design and additional information that is obtained from a displacement-controlled protocol can supplement the information.

Since the load-displacement behavior of the tested anchors was rather similar regardless of the testing scheme (monotonic, force-controlled, or displacement-controlled), it appears that the 40 cycles performed in the first two load phases of the force-controlled protocol had no major influence on the performance of the tested anchors. Although the increased number of cycles likely results in slightly more damage in the base material, the findings suggest that performing three cycles at each displacement level is sufficient to assess the anchor behavior.

The new displacement-controlled testing approach allows the investigation of additional parameters, such as the strength degradation, unloading and reloading stiffness, or the residual displacements of an anchor when unloaded to almost zero displacement. Thereby, the new protocol enables the assessment of these parameters in almost the complete range of the load-displacement curve. Following conclusions can be drawn from the displacement-controlled cyclic tests:

1. Repeated cyclic loading at the same displacement level results in reduced strength in subsequent cycles. With respect to the strength obtained in the first cycle, in the second and third cycle the observed residual strength ranges from 70% - 95%. Thereby, various factors were identified to have an influence on the amount of degradation. The first factor is the damage in concrete which is evident in two ways. On the one hand it was observed that when tested in cracked concrete ($\Delta w = 0.8$ mm), the average strength degradation in subsequent cycles increased compared to tests in uncracked concrete. Thereby, the observed difference between uncracked and cracked concrete is highly related to the type of anchor. On the other hand, it was shown that with increasing displacement level (thus increasing damage in the base material) the amount of degradation increased for most types of anchors. However, the rate at which the strength degradation increases with increasing displacement levels is rather moderate for most anchor systems. The second factor is the type of anchor and thus the load-transfer mechanism. Both in cracked and uncracked concrete, the tested concrete screws showed the largest degradation in subsequent cycles. In uncracked concrete bonded anchors showed the most favorable behavior, although with increasing displacement levels the strength degradation in subsequent cycles increases more rapidly as compared to the other tested anchor systems. This is also reflected in the results for cracked concrete where at lower displacement levels, the initial behavior of bonded anchors was superior

to that of the other anchors. However, at higher levels the strength reduction increased markedly. The third factor is the failure mode. While in uncracked concrete the failure mode appears to have only a negligible influence on the strength degradation, in cracked concrete it was shown that when the failure mode transitions from concrete cone to pull-out failure, the amount of strength degradation increases. However, up to a certain ratio h_{cc} / h_{ef}, the level of degradation is rather constant, similar to the behavior in uncracked concrete. Only for cases where the anchor failure is dominated by pull-out failure, the strength degradation appears more severe.

2. During cyclic loading, the loading, unloading and reloading path of the load-displacement curve is defined by the loading, unloading and reloading stiffness of an anchor. It was shown that the unloading and reloading behavior of the tested anchor systems varies mainly in two ways. First of all, the stiffness of different anchor systems itself varies. Similar to the evaluation of the secant stiffness, the tested bonded anchors are the stiffest anchors while undercut anchors show a softer behavior. However, the stiffness of bonded anchors is more affected by cracks than it is in case of other anchor systems. Particularly undercut anchors and bonded expansion anchors showed only a low susceptibility to cracked concrete. Nonetheless, the initial unloading and reloading stiffness of bonded anchors was higher than that of the other tested anchor systems, even in cracked concrete. The second main finding considers the development of the stiffness with increasing anchor displacement. It was observed that in almost all tests, the stiffness values decreased with increasing displacement level. The only exception being concrete screws in cracked concrete. Thereby, again differences could be found among the tested anchor systems. While bonded anchors have a high stiffness at small displacements which decreases rather fast with increasing displacement levels, the other anchor systems have lower initial stiffness values, but the stiffness reduction is more moderate. This is particularly true for undercut anchors and bonded expansion anchors in cracked concrete.

3. In general, it was found that in the second and third cycle of a particular displacement level, the unloading and reloading stiffness during one cycle is rather similar. Here, the simplified assumption of equal values for unloading and reloading stiffness is considered reasonable. It should be noted that in case of undercut anchors, concrete screws and bonded expansion anchors, a difference between reloading and unloading stiffness is particularly apparent in the first cycle of a displacement level, where the reloading stiffness was markedly smaller compared to the unloading stiffness, and roughly corresponded to the mean initial stiffness, $k_{50\%Nu,m}$, of the respective test series.

4. The evaluation of the residual displacements upon unloading of the anchors is in accordance with the general displacement behavior of the tested anchor systems. The largest residual displacements were observed for undercut

anchors and bonded expansion anchors. The residual displacements in case of concrete screws and bonded anchors were markedly smaller, with bonded anchors having the smallest residual displacements.

Currently, the qualification and design of anchors under seismic actions is mainly dominated by two parameters that is, the capacity of the anchor and the influence of cracked concrete on it. The displacement parameters assessed in this context are mainly intended to avoid large deviations in the anchor behavior. Consequently, bonded expansion anchors or undercut anchors are generally known for their ability to function well in cracked concrete, while for example bonded anchors are deemed less suitable for the use in cracked concrete as the reduction of the ultimate capacity is more critical. However, the evaluation of the hysteretic and displacement characteristics has shown that the displacement behavior of the tested bonded anchors under seismic actions is superior to that of tested undercut anchors or bonded expansion anchors, even in case of cracked concrete. Especially in case of strengthening applications against earthquakes, when post-installed anchors are used to form the connection between the new element and the existing structure, the displacement of the anchorage is of major importance. In this context, a favorable displacement behavior (small total displacements and small residual displacements) may be equally or even more important than the capacity of an anchor alone. Naturally, it always depends on the application for which the anchors are ultimately used.

6 Hysteretic model for tension loaded single anchors

Based on the evaluation of the displacement and hysteretic behavior of single post-installed anchors presented in the previous chapter, a hysteretic model to be used within the framework of nonlinear spring model for anchors will be developed in this chapter. The proposed hysteretic model is able to simulate the cyclic behavior of single anchors under tension load and considers the strength degradation in subsequent cycles of a displacement level and the observed unloading and reloading behavior. Thereby, the envelope curve obtained from the displacement-controlled cyclic tests serves as the upper limit of the load at any given displacement during cyclic loading and thus forms the basis of the proposed model. The model considers the design case where the anchors are only intended to take up tension forces, while they are not loaded in compression. Thus, the anchor itself is not forced back to zero displacement.

6.1 Characteristics of the envelope curve for cyclic anchor springs

The basic framework of modeling of anchors is the nonlinear spring model where the anchor is idealized as a nonlinear spring that follows an assigned load vs. displacement rule. As discussed in Chapter 3, various idealization approaches for the monotonic anchor behavior have been proposed in the literature. As shown in Chapter 5, the envelope curve obtained from cyclic tests basically follows the monotonic reference curve for single anchors. Therefore, in order to idealize the envelope curve obtained from cyclic tests, the herein proposed idealization of the anchor behavior is based on the approaches by Sharma (2013) and Bokor (2021). However, for better accuracy, the envelope curve is idealized using six linear segments, instead of five segments as used by Sharma (2013) and Bokor (2021). Thus, in this work, a hexa-linear format was chosen to describe the envelope curve for the anchor spring. The characteristic points are determined from the curves obtained from displacement-controlled cyclic tension tests. Based on these tests, the characteristic points of the idealized envelope curve are defined by two parameters, namely, load and corresponding displacement value. It is worth mentioning that, in principle, the envelope curve might be determined based on monotonic tension tests as well. However, since the hysteretic characteristics of an anchor system are determined from displacement-controlled cyclic tension tests, such as the one introduced in Chapter 5, it is preferable to directly develop the envelope curve from the results of cyclic tests.

As indicated in Figure 6.1, the hexa-linearization of the envelope curve requires the definition of seven characteristic points (A-G). These points are defined by a load value (N_A – N_G) and a corresponding displacement value (s_A – s_G). Furthermore, the secant stiffness values k_1 – k_5 are used to identify the characteristic points of the curve. The curve starts at point A corresponding to the origin (0, 0) from where loading starts. Point B marks the end of the linear range of the load-displacement curve. In Sharma (2013), the corresponding load is taken as 80% of the ultimate load, $0.8N_u$. However, for certain types of anchors a different value such as $0.5N_u$ or $0.6N_u$, may be more suitable (Bokor, 2021). It is assumed that up to point B, the initial stiffness of the anchors, $k_{50\%N_u}$ is valid. Thus, $k_1 = k_{50\%N_u}$. Points C and D mark the upper limit of the anchor capacity and generally refer to the ultimate capacity obtained in tests, N_u (Sharma, 2013). The displacement corresponding to point C can be calculated by dividing the ultimate load N_u by the corresponding secant stiffness k_{Nu} obtained in tension tests. The displacement of point D is chosen to fit the plateau of the ultimate load obtained in the tension tests. Point E defines the unloading branch of the envelope curve. Point F accounts for the fact that the anchor retains a certain residual strength after the formation of a concrete cone due to ability of concrete to transmit forces across cracks, due to aggregate interlock and friction. The corresponding load is taken as 20% of the ultimate load. Point G marks the end of the envelope curve. For single anchors failing due to concrete cone failure, Table 6.1 summarizes typical values for the characteristic points A-G (based on Sharma, 2013).
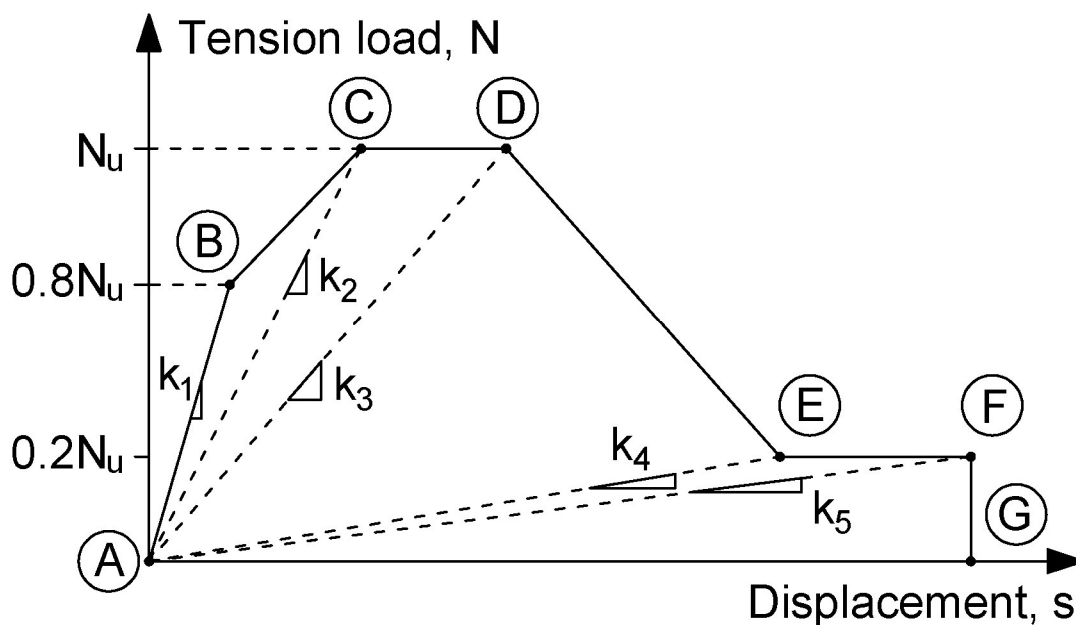
Figure 6.1. Idealization of the cyclic envelope curve for single anchors.

Note that the values provided in Table 6.1 are rather intended as general or indicative values. Depending on the type of anchor and the failure mode, the values may vary from those given in Table 6.1. Based on the load-displacement curve obtained from

tension tests, the idealized envelope curve might be modified to best fit the experimental results. This approach was followed in this chapter.

Table 6.1. Representative values of the characteristic points of the envelope curve for concrete cone failure of single anchors.

Point	Load (N_A – N_G)	Displacement (s_A – s_G)	Secant stiffness (k_1 – k_5)
A	0	$s_A = 0$	0
B	$0.8N_u$	$s_B = 0.8N_u / k_{50\%Nu}$	$k_1 = k_{50\%Nu}$
C	N_u	$s_C = N_u / k_{Nu}$	$k_2 = k_{Nu}$
D	N_u	$s_D = 1.25N_u / k_{Nu}$	$k_3 = 0.8k_{Nu}$
E	$0.2N_u$	$s_E = 2N_u / k_{Nu}$	$k_4 = 0.1k_{Nu}$
F	$0.2N_u$	$s_F = 1.33s_E$	$k_5 = 0.75k_4$
G	0	$s_G = s_F$	0

6.2 Idealization of unloading and reloading stiffness

With respect to the unloading and reloading stiffness, two major conclusions could be drawn from the evaluation of the displacement-controlled single anchor cyclic tests. First, it was shown that the unloading and reloading stiffness changes with increasing displacements of the anchors, whereby the rate of change varied depending on the anchor system. As a consequence, at smaller displacement levels, the unloading and reloading path of the tested anchors was generally steeper compared to higher displacement levels. Second, cycling at the same displacement level resulted in an almost same unloading and reloading path.

The observed hysteretic characteristics in the experiments, in particular the stiffness degradation with increasing displacements, constitute a main feature of the new model. However, in order to be able to consider the change of stiffness in the hysteretic model, it is necessary to idealize the behavior with increasing displacement ratio s_i / s_u based on the experimental results (see Figure 5.30 and Figure 5.31). This idealization should be done in such a way that the same approach can be implemented for different types of anchors. Otherwise, the unloading and reloading behavior of each individual anchor system had to be implemented separately. To this purpose, a tri-linear format was chosen to provide a consistent approach for idealizing the unloading and reloading behavior of all tested anchor systems. A schematic depiction and the relevant parameters to define the idealized curves are given in Figure 6.2. Note that based on the experimental results, the value for unloading and reloading stiffness at a certain displacement level s_i / s_u is considered equal. In this context, k_{cyc} represents both the unloading and reloading stiffness. This assumption simplifies the approach considerably by avoiding the need to define the values for unloading and reloading

stiffness separately. At the same time, this approach provides a sufficient degree of accuracy.
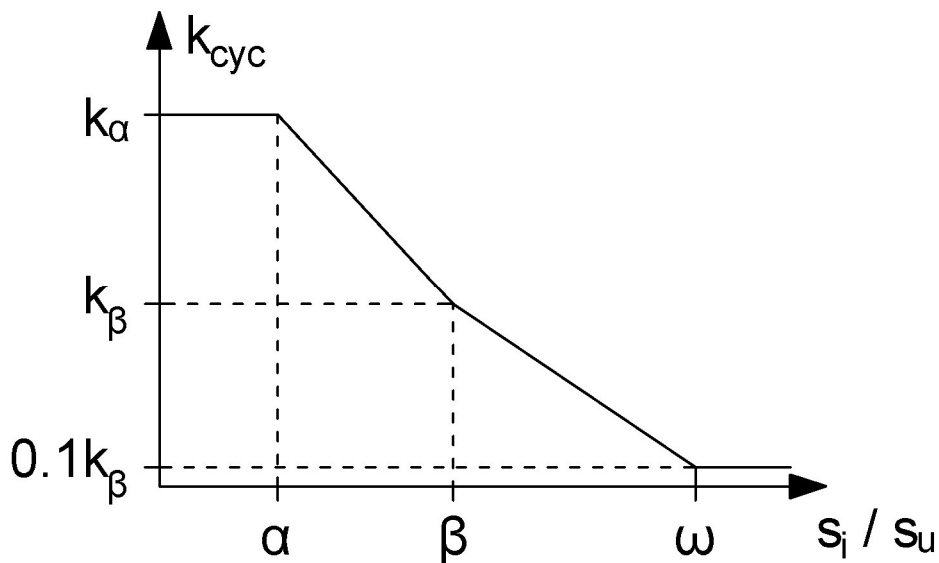
Figure 6.2. Idealization of the unloading and reloading behavior with increasing residual displacement.

As can be seen in Figure 6.2, the unloading and reloading stiffness is defined as a function of the relative displacement s_i / s_u and is characterized by five parameters. As will be shown in the following, these five parameters are sufficient to describe the unloading and reloading behavior of the tested anchor systems with adequate accuracy, while at the same time limiting the required parameters to a reasonable level. The stiffness k_α defines the initial unloading and reloading behavior. It is valid up to a relative displacement of α. Beyond this point the stiffness linearly decreases until it reaches a value of k_β at a relative displacement of β. From here the third branch starts and the stiffness further decreases linearly until it reaches 10% of the value of k_β at a relative displacement of ω. At this point, the stiffness remains constant for further increasing relative displacements. The lower limit of 10% of k_β results mainly from the fact that as the relative displacement approaches the value ω, the unloading and reloading stiffness would become unrealistically small. Moreover, ending the idealized curve at zero stiffness would result in numerical instabilities in the analysis.

Figure 6.3 shows the comparison between the experimental results in uncracked concrete and the idealized progression of the unloading and reloading stiffness with increasing levels of displacement. Note that the experimental results comprise the unloading stiffness of all three cycles of a displacement level and the reloading stiffness of the second and third cycle of a displacement level obtained in one test series. The five parameters which were used to define the idealized curves were determined in such a way that they provide the best fit with the experimental results. The respective values for the tested anchors are provided along the graphs in Figure 6.3. Note,

however, that the parameters for other anchor systems, sizes, or concrete mixtures, may differ from those given in Figure 6.3. For the tested anchor systems, in uncracked concrete the mean value of the ratio between the stiffness obtained in the experiments and the calculated stiffness ranges between 0.91 and 1.01 with a maximum coefficient of variation of 22%. In general, the described approach matches well with the experimental results.
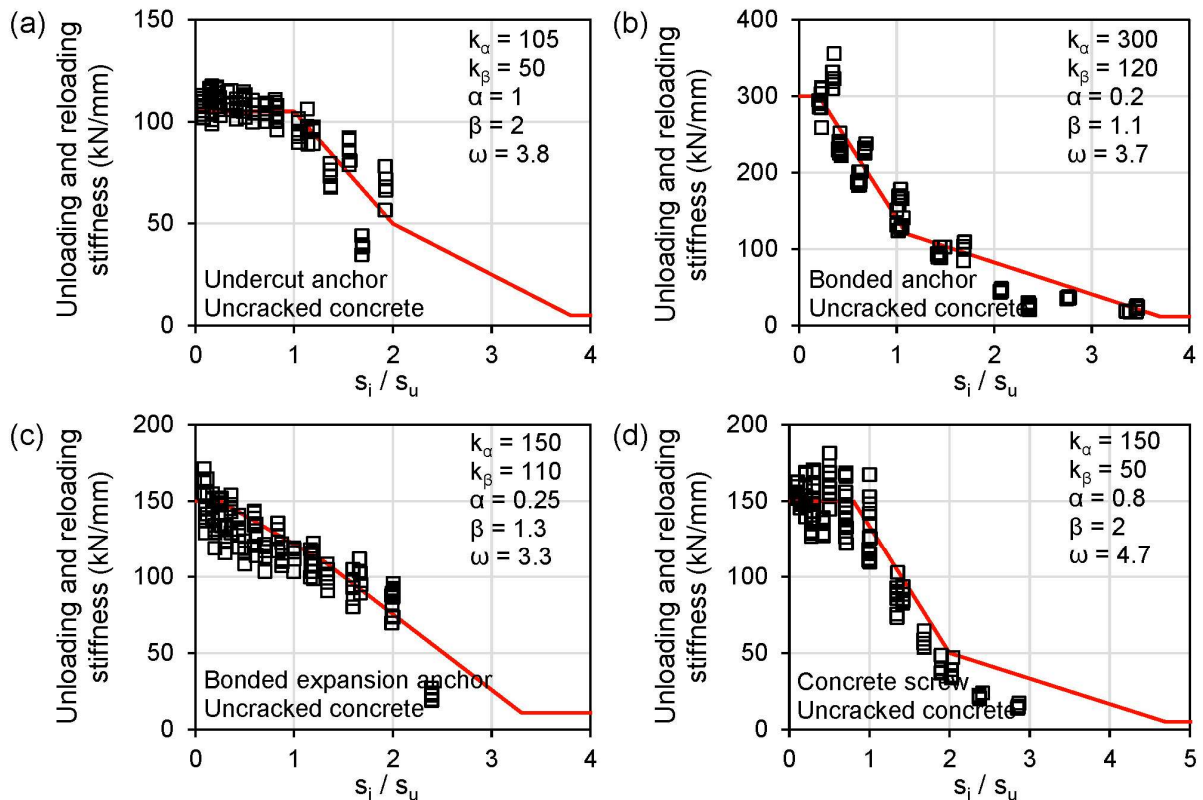
Figure 6.3. Comparison between the idealized unloading and reloading behavior and the behavior observed in the experiments in uncracked concrete.

In the same way, the unloading and reloading behavior was idealized for the tests in cracked concrete (Figure 6.4). Here, the mean value of the ratio between the stiffness obtained in the experiments and the calculated stiffness ranges between 0.96 and 1.02 with a maximum coefficient of variation of 31% for concrete screws. As shown in the previous chapter, the unloading and reloading behavior of concrete screws in cracked concrete is somewhat erratic, which results in a relatively high scatter. This is mainly attributable to one test which deviates from the behavior of the remaining two tests. Note that if the second test is disregarded, the coefficient of variation of the ratio between the stiffness obtained in the experiments and the calculated stiffness is 19%. Therefore, as can be seen in Figure 6.4 (d), the idealization follows the two test series which show an increase in the stiffness up to a relative displacement of approximately 1.5. The behavior of concrete screws thus differs significantly from that of other anchor systems, where a steady reduction in stiffness was observed, similar to the behavior

in uncracked concrete. In general, the main influence of cracked concrete is a reduced stiffness, expressed mainly in the parameter k_α. Nonetheless, the comparisons in cracked and uncracked concrete show that a tri-linearization of the unloading and reloading stiffness allows a sufficiently accurate simplification.
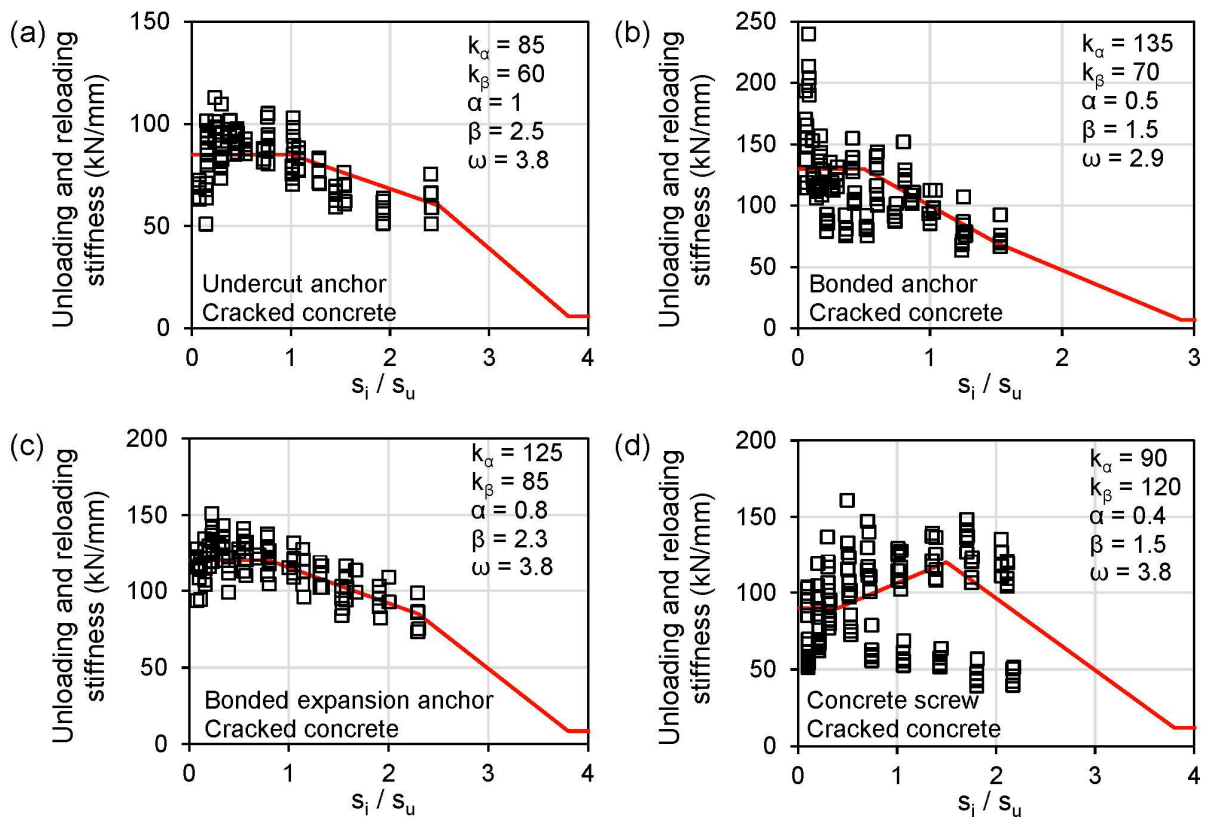
Figure 6.4. Comparison between the idealized unloading and reloading behavior and the behavior observed in the experiments in cracked concrete.

6.3 Development of hysteretic rules

The hysteretic rules presented in this chapter were basically developed at three levels, namely (i) One-parameter model, (ii) Two-parameter model and (iii) Three-parameter model. With each level, the accuracy of the model is increased, by increasing the number of parameters which are required to model the hysteretic anchor behavior. However, the increased accuracy comes at a cost of higher computational effort. It should be noted that not all applications require same level of detailed modeling. In some cases, a rather rough estimation of the anchor behavior might be sufficient. One such example is when the anchorage is modelled as part of the complete structure. In this case, the detailed hysteretic behavior of the anchorage is smeared out in comparison to the overall structural behavior and the application of the model which was developed in the first level might be sufficient. A detailed modelling of the hysteretic behavior of the anchors would be redundant. However, in the case where

for example the behavior of a connection is investigated, a detailed consideration of the anchor behavior might be required. For these cases, the second or third levels should be applied. In order to provide practitioners with the flexibility to decide upon the degree of accuracy for individual tasks, the three levels are therefore presented below.

6.3.1 One-parameter model

The basis of the hysteretic model (in all levels) is the envelope curve presented in Section 6.1 and the unloading and reloading characteristics defined in Section 6.2. Since the unloading and reloading behavior is defined as a function of the relative displacement, the first additional parameter which is required, is the displacement at ultimate load, s_u, which is determined for each individual anchor system, depending on the type of anchor, the size of the anchor and the base material (concrete strength, condition of the concrete member).

In principle, three phases can be distinguished as: (i) a phase where the response follows the envelope curve shown in Figure 6.1, (ii) an unloading phase, and (iii) a reloading phase. Thereby, loading, unloading, and reloading follow a predefined loading or displacement history. As long as no displacement reversal occurs, the response follows the envelope curve by stepwise increasing the displacement in displacement steps $+\Delta s$. Once the displacement is reversed and decreases incrementally by $-\Delta s$, unloading follows a defined unloading path until the load is again reversed and the anchor is reloaded. Thereby, reloading follows the same path as during unloading of the anchor until the envelope curve is encountered. The following is a set of rules which defines the unloading and reloading behavior of an anchor. Figure 6.5 provides a schematic depiction of those rules.

Unloading
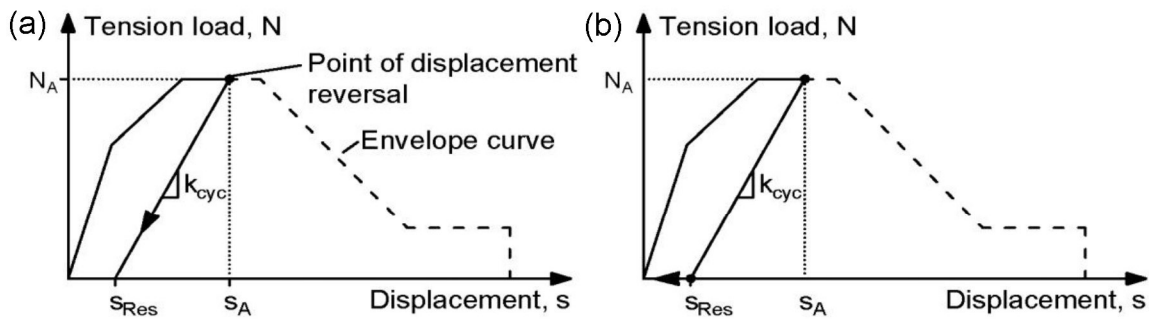
Reloading
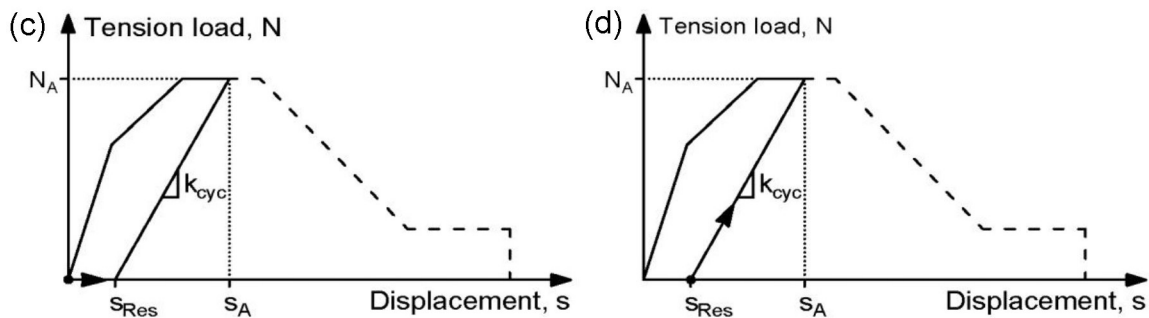
Figure 6.5. Schematic depiction of the (a), (b) unloading rules, and (c), (d) reloading rules for the one-parameter model.

Unloading follows two rules which are schematically depicted in Figure 6.5 (a) and (b). It begins when the displacement is reversed. In Figure 6.5 this point is denoted as point A. From here, up to the point where the anchor is completely unloaded (N = 0 kN), unloading follows a path defined by the unloading stiffness k_{cyc} (see Figure 6.2). Thereby, the stiffness is calculated based on the displacement at which the displacement reversal starts (point A in this example). Note that as long as the response does not encounter the envelope curve again, unloading and reloading paths are defined by the displacement of point A and k_{cyc}. Accordingly, the first rule is:

1. Unloading:
$$s_{i+1} = s_i - \Delta s$$
$$N_{i+1} = N_i - \Delta s \cdot k_{cyc} \geq 0$$
(6.1)

with $s_i \geq 0$

The point where the unloading path crosses the x-axis is defined by the residual displacement, s_{Res}. In real applications, even in case of single anchor tests, the load is transferred to the anchor via a baseplate or fixture. While during unloading, the anchor is not forced back to zero displacement, the baseplate might very well be moved back into its original position (zero displacement). In order to consider this effect in the

model, the force on the anchor remains zero with decreasing displacement steps -Δs as soon as the displacement is smaller than the residual displacement. Thus, if the force calculated according to Equation (6.1) for the next step would be negative, the second rule applies:

$$2.\text{ Unloading:} \qquad \begin{aligned} s_{i+1} &= s_i - \Delta s \\ N_{i+1} &= 0 \end{aligned} \qquad \text{, for } s_{i+1} \leq s_{Res} \qquad (6.2)$$

When the baseplate is reloaded from its original position, it first has to overcome the residual displacement of the anchor before any load can be taken up again. Accordingly, when reloading, the load on the anchor remains zero for displacements smaller than the residual displacement (see Figure 6.5 (c)). This gives the third rule:

$$3.\text{ Reloading:} \qquad \begin{aligned} s_{i+1} &= s_i + \Delta s \\ N_{i+1} &= 0 \end{aligned} \qquad \text{, for } s_{i+1} \leq s_{Res} \qquad (6.3)$$

When the residual displacement is overcome, the anchor is able to take up load again. Thereby, the reloading path follows the previous unloading path until the response encounters the envelope curve (see Figure 6.5 (d)). Thus, the fourth rule is:

$$4.\text{ Reloading:} \qquad \begin{aligned} s_{i+1} &= s_i + \Delta s \\ N_{i+1} &= N_i + \Delta s \cdot k_{cyc} \end{aligned} \qquad \text{, for } s_{i+1} > s_{Res} \qquad (6.4)$$

Once the reloading path encounters the envelope curve, the response follows the envelope curve until the next displacement reversal occurs. The above stated rules describe a rather simple approach for an idealization of the hysteretic behavior of post-installed anchors. It does not consider effects such as strength degradation in subsequent cycles of the same displacement level or softening of the unloading and reloading branch (hysteresis). However, it is reasonable to consider the residual displacements of anchors and the unloading and reloading behavior of different types of post-installed anchors. A more sophisticated approach is presented with the two-parameter model.

6.3.2   Two-parameter model

The two-parameter model is a modification of the previous approach which considers the strength degradation of anchors in subsequent cycles. Thereby, the basic principles of the model remain valid, while it is only necessary to modify the first and the fourth rule, whereas the second and third rule remain the same. It was shown in the experiments that when post-installed anchors are unloaded and again reloaded to the same displacement level, the strength that can be taken up at the same displacement level reduces in subsequent cycles. To simulate the observed

degradation, the parameter η, where $0 \leq \eta \leq 1$ is introduced, which is determined from displacement-controlled cyclic tests. It specifies the load that can be achieved in subsequent cycles relative to the first time a certain displacement level is reached. Typical values for the tested anchor systems in uncracked and cracked concrete are provided in Figure 5.24 and Figure 5.25, respectively. In this work, η is determined as the average strength degradation in the second cycle of a displacement level. Alternatively, for a more conservative approach, the degradation in the third cycle might be considered. A schematic depiction of the modified rules is presented in Figure 6.6.

(a) Unloading
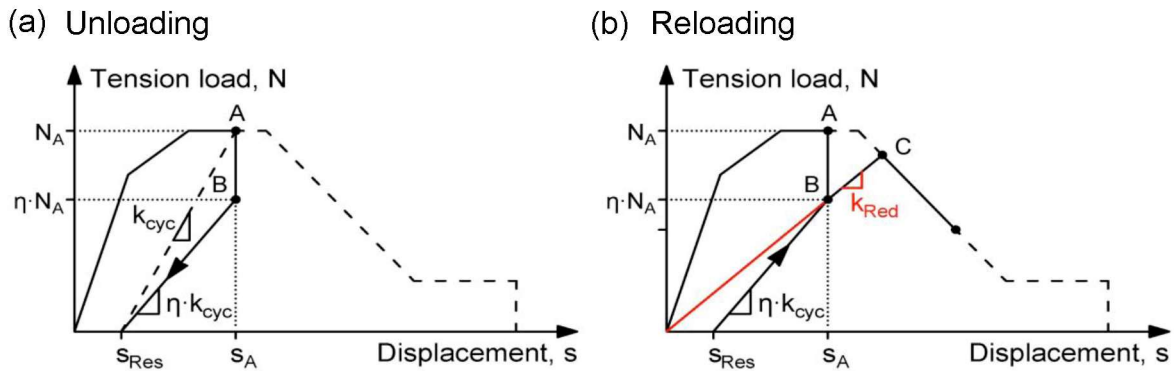
(b) Reloading

Figure 6.6. Schematic depiction of the modified (a) unloading rules, and (b) reloading rules for the two-parameter model.

Upon reversal of the displacement after the response has followed the envelope curve, first the load drops at the same displacement to η times the load at which the load reversal begins. Thereafter, the unloading path is defined by the modified stiffness $\eta \cdot k_{cyc}$. In this way, unloading from a certain displacement level results in the same residual displacement as in the first model. The first step of unloading is thereby defined by the following rule:

5. Unloading: (initial condition)

$$s_{i+1} = s_i$$
$$N_{i+1} = \eta \cdot N_i$$

(6.5)

The first unloading step considers the vertical drop in load when the displacement is reversed. Thereafter, unloading follows the modified path until it crosses the x-axis at s_{Res}. The response is defined as a modification of the first rule:

6. Unloading:

$$s_{i+1} = s_i - \Delta s$$
$$N_{i+1} = N_i - \Delta s \cdot \eta \cdot k_{cyc} \geq 0$$

(6.6)

For $s_{i+1} \leq s_{Res}$ the second and third rule apply. Once the residual displacement is overcome, reloading of the anchor has two parts, which are schematically shown in

Figure 6.6 (b). The first part starts when the residual displacement is overcome (see third rule) and initially follows the modified unloading path until it reaches the displacement level from where the anchor was unloaded. In Figure 6.6 (b), this point is marked as point B, and is defined by the displacement of point A and the load value $\eta \cdot N_A$. Up to this point reloading is defined as:

7. Reloading:
$$\begin{aligned} s_{i+1} &= s_i + \Delta s \\ N_{i+1} &= N_i + \Delta s \cdot \eta \cdot k_{cyc} \end{aligned} \qquad \text{, for } s_{i+1} > s_{Res} \qquad (6.7)$$

From here the second part starts with a softened reloading path and a reduced stiffness k_{Red}, which is valid up to the point where the envelope curve is again encountered. The second part (and k_{Red}) is defined by a straight line extending from the origin through point B, where the second part of reloading starts. Thus, the eight rule is:

8. Reloading:
The load-displacement response moves along a line extending from the origin through point B

Once the reloading path encounters the envelope curve at point C, the response follows the envelope curve until the next displacement reversal occurs. Two special cases should be mentioned.

First, if during reloading of the anchor ($s_{i+1} > s_{Res}$) a displacement reversal occurs at a displacement smaller than the displacement level from where it was previously unloaded (displacement of point A and B), unloading follows the reloading path back to the residual displacement. In other words, the displacement of point A, from where the unloading from the envelope curve started, defines the stiffness $\eta \cdot k_{cyc}$, as long as the displacement level has not been exceeded.

Second, if the anchor is unloaded from a displacement level between point B and C, unloading follows the fifth and sixth rule, where k_{cyc} is defined by the new displacement level (point of displacement reversal).

The main features of the two-parameter model are the strength degradation of anchors in subsequent cycles and the reduced reloading stiffness to the next displacement level observed in the previous chapter. Thereby, the reduced reloading stiffness to the next displacement level is considered by a softening branch during reloading. With this model, it is possible to accurately determine the behavior of anchors that exhibit a rather linear loading and unloading behavior, where practically no hysteretic loops are observed.

6.3.3 Three-parameter model

The extent to which tension loaded anchors might dissipate energy during a seismic event is rather negligible (Hoehler, 2006). Particularly in comparison to the global

energy dissipation of the structure. Nonetheless, some types of anchors exhibit observable hysteretic loops. In order to enable the analysis of the potential hysteretic behavior of post-installed anchors, the last development level defines the unloading in two steps such that after the initial drop of load (fifth rule, $N_i = \eta \cdot N_A$ and $s_i = s_A$), unloading first follows a relatively stiff branch up to a certain load value (defined by the ninth rule). From there, the unloading behavior softens and follows a second unloading branch towards the residual displacement (defined by the tenth rule). In this context, a third parameter is introduced, λ, which defines both the intermediate load level ($\lambda \cdot N_A$) and the stiffness of the two unloading branches. Consequently, two additional rules are given which supersede the sixth rule:

9. Unloading:
$$\begin{aligned} s_{i+1} &= s_i - \Delta s \\ N_{i+1} &= N_i - \Delta s \cdot \frac{1}{\lambda} \cdot k_{cyc} \end{aligned} \qquad , \text{ for } N(s_{i+1}) \geq \lambda \cdot N_A \qquad (6.8)$$

10. Unloading:
$$\begin{aligned} s_{i+1} &= s_i - \Delta s \\ N_{i+1} &= N_i - \Delta s \cdot \frac{\lambda \cdot k_{cyc}}{1 - \lambda(\eta - \lambda)} \end{aligned} \qquad , \text{ for } 0 \leq N(s_{i+1}) \leq \lambda \cdot N_A \qquad (6.9)$$

Figure 6.7 schematically depicts the modified unloading behavior. The response follows the envelope curve up to point A where the displacement is reversed according to the defined loading history. The first unloading step results in the first drop of load to point B. From there, unloading is defined by the ninth rule until the load level $\lambda \cdot N_A$ is reached. Further unloading follows a line towards the residual displacement on the x-axis. When the unloading path crosses the x-axis at s_{Res}, the second and third rule apply. The anchor remains unloaded until the displacement of the anchor exceeds the residual displacement again. Reloading from the residual displacement, follows the same rules as in the two-parameter model.
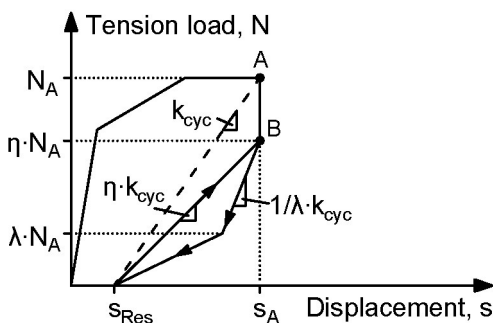
Figure 6.7. Schematic depiction of the modified unloading rules for the three-parameter model.

6.4 Validation against experimental results

In this section, the hysteretic rules established in the previous section are validated against the experimental results obtained from displacement-controlled single anchor cyclic tests, which were presented in Chapter 5. As part of the validation, the three levels of accuracy are compared with each other and with the experimental results. With the practical examples, differences between the three models, which were previously shown only by the theoretically defined rules, will become clearer. It should be noted that the experimental results in terms of load-displacement curves, which are used to compare the experimental behavior to the hysteretic models, have already been shown in Chapter 5. However, to facilitate the comparison, some of the curves will be shown again in this section.

6.4.1 Comparison between one-parameter model and two-parameter model exemplified with undercut anchors

To examine the difference between the one-parameter model and the two-parameter model, the simulated hysteretic behavior is compared to test series UC-DISP-UCR. For this purpose, the idealized envelope curves for the individual tests were obtained in such a way that they best fitted the experimental results. The loading history was defined according to the loading history in the corresponding experiments. However, the limitation of a minimum tension load, which, for practical reasons, was required in the tests, is neglected in the analysis. Here the bottom of the displacement pulses was defined as zero, simulating the case where the fixture is pushed back into its original position. Table 6.2 summarizes the input parameters required for the idealization of the unloading and reloading stiffness (see Section 6.2) and the parameters required for the two hysteretic models (see Section 6.3).

Table 6.2. Required input parameters for test series UC-DISP-UCR.

Unloading and reloading behavior			Model parameters	
k_α	105	kN/mm	Displacement at ultimate load, s_u	
k_β	50	kN/mm	UC-DISP-UCR-1	5.45 mm
α	1		UC-DISP-UCR-2	2.79 mm
β	2		UC-DISP-UCR-3	6.24 mm
ω	3.8		Strength degradation factor, η	0.89

Using the Visual Basic for Applications (VBA) programming language, the rules were scripted into a routine and implemented in the program Microsoft Excel. In the simulations, the displacement step size was chosen as $\Delta s = 0.005$ mm. The output load-displacement curves obtained from the hysteretic models for test UC-DISP-UCR-1 are shown in Figure 6.8. Along with the results of the hysteretic models, the

experimental results are presented to enable a direct comparison between the model behavior and the experimental behavior.

UC-DISP-UCR-1
(a) One-parameter model   (b) Two-parameter model
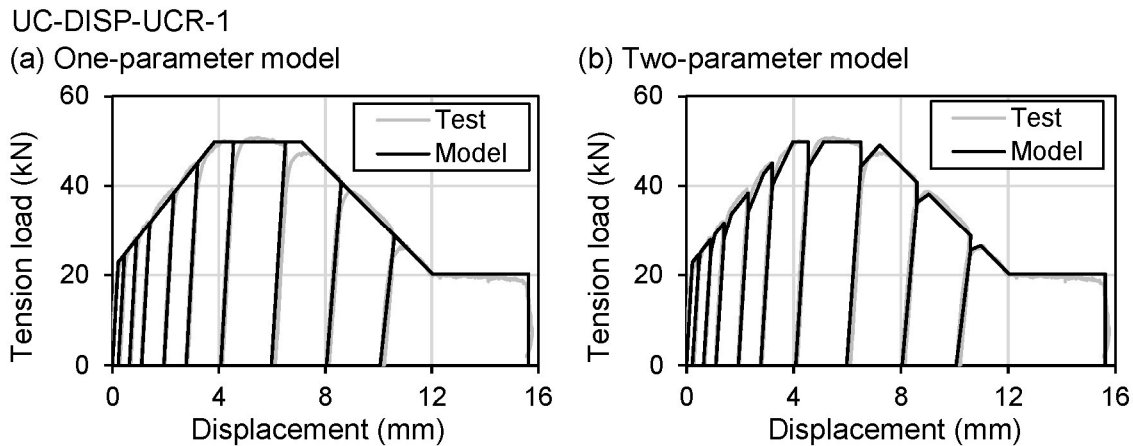
Figure 6.8. Load-displacement curves obtained from experiments and the results of the (a) one-parameter model and the (b) two-parameter model.

The comparison presented in Figure 6.8 shows a good agreement between the experimental and the model results in terms of the load-displacement and hysteretic behavior. The response of the model curves follows the load-displacement curve obtained in the experiments. The comparison shows that both models are able to accurately simulate unloading and reloading of the tested anchors. One of the major differences between the two models is how the envelope curve is approached during reloading. This becomes evident in Figure 6.9.

UC-DISP-UCR-2 - Two-parameter model
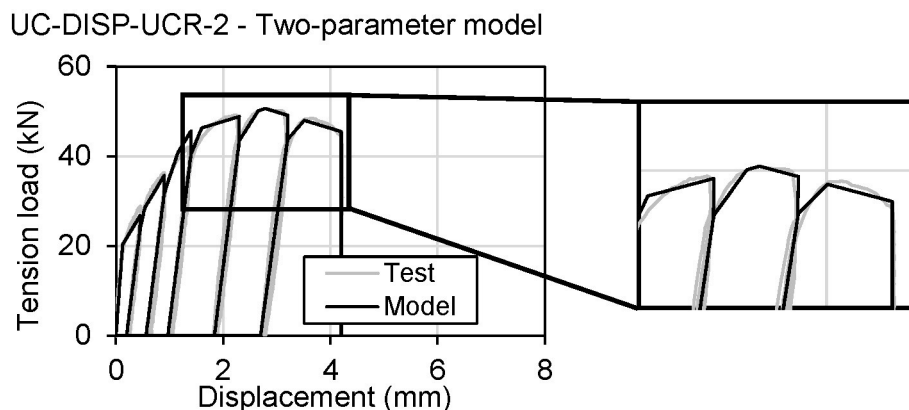
Figure 6.9. Load-displacement curves obtained from test UC-DISP-UCR-2 and the result of the two-parameter model.

While in the one-parameter model, the anchor behavior returns into the position from where it was unloaded from the envelope curve, the two-parameter model considers a softening branch during reloading. It can be seen from the experimental results in Figure 6.9 that reloading to the next displacement level initially follows the unloading

path until the displacement of the previous level is reached. Thereafter, reloading is characterized by a less stiff path. The two-parameter model is able to accurately simulate this behavior. Thereby, it is taken into account that the anchor is not able to regain its full strength when reloaded to the same displacement level. In contrast, the one-parameter model does not consider any strength degradation in subsequent cycles. The definition of the softening branch by means of a line extending from the origin through the point where softening starts, seems to be a viable workaround that eliminates the need to introduce additional parameters.

Figure 6.10 shows the output load-displacement curves obtained from the hysteretic models along with the experimentally obtained load-displacement curves for test UC-DISP-UCR-3. The comparison shows a good agreement between the experimental and the model results in terms of the load-displacement and hysteretic behavior. Again, both models are able to accurately predict the point at which the anchors are completely unloaded, thus the residual displacement. The results suggest that the introduced approach for idealization of the unloading and reloading behavior (see Section 6.2) reasonably well reflects the real anchor behavior. In case of the tested undercut anchors, it can be seen that almost no hysteretic loops are apparent. Therefore, both presented modelling approaches are deemed adequate to realistically represent the hysteretic anchor behavior. However, as expected, the two parameter model results in better accuracy compared to the one parameter model.

6.4.2 Comparison between two-parameter model and three-parameter model exemplified with bonded anchors

In this section, the two-parameter model and the three-parameter model are compared to each other and the test series BA-DISP-CR. In this test series, bonded anchors were tested in cracked concrete and loaded according to the displacement-controlled protocol for pulsating tension load. The idealized envelope curves for the individual tests were obtained in such a way that they best fitted the experimental results. The loading history was defined according to the loading history in the corresponding experiments. Table 6.3 summarizes the input parameters required for the idealization of the unloading and reloading stiffness and the parameters required for the two hysteretic models.

UC-DISP-UCR-3

(a) One-parameter model

(b) Two-parameter model

Figure 6.10. Load-displacement curves obtained from test UC-DISP-UCR-3 and the results of the (a) one-parameter model and (b) two-parameter model, along with the details of the unloading behavior.

Table 6.3. Required input parameters for test series BA-DISP-CR.

Unloading and reloading behavior			Model parameters	
k_α	135	kN/mm	Displacement at ultimate load, s_u	
k_β	70	kN/mm	BA-DISP-CR-1	0.94 mm
α	0.5		BA-DISP-CR-2	1.17 mm
β	1.5		Strength degradation factor, η	0.87
ω	2.9		λ	0.4

Once the parameters are specified, the load-displacement and hysteretic behavior of the anchors is calculated based on the given loading history. For the test BA-DISP-CR-1, the output load-displacement curves of both the models along with the experimental results are presented in Figure 6.11. Both models reproduce the experimental behavior in terms of the load-displacement and the unloading and reloading behavior sufficiently accurate. The response of the model curves follows the load-displacement curve obtained in the experiments. It can be seen that also for rather small displacements, the two-parameter model accurately predicts the point at which

the anchor is completely unloaded (the point where the response encounters the x-axis). In case of the tested bonded anchors, the hysteretic behavior is more pronounced compared to the previously discussed undercut anchors. Hysteretic loops are clearly visible in the experimental load-displacement curves shown in Figure 6.11. These hysteretic loops cannot be simulated using the two-parameter model, since here the definition of the unloading and reloading paths largely coincide with each other. The three-parameter model, on the other hand, addresses potential hysteretic behavior more carefully by splitting the unloading branch into two branches. In this way, the hysteretic loops are represented by triangles as shown in Figure 6.11. The comparison with the experimental results shows a good agreement.
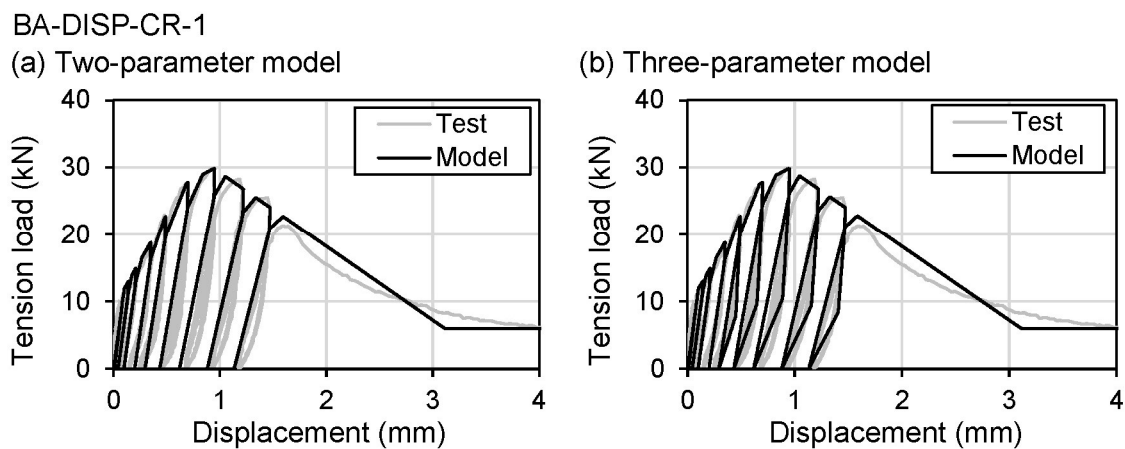
BA-DISP-CR-1

Figure 6.11. Load-displacement curves obtained from test BA-DISP-CR-1 and the results of the (a) two-parameter model and the (b) three-parameter model.

A more detailed view of one of the hysteretic loops in test BA-DISP-CR-2 and the associated model behavior is shown in Figure 6.12. It can be seen that the proposed approach reasonably well represents the hysteretic behavior of the tested anchors. The response follows the envelope curve until the displacement is reversed. After the first drop of strength, the unloading behavior is defined by a first rather steep branch, followed by a rather soft branch towards the point where the response encounters the x-axis. In the model, the fullness of the hysteretic loops is defined by the parameter λ. Smaller values for λ will move the intermediate point between the two branches closer to the x-axis and will increase the stiffness of the first branch. As a results, the hysteretic loops will become fuller.

148

BA-DISP-CR-2 - Three-parameter model
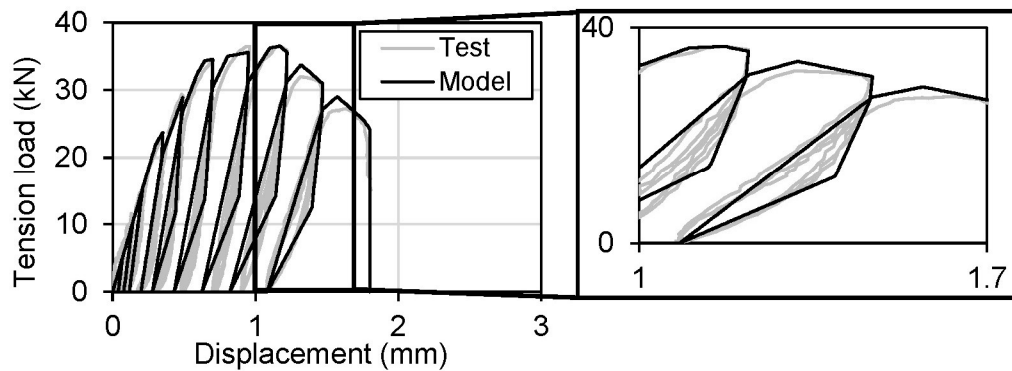
Figure 6.12. Load-displacement curves obtained from test BA-DISP-CR-2 and the result of the three-parameter model.

6.4.3   Validation of the model against further experimental results from this work

In order to emphasize the differences between the individual models, in the previous sections, the anchor behavior was separately modelled for the individual tests of a test series. In this section, a more general approach is followed where the spring characteristics of the tested anchor systems are obtained by the mean spring characteristics determined from the individual tests. For this purpose, the envelope curves were determined for the individual tests and the mean load and stiffness values were used to define the spring characteristics of the mean envelope curve.

6.4.3.1   Concrete screws

In this example, the hysteretic model is validated against the test series CS-DISP-UCR and CS-DISP-CR, where concrete screws were tested in uncracked and cracked concrete. The required input parameters for the idealization of the unloading and reloading stiffness and the parameters required for the hysteretic model are summarized in Table 6.4.

Table 6.4. Required input parameters for test series CS-DISP-UCR and CS-DISP-CR.

Parameters	CS-DISP-UCR	CS-DISP-CR
Unloading and reloading behavior		
k_α	150 kN/mm	90 kN/mm
k_β	50 kN/mm	120 kN/mm
α	0.8	0.4
β	2	1.5
ω	4.7	3.8
Model parameters		
Mean displacement at ultimate load, $s_{u,m}$	1.38 mm	2.61 mm
Strength degradation factor, η	0.86	0.78
λ	0.4	0.4

To simulate the anchor behavior, the three-parameter model was applied for both test series. Once the required parameters are specified, the load-displacement and hysteretic behavior of the anchors is calculated based on the respective loading (displacement) history. The output load-displacement curves of the model along with the experimental results are presented in Figure 6.13. With respect to the unloading and reloading behavior, the model is able to accurately simulate the real anchor behavior. When tested in uncracked concrete it appears that the hysteretic behavior of the tested anchors is somewhat more pronounced compared to their behavior in cracked concrete. Up to certain displacement level in the post-peak range of the load-displacement curve, the model can simulate the hysteretic loops reasonably well. However, particularly the behavior of test CS-DISP-UCR-2 becomes more erratic at larger relative displacements and the model accuracy appears to reduce. The discrepancy between the behavior in the tests and the predicted behavior is rather a consequence of the scatter in the test results, thought. The three tests result in different envelope curves, whereas the model uses the mean envelope curve considering the results in all three tests. If the model parameters were chosen based on the individual test results, it would be able to accurately predict their behavior. Nevertheless, the comparison with experimental results shows that the hysteretic model is suitable to reproduce the behavior of concrete screws and confirms the assumptions made regarding the idealization of the unloading and reloading behavior.
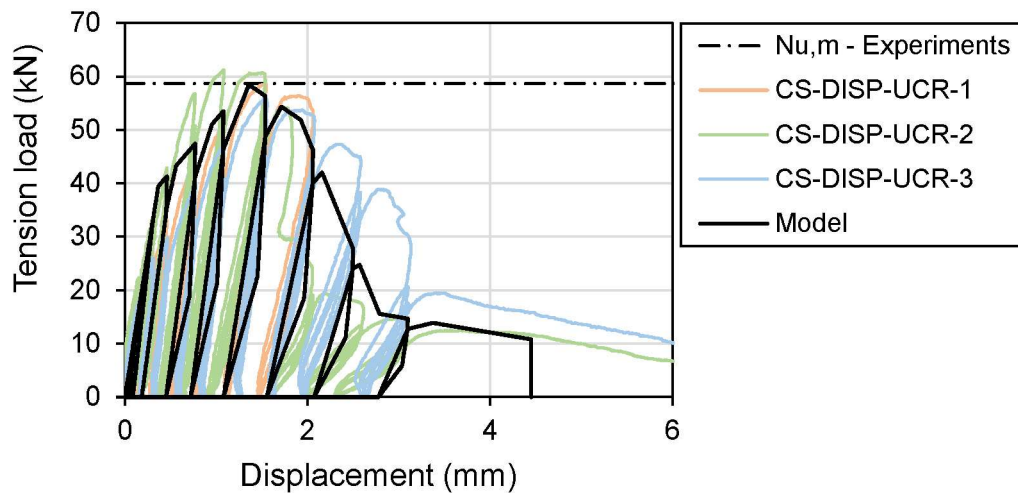
(a)
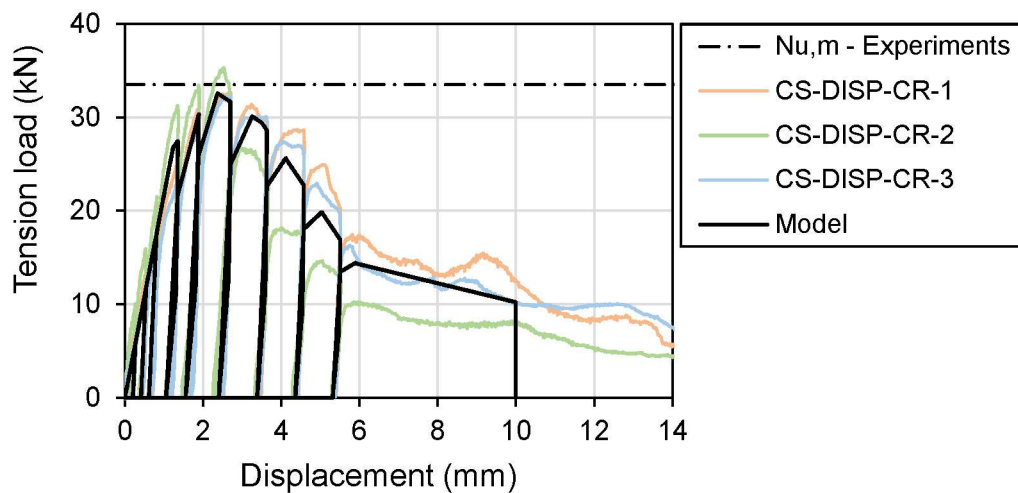
(b)

Figure 6.13. Load-displacement curves obtained from test series (a) CS-DISP-UCR and (b) CS-DISP-CR along with the results obtained from the three-parameter model using mean envelop curve.

6.4.3.2   Bonded expansion anchor

In Chapter 5 also bonded expansion anchors were tested according to the displacement-controlled protocol for pulsating tension load. The curves obtained from these tests in uncracked (BEA-DISP-UCR) and cracked concrete (BEA-DISP-CR) are now used to validate the hysteretic model. A summary of the required input parameters for the idealization of the unloading and reloading behavior and the three parameters required for the hysteretic model are given in Table 6.5.
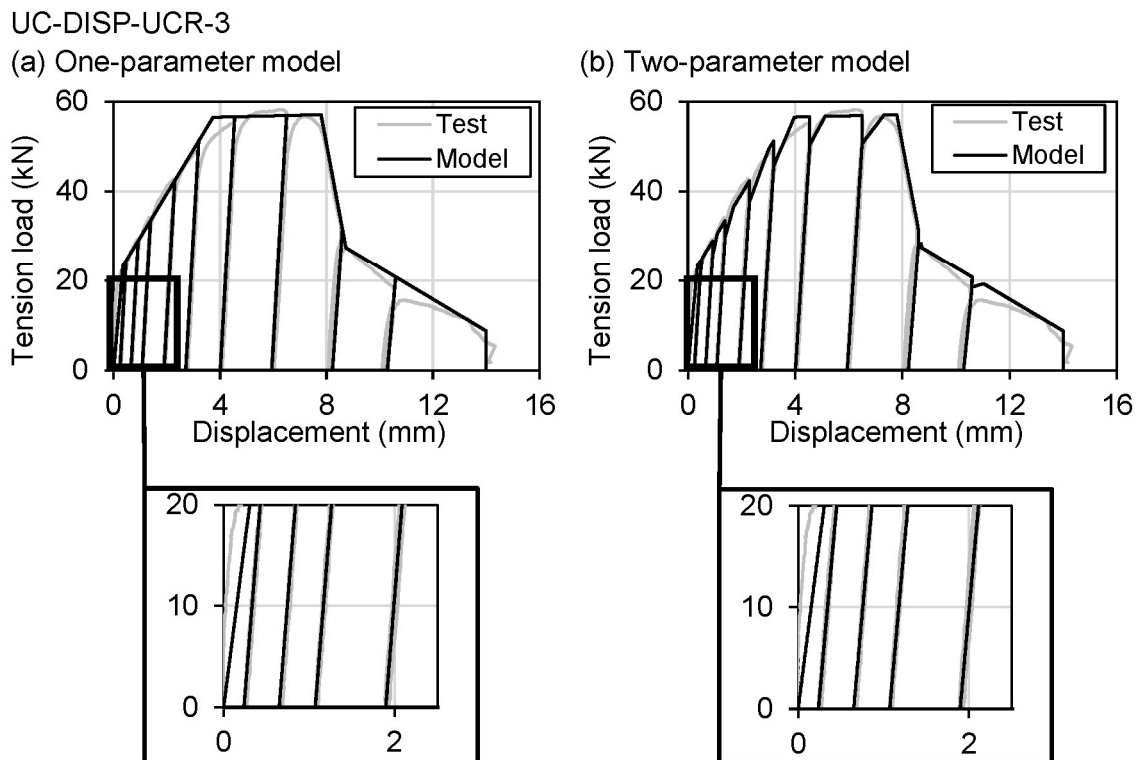
Table 6.5. Required input parameters for test series BEA-DISP-UCR and BEA-DISP-CR.

Parameters	BEA-DISP-UCR	BEA-DISP-CR
Unloading and reloading behavior		
k_α	150 kN/mm	150 kN/mm
k_β	110 kN/mm	50 kN/mm
α	0.25	0.8
β	1.3	2
ω	3.3	4.7
Model parameters		
Mean displacement at ultimate load, $s_{u,m}$	4.47 mm	6.92 mm
Strength degradation factor, η	0.89	0.86
λ	0.5	0.5

Although the hysteretic behavior observed in the experiments was rather moderate, again, the three-parameter model was used to simulate the anchor behavior, as it provides the highest level of accuracy and includes all previous levels. Figure 6.14 shows the output load-displacement curves of the model and the corresponding experimental results. Both examples show that the idealization approach for the unloading and reloading behavior of the anchors leads to an accurate simulation of the behavior observed in the experiments. This also accords with our earlier observations and confirms the validity of the idealization approach introduced in Section 6.2. Furthermore, it also shows that the assumptions made to model the hysteretic behavior largely correspond to the real behavior of the anchors. In general, the progression of the envelope curves matches well. This is particularly true for the ascending branch. It can be seen that in the post-peak range, the experimental behavior is more volatile. Nonetheless, the model even considering the average envelope curve and average model parameters is able to provide a suitable estimation of the behavior.
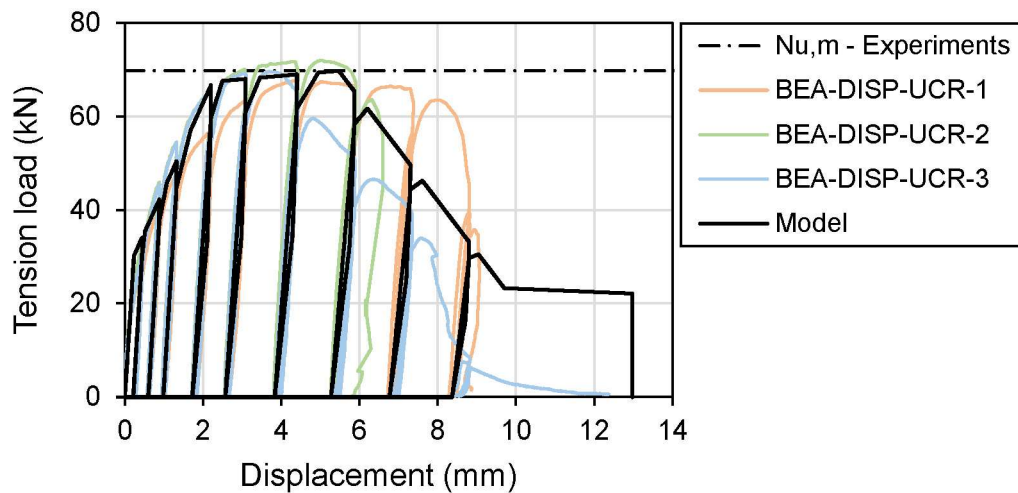
(a)
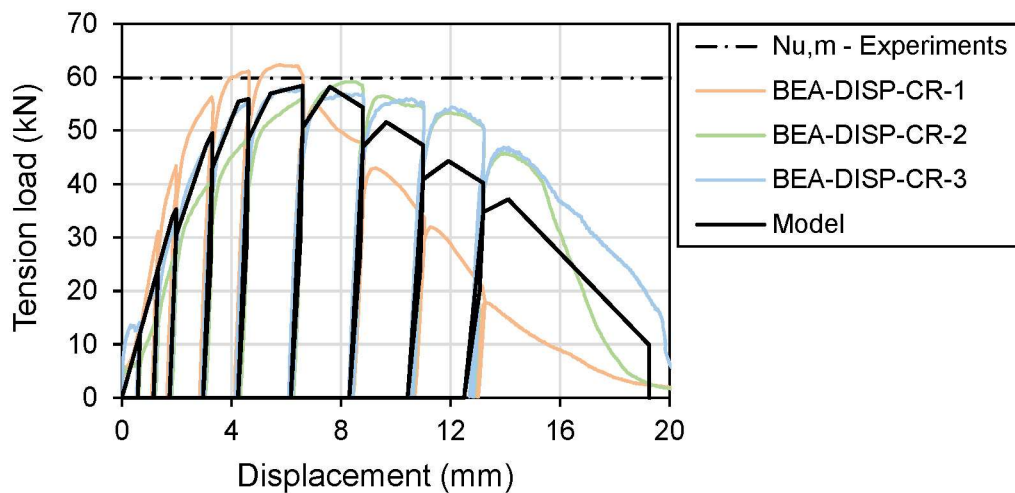
(b)

Figure 6.14. Load-displacement curves obtained from test series (a) BEA-DISP-UCR and (b) BEA-DISP-CR along with the results obtained from the three-parameter model using mean envelope curve.

6.4.4 Validation of the model against experimental results from the literature

Force-controlled cyclic tension tests carried out in accordance with DIBt (2010) Guideline for Fastenings with Anchors in Nuclear Power Plants and Nuclear Facilities, on single undercut anchors are reported in Mahadik and Sharma (2014). In the experiments, FZA undercut anchors with an embedment depth of h_{ef} = 80 mm were tested. Note that this is the same anchor system which was used in the experiments on single undercut anchors in Chapter 5. In their study, the anchors were subjected to cyclic tension load at constant crack width. Three test series with three tests each were performed, whereby the crack width was varied in each test series. The applied crack

widths include $\Delta w = 0.4$ mm, $\Delta w = 0.8$ mm, and $\Delta w = 1.5$ mm. In each test, 15 cycles were performed with a force amplitude of 16.3 kN. Thereafter, a residual pull-out test was performed. The corresponding reproduced load-displacement curves are shown in Figure 6.15. The mean cube concrete compressive strength at the time of testing was $f_{cc,150} = 42.53$ N/mm². The anchors failed due to concrete cone failure during residual testing phase. A detailed description of the experimental program, the experimental setup and results is reported in Mahadik and Sharma (2014).

The model envelope curves were created based on the experimental curves. The required input parameters for the idealization of the unloading and reloading behavior of the anchors were assumed based on the experimental results in this work. For test series FZA-CT-CW-0,8mm with a crack width of $\Delta w = 0.8$ mm, the same parameters were assumed as used in this work for undercut anchors installed in cracked concrete (see Figure 6.4). Since the cycling phase in the force-controlled tests mainly considered the elastic range of the load-displacement curve, basically only the parameter k_α needs to be adjusted in the remaining two test series. Therefore, the stiffness factor proposed by Mahadik et al. (2016) was used. Originally, the stiffness factor modifies the secant stiffness values which define the characteristic points of the envelope curve according to the crack width. In this work, the stiffness factor was used to the determine k_α for $\Delta w = 0.4$ mm and $\Delta w = 1.5$ mm crack widths, based on k_α for $\Delta w = 0.8$ mm crack width. Since undercut anchors showed no pronounced hysteretic behavior, the two-parameter model was used to simulate the anchor behavior. In this regard, two parameters were required that is the mean displacement at ultimate load, which was taken from Mahadik and Sharma (2014) and the strength degradation factor, which was considered equal to the factor taken for a crack width of $\Delta w = 0.8$ mm. A summary of the required input parameter is given in Table 6.6. To define the time history, the experiments were evaluated with respect to the displacements associated with the force amplitudes, as the displacement of the anchor increases with each cycle.

Table 6.6. Required input parameters for force-controlled single anchor cyclic tests by Mahadik and Sharma (2014).

Parameters	FZA-CT-CW-0,4	FZA-CT-CW-0,8	FZA-CT-CW-1,5
k_α	93 kN/mm	85 kN/mm	74 kN/mm
Mean displacement at ultimate load, $s_{u,m}$	7.16 mm	11.88 mm	17.72 mm
Strength degradation factor, η	0.87	0.87	0.87

The results of the modelling approach are shown in Figure 6.15. Due to the displacement-controlled nature of the model and the approximation of the envelope curve, the model has minor difficulty in predicting the exact force amplitudes.

Nonetheless, the hysteretic model is able to simulate the overall unloading and reloading behavior sufficiently well.
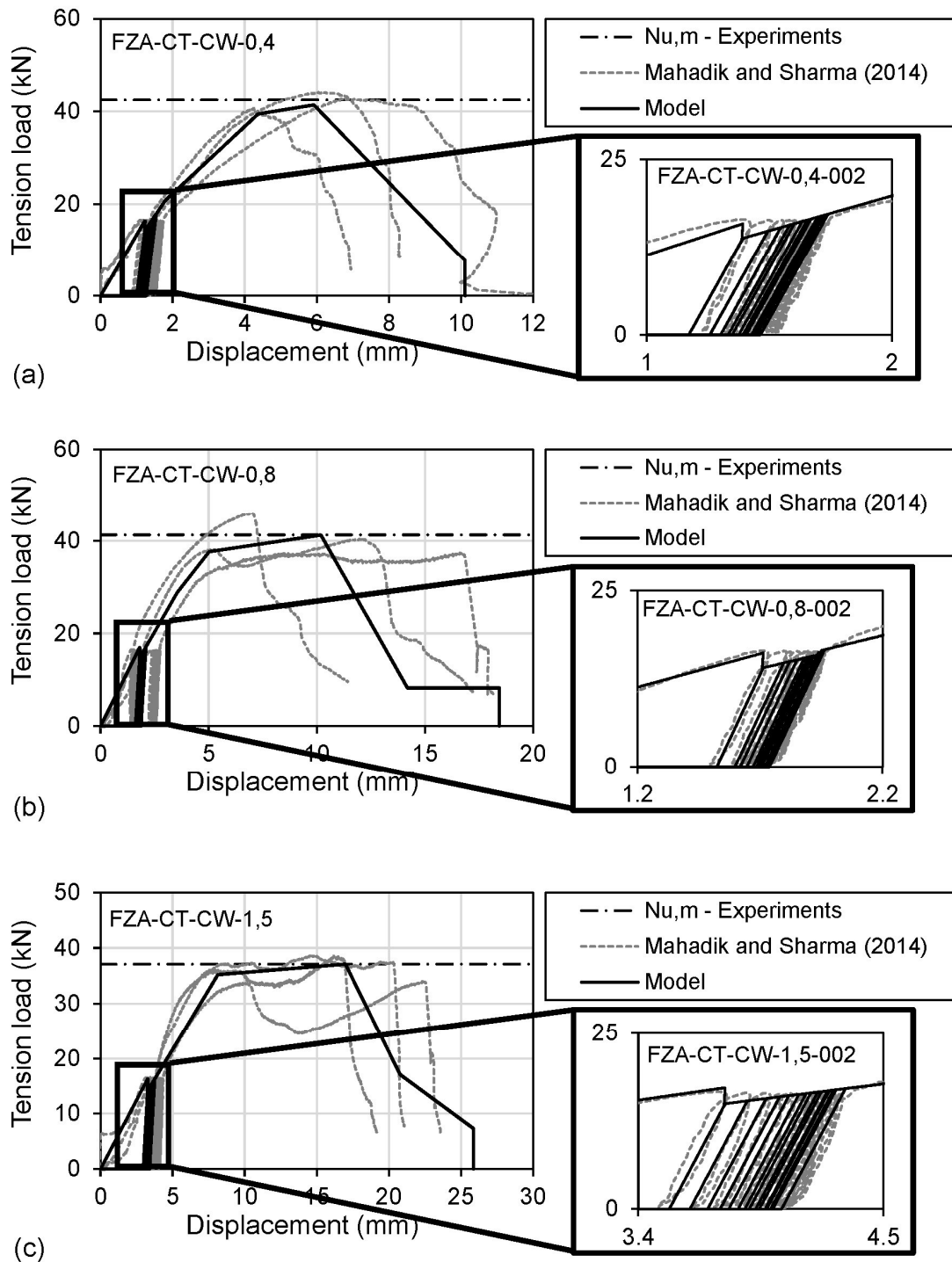
Figure 6.15. Load-displacement curves reproduced from Mahadik and Sharma (2014) compared to the results obtained from the hysteretic model. (a) FZA-CT-CW-0,4 (Δw = 0.4 mm), (b) FZA-CT-CW-0,8 (Δw = 0.8 mm), and (c) FZA-CT-CW-1,5 (Δw = 1.5 mm).

6.5 Summary

In this chapter, a modelling approach for simulation of the cyclic behavior of tension loaded anchors was introduced and successfully validated against experimental results from this work and from the literature. The model is able to simulate the unloading and reloading behavior of various types of anchors, considering softening effects in the unloading and reloading branches, strength degradation in subsequent cycles, and the residual displacements of anchors after unloading.

The basis of the model is an envelope curve which is determined from single anchor tests. This curve encloses the hysteretic loops and can thus be regarded as the upper limit of the cyclic loading. In this work, a hexa-linear format was chosen to idealize the envelope curve obtained from the experiments. Therefore, seven characteristic points need to be defined, each of which is characterized by a load value and a corresponding displacement value.

In the hysteretic model, the unloading and reloading behavior of the anchors is characterized by the stiffness k_{cyc} which changes with increasing displacements of the anchors. However, in the evaluation of the experimental results it became apparent that the alteration of the unloading and reloading stiffness with increasing relative displacement may differ markedly depending on the type of anchor. In order to consider the variations in anchor behavior, while maintaining a simple and consistent approach for modeling, a tri-linear format was proposed in this work. This allows the description of the behavior by using only five parameters. The comparison with the experimental results in this work has shown that the adopted simplification of the unloading and reloading behavior reproduces the real behavior of the tested anchors with a sufficient level of accuracy.

Eventually, a set of rules was introduced which define the anchor behavior during unloading and reloading. Three different levels of accuracy were presented which represent the development levels of the model. At each level, additional features, such as strength degradation in subsequent cycles, were added, resulting in an increasingly accurate representation of the actual anchor behavior. In this way, practitioners can decide upon the level of accuracy depending on the intended application. The difference between these levels was presented in detail using the experimental results from this work as reference examples. A comparison between the experimental results from this work and from the literature has shown that the proposed model is able to accurately simulate the anchor behavior subjected to different types of loading schemes.

7 Recommendations for qualification and design

Based on the previous considerations and results, this chapter presents some thoughts on how the qualification and design of anchors under seismic actions might be evolved. In this context, the main emphasis is on structural connections, where, for example, new structural elements that provide strengthening against seismic loading are connected to the existing structure by means of post-installed anchors. The following suggestions are in no way intended to replace the current qualification procedures or design rules. Rather, they are intended to supplement the information obtained from the current qualification tests and thus provide a basis for the safe design of structural connections against seismic actions.

It should be noted that parts of the discussion in this chapter have previously been published in Stehle and Sharma (2021a).

7.1 Displacement-controlled testing

The relevant force-controlled testing approaches for structural connections according to EOTA TR 049, category C2, feature cyclic loading in a defined range of the load-displacement curve. The maximum forces up to which the cyclic load is applied are defined by the characteristic capacity of a monotonically loaded anchor (Mahrenholtz et al., 2017). In other words, it is assumed here that the cyclic load acting on the anchor during a seismic event will not exceed the characteristic load. Thus, it is assumed that the anchor will behave predominantly within its elastic range during an earthquake. This assumption is based on the premise that the loads acting on the connection can be determined with a reasonable degree of accuracy. However, as pointed out by Stehle and Sharma (2021a), there are some points which should be considered. Current force-based design approaches against seismic actions, such as those specified in EN 1998-1, consider the ability of ductile structural members to dissipate energy through plastic deformations by reducing the seismic demand on the structure. Here the ductility of a member is determined based on the materials used in the construction of the building and the force resisting system against seismic loading, not by computations of the structural behavior or the experimental investigation of the same. If the actual ductility of a structural member is lower than the ductility assumed during the design, it follows that less energy can be dissipated and thus the actual demands are higher than assumed during the design. Consequently, the demands on

structural connections and in turn on the anchors will be notably higher than expected. This is further exaggerated by the over-strength in the material response. Since during an earthquake, structures are expected to undergo deformations in the nonlinear range, plastic hinges will form in some members of the structural system. Although the formation of plastic hinges is intentional in order to dissipate energy, it leads to increased displacement demands on the other structural members and their connections to each other. Besides the increased displacement demands, the formation of plastic hinges results in a redistribution of the forces within the structure. As discussed in Section 4.1, this effect is often ignored in current standards such as EN 1998-1 and might result in notably higher forces on the connection than expected during the design.

Due to these uncertainties with respect to the seismic demands on the structure and thus on the connections itself, insights on the displacement and hysteretic behavior of anchors in a broader range of the load-displacement curve might be useful. In this context, the potential for redistribution of forces within an anchor group can be used to, at least partially, compensate for the increased demands. However, such effects can only be considered if the complete load-displacement behavior of the anchors is known. Furthermore, the experimental results on single anchors have shown that effects such as stiffness degradation or strength degradation become more pronounced with increasing displacement of the anchors. With respect to the high displacement demands during an earthquake and the increasing importance of displacements in the design against earthquakes, a safe design can therefore only be realized if the relevant information is available. The cyclic tests on single anchors carried out in this work show that this additional information can be obtained rather easily and without excessive extra effort by means of displacement-controlled tests such as those presented in this work.

Finally, it should be noted that the concept described for displacement-controlled pulsating tension load tests can in principle also be applied to alternating shear load tests.

7.2   Assessment criteria

The assessment criteria given in the current guideline for qualification of anchors against seismic actions, EOTA TR 049, attempts to harmonize the assessment of anchors for different applications (non-structural and structural applications) and different performance categories (suitability and serviceability). In this context, anchor performance is assessed on the basis of pass/fail criteria, which eventually reveal only little about the actual behavior of an anchor during a seismic event. This might lead to the deceptive assumption that once an anchor is approved it would be suitable for all conceivable applications, which is not necessarily the case.

For instance, bonded anchors are generally considered rather unsuitable for large crack widths, since they exhibit a higher reduction in capacity compared to other anchor systems such as undercut anchors or bonded expansion anchors. However, the experimental results indicate that even in case of rather large crack widths, the tested bonded anchors are markedly stiffer and show a less pronounced displacement behavior compared to the other types of anchors in the experimental program. Moreover, if the displacement of a structural connection is to be limited to a certain degree, the associated capacity of a bonded anchor may be higher than the capacity of an undercut anchor at the same displacement. That is despite the large crack width. In such a case, an application based approval would be more meaningful compared to a general approval.

Furthermore, the experimental results on single anchors have shown that the displacement behavior of different types of anchors may vary significantly. However, whether a more pronounced or a less pronounced displacement behavior is beneficial, again, strongly depends on the application itself and the desired design option (Muciaccia, 2017). In this context, pass/fail criteria are rather unsuitable for choosing the right anchor system. In the design case where for example a plastic hinge is assumed to develop in the baseplate of the connection, EN 1992-4 notes that effects such as redistribution of forces among anchors should be properly considered. This is only possible if the displacement behavior of an anchor is adequately understood. Therefore, the focus should rather be on providing practitioners with as much relevant information as possible. Concomitantly, information such as strength degradation in subsequent cycles or permanent residual displacements upon unloading can be criteria that determine suitability in specific applications.

Finally, the type of application for which anchors form the connection might affect whether the anchor behavior is governed by intersecting cracks or by the hysteretic and displacement behavior of an anchor or whether the behavior is governed by the forces imposed on the connection. In this context, it would be conceivable to distinguish between different demand cases and chose the required tests and assessment criteria accordingly. For example, if post-installed anchors are used to form the connection between a new structural strengthening element against earthquake loads and the existing RC structure, these different demand cases can be illustrated by the following two examples. In case of steel haunches, anchors are simultaneously loaded while cracks in the anchorage zone open (Sharma, 2013). In this case, crack cycling tests are more suitable to obtain the relevant information for a safe design. On the other hand, in case of steel bracings, the cracks in the anchorage zone are actually closed or about to close when the anchors are activated (Mahrenholtz et al., 2015). In this case, the relevant information for the design may rather be obtained in cyclic tension and shear load tests at constant crack width.

7.3 Displacement based design for anchors

As highlighted in Sharma (2017) and Sharma (2019), a solely force-based design for anchors is deemed inadequate for structural connections subjected to seismic loading. Based on the experimental example in Genesio (2012) and Sharma (2013), it was shown that a force-based design alone is not sufficient to ensure the effectiveness of a strengthening solution, since the displacement behavior of different types of anchors has a major influence on the performance of the attached element itself (Sharma, 2017; Sharma, 2019). Therefore, the urgency and the need for a displacement based approach for anchors was clearly emphasized.

To implement a displacement based approach for the design of anchors, certain design tools must be available. The first tool which is required, is the information on the complete load-displacement behavior of an anchor and the description of the behavior in terms of adequate models. One such example is the equivalent spring model introduced in Sharma (2013). The availability of such models to describe the anchor behavior becomes essential for two reasons. For one, it has already been repeatedly pointed out that different anchor systems have different displacement characteristics and that these differences may also have a pronounced effect on the performance of the attached elements. The second point is that effects, such as the redistribution of forces in an anchor group, can only be considered in the design if it is possible to accurately reproduce them. With regard to the last mentioned point, a second tool is needed, that is, the consideration of the baseplate stiffness (Sharma, 2017). An implementation of the first two tools is provided by the nonlinear spring modelling approach proposed by Bokor (2021) for the design of monotonically loaded anchor groups failing due to concrete related failure modes. With the hysteretic rules proposed in the last chapter, a third tool is provided which allows the description of the hysteretic behavior of anchors. Combining these tools results in a toolkit that can be used to describe the cyclic behavior of an anchor group. Using this toolkit, for example, the connection between steel bracing and concrete corner can be modeled. Loading of the entire connection results in turn in a single spring which is characterized by the resulting load-displacement behavior of the model. The spring can then be incorporated into a global structural model. This approach provides two main benefits. First, by considering the displacement behavior and the stiffness of the connections in more detail, the global structural models become more accurate. Second, the incorporation in the global structural model allows for a more reliable estimation of the demands imposed on the connections during an earthquake. On the whole, this results in a safer and more practical design.

Part II

Anchor group level

8 Experimental investigations on anchor groups under displacement-controlled monotonic and cyclic tension load

In Chapter 5, the cyclic behavior of single anchors was presented and discussed. However, in practical applications, more than one anchor is required to fasten additional elements to the RC structure. Generally, several anchors are combined to form an anchor group by means of a steel baseplate or a fixture. In this case, several aspects may influence the load-displacement behavior of the anchor group as a whole. Alongside the individual anchor behavior, the arrangement of the anchors in the group (number of anchors and anchor spacing), the stiffness of the baseplate, and the point and nature of load application are of particular relevance for anchorages under tension as shown in Bokor et al. (2019a).

In force-based design approaches, the anchor spacing is particularly important in case of concrete related failure modes such as concrete cone failure. While in case of pull-out failure (other than for bonded anchors) or steel failure the capacity is unaffected by the anchor spacing, in case of concrete cone failure, the individual cones of the anchors are overlapping when the spacing is too small (Eligehausen et al., 2006). This results in a reduction of the induvial anchor capacity and consequently in the reduction of the group capacity (Eligehausen et al., 2006). On the other hand, when the spacing is rather large, the flexibility of the baseplate increases, which results in larger total displacements of the anchor group. Furthermore, the anchor spacing influences the stiffness of the baseplate, which may in turn determine how the applied tension load is distributed among the anchors as shown in Bokor et al. (2019b).

The experimental program presented in this chapter aims to further investigate the above mentioned aspects for monotonic loading and extend the investigation to the case where the anchor groups are subjected to displacement-controlled pulsating tension load. Therefore, experiments on various anchor groups with different anchor configurations have been performed. The groups were loaded monotonically in tension or according to the displacement-controlled protocol for pulsating tension load presented earlier. Besides the overall behavior of the anchor groups and the influence of cyclic loading thereon, the focus is set on the displacement and hysteretic behavior of the individual anchors within the group.

Note that parts of this chapter have been previously published in Stehle and Sharma (2021b).

8.1 Experimental program

Table 8.1 provides an overview of the experimental program. In total, 18 test series were carried out, with 3-4 tests per series to verify repeatability. Four test series were performed on single anchors, including six tests with monotonic loading and seven with cyclic loading. These single anchor tests were performed as reference for the behavior of anchor groups and the individual behavior of anchors within the group. The investigated anchor configurations include 2 x 1 anchor groups, 2 x 2 anchor groups and 3 x 2 anchor groups with varying anchor spacing and baseplate dimensions (see Table 8.1). Each configuration was tested under monotonic tension load and displacement-controlled pulsating tension load. Eccentric loading was investigated in one test series on 3 x 2 anchor groups. In this test series the load was applied at a distance $e_1 = 40$ mm away from the center of gravity of all anchors within the group. The same configuration was also tested in another test series with centric loading, which allows a direct comparison of the influence of eccentricity on the anchorage behavior. In all tests, the baseplate was fastened to the concrete slab by means of a bonded anchor system, which comprises a two-component injection system and a high-strength threaded rod. The threaded rods had a size of M16 and strength class 8.8. The anchors were embedded in the concrete with an effective embedment depth of $h_{ef} = 80$ mm. The embedment depth of the anchors was kept constant in all tests to allow the direct comparison of various anchor configurations. The tests were performed in uncracked and unreinforced slabs made of normal strength concrete (C20/25). Thereby, the anchor groups were positioned in a way to exclude any influence of neighboring anchor groups or close edges. In general, the clear distance between the closest anchors of different anchor groups or to the edge was at least $4h_{ef}$. This approach was also followed in Bokor et al. (2019a). As mentioned at the beginning, the focus of the investigation is on the concrete breakout failure, which is why parameters, such as the diameter of the anchors, the embedment depth of the anchors, or the concrete strength were designed, as well as an unconfined tests setup was employed to facilitate the formation of desired failure mode.

The designation of the individual test series indicates the type of anchor system used in the tests (BA for bonded anchor), the layout of the anchor group (m x n, where m is the number of anchor rows and n is the number of anchors in a row), and the type of loading (stat for monotonic loading and cyc for cyclic loading). The letters A, B, and C distinguish between anchor configurations with the same layout in case of 2 x 1 and 2 x 2 configurations. Here, A implies that the spacing between the anchors in the orthogonal directions equals the effective embedment depth ($s_1 = s_2 = h_{ef}$); B implies that the spacing between the anchors in the orthogonal directions equals twice the effective embedment depth ($s_1 = s_2 = 2h_{ef}$); and C implies that in one direction the anchor spacing equals the effective embedment depth ($s_2 = h_{ef}$) while in the other direction the spacing equals twice the effective embedment depth ($s_1 = 2h_{ef}$).

Alternatively, the letters C and E specify the point of load application in case of 3 x 2 anchor groups, where C implies centric loading and E implies eccentric loading.

Table 8.1. Experimental program on anchor groups subjected to monotonic and cyclic tension load.

Test ID	Group layout	Baseplate dimensions (mm)	$s_1^{(1)}$ (mm)	$s_2^{(1)}$ (mm)	$e_1^{(2)}$ (mm)	$f_{c,m}^{(3)}$ (N/mm²)	Number of tests
BA-1x1-stat-A		-	-	-	-	21.98	3
BA-1x1-cyc-A			-	-	-	21.98	3
BA-1x1-stat-B		-	-	-	-	22.26	3
BA-1x1-cyc-B			-	-	-	22.26	4
BA-2x1-A-stat		160x80x25	80	-	-	21.98	3
BA-2x1-A-cyc			80	-	-	21.98	3
BA-2x1-B-stat		240x80x25	160	-	-	21.98	3
BA-2x1-B-cyc			160	-	-	21.98	3
BA-2x2-A-stat		160x160x25	80	80	-	21.98	3
BA-2x2-A-cyc			80	80	-	21.98	3
BA-2x2-B-stat		240x240x25	160	160	-	22.26	3
BA-2x2-B-cyc			160	160	-	22.26	4
BA-2x2-C-stat		240x160x25	160	80	-	22.26	3
BA-2x2-C-cyc			160	80	-	22.26	4
BA-3x2-C-stat		240x160x25	80	80	-	22.28	3
BA-3x2-C-cyc			80	80	-	22.28	4
BA-3x2-E-stat		240x160x25	80	80	40	22.26	3
BA-3x2-E-cyc			80	80	40	22.26	4

(1) Anchor spacing
(2) Load eccentricity
(3) Mean cylinder concrete compressive strength at the time of testing

8.2 Description of the tested anchor configurations and test specimen

To fasten the baseplates to the concrete slabs, the same two-component injection system, FIS EM Plus, was used as in the experimental part on single anchors. For this reason, no detailed description of the bonded anchor system is given here, and reference is made to the description provided in Chapter 5. The high-strength threaded rods had a size of M16 and strength class 8.8 with a specified yield strength of $f_y = 640$

N/mm² and specified ultimate strength of f_u = 800 N/mm². The baseplates used to connect the individual anchors were made of S235JR steel with a characteristic yield strength of f_y = 235 N/mm². In all tests, the baseplates had a thickness of 25 mm, while the remaining dimensions were varied as required by anchor configuration. Holes with a diameter of 18 mm were cut into the steel to allow the anchor rods to pass through the baseplate and to comply with the stipulated hole clearance for M16 anchor rods. The baseplates were loaded at a single point, using a M20 threaded rod, which was connected to the servo-hydraulic cylinder. Therefore, a M20 internally threaded hole was cut into the baseplate. In case of centric loading, the internal thread was cut at the center of gravity of all anchors within the group. Figure 8.1 shows the dimensions of the baseplates used in the respective test series. Note that the circle marks the point of load application.
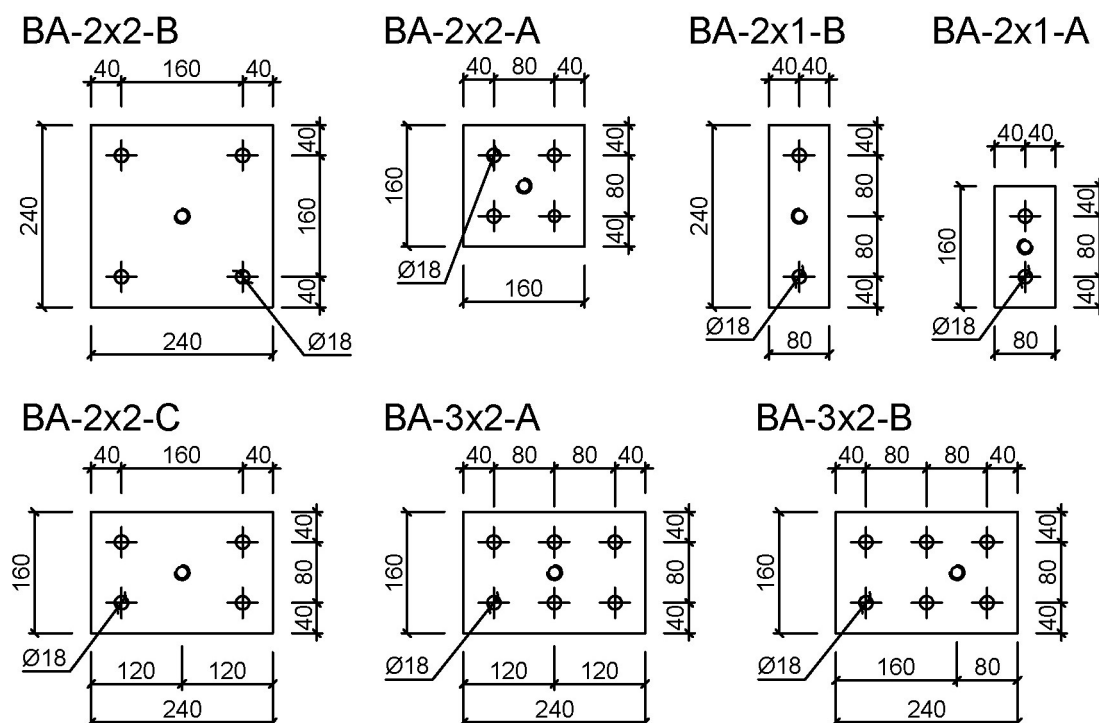
Figure 8.1. Dimensions of the anchor group configurations used in the experiments. (Note: All dimensions are in mm).

The tests were performed in uncracked concrete slabs with a side length of 1635 mm and a thickness of 300 mm. Besides nominal reinforcing bars with a diameter of 6 mm on the edges of the concrete slabs to facilitate handling of the specimens, no reinforcement was provided. The slabs were produced using concrete in accordance with DIN EN 206, whereby the composition of the aggregates was chosen in such a way that a grading curve between the standard grading curves A16 and B16 according to DIN EN 206 was obtained. The concrete mixture included a Portland cement CEM I 32.5 R. Due to the number of required concrete slabs, three concrete batches were needed for casting the specimens. When conducting the experiments, it was made

sure that all tests of a particular test series were carried out in specimens of the same concrete batch. For each concrete batch the concrete cube compressive strength was measured at the time of testing. For this purpose, six additional concrete cubes with a side length of 150 mm were cast for each batch, which were used to determine the compressive strength at the time of testing. The respective converted cylinder concrete compressive strength, $f_{c,m}$, for each test series is given in Table 8.1. Note that the conversion factor $k_{cyl/cube} = 0.82$ was applied (see Section 5.3 and DIN EN 206, Fingerloos et al. (2015), and Loch (2014)).

8.3   Description of the experimental setup and testing procedure

8.3.1   Experimental setup

Figure 8.2 shows the experimental setup utilized to execute the tests. Two I-beams were placed directly on the concrete slabs which were used as supports on both sides of the anchor groups. The beams were placed in such a way that the clear distance to the outermost anchors was at least $2h_{ef}$ as stipulated in EOTA TR 048 for an unconfined test setup. On top of the two I-beams, the test rig is placed, on which the servo-hydraulic cylinder is mounted. The servo-hydraulic cylinder has a capacity of 250 kN and was used to apply the tension load to the baseplate. To this purpose the servo-hydraulic cylinder and the baseplate were connected via a high-strength M20 threaded rod, and a special hinge as shown in Figure 8.2 (a). The interposition of the hinge between the servo-hydraulic cylinder and the baseplate provides for unobstructed rotation of the baseplate. In this way a redistribution of forces among the anchors is facilitated, which is particularly important in case of eccentric loading.
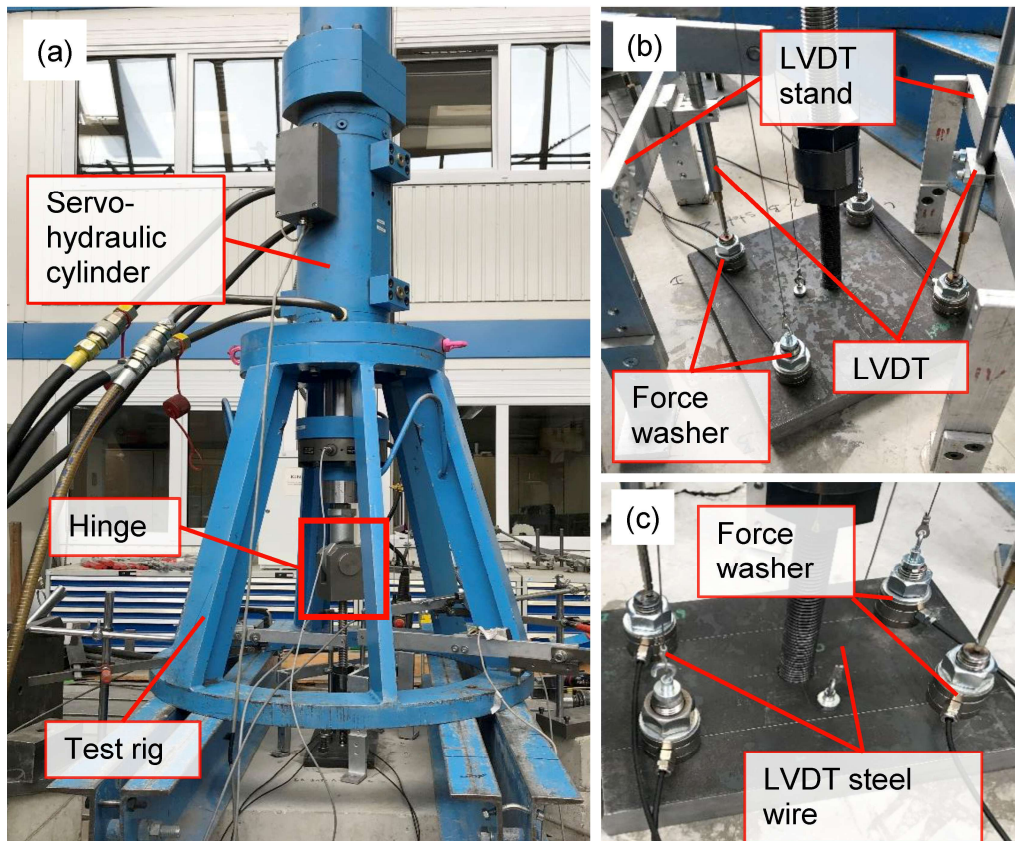
Figure 8.2. Experimental setup.

8.3.2   Instrumentation

Throughout the experiments, the total force on the anchor group, the displacements of the anchor group and the individual anchors in the direction of loading, as well as the individual axial anchor forces were constantly monitored via a data acquisition system. A calibrated load cell with a measuring range up to 250 kN was used to measure the total force on the anchor group. Strain gauge-based force washers with two additional hardened washers were mounted on the individual anchors just above the baseplate and beneath the nut. These strain gauge-based force washers were able to monitor the axial forces of individual anchors within a group up to a load of 200 kN. However, it should be noted that the individual anchor forces were only measured in test series BA-2x2-B, BA-2x2-C, BA-3x2-C, and BA-3x2-E. The total displacement of the anchor groups was measured as close to the point of load application as practically possible as shown in Figure 8.2 (b) and (c). Thereby, an indirect measurement approach was applied, where the LVDT was mounted to a separate stand and connected to the baseplate by means of a steel wire. In case of the 2 x 1 anchor groups, the individual anchor displacements were measured directly on top of the anchors. To be able to measure the displacement directly, the LVDTs were mounted on special bridge-like stands, which were then fixed to the concrete slab. A figure of these bridge-like stands is shown in Figure 8.2 (b). In case of 2 x 2 anchor groups, for practical reasons, both

direct and indirect measurement of the anchor displacement was applied. It can be seen in Figure 8.2 (b) that the displacements of each two diagonally opposed anchors were measured either directly or indirectly. In a similar way, the anchor displacements and individual axial forces were measured in case of the 3 x 2 groups. However, due to practical considerations, only four anchors were considered. The point of reference for the measurement of the displacement is the surface of the concrete slab.

8.3.3 Testing procedure

After the installation of the anchors following the manufacture's installation instructions (ETA-17/0979), the experimental setup was assembled, and the test was started. In the monotonic tension tests, the load was applied under a quasi-static loading rate in such a way that the ultimate load of the anchor groups was reached within one to three minutes. In the cyclic tension tests, the displacement-controlled protocol for pulsating tension load, introduced above, was applied. However, some adjustments had to be made. While in case of the single anchor tests, the displacement values required for defining the loading protocol, s_u and s_{max}, refer to the anchor displacement, in case of anchor groups the individual anchor displacements and the displacement of the baseplate were too small to control the hydraulic system with these displacement values. This is attributable to the bonded anchors which show a rather stiff behavior and the increased stiffness of the complete system due to the increased number of anchors. Instead, the displacement of the servo-hydraulic cylinder itself was used as the control parameter for the test protocol. However, the displacements of the baseplate and individual anchors were continuously recorded. Note that when referring to the displacement of the anchor group in the discussion section, the displacement measured on the baseplate as close to the point of loading as possible is meant.

In the first cyclic tests on anchor groups, it was observed that the displacements obtained in the first displacement level were too small to derive any meaningful information from it. Therefore, the cyclic loading protocol in test series BA-2x2-B-cyc, BA-2x2-C-cyc, BA-3x2-C-cyc, and BA-3x2-E-cyc was altered. More precisely, this means that the initial displacement levels were modified, and a seventh displacement level was added in the ascending branch of the load-displacement curve, increasing the total number of displacement levels to ten. As a result, the modified displacement levels in the initial phase correspond to 20%, 40%, 60%, 70%, 80%, 90% and 100% of s_u. The three subsequent displacement levels in the post-peak phase were not altered and follow the same principles as described before.

8.4 Experimental results and discussion

A summary of the results in terms of loads, displacements, and stiffness values is given in Table 8.2. Furthermore, Table 8.2 shows the coefficients of variation of the ultimate loads for each test series. It can be seen that the scatter of the test results in terms of the capacities is rather low.

The following subsections will discuss the behavior of anchor groups with respect to the influence of the anchor spacing and the number of anchors, the influence of eccentric loading, and the performance of the individual anchors in a group. Where required for the discussion, the respective load-displacement curves are presented. Note that the load-displacement curves shown in this section represent the total force on the anchor group and the displacement measured on the baseplate as close to the point of loading as possible.

Table 8.2. Summary of experimental results (Stehle and Sharma, 2021b).

Test ID	Ultimate load, N_u (kN)				$N_{u,m}$[1] (kN)	$CV(N_u)$ (%)	$s_{u,m}$[2] (mm)	$k_{Nu,m}$[3] (kN/mm)	$k_{50\%Nu,m}$[4] (kN/mm)
	1	2	3	4					
BA-1x1-stat-A	50.5	44.0	53.4	-	49.3	8.0	0.56	94.3	347.2
BA-1x1-cyc-A	53.3	57.0	48.8	-	53.0	6.3	0.64	91.6	324.9
BA-1x1-stat-B	42.4	47.4	42.6	-	44.2	5.2	0.57	82.3	323.5
BA-1x1-cyc-B	51.8	48.0	44.3	48.9	48.3	5.6	0.60	89.7	272.9
BA-2x1-A-stat	65.2	55.5	62.4	-	61.0	6.7	0.44	148.3	494.2
BA-2x1-A-cyc	60.7	59.9	59.5	-	60.0	0.8	0.35	178.3	478.6
BA-2x1-B-stat	70.5	65.8	68.3	-	68.2	2.8	0.64	109.7	-
BA-2x1-B-cyc	70.1	72.0	71.4	-	71.2	1.1	0.55	129.9	259.9
BA-2x2-A-stat	78.0	78.9	69.5	-	75.5	5.6	-	-	-
BA-2x2-A-cyc	88.4	79.6	78.3	-	82.1	5.5	0.27	292.6	767.4
BA-2x2-B-stat	134.1	132.4	131.8	-	132.8	0.7	0.59	224.8	314.8
BA-2x2-B-cyc	125.0	131.2	133.3	129.0	129.6	2.4	0.49	272.0	372.8
BA-2x2-C-stat	100.5	93.7	100.3	-	98.2	3.2	0.40	247.1	456.4
BA-2x2-C-cyc	106.3	96.0	94.4	96.3	98.2	4.8	0.41	247.7	439.4
BA-3x2-C-stat	98.8	109.0	98.4	-	102.1	4.8	0.30	424.6	764.9
BA-3x2-C-cyc	86.4	94.5	94.1	98.0	93.2	4.6	0.29	385.7	807.4
BA-3x2-E-stat	84.9	80.9	80.2	-	82.0	2.5	1.04	214.9	498.9
BA-3x2-E-cyc	83.6	82.6	75.6	80.6	80.6	3.9	0.72	161.5	441.8

(1) Mean ultimate load
(2) Mean displacement at ultimate load
(3) Mean secant stiffness at ultimate load
(4) Mean secant stiffness at $0.5N_u$ in the ascending branch of the load-displacement curve

Figure 8.3 shows typical failure modes obtained from monotonic and cyclic tests. In all tests on anchor groups, the observed failure mode was concrete cone failure. In the single anchor tests, besides concrete cone failure, also a mixed concrete cone and pull-out failure was observed in some tests. With respect to the failure mode, generally no significant differences were found between monotonic and cyclic loading.

Figure 8.3. Typical failure modes obtained from monotonic and cyclic tension tests.

8.4.1 Comparison of the behavior of monotonically and cyclically loaded anchor groups

In accordance with the observations in the single anchor tests, cyclic loading had no significant adverse effect on the overall behavior of the tested anchor groups. Comparing the mean ultimate loads in Table 8.2, in principle, no major difference is discernable between cyclically and monotonically loaded anchor groups of the same configuration. In no cyclic test series did the deviations exceed 10% of the corresponding monotonic mean ultimate load, which is within the limits generally observed in the scatter of ultimate loads for post-installed anchors.

Figure 8.4 compares typical load-displacement curves obtained from monotonically and cyclically loaded single anchors and anchor groups. As can be seen, the envelopes of the cyclic curves match well with the monotonic load-displacement curves. Moreover, the mean secant stiffness values at ultimate load are in good agreement (see Table 8.2). Altogether the findings suggest that also with respect to the displacement behavior of single anchors and anchor groups, tension cycling appears to have no negative effect in case of concrete breakout failure.
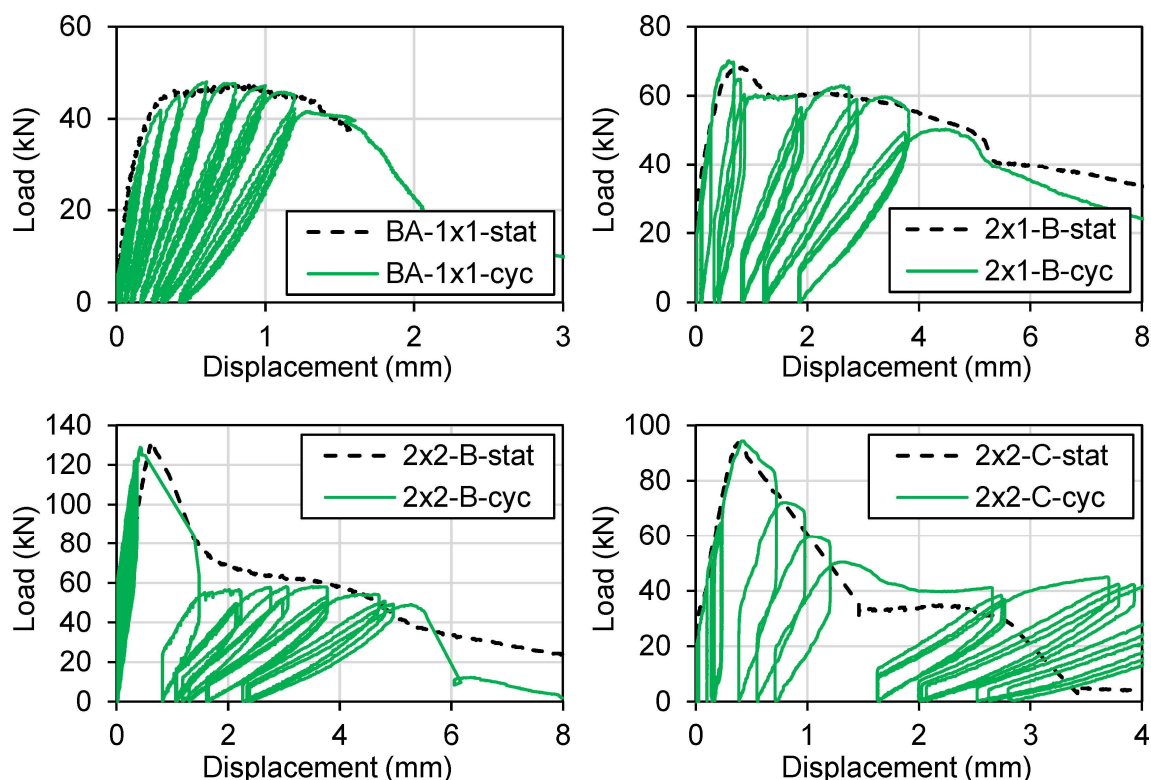
Figure 8.4. Comparison of the load-displacement behavior of single anchors and anchor groups when subjected to monotonic and cyclic loading.

8.4.2 Behavior of anchor groups with varying anchor spacing

In case of concrete cone failure, the spacing of anchors in a group has a strong influence on both the load capacity and the load-displacement behavior of anchor groups. While the impact on the capacity of the group is relatively well understood and described comprehensively in standard literature (Eligehausen et al., 2006), experimental investigations regarding the influence on the displacement behavior is rather limited. This is particularly true for anchor groups subjected to cyclic loading. Therefore, this section investigates the influence of anchor spacing on the overall displacement behavior and stiffness of an anchor group, as well as the impact on the distribution of forces among the anchors for anchor groups subjected to displacement-controlled pulsating tension load.

Figure 8.5 shows typical load displacement curves obtained from test series BA-2x1-A-cyc, BA-2x1-B-cyc, BA-2x2-A-cyc, and BA-2x2-B-cyc. In these test series, the 2 x 1 and 2 x 2 anchor groups were subjected to displacement-controlled pulsating tension load. In all four configurations, the anchor spacing is smaller than the critical anchor spacing for which individual anchors within a group would develop the full capacity of a single anchor. The upper graph in Figure 8.5 compares the behavior of 2 x 1 anchor groups in configuration A and B, where in configuration B the anchor spacing is twice

the spacing of configuration A. The larger anchor spacing results in a moderate increase of the total capacity of the anchor group, by around 10 kN. At the same time, it becomes apparent that the displacement behavior in the ascending branch and the stiffness of the anchor groups differ strongly. The increased anchor spacing in configuration 2x1-B causes larger initial displacements and a reduced initial stiffness of the complete anchor group (see Table 8.2), which is attributed to reduced flexural rigidity of the baseplate with increased anchor spacing. The mean secant stiffness at ultimate load obtained from tests with configuration 2x1-A is almost two times the value obtained in the corresponding single anchor reference tests. It appears that for this case, the two anchors dominate the displacement behavior of the group, while the deformation of the baseplate seems rather low. It can therefore be assumed that due to the rather small ratio between the spacing of 80 mm and the thickness of the baseplate, t = 25 mm, the baseplate is relatively rigid.
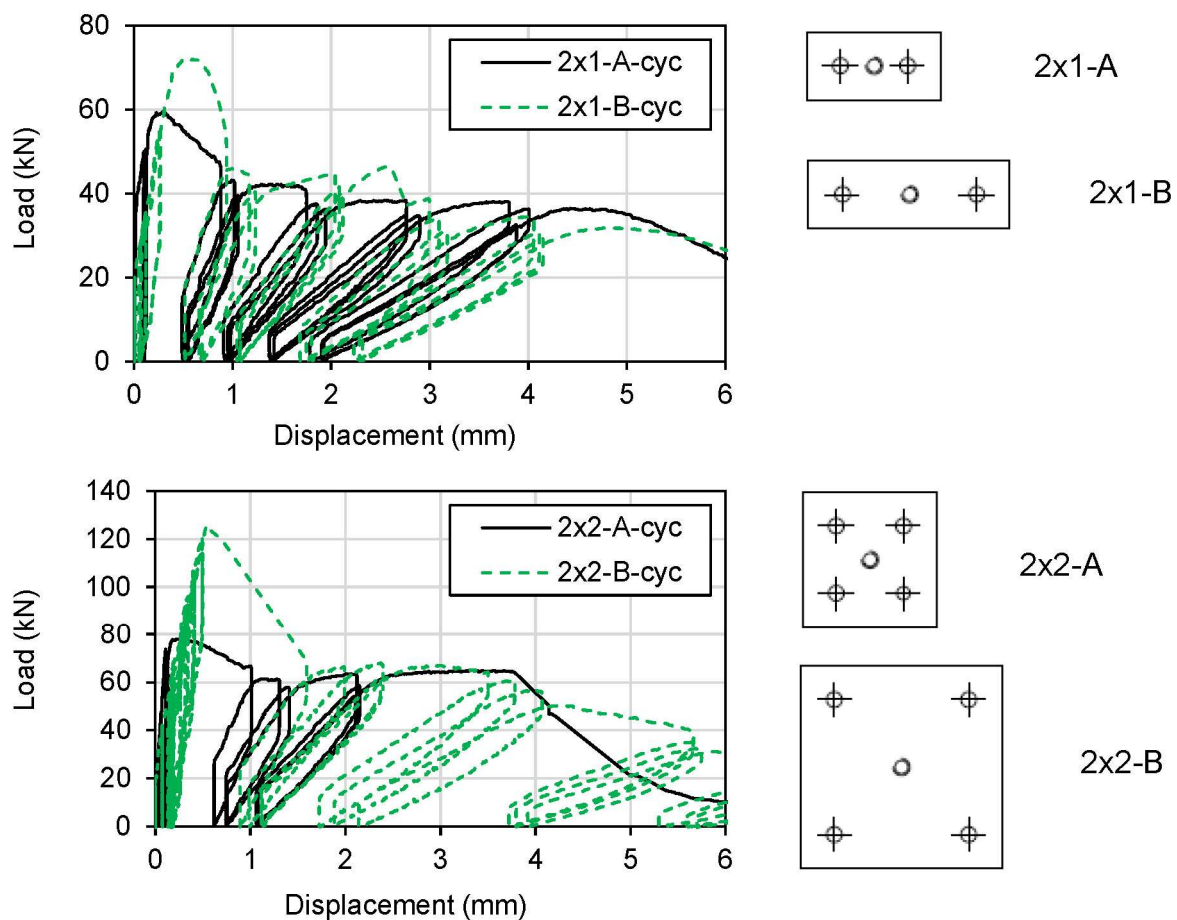
Figure 8.5. Typical load-displacement curves obtained from cyclic tests on 2 x 1 and 2 x 2 anchor groups. Comparison between configuration A and B (Stehle and Sharma, 2021b).

In case of the 2 x 2 anchor groups, the anchor spacing has a more pronounced effect on the capacity of the groups as can be seen in the lower graph in Figure 8.5. Doubling

the anchor spacing in both directions yields an increase in the peak load of almost 60% on average. At the same time, the initial stiffness at 50% of the ultimate load in the ascending branch reduces to approximately half by doubling the spacing. Since the anchor stiffness of anchors should be practically equal in both cases, the reduced stiffness for case B is attributed to the reduced flexural rigidity of the baseplate.

To exemplarily investigate the ratio between anchor stiffness and baseplate stiffness in more detail, the baseplates in case of the 2 x 1 configurations are simplified as a simply supported beam loaded centrically in tension. In this case the baseplate stiffness can be calculated as:

$$k_{Baseplate} = \frac{48 E_s I_{Baseplate}}{s_1^3},$$
(8.1)

where s_1 is the spacing between the anchors, E_s is Young's Modulus for steel and $I_{Baseplate}$ is the second moment of area. Considering E_s = 210000 N/mm², the baseplate stiffness for configuration 2x1-A and 2x1-B is 2051 kN/mm and 256 kN/mm, respectively. The theoretical consideration for the baseplate stiffness supports the previous findings. In case of configuration 2x1-A, the stiffness of the baseplate is significantly higher than the initial stiffness of a single anchor (on average around 300 kN/mm, see Table 8.2). Therefore, the stiffness of the complete group is dominated by the stiffness of the two anchors. In contrast, the stiffness of the baseplate in case of configuration 2x1-B is lower than the initial stiffness of a single anchor, which is why the contribution of the baseplate to the displacement behavior of the complete group is more relevant.

Figure 8.6 compares typical load-displacement curves obtained from test series BA-2x2-C-cyc and BA-3x2-C-cyc. In the corresponding configurations 2x2-C and 3x2-C the baseplate dimensions and the spacing of the outermost anchors are the same. However, in configuration 3x2-C, two more anchors are used to fasten the baseplate to the concrete specimen. These are placed in the middle of the baseplate, resulting in a reduced spacing between the anchors on the longer side (see Figure 8.1). When calculating the capacity of the two anchor groups according to the CCD method, in this case, the two additional anchors do not increase the capacity of the anchor group. This is due to the fact that in the event of concrete related failure, if the spacing between the anchors is not large enough (s < s$_{cr}$ = 3h$_{ef}$ according to EN 1992-4), the breakout cones of the individual anchors will overlap and form a common breakout body (Eligehausen et al., 2006). Accordingly, with decreasing anchor spacing, the capacity of the individual anchors reduces. The total capacity of the group, however, remains constant if the projected area is maintained. The design approach for anchor groups matches very well with the experimental results. In Figure 8.6 and by comparing the ultimate loads in Table 8.2, it can be seen that the ultimate loads obtained for both configurations are in a good agreement. While the capacity of the group remains the same if only the projected area is the same, the additional anchors will affect the

stiffness of the anchor group as becomes apparent from Figure 8.6. Thereby, the stiffness of the anchor groups is significantly higher in case of configuration 3x2-C with six anchors compared to configuration 2x2-C with four anchors. On average, considering both monotonic and cyclic loading, the initial stiffness increases by around 76% and the secant stiffness at ultimate load increases by around 64%. Assume that the entire group is simplified by two springs in series. Where one spring is characterized by the stiffness of the baseplate and the second spring is characterized by an equivalent spring, which represents the springs of the individual anchors in parallel. Then the stiffness of the baseplate can be back calculated as 715 kN/mm and 1396 kN/mm for configuration 2x2-C and 3x2-C, respectively. This much simplified approach is a rough approximation of the actual behavior. Mainly due to the fact that in case of the 3x2-C configuration, the anchors are not loaded uniformly, as will be shown below. Thus, following the results from the single anchor experiments, the varying load levels may result in different values for the anchor stiffness. However, it shows in a simplified way that the higher stiffness in configuration 3x2-C can be attributed on the one hand to the additional stiffness due to the two additional anchors, but on the other hand also to the reduced compliance of the baseplate resulting from the reduced anchor spacing.
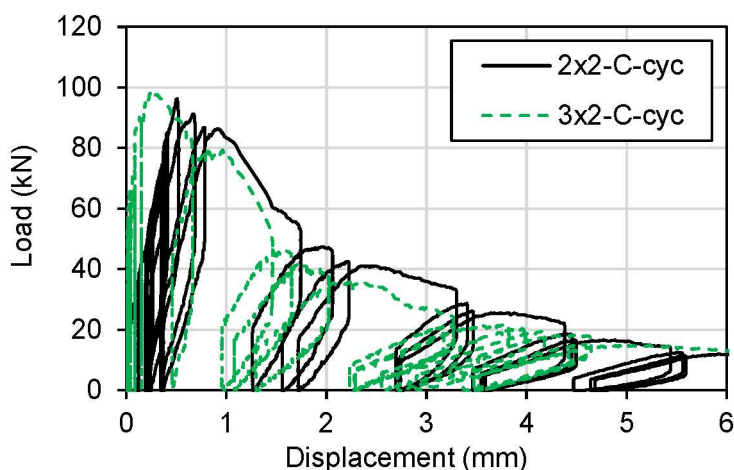
Figure 8.6. Comparison of typical load-displacement curves obtained from cyclic tests in test series BA-2x2-C-cyc and BA-3x2-C-cyc (Stehle and Sharma, 2021b).

Figure 8.7 (a) shows the force-time history with regards to the total forces on the anchor group and the individual axial anchor forces over the course of the experiments for configuration 2x2-C. For both monotonic and cyclic loading, the forces are equally distributed among the four anchors. The results show that cycling has no major influence on the distribution of forces among the anchors and all four anchors are simultaneously taking up the load. In case of 2 x 2 anchor groups the even distribution of forces might be attributed to the symmetric behavior under centric loading.

(a) Configuration BA-2x2-C

(b) Configuration BA-3x2-C

Figure 8.7. Total force on the anchor group and axial anchor forces measured over the duration of the experiment in case of monotonic and cyclic loading. (a) Configuration BA-2x2-C and (b) configuration BA-3x2-C. Time represents the recording time and not the loading time (Stehle and Sharma, 2021b).

In the same way, Figure 8.7 (b) shows the force-time history for configuration 3x2-C. Similarly, all anchors participate in the load transfer. However, it can be seen that the two anchors in the middle (anchor C and D) take up more load than the outer anchors. These two anchors are also loaded somewhat prior to the outer anchors. The delayed activation of the outer anchors is due to the fact that the point where the load is applied on the anchor group is very close to anchor C and D, while the distance from the outer anchors to the point of load application is larger. Therefore, the load is first transferred to the middle anchors while the activation of the outer anchors is shortly delayed. The uneven distribution of forces among the anchors suggests that the baseplate is not rigid. With a sufficiently stiff or rigid baseplate, all anchors would have taken almost the same load, which could have resulted in a higher capacity of the group. However, in order to achieve a sufficiently stiff baseplate according to the CCD method, where the forces are evenly distributed, it would have been required to significantly increase the thickness of the baseplate as indicated in a numerical study on a 4 x 1 anchor group conducted by Bokor et al. (2018). The results highlight the importance of considering

the behavior of the baseplate, even for conventional anchor configurations. Not considering the stiffness of the baseplate might result in an unfavorable behavior of the overall group and affects the distribution of forces among the anchors.

8.4.3   Behavior of anchor groups subjected to eccentric loading

The influence of eccentrically applied tension load was investigated on the 3 x 2 anchor groups in test series BA-3x2-E. The anchor configuration used in these test series is the same as in test series BA-3x2-C. Thus, the anchor spacing, and baseplate dimensions were the same. Only the point of load application was changed as illustrated in Figure 8.1. It is evident from the comparison of the load-displacement curves obtained from configuration BA-3x2-C and BA-3x2-E in Figure 8.8 that the load reduces due to eccentric loading. By applying the tension load with an eccentricity of e_1 = 40 mm, the mean ultimate load reduces by around 20% in case of monotonic loading and by around 14% in case of cyclic loading. As can be seen from the results presented in Table 8.2, the mean ultimate loads obtained in the monotonic and cyclic test series with configuration 3x2-E are almost equal, while the differences between monotonic and cyclic loading is more pronounced in case of configuration 3x2-C, where the mean ultimate load in the cyclic tests is around 10% lower than in the monotonic tests. Hence, the greater reduction in load due to load eccentricity observed in monotonic tests can be explained by the lower mean capacity in test series BA-3x2-C-cyc.

The fact that eccentric tension loading has a marked negative effect on the capacity of an anchor group is relatively well known (Eligehausen et al., 2006). Equally important, the comparison of the load-displacement behavior in Figure 8.8 indicates that also the stiffness of the anchor group reduces significantly when loaded eccentrically in tension. Note that the displacement is measured close to the point of loading in both centric and eccentric loading cases.
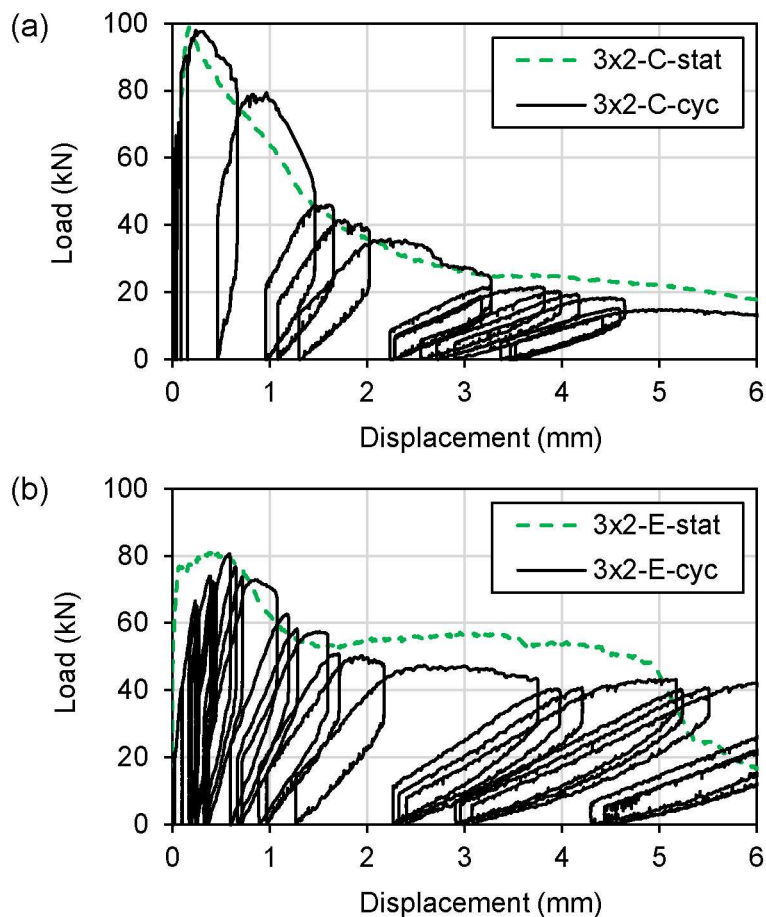
Figure 8.8. Typical load-displacement curves obtained for configuration (a) BA-3x2-C (upper graph) and (b) BA-3x2-E (lower graph) for monotonic and cyclic loading (Stehle and Sharma, 2021b).

In Table 8.2, the mean secant stiffness at ultimate load and at 50% of the ultimate load are given for the corresponding test series. At ultimate load, the secant stiffness for BA-3x2-E under eccentric loading reduces by around 49% - 58% and at $0.5N_u$ in the ascending branch, the secant stiffness reduces by around 35% - 45% compared to the corresponding values obtained for BA-3x2-C under centric tension. This severe reduction of the stiffness suggests that not all anchors in the group are simultaneously activated and thus the contribution of the individual anchors to the overall stiffness of the anchor group might vary significantly throughout the course of the experiment. Figure 8.9 shows the force-time history for the eccentrically loaded 3 x 2 anchor group under cyclic loads. It should be noted that in each test, the axial forces were only monitored on four anchors. In the upper graph (monotonic loading), the four anchors closest to the point of load application were monitored. It can be seen that primarily the outer anchors A and B are taking up the load. With delay, also the middle anchors C and D are activated and participate in the load transfer. However, the contribution of anchor C and D is markedly lower, which is particularly evident at the point where the group reaches its ultimate load. The lower graph shows the force-time history for the

cyclic loading case, where in one test also anchor F was monitored. Anchors E and F are located farthest away from the point of load application, and as can be seen in Figure 8.9, anchor F carries almost no load. The experimental results indicate that in case of eccentric loading of the tested 3 x 2 groups, only four anchors are activated while the outermost two anchors do not take up any tension forces. The influence which the sequence of activation of the anchors has on the stiffness of the anchor group may also be determined by comparing the stiffness values obtained from configuration BA-3x2-E to the values obtained from configuration BA-2x1-A. Initially, the stiffness of both configuration matches rather well. As shown before, the stiffness of configuration BA-2x1-A is mainly dominated by the stiffness of the two anchors, which indicates that in case of BA-3x2-E, mainly anchors A and B are initially activated. At ultimate load, the secant stiffness observed for configuration BA-3x2-E is higher than the secant stiffness of configuration BA-2x1-A, indicating that at this point also anchors C and D are activated. In conclusion, both the sequence of activation and the contribution of only four anchors explains the reduced stiffness of the eccentrically loaded anchor groups.

8.4.4   Investigation on the individual anchor behavior

So far, the discussion was mainly focused on the overall behavior of the anchor groups. However, in order to fully understand the behavior of an anchor group, it is necessary to know the behavior of the individual anchors within the group. Therefore, this section deals with the displacement behavior of individual anchors within the group and compares their behavior to the behavior of the reference single anchors. Similar to the evaluation of the single anchors in Chapter 5, the evaluation focuses on the secant stiffness of the anchors and their unloading and reloading behavior.

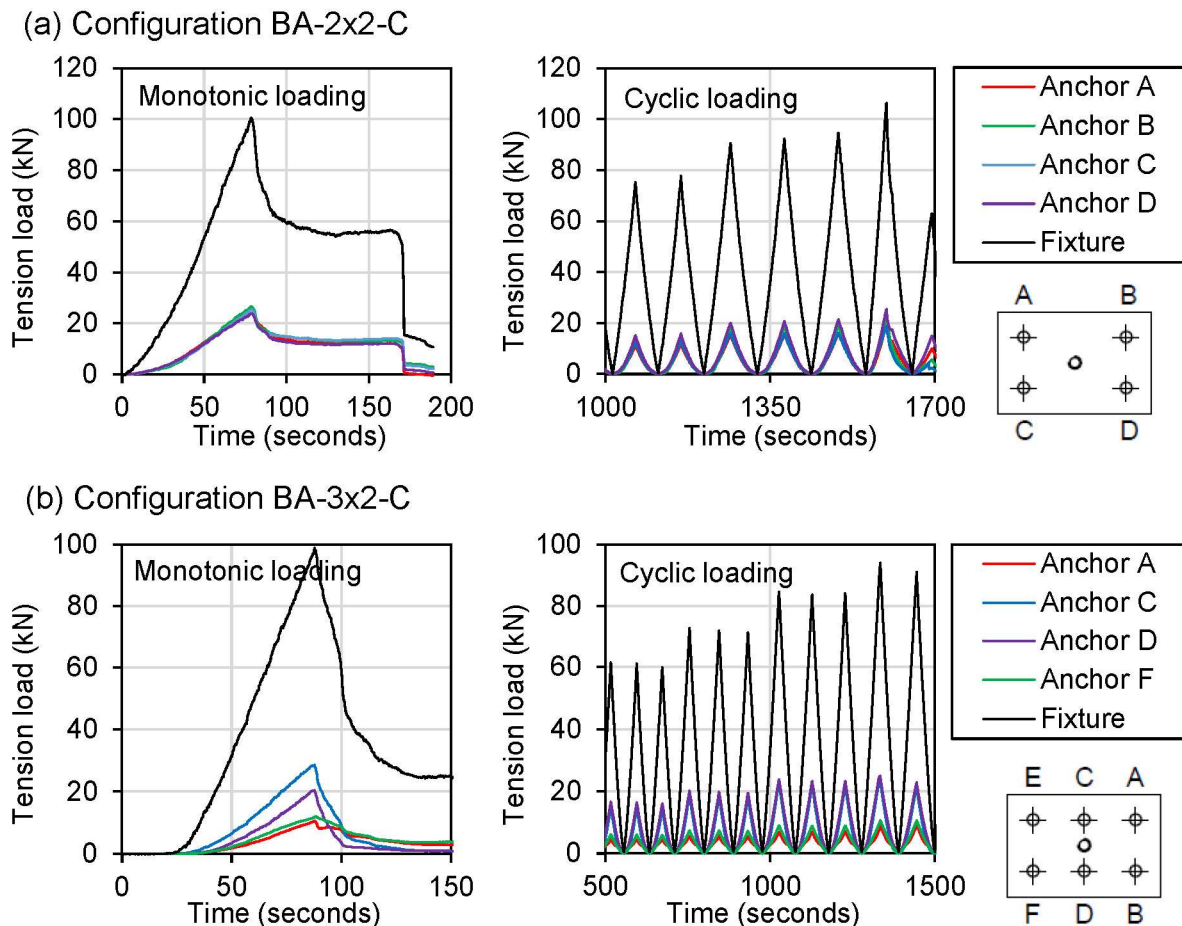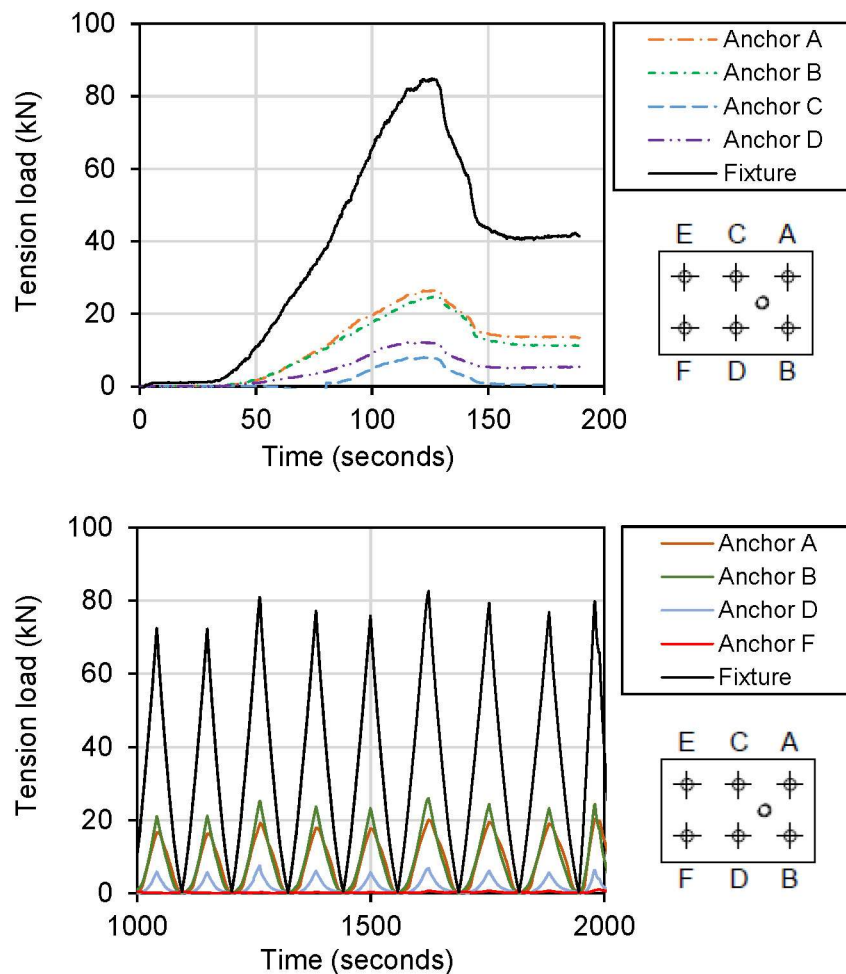Figure 8.9. Typical force-time history for configuration BA-3x2-E. Total force on the anchor group and axial anchor forces measured over the duration of the experiment in case of monotonic (upper graph) and cyclic loading (lower graph). Time represents the recording time and not the loading time (Stehle and Sharma, 2021b).

8.4.4.1 Evaluation of the secant stiffness

Figure 8.10 shows the secant stiffness obtained from single anchor tests and from the individual anchors within the tested groups at (a) 50% of the ultimate load in the ascending branch and (b) at ultimate load. Thereby, both monotonic and cyclic tests are considered. The stiffness values are presented as a function of the ratio between the ultimate axial anchor force, $N_{u,i}$, and the mean ultimate load obtained from the single anchor reference tests, $N_{u,m,ref}$. Thus, if an anchor cannot achieve its full capacity due to the presence of neighboring anchors within a group, the ratio decreases the closer the anchors are placed to each other. Note that in test series BA-2x1-A-stat, BA-2x1-A-cyc, BA-2x1-B-stat, BA-2x1-B-cyc, BA-2x2-A-stat, and BA-2x2-A-cyc, no force washers were applied to measure the individual axial anchor forces. However, in order to evaluate the secant stiffness values, an equal distribution of forces among the anchors is assumed. Considering the results discussed so far and the symmetry of the

groups with respect to the configuration and loading, it can be assumed that this approach reflects the real behavior with a sufficient degree of accuracy. Figure 8.10 (a) shows the secant stiffness at 50% of the ultimate load. It can be seen that the stiffness values range between 200 kN/mm and 400 kN/mm with a mean value of around 300 kN/mm. Thereby, the stiffness of the individual anchors within a group generally matches the stiffness observed in the reference single anchor tests. From the linear regression over all test results (black line), it appears that the initial stiffness slightly increases with increasing load received by an anchor of the group relative to the mean ultimate load obtained from the single anchor reference tests. However, due to the relatively large scatter of the test results, the increase is considered as negligible. Figure 8.10 (b) shows the secant stiffness of the anchors at ultimate load. The stiffness values with respect to anchors in a group range between 50 kN/mm and 200 kN/mm with a mean value of around 125 kN/mm. Thus, the values are rather in the upper range of the stiffness determined in the single anchor tests, where the values for k_{Nu} in the tests ranged between 50 kN/mm and 115 kN/mm. The deviation is partly attributable to the high scatter of the test results. Including the single anchor tests, the coefficient of variation of the secant stiffness at ultimate load is 34%. The large scatter, which is particularly evident for the anchors in the group (even smaller displacements than in the single anchor tests), can be explained by the probable errors of measurement at small displacement levels and lower accuracy of washer load cells compared to global load cells. Note however, that the coefficient of variation is smaller than the limit value for the displacement at 50% of the ultimate load in the residual pull-out test stipulated by EOTA TR 049. In summary, it seems that the overall displacement behavior and the stiffness of an anchor is rather unaffected by the anchor configuration or neighboring anchors. In principle the behavior of anchors in a group matches the behavior observed in single anchor tests. Nonetheless, given the relatively large scatter, a note of caution is due here with respect to the interpretation of the results.

(a)

(b)
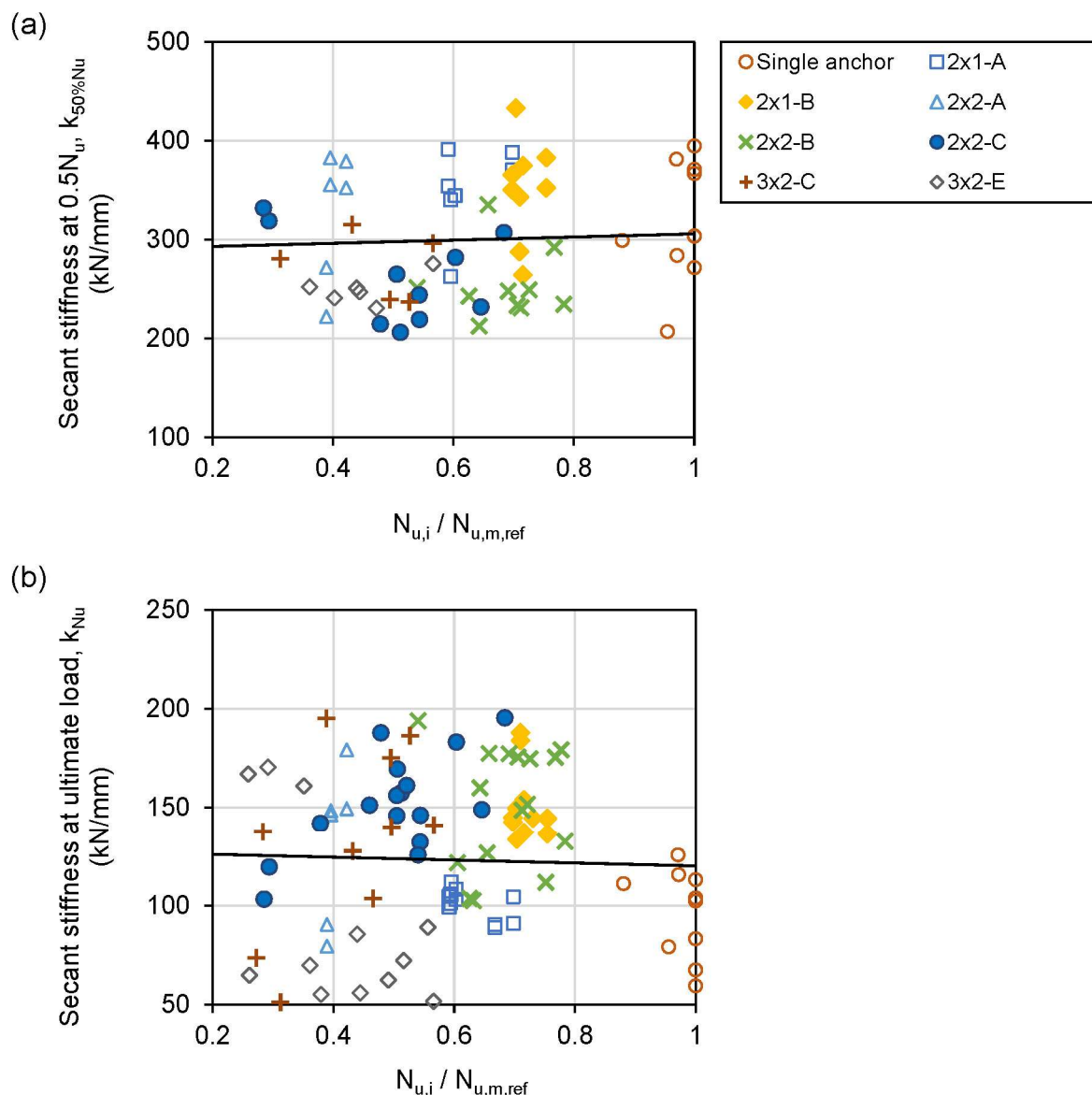
Figure 8.10. Anchor stiffness as a function of the ratio between the individual ultimate axial anchor force and the mean ultimate load obtained for the reference single anchors. (a) Secant stiffness at 50% of the ultimate capacity and (b) secant stiffness at ultimate load (Stehle and Sharma, 2021b).

8.4.4.2 Evaluation of unloading and reloading stiffness

The evaluation of the unloading and reloading stiffness follows the principles described above for the evaluation of different types of post-installed anchors. First, the single anchor tests are evaluated to provide a basis for the comparison of the behavior of individual anchors in a group. The stiffness values are plotted in Figure 8.11 (a) as a function of the ratio between the maximum displacement s_i in the respective cycle "i" and the ultimate load obtained in the corresponding cyclic test, s_u. Accordingly, a ratio smaller than one implies a displacement level in the ascending branch of the load-displacement curve, whereas a ratio greater than one implies a displacement level in

the post-peak range of the load-displacement curve. It is worth mentioning that the evaluation includes more than 160 stiffness values for both unloading and reloading stiffness. The hysteretic behavior observed in the single anchor tests matches very well with the behavior previously observed for the same type of anchor (see Chapter 5). In the beginning, at smaller displacement levels, the tested anchors show a high unloading and reloading stiffness. With increasing displacement of the anchors, a strong reduction of the stiffness can be observed. At a displacement level of around $0.5s_u - 1.0s_u$, the regression curve starts to flatten, and the stiffness degradation becomes more gradual. Figure 8.11 (b) presents the unloading and reloading stiffness for individual anchors in a group in various configurations. The two graphs show the evaluation of more than 500 stiffness values. In addition, the regression curves are plotted for each configuration, respectively. It can be seen that in general, the behavior of the individual anchors in a group agrees well with the behavior observed in the single anchor tests. However, the observed scatter is significantly higher. Whereby especially anchors in configuration BA-3x2-C and BA-3x2-B deviate from the behavior of single anchors. In particular, the stiffness degradation in the beginning is stronger. Again, the large scatter is mainly attributable to the accuracy of measurement at small displacement levels. Especially in case of individual anchors in a group, the corresponding displacements are notably smaller than the displacements of anchors determined from single anchor tests. This may also explain (in parts) the deviation between the stiffness of anchors in a group and the stiffness obtained in the single anchor tests. Despite the larger scatter, the experimental results show a clear tendency of the behavior of individual anchors in a group towards the behavior observed in the single anchor reference tests.
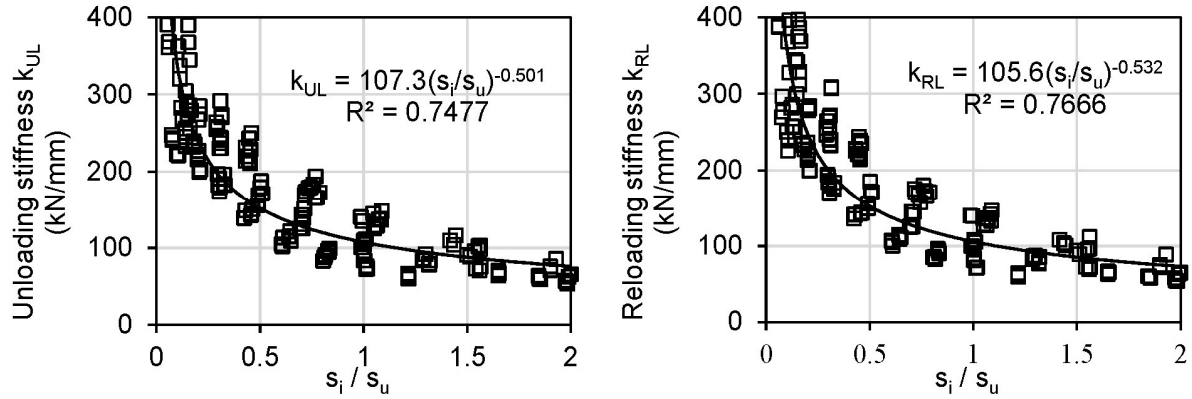
(a) Single anchor reference tests
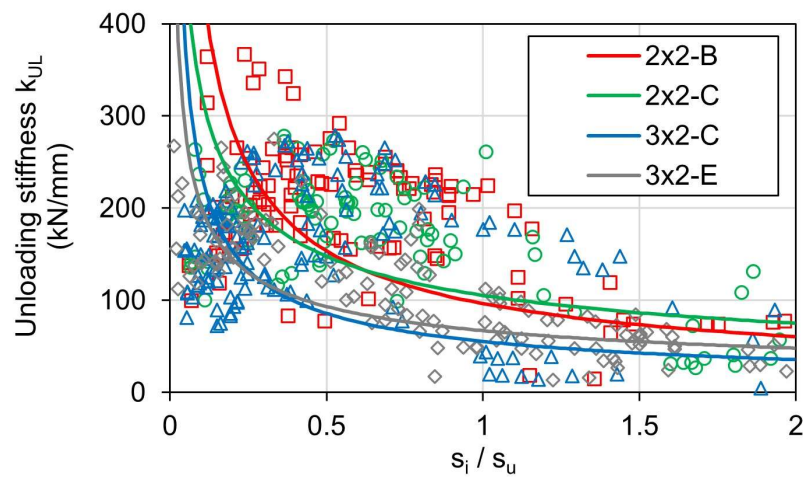
(b1) Individual anchors in a group – Unloading stiffness
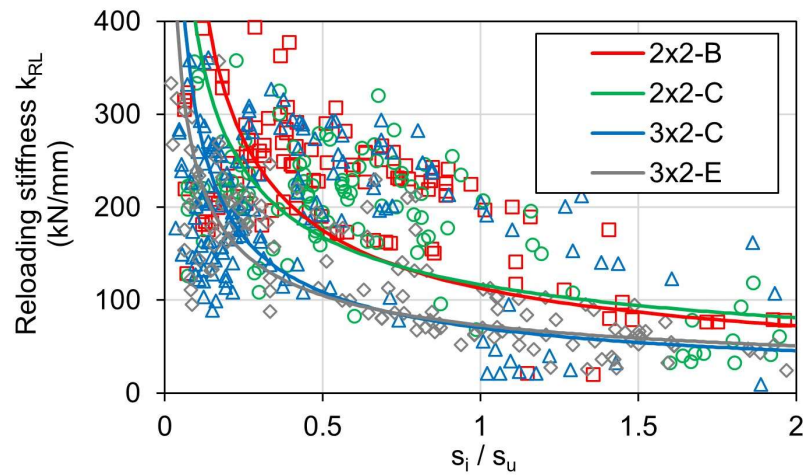
(b2) Individual anchors in a group – Reloading stiffness

Figure 8.11. (a) Unloading (left) and reloading (right) stiffness obtained from single anchor tests and (b1) unloading stiffness and (b2) reloading stiffness obtained from individual anchors in a group in configuration BA-2x2-B, BA-2x2-C, BA-3x2-C, and BA-3x2-E (Stehle and Sharma, 2021b).

From the results given in Figure 8.11, it can be seen that the progression of the unloading and reloading stiffness of the tested anchors (both in a group and single anchor) is rather similar. This accords with the earlier observations in Chapter 5, where in case of bonded anchors a similar unloading and reloading behavior was observed. Figure 8.12 shows the ratio between unloading and reloading stiffness for single anchors (red circles) and individual anchors in a group (black squares). The results are plotted as a function of the displacement ratio s_i/s_u, described above. It should be noted that the results given in Figure 8.12 only consider values for $s_i/s_u \geq 0.2$. As suspected, the unloading and reloading stiffness determined from single anchor tests correspond well. The values are evenly distributed above and below a line corresponding to k_{UL}/k_{RL} = 1. For single anchors the average of the stiffness ratio is 1.01 with a coefficient of variation of 5%. It can be seen that in case of individual anchors in a group, the scatter increases markedly. In particular at smaller displacement levels, the values are rather distributed below the line corresponding to k_{UL}/k_{RL} = 1. The larger scatter is also evident from the coefficient of variations which increases to 20%. However, the value for the stiffness ratio does not deviate from one by more than 10%. Therefore, the experimental results support the conclusion that for the tested bonded anchors, the unloading and reloading stiffness at the same displacement is almost identical.
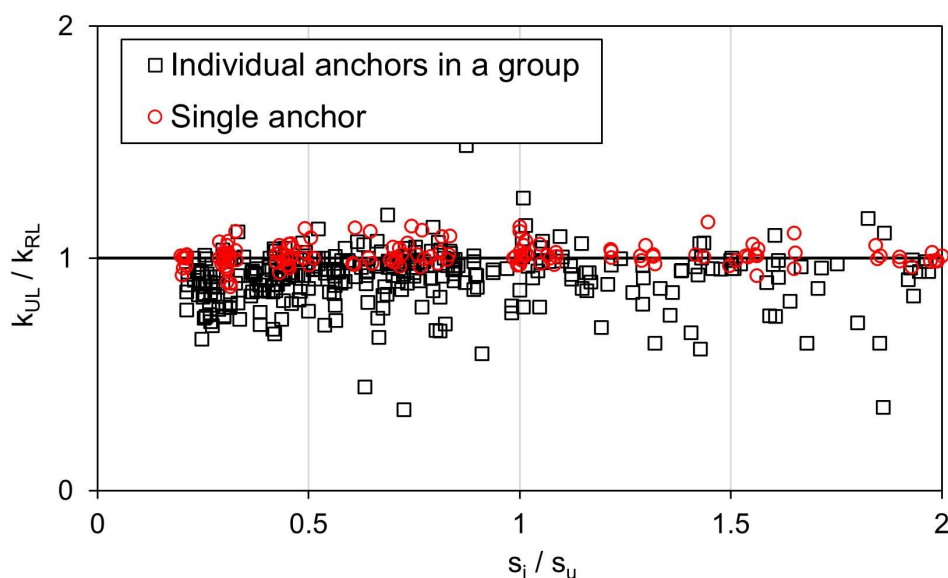
Figure 8.12. Comparison of the unloading stiffness k_{UL} and the reloading stiffness k_{RL} for the tested bonded anchors (Stehle and Sharma, 2021b).

8.5 Summary

Similar to the behavior of single anchors, the experimental results indicate that the behavior of anchor groups subjected to displacement-controlled pulsating tension load does not significantly deviate from the behavior under monotonic loading. The envelope of the cyclic load-displacement curves essentially follows the respective

monotonic curves and the mean ultimate loads and secant stiffness values obtained from cyclic tests are in a good agreement with the results obtained in the monotonic tests. Therefore, the following conclusion can be drawn for both monotonically and cyclically loaded anchor groups:

1. Comparing the behavior of anchor groups with varying anchor spacing but same number of anchors in the group has shown that the stiffness or flexibility of the baseplate has a significant influence on the displacement behavior of the tested anchor groups and the distribution of forces among the anchors. This finding is in accordance with the findings reported in Bokor (2021). Thereby, increasing the anchor spacing in the experiments resulted in a marked reduction of the overall stiffness of the anchor groups. Moreover, the experimental results showed that in test series 3x2-C the forces were not equally distributed among the individual anchors, thus indicating that, although the baseplate thickness may be presumed as rather thick, the rigidity of the baseplate was not high enough to guarantee an even distribution of forces.

2. Eccentrically applied tension load affects not only the capacity of an anchor group but also its displacement behavior and stiffness. The resulting reduction of the overall stiffness is attributable to the observation that the anchors in the group are not activated simultaneously. Moreover, the anchors placed farthest away from the point of loading in the tested 3 x 2 anchor groups were barely activated at all.

3. A comparison between the secant stiffness values of individual anchors in a group and single anchors suggests that the displacement behavior of anchors is essentially unaffected by neighboring anchors in a group. This finding is in accordance with the findings reported in Bokor (2021).

The displacement-controlled protocol for pulsating tension load further allowed the evaluation of the hysteretic behavior of single anchors and individual anchors within an anchor group with respect to the unloading and reloading behavior. The following conclusions can be drawn from the experimental results:

4. In the initial loading phase, the tested bonded anchors show a very stiff behavior. However, both unloading and reloading stiffness degrade rather strong with increasing anchor displacement. Thereby, the behavior of individual anchors in a group and the behavior of single anchors principally matches well.

5. In case of the tested bonded anchors, regardless of whether they were arranged in an anchor group or tested alone, the unloading and reloading stiffness at the same displacement level is rather similar.

9

Experimental investigation on anchor groups in narrow concrete members under monotonic tension load

In the experiments reported earlier in the thesis, the anchors and anchor groups were placed in concrete slabs such that there was no influence of any nearby edge on the behavior of the anchorages. These tests represent the behavior of anchorages installed in reinforced concrete slabs or walls. In seismic retrofitting applications such as seismic bracing systems, the anchorages need to be installed in structural members (beams and columns) that have limited cross-sectional dimensions. Therefore, it is important to understand the influence of the nearby edges on the behavior of anchorages under tension forces. To understand the influence of only nearby edges while precluding other effects, the tests were carried out on 2 x 2 and 3 x 2 anchor groups of the same configurations as those reported in Chapter 8, however in narrow concrete members. This chapter provides the details of the experimental program carried out on anchor groups in narrow concrete members under monotonic tension load.

9.1   Available data from the literature

This section provides a brief overview of the available studies regarding the breakout behavior of tension loaded anchors and anchor groups close to the edge. To begin with, the data on single anchors is summarized. It is worth mentioning that, in comparison to tension loaded anchor groups, the breakout behavior of tension loaded single anchors located close to one or more free edges is well described in the literature. Whereby, the main focus of experimental studies was on the behavior of anchors located close to one edge. In general, the data on single anchors or anchor groups installed in narrow concrete members (two parallel close edges) is rather limited.

When single anchors are located close to an edge and loaded in tension, the concrete breakout capacity reduces if a critical edge distance, c_{cr}, cannot be maintained (Eligehausen et al., 2006). Based on a large experimental database, the critical edge distance for tension loaded single metal anchors (Eligehausen et al., 1987) and single headed studs (Eligehausen et al., 1992) located close to one edge was determined as $c_{cr} = 1.5h_{ef}$. Correspondingly, if the edge distance is larger than the critical value, an anchor is able to develop the full capacity of a single anchor without edge influence. In

Eligehausen et al. (1987) and Eligehausen et al. (1992), this marks the upper limit of the single anchor capacity (no edge influence). To define the lower limit of the single anchor capacity, they assumed a theoretical edge distance of c = 0. For this theoretical case, they considered two effects which influence the anchor capacity. First, the close edge reduces the available concrete to resist the tension load. This effect was considered by the projected area approach, whereby the area is reduced by half, in turn reducing the capacity of a single anchor by half. Second, the disturbance of the rationally symmetrical stress field in the concrete was considered analogous to cracked concrete. Therefore, the reduction factor for cracked concrete was applied to determine the lower limit of the single anchor capacity. For an edge distance between the critical edge distance and the theoretical edge distance c = 0, they assumed that the capacity of a single anchor may simply be linearly interpolated between the upper and lower limit of the capacity.

It is worth mentioning that the value for $c_{cr} = 1.5h_{ef}$ has been adopted in standards and guidelines such as EN 1992-4. Furthermore, the lower limit for the reduction factor for close edges, $\psi_{s,N}$ (see Equation (3.14)), is based on the considerations regarding the disturbance of the stress field in cracked concrete (Eligehausen et al., 2006). Typically, the observed breakout behavior for metal anchors and headed studs is characterized by a shell shaped breakout body as indicated in Figure 9.1, case (1).
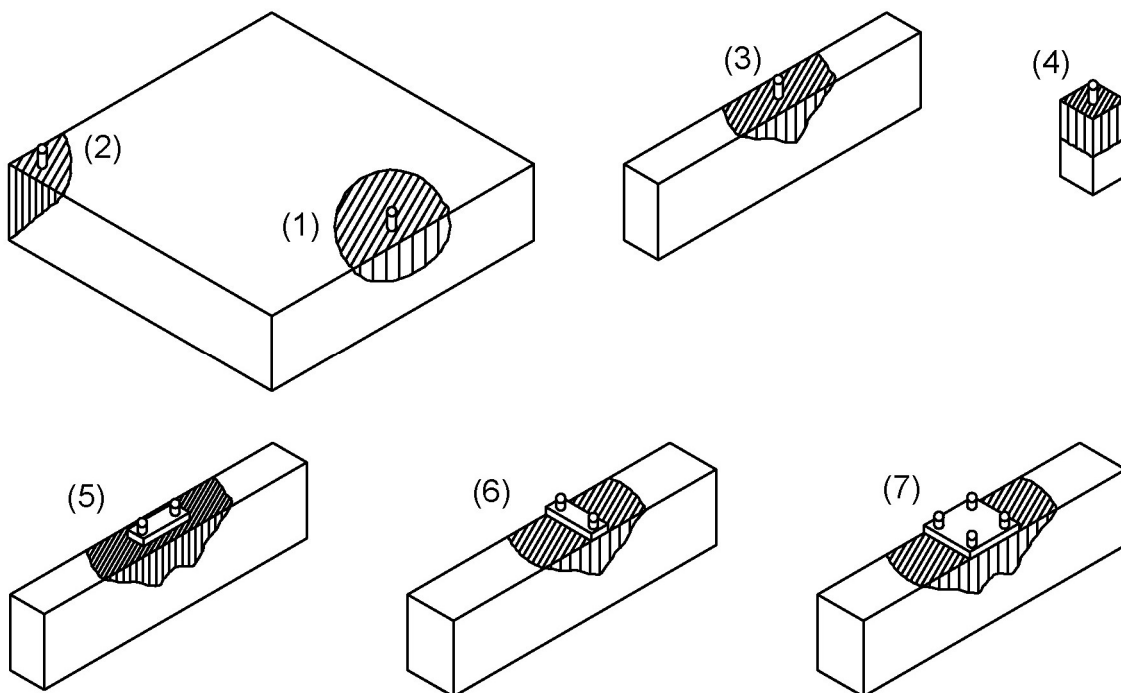
Figure 9.1. Schematic depiction of the concrete breakout bodies observed for single anchors and anchor groups loaded centrically in tension.

In Popo-Ola and Newman (1995) tests on tension loaded single bonded anchors under the influence of one close edge and two perpendicular close edges (anchors placed in

the corner of a slab) are reported. The experimental results were evaluated by Lehr (2003). When located close to one edge, in accordance with the observation on headed studs and metal anchors, the breakout behavior was characterized by a shell-shaped breakout body, where the single anchor capacity reduces with decreasing edge distance. However, the presence of a second perpendicular close edge (see Figure 9.1, case (2)) appeared to have only a minor additional negative effect on the anchor capacity, while Lehr (2003) observed that the stiffness of the anchor reduced further. Lehr (2003) assumes that only with very small edge distance the second perpendicular edge will have an additional negative effect on the anchor capacity. It should be noted thought that the observations for anchors in the corner were based on a limited number of test results.

An experimental study on single headed anchors located close to four edges was conducted by Delhomme et al. (2010). The anchors were placed in the middle of a concrete specimen with equal edge distance to each side of the specimen, whereby the edge distance was less than half the embedment depth. When loaded in tension, strain measurements in the concrete specimen indicated a failure mechanism which is characterized by horizontal cracks forming between the head of the anchor and the free edges. Figure 9.1, case (4) schematically depicts such a breakout behavior. In other words, the crack formation followed the shortest path through the cross section of the concrete specimen (Delhomme et al., 2010). A similar crack propagation was observed in a numerical study conducted by Di Nunzio (2020), where in case of cast-in-place fasteners located close to two parallel edges (Figure 9.1, case (3)) and close to four edges, the failure mechanism was characterized by horizontal cracks towards the free edges.

In Bujňák and Farbák (2018), headed studs were tested for their tension capacity in narrow RC members to investigate the beneficial effect of supplementary (anchor) reinforcement. In the reference tests in concrete slabs without supplementary reinforcement, the investigated anchors failed in concrete cone failure. A comparison of the obtained ultimate capacities between both anchors with and without supplementary reinforcement and the calculated capacities according to the standards has shown that the calculated values were well below the experimentally obtained capacities, thus indicating the conservatism of the current design approach for anchors installed in narrow concrete members.

In conclusion, the experimental and numerical data on tension loaded single anchors close to the edge has shown that both the capacity and stiffness of anchors are markedly influenced by the vicinity of close edges, and that the failure mechanism is characterized by horizontal cracks starting from the tips of the embedded end of the anchor towards the free edges. For single anchors installed in narrow concrete members, the available test data is rather limited. Nevertheless, it indicates that the current design approach, which was mainly developed based on experimental data on

anchors close to one edge, yields conservative results in case of single anchors close to two parallel edges.

The available experimental data on predominantly tension loaded anchor groups installed close to the edge is rather limited. In an experimental study conducted by Laichinger and Bergmeister (2014), groups of bonded anchors were installed close to one edge and loaded simultaneously in tension and shear, whereby the angle of the total force was varied. Thereby, the shear load was acting in the direction perpendicular to the free edge. Similarly, Sharma et al. (2019) carried out experimental investigations on quadruple anchor groups installed close to one edge subjected to tension, shear (perpendicular to the free edge) and combined tension and shear loads with and without supplementary reinforcement. Zeng et al. (2013) studied the behavior of anchor groups installed in narrow concrete members which were loaded simultaneously in shear and tension, whereby again the shear load was acting perpendicular to the free edges.

Tests where anchor groups were installed in narrow concrete members and loaded centrically in tension are reported in Anderson et al. (2017). The dominant failure mode observed in the experiments was concrete cone failure. As indicated in Figure 9.1, case (3) and (6), it was reported that a typical concrete cone formed in the direction parallel to the edges, while similar to the behavior of single anchors, a horizontal crack formed between the embedded ends of the anchors towards the free edge. Furthermore, Anderson et al. (2017) compared the obtained experimental capacities to the calculated capacities according to ACI 318-14. In accordance with the findings of Bujňák and Farbák (2018), it was found that the calculated capacities are significantly lower than the actual capacities obtained in the experiments, thus rendering the current design approach as relatively conservative for the cases where anchors are installed in narrow concrete members. Although the test program was rather limited in terms of tested configurations and the total number of performed tests, the experimental results clearly highlight the need for further investigation on the behavior of anchor groups close to parallel edges.

9.2 Experimental program

The experimental investigation in this work focuses on the behavior of anchor groups close to two parallel edges. This means that on two parallel sides of an anchor group, the distance from the outermost anchors to the edge is smaller than the critical edge distance according to EN 1992-4. The narrow members simulate the structural members such as beams or columns where the connections are usually formed in case of seismic retrofit solutions. The experimental program comprises 15 test series with various anchor configurations and embedment depths. The investigated configurations include single anchor tests which serve as a reference for the behavior of the anchor groups, one configuration with a 2 x 1 anchor group, two configurations with a 2 x 2

anchor group and two configurations with a 3 x 2 anchor group. Note that in this context, configuration refers to the mutual position of the anchors within the group (anchor spacing) and the number of anchors in a group. The tested anchors were embedded in the concrete with an embedment depth of h_{ef} = 80 mm and h_{ef} = 110 mm and loaded both centrically and eccentrically in tension, with eccentricity parallel to the free edges. Eight test series were performed with anchor groups located close to two parallel edges where the edge distance is smaller than the critical edge distance and one test series on a 2 x 1 anchor group was performed where the edge distance equals the critical edge distance. Thereby the dimensions of the concrete specimens were the same in each test and only the layout of the anchor groups and the effective embedment depth was altered. In this way the influence of different edge distances is investigated while the available concrete to resist the tension load essentially remains the same. Out of these tests, two test series are performed where the simultaneous influence of eccentric loading and close edges is investigated on a 2 x 2 and a 3 x 2 anchor group. Two test series investigate the influence of a deeper embedment depth. In order to compare the performance of anchor groups close to two parallel edges to the behavior of anchor groups without edge influence, the same anchor configurations are used as in the tests in Chapter 8. For the configurations, which were not investigated in Chapter 8, the experimental program includes additional four test series where the anchor groups were installed away from the edge. Each test series comprises two to four tests. In all tests a bonded anchor system is used, whereby the anchor diameter is kept constant in all tests (d = 16 mm). The details of the experiments along with the baseplate dimensions of each configuration are given in Table 9.1. The tests were performed in normal strength uncracked concrete specimens (C20/25). To exclude any influence of neighboring anchor groups, they are positioned in a way that the clear distance between the outermost anchors of neighboring anchor groups is at least $4h_{ef}$. A static tension load is applied in hydraulic (oil pressure) control on the anchor groups to pull the groups out of the concrete. The experimental program aims to investigate concrete cone failure and hence, an unconfined experimental setup is used to obtain the desired failure mode and the test parameters like the diameter of the anchors, spacing and the embedment depth of the anchors as well as the concrete strength were chosen accordingly. Note that in the following the term "tests in wide slabs" refers to tests on single anchors or anchor groups in unreinforced concrete slabs, where the distance to the free edges was large enough to exclude any influence of the edges on the load-displacement behavior.

Table 9.1. Experimental program on anchor groups in narrow concrete members.

Test ID	h_{ef}[1] (mm)	Baseplate dimensions (mm)	s_1[2] (mm)	s_2[2] (mm)	c_2[3] (mm)	e_1[4] (mm)	$f_{c,m}$[5] (N/mm²)	Number of tests
C-10A	80	-	-	-	≥4h_{ef}	-	24.5	3
C-10B	110	-	-	-	≥4h_{ef}	-	24.0	3
C-60	110	240x160x25	160	80	≥4h_{ef}	-	24.0	3
C-70	80	240x240x25	80	160	≥4h_{ef}	-	24.0	3
C-80	110	240x240x25	160	160	≥4h_{ef}	-	24.0	3
C-22	80	240x80x25	160	-	120	-	24.5	3
C-32	80	240x160x25	160	80	80	-	24.5	3
C-42	80	240x240x25	160	160	40	-	24.5	3
C-52	80	240x160x25	80	80	80	-	24.5	4
C-62	110	240x160x25	160	80	80	-	24.5	4
C-72	80	240x240x25	80	160	40	-	24.5	3
C-82	110	240x240x25	160	160	40	-	24.5	2
E-30	80	240x160x25	160	80	≥4h_{ef}	40	24.5	4
E-32	80	240x160x25	160	80	80	40	24.5	3
E-52	80	240x160x25	80	80	80	40	24.5	3

(1) Effective embedment depth
(2) Anchor spacing
(3) Edge distance
(4) Load eccentricity
(5) Mean cylinder concrete compressive strength at the time of testing

The designation of the individual test series is composed of a letter and two digits, such as C-22. The letter (C or E) identifies whether the tension load is applied centrically (C) or eccentrically (E) – the first digit identifies a certain anchor configuration – the second digit identifies whether the anchor group is placed away from edge (0) or close to two parallel edges (2). In case of the single anchor reference tests, the additional letter A implies an effective embedment depth of h_{ef} = 80 mm and B implies an effective embedment depth of h_{ef} = 110 mm. Figure 9.2 provides a schematic description of the geometrical parameters of the anchor groups when installed in narrow concrete members. As indicated in Figure 9.2, the anchor groups were placed in the middle of the narrow side of the concrete specimen. Thus, the edge distance on both sides of the anchor group is equal. In this way, geometrical eccentricities in the direction perpendicular to the edge were obviated.
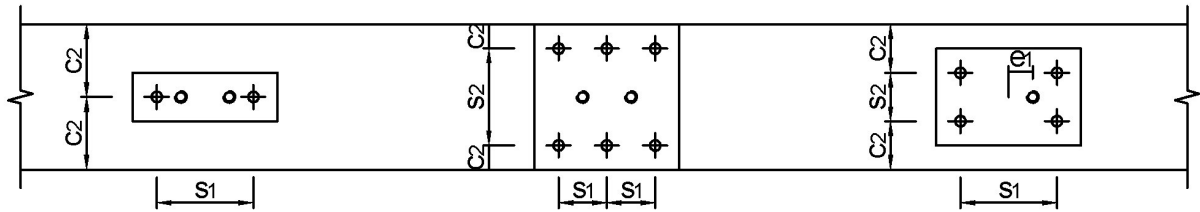
Figure 9.2. Schematic depiction of anchor groups installed close to parallel edges and designation of the geometrical parameters.

9.3 Description of the tested anchor configurations and test specimen

9.3.1 Anchor configurations

To fasten the baseplates to the concrete specimen, the same two-component injection system, FIS EM Plus, was used as in the previous experimental parts. Therefore, no detailed description of the bonded anchor system is given here, and reference is made to the description provided in Chapter 5. The high-strength threaded rods had a size of M16 and strength class 8.8 with a specified yield strength of $f_y = 640$ N/mm² and an ultimate strength of $f_u = 800$ N/mm². The baseplates themselves, which were used to connect the individual anchors, were made of S235JR steel with a specified yield strength of $f_y = 235$ N/mm². The dimensions of the baseplates used in the experimental program are given in Table 9.1 and Figure 9.3. In all tests the thickness of the baseplate was 25 mm. To allow the anchor rods to pass through the baseplates, holes with a diameter of 18 mm were cut into the steel plates. The tension load on the baseplates is applied via two threaded rods of size M20 in case of centric loading and via one threaded rod of size M20 in case of eccentric loading. In Figure 9.3 the point of load application is marked by a circle where the internal threads are cut into the steel.
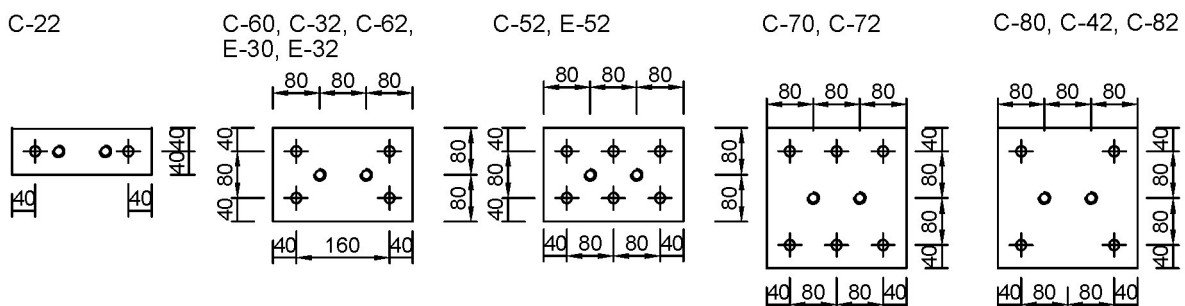
Figure 9.3. Dimensions of the baseplates used in the experiments and indication in which particular test series they were used.

9.3.2 Design considerations for the concrete specimen used for the tests with two parallel edges

In order to investigate the influence of the edge distance, the width of the concrete specimen is kept constant for each configuration. Thus, the part of the concrete activated for taking the load remains the same for equal embedment depths and equal spacing between the outermost anchors in the direction parallel to the edges. Only by altering the layout of the anchor configuration by placing the anchors closer to the edges, the edge distance is varied. In this way the actual influence of the edge distance can be evaluated.

When the anchor groups are loaded in tension, forces are transferred to the concrete specimen resulting in bending moments, shear forces and splitting forces in the specimen. These demands can lead to pronounced cracking and splitting of the concrete specimen which has a significant negative effect on the load-displacement behavior and performance of the anchor groups. The height of the specimen was determined in such a way that severe crack formation would be prevented, and two tests could be performed on each of the opposite narrow sides. Hence, the required specimen height was calculated as 630 mm.

The dimensions of the concrete specimen and the reinforcement details are given in Figure 9.4. The position of one anchor group is indicated in Figure 9.4. It can be seen that the anchor group is located between the cross ties and correspondingly another three anchor groups are positioned on the specimen. In this way four tests could be performed in one concrete specimen. Therefore, additional longitudinal reinforcement with a diameter of 10 mm was provided beneath the embedded anchors to avoid any influence on the anchors. The shear forces in the concrete specimen are taken up by stirrups with a diameter of 8 mm enclosing the longitudinal reinforcement. In order to prevent extensive longitudinal splitting at the surface of the specimen, cross ties with a diameter of 6 mm are provided on both sides of the specimen. The cross ties are located in a way to inhibit interaction with the anchor groups. However, longitudinal reinforcement is required to hold the cross ties in place during casting. Therefore, on both sides of the specimen, two additional reinforcing bars with a diameter of 6 mm are located close to the surface. The horizontal placement of the longitudinal surface reinforcement had to be adjusted depending on the anchor configuration. As can be seen in Figure 9.4, a distinction is made between specimen A and B, which differ only in the position of the longitudinal surface reinforcement. Specimen A was used for configurations with an edge distance of 80 mm and specimen B was used for configurations with an edge distance of 40 mm. The concrete specimens were made of normal strength concrete (C20/25) and were produced according to the state of the art in accordance with DIN EN 206. The composition of the aggregates was chosen such that a grading curve between the standard grading curves A16 and B16 was obtained with a maximum aggregate size of 16 mm. The specimens were cast from two concrete batches, whereby the slabs used to perform the tests in narrow concrete

members were cast from the same batch. Only the specimen for the additional reference tests in wide slabs were cast from the second batch. The corresponding concrete strength values for each test series at the time of testing are given in Table 9.1. The hardened concrete compressive strength at the time of testing was determined on six concrete cubes with a side length of 150 mm for each concrete batch, respectively. The measured mean cube concrete compressive strength was converted into the mean cylinder concrete compressive strength, $f_{c,m}$, using the conversion factor $k_{cyl/cube}$ = 0.82 (see Section 5.3 and DIN EN 206, Fingerloos et al. (2015), and Loch (2014)).
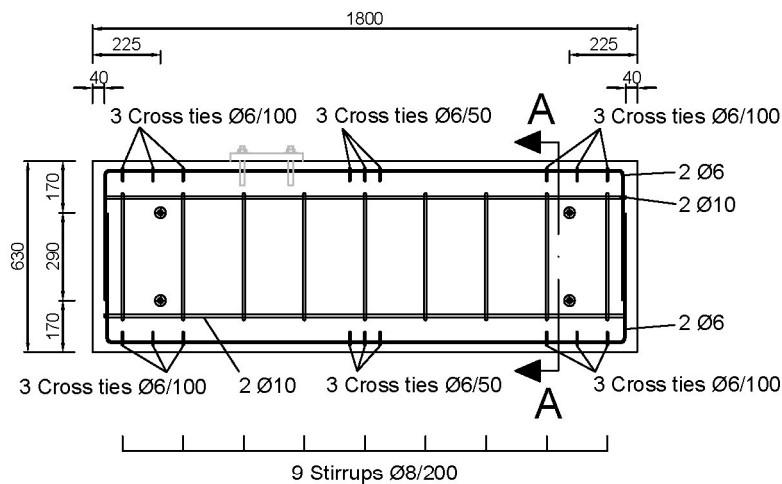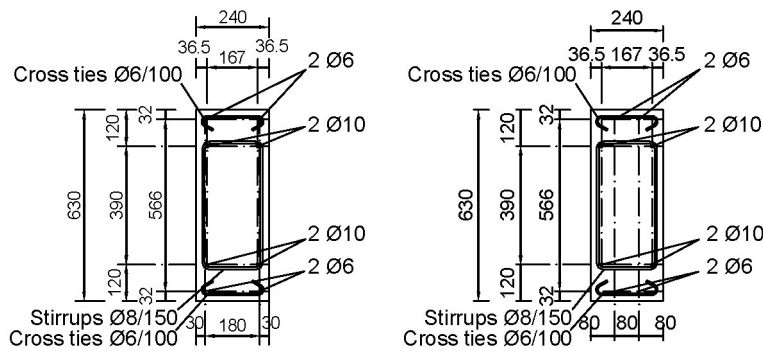
Figure 9.4. Dimensions and reinforcing details of the concrete specimen used for the tests with anchor groups located close to parallel edges. (Note: All dimensions are in mm).

9.4 Description of the experimental setup and testing procedure

9.4.1 Experimental setup

In the experiments an unconfined experimental setup was used to facilitate the desired concrete breakout failure. Therefore, in accordance with EOTA TR 48, a clear distance

of at least $2h_{ef}$ is kept between the supports and the outer most anchors of the groups in the direction parallel to the edges. This allowed the formation of an unrestricted concrete cone in the direction parallel to the edges. Figure 9.5 shows the setup that was used in the experiments. It can be seen that two steel I-beams were used as supports. To keep the system stable, four additional concrete support blocks were arranged adjacent to the concrete test specimen. In this way, the reaction forces were distributed via the I-beams on the support blocks and the test specimen. In the centric loading case, the load was applied onto the baseplates by means of two high strength M20 threaded rods. The two rods were in turn attached to a fixture which was connected to the 200 kN hydraulic cylinder by another M20 threaded rod. In the eccentric loading case, the load was applied by means of one M20 threaded rod. In addition, a special hinge was used which provides for unobstructed rotation of the baseplate and thus allowed a redistribution of forces, if any.

9.4.2 Instrumentation

To measure the total force on the connection, a calibrated load cell with a measuring range up to 200 kN was used. As in the experiments described in Chapter 8 and in Stehle and Sharma (2021b), the axial anchor forces were monitored via strain gauge-based force washers, which enable monitoring up to a load of 200 kN. The strain gauge-based force washers along with two additional hardened washers were mounted on the individual anchors just above the baseplate and beneath the nut (see Figure 9.6 (b)). Displacement transducers (LVDT) were utilized to measure the anchor displacements, the crack width at the side surface of the concrete test specimen and the displacement of the baseplate. Thereby, the displacement of the baseplate was measured as close to the point of loading as possible. The anchor displacements were measured directly on top of the anchors using two bridge-like stands as shown in Figure 9.6 (a). The LVDTs to measure the anchor displacements and the baseplate displacement are fixed to these stands which are in turn fixed to the concrete specimen. Thus, the reference point for the anchor displacements and the baseplate displacement is the upper surface of the concrete specimen. The measuring range of the LVDTs is up to 25 mm. The total force, the displacement of the anchor group in the direction of loading, the individual anchor axial forces, the anchor displacements, and the crack width on the side of the concrete test specimens were constantly monitored throughout the experiments by means of a data acquisition system. In case of the 2 x 1 configuration and the 2 x 2 configurations the anchor axial forces and displacements were monitored on each individual anchor. However, due to practical considerations, the measurement was limited to four anchors in case of the 3 x 2 anchor configurations. In order to obtain the best possible overview of the anchor behavior, three anchors in a row and an additional anchor in the second row were monitored. At the side surface of the concrete specimen the crack width and propagation of the concrete cone was measured using four LVDTs as shown in Figure 9.6 (b). The LVDTs were arranged in such a way that two of them measured the width of the crack between the anchors at

the bottom of the concrete breakout body and two LVDTs measured the crack width at the side of the concrete cone.
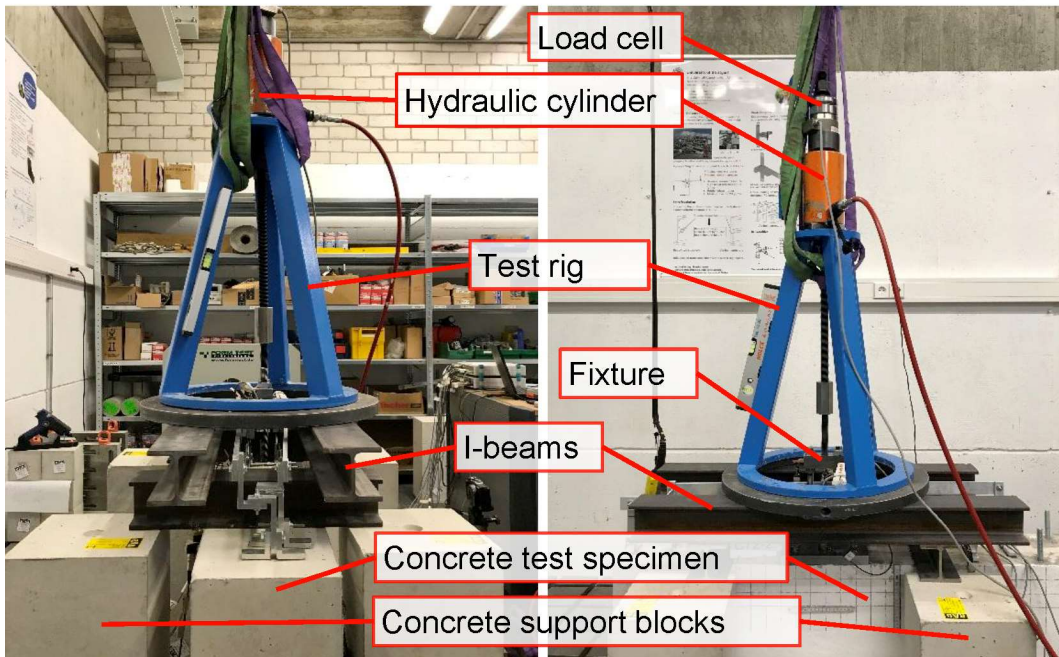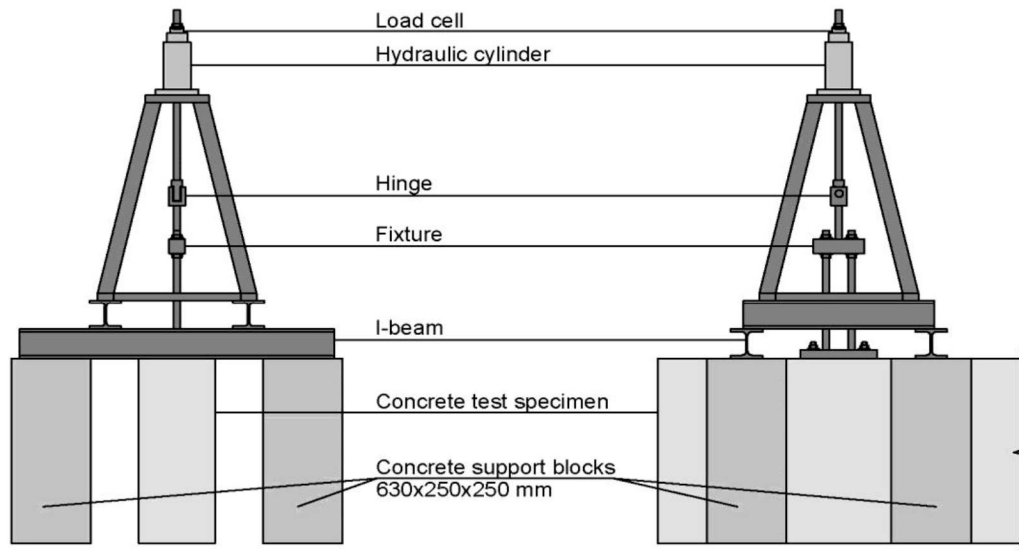
Figure 9.5. Experimental setup – Depiction of the individual parts of the setup.
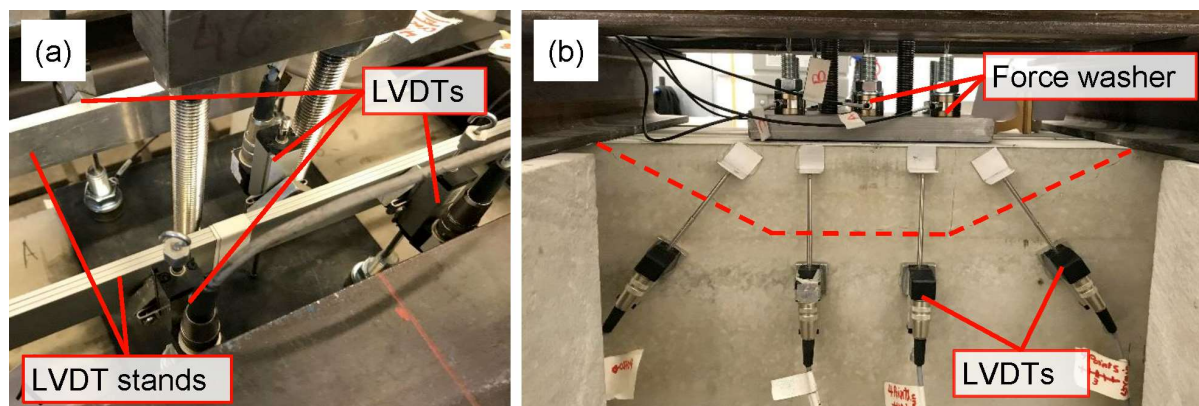
Figure 9.6. Experimental setup – Measurement of displacements and anchor axial forces: (a) Anchor displacement and (b) crack width at the side surface of the concrete specimen and anchor axial forces.

9.4.3   Testing procedure

The anchors were installed according to the manufacturer's printed installation instructions (ETA-17/0979) which includes drilling of the holes, cleaning of the holes, application of the adhesive and the installation of the threaded rods. After the specified curing time the baseplate was fixed by the nuts. Thereby the nuts were hand-tightened. After assembling of the experimental setup, the anchor groups were loaded monotonically in tension according to EOTA TR 48. The load was applied in hydraulic (oil pressure) control in a way that the ultimate load is reached within one to three minutes. The anchor groups were loaded until failure. It should be noted that the failure happens so rapidly that the hydraulic control cannot control the post-peak behavior sufficiently accurate. Therefore, only a few points are actually measured in the post-peak range of the load-displacement curve, which is why the post-peak results should be treated with caution.

9.5   Experimental results and discussion

To provide a better understanding of the behavior of anchor groups installed close to two parallel edges, the experimental results are discussed with respect to the obtained ultimate capacities, the observed load-displacement behavior, the failure mechanism, and the simultaneous influence of eccentric loading and parallel close edges. Table 9.2 summarizes the experimental results in terms of the obtained ultimate loads, the mean displacements at ultimate load and the corresponding mean secant stiffness. Along with the experimental results, the scatter of ultimate loads and displacements is given in terms of the coefficient of variation. Typical load-displacement curves of the respective test series are provided where relevant for the discussion.

As intended, concrete breakout failure was the observed failure mode in all tests where the anchor groups were installed close to parallel edges. It was also the observed

failure mode in tests on anchor groups installed in wide slabs (no edge influence). In the single anchor reference tests both concrete cone failure and mixed concrete cone and pull-out failure was observed.

Table 9.2. Experimental results.

Test ID	Ultimate load, N_u (kN)				$N_{u,m}$[1] (kN)	$CV(N_u)$ (%)	$s_{u,m}$[2] (mm)	$CV(s_u)$ (%)	$k_{Nu,m}$[3] (kN/mm)
	1	2	3	4					
C-10A	65.4	57.4	58.9	-	60.5	5.8	0.93	23.7	69.7
C-10B	95.4	92.1	86.2	-	91.2	4.1	1.30	35.0	79.0
C-60	153.1	138.1	142.6	-	144.6	4.3	0.79	23.0	266.3
C-70	149.6	150.8	145.3	-	148.6	1.6	0.50	8.1	300.5
C-80	187.3	183.8	186.8	-	185.9	0.3	0.84	6.4	221.1
C-22	72.6	73.5	76.2	-	74.1	2.1	0.81	0.7	91.1
C-32	104.4	102.7	101.1	-	102.7	1.3	0.73	13.7	144.3
C-42	92.0	92.2	92.1	-	92.1	0.1	0.52	2.9	176.0
C-52	85.2	88.8	103.3	99.2	94.1	7.8	0.50	16.6	195.1
C-62	129.6	136.5	118.0	132.2	129.1	5.3	0.68	33.3	196.8
C-72	96.9	96.2	110.2	-	101.1	6.4	0.50	8.8	206.8
C-82	116.3	123.6	-	-	120.0	3.1	0.68	2.9	177.0
E-30	92.3	83.7	76.0	82.6	83.6	6.9	0.67	5.9	124.9
E-32	70.8	68.3	68.1	-	69.1	1.8	0.66	5.9	104.3
E-52	81.5	78.6	74.1	-	78.1	3.9	0.43	7.0	182.2

(1) Mean ultimate load
(2) Mean displacement at ultimate load
(3) Mean secant stiffness at ultimate load

9.5.1 Failure mechanism of anchor groups installed in narrow concrete members

Figure 9.7 shows typical crack patterns observed on the side surface of the concrete specimen for anchor groups installed with an embedment depth of $h_{ef} = 80$ mm. The displayed crack patterns were obtained in test series C-22, C-32, and C-42 after the ultimate load of the anchor group has been reached. Note that the black squares, which were drawn onto the surface, have a side length of 40 mm and were marked on the test specimen to facilitate the visual observation of the crack propagation. In test series C-22, where the distance to the edge equals the critical edge distance ($c_{cr,N} = 1.5h_{ef}$), it was observed that upon failure, the cracks which emerged on the side surface were located relatively close to the top edge of the concrete specimen. The corresponding breakout body indicates that the crack propagation initially followed an inclined path towards the free edges, which flattens and turns into a horizontal crack as it approaches the free edge. In contrast, in test series C-32 and C-42, where the anchors are located closer to the edges, it can be seen that at the level of the embedded ends

of the anchors, the distance between the top edge of the specimen and the crack, which emerges on the surface, is around the embedment depth of the anchors. For anchors where the edge distance is smaller than the critical edge distance, it can be concluded that the crack propagation, which starts at the tips of the embedded ends of the anchors, follows an almost horizontal path towards the free edges. The observed breakout behavior of anchor groups close to the edge is consistent with the reported behavior in Delhomme et al. (2010) and Anderson et al. (2017). It seems that the crack propagation, and thus the stress distribution in the concrete, is to some extend influenced by the distance between the maximum tensile stress at the tip of the crack and the free edge. In the direction parallel to the free edges, a regular concrete cone has formed.
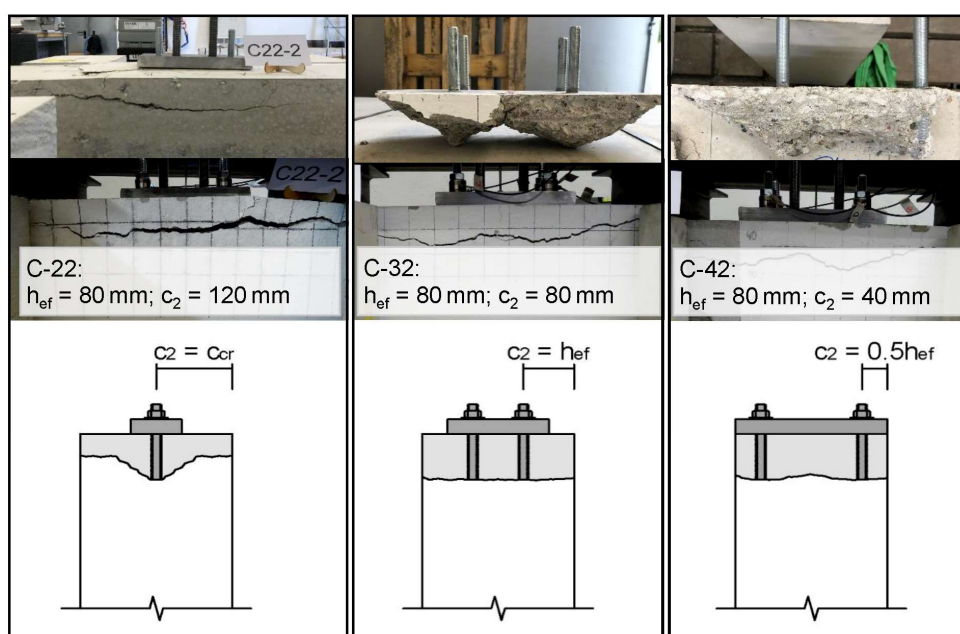
Figure 9.7. Typical crack patterns at the side surface of the concrete specimen upon failure in test series C-22, C-32, and C-42.

Similar breakout behavior was observed for anchor groups in narrow members with an embedment depth of h_{ef} = 110 mm. Figure 9.8 shows typical crack patterns obtained from test series C-62 and C-82. At the level of the embedded ends of the anchors, the crack appears on the concrete surface at a distance from the top of the concrete specimen that is approximately equal to the effective embedment depth of the anchors. In some tests it was observed that the crack on the concrete surface which forms between the anchors is somewhat deeper than the actual embedment depth itself. This observation was particularly apparent in test series C-82, which had the smallest relative edge distance. A likely explanation for this might be that aggregates are in the way of the crack, causing it to branch downward. In the direction parallel to the free edges, a regular cone has formed.
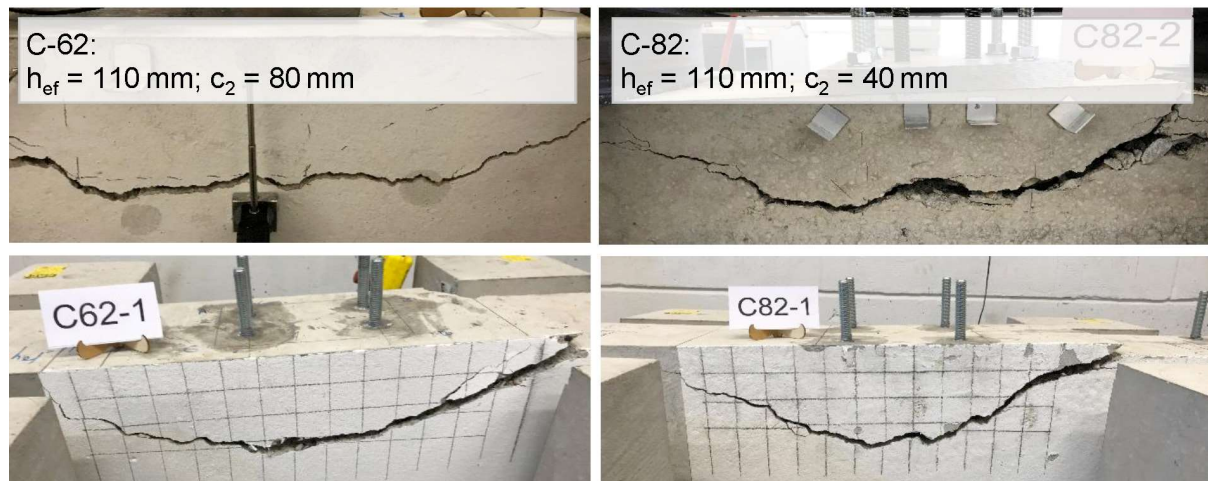
Figure 9.8. Typical crack patterns at the side surface of the concrete specimen upon failure in test series C-62, and C-82.

As mentioned above the breakout failure occurred rather abruptly. This is also evident from the crack measurements on the side surface of the concrete specimen shown in Figure 9.9. The figure shows the crack measurements for test C-72-2. Before reaching the ultimate load, the crack width is negligibly small (< 0.05 mm). Upon reaching the ultimate load however, the breakout body is almost immediately forming as can be seen from the fast enlarging crack width in the right graph. It should be noted that the results shown in Figure 9.9, are one of the few tests where actually a crack width was measured before reaching the ultimate load of the anchor group. In most tests, no crack width was measured before the ultimate load has been reached. However, all tests showed rapidly enlarging cracks either upon reaching the ultimate load or shortly thereafter. These results indicate that upon reaching the ultimate load, the fracture process zone and micro cracks have reached the concrete surface, while the discrete crack has not yet formed upon reaching ultimate load. Furthermore, the rapid formation of the cracks on the surface highlights the unstableness of the crack growth after the ultimate load has been reached, as also the cracks in the direction parallel to the free edges form rather fast.

This is understandable from the fracture area of concrete available in these cases. It is well-known from Eligehausen and Sawade (1989) that for an anchor group away from any edge under tension loads, the peak load is reached when the concrete cone crack is approximately 30% of its final crack length. After reaching peak load, as the concrete further fractures and the crack propagates toward the concrete surface, the load-displacement curve gradually drops down. However, in case of narrow members, due to the absence of concrete to further fracture upon reaching peak load, the breakout of concrete surface is more sudden resulting in brittle fracture.

These results suggest that since the cracks appear close to peak load only, in terms of serviceability, anchor groups installed in narrow concrete members do not pose any serviceability issues.
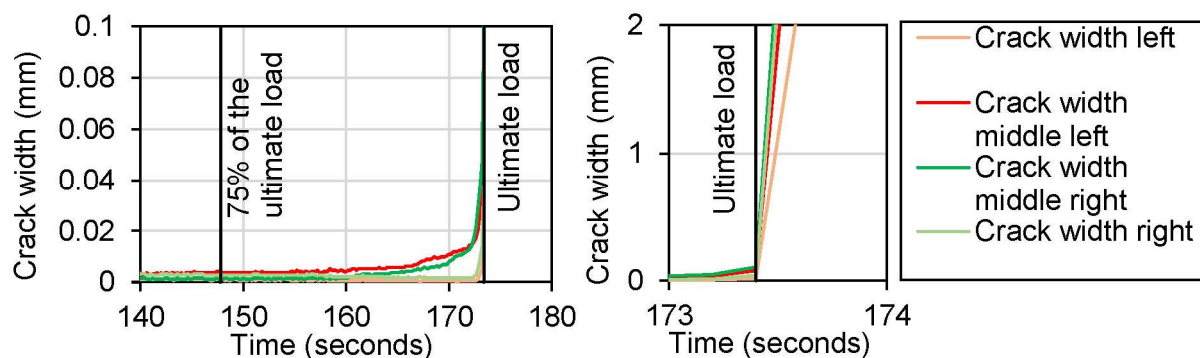
Figure 9.9. Crack width on the side surface of the concrete specimen as a function of the elapsed time. The designation of the curves corresponds to the position of the respective LVDTs in Figure 9.6 (b) from left to right.

9.5.2 Load-displacement behavior

Figure 9.10 (a) shows typical load-displacement curves obtained from test series in narrow members with an embedment depth of h_{ef} = 80 mm (C-22, C-32, C-42, C-52, and C-72). It should be mentioned that the information on the descending branch of the measured load-displacement curves is rather limited. This is due to brittle failure of the anchor groups in narrow concrete members and the hydraulic (oil pressure) controlled testing approach, which made it difficult to control the post-peak behavior shortly after the failure occurred. For this reason, only few points where actually measured in the descending branch.

The anchor configurations used in these test series feature the same total anchor spacing in the direction parallel to the edges, $s_{1,tot}$ = 160 mm (see Figure 9.3). Due to the equal width of the concrete specimen in all tests, this results in the same projected area according to EN 1992-4 for all five test series. In case of the 2 x 1 anchor groups in C-22, the distance to the edges matches the theoretical critical edge distance ($c_{cr,N}$ = 1.5h_{ef}) for which the anchor groups are able to develop their full capacity without the negative influence of close edges. In case of the 2 x 2 and 3 x 2 anchor groups, the edge distance is smaller than the required critical edge distance. Here the applied distance to the edges is either 80 mm (= h_{ef}) or 40 mm (= 0.5h_{ef}), whereby the distance is reduced by increasing the anchor spacing in the direction perpendicular to the edges as discussed above. Similarly, Figure 9.10 (b) shows typical load-displacement curves obtained from test series C-62 and C-82 where the embedment depth was increased to h_{ef} = 110 mm. Here the distance to the free edges is 80 mm (= 0.73h_{ef}) and 40 mm (= 0.36h_{ef}), respectively. While due to the equal width of the test specimen, again the projected area of these two configurations is the same according to EN 1992-4, the projected area is larger compared to the one for an embedment depth of h_{ef} = 80 mm as the development of a full concrete cone is not restricted in the direction parallel to the edges.
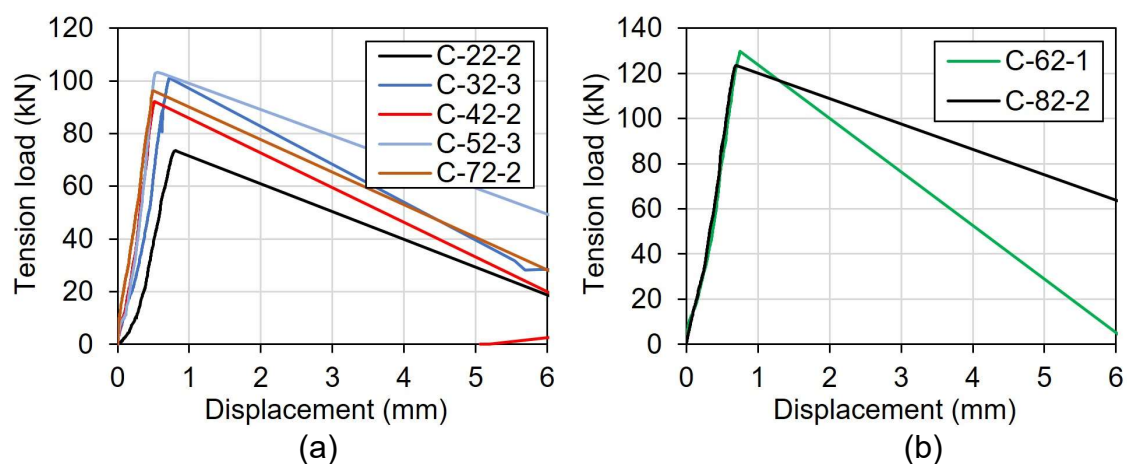
Figure 9.10. Typical load-displacement curves obtained in test series (a) C-22, C-32, C-42, C-52, and C-72, and (b) C-62 and C-82.

9.5.2.1 Ultimate capacity in narrow members

First, the results of the 2 x 1 groups are discussed, where the edge distance according to the CCD method is just enough (c_2 = 1.5h_{ef}) to prevent a negative influence on the breakout capacity. The mean ultimate load in test series C-22 is compared to the corresponding normalized mean ultimate load in test series BA-2x1-B-stat (see Table 8.2), where the anchor groups were installed in wide slabs. The load is normalized to the mean cylinder concrete compressive strength of test series C-22. The normalized mean ultimate load in test series BA-2x1-B-stat is 72.0 kN, thus matching very well with the mean ultimate capacity obtained in test series C-22 ($N_{u,m}$ = 74.1 kN). The comparison of the ultimate loads in the two test series shows that also in the case where anchor groups are installed in narrow concrete members with the edge distance exactly equal to the critical edge distance (c = $c_{cr,N}$ = 1.5h_{ef}), two parallel edges have no negative influence on the load carrying capacity of the anchorage.

From Figure 9.10 (a) and Table 9.2, it can be seen that the ultimate capacity in C-22 is markedly lower than the capacities obtained in the other four test series with the same projected area according to the EN 1992-4 (C-32, C-42, C-52, and C-72). From a theoretical perspective one could assume that the ultimate load in the narrow member is limited by the capacity of the 2 x 1 configuration (see CCD method). However, it appears that the anchor groups with additional anchors and smaller distance to the edges are capable to exploit the concrete capacity more efficiently than the 2 x 1 anchor groups. One possible explanation for this phenomenon is that due to the second anchor row in the 2 x 2 and 3 x 2 anchor groups, more core concrete between the anchors is activated, which results in the observed higher capacities. Additionally, the change of the failure mechanism from an inclined crack propagation to a roughly horizontal propagation towards the free edges, and the corresponding (re-) distribution of stresses in the concrete, might have a beneficial effect on the breakout capacity.

It can be seen in Figure 9.10 that in the test series, where the edge distance is smaller than the critical edge distance, the observed behavior of the tested anchor groups with the same embedment depth is rather similar despite the varying configuration of the anchors and the varying distance to the free edges. Figure 9.11 (a) compares the ultimate loads obtained in the individual tests for anchor groups with an embedment depth of h_{ef} = 80 mm. It can be seen that the obtained failure loads are rather similar. However, there are some differences between anchor groups with varying edge distance or configuration. Comparing test series C-32 and C-42, it can be seen that when the anchors are placed closer to the edges, the failure loads reduced on average by around 10%. A similar observation was made in test series C-62 and C-82 (Figure 9.11 (b)) with an embedment depth of h_{ef} = 110 mm, where the failure loads in test series C-82 with smaller edge distance were around 7% smaller than in test series C-62. When comparing test series C-42 and C-72, it can be seen that an additional middle anchor resulted in somewhat higher failure loads. On the other side, the failure loads in test series C-32 are higher than those in test series C-52 despite the additional middle anchor.

In principle, the failure loads obtained in the tests with two parallel close edges and an edge distance to both sides which is smaller than the critical edge distance appear rather similar despite the varying configurations and edge distance. The obtained failure loads are within a certain scatter range typically observed in fastening technology for concrete related failure. The test results suggest that the actual distance to the free edges had only a minor effect on the capacity of the tested anchor groups. It rather seems that the capacity depends on the available concrete to resist the tension load and the available fracture area.
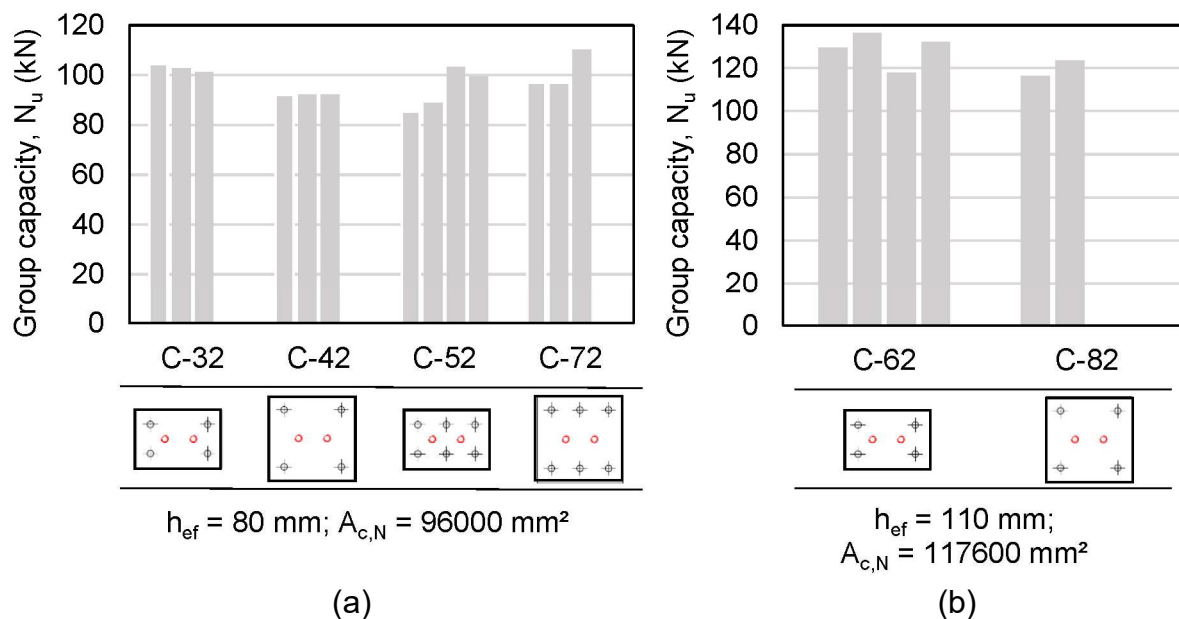
Figure 9.11. Comparison of the ultimate loads obtained in the individual tests for (a) an embedment depth of 80 mm and (b) an embedment depth of 110 mm.

9.5.2.2   Stiffness of anchor groups in narrow concrete members

In general, it was observed that the deviation in terms of the stiffness behavior of the individual anchor groups in narrow members was relatively small. This may be partly explained by the high variation of stiffness values in anchor technology. Nevertheless, some differences were identified. As shown in the previous chapter, additional anchors in a configuration lead to an increased stiffness of the connection (comparison between BA-2x2-C and BA-3x2-C). Comparing the same configurations when installed in narrow members, namely C-32 and C-52, the addition of two anchors also leads to an increase of the secant stiffness at ultimate load by around 35%, as can be seen from Table 9.2. However, when installed in narrow concrete members the effect appears to be smaller than in wide slabs. This might be attributed to the varying points of load application in the two experimental campaigns. In the experiments presented in Chapter 8 the load was applied at a single point at the geometric center of the baseplate, while in the experiments in this chapter, the load on the baseplate was applied at two points as indicated in Figure 9.3. Furthermore, the varying concrete mixture may also have an influence on the anchor behavior. The anchor groups in test series C-42 and C-72 have the same baseplate dimensions and only vary by means of the number of anchors. A comparison of the secant stiffness values at ultimate load shows that in this case the beneficial effect is rather moderate as the stiffness increased only by around 18%. The reduced impact might be explained by the larger anchor spacing in the direction perpendicular to the edges, which may dominate the displacement behavior.

Reducing the edge distance by simultaneously increasing the anchor spacing in the direction perpendicular to the edges had a mixed effect on the stiffness of the anchor groups. In case of anchor groups with an embedment depth of h_{ef} = 80 mm, the secant stiffness at ultimate load slightly increased when the anchors were placed closer to the edge. In contrast, in case of anchor groups with an embedment depth of h_{ef} = 110 mm, the secant stiffness of the tested anchor groups reduced when the anchors were placed closer to the edge while simultaneously increasing the anchor spacing in the respective direction. However, the variation of the stiffness values over all cases is within the scatter typically observed for the displacements, rendering a conclusive evaluation rather difficult.

9.5.3 Eccentric loading

When anchor groups are used to connect additional components to an existing structure, for practical reasons it is often not possible to ensure centric loading of the anchor groups. If, in such a case, the anchor group is additionally installed in a narrow concrete member, this poses a particular challenge for the connection. Therefore, two test series, E-32, and E-52, have been conducted to investigate the behavior of anchor groups simultaneously subjected to eccentric loading and parallel close edges. The configuration used in E-32 features a 2 x 2 anchor group with 80 mm anchor spacing in the direction perpendicular to the edges and 160 mm anchor spacing in the direction parallel to the edges. The configuration used in E-52 uses the same baseplate dimensions and has equal anchor spacing in the direction perpendicular to the edges. E-52 differs from E-32 insofar as, while the distance between the outermost anchors in the direction parallel to the edges is equally 160 mm, two additional anchors are placed in between, halving the actual anchor spacing to 80 mm. The test series E-30, where the behavior is not influenced by the vicinity of edges, serves as a reference for test series E-32. In case of E-52, test series BA-3x2-C will serve as the reference without edge influence. The results of the test series have been presented in the previous chapter. The corresponding ultimate load normalized to the mean cylinder concrete compressive strength in this study is 86.0 kN and the mean secant stiffness at ultimate load is 214.9 kN/mm. Typical load-displacement curves obtained in test series E-30, E-32, and E-52 are shown in Figure 9.12. By comparing the load-displacement curves of E-30 and E-32 it becomes evident that placing the anchor groups close to parallel edges has a negative influence on both the total capacity and the stiffness of the anchor groups. Similarly, the capacity and the stiffness of the anchor groups in E-52 are reduced in comparison to the tests in wide slabs.
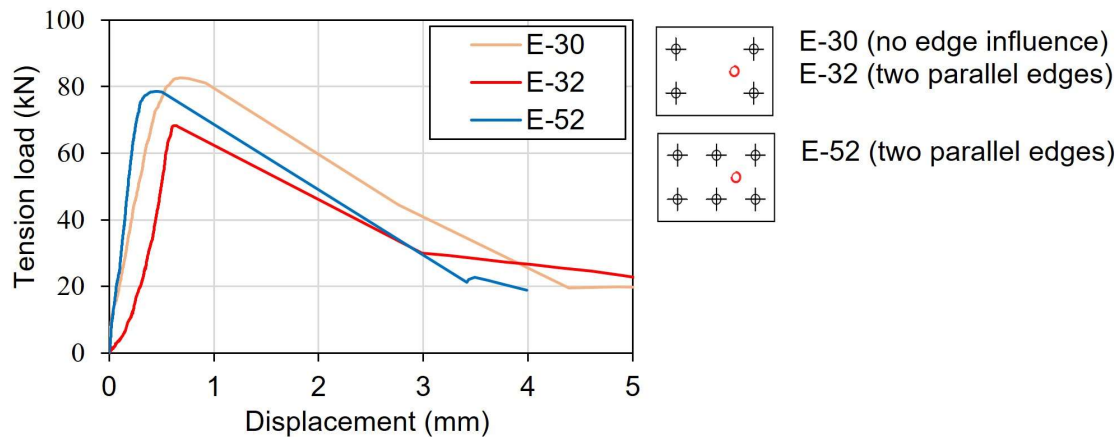
Figure 9.12. Typical load-displacement curves obtained in test series E-30, E-32, and E-52.

In the previous chapter it was shown that in case of centrically loaded anchor groups without any edge influence, the investigated 2 x 2 and 3 x 2 configurations yield approximately the same ultimate capacities despite the varying number of anchors in the group. That is because the baseplate dimensions and the anchor spacing of the outermost anchors are identical and the additional anchors only have an effect on the stiffness of the anchor group and the flexibility of the baseplate. Correspondingly, in case of eccentric tension load, the ultimate capacities obtained from the two configurations without the influence of close edges (E-30 and BA-3x2-C) are similar. With respect to the stiffness of the anchor groups, analogous to the centrically loaded tests, the 3 x 2 anchor groups behaved markedly stiffer due to the presence of additional middle anchors. When it comes to anchor groups that are simultaneously placed close to parallel edges and loaded eccentrically in tension, it was observed that the 3 x 2 anchor groups in E-52 where capable of taking up around 12% more load than the 2 x 2 anchor groups in E-32. With respect to the stiffness of the anchor groups, the ratio of the stiffness values of the two configurations is similar to the one which was observed in case of anchor groups without edge influence.

In order to investigate to which extent, the parallel edges have an influence on the redistribution of anchor forces in the group, Figure 9.13 shows the distribution of forces among the individual anchors in E-30 and E-32. In both cases, as expected, the anchors which are closer to the point of load application (anchor B and D) take up most of the load. With a short delay, also anchors A and C take up a smaller part of the load. In general, it can be seen that the behavior of anchorages in wide slabs and in narrow members is rather similar. However, it was observed that the proportional contribution of anchor A and C was slightly higher when the anchor groups were installed in narrow members. The experimental results suggest that anchors A and C take up the load slightly earlier when installed in a narrow member, thus the distribution of forces to the anchors away from the point of load application is somewhat more pronounced. The reduced capacity of eccentrically loaded anchor groups is therefore mainly a

consequence of the reduced capacity of the anchors closest to the point of load application (B and D). In both cases, the anchor group fails when the highest loaded anchors fail. A similar behavior was observed in case of the 3 x 2 configuration in E-52. The observed higher ultimate capacity in this test series might be attributed to the fact that due to the two additional anchors in the 3 x 2 anchor groups, the total force acting on the anchor group is more evenly distributed, resulting in a delayed failure of the highest loaded anchors. However, the differences between the two configurations are within a certain scatter for the ultimate capacity and the experimental results are limited. Therefore, the potential beneficial effect of additional anchors which would help distributing the forces more evenly in case of narrow members needs further investigation and the data should be treated with caution.
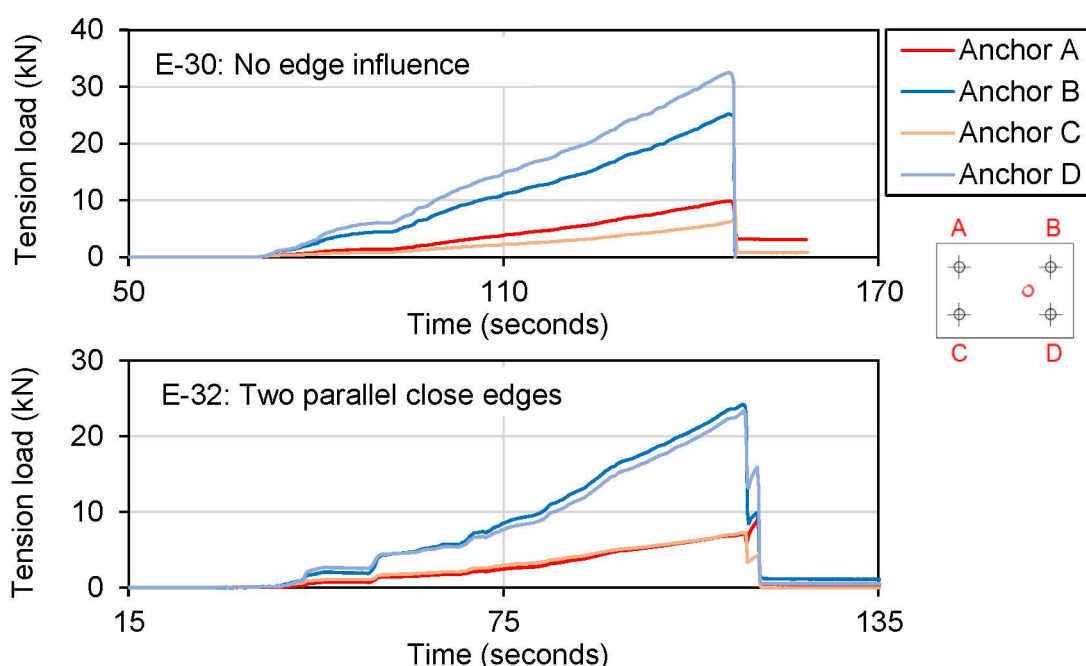
Figure 9.13. Distribution of anchor forces as a function of the elapsed time over the duration of the experiment for test series E-30 (top graph) and E-52 (bottom graph). Time represents the recording time and not the loading time.

9.6   Summary

The aim of the experimental work discussed in this chapter was to establish a database and study the breakout behavior of tension loaded anchor groups installed in narrow concrete members. Therefore, a systematic and extensive experimental campaign has been carried out comprising 28 tests on anchor groups installed in narrow concrete members and additional reference tests with no edge influence. In this chapter, the details of the experimental program, the tested fasteners, the design of the concrete specimen, and the experimental setup are described, and the experimental results are presented. The evaluation of the results focused on the failure mechanism and

breakout behavior of anchor groups in narrow members, as well as the load-displacement behavior in case of centric and eccentric tension load. The following conclusions can be drawn from the experimental investigations:

1. In case of anchor groups with an edge distance smaller than the critical edge distance, the breakout behavior of the tested anchors groups is governed by horizontal cracks starting from the embedded ends of the anchors towards the free edge. In the case where the anchor groups were installed in narrow concrete members, but where the edge distance equaled the critical edge distance, the initial crack propagation followed an inclined path towards the surface of the concrete specimen which turned into a horizontal path when it approached the free edge.

2. The failure in narrow concrete members happens abruptly and is brittle in nature. This is attributed to the relatively small fracture surface of the concrete breakout body. However, it appears that in terms of serviceability, installing anchor groups in narrow members is rather unproblematic as basically no cracking was observed on the concrete surface before the failure of the anchor groups.

3. The tested 2 x 1 anchor groups installed in narrow members with an edge distance equal to the critical edge distance, yielded almost the same mean ultimate capacity as compared to the same configuration in wide concrete slabs with no edge influence.

4. The tested 2 x 2 and 3 x 2 configurations installed in narrow concrete members with an edge distance smaller than the critical edge distance yielded approximately the same ultimate capacities when their projected area according to the CCD method was identical. The experimental results provide evidence that only considering the projected area for the design of anchor groups in narrow members would suffice for a practical and safe design. However, this is only valid for tension loaded anchor groups with equal distance to both close edges and no load eccentricity towards one of the two parallel edges.

5. The behavior of eccentrically loaded anchor groups in narrow members is similar to the behavior of eccentrically loaded anchor groups without the influence of close edges, provided the eccentricity is applied in the direction parallel to the edges. The parallel edges have an influence in so far as the ultimate capacity of the anchor groups and the stiffness is further reduced. Thereby, similar to the behavior in wide slabs, the additional anchors in the tested 3 x 2 configuration result in a higher stiffness of the complete anchor group compared to the respective 2 x 2 configurations.

10 Numerical investigations on anchor groups

The experimental studies presented in previous chapters were augmented by the 3D finite element numerical simulations for better understanding of the behavior of anchor groups and also to conduct numerical parametric studies.

10.1 Numerical program

The numerical study is set out with the aim of further investigating the influence of close edges on the concrete breakout behavior, the capacity, and the load-displacement behavior of anchor groups. The basis of the numerical investigation are three anchor configurations which were already applied in the experimental part. The simulated configurations comprise a 2 x 1 configuration (which has been applied in test series BA-2x1-B and C-22), a 2 x 2 configuration (which has been applied in test series BA-2x2-C, C-32, and E-32), and a 3 x 2 configuration (which has been applied in test series BA-3x2-C, BA-3x2-E, C-52, and E-52). Figure 10.1 provides a schematic depiction of the respective configurations along with the corresponding definitions of anchor spacing, edge distance, and eccentricities. The anchor groups comprise bonded anchors with a diameter of 16 mm. The embedment depth, applied in the numerical study was 80 mm, 110 mm, and 150 mm. The baseplate dimension applied in the numerical study are identical to those used in the respective configurations in the experimental part.
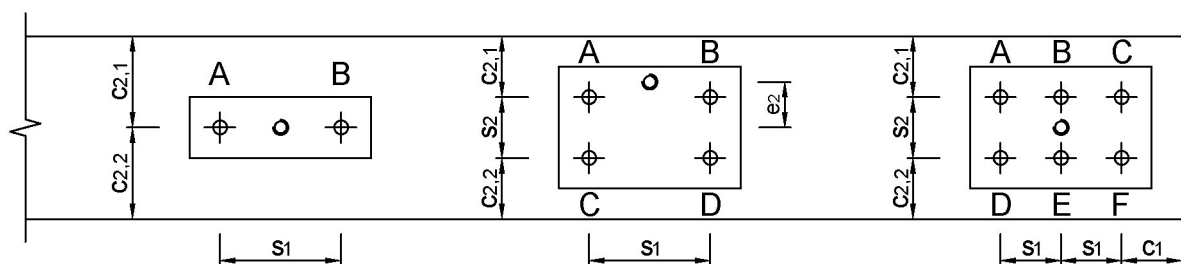
Figure 10.1. Schematic depiction of the configurations used in the numerical study located close to two parallel edges and three close edges along with the designation of the geometrical parameters.

The first part of the numerical program is summarized in Table 10.1. In these simulations the distance to the parallel edges is equal on both sides of the anchor group. In simulations where the anchor groups are placed close to two parallel edges,

the designation of the individual simulations comprises a letter and two digits, each separated by a hyphen (e.g., L-2-120). The letters L, M, and H specify the embedment depth of the anchors. The letter L (low) implies an embedment depth of h_{ef} = 80 mm, the letter M (medium) implies an embedment depth of h_{ef} = 110 mm, and the letter H (high) implies an embedment depth of h_{ef} = 150 mm. The first digit indicates the number of anchors of the group, thus specifies the anchor configuration. The second digit gives the distance to the two parallel edges. In some simulations, the anchor groups are placed close to three edges. In this case a third digit is added, which implies the distance to the third (perpendicular) close edge (e.g., L-6-40-40).

Table 10.1. Numerical program: Part 1.

ID	h_{ef}[1] (mm)	Edge distance (mm)			$f_{c,m}$[2] (mm)	Slab dimensions (mm)			Ultimate load, N_u (kN)
		c_1	$c_{2,1}$	$c_{2,2}$		L	W	H	
L-2-120	80	-	120	120	24.5	1200	240	300	65.6
L-4-80	80	-	80	80	24.5	1200	240	300	94.4
L-4-80-R	80	-	80	80	24.5	1200	240	300	94.2
L-6-85	80	-	85	85	22.3	1200	250	300	94.1
L-6-40	80	-	40	40	22.3	1200	160	300	79.5
L-6-85-80	80	80	85	85	22.3	760	250	300	93.1
L-6-85-40	80	40	85	85	22.3	720	250	300	90.6
L-6-40-40	80	40	40	40	22.3	720	160	300	74.5
M-6-85	110	-	85	85	22.3	1200	250	300	123.8
M-6-40	110	-	40	40	22.3	1200	160	300	100.7
M-6-55	110	-	55	55	22.3	1200	190	300	112.7
M-6-117	110	-	117	117	22.3	1200	314	300	122.1
H-6-85	150	-	85	85	22.3	1200	250	300	150.9
H-6-40	150	-	40	40	22.3	1200	160	300	116.5
H-6-75	150	-	75	75	22.3	1200	230	300	148.5
H-6-160	150	-	160	160	22.3	1200	400	300	164.3

(1) Effective embedment depth
(2) Mean cylinder concrete compressive strength

To begin the numerical study, the numerical modeling approach is validated against the experimental results, and the question is addressed to what extent the surface reinforcement in the experimental part on narrow members (see Chapter 9) had an influence on the capacities of the anchor groups. For this purpose, simulations L-2-120, L-4-80 and L-4-80-R were carried out. The letter R in the designation of simulation L-4-80-R implies that longitudinal surface reinforcement was modelled (two rebars with

diameter of 6 mm) to investigate any potential influence. The modelled concrete members simulate the case where the anchor groups are located close to two parallel edges with equal edge distance to both sides. The specimens were modelled with a length of 1200 mm, a height of 300 mm and a width of 240 mm. Thus, the width of the specimen corresponds to the width of the specimen used in the experiments.

Subsequently, the behavior of anchor groups close to more than one edge is investigated with respect to the failure mechanism, the load-displacement behavior, and the obtained ultimate capacity. Besides anchor groups in narrow members, also anchor groups close to three edges are examined. The main emphasis is on the 3 x 2 configuration with varying embedment depth (80 mm, 110 mm, and 150 mm). However, also the 2 x 1 configuration in L-2-120 is studied with respect to the failure mechanism. Analogous to the experiments, the anchor groups are positioned in such a way that the distance to the parallel edges is equal on both sides. Furthermore, the case is investigated where the anchor groups are loaded centrically in tension. Therefore, in these cases, a certain symmetry of the stress condition in the concrete can be assumed, which, however, might be disturbed in case of different edge distances or eccentric loading towards the parallel edges. In contrast to the experimental study, the edge distance is varied by altering the width of the concrete specimen itself. Therefore, depending on the desired edge distance, the specimens in the individual simulations differ in width. The exact dimensions of the specimens used in the individual simulations, the embedment depth of the anchors, and the edge distance are summarized in Table 10.1.

At last, the case is investigated where the symmetry of the stress condition in the concrete might be disturbed by unequal edge distances on either side of the anchor group or eccentrically applied tension load in the direction perpendicular to the free edges. Therefore, a 2 x 2 configuration with an embedment depth of h_{ef} = 80 mm is studied which is installed in a narrow member with a width of 220 mm. While the width of the concrete member is kept constant, the position of the anchor group is varied in the direction perpendicular to the free edges. In this way, the edge distance is increased to one edge and is decreased to the second edge. In addition, simulation L-4-70/70-E investigates the case where the anchor group is positioned in the middle of the specimen and loaded with an eccentricity in the direction perpendicular to the edges. L-4-70/70 simulates and anchor group with equal edge distance to both sides and centric loading. It serves as the reference case for the other cases. Table 10.2 summarizes the respective simulations. The nomenclature in the second part is similar to the first part (first letter specifies the embedment depth and first digit specifies the number of anchors of the group). Differently, $c_{2,1}/c_{2,2}$ indicates the respective distance to the free edges (e.g., 40/100) and the letter E signifies that the anchor group is loaded by an eccentric tension force.

Table 10.2. Numerical program: Part 2.

ID	h_{ef}[1] (mm)	Edge distance (mm)			e_2[2] (mm)	$f_{c,m}$[3] (mm)	Slab dimensions (mm)			Ultimate load, N_u (kN)
		c_1	$c_{2,1}$	$c_{2,2}$			L	W	H	
L-4-70/70	80	-	70	70	-	24.5	1200	220	300	91.6
L-4-40/100	80	-	40	100	-	24.5	1200	220	300	84.1
L-4-20/120	80	-	20	120	-	24.5	1200	220	300	74.0
L-4-70/70-E	80	-	70	70	67	24.5	1200	220	300	74.1

(1) Effective embedment depth
(2) Load eccentricity in the direction perpendicular to the parallel edges
(3) Mean cylinder concrete compressive strength

10.2 The 3D finite element software MASA

To perform the numerical simulations, the 3D finite element (FE) software MASA (Macroscopic Space Analysis) is used. MASA was developed by Ožbolt et al. (2001) at the Institute of Construction Materials, University of Stuttgart to provide a tool to study the nonlinear behavior of concrete and RC structures. To realistically simulate the formation and propagation of cracks and the associated deterioration of concrete, a smeared crack approach is applied where the constitutive law for concrete is the microplane model with relaxed kinematic constraint proposed by Ožbolt et al. (2001). As indicated in Figure 10.2, this model is based on the assumption that in the concrete matrix planes of various orientation can physically be interpreted as what Ožbolt et al. (2001) call damage planes on a microstructural level (e.g., the interface zone between the aggregates in the concrete matrix as shown in Figure 10.2).
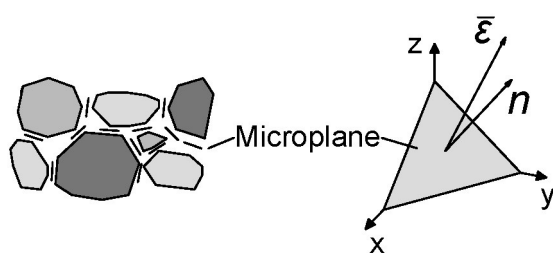
Figure 10.2. The left figure indicates the damage planes (microplanes) between the aggregates and the right figure shows the strain and normal vector of the microplane. Redrawn on the basis of Ožbolt et al. (2001).

The basic concept of the microplane model is schematically illustrated in Figure 10.3. The known macroscopic strain tensor in the integration point of a finite element is applied to a spatial polygon idealizing a sphere. The surfaces of the sphere are discretized by microplanes of various orientations which are defined by their respective normal vector n_j (see Figure 10.2). Note that MASA uses 21 microplanes to discretize

the surfaces on the half sphere (utilizing symmetry, which works out as 42 microplanes for the full sphere). The microplane strain tensors are divided into a normal (ε_N) and two shear components (ε_K and ε_M) as indicated in Figure 10.3. Using uniaxial stress-strain relations, the corresponding microplane stress are then calculated (Ožbolt et al., 2001). In short, the macroscopic strain tensor in the integration point of the finite element is first converted to each microplane and divided into its strain components, which are then used to determine the associated stress components. Once the stress components are determined for each microplane of a sphere, the macroscopic stress tensor, σ_{ij}, can be calculated by numerical integration over all microplane directions using virtual work approach (Ožbolt et al., 2001):

$$\sigma_{ij} = \sigma_V \delta_{ij} + \frac{3}{2\pi} \int_S \left[\sigma_D \left(n_i n_j - \frac{\delta_{ij}}{3} \right) + \frac{\sigma_K}{2} \left(k_i n_j + k_j n_i \right) + \frac{\sigma_M}{2} \left(m_i n_j + m_j n_i \right) \right] dS. \qquad (10.1)$$

In Equation (10.1), n_i is the normal vector, k_i and m_i are the directions of the shear components, δ_{ij} is the Kronecker delta, and dS is the surface of the respective sphere.
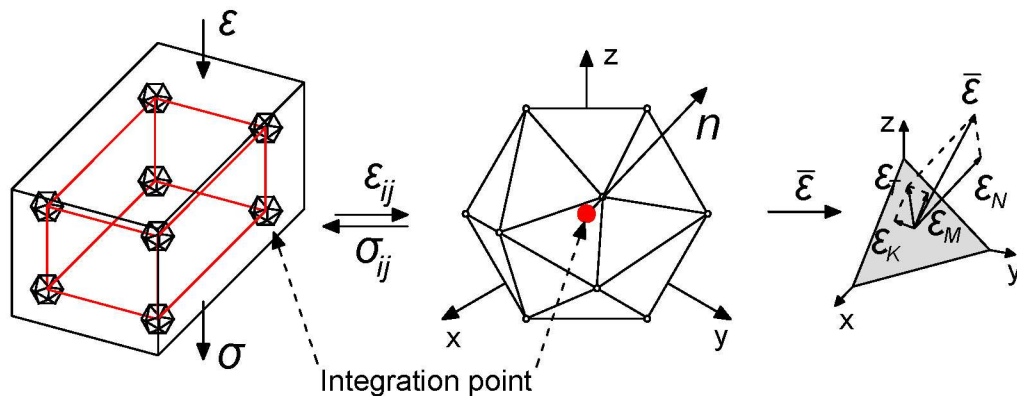
Figure 10.3. Schematic concept of the microplane model. Redrawn on basis of Ožbolt (2009).

According to Ožbolt et al. (2001) the normal component needs to be further divided into a volumetric and a deviatoric component to allow the model to make a viable prediction of the behavior of confined concrete and concrete that is mainly subjected to compression loads. However, it was found that this results in an incorrect behavior in case of dominant tensile loading, which is for example expressed by lateral expansion in case of uniaxial tensile loading. In order to overcome the problem for dominant tensile loads, the microplane strain components were further modified in a way to relax the kinematic constraint by maintaining a constant ratio between the deviatoric and volumetric stiffness. As shown in Ožbolt et al. (2001), this can be achieved by the introduction of the discontinuity function, which is taken into account in the determination of microplane strains (with the exception of volumetric strain).

In finite element simulations a well-known phenomenon is the sensitivity of the analysis towards the element mesh. This phenomenon is also observed when using a smeared crack approach for the simulation of concrete members, causing the load that the modelled member can withstand to increase or decrease depending on the mesh size. To overcome this issue, in MASA, the crack band method (Bažant and Oh, 1983), a so-called localization limiter, is implemented to ensure that the validity of the results is not influenced by the chosen element mesh (MASA Manual).

In this study, the numerical investigation is focused on the concrete cone failure mode. Hence, for the given problem, concrete cone failure is expected before yielding of the steel elements. In order to reduce computational time, the steel elements, such as the anchor rods and the baseplate, are therefore modeled assuming linear-elastic material behavior. The bond between the steel anchors and concrete is discretized using the bond stress-slip behavior as illustrated in Figure 10.4.

For pre- and post-processing, the software FEMAP (Siemens) is utilized. In here the model is prepared (defined through e.g., elements, nodes, material), boundary conditions are defined, and loads (displacements) are applied. These data can be extracted and converted into the input data for MASA. After the analysis, the results from MASA can be in turn converted and imported back to FEMAP for post-processing.
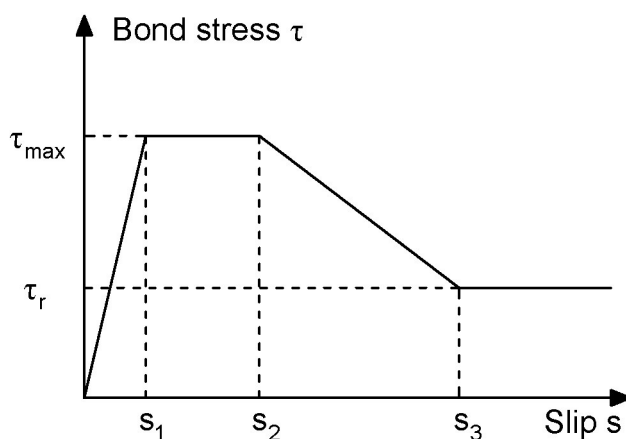
Figure 10.4. Idealization of bond stress-slip relation.

10.3 Numerical modelling approach

Figure 10.5 exemplarily shows the discretization of the concrete specimens for the simulations with two and three close edges and the discretization of the 3 x 2 anchor groups. The concrete specimens were modeled using 4-node tetrahedral elements. Steel elements, such as the anchor rods and the baseplate, were modeled using 8-node hexahedral elements. To simulate the bond between anchor rods and concrete, 2-node bar elements were utilized which are only able to transfer compression and shear forces (see Figure 10.5 (c)). Compression-only 2-node bar elements were used

to model the contact between the baseplate and the concrete. In general, the concrete specimens were modelled as unreinforced specimen. Only in simulation L-4-80-R, the surface reinforcement was also modelled using 2-node bar elements, whereby the bond stress-slip model by Lettow (2007) was applied.

The loads and constraints were directly applied onto the nodes. The anchor groups were loaded in displacement-control by stepwise increasing the displacement by increments of 0.01 mm. In this way, generally more than 10-20 steps were required to reach the ultimate load of the anchor group. The total force acting on the anchor group is calculated from the sum of forces on the loaded nodes in the direction of loading. In order to simulate experimental support conditions, two straight curves were modeled on the upper surface of the concrete specimen. In case of simulations with two close edges, the curves are located on both sides of the anchor group at a distance of twice the embedment depth, $2h_{ef}$, away from the outermost anchors (following the prescribed testing conditions for unconfined tension tests according to EOTA TR 048). In case of simulations with three close edges, only one curve was required. Constraints in the direction of loading were directly applied onto these curves (Figure 10.5 (a)). The bottom surface of the concrete specimens was constraint in all directions to prevent the specimens from sliding and to prevent the negative influence due to bending.
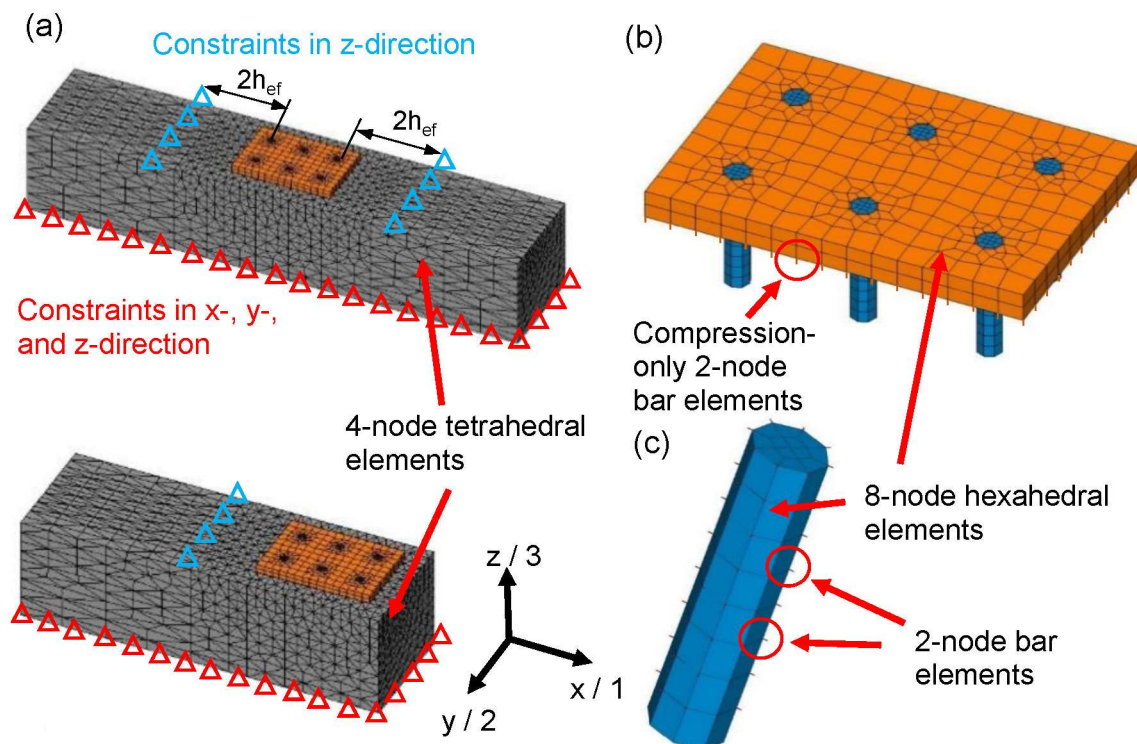
Figure 10.5. (a) Discretization of complete model, (b) discretization of 3 x 2 anchor group, and (c) discretization of anchor rod with 2-node bar elements for bond.

Table 10.3 provides an overview of the material properties for steel and concrete. The steel parts were assumed to behave linear-elastic since concrete failure was expected

before yielding of the steel. Thus, only Young's modulus and Poisson's ratio were given. The concrete properties were calculated based on the mean cylinder concrete compressive strength obtained from the experimental parts. Note that in the numerical study two different values for the concrete compressive strength were applied. Young's modulus of concrete is calculated as $E_c = 22000 \cdot \left(f_{c,m}/10\right)^{0.3}$ (EN 1992-1-1), the tensile strength of concrete as $f_{ctm} = 0.3 \cdot f_{c,m}^{2/3}$ (EN 1992-1-1), and the fracture energy of concrete as $G_F = \alpha_F \cdot f_{c,m}^{0.7}$ (Karihaloo, 1995). The expressions are valid in N and mm units.

Table 10.3. Material properties for concrete and steel.

Material	Compressive strength, f_c (N/mm²)	Young's modulus, E (N/mm²)	Poisson's ratio, v	Tensile strength, f_t (N/mm²)	Fracture energy, G_F (N/mm)
Concrete 1	22.3	28000	0.18	2.40	0.070
Concrete 2	24.5	28800	0.18	2.53	0.065
Steel	-	200000	0.33	-	-

Referring to Figure 10.4, five parameters are required to define the bond between the steel anchors and concrete, which simulates the epoxy mortar layer in the experiments. To define the bond stress-slip behavior two values for bond stress are required, namely the maximum bond strength τ_{max}, and the residual bond strength τ_r. The three required parameters for the corresponding slip are s_1, s_2, and s_3, where s_1 specifies the initial stiffness, s_2 defines the plateau of the maximum bond strength and s_3 corresponds to the point where the residual bond strength in the post-peak phase is reached (see Figure 10.4). The parameters for an epoxy mortar applied in this work are taken from Bokor (2021) as: $\tau_{max} = 32.5 \ N/mm^2$, $\tau_r = 8 \ N/mm^2$, $s_1 = 0.01 \ mm$, $s_2 = 0.2 \ mm$, and $s_3 = 2 \ mm$.

10.4 Validation of the numerical modelling approach

To validate the numerical modelling approach, the results of simulation L-2-120 and L-4-80 are compared to the experimental results obtained in test series C-22 and C-32, respectively. The results are compared in terms of the load-displacement behavior and the observed crack pattern. The respective simulations and experiments involve centrically loaded anchor groups installed in narrow concrete members.

In Figure 10.6, the load-displacement behavior observed in the experiments is compared to the behavior in the numerical analysis. In both cases, L-2-120 and L-4-80, the numerical behavior appears to be slightly stiffer in the ascending branch, which is attributable to the unavoidable slips in the tests that affect the initial part of the

experimental curves. However, the actual stiffness is quite similar in tests and numerical simulations. This is evident from the comparison of the slope of the curves between 50% of the ultimate load and ultimate load. For the 2 x 1 anchor group, the mean secant stiffness $k_{50\%-100\%}$ is 112 kN/mm and 91 kN/mm in tests and numerical simulation, respectively. For the 2 x 2 anchor group, the mean secant stiffness $k_{50\%-100\%}$ is 180 kN/mm and 218 kN/mm in tests and numerical simulation, respectively. The discrepancy between numerical and experimental results in the post-peak range of the load-displacement curve is attributable to the limits of accuracy of measurement and data acquisition in the experiments due to the very brittle failure of the anchor groups in narrow members and the hydraulic-controlled testing approach which made it difficult to control the post-peak behavior shortly after the failure occurred (only very few points are actually measured in the descending branch). On contrary, the numerical analysis is carried out in displacement control using a secant stiffness approach and therefore allow the load to be dropped when the significant event (failure) happens and then regain the stiffness in the next branch. As can be seen, the numerical results somewhat underestimate the actual capacity. In L-2-120, the experimental mean ultimate load is 74.1 kN, while the obtained ultimate load from analysis is 65.6 kN (~11% lower than tests). In case of L-4-80, the discrepancy is less severe with a numerical capacity of 94.4 kN, approximately 8% lower than the experimental mean ultimate load of 102.7 kN.
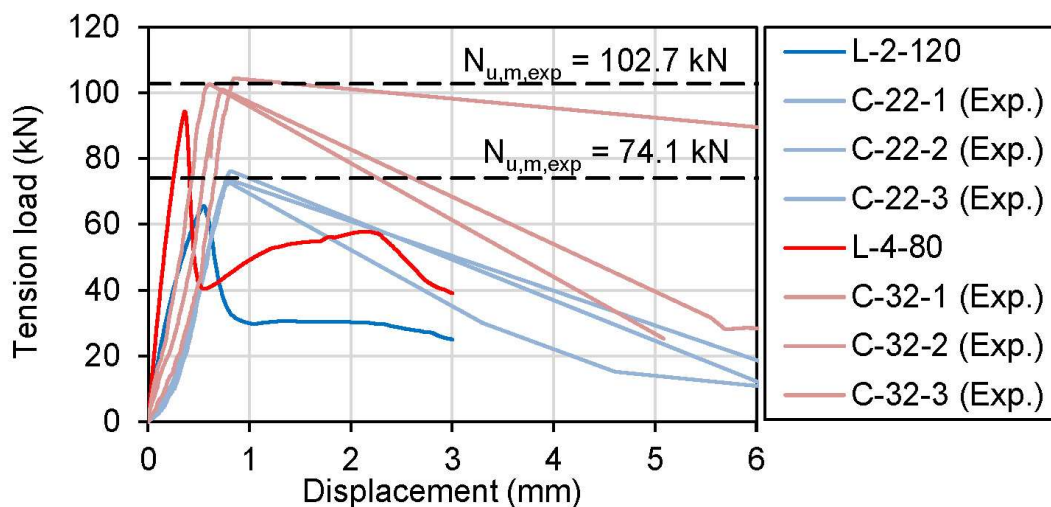
Figure 10.6. Comparison of the load-displacement behavior obtained in the numerical analysis and the experiments.

Figure 10.7 shows a comparison between the crack pattern obtained in the experiments and the numerical analysis. The comparison is made by reflecting the numerically obtained crack patterns to the experimental photographs of the failure modes. In the simulation, the crack pattern is depicted in terms of principle tensile strain where red elements represent a crack width larger than 0.1 mm. From the comparison, it can be seen that the numerical and experimental failure modes are in a good

agreement. Overall, the comparison showed that the numerical simulations reflect the real anchor behavior with a sufficient degree of accuracy.
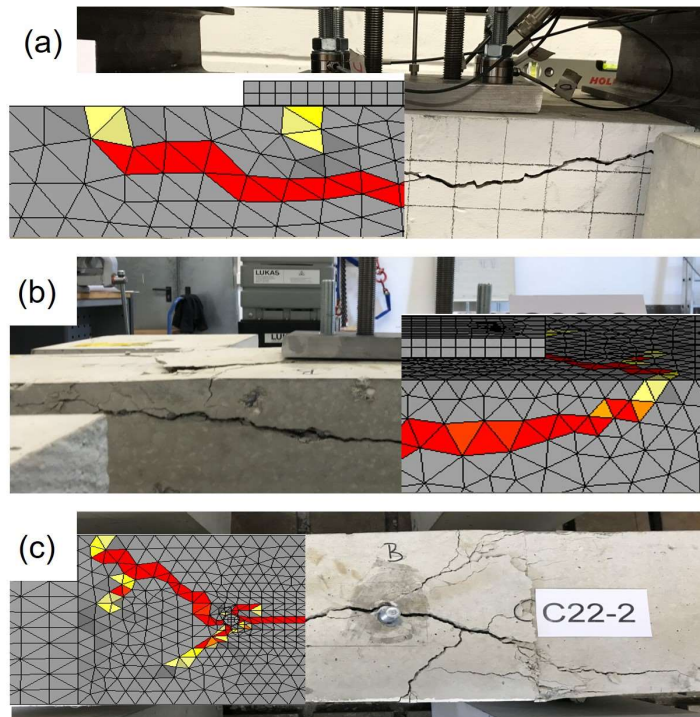
Figure 10.7. Comparison of the crack patterns obtained in the numerical analysis and the experiments (a) side view of L-4-80 and C-32, (b) side view of L-2-120 and C-22, and (c) top view of L-2-120 and C-22.

10.5 Results of numerical parametric studies and discussion

10.5.1 Influence of surface reinforcement

In the experiments, two rebars with a diameter of 6 mm were provided relatively close to the concrete surface which are located in the anchorage zone of the tested anchor groups (see Chapter 9). Therefore, this section deals with the question whether the longitudinal reinforcement had any influence on the capacity of the tested anchor groups. For that purpose, the concrete specimen used in L-4-80 has additionally been modelled with reinforcement as shown in Figure 10.8 (a). The position of reinforcement with respect to the top surface and the free edges is identical to the position of the longitudinal reinforcements in the respective experiments (see Figure 9.4). Mesh size, loading, and constraints of L-4-80 and L-4-80-R were otherwise identical. With respect to the obtained ultimate capacity, the longitudinal reinforcement had basically no significant influence (see Table 10.1). This also applies to the observed load-displacement behavior as can be seen in Figure 10.8 (b). According to the numerical results, it can be assumed that the surface reinforcement that was provided in the experiments had no major influence on the behavior of the tested anchor groups.

Furthermore, the numerical results show that the modelling of unreinforced concrete specimens represents a valid simplification.
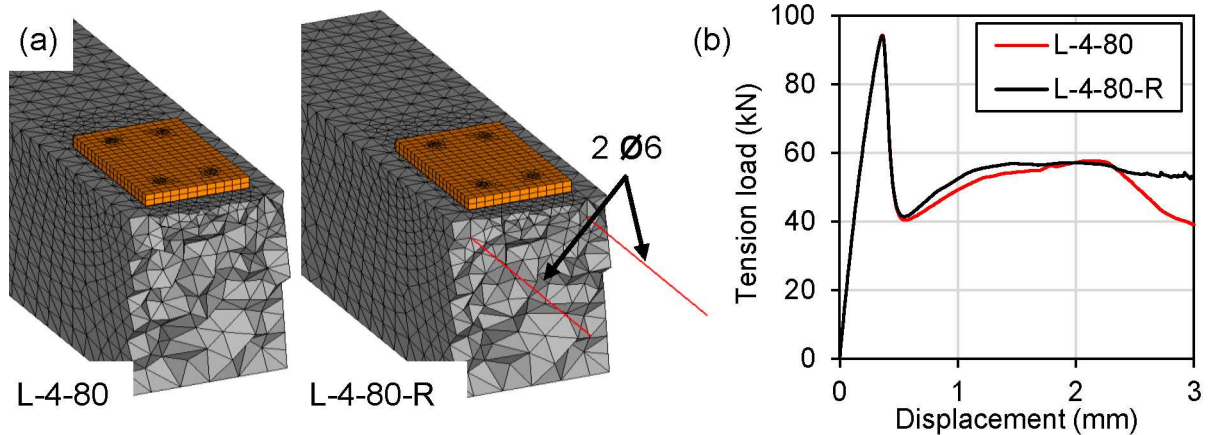
Figure 10.8. Comparison of the behavior with and without surface reinforcement (a) numerical models and (b) load-displacement curves.

10.5.2 Failure mechanism of anchor groups located close to more than one edge

To investigate the failure mechanism of anchor groups in narrow members with two parallel or three close edges in more detail, the crack patterns obtained from the numerical analysis are evaluated. The numerical simulation allows to examine the fracture process in the concrete, while in the experiments only the cracks on the surface become visible. For this purpose, a 2 x 1 configuration with two close parallel edges (L-2-120) and a 3 x 2 configuration with two parallel (L-6-40) and three close edges (L-6-40-40), respectively, are investigated.

Figure 10.9 shows the failure mechanism observed in simulation L-2-120 with centric loading. The figure shows a section cut through the concrete specimen, allowing to identify the crack propagation towards the free edges. At ultimate load, discrete cracks have formed both close to the concrete surface and at the embedded ends of the anchor rods. The shallow cone which formed relatively close to the concrete surface has a depth of approximately 30 mm (40% of the embedment depth). The crack at the embedded end has a length equal to about 20% of the length of the fully developed concrete cone, with an inclination of 20° - 30° against the concrete surface. With increasing displacement of the anchor group, the crack propagation at the surface stops while at the embedded end, initially the inclined crack growth continues. However, with further increasing displacement, the inclined crack turns into an almost horizontal crack towards the free edges. The lower capacity of the 2 x 1 groups compared to the other tests at the same embedment depth and with the same projected area, which was already observed in the experimental part, might be

attributed in part to the fact that at ultimate load, the behavior is governed by the shallow cone forming close to the concrete surface.

N = 65.6 kN
s = 0.55 mm
(Ultimate load)

N = 61.7 kN
s = 0.59 mm

N = 36.7 kN
s = 0.75 mm
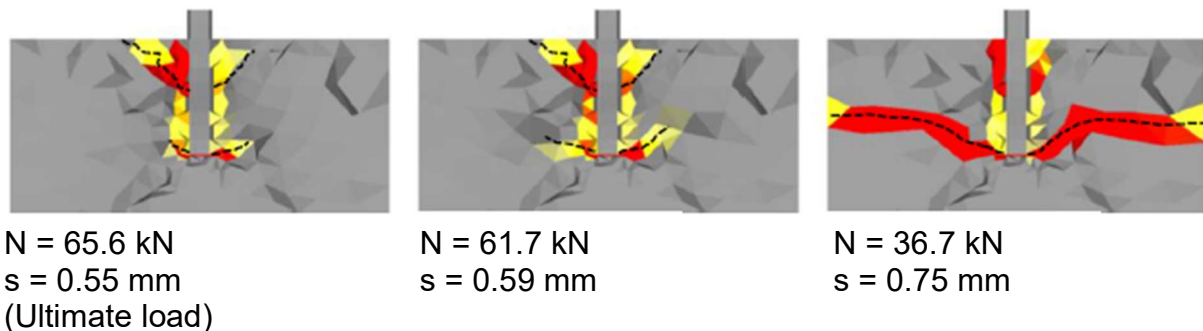
Figure 10.9. Failure mechanism observed in simulation L-2-120 with two parallel close edges (h_{ef} = 80 mm; c_2 = 120 mm).

Figure 10.10 (a) shows the failure mechanism observed in simulation L-6-40 with two close parallel edges and centrical tension load. The edge distance is 40 mm on both sides. Circumferential cracking starts at the embedded ends of the two middle anchors, from where horizontal cracks start propagating towards each other, the outer anchors, and the free edges. When the anchor group reaches its ultimate capacity, the cracks between the middle anchors merge and horizontal discrete cracks have almost reached the free edges. At this point circumferential cracking starts at the embedded ends of the outer anchors as well. Upon further loading, the crack propagation becomes unstable as the cracks which started from the two middle anchors reach the free edges. Thereafter, the horizontal cracks between the outer and the middle anchors merge and then the horizontal cracks that started from the embedded ends of the outer anchors reach the free edges. While with increasing displacements the already existing horizontal cracks at the bottom of the breakout body become wider, conical cracks start propagating from the embedded ends of the outer anchors towards the concrete surface in the direction parallel to the edges and the final concrete cone forms. The staggered initiation of cracking between outer and inner anchors suggests that the load is initially mainly taken up by the two inner anchors, while the outer anchors are initially less involved in the load transfer. The numerical findings support the previous observations made in the experiments with respect to the load transfer and failure mechanism.

In Figure 10.10 (b), the observed failure mechanism for simulation L-6-40-40 with three close edges and centrical tension load is illustrated. Initially, before the ultimate load of the anchor group is reached, circumferential cracks form at the tip of the embedded ends of the middle anchors while the outer anchors show no cracks. At ultimate load, cracking is mainly governed by the two middle anchors, while the outer anchors only show initial circumferential cracking at the tip of the anchor rod. Discrete circumferential cracks which started from the middle anchors have propagated horizontally towards each other and towards the outer anchors. Furthermore, a

horizontal crack has propagated towards the free edge. However, at ultimate load, the discrete cracks have neither merged between the anchors nor reached to concrete surface at the free edges. Upon further increasing the displacement after reaching the ultimate load, the horizontal cracks that started at the embedded ends of the middle anchors towards each other merge and form a single crack. Simultaneously, cracks form at the embedded ends of the anchors closest to the third free edge and propagate horizontally towards the free edges and towards the middle anchors. Crack propagation upon reaching ultimate load is mainly governed by the cracks that started from the two anchors closest to the third free edge, where larger discrete cracks propagate relatively fast towards the three close edges. When the cracks approach these free edges, typical cone like cracks in the direction parallel to the free edges start propagating from the embedded ends of the anchors which are farthest away from the third edge towards the upper surface of the concrete specimen.

(a) Anchor group located close to two parallel edges

N = 79.2 kN	N = 79.5 kN	N = 66.7 kN	N = 34.3 kN
s = 0.10 mm	s = 0.11 mm	s = 0.12 mm	s = 0.15 mm
	(Ultimate load)		

(b) Anchor group located close to three edges

N = 72.7 kN	N = 74.5 kN	N = 62.5 kN	N = 15.6 kN
s = 0.10 mm	s = 0.11 mm	s = 0.12 mm	s = 0.17 mm
	(Ultimate load)		
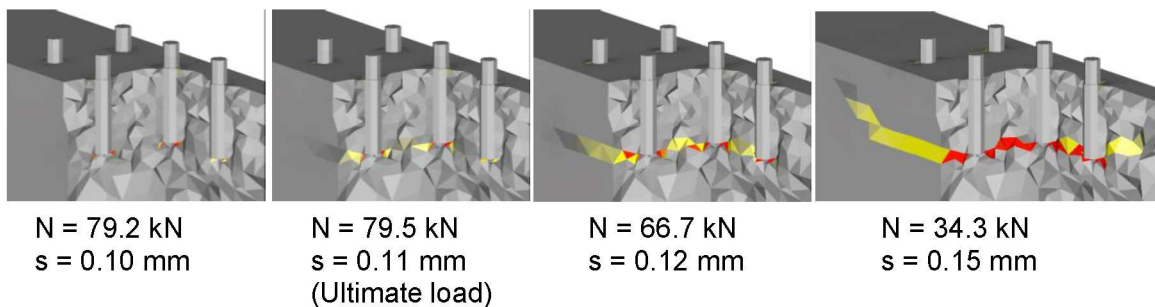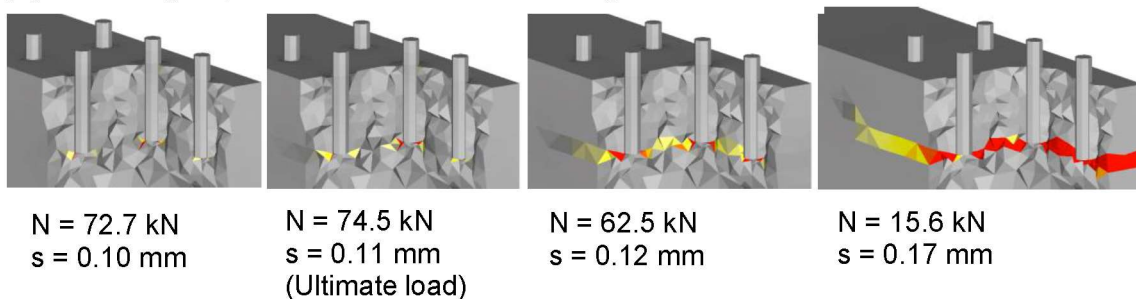
Figure 10.10. Failure mechanism observed in (a) simulation L-6-40 with two parallel close edges (h_{ef} = 80 mm; c_2 = 40 mm) and (b) simulation L-6-40-40 with three close edges (h_{ef} = 80 mm; c_1 = c_2 = 40 mm).

10.5.3 Influence of two parallel close edges and three close edges on the load-displacement behavior of anchor groups

Figure 10.11 shows the load-displacement curves obtained from simulations where 3 x 2 anchor groups were placed close to two parallel edges and close to three edges. Thereby, the distance to the free edges was varied in each simulation. The results shown, are limited to the case where the anchor group is loaded centrically in tension.

The first general observation that stands out is that the descending branch of the curves in case of close edges shows a severe drop after reaching the ultimate load. It can be observed that the descending branch becomes steeper with smaller edge distance and additional close edges, whereby it appears that the edge distance has the greater influence on the post-peak behavior. While the post-peak behavior obtained from the experiments is rather inconclusive as only few points were measured after reaching the ultimate load, the numerical results clearly highlight the brittle behavior of anchor groups installed in narrow members.

To evaluate the numerical results with anchor groups located close to the edge, the results of the experiments without any edge influence are used. Test series BA-3x2-C-stat has the same anchor configuration and the same mean cylinder concrete compressive strength as used in the numerical analysis. The corresponding mean ultimate load is 102.1 kN. In those cases where the edge distance was relatively large (approximately equal to the effective embedment depth), the negative effect on the load-bearing capacity was comparatively small. As can be seen in the simulations L-6-85, L-6-85-80, and L-6-85-40 the ultimate capacity is reduced by around 8% - 11% when compared to BA-3x2-C-stat. The numerical results show that placing the anchor group close to an additional third edge has only a minor effect on the group behavior. Comparing simulation L-6-85 with two close edges and large edge distance (c_2 = 85 mm) to simulation L-6-85-80 with three close edges and large edge distance (c_1 = 80 mm; c_2 = 85 mm), it can be seen that the behavior of the anchor groups and their capacity is almost identical. Again, further reducing the distance to the additional third edge to c_1 = 40 mm in simulation L-6-85-40 has only a small impact on the overall behavior. Regarding L-6-85 and L-6-85-40, the ultimate load obtained from L-6-85-40 reduces by around 4% compared to L-6-85. In contrast, reducing the distance to the parallel edges has a more pronounced influence on the overall behavior as can be seen from simulation L-6-40 and L-6-40-40 (c_2 = 40 mm). A notable reduction in the ultimate capacities can be observed and also the stiffness is reduced compared to the cases with large edge distance. As shown in the previous section, when reaching the ultimate load, cracking is dominated by the middle anchors of the group, which are nearest to the point where the load was applied onto the group. This was observed for anchor groups close to two edges as well as for anchor groups close to three edges. In both cases, at ultimate load, the horizontal cracks have not yet reached the surface of the free edge and initial circumferential cracking at the tips of the remaining anchors has just begun. Since the ultimate load appears to be related to the length of the crack towards the parallel edges, this observation might provide an explanation for the similar behavior of the anchor groups in L-6-85, L-6-85-80, and L-6-85-40 (equal distance to the parallel edges). At ultimate load, although all anchors participate in the load transfer, the two middle anchors take up the highest load. When the horizontal cracks which propagated form the middle anchors towards the free edges reach a certain length, the middle anchors reach their ultimate capacity. This is similar to the behavior of single anchors, which reach their ultimate capacity when the conical crack towards

the concrete surface has a certain length (Eligehausen et al., 2006). Thereafter, crack propagation becomes unstable, and the forces are redistributed to the outer anchors. However, the capacity of the anchor groups does not increase further. The slightly reduced capacity and the more brittle behavior in case of an additional third edge might be explained by the reduced capacity of the two anchors closest to the third edge and the internal eccentricity formed due to asymmetry of the hoop stresses. After reaching the ultimate capacity, the forces are distributed to the outer anchors. In the case of two parallel edges, due to symmetry, the load capacity of the outer anchors is the same on both sides and the hoop stresses are in balance. In the case of a third edge, however, the hoop stresses get disturbed due to the presence of the third edge and the symmetry is lost. The load capacity of the group is limited by the reduced capacity of the anchors close to the third edge.
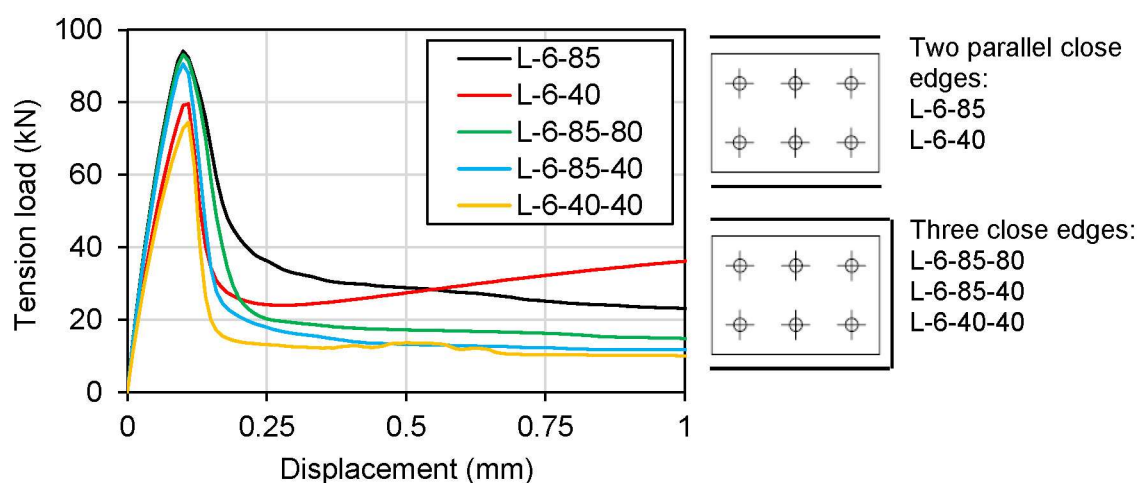
Figure 10.11. Load-displacement curves obtained from the numerical analysis of centrically loaded anchor groups with same embedment depth (h_{ef} = 80 mm) but varying number of close edges and varying edge distance.

10.5.4 Influence of the embedment depth on the ultimate capacity of anchor groups located close to two parallel edges

First, the behavior of the anchor group is investigated when the dimensions of the concrete specimen remain the same (thus the distance to the edges is kept constant) while only the embedment depth is increased. This means that the relative edge distance, that is the ratio between edge distance, c_2, and embedment depth, h_{ef}, is decreasing with increasing embedment depth. To this purpose, two concrete specimens with a width of 250 mm and 160 mm were modelled, where the installed anchor groups have an equal edge distance to both parallel edges of 85 mm and 40 mm, respectively. The simulations which were evaluated for an edge distance of 85 mm include L-6-85, M-6-85, and H-6-85. The simulations L-6-40, M-6-40, and H-6-40 have an edge distance of 40 mm. Figure 10.12 shows the obtained ultimate loads as a function of the effective embedment depth of the anchors. The data points can be

fitted by a power function. As can be seen, the exponent takes a value smaller than one, which is due to the size effect. From the small number of data points, however, it appears that for the investigated cases, the ultimate capacity, N_u, increases rather linearly with increasing embedment depth when the width of the concrete specimen remains the same. This observation may be attributable to the fact that the larger embedment depth and thus the corresponding larger side length of the concrete cone is only effective in the direction parallel to the edges. In other words, if the width of the concrete specimen is kept constant, with increasing embedment depth the fracture surface does not increase by the same extent as when installed in wide slabs. Therefore, the size effect is not as pronounced as assumed by the CCD method.
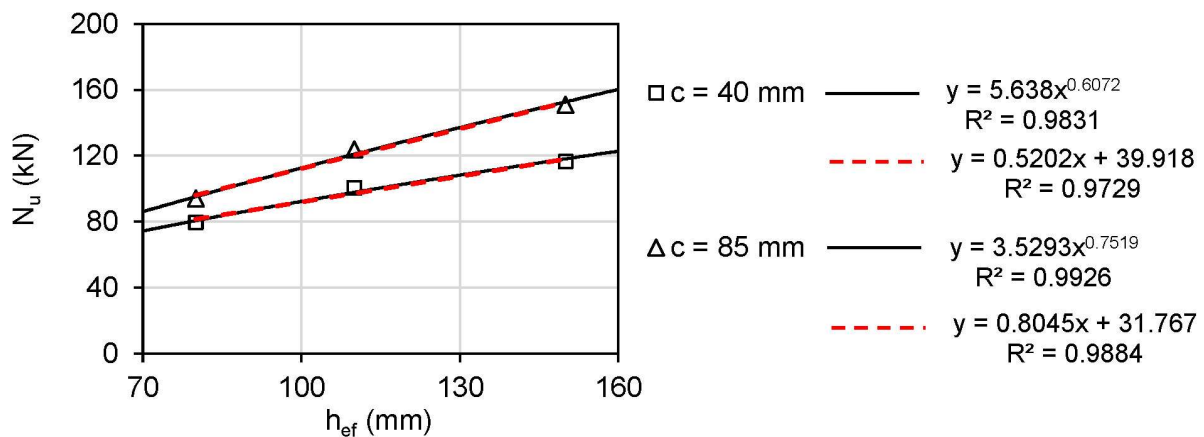
Figure 10.12. Influence of embedment depth: Ultimate load as a function of the embedment depth for constant edge distance.

Additional simulations with an embedment depth of 110 mm and 150 mm have been performed, where the width of the concrete specimen resulted in a relative edge distance of c/h_{ef} = 0.5 and 1.06 (M-6-55, M-6-117, H-6-75, and H-6-160). This corresponds to the relative edge distances of simulations L-6-85 and L-6-40. Along with the other results for the 3 x 2 configuration with two parallel edges, the obtained ultimate loads are shown in Figure 10.13 as a function of the relative edge distance. Note that in most cases, the relative edge distance was larger than 0.3. One simulation with an embedment depth of 150 mm was performed with a relative edge distance of 0.267, which is identified by a filled triangle. Considering only the cases where the relative edge distance is larger than 0.3, it can be seen that for the same embedment depth of the anchors, the obtained ultimate load increases linearly with increasing relative edge distance. Since the edge distance is increased by increasing the width of the concrete specimen, the linearly increasing capacity is attributable to the additional concrete available in the direction perpendicular to the edges. In other words, if the embedment depth of the anchors is kept constant, the projected area increases linearly with increasing width of the concrete specimen. This also means that the upper limit for the capacity is reached when the relative edge distance to the parallel edges is 1.5 (critical edge distance). If the relative edge distance falls below the value 0.3, it appears

that the load reduction no longer follows a linear regression. From Figure 10.13 it can be seen that for an embedment depth of 150 mm, the load is affected by a notably higher reduction when moving from a relative edge distance of 0.5 to 0.267. The numerical results imply that if the relative edge distance falls below a critical value, the close parallel edges might have an additional negative effect on the capacity of an anchor group.
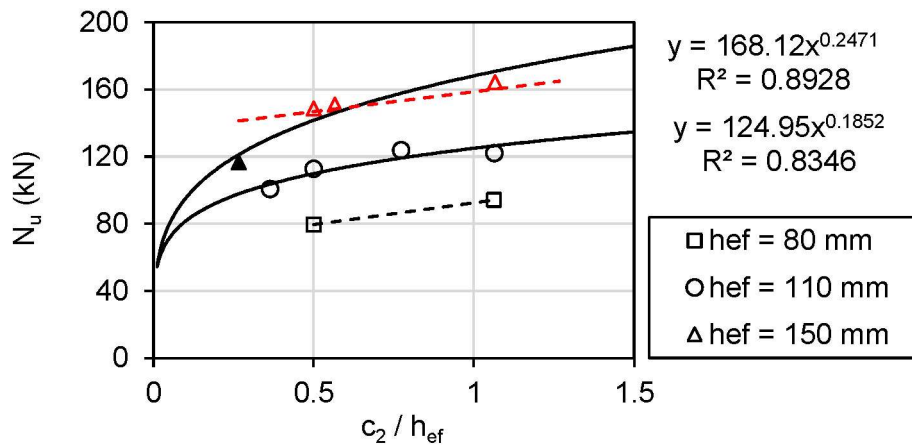
Figure 10.13. Influence of embedment depth: Ultimate load as a function of the relative edge distance for various embedment depths.

10.5.5 Influence of asymmetry in narrow concrete members (unequal edge distance)

In the previously discussed simulations where the anchor groups were placed between two parallel edges and loaded centrically in tension, only the case where the edge distance was identical on both sides was considered. In these cases, it can be assumed that the rotational stress condition in the concrete is symmetrical. Accordingly, a disturbance of the stress field could be assumed if either the distance to the edges on both sides of the group were different or if an eccentric tension load were applied in the direction perpendicular to the free edges. In order to investigate a potential asymmetric stress condition, two special cases for anchor groups installed in narrow members were studied on a 2 x 2 anchor group with an embedment depth of 80 mm. The first case considers a narrow concrete member with constant width, where the centrically loaded anchor group is stepwise placed closer to one of the edges, while the distance to the second edge increases accordingly (L-4-40/100 and L-4-20/120). Note however that the edge distance to both sides is always less or equal to the critical edge distance. Therefore, the total projected area is the same in all simulations as per the CCD method. Also, since the load is applied centric to the group, no eccentricity factor shall be applicable. However, as the edge distance varies, the eccentricity factor as per the CCD method would vary as well.

The second case considers a variation of load eccentricity with load being moved towards one of the free edges (uniaxial eccentricity) while the anchor group is placed in the middle of the narrow member with equal edge distance on both sides (L-4-70/70-E). As a reference, one simulation was performed where the anchor group is placed in the middle of the narrow member and loaded centrically in tension (L-4-70/70). Details of the simulations are given in Table 10.2. The results in terms of load-displacement curves are shown in Figure 10.14. Placing the anchor group closer to one edge results in a reduction of the ultimate capacity. Thereby it seems that the load reduction increases as the difference between the two edge distances increases. However, the initial stiffness of the anchor groups appears to be unaffected by their position. From the crack propagation at ultimate load shown in Figure 10.15 (a) and (b), it can be seen that at ultimate load the forces are rather equally distributed among the anchors. This was also evident from the comparison of the stresses in the anchor rods at ultimate load and explains why the initial stiffness of the anchor groups is quasi identical. Failure is initiated when the anchors adjacent to the closer edge reach their ultimate capacity, whereby the crack towards the free edge swiftly propagates towards the concrete surface. At this point, the forces are distributed to the remaining two anchors from where a conical crack propagates towards the second free edge and in the direction parallel to the edges.
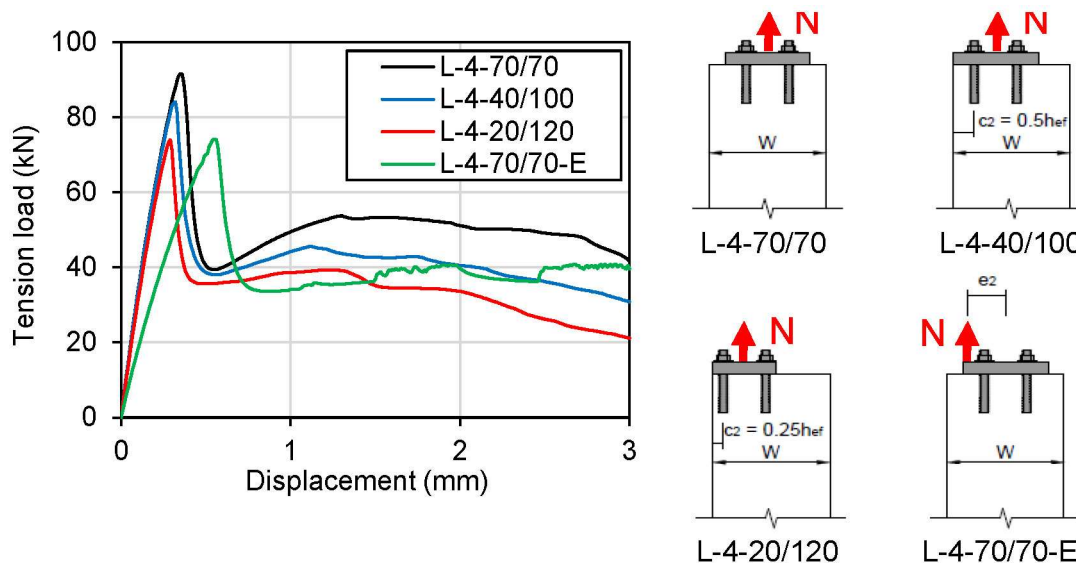
Figure 10.14. Load-displacement curves obtained from simulations L-4-70/70, L-4-40/100, L-4-20/120, and L-4-70/70-E.

In case of an eccentrically applied tension load towards one of the parallel edges, both the ultimate capacity and the stiffness of the anchor group decreases markedly. From the crack pattern shown in Figure 10.15 (c) it becomes apparent that the anchors closest to the point of load application are loaded prior to the remaining two anchors. The deferred activation of the anchors explains the reduced stiffness of the anchor groups in comparison to the previously discussed simulations.
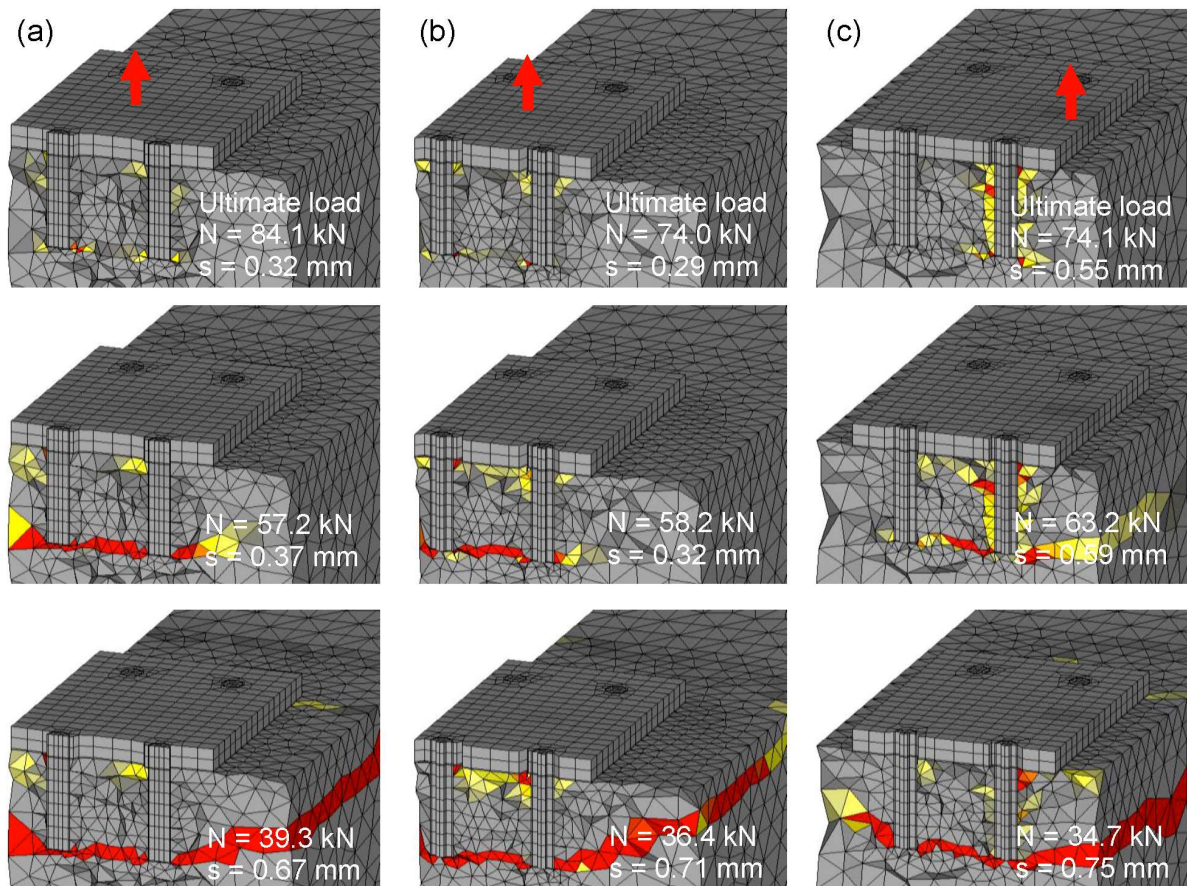
Figure 10.15. Section cut through a narrow concrete member at the position of the anchors in a 2 x 2 group. Crack pattern obtained from simulation (a) L-4-40/100, (b) L-4-20/120, and (c) L-4-70/70-E.

10.6 Summary

In order to support the findings of the experimental work and to gain a deeper understanding of the behavior of anchor groups installed close to more than one edge, an extensive numerical investigation was conducted. The main findings of the numerical study are:

1. The numerical modelling approach was successfully validated against the experimental results, and it was shown that the 3D finite element software MASA is able to accurately simulate the load-displacement behavior of anchor groups installed in concrete.

2. The simulation with an unreinforced and a reinforced concrete specimen have shown that the longitudinal surface reinforcement that was provided in the experiments has no significant influence on the load-displacement behavior or the crack pattern of the tested anchor groups.

3. In the numerical analysis, cases with two and three close edges and with varying edge distances were investigated. It was observed that in those cases with a relatively large edge distance the negative effect on the load-bearing capacity was rather small. An additional third edge had only a minor influence on the group capacity as the behavior of the modelled 3 x 2 anchor group appears to be dominated by the crack formation starting from the middle anchors towards the parallel edges. By reducing the distance to the two parallel edges, the capacity and stiffness decreased notably compared to the cases with large edge distance.

4. The investigation on the failure mechanism of centrically loaded anchor groups located close to the edge support the findings of the experimental work. At ultimate load, the investigated 2 x 1 anchor group showed an inclined cracking at the embedded end of the anchor rods while a shallow cone had formed close to the concrete surface. After the ultimate load has been reached the inclined crack growth at the embedded end continues and turns into a horizontal crack towards the free edges with increasing displacements. In case of the investigated 3 x 2 anchor group, cracking starts from the tips of the embedded ends of the middle anchors where horizontal cracks start to propagate towards each other, the outer anchors, and the free edges. Thereafter the outer anchors are also activated. The ultimate capacity of the group is reached when the horizontal crack towards the free edge has reached a certain length.

5. Both geometrical asymmetry and asymmetry of loading in the direction perpendicular to the edges results in an additional reduction of the capacity of anchor groups installed in narrow concrete members. Moreover, asymmetry of loading results in a significant reduction of the stiffness.

11 Modified design concepts for anchor groups in narrow concrete members

11.1 Experimental results vs. CCD method

In case of concrete cone failure of single anchors or anchor groups which are installed in narrow RC members such as beams and columns, the vicinity of two close edges hinders the development of a full concrete cone breakout body and thus reduces the capacity. As mentioned before, the CCD method (Fuchs et al., 1995), which is included in all major guidelines and standards such as EN 1992-4 , ACI 318-14, and fib Bulletin 58 for the design against concrete cone failure, considers the influence of close edges in two ways. One is through the projected surface area of the group which is reduced according to the close edges. The other is through the reduction factor $\psi_{s,N}$, which considers a reduction of the capacity due to the disturbance of the rotationally symmetric stress conditions in the concrete. However, in experimental studies on single anchors (Bujňák and Farbák, 2018) and anchor groups (Anderson et al., 2017) which were placed adjacent to two parallel edges with equal edge distance, it was found that the calculated capacities for concrete cone breakout failure according to current standards and guidelines are well below the capacities obtained in the experiments.

Figure 11.1 shows the ratio between the ultimate capacities obtained from the experiments presented in the previous chapters and from Anderson et al. (2017), $N_{u,exp}$, and the calculated mean capacity according to EN 1992-4, N_{EN2-4}. The ratio is plotted as a function of the relative edge distance, c_2 / h_{ef}. Note that the experimental results only consider the case where anchor groups were installed in narrow members with equal edge distance to both sides and which were loaded centrically in tension. The mean capacity according to EN 1992-4 was calculated using the mean cylinder concrete compressive strength at the time of testing of the respective tests. The results are in accordance with the previous findings from the literature with respect to the conservatism of the current design approach. Figure 11.1 shows that the calculated values are in part well below the experimentally obtained capacities. This is particularly true for rather small relative edge distances where, according to EN 1992-4, only around 60% of the actual capacity of the anchor group is utilized. The conservatism of the current design approach increases linearly with decreasing relative edge distance. Thus, with decreasing relative edge distance, the current approach becomes less accurate in capturing the actual capacity of anchor groups in narrow members.
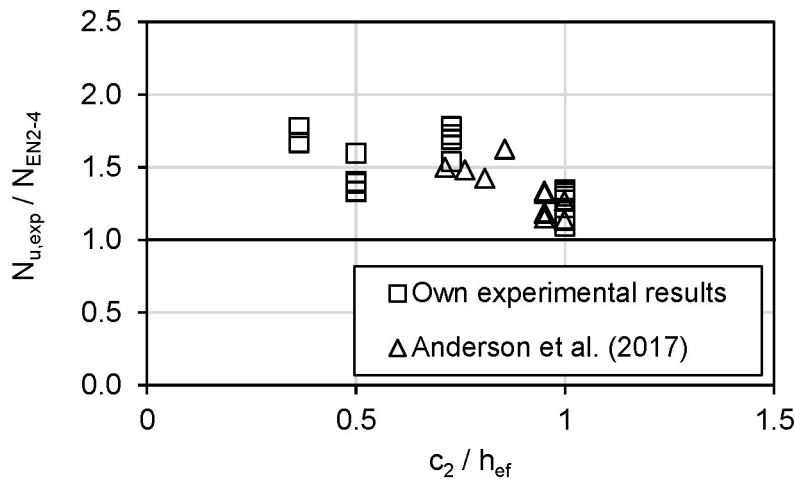
Figure 11.1. Ratio between the ultimate capacities obtained from the own experimental work and from Anderson et al. (2017) and the calculated mean capacity according to EN 1992-4. The ratio is plotted as a function of the relative edge distance, c_2 / h_{ef}.

In order to overcome the over-conservatism of the current analytical design approach (Bujňák and Farbák, 2018; Anderson et al., 2017), in this chapter, four concepts will be discussed which aim on modifying the current design approach. Three concepts consider a modification factor which increases the calculated tension capacity according to the current approach for anchor groups in narrow members. The first modification factor was proposed by Anderson et al. (2017) and is based on the ratio between the spacing in the direction perpendicular to the free edges, s_2, and the edge distance, c_2. The second modification factor considers the relative edge distance. As shown in Figure 11.1, the conservatism clearly increases with decreasing relative edge distance. The third approach that will be discussed is based on the assumption that, in case of identical edge distance on both sides and centric loading, there is no disturbance of the rotationally symmetric stress conditions in the concrete. In this case, the reduction factor $\psi_{s,N}$ becomes rather superfluous and might be neglected to avoid an immoderate conservatism. Finally, a third modification factor is discussed based on the factor $\psi_{h,V}$ for concrete edge failure of shear loaded anchors according to EN 1992-4. Thus, it is assumed that the capacity of single anchors or anchor groups installed in narrow concrete members does not decrease as strongly with decreasing width of the concrete member as determined by the ratio $A_{c,N}/A_{c,N}^0$.

Note that the discussed analytical approaches are strictly only valid for the tested anchor groups with centrical tension load and where the distance to the two close parallel edges is equal on both sides.

Besides the analytical approaches, the spring modelling approach proposed by Bokor (2021) is applied to anchor groups in narrow members and compared to the experimental results. In addition to the ultimate capacity of anchor groups, this

approach allows the evaluation of the load-displacement behavior of anchor groups which fail due to concrete cone breakout (Bokor, 2021).

11.2 Modification of analytical design concept

11.2.1 Approach 1: Modification factor according to Anderson et al. (2017)

In Anderson et al. (2017) the issue of over-conservatism in case of parallel edges is addressed by means of a modification factor, $\psi_{||,N}$, which increases the calculated capacity for the concrete cone failure mode. However, it should be noted that the proposed modification factor is based on a limited number of tests and only anchor groups comprising headed studs with an embedment depth of h_{ef} = 66.8 mm were tested. Furthermore, the tested configurations were limited to 2 x 1 and 2 x 2 anchor groups. The modification factor proposed by Anderson et al. (2017) is solely a function of the ratio between the anchor spacing in the direction perpendicular to the free edges, s_2, and the distance to the free edges, c_2:

$$\psi_{||,N} = 1.0 + \left(\frac{s_2}{4c_2}\right). \tag{11.1}$$

Other parameters such as the influence of the embedment depth or the relative edge distance were not considered. In Figure 11.2 the experimental results (including the results by Anderson et al. (2017)) are plotted along with the proposed equation (solid black line). It can be seen that if the anchor spacing is rather large in comparison to the edge distance, the modification factor actually results in an overestimation of the capacity. In fact, the experimental results obtained in this work imply a rather small or even no impact on the discrepancy between the calculated value and the actual behavior. This can be seen from the linear regression curve of the experimental results, which is plotted as the dashed red line. It appears that the ratio between spacing s_2 and edge distance c_2 is not suitable to define a modification factor for the calculated capacity in case of two parallel edges.
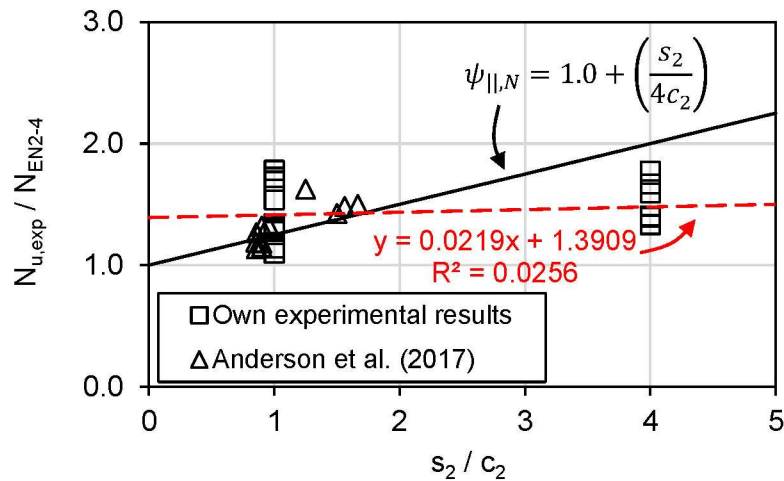
Figure 11.2. Discrepancy between experimental capacities and the calculated mean capacity according to EN 1992-4 as a function of the ratio between anchor spacing in the direction perpendicular to the edges and the edge distance.

11.2.2 Approach 2: Modification factor based on the relative edge distance

As seen in Figure 11.1, the discrepancy between the calculated capacities and the behavior observed in the experimental work increases with decreasing relative edge distance. Therefore, the second approach considers a modification factor based on the ratio c_2 / h_{ef}. The approach is linked to the experimental results, which showed that, for a constant projected area (constant width of the concrete specimen), the ultimate load does not significantly change, even for smaller edge distances. Correspondingly, the reduction factor $\psi_{s,N}$, which is defined in particular by the edge distance, has an increasingly conservative effect. The proposed modification factor therefore counteracts this excessive reduction of the ultimate load. Figure 11.3 shows the experimental results obtained in this work and by Anderson et al. (2017) as a function of the relative edge distance. The red dashed line represents the linear regression over the results.
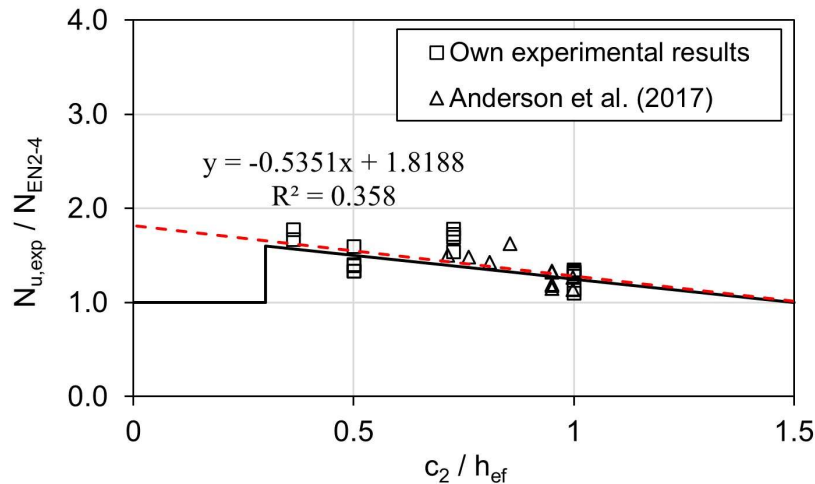
Figure 11.3. Discrepancy between experimental capacities and the calculated mean capacity according to EN 1992-4 as a function of the relative edge distance.

The numerical analyses indicated that if the relative edge distance falls below the value 0.3, the close edges may indeed have an additional negative effect. Moreover, the experimental data is limited to cases where the relative edge distance is larger than 0.3. Therefore, the applicability of the second modification factor should be limited from this relative edge distance. In addition, the maximum capacity is reached when the relative edge distance reaches the value 1.5 (critical edge distance). Based on these considerations and the linear regression in Figure 11.3, following equation is proposed to modify the calculated tension capacity of anchor groups with two parallel edges:

$$
\psi_{||,Approach2} = \begin{cases} -0.5 \cdot \dfrac{c_2}{h_{ef}} + 1.75, & 0.3 \le c_2/h_{ef} \le 1.5 \\ 1.0, & c_2/h_{ef} > 1.5 \end{cases}
\tag{11.2}
$$

The solid black line in Figure 11.3 presents the proposed equation. It can be seen that the curve fits well with the experimental results.

11.2.3 Approach 3: Assumption of rotationally symmetric stress condition

The third approach is based on the assumption that, if both geometrical conditions and loading conditions are symmetrical in the direction perpendicular to the free edges, thus if there is equal distance to both sides and no load eccentricity towards one of the two edges, then the rotationally symmetric stress condition in the concrete is not disturbed. Consequently, the reduction factor $\psi_{s,N}$ can be taken equal to 1.0.

The assumption can be justified by the fact that a symmetric breakout behavior was observed in the experiments as well as in the numerical analysis, provided that the above mentioned conditions apply. Furthermore, it was shown in the experiments that the relative edge distance had basically no influence on the capacity of an anchor group if the amount of concrete to resist the tension load was the same (defined by the

same projected area). On the other hand, in case of an asymmetry in the direction perpendicular to the parallel edges (either unequal edge distances or eccentric loading), the ultimate load reduced in comparison to corresponding case with equal projected area and with symmetric conditions. In these asymmetric cases, the assumption of a disturbed rotationally symmetric stress condition is justified and application of the reduction factor ψs,N is required.

It will be shown in Section 11.3 that in case of anchor groups installed in narrow concrete members with symmetric conditions, assuming the reduction factor ψs,N = 1.0 will still result in conservative design resistances.

11.2.4 Approach 4: Modification factor based on the width of the concrete member

The resistance of shear loaded single anchors or anchor groups in case of concrete edge failure is reduced when the thickness of the concrete member is not sufficiently large. In EN 1992-4, this is accounted for by the ratio $A_{c,V}/A_{c,V}^0$. However, it was shown in experimental and numerical studies (Zhao et al., 1989; Hofmann, 2005; Eligehausen and Grosser, 2007) that the resistance in case of concrete edge failure does not reduce as strongly with decreasing thickness of the concrete member as would be expected by the ratio $A_{c,V}/A_{c,V}^0$. To overcome the conservatism of the design approach, current standards, such as EN 1992-4, consider the factor ψh,V when calculating the resistance of shear loaded single anchors or anchor groups in case of concrete edge failure. The factor ψh,V increases the calculated capacity based on the ratio of the edge distance, c1, and the thickness, h, of the concrete member (Zhao and Eligehausen, 1992; Eligehausen et al., 2006; EN 1992-4).

In an analogous way, the design of single anchors and anchors groups in narrow concrete members subjected to tension loads can be considered in case of concrete cone failure. Based on the assumption that the resistance does not reduce as strongly with decreasing width of the concrete member as would be expected by the ratio $A_{c,N}/A_{c,N}^0$, the modification factor given in Equation (11.3) is proposed.

$$\psi_{w,N} = \left(\frac{3h_{ef}+s_{tot}}{w}\right)^{0.5} \geq 1, \tag{11.3}$$

where s_{tot} is the spacing between the outermost anchors in the direction perpendicular to the parallel close edges, and w is the width of the concrete member.

Figure 11.4 shows the ratio of failure loads measured in the experiments reported in this work and by Anderson et al. (2017) to the calculated capacities according to EN 1992-4 as a function of the ratio between the width of the projected area without edge influence, $3h_{ef} + s_{tot}$, and the width of the concrete members in the tests. The dashed red line shows the regression of the results using a power function. The solid black line shows the proposed factor $\psi_{w,N}$ (Equation (11.3)). It can be seen that the proposed

factor matches reasonably well with the experimental results. From Figure 11.4 it appears that with increasing ratio $(3h_{ef} + s_{tot})/w$, the prediction according to the factor $\psi_{w,N}$ becomes more conservative.
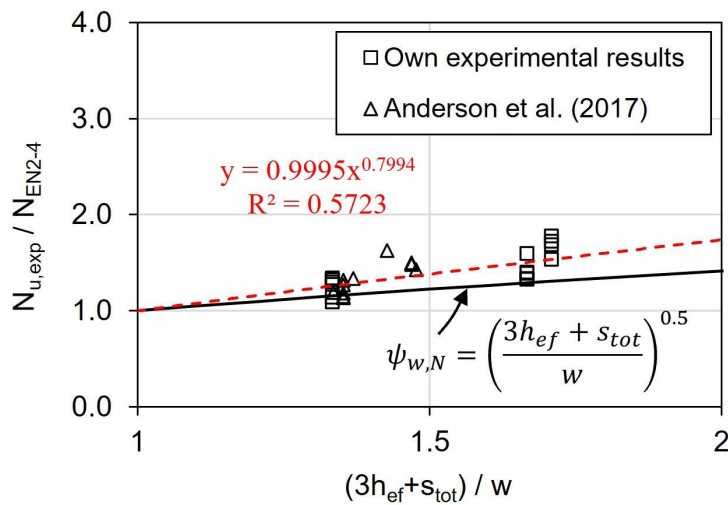
Figure 11.4. Ratio of the failure loads measured in the experiments reported in this work and by Anderson et al. (2017) to the calculated capacities according to EN 1992-4 as a function of the ratio between the width of the projected area without edge influence, $3h_{ef} + s_{tot}$, and the width of the concrete members in the tests.

11.3 Comparison of the modified approaches

Figure 11.5 shows the comparison between the ultimate loads obtained from the modified analytical approaches and the ultimate loads obtained from the own experimental work and reported in Anderson et al. (2017). Table 11.1 summarizes the comparison between the mean ultimate loads obtained in the individual test series in Chapter 9 and the ultimate loads obtained from the modified analytical approaches. As discussed above, the first approach results in a significant overestimation of the capacity in cases where the ratio s_2 / c_2 is rather large, which may result in an unsafe design. Considering all test results, the mean value of the ratio $N_{u,exp} / N_{Approach1}$ is 0.99 with a coefficient of variation of 21%. For the second approach, the mean value of the ratio $N_{u,exp} / N_{Approach2}$ is 1.03 with a coefficient of variation of 11%. On average the second approach slightly underestimates the actual capacity of the anchor groups, nonetheless in most cases, it shows a good agreement. Most importantly, there are no pronounced outliers in the calculation of the loads in comparison to the tested anchor groups. It can be seen that for the available experimental data, application of the third approach results in a rather conservative design for all test series. The mean value of the ratio $N_{u,exp} / N_{Approach3}$ is 1.19 with a coefficient of variation of 12%. The fourth approach lies somewhat between the second and third approach. The ratio $N_{u,exp} / N_{Approach4}$ is 1.14 with a coefficient of variation of 10%.

(a) Approach 1

(b) Approach 2

☐ Own experimental results
△ Anderson et al. (2017)

Mean ($N_{u,exp}$ / $N_{Approach1}$) =0.99
CV = 21%
n = 30

Mean ($N_{u,exp}$ / $N_{Approach2}$) = 1.03
CV = 11%
n = 30

(c) Approach 3

(d) Approach 4

Mean ($N_{u,exp}$ / $N_{Approach3}$) = 1.19
CV = 12%
n = 30

Mean ($N_{u,exp}$ / $N_{Approach4}$) = 1.14
CV = 10%
n = 30
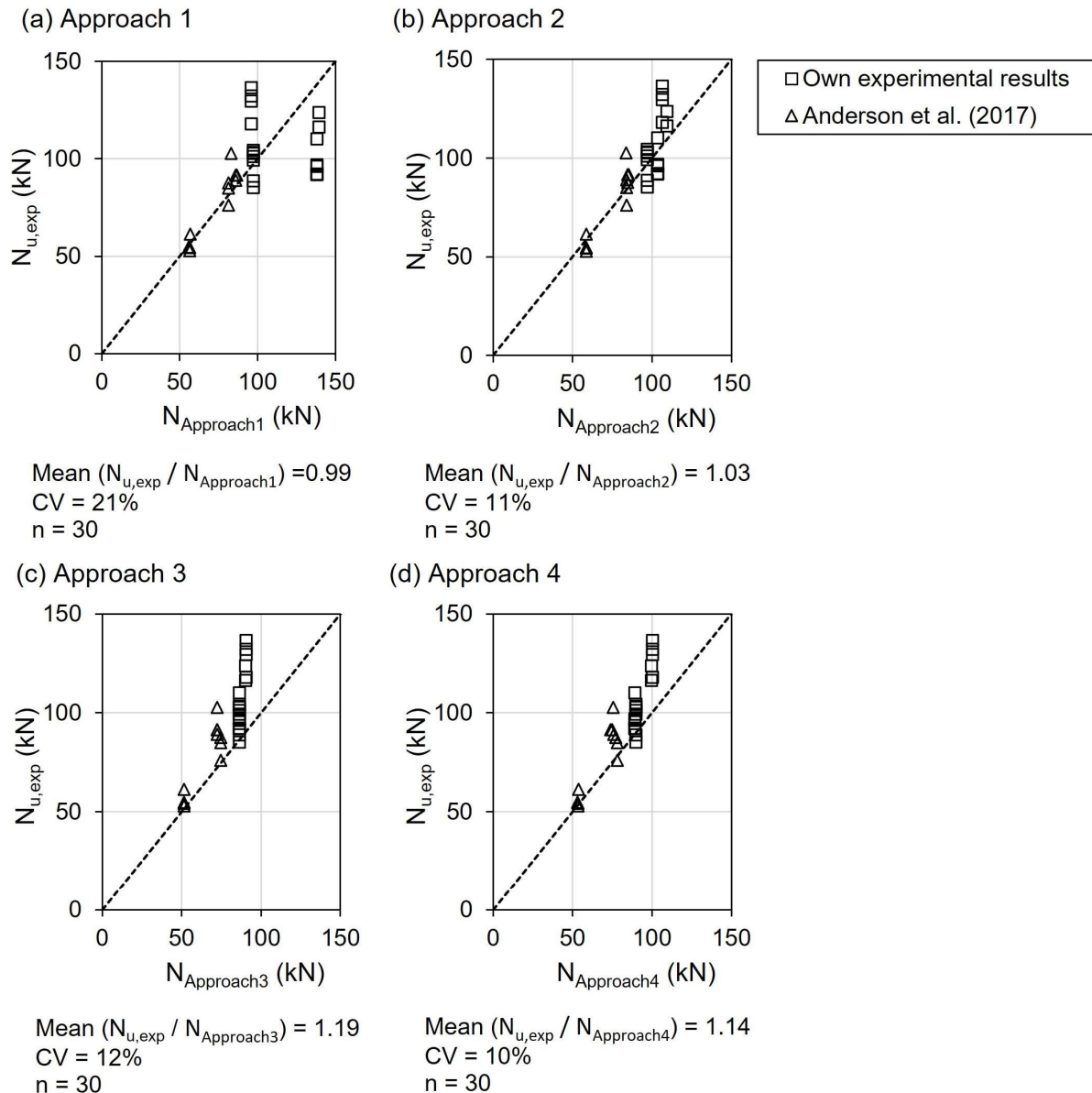
Figure 11.5. Comparison of the ultimate loads obtained from the modified analytical approaches and the experimental data.

A comparison of the four approaches has shown that the first approach is rather unsuitable. Besides the observation that the parameter s_2 / c_2 alone appears to be inconclusive to modify the current design approach as indicated by the experimental results in this work, it may even result in an unsafe design. The second approach shows a good agreement with the experimental results and is deemed more suitable for modification of the current design of anchor groups with two parallel close edges. This approach provides a way to address the over-conservatism of the current design approaches according to the CCD method (Bujňák and Farbák, 2018; Anderson et al., 2017), while at the same time the comparison with the experimental results shows that the capacity of the tested anchor groups is not wildly overestimated. The third approach

is still rather conservative. The actual capacity of the tested anchor groups was on average around 19% higher than the calculated values. However, its application is straightforward and does not require an additional modification factor. Also, the predicted failure loads according to the fourth approach are rather conservative for the investigated cases. Unlike the other approaches, however, both the (relative) edge distance and the spacing of the anchors in the direction perpendicular to the parallel edges is taken into account.

Table 11.1. Comparison of the experimental results and the modified analytical approaches.

Test ID	c_2 / h_{ef}	s_2 / c_2	$N_{u,m} / N_{Appraoch1}$	$N_{u,m} / N_{Appraoch2}$	$N_{u,m} / N_{Appraoch3}$	$N_{u,m} / N_{Appraoch4}$
C-32	1.00	1.0	1.06	1.06	1.19	1.14
C-42	0.50	4.0	0.67	0.89	1.07	1.03
C-52	1.00	1.0	0.97	0.97	1.09	1.05
C-62	0.73	1.0	1.35	1.21	1.42	1.29
C-72	0.50	4.0	0.73	0.98	1.17	1.13
C-82	0.36	4.0	0.86	1.10	1.33	1.20

11.4 Application of the nonlinear spring modelling approach for narrow concrete members

So far, the focus in terms of anchorage design laid on the ultimate capacity of the anchor groups. However, the displacement behavior of anchor groups is an equally important topic, which increasingly receives attention in the engineering community. This is especially true when it comes to performance-based design solutions (Sharma, 2017). In Bokor et al. (2019b) and Bokor (2021) the nonlinear spring modelling approach was introduced, which can be used to determine the resistance of tension loaded anchor groups in case of concrete cone failure. This approach considers the flexibility of the baseplate, anchor spacing, number of anchors, point of loading, distribution of forces, and the vicinity to free edges by directly modelling the load and deformation behavior of the essential elements of an anchor group (e.g., anchors with tension-only springs, transfer of compression forces from the baseplate to the concrete with compression-only springs and the baseplate using 2D shell or 3D solid elements (see Section 3.2.4)). The spring model characteristics for the anchors are determined by idealizing the experimentally obtained behavior of single anchors. To this purpose, a hexa-linearization was chosen in this work. The hexa-linearization of the experimentally obtained load-displacement curves in test series C-10A along with the experimental results are shown in Figure 11.6. Table 11.2 summarizes the corresponding spring characteristics of the single anchors. As can be seen, the hexa-linearization describes the experimental behavior with a sufficient degree of accuracy.
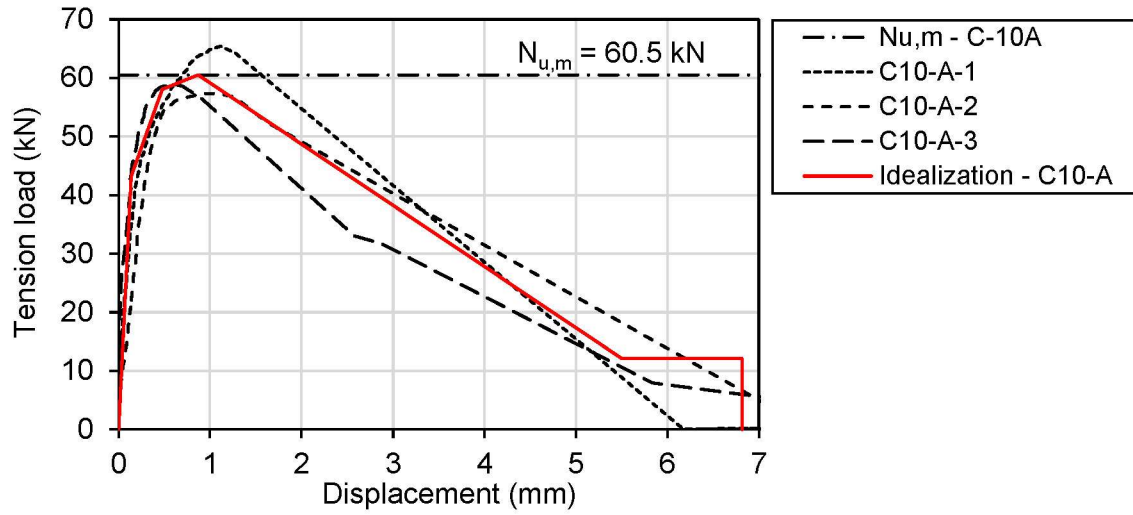
Figure 11.6. Idealized load-displacement curve for test series C-10A.

Table 11.2. Spring model characteristics for single anchor and individual anchors within the anchor groups in test series C-52 and E-52.

	Load $N_{Rm,c,A\text{-}G}$ (kN)	Secant stiffness $k_{1\text{-}5}$ (kN/mm)	Displacement, $s_{A\text{-}G}$ (mm)
Single anchor			
A	0.0	0.0	0.00
B	43.2	311.4	0.14
C	58.1	121.6	0.48
D	60.5	69.7	0.87
E	12.1	2.2	5.50
F	12.1	1.8	6.82
G	0.0	0.0	6.82
Anchors A, C, D, and F			
A	0.0	0.0	0.00
B	14.4	311.4	0.05
C	19.4	121.6	0.16
D	20.2	69.7	0.29
E	4.0	2.2	1.83
F	4.0	1.8	2.27
G	0.0	0.0	2.27
Anchors B and E			
A	0.0	0.0	0.00
B	7.2	311.4	0.02
C	9.7	121.6	0.08
D	10.1	69.7	0.14
E	2.0	2.2	0.92
F	2.0	1.8	1.14
G	0.0	0.0	1.14

To verify the applicability of the spring modelling approach for anchor groups installed in narrow concrete members, it is exemplarily applied to simulate the behavior of the 3 x 2 anchor groups in test series C-52 and E-52 using the finite element software SAP2000. The spring model characteristics of the individual anchors in a group are determined according to Section 3.2.4. In this way, anchor spacing, and close edges are directly considered. Via the tributary area approach only the capacities of the individual anchors within a group are modified. The secant stiffness values for the characteristic points of the hexa-linear curve are the same as those determined for the single anchor (Bokor, 2021). It is worth mentioning that no additional reduction factors are required. Figure 11.7 shows the respective 3 x 2 anchor configuration and the segmentation into the individual tributary areas.
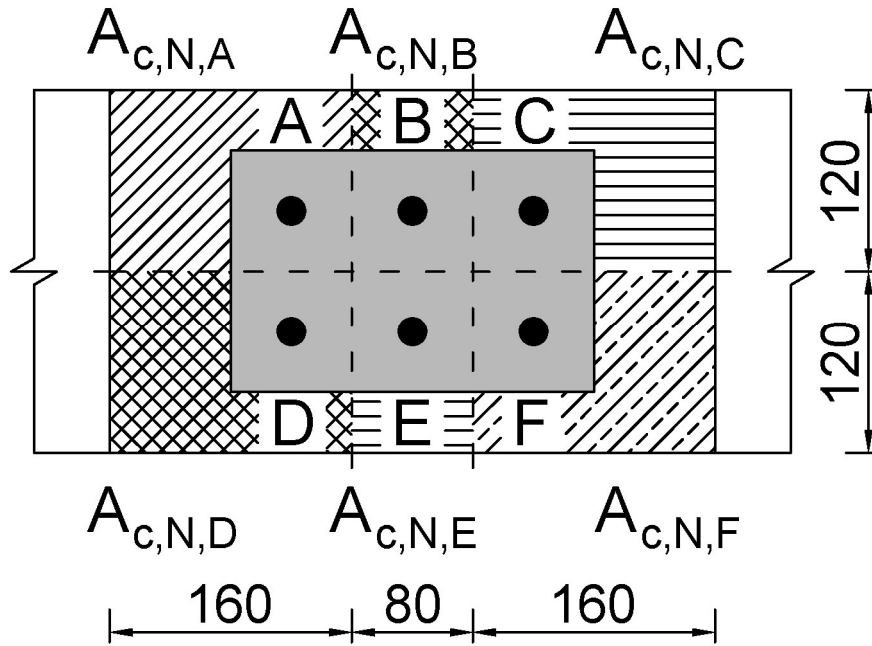
Figure 11.7. Segmentation into tributary areas for the 3 x 2 anchor configuration in test series C-52 and E-52. (Note: All dimensions are in mm).

As can be seen, anchors A, C, D and F have the same tributary area, and anchors B and E have the same tributary area. The corresponding tributary areas, the unrestricted area of a single anchor, $A_{c,N}^0$ (according to CCD method), and the ultimate loads of the individual anchors are calculated as follows:

$$A_{c,N}^0 = 9h_{ef}^2 = 57600 \ mm^2, \tag{11.4}$$

$$A_{c,N,A} = A_{c,N,C} = A_{c,N,D} = A_{c,N,F} = 120 \cdot \left(1.5h_{ef} + 0.5s_1\right) = 19200 \ mm^2, \tag{11.5}$$

$$A_{c,N,B} = A_{c,N,E} = 120 \cdot s_1 = 9600 \ mm^2, \tag{11.6}$$

$$N_{Rm,c,A} = N_{Rm,c,C} = N_{Rm,c,D} = N_{Rm,c,F} = \frac{A_{c,N,A}}{A_{c,N}^0} \cdot N_{Rm,c}^0 = 20.2 \ kN, \tag{11.7}$$

$$N_{Rm,c,B} = N_{Rm,c,E} = \frac{A_{c,N,B}}{A_{c,N}^0} \cdot N_{Rm,c}^0 = 10.1 \ kN. \tag{11.8}$$

The spring model characteristics of the individual anchors within the group are summarized in Table 11.2. The baseplate was modelled using shell elements with a Young's Modulus for steel of E_s = 200000 N/mm². The loads were directly applied onto the nodes with respect to the point of load application in the respective test series. The

243

load was applied in displacement-control by incrementally increasing the displacement. Figure 11.8 shows the load-displacement curves obtained through the spring modelling approach compared to the respective curves obtained in the experiments. It can be seen that for both the centric and the eccentric loading case, in terms of ultimate loads, the results match well with the experimentally obtained ultimate loads. In case of centrically loaded anchor groups (test series C-52) the behavior in the ascending branch is reflected quite well although the behavior in the simulation is slightly stiffer. In the post-peak range of the load-displacement curve, the simulated behavior appears markedly more brittle than the experimental behavior. However, it should be considered that owing to the abrupt failure, only few points of the post-peak phase of the load-displacement curve were really measured in the experiments. As a result, the behavior in this range cannot be identified conclusively from the experimental results. In fact, the numerical simulations on tension loaded anchor groups in narrow members indicate a rather brittle failure in case of concrete breakout failure and support the validity of the spring modelling approach. In case of the eccentrically loaded anchor groups, the behavior up to ultimate load is somewhat stiffer than the behavior obtained in the experiments. In the post-peak range, the results obtained by using the spring modelling approach show a somewhat more brittle failure. Again, this discrepancy is rather attributable to the measurement accuracy in the experiments. In summary, the spring modelling approach reflects the experimental behavior with a good degree of accuracy. With respect to the ultimate capacity, the spring modelling approach matches very well with the experimental results. In terms of the load-displacement behavior, initially the predicted behavior is stiffer compared to the behavior observed in the experiments. Furthermore, the predicted post-peak behavior appears to be more brittle. However, breakout failure is often very brittle in nature and happens relatively fast. This renders the control of the post-peak behavior in force-controlled tests rather difficult, which is why the measurement of the post-peak behavior is less reliable. This problem can be overcome either by performing displacement-controlled tests or by carrying out complex FE calculations. Here the nonlinear spring modelling approach offers a comparatively simple alternative, with which the behavior of an anchor group in the post-peak range can be estimated with little effort.
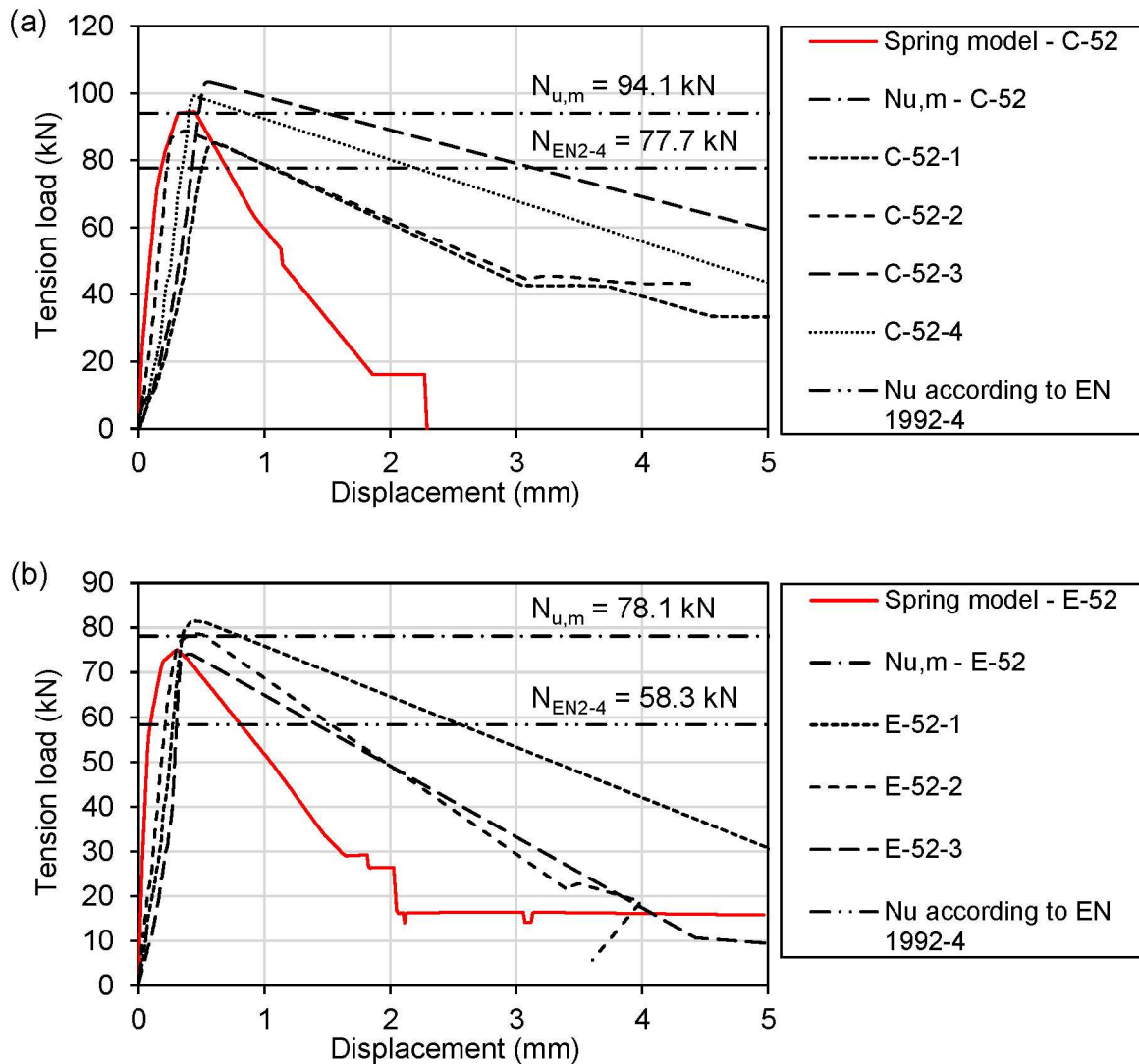
Figure 11.8. Comparison between nonlinear spring modelling approach and experimentally obtained load-displacement curves for test series (a) C-52 and (b) E-52.

11.5 Summary

Based on the experimental results in this work and the experimental data available in the literature, it was shown that the current analytical design approach for the concrete cone breakout failure of anchor groups (CCD method) is quite conservative when it comes to anchor groups installed in narrow members. In this context, four approaches were presented and evaluated which are aimed at modifying the current design approach. Note that the discussed modification approaches are based on the available experimental data, where anchor groups are loaded centrically in tension and have equal edge distance to both parallel edges. Therefore, the approaches are strictly only valid for the tested configurations and anchor systems.

The first approach was introduced by Anderson et al. (2017) and considers a modification factor which increases the calculated capacities according to the CCD method. This factor is a function of the ratio s_2 / c_2. However, experimental findings in this work suggest that this parameter is less meaningful, especially for larger ratios between s_2 and c_2, in which case the proposed factor may even lead to unreliable or unsafe predictions.

The second approach also considers a modification factor, which is based on the relative edge distance, c_2 / h_{ef}. The experimental results showed that for the tested anchor configurations, the conservatism of the current design approach increases with decreasing relative edge distance. This observation is likely to be related to the reduction factor $\psi_{s,N}$, which considers the disturbance of the rotationally symmetric stress condition in the concrete due to close edges, and which is a function of the edge distance. The comparison with the experimental data showed a good agreement between the proposed modification factor and the results obtained from the tested anchor groups.

In the third approach, the reduction factor $\psi_{s,N}$ is omitted, which results in a better estimation of the actual capacity of the anchor groups in narrow members. At the same time, it was shown that this approach maintains a certain degree of conservatism. It is arguable whether in the case of parallel edges with equal edge distance on both sides of the anchor groups, a disturbance of the symmetry should be assumed at all, which is why the omission of the reduction factor can be justified in this case. Although this approach remains conservative, its advantage is the simplicity, without the requirement of adding further factors to the current approach.

The fourth approach is similar to the existing design approach for concrete edge failure of shear laded anchors, where the factor $\psi_{h,V}$ considers that the resistance in case of concrete edge failure does not reduce as strongly with decreasing thickness of the concrete member as determined by the ratio $A_{c,V}/A_{c,V}^0$ (EN 1992-4). Hence, based on the assumption that in case of anchors installed in narrow concrete members, the resistance does not reduce as strongly with decreasing width of the concrete member as determined by the ratio $A_{c,N}/A_{c,N}^0$, the modification factor $\psi_{w,N}$ given in Equation (11.3) is proposed. The comparison with the experimental data showed the suitability of the proposed modification factor for the investigated cases. The fourth approach is more conservative than the second approach and less conservative than the third approach.

The main disadvantage of modification factors is that another parameter is introduced, which renders the existing method more complicated. It is therefore more desirable to have a holistic solution that also includes the cases where, for example, only one close edge is present or the edge distances to the parallel edges are of different values. An approach that is used as soon as an anchor group is placed in the vicinity of one or more edges and that would then make the use of reduction and modification factors

superfluous. This work, however, can only offer a modification of the current analytical design approach and not a new one. This is especially due to the fact that further investigations would be required which are out of the scope of the current work.

In this context, the spring modelling approach (Bokor et al., 2019b; Bokor, 2021) offers a solution which predicts the capacity of anchor groups in narrow member with a sufficient degree of accuracy without the necessity of any reduction or modification factors. Moreover, this approach is able to adequately predict and assess the load-displacement behavior of the investigated anchor groups in narrow concrete members (see Figure 11.8).

12 Applicability of the hysteretic model to anchor groups

12.1 Opening remarks

In principle, the hysteretic rules for single anchors which were introduced in Chapter 6 can be implemented in any FE software. In doing so it would be possible to directly model an anchor group considering the hysteretic behavior of the individual anchors within the group. This means, for example, with regard to the nonlinear spring modelling approach proposed by Bokor (2021), once the rules are implemented in a software, the required input parameters for the idealization of the unloading and reloading behavior and for the hysteretic model can be applied to the individual springs of an anchor group and a nonlinear analysis can be performed, which considers the hysteretic behavior of the individual anchors separately.

However, the implementation of these rules in a commercial FE software is out of the scope of this work. Therefore, to show the applicability of the hysteretic model to anchor groups, an alternative approach is presented in this chapter. The basic idea is to replace the single anchor envelope curve with the envelope curve of the complete anchor group. Thereby, again, the envelope curve is the upper limit of cyclic loading. In the case of anchor groups, however, the envelope curve accounts for the overall behavior of the group, which reflects the interaction between the behavior of the baseplate and that of the individual anchors. The hysteretic model which was developed for single anchors has then to be adjusted to the number of anchors in the group, whereby it is assumed that the unloading and reloading stiffness is directly proportional to the number of anchors. The details of this assumption will be discussed in the following section. In this context, it is worth mentioning that the hysteretic behavior of an anchor group is directly calculated from the hysteretic behavior of the individual anchors. Thus, this approach does not require an extensive additional evaluation of the hysteretic behavior of anchor groups per se.

There are two main approaches how the envelope curve of an anchor group can be determined. Either through experiments or detailed finite element analysis on anchor groups, or through advanced modelling methods such as the nonlinear spring modelling approach by Bokor (2021). In the latter case, in order to simulate the behavior of an anchor group, only the experimental results of cyclic single anchor tests are required. First, to identify the hysteretic characteristics of the individual anchors. Second, to obtain the characteristic points for the anchor springs which are required to model the anchor group (idealized envelope curve or load-displacement curve). The

envelope curve of the complete group is then calculated through a monotonic analysis. In this work the envelope curves were directly determined from the respective experimental results. In this way, the accuracy of the whole model can be increased. This allows to focus on the hysteretic behavior itself, which is the main objective of this work.

In conclusion, the following approach assumes that the overall behavior of an anchor group, which is defined by the envelope curve, is known. With the known envelope curve as the upper limit for cyclic loading, the hysteretic model can be used to simulate the hysteretic behavior of the group based on the unloading and reloading behavior determined for single anchors.

12.2 Adaptation of hysteretic model for anchor groups

In case of single anchors, the response follows the envelope curve until the displacement is reversed. With respect to this point, or rather based on the corresponding displacement, the subsequent unloading and reloading behavior is determined, following the rules given in Chapter 6. In the same way, the response follows the envelope curve in case of anchor groups until the displacement is reversed. Thereby, the envelope curve already considers the nonlinear behavior of the complete anchor group, including the behavior and interaction of the individual anchors and the stiffness of the steel baseplate. Similarly, the interaction between the baseplate and the individual anchors must also be considered when calculating the unloading and reloading stiffness of the anchor groups. To do so, the hysteretic model must be adapted. The adaption to anchor groups requires some assumptions which allow to retain the simplicity (limitation of additional parameters) and adequate accuracy of the model. These can also be considered as prerequisites or limitations for the use of the model, which are required in its present form. The modification of the hysteretic model and the corresponding assumptions are described in the following.

12.2.1 Consideration of multiple anchors

Like individual anchors contribute to the overall stiffness of the anchor group in case of monotonic loading, individual anchors contribute to the unloading and reloading stiffness of the group in case of cyclic loading (Stehle and Sharma, 2021b). However, at what time an anchor is activated, how much load it takes, and what its contribution to the stiffness is, depends largely on the layout of the anchor group, the position of the anchor within the group, the point of load application, the attached element, and the stiffness of the baseplate (Bokor, 2021). While these effects can be considered in a step-by-step nonlinear analysis, where the stiffness matrix is updated after each step as shown by Bokor (2021), the simplified approach followed in this chapter is only able to simulate cases where the anchors are equally loaded. This essentially means that this approach is limited to the case where at the same time all anchors in a group have (approximately) the same displacement.

In principle, the resulting behavior of all anchors is expressed by an equivalent spring which represents the springs of the individual anchors in parallel. Thereby, the behavior of individual anchors is characterized by the stiffness $k_{cyc,ind}$. The resulting unloading and reloading stiffness of all anchors is calculated as:

$$k_{cyc,res} = \text{n} \cdot k_{cyc,ind} \; . \tag{12.1}$$

Where n is the number of anchors in the group. The stiffness $k_{cyc,ind}$ follows the same rules which were defined in Chapter 6 for single anchors. Thus, the unloading and reloading behavior of the individual anchors depends on the maximum displacement reached so far in the analysis. For simplicity, it is assumed that the displacement of the individual anchors corresponds to the total displacement of the anchor group. In other words, the flexibility of the baseplate is neglected at this point. As shown in Chapter 8, with increasing relative displacement, the progression of the unloading and reloading stiffness of individual anchors in an anchor group is rather similar to the progression observed in single anchor tests. Therefore, the required input parameters to define the unloading and reloading behavior can be determined from single anchor reference tests.

12.2.2 Consideration of baseplate stiffness

Besides the individual anchors, also the baseplate contributes to the overall unloading and reloading behavior. However, in contrast to the anchors, it is assumed that the baseplate remains in the elastic range throughout the analysis. Note that this assumption limits the scope of the model to design cases where no plastic hinge is considered in the baseplate. The elastic stiffness of the baseplate for a given global load-displacement behavior of an anchor group can be back calculated assuming the anchors and the baseplate as springs that are connected in series. To this purpose, the initial stiffness of the individual anchors and the initial stiffness of the complete group including the baseplate must be known. The initial stiffness of the complete group can be determined from the envelope curve, as the secant stiffness k_1 associated with point B of the idealized curve (see Chapter 6). The initial stiffness of individual anchors is assumed equal to the initial stiffness obtained in the single anchor tests (Bokor, 2021). Thus, the stiffness corresponding to the point where 50% of the ultimate load is reached in the ascending branch, $k_{50\%Nu}$. This value has to be given as an additional input parameter. With regards to the number of anchors in the group, n, the stiffness of the baseplate can be calculated as follows:

$$k_{baseplate} = \frac{1}{(1/k_1) - (1/(n \cdot k_{50\%Nu}))} \; . \tag{12.2}$$

The elastic baseplate stiffness is calculated at the beginning of the analysis and is valid throughout the procedure. Finally, using Equation (12.1) and (12.2), the unloading and reloading stiffness at any point in the analysis can then be calculated as follows:

$$k_{cyc,grp} = \frac{1}{(1/k_{baseplate})+(1/k_{cyc,res})} \ . \qquad\qquad (12.3)$$

This procedure allows both the elastic behavior of the baseplate and the number of anchors to be accounted for in the calculation of the unloading and reloading stiffness. As already mentioned, the simplicity of the approach comes with some limitations though. In summary it is only applicable to anchor groups where all anchors yield at the same displacement and to design cases where the baseplate is intended to remain in the elastic range.

12.3 Validation of the modelling approach against experimental results from this work

This section serves two purposes. Based on the experimental results, it is first described how the required input parameters for modelling of anchor groups are determined. For this purpose, the single anchor cyclic tests will be evaluated in accordance with the approach described in Chapter 6, and the results will be partly adapted to the requirements of anchor groups. Once the required parameters have been determined, an analysis is performed for the individual tests with anchor groups and the calculated load-displacement response is compared to the experimental results. Note that the three-parameter model is used for the analysis as it provides the highest level of accuracy. Some of the experimental results used in this chapter have already been shown in Chapter 8. However, to improve the comprehensibility in this section, some of the data are reproduced.

12.3.1 Determination of required input parameter from single anchor tests

To describe the unloading and reloading behavior of an anchor at any point of the load-displacement curve, the corresponding unloading and reloading stiffness are defined as a function of the relative displacement. As shown in Chapter 6, both the unloading and reloading stiffness can be described with reasonable degree of accuracy using only a single stiffness value, k_{cyc}. For the idealization of this value as a function of the relative displacement, five parameters are required. In Chapter 8 it was shown that the behavior of individual anchors in the group is rather similar to the behavior observed in single anchor tests. However, the scatter was notably larger for anchors in a group. In case of single anchors, the unloading and reloading behavior within one test series is rather stable, which is why five parameters are sufficient to describe the behavior of particular tests with sufficient degree of accuracy. However, when it comes to the behavior of individual anchors within a group, the situation becomes more complex,

which leads to a more volatile behavior. To account for the observed variability in the modelling of anchor groups, instead of a single data set of five parameters, a range is defined from which the five parameters can be selected. This range is defined by an upper and lower bound, which are graphically represented in Figure 12.1 (a) along with the test results obtained from displacement-controlled single anchor cyclic tests. Note that the values for both unloading and reloading stiffness obtained from the seven cyclic tests on single anchors described in Chapter 8 are plotted. The values which define the upper and lower bound are given in Table 12.1.

Table 12.1. Parameters for defining the unloading and reloading stiffness for BA-1x1-cyc.

Parameter	Single anchor[1]	Upper bound	Lower bound
k_α	250	400	220
k_β	80	120	50
α	0.15	0.4	0.1
β	1	1.5	0.7
ω	11	13	3.5

(1) Mean values of all test results

Besides the upper and lower bound, Figure 12.1 (a) shows the idealization of the unloading and reloading behavior which was used to model the hysteretic behavior of single anchors in Figure 12.1 (b)-(d). The corresponding values are also given in Table 12.1. It can be seen that for the idealization of the single anchor behavior, the five parameters were chosen in such a way that the curve lies between the upper and lower bound. Thereby, the parameters k_α, k_β, α and β are in good agreement with those defined in Chapter 6 for the tested bonded anchors in uncracked concrete. However, a significantly higher value was selected for the parameter ω. The variation of ω might be explained by the fact that the overall stiffness of an anchor group is markedly higher than the stiffness of a single anchor. Consequently, the displacement s_u at ultimate load is smaller. At the same time, the observed ultimate displacements of the tested anchor groups are equal or even larger than those of single anchors. In other words, the post-peak displacement behavior appears to be somewhat more pronounced when the tested bonded anchors were arranged in a group.

Since in case of bonded anchors, ω essentially defines how fast the stiffness decreases after the ultimate load is reached, small values for ω cause the stiffness in the descending branch of the load-displacement curve to decrease too fast in case of anchor groups. This also has to do with the fact that the stiffness values are determined on the basis of the relative displacement, which is in turn defined by the displacement at ultimate load. To counteract this, a larger value for ω was chosen. It is worth mentioning at this point, that the hysteretic behavior of single anchors can still be simulated using larger values of ω compared to the ones used in Chapter 6. However,

this may have a negative influence on the accuracy of the idealized unloading and reloading stiffness. This becomes evident when comparing the experimental load-displacement curves to the output curves of the model in Figure 12.1 (b)-(d).
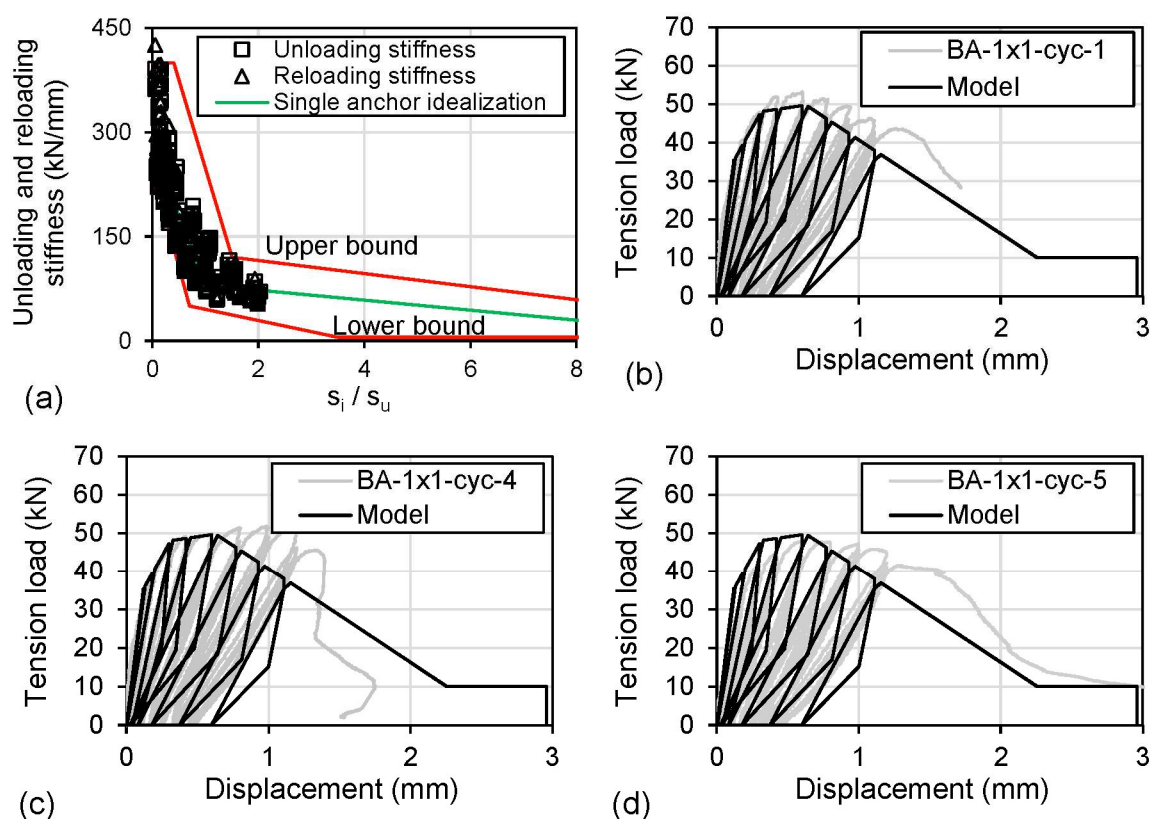
Figure 12.1. Experimental results and modelling of single anchors: (a) Idealization of unloading and reloading behavior, (b)-(d) comparison between experimental results and calculated response.

The model response is based on the mean envelope curve obtained from the seven single anchor tests (according to the procedure described in Section 6.1). The remaining input parameters for the hysteretic model are the mean displacement at ultimate load, $s_{u,m} = 0.62\ mm$, the strength reduction factor $\eta = 0.93$, and $\lambda = 0.4$. In general, the model response is able to simulate the experimental behavior with a sufficient degree of accuracy. Nonetheless, it can be seen that the model response in the post-peak range is stiffer than the experimental behavior. Note that in this case, higher values for unloading and reloading stiffness will result in larger residual displacements. In many structural strengthening applications, it is favorable to have small residual displacements in order to ensure a safe load transfer between the structural element and the strengthening element in case of reversed loading. Furthermore, large residual displacements can cause local geometrical asymmetries, which may result in local buckling of the steel elements (Mazzolani et al., 2009; Mahrenholtz et al., 2015). In such applications, the simulated response using larger values for ω may be considered as a more conservative approach.

As already noted, the tested anchor groups reach the ultimate load at smaller displacements due to the generally higher stiffness of groups compared to single anchors. This in turn means that also the individual anchors within a group have a smaller displacement at ultimate load than anchors in single anchor tests, which is also a result of the altered load-displacement behavior owing to the presence of nearby anchors in the group (Bokor, 2021). When modelling the single anchor behavior, the displacement at ultimate load obtained from the tests is given as an input parameter to define the relative displacement and thus the unloading and reloading stiffness at a given anchor displacement. It is evident that, since the displacement of individual anchors in groups is smaller, the input parameter has to be adjusted accordingly. To do so, the tributary area approach (Bokor, 2021) is applied. Since only the capacities of individual anchors within a group are modified while the secant stiffness values for the characteristic points remain the same, the corresponding displacements are reduced accordingly. Thus, the displacement of anchors in a group at ultimate load can be estimated based on the layout of the anchor group (tributary area), the ultimate load obtained from single anchor tests and the corresponding secant stiffness at ultimate load. Note that the ultimate load and the corresponding secant stiffness for single anchors is already required for idealization of the load-displacement curve or the envelope curve. The method of adjusting the required displacement value for individual anchors in a group is described using test series BA-2x2-C-cyc as an example. Figure 12.2 shows the corresponding anchor configuration and the segmentation into the individual tributary areas as well as the idealized load-displacement curves of the reference anchor and the individual anchors of the group.

(a) Tributary areas

(b) Idealized load-displacement curves
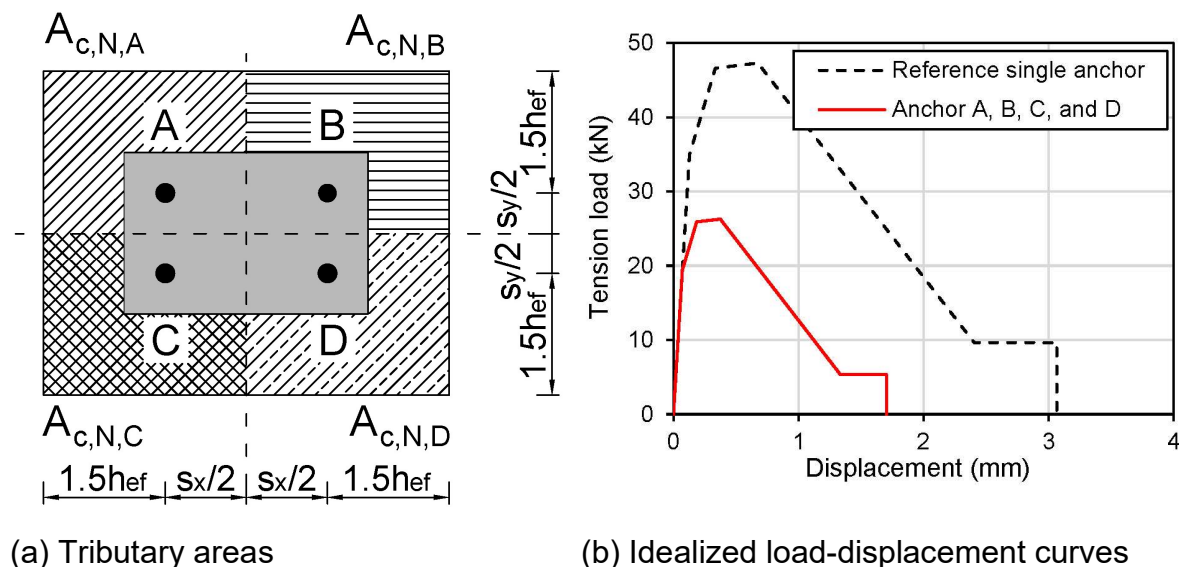
Figure 12.2. (a) Segmentation into tributary areas for the 2 x 2 anchor configuration in test series BA-2x2-C-cyc and (b) idealized load-displacement curves of the reference anchor and the individual anchors of the group based on the tributary area approach.

The equal tributary area of all anchors, A, B, C, and D, the unrestricted area of a single anchor, $A_{c,N}^0$ (according to CCD method), and the ultimate loads of the individual anchors are calculated as follows:

$$A_{c,N}^0 = 9h_{ef}^2 = 57600 \ mm^2, \tag{12.4}$$

$$A_{c,N,A} = A_{c,N,B} = A_{c,N,C} = A_{c,N,D} = 200 \cdot 160 = 32000 \ mm^2, \tag{12.5}$$

$$N_{Rm,c,A} = N_{Rm,c,B} = N_{Rm,c,C} = N_{Rm,c,D} = \frac{A_{c,N,A}}{A_{c,N}^0} \cdot N_{u,m} = 27.9 \ kN. \tag{12.6}$$

Where $N_{u,m}$ is the mean ultimate load obtained in the single anchor tests. The mean secant stiffness at ultimate load considering all the single anchor tests (cyclic loading) in Chapter 8, is $k_{Nu,m} = 90.5 \ kN/mm$. Thus, the displacement at ultimate load for the individual anchors of a group can be calculated as follows:

$$s_{u,m,A} = s_{u,m,B} = s_{u,m,C} = s_{u,m,D} = \frac{N_{Rm,c,A}}{k_{Nu,m}} = 0.31 \ mm. \tag{12.7}$$

In the following, using the hysteretic model, test series BA-2x1-A-cyc, BA-2x1-B-cyc, BA-2x2-A-cyc, BA-2x2-B-cyc, and BA-2x2-C-cyc are analyzed and the calculated model responses are compared to the experimental results. For each of these test series, the corresponding individual anchor displacements at ultimate load were calculated according to the above described procedure. The values are summarized in Table 12.2. The remaining input parameters for the hysteretic model can directly be taken from the single anchor reference tests and are also given in Table 12.2.

Table 12.2. Required model parameters.

Test ID	$s_{u,m,i}$ (mm)	$k_{50\%Nu,m}$ (N/mm²)	η	λ
BA-2x1-A-cyc	0.37			
BA-2x1-B-cyc	0.46			
BA-2x2-A-cyc	0.25	295.2	0.93	0.4
BA-2x2-B-cyc	0.39			
BA-2x2-C-cyc	0.31			

12.3.2 Test series BA-2x1-A-cyc

In the first example, the results of the hysteretic model are compared with the results of the test series BA-2x1-A-cyc. In this test series, the anchors were embedded in the concrete with an embedment depth of h_{ef} = 80 mm. The anchor groups comprise two anchors with a spacing of s_1 = 80 mm. The required parameters for defining the

unloading and reloading stiffness are summarized in Table 12.3 for each test respectively.

Table 12.3. Parameters for defining the unloading and reloading stiffness for BA-2x1-A-cyc.

Parameter	BA-2x1-A-cyc-1	BA-2x1-A-cyc-2	BA-2x1-A-cyc-3
k_α	300	300	300
k_β	50	50	50
α	0.1	0.1	0.1
β	1.2	1.2	1.2
ω	12	10	12

To simulate the hysteretic behavior, the three-parameter model (see Section 6.3.3) was used. Figure 12.3 shows the reproduced load-displacement curves obtained in the experiments and the corresponding model response. The comparison of experimental and numerical results shows that the proposed modelling approach can simulate the overall load-displacement behavior and the hysteretic behavior of anchor groups very well. Since in this case, tests were also performed in displacement control, the numerical results match the experimental results in the post-peak branch also very well. The model captures the softening of the unloading and reloading paths at larger displacement levels quite well. However, the idealization of the unloading and reloading behavior generally results in a slightly stiffer behavior. Nonetheless, the applied approach proves effective, and the comparison supports the assumption of a similar unloading and reloading behavior of single anchors and individual anchors in a group.
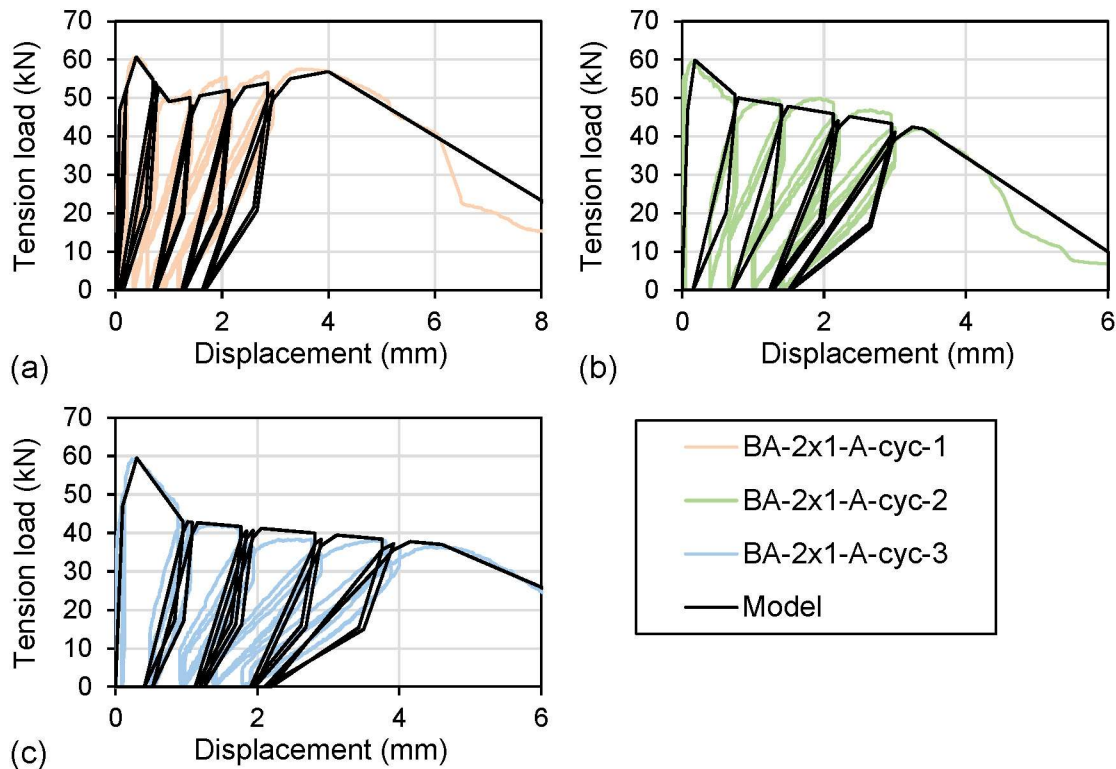
Figure 12.3. Load-displacement curves obtained from test series BA-2x1-A-cyc along with the results obtained from the three-parameter model.

12.3.3 Test series BA-2x1-B-cyc

In the second example, the results of the hysteretic model are compared with the results of the test series BA-2x1-B-cyc. In this test series, the anchors were embedded in the concrete with an embedment depth of h_{ef} = 80 mm. The anchor groups comprise two anchors with a spacing of s_1 = 160 mm. The required parameters for defining the unloading and reloading stiffness are summarized in Table 12.4 for each test respectively.

Table 12.4. Parameters for defining the unloading and reloading stiffness for BA-2x1-B-cyc.

Parameter	BA-2x1-B-cyc-1	BA-2x1-B-cyc-2	BA-2x1-B-cyc-3
k_α	300	300	300
k_β	50	50	50
α	0.1	0.1	0.1
β	1.2	1.2	1.2
ω	10	10	12

Again, the three-parameter model was used to simulate the hysteretic behavior of the anchor groups. Figure 12.4 shows both the experimental load-displacement curves

and the corresponding output curves of the model. In general, the model response matches rather well with the experimental results.
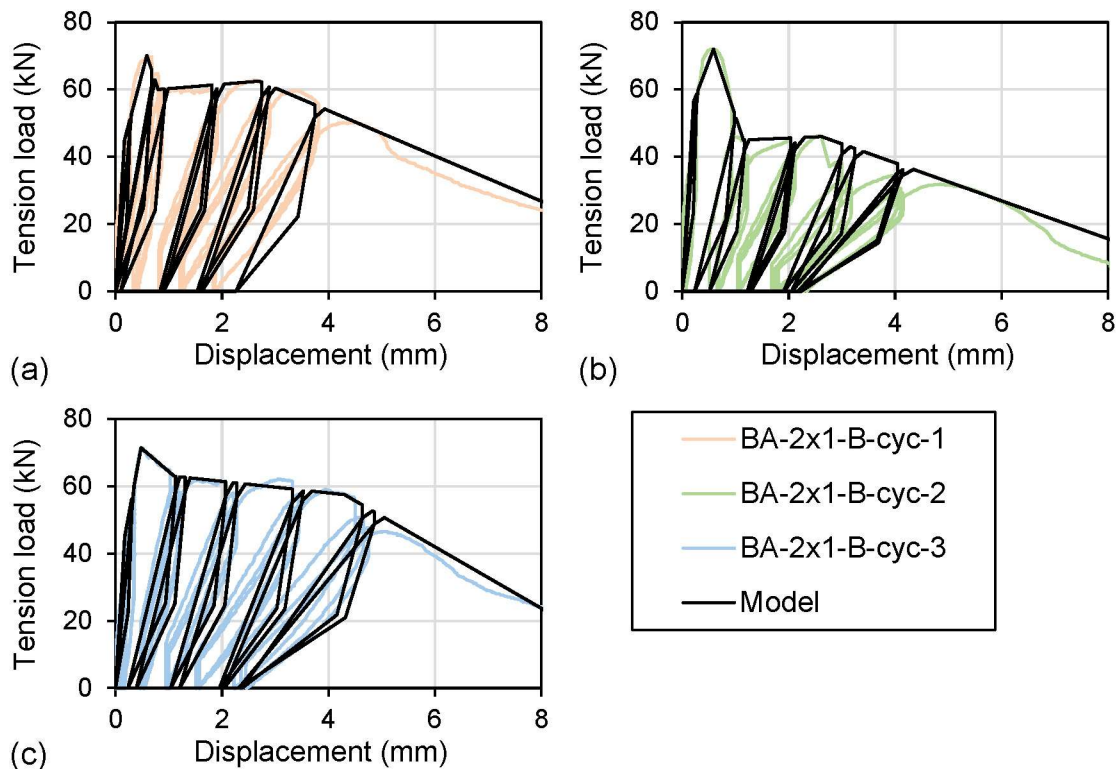
Figure 12.4. Load-displacement curves obtained from test series BA-2x1-B-cyc along with the results obtained from the three-parameter model.

12.3.4 Test series BA-2x2-A-cyc

The third example compares the results of the hysteretic model with the results of the test series BA-2x2-A-cyc. In this test series, the anchors were embedded in the concrete with an embedment depth of h_{ef} = 80 mm. The anchor groups comprise four anchors with a spacing of s_1 = s_2 = 80 mm. The required parameters for defining the unloading and reloading stiffness are summarized in Table 12.5 for each test respectively.

Table 12.5. Parameters for defining the unloading and reloading stiffness for BA-2x2-A-cyc.

Parameter	BA-2x2-A-cyc-1	BA-2x2-A-cyc-2	BA-2x2-A-cyc-3
k_α	300	300	300
k_β	50	50	50
α	0.1	0.1	0.1
β	1.2	1.2	1.2
ω	10	12	12

Figure 12.5 shows the experimental load-displacement curves obtained in test series BA-2x2-A-cyc and the corresponding simulations using the three-parameter model. The simulated unloading and reloading behavior match well with the experimental behavior. The comparison shows that the overall behavior of a 2 x 2 anchor group can be simulated using the hysteretic characteristics obtained in single anchor reference tests. With respect to the hysteretic loops, the unloading path reflects the real behavior quite well. However, in case of anchor groups, the beginning of the reloading path observed in the experiments is significantly stiffer compared to the model response.

(a)

(b)

(c)

Figure 12.5. Load-displacement curves obtained from test series BA-2x2-A-cyc along with the results obtained from the three-parameter model.

12.3.5 Test series BA-2x2-B-cyc

The test series configuration BA-2x2-B-cyc comprises four anchors with an embedment depth of h_{ef} = 80 mm. The spacing between the anchors is s_1 = s_2 = 160 mm. The required parameters for defining the unloading and reloading stiffness are summarized in Table 12.6 for each test respectively.

Table 12.6. Parameters for defining the unloading and reloading stiffness for BA-2x2-B-cyc.

Parameter	BA-2x2-B-cyc-1	BA-2x2-B-cyc-2	BA-2x2-B-cyc-3	BA-2x2-B-cyc-4
k_α	300	300	300	300
k_β	50	50	50	105
α	0.1	0.1	0.1	0.1
β	1.2	1.2	1.2	1.2
ω	12	12	12	5

The model output load-displacement curves and the corresponding experimental results shown in Figure 12.6 are in good agreement. This is particularly true for the first test (Figure 12.6 (a)). In the second and third tests, shown in Figure 12.6 (b) and (c), it can be seen that in the cases where the soft unloading and reloading behavior in the last cycle is accurately simulated, the previous cycles are somewhat stiffer than in the experiments. On the other hand, in the cases where the intermediate behavior is accurately simulated, the behavior in the last cycles can be too stiff. This becomes apparent in the fourth test in Figure 12.6 (d).
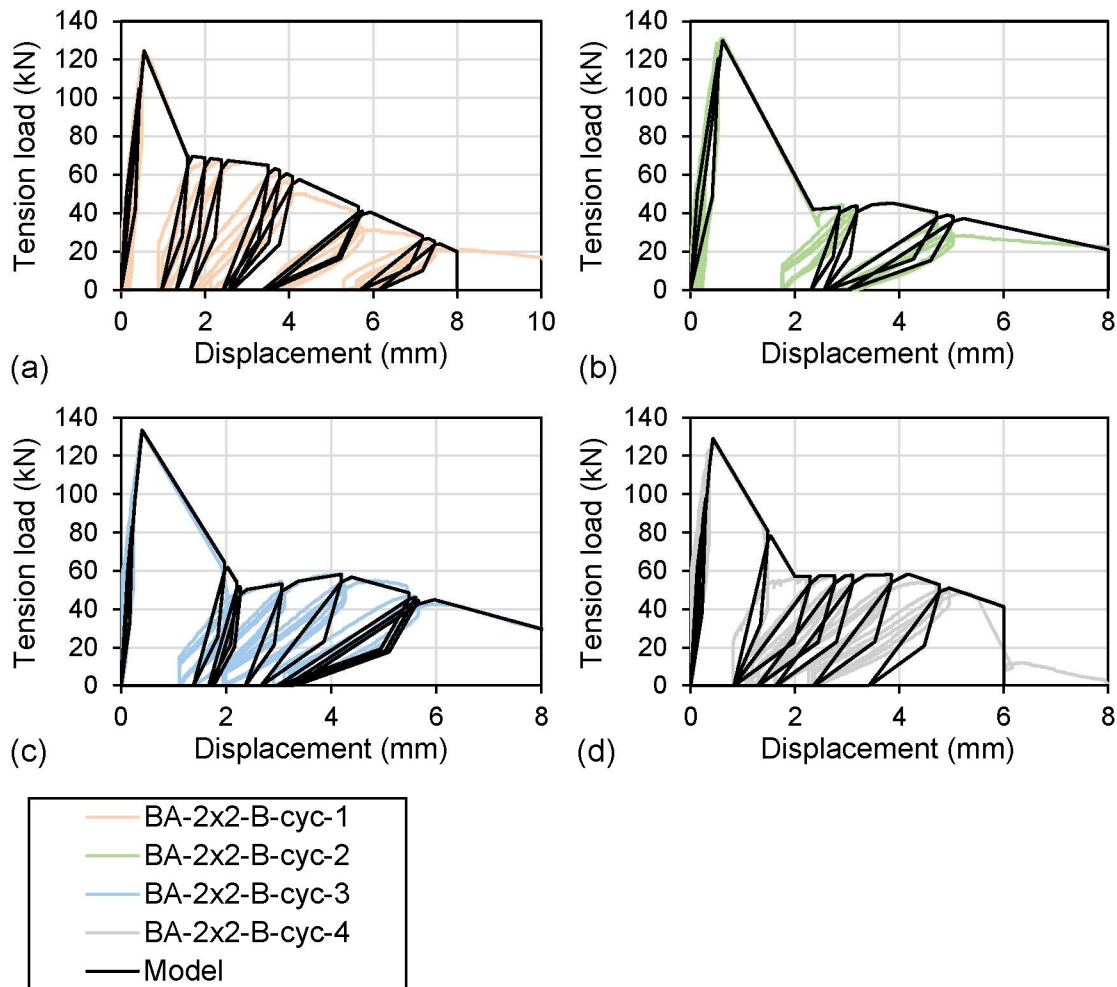
Figure 12.6. Load-displacement curves obtained from test series BA-2x2-B-cyc along with the results obtained from the three-parameter model.

12.3.6 Test series BA-2x2-C-cyc

In the last example, the hysteretic model is compared to test series BA-2x2-C-cyc. In this test series, the anchors were embedded in the concrete with an embedment depth of h_{ef} = 80 mm. The anchor groups comprise four anchors with a spacing of s_1 = 160 mm and s_2 = 80 mm. The required parameters for defining the unloading and reloading stiffness are summarized in Table 12.7 for each test respectively.

Table 12.7. Parameters for defining the unloading and reloading stiffness for BA-2x2-C-cyc.

Parameter	BA-2x2-C-cyc-1	BA-2x2-C-cyc-2	BA-2x2-C-cyc-3	BA-2x2-C-cyc-4
k_α	300	300	300	300
k_β	80	55	50	50
α	0.1	0.1	0.1	0.1
β	1.2	1.2	1.2	1.2
ω	9.4	13	13	13

Figure 12.7 shows the reproduced load-displacement curves obtained in the experiments and the corresponding model response. The comparison of experimental and model results shows that the model is able to simulate the behavior of anchor groups with four anchors and varying spacing in the two directions with adequate degree of accuracy. In the fourth test, shown in Figure 12.7 (d), the experimental curves feature cycling in almost the entire range of the load-displacement curve. Thereby, the unloading and reloading behavior clearly softens with increasing displacements. The comparison to the output load-displacement curve obtained through the modelling approach shows that the proposed model is quite capable of reproducing the hysteretic behavior of the group in the entire range of the load-displacement curve. The findings support the assumption that the hysteretic behavior of a group can be determined based on the characteristics of the individual anchors.

12.4 Summary

In this chapter, a modelling approach was presented for the simulation of the hysteretic behavior of multiple anchor groups without the requirement of implementing the hysteretic rules in a commercial FE software. This requires that the monotonic load-displacement behavior of the anchor group is already known in the form of the envelope curve, which can be determined using the nonlinear spring model.

Since the interaction between anchors and baseplate is not directly considered, as it can be done in a step-by-step FE analysis, some assumptions were needed which limit the use of the model. At the same time, only information and parameters that can be derived from single anchor reference tests under pulsating tension load should be required for modeling of the hysteretic behavior. In order to consider the interaction of the individual anchors, or to be more precise, the combined unloading and reloading behavior, it is assumed that the anchors act like springs which are connected in parallel. This assumption limits the use of the model to anchor groups, where all anchors are equally loaded. Thus, all anchors have the same displacement. Knowing the overall behavior of an anchor group in terms of the envelope curve, also the flexibility of the baseplate is considered in the modelling approach. To this purpose, it is assumed that the anchors and the baseplate are connected in series, whereby the

baseplate remains elastic. Note that the approach proposed here is general and if the hysteretic rules are implemented in a FE analysis software, the model should be able to capture the hysteretic behavior of eccentric loading groups as well and even should be able to consider yielding of the baseplate through appropriate material modeling. However, this is out of scope of this work and should be looked into in the future.
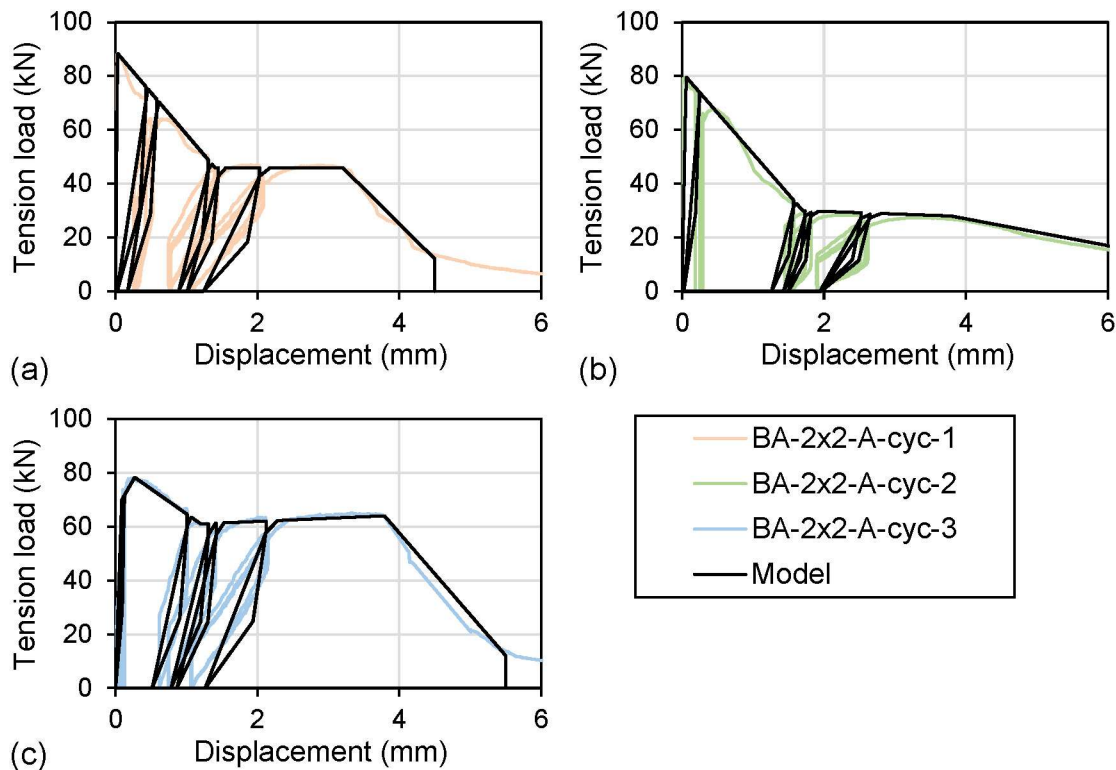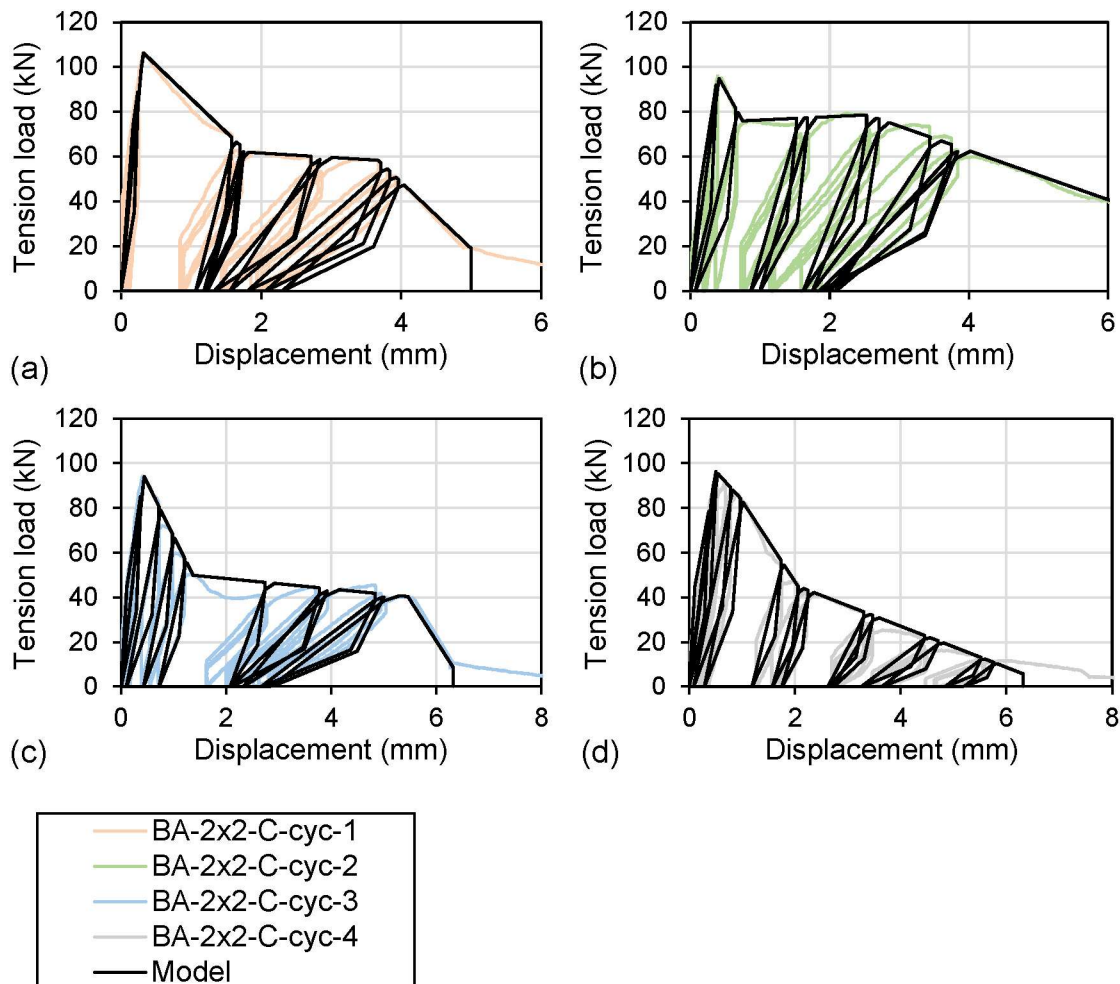

Figure 12.7. Load-displacement curves obtained from test series BA-2x2-C-cyc along with the results obtained from the three-parameter model.

Finally, the modelling approach was validated against experimental results from this work. In general, the comparison between the experimental results and the model results showed a good agreement. The unloading and reloading behavior and the general hysteretic behavior of anchor groups could be simulated with adequate level of accuracy. The comparison showed that the hysteretic rules, which were established to define the unloading and reloading paths in case of single anchors, are, in principle, applicable to anchor groups as well. However, it should be mentioned that the hysteretic loops in the model are less prominent compared to the experimental results. This is mainly a result of the simplified reloading approach. Nonetheless, the hysteretic rules can be adopted without further modification. Furthermore, the comparison

verified the assumptions which were made for the combined unloading and reloading behavior of the anchors and the baseplate.

In some examples, it has been shown that the progression of the unloading and reloading stiffness with increasing displacement was not consistently accurate. One explanation for this could be that even though in theory the anchors are loaded uniformly, the individual anchor behavior may differ in reality. For instance, this may result from imperfections associated with installation. In these cases, the relatively simple idealization of the unloading and reloading behavior of the individual anchors can lead to a decrease in the accuracy of the overall behavior of the group. In this case, using a higher grade idealization approach would result in a more accurate description of the hysteretic behavior of anchor groups.

Part III

Subassembly level

13 Experimental investigations on anchorages in a corner configuration

Several bracing configurations, such as diagonal bracing or X-bracing, require an installation of the connection element in the corner of the frame. One example of such a connection is found in Mahrenholtz et al. (2015) (see Figure 2.9 and Figure 13.1 (a)). When the steel braces are directly attached to the RC frame and post-installed anchors are used to form the connection between them, the anchors are arranged in a spatial configuration in the corner of the frame, which is not covered in current standards and guidelines. Moreover, to the best of the author's knowledge, there is barely any experimental data on the performance of such an anchor configuration per se. Note that experiments have been performed where post-installed anchors were used to fasten the steel braces to the RC frame structure. However, the target of these experiments was to investigate the performance of the steel braces and the strengthened structure. With respect to the anchors, these experiments could only show that they provide a feasible solution.

Since the geometrical conditions of such a configuration is only little understood, an experimental investigation on the breakout behavior of anchorages in such a corner configuration was conducted. Since the focus of this study was on anchorages set in the concrete corner, the test specimen was designed in a way that other effects, such as bending of the RC members or the frame action effect on the gusset plate would not compromise the evaluation of the concrete breakout behavior.

This chapter presents a detailed description of the executed experimental program, the experimental setup, the design of the test specimens and the experimental results. The results are discussed with respect to the load-displacement behavior and the observed failure mechanism of the configuration. In addition, the distribution of forces in the connection element and among the anchors is investigated.

Note that in the following, the terms bracket-to-gusset plate connection, bracket configuration and corner configuration are used synonymously and describe the complete connecting element between steel brace and RC frame including the anchorage. It comprises a gusset plate, an anchor bracket and the post-installed anchors which are used to fasten the steel elements to the base material. A detailed description is given below.

13.1 Experimental program

The experimental program comprises two test series with three tests each on anchor groups of 8 bonded anchors installed in a corner configuration (4 anchors in each plane), as shown in Figure 13.1 (b). The dimensions of the concrete specimen and the steel parts of the bracket-to-gusset plate connection were the same in each test. The two test series differed solely with respect to the embedment depth of the anchors. In test series BGC-80, the anchors were embedded in the concrete with an embedment depth of h_{ef} = 80 mm and in test series BGC-110 with an embedment depth of h_{ef} = 110 mm. Each test was performed in a separate concrete specimen made of normal strength concrete (C20/25). The steel element comprising the gusset plate and the anchor bracket was fabricated twice. This allowed two elements to be installed and prepared at the same time, resulting in a more practical and efficient experimental procedure due to the curing time of the epoxy mortar. The bracket configuration was monotonically loaded in displacement-control until failure using a servo-hydraulic actuator. The loading speed was maintained at 0.02 mm/sec. This allowed an accurate capture of the post-peak behavior of the load-displacement curve, after reaching the ultimate capacity. The bonded anchor system comprised a two-component injection system and a high-strength threaded rod. The threaded rods had a size of M16 and strength class 8.8.
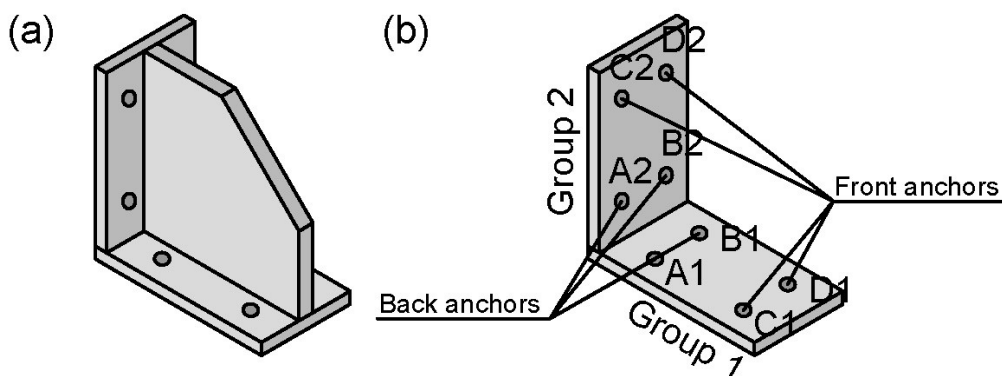
Figure 13.1. Schematic depiction of (a) the bracket-to-gusset plate connection (spatial group of eight anchors) and (b) segmentation of the spatial group with eight anchors into two groups with four anchors in each plane.

13.2 Description of the connection element

The investigated connection comprises a gusset plate which is welded to an L-shaped anchor bracket. The anchor bracket is in turn fastened to the concrete specimen by means of post-installed bonded anchors such that two standard anchor groups of 4 anchors each (2 x 2 anchor groups) orthogonal to each other are formed (see Figure 13.1 (b)). Gusset plate and anchor bracket are made of S235JR steel with a specified

yield strength of f_y = 235 N/mm² and a specified ultimate strength of f_u = 360 N/mm². The dimensions of the connection element are given in Figure 13.2. The gusset plate has a thickness of 25 mm, and the anchor bracket has a thickness of 20 mm. The gusset plate is welded to the anchor bracket using double-bevel-groove and double fillet welds with a weld size of 5 mm.

The anchor configuration requires a push through installation of the bonded anchors. Thus, eight holes with a diameter of 20 mm are cut into the steel to allow the M16 threaded rods to pass through the anchor bracket. The anchor bracket is basically composed of two steel plates, which are fastened to the concrete specimen. In simplified terms, the connection can be considered as two perpendicular anchor groups. Thus, the anchor bracket is also referred to as two perpendicular anchor groups. In these anchor groups, the anchors are distinguished according to their position. The two anchors closest to the corner are referred to as back anchors and the two anchors farthest away are referred to as front anchors. To fasten the bracket-to-gusset plate connection element to the concrete specimen the same two-component injection system, FIS EM Plus, was used as in the experimental part on single anchors. For this reason, no detailed description of the bonded anchor system is given here, and reference is made to the description provided in the respective chapter.

In one test series, the threaded rods were embedded in the concrete with an embedment depth of 80 mm and in the second test series with an embedment depth of 110 mm. The threaded rods were made of steel with strength class 8.8. Therefore, the specified yield and ultimate strength were 640 N/mm² and 800 N/mm², respectively. In all test series the anchor spacing in the direction perpendicular to the parallel edges is 80 mm and the anchor spacing parallel to the free edges is 160 mm (see Figure 13.2). The distance from the back anchors to the concrete corner was 80 mm in all tests and thus corresponds to the effective embedment depth in test series BGC-80. Accordingly, in test series BGC-110, the distance is smaller than the embedment depth of the anchors. The individual anchor groups correspond to the 2 x 2 anchor groups tested in Chapter 9 in narrow concrete members.
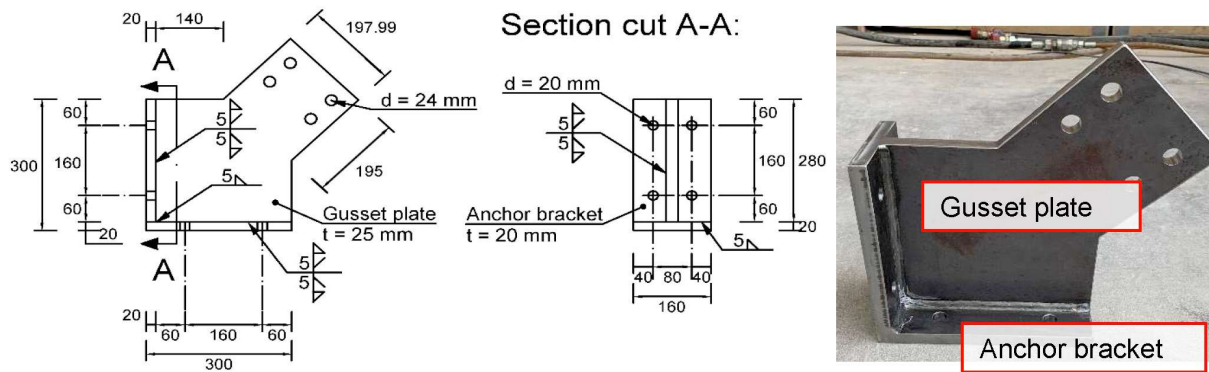
Figure 13.2. Dimensions of the bracket-to-gusset plate connection element comprising the anchor bracket and the gusset plate. (Note: All dimensions are in mm).

The load on the connection was applied via an additional U-shaped fixture made of S235JR steel, which was connected to the gusset plate by means of four pins. A depiction of the U-shaped fixture and the assembly is given in Figure 13.3. The bolted connection was chosen for practical reasons as it facilitates the assembly and disassembly of the experimental setup. The U-shaped fixture is connected to the servo-hydraulic cylinder using a M30 threaded rod of strength class 12.9.
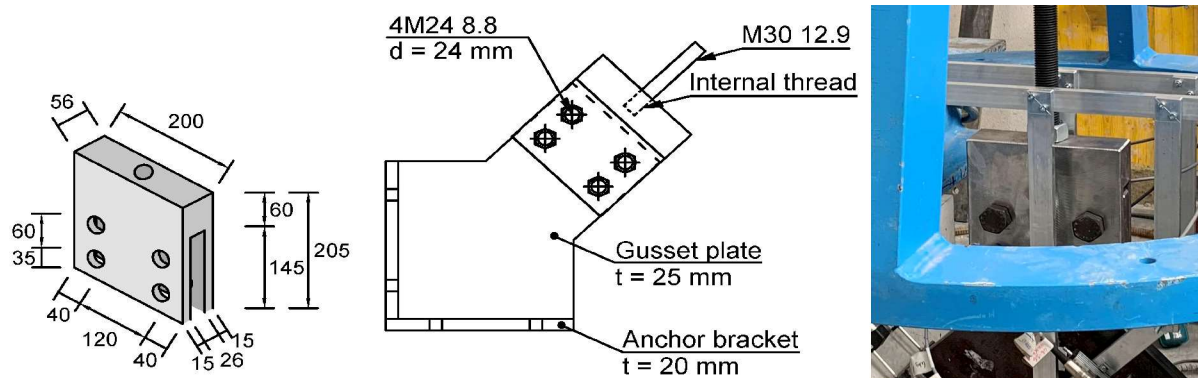
Figure 13.3. Dimensions of the U-shaped fixture and schematic description of the load application. (Note: All dimensions are in mm).

13.3 Design of the connection element

Since the main focus of the experimental program is set on the failure of the anchorage, the steel elements of the connection were designed in a way to ensure that concrete breakout failure of the anchorage dominates the overall behavior. This essentially means that the steel parts of the connection were designed to withstand the maximum expected capacity of the anchorage without yielding. As mentioned above, for such a spatial anchor configuration, no design recommendations are available in current standards and guidelines. This renders an estimation of the ultimate capacity of the

anchorage rather difficult. For this reason, a preliminary numerical analysis was performed to estimate the forces acting on the bracket configuration. A detailed description of the numerical study is found in Stehle and Sharma (2021c). In this numerical analysis, the steel elements were modeled assuming a linear-elastic behavior. In this way, a failure of the anchors was provoked which resulted in a concrete breakout failure of the connection, which is the type of failure also targeted in this experimental study. The ultimate capacity of the configuration obtained in the numerical analysis for an embedment depth of 110 mm, P_u = 292 kN, was considered for the design of the bracket-to-gusset plate connection. It should be noted however that the dimensions of the connection element and the concrete specimen in the numerical analysis slightly differed from the dimensions in this study. The main difference is the distance from the back anchors to the concrete corner. In the numerical study the distance was 60 mm, while in this study, for practical reasons, the distance is 80 mm (see Figure 13.2).

The applied design approach for the bracket-to-gusset plate connection basically follows the principles in steel construction discussed in Chapter 2. The associated design checks include the welds at the gusset interfaces, yield strength at the Whitmore section, gusset plate buckling below the Whitmore section, block shear failure, von Mises yield criteria at the interfaces, tensile rupture at the interfaces and shear rupture at the interfaces. Since the connection is only loaded in tension, some design checks, such as buckling of the gusset plate are not required. On the other hand, due to the load application by means of a bolted connection, additional design checks are required, that are the shear resistance of the bolts, hole bearing in the gusset plate and in the flanges of the fixture, block tearing in the gusset plate and in the fixture and yielding in the flanges of the fixture. The forces acting on the gusset-to-bracket interfaces were calculated based on the UFM. Thereby it was assumed that the column and beam dimensions were equal. For a total force on the bracket configuration which is applied at a load angle of 45°, the tension and shear forces acting on the interfaces were calculated as N = 113.2 kN and V = 93.3 kN, respectively.

In the following, the individual design checks are performed, and the corresponding design-to-capacity ratios (DCR) are determined.

13.3.1 Welds at gusset-to-bracket interfaces

The welds are designed according to EN 1993-1-8. A fillet weld and bevel-groove weld on both sides of the gusset plate was chosen with a weld length, l_w = 28 cm at both interfaces. The minimum weld size, a_w, for the 25 mm thick gusset plate is 4.5 mm and the minimum length is 3 cm. The tension and shear demand on the weld per unit length is calculated as follows:

$$F_\perp = \frac{N}{l_w} = 4.04 \ kN/cm, \tag{13.1}$$

$$F_{\parallel} = \frac{V}{l_w} = 3.33 \ kN/cm.$$

(13.2)

The combined demand is calculated as:

$$F_w = \sqrt{F_{\perp}^2 + F_{\parallel}^2} = 5.24 \ kN/cm.$$

(13.3)

Using a weld size of a_w = 5 mm, the design capacity of the welds is calculated as follows:

$$F_{w,Rd} = \frac{f_u \cdot 2 \cdot a_w}{\sqrt{3} \cdot \beta_w \cdot \gamma_{M2}} = 20.78 \ kN/cm.$$

(13.4)

Where β_w is 0.8 for S235JR steel and the safety factor for connections, γ_{M2}, is 1.25. The demand-to-capacity ratios for the interface welds are determined as:

$$DCR_{w,1} = DCR_{w,2} = \frac{F_w}{F_{w,Rd}} = 0.25.$$

(13.5)

13.3.2 Yield strength at Whitmore section

For the problem at hand, the resulting Whitmore width for a distance between the two rows of 60 mm is w_w = 189.3 mm. With a gusset plate thickness of t_g = 25 mm, the stress in this section is calculated as σ_T = 61.7 N/mm². Accordingly, the DCR is calculated as:

$$DCR_{wy} = \frac{\sigma_T}{f_y} = 0.26.$$

(13.6)

13.3.3 Von Mises yield criteria and tensile and shear rupture at interfaces

Besides the yield strength at the Whitmore section, the gusset plate is checked for the stresses at the interfaces to the anchor bracket. For this purpose, a horizontal section cut through the gusset plate just above the interface weld is considered. One approach to determine the distribution of stresses and the maximum normal and shear stresses in this section is the application of the beam formulas. Hence a uniform distribution of the normal stresses and a parabolic pattern for the shear stress distribution with the maximum shear stress at the center of the section. However, a numerical study on gusset plates conducted by Lin et al. (2014) has shown that the assumption of equal normal stresses along the interface can be considered adequate, whereas the maximum shear stress was rather observed at the corner from where the stresses decrease linearly to zero in the direction towards the free end of the gusset plate. In

this case the maximum normal and shear stresses in the interface section are calculated using following equations (Lin et al., 2014):

$$\sigma_{max} = \frac{N}{t_g \cdot L_{gusset}} = 16.2 \ N/mm^2, \tag{13.7}$$

$$\tau_{max} = \frac{2 \cdot V}{t_g \cdot L_{gusset}} = 26.7 \ N/mm^2. \tag{13.8}$$

Where L_{gusset} is the length of the gusset-to-bracket interface and t_g is the thickness of the gusset plate. It is worth mentioning that the maximum shear stress obtained from Equation (13.8) is higher than the one obtained from the beam formulas. Furthermore, it should be noted that according to Lin et al. (2014), the distribution of normal and shear stresses again changes when the frame action effect is considered. The respective DCRs for the von Mises yield criteria, tensile rupture and shear rupture are as follows (Lin et al., 2014):

$$DCR_{m,1} = DCR_{m,2} = \frac{\sqrt{\sigma_{max}^2 + 3 \cdot \tau_{max}^2}}{f_y} = 0.21, \tag{13.9}$$

$$DCR_{t,1} = DCR_{t,2} = \frac{\sigma_{max}}{\psi \cdot f_u} = 0.06, \tag{13.10}$$

$$DCR_{s,1} = DCR_{s,2} = \frac{\tau_{max}}{\psi \cdot 0.6 \cdot f_u} = 0.17. \tag{13.11}$$

13.3.4 Bolted connection

The bolted connection between the U-shaped fixture and the gusset plate with four pins (see Figure 13.3) is a double shear connection of category A (bearing type) with four M24 bolts of strength class 8.8. The diameter of the bolts was chosen to fit just through the holes in the gusset plate and the U-shaped fixture to keep the hole clearance as small as possible, thus facilitating an even distribution of the forces on the bolts. It is designed according to EN 1993-1-8. The design checks for the connection include the shear resistance of the bolts, hole bearing in the gusset plate, hole bearing in the flanges of the fixture, block tearing in the gusset plate and block tearing in the flanges of the fixture. In addition, the tensile stresses in the flanges of the fixture are checked to exclude yielding. For simplification, the effective cross-sectional area (subtracting the holes of the bolts) of one flange is taken to calculate the maximum tensile stress, thus $A_{eff} = (200 - 2 \cdot 24) \cdot 15 = 2280 \ mm^2$. A summary of the DCRs for the above mentioned design checks is provided in Table 13.1. For the bolted connection, the highest utilization is determined for hole bearing in the gusset plate

with a DCR of 0.34. Therefore, it can be safely assumed that the gusset plate will remain linear-elastic during the tests.

Table 13.1. Overview of the demand-to-capacity ratios of the double shear connection.

Description of design checks	DCR
Shear resistance of the bolts	0.21
Hole bearing in the gusset plate	0.31
Hole bearing in the flanges of the fixture	0.29
Block tearing in the gusset plate	0.26
Block tearing in the flanges of the fixture	0.22
Yielding in the flanges of the fixture	0.27

13.3.5 Anchor bracket

The CCD method requires that the steel fixture, which combines a number of individual anchors to an anchor group is rigid enough to ensure a uniform distribution of the total load to the individual anchors. Although this requirement applies to the CCD method and not to the anchor bracket per se, it is intended to ensure that the anchor bracket remains linear elastic during testing.

In order to check the stresses in the anchor bracket, it is considered as two separate anchor groups. For these two steel plates the maximum stresses are determined using the beam formulas. Thereby, the steel plates are considered as simply supported beams with overhanging, where the two directions of the steel plate are examined separately. The maximum obtained design-to-capacity ratio for steel yielding is $DCR_{ab} = 0.53$. Therefore, it can be safely assumed that the anchor bracket will remain linear elastic during the test.

13.3.6 Overview of the DCRs for the bracket-to-gusset plate connection

Table 13.2 provides a summary of the design-to-capacity ratios of the gusset plate and anchor bracket connection.

Table 13.2. Overview of the demand-to-capacity ratios of the connection element.

Description of design checks	DCR
Weld at gusset-to-beam interface	0.25
Weld at gusset-to-column interface	0.25
Yield strength at Whitmore section	0.26
von Mises yield criteria at gusset-to-beam interface	0.21
von Mises yield criteria at gusset-to-column interface	0.21
Tensile rupture at gusset-to-beam interface	0.06
Tensile rupture at gusset-to-column interface	0.06
Shear rupture at gusset-to-beam interface	0.17
Shear rupture at gusset-to-column interface	0.17
Double shear bolted connection	0.34
Anchor bracket	0.53

13.4 Description of the concrete test specimen

The experimental study investigates the connection of steel braces in the corner of RC frames by means of post-installed anchors. Under seismic actions, the steel brace and thus the connection element is alternately loaded in tension and compression. However, for the investigated application, the anchors are only intended to be activated and transfer the load to the RC frame structure, when the steel brace is loaded in tension. When loaded in compression, the forces are expected to be directly transferred to the RC frame by the anchor bracket. As shown in Section 2.3.3, the RC members in which the anchors are installed, are expected to bend inwards and the anchorage zone is under compression when the brace is loaded in tension. Consequently, cracks in the anchorage zone have mostly closed as shown in Mahrenholtz et al. (2015). Furthermore, bending of the RC members would also trigger a frame action effect on the gusset plate.

As the main focus of this study is to examine the behavior of a such a spatial anchor configuration in the corner, the investigation of a full-scale RC frame or a RC frame subassembly would hinder the assessment of the mere geometrical influence of the corner due to the additional effects. To enable a clear distinction between the various effects on the connection, it is required to perform initial tests in a concrete specimen where only the effects of the corner are relevant. Within this framework, the test specimen shown in Figure 13.4 was designed.
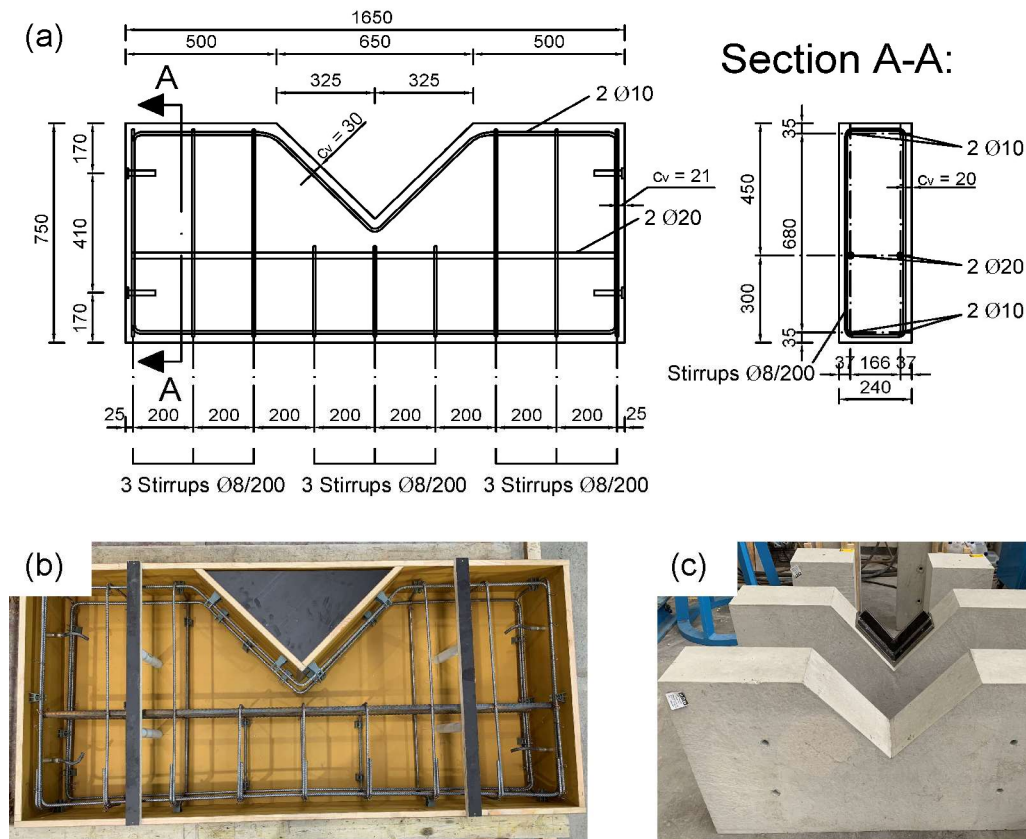
Figure 13.4. (a) Dimensions and reinforcement details of the concrete specimen used in the experiments, (b) formwork with reinforcement cage and (c) concrete specimen after construction. (Note: All dimensions are in mm).

The concrete specimen has a length of 1650 mm, a height of 750 mm and a width of 240 mm. The width resembles the width of the concrete specimen used in the experimental part on narrow concrete members. This enables a direct comparison between the two experimental programs. With respect to the width, the connection element is placed centered and so the distance of the anchors to the free edges on both sides is 80 mm. The concrete specimen features a triangular recess simulating the inner corner of a RC frame with a 90° angle. The sides of the recess have a length of 460 mm (hypotenuse of the right angled isosceles triangle of sides 325 mm as shown in Figure 13.4 (a)). The distance from the back anchors to the corner is 80 mm, the spacing in the direction parallel to the free edges is 160 mm, and the distance from the front anchors to the base of the recess is 220 mm. The distance of 220 mm was chosen on basis of EOTA TR 048 which stipulates a distance of at least $2h_{ef}$ from the outermost anchors to the supports in case of an unconfined test setup. Note, the details of the test setup will be discussed in detail in a later section.

Figure 13.4 provides the reinforcement details used in the test member. Note that the sole purpose of the reinforcement was to prevent splitting or bending cracks in the concrete specimen and to facilitate handling. The reinforcement was provided such that it will not have any influence on the behavior of the anchorages. Two longitudinal

reinforcing bars with a diameter of 20 mm are provided beneath the embedded anchors to prevent bending cracks being developed in the concrete specimen. In the anchorage zone rebars with a diameter of 10 mm are provided relatively close to the concrete surface to prevent splitting. The longitudinal reinforcement is enclosed by stirrups with a diameter of 8 mm which are supposed to take up the shear forces in the concrete specimen.

The slabs are made of normal strength concrete C20/25 and were cast from a single batch of concrete mixture in accordance with DIN EN 206. The grading curve was chosen between the standard grading curves A16 and B16 with a maximum aggregate size of 16 mm. The cube concrete compressive strength of the hardened concrete at the time of testing was determined on six concrete cubes with a side length of 150 mm. The measured mean cube concrete compressive strength was $f_{cc,m}$ = 30.5 N/mm². The mean cylinder concrete compressive strength is determined as $f_{c,m}$ = 25.0 N/mm² using the conversion factor $k_{cyl/cube}$ = 0.82 (see Section 5.3 and DIN EN 206, Fingerloos et al. (2015), and Loch (2014)).

13.5 Description of the experimental setup and testing procedure

13.5.1 Experimental setup

The experimental setup is shown and explained in Figure 13.5. Four concrete support blocks were placed adjacent to the test specimen, two blocks on each side. On top of the support blocks and the test specimen, two I-beams were situated in a way that they were located at the edge of the triangular recess. The I-beams serve as the supports for the test rig and the servo-hydraulic cylinder, and they are intended to distribute the weight of the servo-hydraulic cylinder and the reaction forces to the support blocks and the test specimen. In this way, the test specimen did not have to carry the entire load alone, which would otherwise have resulted in high stresses in the test specimen. Moreover, the setup provides the necessary stability during the experiments. The load on the connection is applied via the U-shaped fixture shown in Figure 13.3. The fixture is in turn connected to the servo-hydraulic cylinder by means of a M30 threaded rod with strength class 12.9 and a special hinge (see Figure 13.5 (d)). Similar to the tests on anchor groups, the purpose of the hinge is the free rotation of the connection element which enables a redistribution of forces. Furthermore, the assembly and disassembly of the setup is facilitated. The servo-hydraulic cylinder has a load capacity of up to 400 kN.
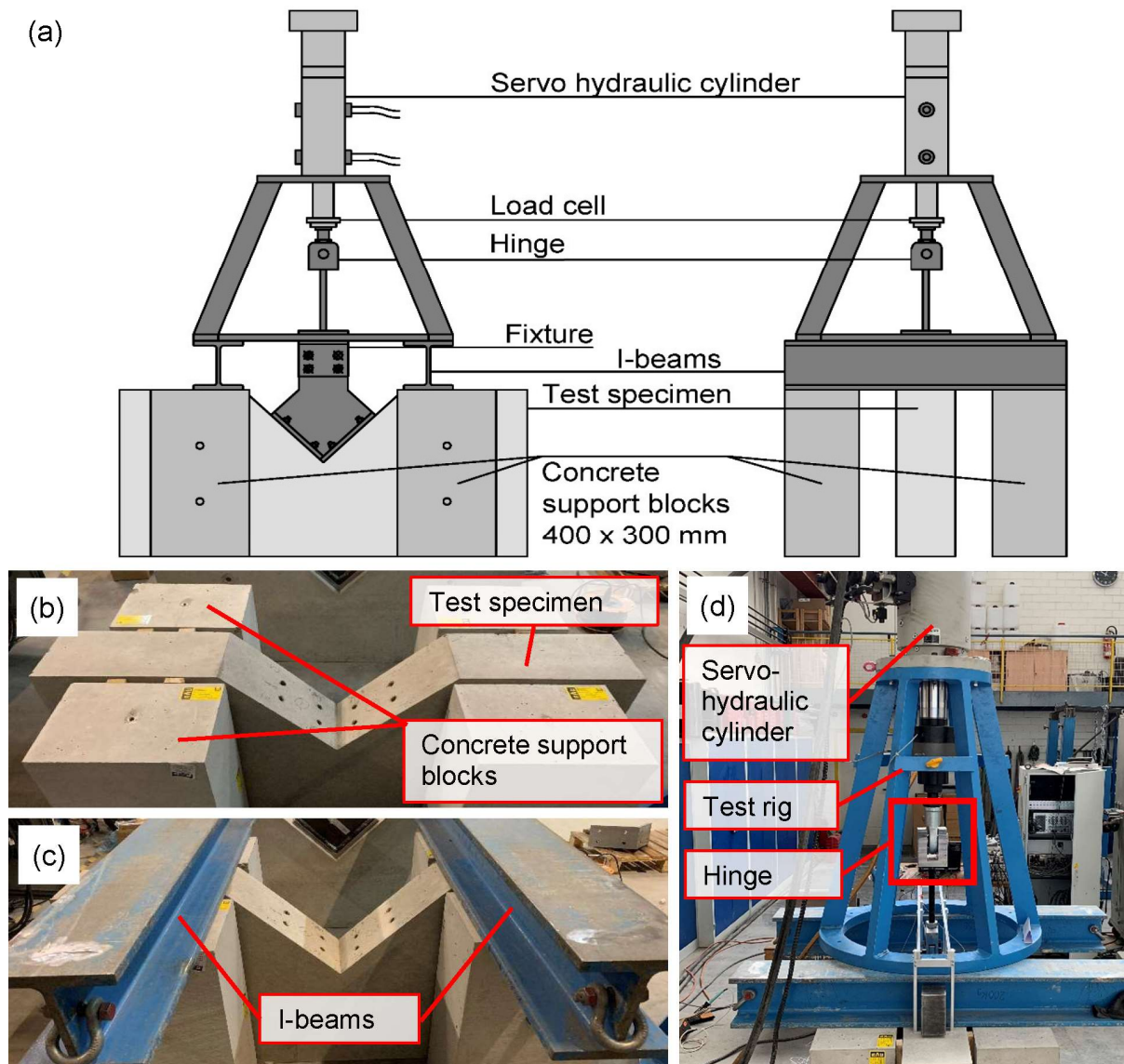
Figure 13.5. Experimental setup – Depiction of the individual parts of the setup. (a) Schematic depiction, (b) Test specimen and concrete support blocks, (c) I-beams on support blocks, and (d) test rig and servo-hydraulic cylinder.

13.5.2 Instrumentation

The total force demand on the connection was measured using a calibrated load cell with a measuring range up to 400 kN. As indicated in Figure 13.6 (b), the anchor bracket is conceptually split into two groups comprising four anchors each. In Group 1, strain gauge-based force washers with a measuring range up to 200 kN were applied to measure the axial forces of the four anchors. On the same anchors, also the axial displacements were measured directly on top of the anchor head using four LVDTs. These LVDTs are mounted on a special stand as seen in Figure 13.6 (a). This stand is fixed to the upper surface of the concrete specimen outside the I-beams as can be seen in Figure 13.5 (d). Two LVDTs measured the shear displacement of the anchor

bracket on each side in the direction parallel to the sides of the triangular recess (the horizontal displacement of the individual groups, perpendicular to the anchor axis of the individual groups). The displacement of the connection, in the direction of load application, was measured on top of the fixture as close to the point of loading application as possible. Additional five LVDTs were fixed to the side surface of the concrete specimen to measure the crack width of the anticipated breakout body (see Figure 13.6 (b)). All LVDTs used in the tests have a measuring range up to 25 mm. In order to determine the stresses in the gusset plate, strain gauges were used. They were glued to the surface of the gusset plate. The main intention was on the evaluation of normal stresses at the interface between the gusset plate and the anchor bracket. Throughout the tests, the total load, the displacement of the connection, the individual axial anchor forces, the axial anchor displacements, the shear displacement of the anchor bracket, and the crack width on the side of the concrete slabs were continuously recorded.
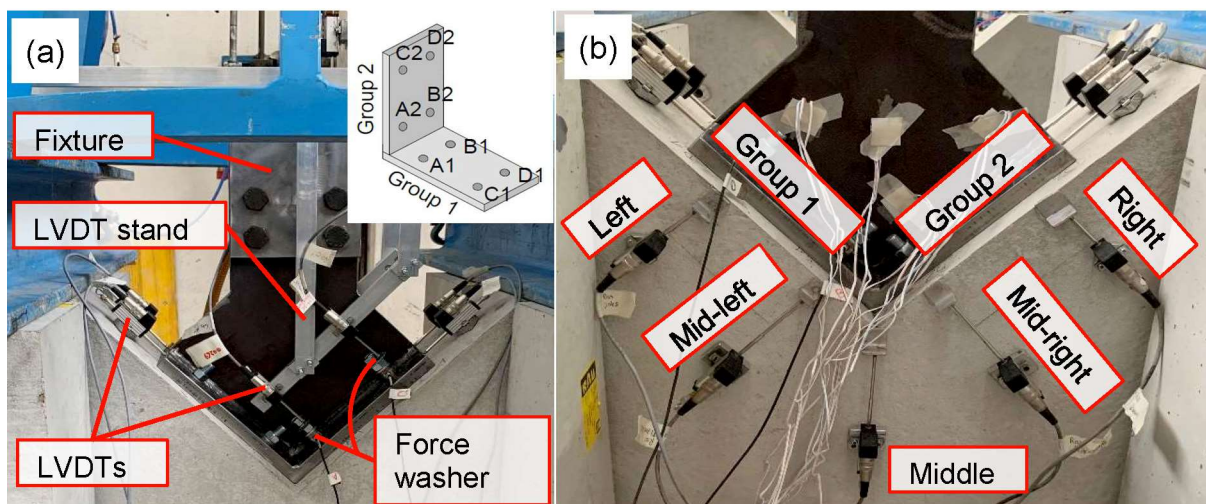
Figure 13.6. Experimental setup – Instrumentation. (a) Measurement of anchor axial forces and displacements and the shear displacement of the bracket and (b) measurement of the cracks on the side surface of the concrete specimen.

13.5.3 Testing procedure

The installation of the anchors followed the installation instructions provided in ETA-17/0979. The anchor holes were drilled using a mounted rotary hammer with a nominal drill hole diameter of 18 mm. Thereafter, the holes were cleaned according to the installation instruction provided by the manufacturer (ETA-17/0979). After cleaning, the connection element was placed in its position and the anchors were installed in push through installation. Thereby, the annular gap was filled with mortar. After the specified curing time, the connection was fixed by the nuts, and the nuts were hand-tightened. After assembling of the experimental setup, the bracket configuration was loaded monotonically using the servo-hydraulic actuator. The load was applied in displacement-control in a way that the ultimate load was reached within two to six

minutes, depending on the embedment depth. Due to the displacement-controlled loading it was possible to accurately capture the post-peak behavior of the load-displacement curve, after reaching the ultimate capacity.

13.6 Experimental results and discussion

To begin with, the behavior of the complete connection is discussed on basis of the obtained load-displacement curves. Once the overall behavior has been established, the individual tests are evaluated on the basis of the axial displacements of the anchors, the shear displacements of the bracket, and in terms of the crack propagation on the side surface of the concrete specimen. Based on the evaluation, the failure mechanism of such a configuration is determined. Finally, the stresses in the gusset plate are evaluated.

Note that the force washer readings were somehow corrupted, which is why a quantitative statement on the axial forces of the anchors is not meaningful. Nonetheless, the results are briefly discussed.

13.6.1 Load-displacement behavior of the complete connection

Figure 13.7 shows the load-displacement curves obtained in the individual tests. The x-axis refers to the displacement measured on top of the fixture and the y-axis refers to the total force applied on the connection which was measured using the load cell. The black lines mark the tests where the anchors were embedded with an embedment depth of 80 mm. The green lines mark the tests with 110 mm embedment depth. It can be seen that in all tests, regardless of the embedment depth of the anchors, the load-displacement behavior is characterized by a first distinct peak, with the corresponding peak load, P_{first}, and a subsequent peak which marks the ultimate capacity of the connection, P_u.
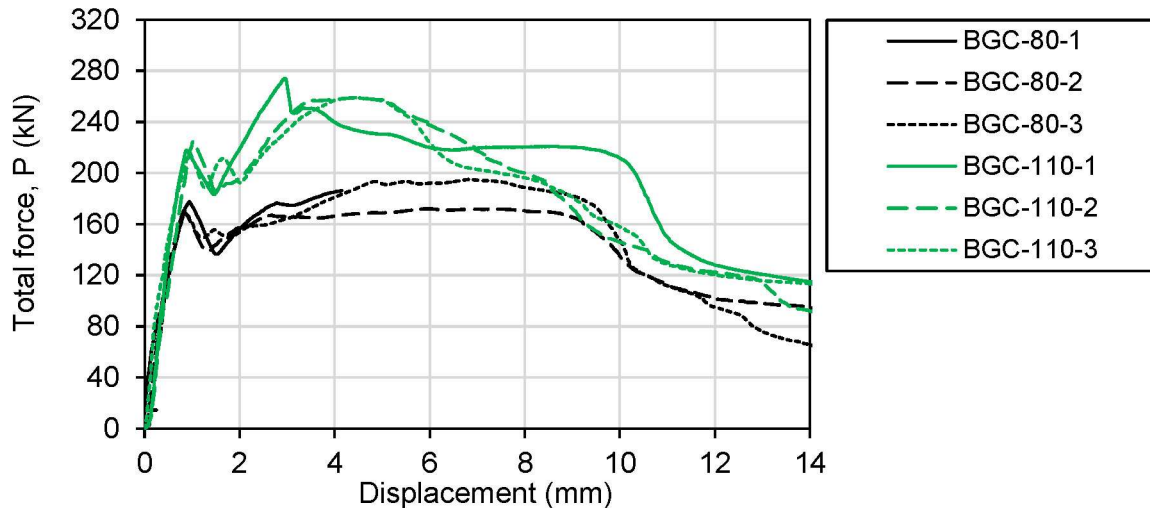
Figure 13.7. Load-displacement curves obtained in test series BGC-80 and BGC-110.

It can be seen that in both test series, the initial behavior of the bracket configuration is rather similar. That is despite the varying embedment depth of the anchors. A comparison of the initial stiffness of the connection at 50% of the load corresponding to the first peak shows a good agreement. In test series BGC-80, the average initial stiffness is 253 kN/mm and in test series BGC-110, the average initial stiffness is 273 kN/mm. At first peak, the difference is somewhat more pronounced. The corresponding mean secant stiffness is 199 kN/mm and 231 kN/mm for BGC-80 and BGC-110, respectively. The results indicate that with increasing embedment depth of the anchors, the behavior of the complete connection becomes stiffer. Besides the stiffness, also the load at first peak increases with increasing embedment depth of the anchors. At an embedment depth of 80 mm, on average, the bracket configuration reaches a load of 172.6 kN. Increasing the embedment depth of the anchors to 110 mm leads to an increase of the load to 219.6 kN. Upon reaching the first peak, the load drops to a local minimum. Thereby, the load decreases by around 13% - 23% compared to the load corresponding to first peak. Thereafter, the tested bracket configurations regain their strength, whereby the load increases to a level higher than the first peak. At this point, the connection reaches its ultimate capacity. It can be seen from the load-displacement curves that the displacement behavior in this second phase is significantly more pronounced than the behavior up to the first peak. This is also apparent from the comparison between the mean displacements at first peak, $s_{first,m}$, and the mean displacements at ultimate load, $s_{u,m}$, given in Table 13.3. Moreover, depending on the embedment depth of the anchors, the behavior of the bracket configuration differs more significantly in the second phase of the load-displacement curves. For an embedment depth of 80 mm, the ultimate load is only marginally higher compared to the load at first peak. As a result, the load-displacement behavior is mainly characterized by a pronounced load plateau with a rather soft

behavior up to the ultimate capacity. For an embedment depth of 110 mm, the ultimate load increases by around 20% compared to the load at first peak. Thereby the load-displacement behavior upon regaining the strength is significantly stiffer. This can also be seen by comparing the mean displacements at ultimate load obtained from the two test series. With an embedment depth of 110 mm, the bracket configuration reaches its ultimate load at markedly smaller displacements.

Table 13.3. Overview of the experimental results.

Test series	Test no.	P_{first} (kN)	$P_{first,m}$ (kN)	$CV(P_{first})$ (%)	$s_{first,m}$ (mm)	P_u (kN)	$P_{u,m}$ (kN)	$CV(P_u)$ (%)	$s_{u,m}$ (mm)
	1	177.8				187.4			
BGC-80	2	169.2	172.6	2.6	0.87	172.1	184.9	6.3	6.36
	3	170.8				195.1			
	1	218.0				274.2			
BGC-110	2	225.1	219.6	2.2	0.95	259.0	264.1	3.3	3.93
	3	215.8				259.1			

13.6.2 Evaluation of individual tests

13.6.2.1 BGC-80-1

Figure 13.8 (a) shows the axial displacements of the anchors in the first group as a function of the elapsed time. Figure 13.8 (b) shows the shear displacement of the two perpendicular anchor groups which were measured in line with anchor C and D, in the direction parallel to the inclined concrete surface and to the two close edges (see Figure 13.6). The red lines mark the shear displacement of the first group, and the green lines mark the shear displacement of the second group. In Figure 13.8 (c), the crack width which was measured on the side surface of the concrete specimen is plotted as a function of the elapsed time. The points where the bracket configuration reaches its first peak, and the ultimate load are marked by dotted lines. Up to the first peak, the behavior of the bracket configuration is relatively uniform. The individual anchors in one group yield practically the same displacements. Although it should be noted that anchor B and D show slightly larger displacements. The shear displacement of both groups progresses uniformly. No cracking on the concrete surface is apparent up to the first peak.

Figure 13.8. Results obtained in test BGC-80-1 as a function of the elapsed time: (a) Axial displacement of the anchors, (b) shear displacement of the anchor bracket, and (c) crack width on the side surface of the concrete specimen.

Shortly after the first peak is reached, cracks occur on the side surface of the concrete specimen at the level of the embedded ends of the anchors. As can be seen in Figure 13.8 (c), the crack width in the anchorage zone of the first group is notably larger compared to the crack width of the second group. As a result, the shear displacement of the second group which is perpendicular to the crack opening of the first group increases further, while the shear displacement of the first group reduces. With increasing load, also a crack in the corner of the concrete specimen opens up. Upon the initial crack opening, a sudden increase of axial displacements of the anchors is apparent. Thereafter, the anchor axial displacement increases steadily until the ultimate load is reached, whereby the rate of change is somewhat higher in the second

phase. Nonetheless, similar to the initial phase, the axial displacement of the individual anchors progresses rather equally. However, anchor B and D show somewhat larger axial displacements, indicating a slight distortion of the connection element.

13.6.2.2   BGC-80-2

Figure 13.9 shows the results obtained in test BGC-80-2 as a function of the elapsed time. Figure 13.9 (a) shows the axial displacements of the anchors in the first group. Figure 13.9 (b) shows the shear displacement of the two perpendicular anchor groups which were measured in line with anchor C and D, in the direction parallel to the inclined concrete surface and to the two close edges. The red lines mark the shear displacement of the first group, and the green lines mark the shear displacement of the second group. In Figure 13.9 (c), the crack width which was measured on the side surface of the concrete specimen is plotted. The points where the bracket configuration reaches its first peak, and the ultimate load are marked by dotted lines.

In accordance with the results in test BGC-80-1, the behavior of the bracket configuration is relatively uniform until the first peak is reached. The individual anchors in one group yield practically the same axial displacements. Also, the shear displacement of the bracket progresses uniformly at both sides. No cracking on the concrete surface is apparent up to the first peak.

Shortly after the first peak has been reached, cracks occur on the side surface of the concrete specimen in the anchorage zone of the first group, at the level of the embedded ends of the anchors. Also, a crack has opened between the back anchors of the two groups, in the corner of the concrete member. In contrast to the first test, at this point, no cracking on the surface was apparent in the anchorage zone of the second group. As a result of the cracking in the anchorage zone of the first group, the shear displacement of the second group, which is perpendicular to the crack opening of the first group, exhibits an abrupt increase and rises steadily thereafter, while the shear displacement of the first group shows a sudden drop. With increasing load, cracks also occur on the side surface at the level of the embedded ends of the anchors of the second group. Analogous to the previous test, a sudden increase of axial displacements of the anchors is apparent upon initial crack opening. Thereafter, the anchor axial displacement increases steadily until the ultimate load is reached. Thereby, the axial displacement of the individual anchors is rather similar.

In contrast to test BGC-80-1, the increase of the shear displacement of the second group is more pronounced after the first peak has been reached. This might be attributed to the fact, that the cracks at the location of the second group have not yet opened. Thus, the formation of the breakout body on this side was somewhat delayed. The observations suggest that in this test, after the first peak has been reached, the overall displacement behavior of the bracket configuration is dominated by cracking in the anchorage zone of the first group, which fails first. This is also apparent from the lower capacity of the bracket configuration. After its failure, the bracket configuration is

only partly able to distribute the loads to the second group, which results in the rather flat load-displacement behavior in the second phase. Here the overall ultimate capacity is only slightly larger compared to the capacity at first peak.
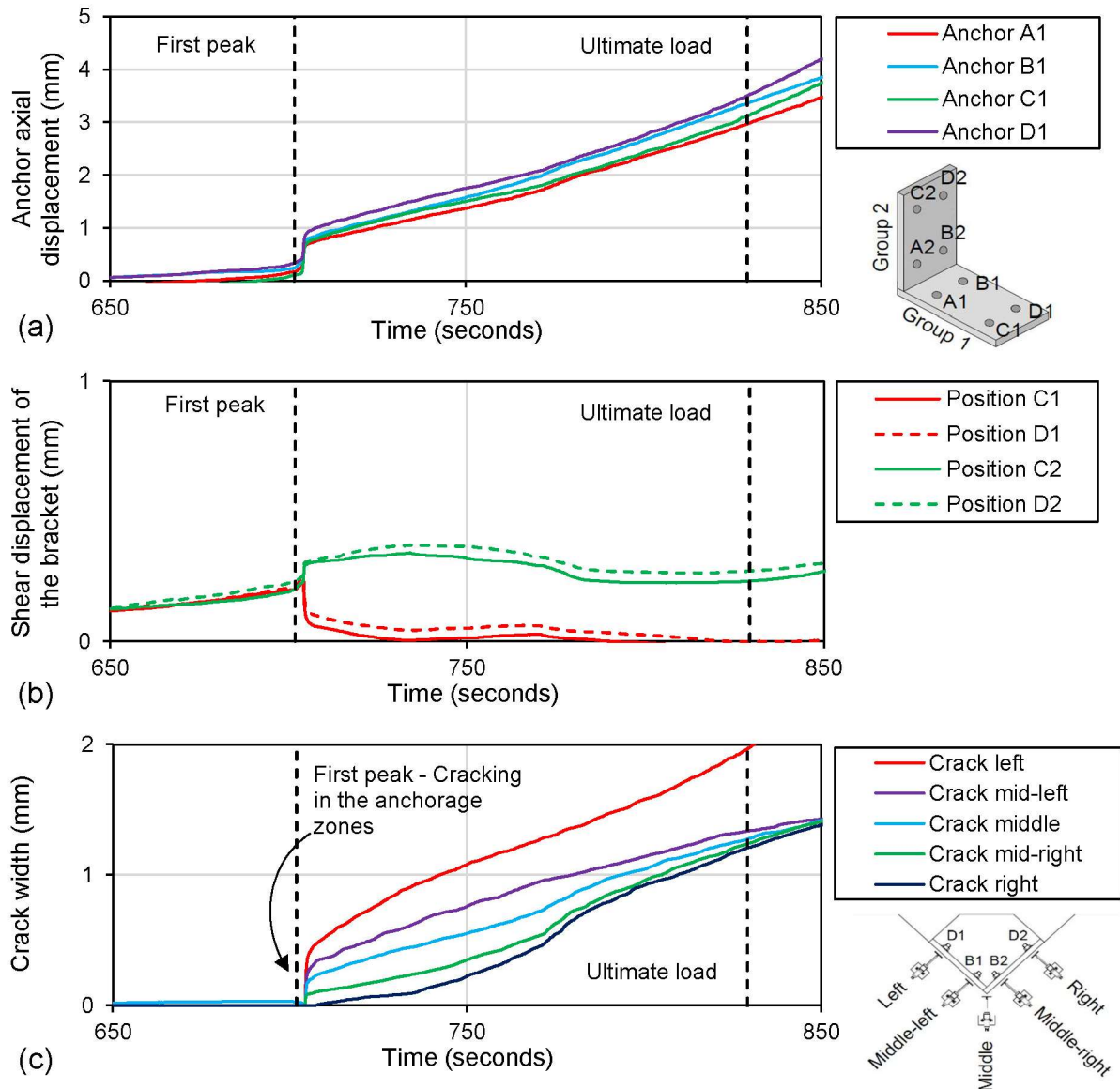

(a)

(b)

(c)

Figure 13.9. Results obtained in test BGC-80-2 as a function of the elapsed time: (a) Axial displacement of the anchors, (b) shear displacement of the anchor bracket, and (c) crack width on the side surface of the concrete specimen.

13.6.2.3   BGC-80-3

Figure 13.10 shows the results obtained in test BGC-80-3 as a function of the elapsed time. Figure 13.10 (a) shows the axial displacements of the anchors in the first group. Figure 13.10 (b) shows the shear displacement of the two perpendicular anchor groups which were measured in line with anchor C and D, in the direction parallel to the inclined concrete surface and to the two close edges. The red lines mark the shear

displacement of the first group, and the green lines mark the shear displacement of the second group. In Figure 13.10 (c), the crack width which was measured on the side surface of the concrete specimen is plotted. The points where the bracket configuration reaches its first peak, and the ultimate load are marked by dotted lines.
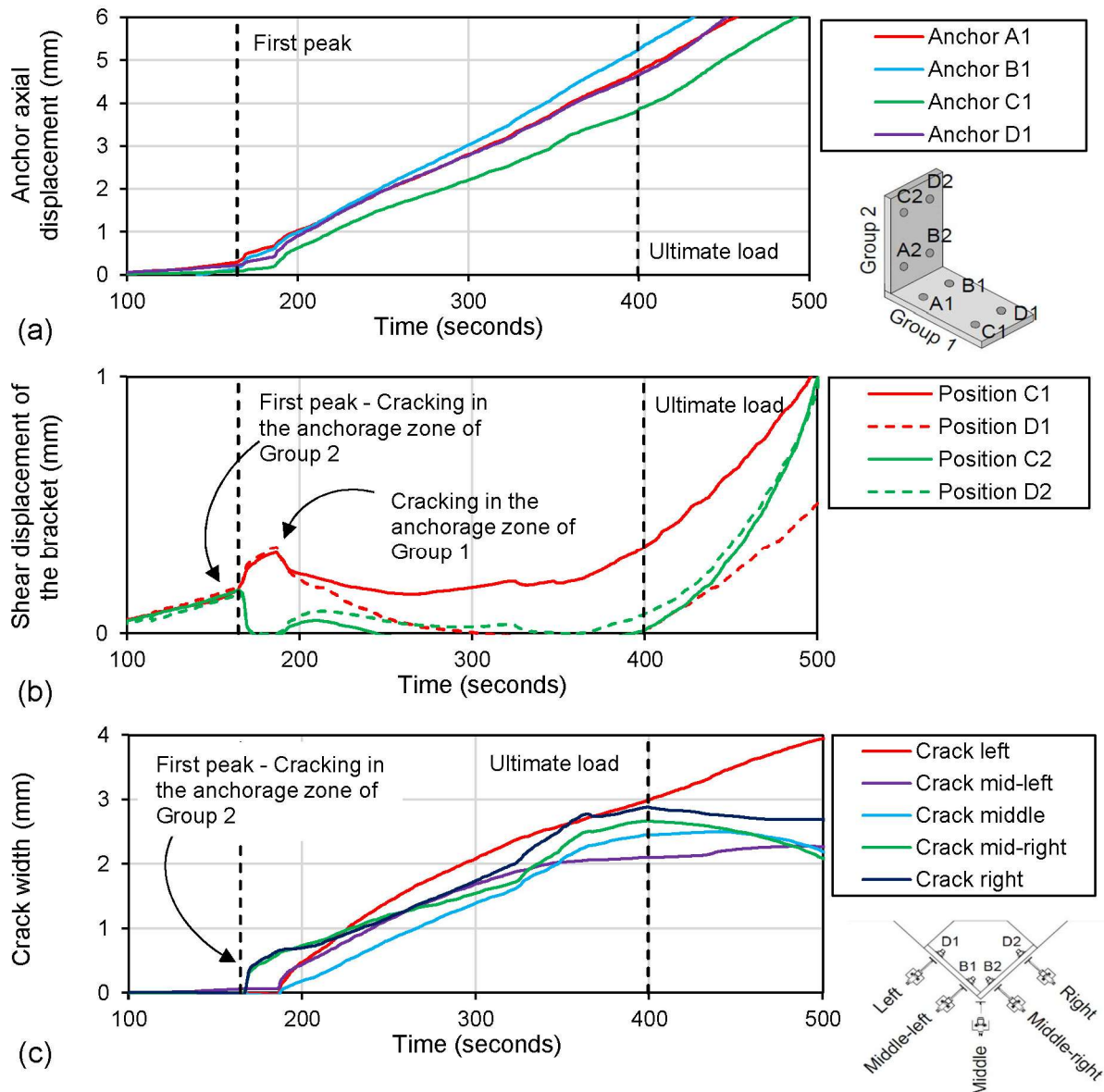
Figure 13.10. Results obtained in test BGC-80-3 as a function of the elapsed time: (a) Axial displacement of the anchors, (b) shear displacement of the anchor bracket, and (c) crack width on the side surface of the concrete specimen.

In accordance with the previously discussed test results, the behavior of the bracket configuration is relatively uniform until the first peak has been reached. The individual anchors in one group yield practically the same axial displacements. The shear displacement of the bracket progresses uniformly on both sides. Basically, no cracking on the concrete surface is apparent up to the first peak.

Similar to test BGC-80-2, at first peak, cracks at the side surface of the concrete specimen initially occurred only in the anchorage zone of one of the groups. In BGC-80-3, cracking occurs first at the level of the embedded ends of the anchors in the anchorage zone of the second group. At this point, no cracks on the concrete surface were apparent in the anchorage zone of the first group or in the corner of the concrete specimen. As a result of the cracking in the anchorage zone of the second group, the shear displacement of the first group which is perpendicular to the crack opening of the second group increases further, while the shear displacement of the second group becomes zero. With increasing load, cracks also occur on the side surface at the level of the embedded ends of the anchors of the first group and slightly delayed also in the corner of the concrete specimen. At this point, the shear displacement at both groups reversed. A sudden increase of the axial displacements of the anchors is apparent upon the first crack opening at the location of the second group and again when the surface cracks open at the location of the first group. Thereafter, the axial displacements increase steadily until the ultimate load is reached. Although there are minor deviations between the axial displacements of the individual anchors, no clear pattern is apparent which would indicate a certain distribution of loads among the anchors of one group. In principle the rate of change of the axial displacements of the individual anchors is rather similar.

When the cracks also open up in the anchorage zone of the first group, the crack width grows rather fast to the same size as observed at the location of the second group (initial cracking location). Thereupon, crack growth at all locations is rather equal. This observation indicates that the bracket configuration was able to effectively redistribute forces among the two groups after the initial preliminary failure of the second group. Considering the overall load-displacement behavior in the second phase (see Figure 13.7), the complete connection is able to stabilize again and exhibit considerable increase in its strength after the first peak.

13.6.2.4 BGC-110-1

Figure 13.11 shows the results obtained in test BGC-110-1 as a function of the elapsed time. Figure 13.11 (a) shows the axial displacements of the anchors in the first group. Figure 13.11 (b) shows the shear displacement of the two perpendicular anchor groups which were measured in line with anchor C and D, in the direction parallel to the inclined concrete surface and to the two close edges. The red lines mark the shear displacement of the first group, and the green lines mark the shear displacement of the second group. In Figure 13.11 (c), the crack width which was measured on the side surface of the concrete specimen is plotted. The points where the bracket configuration reaches its first peak, and the ultimate load are marked by dotted lines.
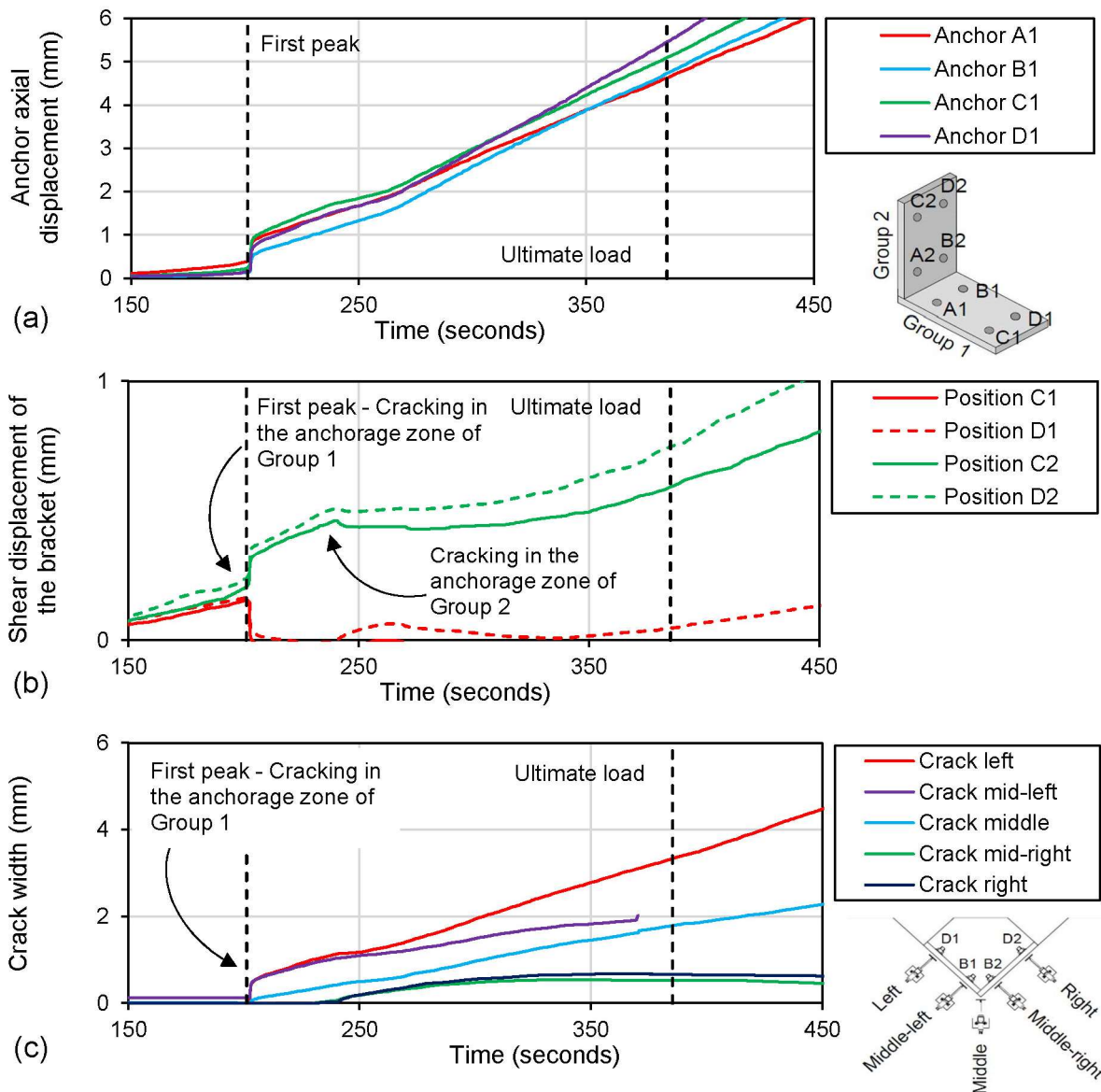
Figure 13.11. Results obtained in test BGC-110-1 as a function of the elapsed time:
(a) Axial displacement of the anchors, (b) shear displacement of the anchor bracket,
and (c) crack width on the side surface of the concrete specimen.

Similar to the behavior observed in test series BGC-80, the initial behavior of the
bracket configuration with an embedment depth of h_{ef} = 110 mm, is rather uniform until
the first peak has been reached. The individual anchors in one group display practically
the same displacements. The shear displacement of the bracket configuration
progresses uniformly at both sides. No cracking on the concrete surface is apparent
up to the first peak.

Upon the first peak, rather large cracks on the concrete surface open up in the
anchorage zone of the first group and smaller cracks open in the corner of the concrete
specimen. Thereby, the crack opening happens quite abruptly. At first peak, no
cracking is apparent on the concrete surface in the anchorage zone of the second

group. The crack opening in the anchorage zone of the first group leads to a further increase of the shear displacement of the second group which is perpendicular to the crack opening of the first group. At the same time, the first group returns into its original position. Also, a sudden increase of the axial anchor displacements is apparent upon reaching the first peak. With increasing load on the bracket configuration, the width of the already opened cracks, the shear displacement of the second group, and the anchor axial displacements increase steadily until the ultimate capacity is reached. No cracking is apparent in the anchorage zone of the second group up to the ultimate capacity, where the cracks suddenly open. At this point, the overall load-displacement behavior of the bracket configuration is characterized by a sudden drop of the load.

13.6.2.5   BGC-110-2

Figure 13.12 shows the results obtained in test BGC-110-2 as a function of the elapsed time. Figure 13.12 (a) shows the axial displacements of the anchors in the first group. Figure 13.12 (b) shows the shear displacement of the two perpendicular anchor groups which were measured in line with anchor C and D, in the direction parallel to the inclined concrete surface and to the two close edges. The red lines mark the shear displacement of the first group, and the green lines mark the shear displacement of the second group. In Figure 13.12 (c), the crack width which was measured on the side surface of the concrete specimen is plotted. The points where the bracket configuration reaches its first peak, and the ultimate load are marked by dotted lines.

In test BGC-110-2, a reasonably uniform behavior is observed until the first peak is reached, very similar to the behavior observed in the previous tests. As can be seen from the detailed view of the first phase in Figure 13.12 (a), the individual anchors in one group yield practically the same axial displacements, indicating a rather even distribution of loads among the anchors. At first peak the individual anchor displacement ranges between 0.15 mm – 0.29 mm with a coefficient of variation of 27%. This is within the generally observed scatter for bonded anchors. The shear displacements of the bracket progress rather uniformly on both sides. No cracking on the concrete surface is apparent up to the first peak.

Upon the first peak, cracks open in the anchorage zone of the second group. Thereby, rather large cracks appear on the concrete surface at the level of the embedded ends of the outermost anchors and smaller cracks open at the level of the embedded ends of the anchors closest to the corner. Additionally, a crack with smaller crack width opens in the corner of the concrete specimen. Thereby, the crack opening happens quite abruptly. At first peak, no cracking is apparent on the concrete surface in the anchorage zone of the first group. The crack opening at the second group leads to a further increase of the shear displacement of the first group which is perpendicular to the crack opening of the second group. At the same time, the shear displacement of the second group is reversed, and the group returns into its original position. Also, a sudden increase of the axial anchor displacements is apparent upon reaching the first

peak. Shortly after the first peak has been reached, cracks also open at the level of the embedded ends of the anchors in the first group. At this point, the shear displacement of the second group is again reversed, and the shear displacement of the first group starts to reduce. Up until the ultimate load is reached, the shear displacement of the two groups converges, while the crack width steadily increases. The axial displacements of the anchors gradually increase, whereby the gradient is markedly steeper comparted to the gradient up to the first peak. Nonetheless, the displacement measured on the individual anchors is quite similar.

In comparison to test BGC-110-1, where after one group fails, the other group is able to resist failure until the ultimate load has been reached, it appears that the rather fast successive failure of the two groups, indicated by the crack opening on the concrete surface, has a negative effect on the overall capacity of the bracket configuration.
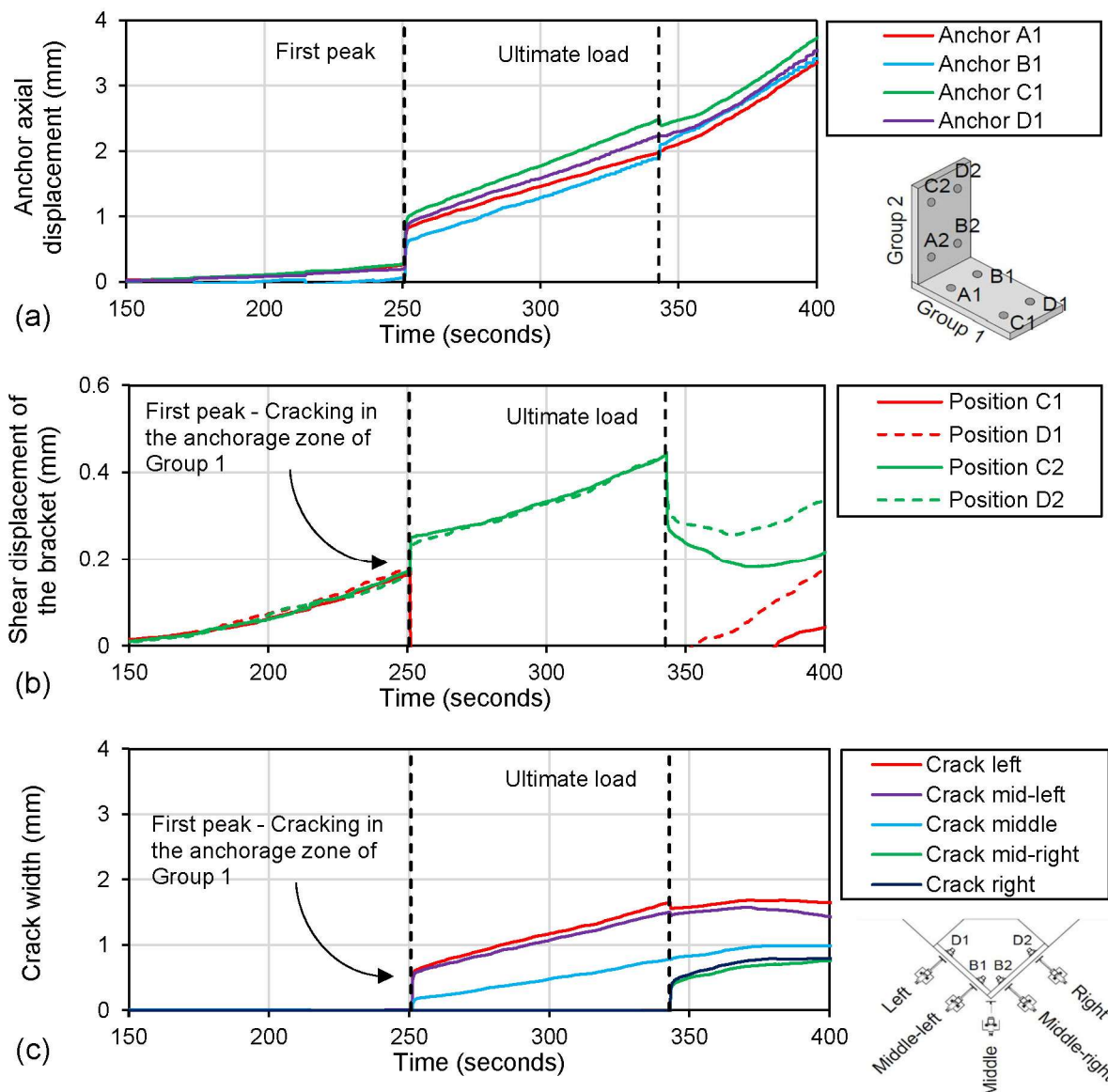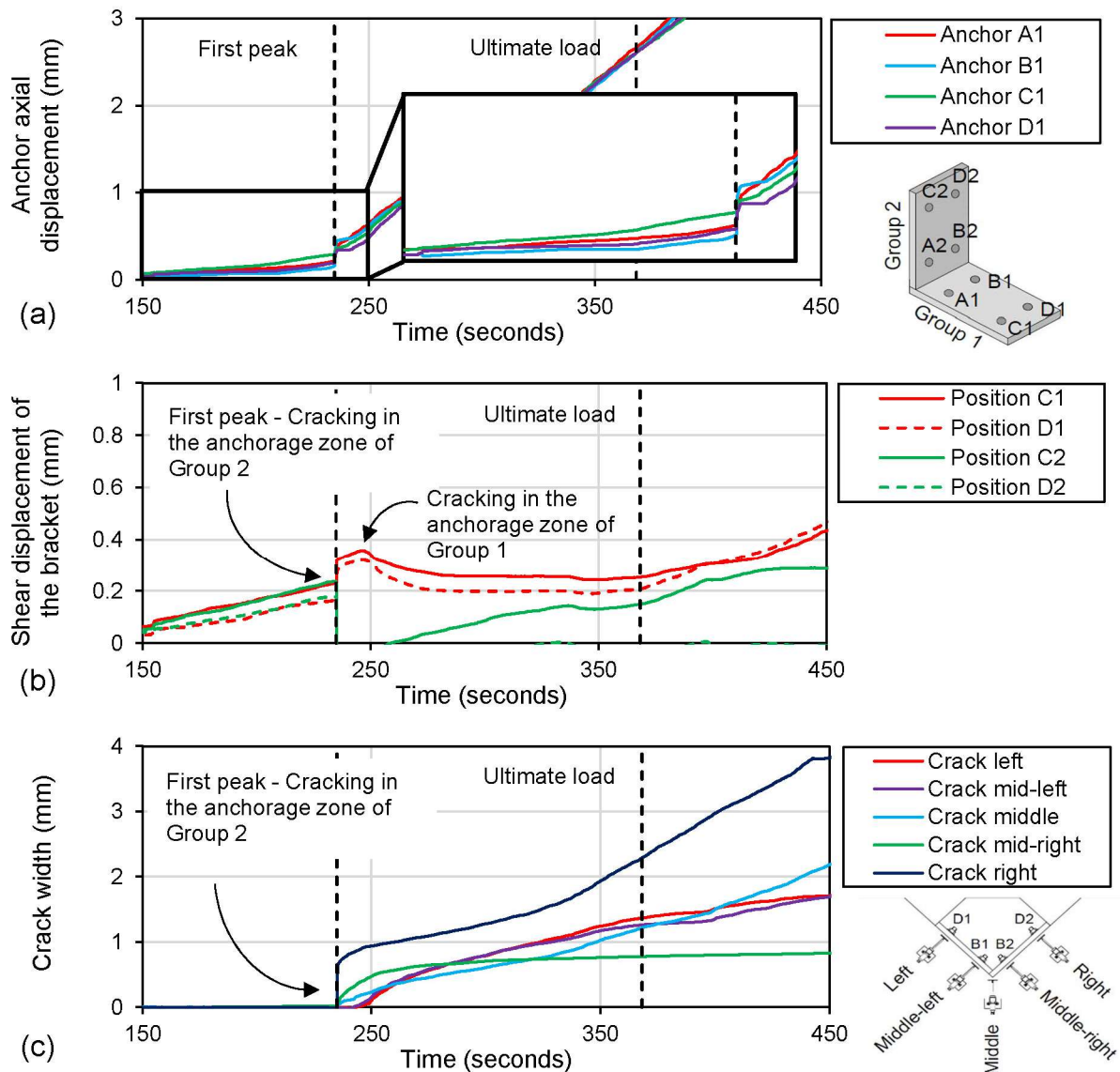
Figure 13.12. Results obtained in test BGC-110-2 as a function of the elapsed time: (a) Axial displacement of the anchors, (b) shear displacement of the anchor bracket, and (c) crack width on the side surface of the concrete specimen.

13.6.2.6   BGC-110-3

Figure 13.13 shows the results obtained in test BGC-110-3 as a function of the elapsed time. Figure 13.13 (a) shows the axial displacements of the anchors in the first group. Figure 13.13 shows the shear displacement of the two perpendicular anchor groups which were measured in line with anchor C and D, in the direction parallel to the inclined concrete surface and to the two close edges. The red lines mark the shear displacement of the first group, and the green lines mark the shear displacement of the second group. In Figure 13.13 (c), the crack width which was measured on the side

surface of the concrete specimen is plotted. The points where the bracket configuration reaches its first peak, and the ultimate load are marked by dotted lines.

(a)

(b)

(c)
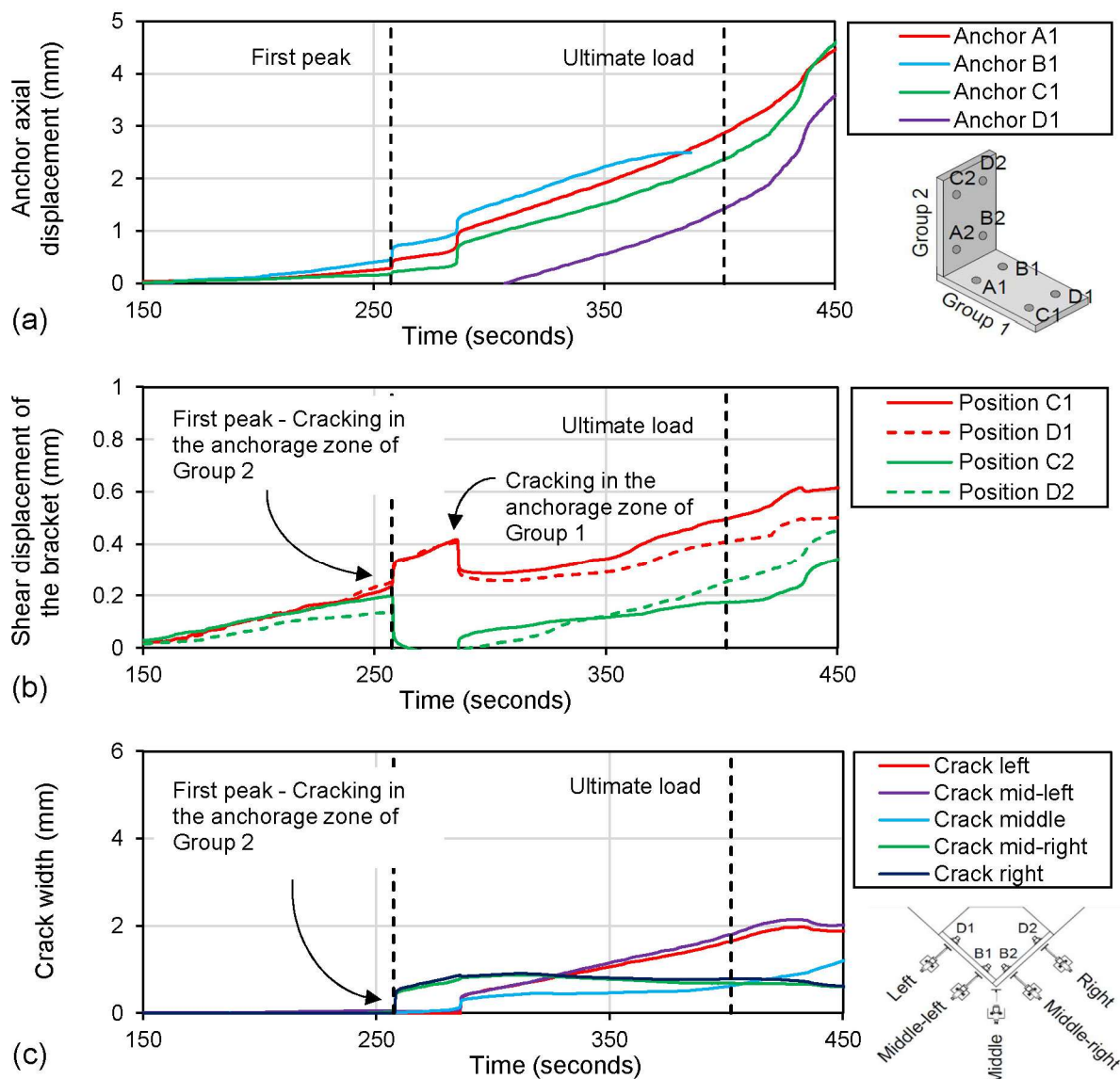
Figure 13.13. Results obtained in test BGC-110-3 as a function of the elapsed time: (a) Axial displacement of the anchors, (b) shear displacement of the anchor bracket, and (c) crack width on the side surface of the concrete specimen.

In test BGC-110-3, a rather uniform behavior is observed until the first peak is reached, very similar to the behavior observed in the previous tests. The individual anchors in one group yield practically the same axial displacements, indicating a rather even distribution of forces among the anchors. Only the axial displacement of anchor D1 appears to be significantly smaller compared to the remaining three anchors. However, this observation is likely to be related to instrumentation problems. The shear displacement of the bracket progresses rather uniformly at both sides. No cracking on the concrete surface is apparent up to the first peak.

When the first peak is reached, cracks on the concrete surface open at the level of the embedded ends of the anchors of the second group. At this point, only minor cracking is observed on the concrete surface in the corner of the concrete specimen and in the anchorage zone of the first group. Crack opening in the anchorage zone of the second group leads to a further increase of the shear displacement of the first group which is perpendicular to the crack opening of the second group. At the same time, the shear displacement of the second group reverses and returns into is original position. Along with the first visible crack opening on the concrete surface, the axial displacements of the anchors exhibit a sudden increase as can be seen in Figure 13.13 (a). After the first peak, the bracket configuration in test BGC-110-3 undergoes a sudden drop of load, after which it regains its strength until it reaches a second peak. Up to this point, the axial displacements of the anchors, the shear displacement of the first group and the width of the already opened cracks increase gradually. At the second peak, cracks on the concrete surface also open at the level of the embedded ends of the anchors of first group. Simultaneously, the shear displacement of the first group reduces suddenly while the shear displacement of the second group starts to increase again. This also causes another sudden increase in the axial displacements of the anchors. Further increasing the load on the bracket configuration results in a steadily increasing crack width at the location of the first group, while the crack width at the second group and in the corner remains essentially the same. Up to the ultimate capacity, the axial displacements of the anchors steadily increase, whereby the gradient is markedly steeper comparted to the gradient up to the first peak. The shear displacement of both groups also increases steadily with about the same gradient as observed up to the first peak.

13.6.3 Failure mechanism derived from the evaluation of the individual tests

Based on the evaluation of the individual tests, general failure characteristics are described in this section. In the initial phase before the first peak is reached, no cracking was observed on the side surface of the concrete specimens. The shear displacement of both groups, thus the displacement in the direction parallel to the concrete surface and the close edges, is equal on both sides. So are the axial displacements of all four anchors measured on one group. The relatively equal displacements of the anchors in one group indicates a rather even distribution of axial forces among the individual anchors at the beginning of the tests. The uniform shear displacement observed at both groups suggests that the total force on the bracket configuration is rather evenly distributed to the two groups and thus to all anchors of the configuration. For the investigated cases, the observed behavior up to the first peak was rather similar, indicating a uniform load bearing mechanism of the bracket configuration up to the point where the complete connection reaches the first peak.

It has already been shown that the overall load-displacement behavior of the bracket configuration is characterized by a first peak after which the load drops to a local

minimum. Thereafter the bracket configuration is able to regain its strength, whereby the load increases to a level higher than the first peak, where the connection reaches its ultimate capacity. In all but one test it was observed that when the first peak is reached, cracks on the concrete surface abruptly open at the level of the embedded ends of the anchors of one group. This can be seen in Figure 13.14 (a). Considering the behavior of anchor groups installed in narrow concrete members, where failure was followed by immediate and severe cracking on the side surface of the concrete specimen after the ultimate tension capacity has been reached, it is reasonable to assume that the observed cracking at the location of one group indicates that it has reached its tension capacity.

In one test, BGC-80-1, cracking at first peak occurred at both groups. In this case where both groups fail at the same time, the corresponding capacity at first peak was around 5% larger compared to the other tests in the test series. In some tests, in addition to the cracking in the anchorage zone of one of the groups, also cracks in the concrete corner occurred upon the first peak. However, this had no notable effect on the capacity at first peak. The corresponding crack widths observed shortly after the first peak has been reached, are around 0.4 mm to 0.7 mm. Simultaneously with the opening of the cracks at first peak, the axial displacements of the anchors suddenly increase. Furthermore, cracking in the anchorage zone of the first group leads to a sudden increase of the shear displacement of the second group in the direction perpendicular to the crack opening of the first group. At the same time, the shear displacement of the first group reverses and the group returns into its original position. This behavior indicates that the entire bracket configuration is slightly distorted after initial crack opening.

In the second phase, as the bracket configuration regains its strength, the already opened cracks become wider and the shear displacement of one group increases further. During the second phase, generally before the ultimate capacity is reached, cracks also open at the level of the embedded ends of the anchors of the second group. This can be seen in Figure 13.14 (b). As these cracks open, the shear displacement of the first group starts to decrease, while the shear displacement of the second group starts increasing again. From this point on, the potential ultimate capacity of the complete bracket configuration appears to depend on whether the loads can be redistributed among the two groups. This is indicated by comparing the performance of tests BGC-80-2 and BGC-80-3. In BGC-80-2, cracking is dominated in the anchorage zone of the first group, where the first opening of cracks on the concrete surface was observed. As soon as these cracks were opened, the crack width continuously increases throughout the experiment. When the cracks open in the anchorage zone of the second group, however, the crack width remains almost constant after the initial opening. In BGC-80-3, cracking is initiated in the first group when the first peak is reached. When the cracks open in the anchorage zone of the second group, they swiftly grow to the same crack width as in the anchorage zone of

the first group, from where in both groups the crack width increases rather uniformly. In both tests, the capacity at first peak matches very well. However, in the first case, the ultimate load is only around 2% larger than the capacity at first peak, while in the latter case, the ultimate load is around 14% larger. Thus, the experimental results clearly indicate the beneficial effect of symmetrical behavior and an even distribution of forces. It also highlights the beneficial effect of force redistribution among the anchors. With respect to the axial displacements of the anchors, it was observed that they steadily increase in the second phase until the ultimate capacity is reached. Thereby, all anchors displace rather evenly. However, the gradient is markedly steeper comparted to the gradient up to the first peak. Upon reaching the ultimate capacity, a common breakout body has formed as can be seen in Figure 13.14 (c). The final breakout body is shown in Figure 13.14 (d) and (e). Clearly the anchorage zone of the bracket configuration is vastly damaged.
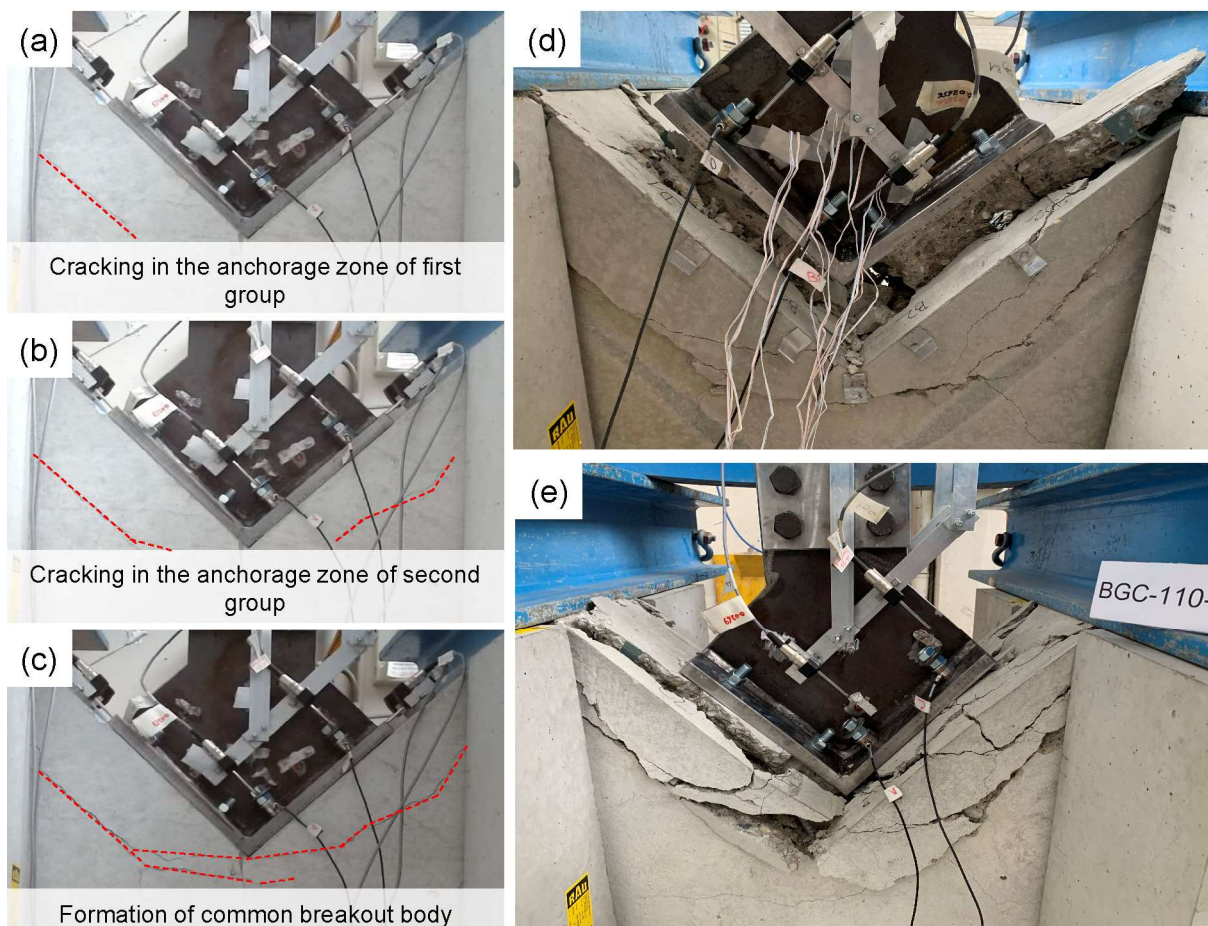
Figure 13.14. Failure mechanism: (a) Initial cracking in the anchorage zone of the first group, (b) beginning of cracking in the anchorage zone of the second group with increasing displacement of the configuration, (c) cracks merge between the groups, (d) and (e) common breakout body.

The described failure mechanisms suggests that in the beginning the total load on the bracket configuration is withstood by both groups uniformly. Upon reaching the first

peak, one of the two groups first loses some of its load-bearing capacity which results in the drop of load observed in the load-displacement curves (see Figure 13.7). The unilateral behavior may be attributed to a number of factors, such as installation differences regarding the actual embedment depth of the anchors, unevenness of the concrete surface, initial misalignment of the connection, or the location of aggregates in the anchorage zones. At the beginning of the strength-regaining phase, the load is generally redistributed to the second group until cracking is also visible on this side. Thereafter, the performance of the bracket configuration appears to rely on its ability to evenly distribute the loads to both groups. The observed failure mechanism is consistent with the obtained load-displacement behavior of the corner configurations. Up to the first peak, the behavior of the corner configurations is rather similar in all tests. In the second phase however, the behavior differs depending on the embedment depth of the anchors and the ability of the connection to evenly distribute the loads. Therefore, it is recommended that for an analytical force-based design approach, which is not accounting for the load-displacement behavior, only the capacity at first peak is considered. In addition, up to the first peak, no cracks were apparent on the concrete surface. Thus, serviceability of such a connection is assured up to this point. Thereafter, cracks open and grow relatively fast until the connection fails.

13.6.4 Evaluation of stresses in the gusset plate

Uniaxial strain gauges were used to assess the stresses in the gusset plates. Although the state of stresses in the gusset plate is biaxial, only the uniaxial strains and stresses were measured. This approach was chosen to keep the measurements and evaluation simple. Moreover, since the axial stiffness of bonded anchors is much higher than their shear stiffness, this simplification seems reasonable.

The stresses were calculated from the measured strains assuming a linear elastic behavior of the gusset plate. For the calculation, Hooke's law (Equation (13.12)) was used, and Young's modulus for steel was assumed as E_S = 200000 N/mm². The maximum stress value determined in this way was 50 N/mm² in test BGC-110-1, which was measured around 10 cm below the Whitmore section. Considering the ultimate load in test BGC-110-1, the stresses at the Whitmore section are calculated as 58 N/mm². It can therefore be assumed that the calculation of stresses in this section provides a reasonable approximation for design purposes. Moreover, the design goal to prevent yielding of the steel elements before the failure of the anchorage has been achieved. Therefore, the assumption of a linear elastic behavior of the gusset plate and the anchor bracket is justified. In the following, the results of test BGC-110-1 and BGC-110-3 will be discussed with regard to the measured normal stresses at the gusset-to-bracket interfaces.

$$\sigma = E_S \cdot \varepsilon. \tag{13.12}$$

Figure 13.15 shows the stresses calculated from the measured strains in test BGC-110-1 as a function of the elapsed time. The corresponding locations to the measurements are shown in the figure next to the graph. The values correspond to the normal stresses at the gusset plate-to-bracket interface. As shown in Lin et al. (2014), the normal stresses along the interface may be assumed to be uniformly distributed in case of steel structures. This finding is consistent with the evaluation of the axial displacements of the anchors in this work. It can therefore be assumed that the normal stresses shown in Figure 13.15 roughly reflect the tensile forces acting on the two groups which form the bracket.

It can be seen that in the beginning of load application, the stresses at both interfaces progress rather evenly, indicating a uniform distribution of tensile forces among the two groups. Before the first peak is reached, the first group appears to have reached its tension capacity as the normal stresses at the corresponding interface remain almost constant until the first peak is reached. At the same time, forces are redistributed to the second group, which continues to be subjected to increasing tensile loads. At peak load, a sudden drop of normal stresses at the interface of first group indicates a loss of tension capacity of the group. These stress measurements are in accordance with the previous findings where cracking on the concrete surface was first apparent in the anchorage zone of the first group. It should be noted however that although the first group has lost its ability to take up tension load, it continues to provide shear resistance. Until reaching the ultimate load, the normal stresses at the second group increase gradually while the normal stresses at the first group decrease. At ultimate load, also the second group reaches its tension capacity, marked by a sudden drop of normal stresses in Figure 13.15. This observation corresponds to the appearance of surface cracks in the anchorage zone of the second group at ultimate load.
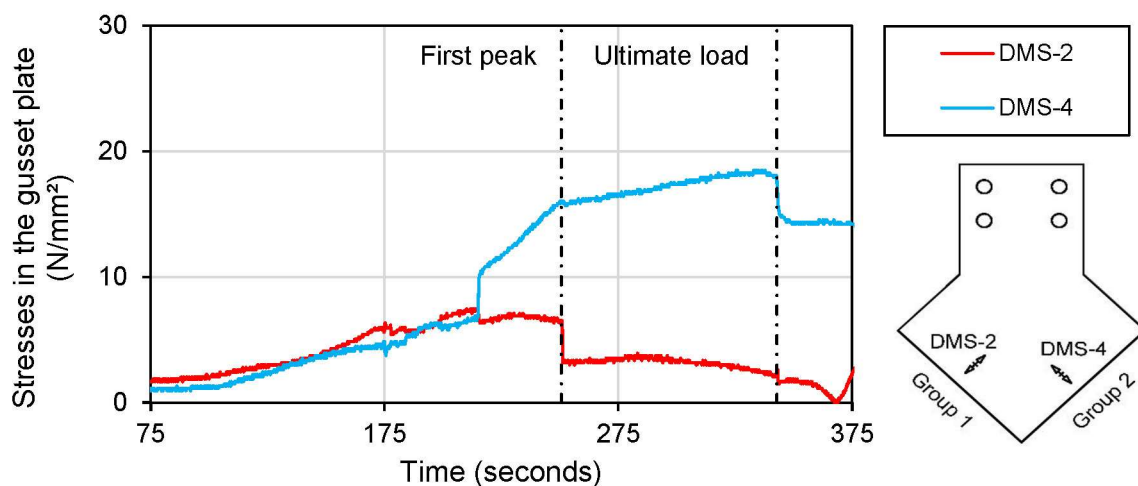
Figure 13.15. Normal stresses in the gusset plate as a function of the elapsed time obtained in test BGC-110-1.

Figure 13.16 shows the stresses calculated from the measured strains in test BGC-110-3 as a function of the elapsed time. The corresponding locations to the measurements are shown in the figure next to the graph. The values correspond to the normal stresses at the gusset plate-to-bracket interface.

Up to the first peak, the normal stresses at both interfaces progress rather similarly. The stress distribution up to the first peak corresponds well with the previous findings, indicating a uniform behavior of the overall bracket configuration with equal axial displacements of the anchors and equal shear displacement of both groups. Considering a uniform distribution of normal stresses along the gusset plate-to-bracket interfaces, the tension forces N_1 and N_2 acting on the first and second group, respectively, can be calculated as follows:

$$N_1 = \sigma_{N,1,first} \cdot L_1 \cdot t_g = 16.2 \cdot 280 \cdot 25 = 113 \ kN, \tag{13.13}$$

$$N_2 = \sigma_{N,2,first} \cdot L_2 \cdot t_g = 16.0 \cdot 280 \cdot 25 = 112 \ kN. \tag{13.14}$$

L_1 and L_2 are the length of the gusset plate interfaces at both groups. $\sigma_{N,1,first}$ and $\sigma_{N,2,first}$ are the normal stresses at the interfaces at first peak.
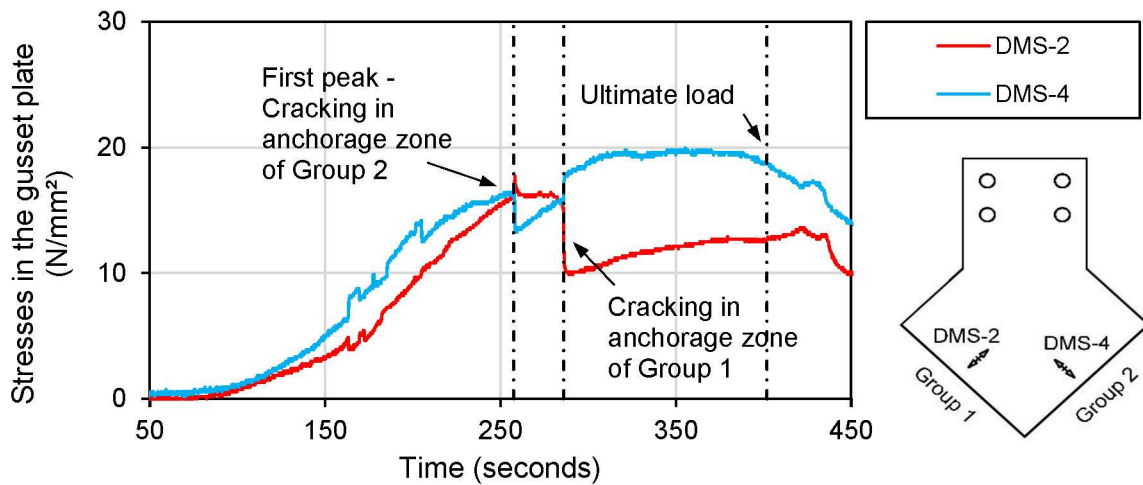
Figure 13.16. Normal stresses in the gusset plate as a function of the elapsed time obtained in test BGC-110-3.

Assuming both groups take up equal shear loads ($V_1 = V_2 = V$), the corresponding forces acting on both groups can be calculated using following equation:

$$P_{tot}^2 = (N_1 + V)^2 + (N_2 + V)^2. \tag{13.15}$$

Where P_{tot} is the total force on the bracket configuration. The formula is derived from the equilibrium of forces on the gusset plate as indicated in Figure 13.17. This results

in a shear load of around 40 kN for both groups. Consequently, the experimental results suggest that the behavior of the bracket configuration up to the first peak is dominated by the tensile behavior of the two groups which form the bracket. Or rather the tensile behavior of the anchors.
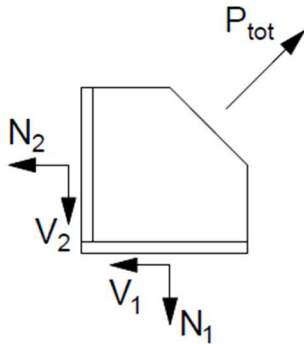
Figure 13.17. Forces acting on the bracket configuration.

Upon arriving at the first peak, the second group seems to reach its tensile load-bearing capacity as a distinct drop of normal stresses is observed in Figure 13.16. Correspondingly, cracks on the concrete surface open in the anchorage zone of the second group. Upon further loading of the bracket configuration, however, the stresses at the second group are again increasing after the sudden drop. Thus, despite the initial cracking and the apparent loss of tensile load-bearing capacity, the group is still able to resist tension loads and even regain its strength. At the same time, the stresses measured at the first group are slightly decreasing. Simultaneously with the occurrence of surface cracks in the anchorage zone of the first group, a distinct drop is observed for the corresponding normal stresses. It can be seen that from here the second group is taking more tension load than the first group. This accords with the previously discussed evaluation of the crack widths on the concrete surface. It is interesting to see that after cracking in the anchorage zone of the first group, the normal stresses at both interfaces remain at a rather constant level, with a slight increase in the first group. At the same time, the total load on the bracket configuration increases considerably. This observation suggests that the anchors, which were predominantly loaded in tension in the first phase, are now increasingly loaded in shear.

Although the total load is applied to the bracket configuration at an angle of 45° with respect to both anchor groups, the anchors are not equally loaded in tension and shear, as might be expected. This can be explained by the fact that the axial stiffness of bonded anchors is significantly higher than their shear stiffness (Mahrenholtz, 2011; Bokor, 2021). Thus, in the initial phase up to the first peak, the resistance of the bracket configuration comes predominantly from the tension capacity of the anchors. Upon first peak the tension capacity of the anchors or anchor groups is almost reached, which is apparent from the cracking at the concrete surface and also from the normal stresses in the gusset plate. Presumably the beneficial effect of the perpendicular concrete

members (the corner) prevents a premature failure of the complete connection which would otherwise be expected when the capacity is reached. Due to the severe cracking in the base material, however, the axial stiffness of the anchors reduces significantly (Mahrenholtz and Eligehausen, 2010; Bokor, 2021). As the anchor behavior in shear is not that much influenced by cracking, the total load on the connection is now dominated by the shear resistance of the anchors. This might also explain the ability of the bracket configuration to regain its strength in the second phase, even beyond the strength in the first phase, as the shear capacity of the anchors at the tested embedment depths is generally higher than their tension capacity. In this context, it should be noted that the behavior of the bracket configuration might differ significantly for other types of anchors, where the difference between the axial and shear stiffness is not that much pronounced.

13.6.5 Evaluation of force washer readings

In the experiments, force washers were used for the intended purpose of monitoring the axial anchor forces. Thereby, due to practical reasons, the force washers were only used on one group. The utilization of force washers for this particular task, however, has proven rather unsuitable to obtain a quantitative statement on the axial anchor forces. This becomes particularly evident in the, often large, deviations in the measured axial anchor forces, as well as in the total tension force resulting from the individual anchor measurements.

Both the scatter of axial anchor forces within one test and the scatter of axial forces of particular anchors (A, B, C, and D) in one test series is rather large. At first peak, the minimum scatter in terms of the coefficient of variation (CV) for anchor forces in one test was 47%. The minimum scatter for forces measured on a particular anchor in three tests was CV = 39%. The comparison shows that the results are rather unsuitable for a quantitative conclusion on the actual axial forces of the anchors.

Besides the large scatter of axial anchor forces at first peak, another indicator for the unsuitability of force washers in this particular setup is the total tension force resulting from the individual anchor measurements compared to the approximated tension load on one group. For this purpose, the tension load on one group was back-calculated from the total load on the bracket configuration assuming equilibrium of forces on the bracket configuration (see Figure 13.17), the possibility of calculating the capacity of the two groups individually and a combined tension and shear load, where the tension load component is dominant. It should be noted that in Equation (13.16) an internal load angle of $\alpha = 65°$ is assumed. This was done to account for the observed behavior of the tested bracket configuration discussed in Section 13.6.4, which indicates that in the initial phase, the resistance of the bracket configuration comes mainly from the tension capacity of the anchors. An internal load angle of around 62° - 65° is also derived from the numerical investigation in Chapter 14 for the investigated cases with an embedment depth of h_{ef} = 80 mm and h_{ef} = 110 mm.

Following equation is used to back-calculate the tension load on one group on basis of the total load, P_{tot}, acting on the bracket configuration:

$$N = \frac{P_{tot}}{\sqrt{2} \cdot (1 + \cos(65°)/\sin(65°))}.$$

(13.16)

Figure 13.18 (a) exemplarily shows the tension load on one group as a function of the elapsed time for test BGC-80-2. The green line shows the sum of axial forces of the individual anchors, which were measured during the experiment by means of the force washers. The black line shows the approximated tension load on basis of Equation (13.16). It can be seen that the two curves clearly do not match, indicating a severe underestimation of the actual anchor forces. On the other hand, the progression of the two curves, from a qualitative point of view, seems to match relatively well. This can also be seen from Figure 13.18 (b), where the relative tension load with respect to the maximum tension load for both cases is compared. Clearly the curves match well, particularly in the first phase up to the first peak. Thereafter, the deviation increases again.
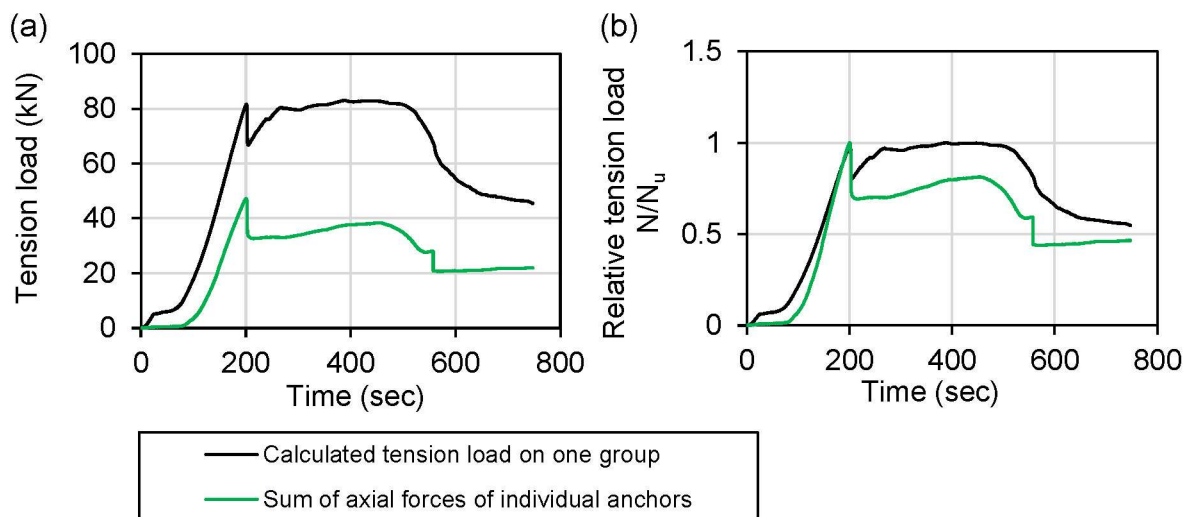
Figure 13.18. (a) Absolute and (b) relative tension load on one anchor group as a function of the elapsed time obtained from test BGC-80-2.

Despite the previously discussed findings with respect to the quantitative significance, the results allow a cautious qualitative interpretation. Two points might be concluded. First, on average, the measured load on the front anchors (C and D) was slightly higher than the measured load on the back anchors (A and B). This finding suggests that the front anchors take up the load prior to the back anchors. The crack measurements on the side surface of the concrete specimen support this assumption as in some tests it was observed that upon reaching the first peak, crack growth was larger at the embedded end of the front anchors of a group. Second, the comparison of the relative tension load showed a good agreement up until the first peak, indicating that the

assumption of a tension dominant behavior is valid up to this point. However, after the first peak, the behavior of the bracket configuration cannot be described by the same means as in the first phase.

In conclusion, besides a qualitative statement on the anchor behavior, force washers appear to be less suitable for measuring the axial anchor forces in these applications or setups. One possible explanation for the observed discrepancies and inaccuracies might be that the anchors were not solely loaded in tension but that they were subjected to inclined loading. The additional shear load and bending of the anchors might have interfered with the measurements and have possibly corrupted the readings.

13.7 Summary

In this chapter, the connection element between a steel brace and a RC frame was investigated where post-installed anchors were used to fasten the bracket-to-gusset plate connection to the concrete corner. The focus of the investigation was on the geometrical influence of the corner and the behavior of the anchorage. Based on the detailed evaluation of the load and displacement behavior of the overall connection and the individual elements, the following conclusions can be drawn:

1. Even for a relatively small embedment depth of 80 mm, and being installed in a narrow member, the connection using post-installed anchors is able to withstand substantial loads before the anchorage fails. In case of h_{ef} = 80 mm, the mean ultimate capacity was 184.9 kN and for an embedment depth of h_{ef} = 110 mm the mean ultimate capacity of the connection was 264.1 kN.

2. With respect to both the loads at first peak and the ultimate loads of the connection, the experimental results showed only little variation, indicating a reliable performance of the connection with post-installed anchors.

3. The investigation of the load-displacement curves for different embedment depths showed a similar behavior of the connection until the first peak is reached. Upon reaching the first peak, the behavior differs depending on the embedment depth of the anchors.

4. The observed overall behavior and failure mechanism of the connection up to the first peak is rather similar in all tests. Thereafter, the behavior becomes more erratic and appears to depend largely on whether the connection is able to redistribute the forces among the anchors.

5. The stresses in the gusset plate suggest that at first peak, the behavior of the gusset plate is dominated by the behavior of the anchors in tension rather than in shear.

6. Up to the first peak, no cracks were apparent on the concrete surface. Thus, serviceability of such a connection is not a problem up to this point. Thereafter, cracks open and grow relatively fast until the connection finally fails.

In summary, the tested connection shows a stable and reliable behavior up to the first peak, with no cracking on the surface of the concrete member. Although the behavior of the connection, with respect to the loads, remains relatively reliable in the second phase, where it shows only little variation in the obtained ultimate loads, the displacement behavior becomes somewhat more erratic. Moreover, large cracks occur on the concrete surface upon reaching the first peak. Therefore, an analytical design approach following design concepts according to current standards and guidelines should only consider the behavior and capacity up to the first peak.

14 Numerical investigations on anchorages in a corner configuration

14.1 Numerical program

In addition to the experimental investigations on the corner configuration presented in the previous chapter, numerical simulations were performed to augment the experimental observations and thus gain a more comprehensive understanding of this type of connection. The main focus of the numerical study is on the distribution and redistribution of forces to the individual anchors, the influence of the corner on the capacity and displacement behavior of the connection, and the influence of varying embedment depths. The basis of the numerical investigation is the concrete specimen and the bracket-to-gusset plate connection introduced in the previous chapter. Thus, the dimensions applied in the numerical models largely correspond to the dimensions in the experimental program (see Chapter 13). The single difference between the connection element in the numerical study and the one which was used in the experiments is the geometry of the gusset plate. In the experiments, the gusset plate featured an extended part for the bolted connection, which was required for practical reasons. In the numerical study, this extended part was omitted as can be seen in Figure 14.1. Besides the addressed modification, the geometry and dimensions of the connection element remain essentially the same.
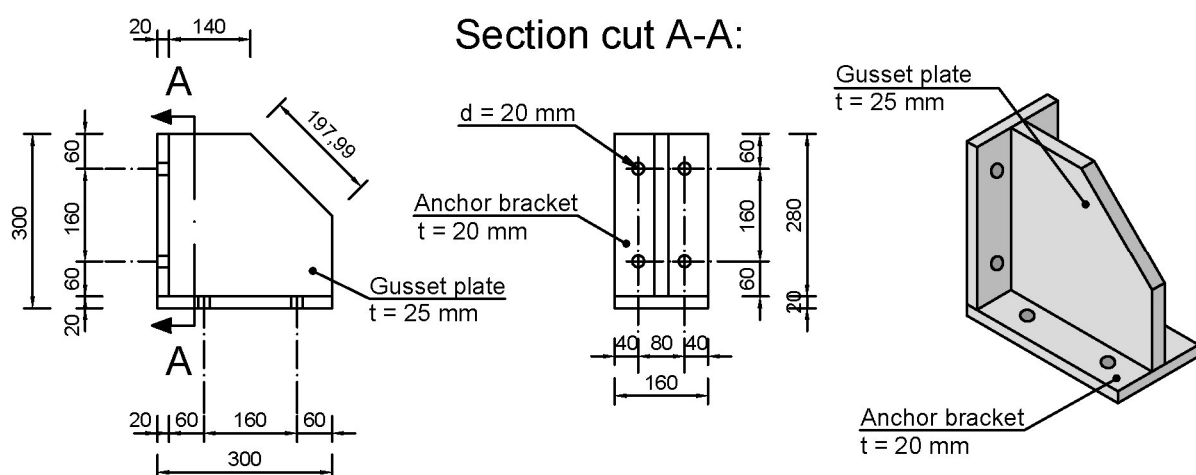
Figure 14.1. Dimensions of the bracket-to-gusset plate connection element comprising the anchor bracket and the gusset plate. (Note: All dimensions are in mm).

306

In accordance with the experimental investigations, a bonded anchor system was simulated featuring a steel rod with a diameter of 16 mm. The steel rod was embedded in the concrete with varying embedment depths, namely 60 mm, 80 mm, 110 mm, and 160 mm. The behavior of the corner configuration using anchors with 80 mm and 110 mm embedment depth were already investigated in the experimental part. The corresponding numerical analysis is used to validate the numerical modelling approach against the experimental results and to further investigate the behavior of the connection.

In the experimental part it was observed that for an embedment depth of h_{ef} = 80 mm (equal to the corner distance) the ultimate load was only marginally higher than the load obtained at first peak, while for a larger embedment depth (h_{ef} = 110 mm) the load in the second phase increased markedly compared to the first peak. Therefore, two additional simulations were performed investigating the behavior at an embedment depth smaller than the distance between the concrete corner and the closest anchors (h_{ef} = 60 mm) and the behavior at an increased embedment depth (h_{ef} = 160 mm).

Of particular interest is the influence of the corner and the mutual influence of the perpendicular anchor group arrangement. For this purpose, a step-by-step parametric study was performed based on the fully attached (FA) connection in the previous chapter. A schematic overview of the parametric study is provided in Figure 14.2. In the first step, the dimensions of the concrete specimen and the bracket-to-gusset plate element remain the same. Again, the complete connection element was placed in the corner of the concrete member and loaded at an angle of 45°. However, only one group was fastened to the concrete specimen (see Figure 14.2 in the middle). In the following, this step is referred to as partly attached in concrete corner (PA). In the last step, one of the two concrete members which from the corner was removed. Thus, the connection element was only fastened to a narrow concrete member and loaded at an angle of 45° as indicated in the schematic on the right-hand side in Figure 14.2. In real applications this would mean that either the beam or column was removed.

Fully attached in concrete corner (FA)

Partly attached in concrete corner (PA)

Partly attached in narrow member (NM)
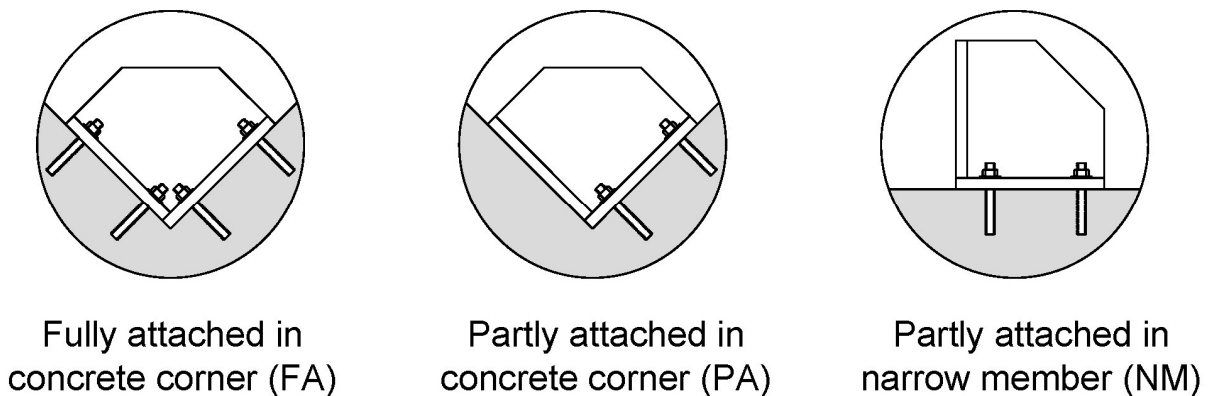
Figure 14.2. Schematic depiction of the attachments considered in the numerical parametric study.

The connection element which was investigated so far considers the case were a steel brace would be fastened to the RC frame at an angle of 45°. As a starting point for a systematic investigation of such connections, it is particularly suitable due to its symmetry, a rather clear force path and the presumably even distribution of forces among the anchors. However, this is often not possible in real applications. Particularly in case of strengthening, where the strengthening solutions has to be adapted to the geometrical and structural conditions of the existing building. Thus, steel braces may also be attached to the RC frame at smaller angles. A detailed analysis of various load angles is however, beyond the scope of this dissertation. Nonetheless, in order to get an initial idea of how the behavior changes at other angles, an additional simulation is performed assuming a load angle of 30°. For this purpose, the geometry of the connection element was altered as shown in Figure 14.3. Note that the concrete specimen and the dimensions of the anchor bracket remain the same. Basically, only the geometry of the gusset plate was altered. The embedment depth of the anchors in the simulation was $h_{ef} = 110$ mm and the connection was fully attached to the concrete specimen.
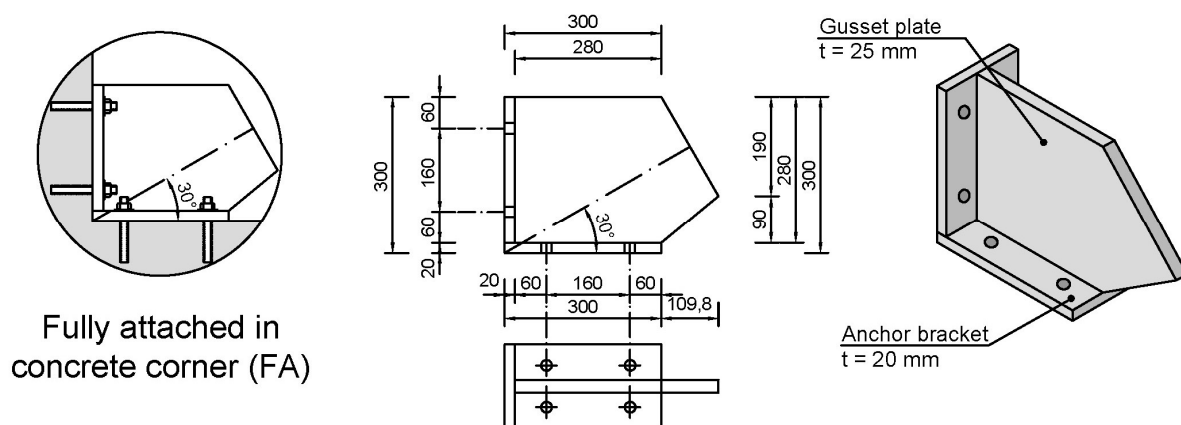
Figure 14.3. Dimensions of the bracket-to-gusset plate connection element for fastening of steel braces at an angle of 30°considered in the numerical study. (Note: All dimensions are in mm).

Again, the numerical simulations were performed using the 3D FE software MASA. Pre- and post-processing were carried out using the software FEMAP (Siemens). A detailed summary of the numerical program is given in Table 14.1.

Note that similar numerical studies have already been published in Stehle and Sharma (2021c) and Stehle and Sharma (2021d). In these studies, the dimensions of the connection element and the concrete specimen slightly differed from the dimensions applied in this study. However, the results presented in the following sections mostly reflect those already published in Stehle and Sharma (2021c) and Stehle and Sharma (2021d).

Table 14.1. Overview of the numerical program and main results.

ID	h_{ef} (mm)	Load angle, θ	Type of attachment	P_{first} (kN)	Ultimate load, P_u (kN)
BGC-N-60-FA	60	45°	FA	144.0	172.8
BGC-N-80-FA	80	45°	FA	182.8	199.0
BGC-N-80-PA	80	45°	PA	92.8	158.9
BGC-N-80-NM	80	45°	NM	-	93.4
BGC-N-110-FA	110	45°	FA	230.4	261.9
BGC-N-160-FA	160	45°	FA	301.3	356.0
BGC-N-110-30°	110	30°	FA	219.5	247.4

14.2 Numerical modelling approach

In principle, the applied modelling approach follows the approach presented in Chapter 10. Figure 14.4 shows the discretization of the concrete specimen and the corner configuration used in the numerical analysis. The dimensions of the concrete specimen shown in Figure 14.4 (a) are identical to the dimensions used in the experimental part. The specimen used for simulating a partly attached connection installed in a narrow concrete member is shown in Figure 14.4 (b). It has a length of 1700 mm, a height of 750 mm and a width of 240 mm. Hence, the width is identical to the width used in the other simulations and in the experiments. The concrete specimens were modelled without considering any reinforcements. Instead, excessive bending of the concrete specimen was hindered by applying constraints on the bottom side of the specimens. For modelling the support conditions, additional constraints were applied on the top surface of the concrete specimens. In the models which simulate the specimen used in the experiments, constraints were applied close to the triangular recess as indicated in Figure 14.4 (a) to simulate the I-beams which were used as supports. Note that the constraints were not directly applied onto the nodes closest to the triangular recess, but at a distance which equals the distance from the web of the I-beam to the triangular recess in the experiments. A parametric study with varying support distance has shown that the adopted support conditions best reflect those of the experimental setup. For the models simulating the behavior in narrow concrete members, constraints were applied at a distance of $2h_{ef}$ from the outermost anchors similar to the numerical models in Chapter 10. The connection element was loaded in displacement control by directly applying the displacements onto the nodes of the upper surface of the gusset plate as indicated in Figure 14.4. The displacements were stepwise increased in increments of $\sqrt{1/2} \cdot 10^{-2}$ mm (0.005 mm per step applied equally to each anchor group). The total forces acting on the anchor group is calculated from the sum of forces on the loaded nodes in the direction of loading.
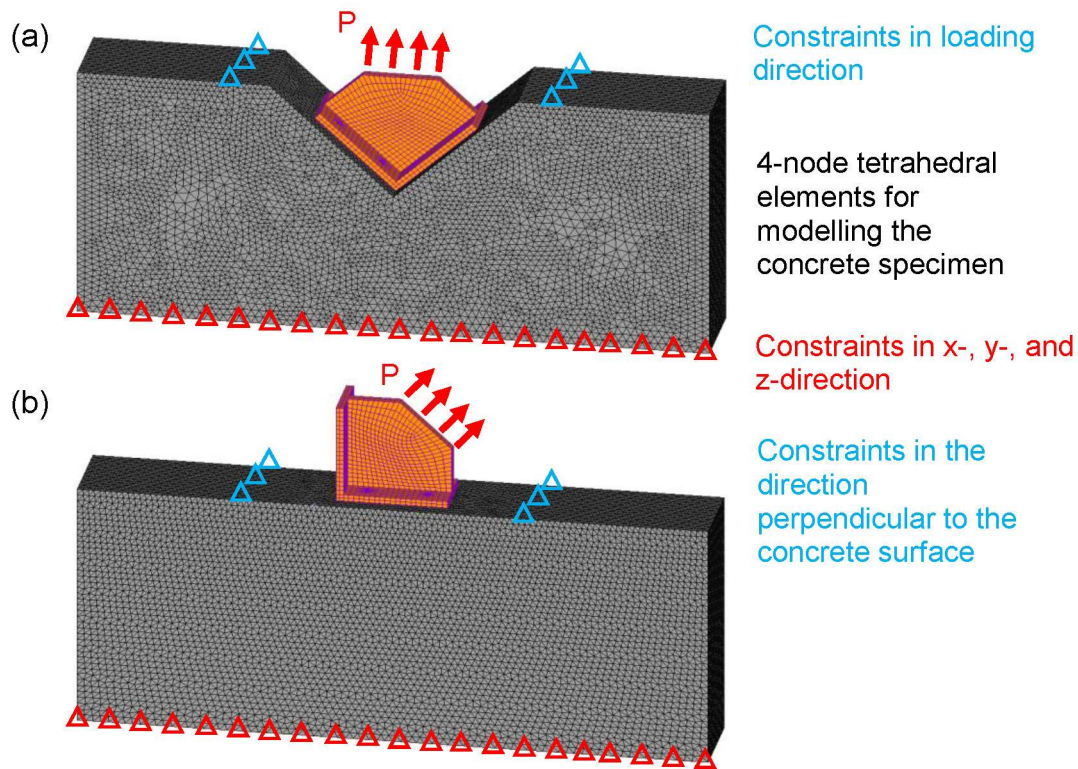
Figure 14.4. (a) Discretization in case of fully and partly attached connection installed in the corner of the concrete specimen and (b) discretization in case of partly attached connection installed in a narrow concrete member.

The concrete specimens were modeled using 4-node tetrahedral elements. Steel elements, such as the anchor rods, the anchor bracket, and the gusset plate, were modeled using 8-node hexahedral elements. To simulate the bond between anchor rods and concrete, 2-node bar elements were utilized which are only able to transfer compression and shear forces (see Figure 14.5). Compression-only 2-node bar elements were used to model the contact between the baseplate and the concrete. The 2-node bar elements are embedded in a weak contact layer of 8-node hexahedral elements to identify them as interface elements.

In accordance with the experiments, the mean concrete cylinder compressive strength of concrete was considered as $f_{c,m} = 25 \, N/mm^2$. Further material properties for concrete that need to be specified are the tensile strength of concrete $f_{ctm} = 2.56 \, N/mm^2$, Young's modulus of concrete $E_c = 23650 \, N/mm^2$, the fracture energy of concrete $G_F = 0.045 \, N/mm$, and Poisson's ratio $\mu_c = 0.18$. As shown in the experiments, the connection was failing due to concrete breakout failure before yielding of the steel elements. Therefore, in case of the fully attached connection model, the steel elements were modelled assuming linear-elastic material behavior with Young's modulus of steel $E_s = 200000 \, N/mm^2$, and Poisson's ratio $\mu_s = 0.33$. In the models where the connection was only partly attached to the concrete specimen, however, the nonlinear behavior of the anchor rods was considered assuming von

Mises plasticity criteria. Here the yield stress was taken as $f_y = 640 \, N/mm^2$ and the ultimate strength was taken as $f_u = 800 \, N/mm^2$. The bond between the anchor rods and concrete, which simulates the epoxy mortar layer in the experiments, is defined according to Chapter 10 with a maximum bond strength of $\tau_{max} = 32.5 \, N/mm^2$.

(a)

(c)

8-node hexahedral elements for steel parts

(b)

8-node hexahedral elements for contact
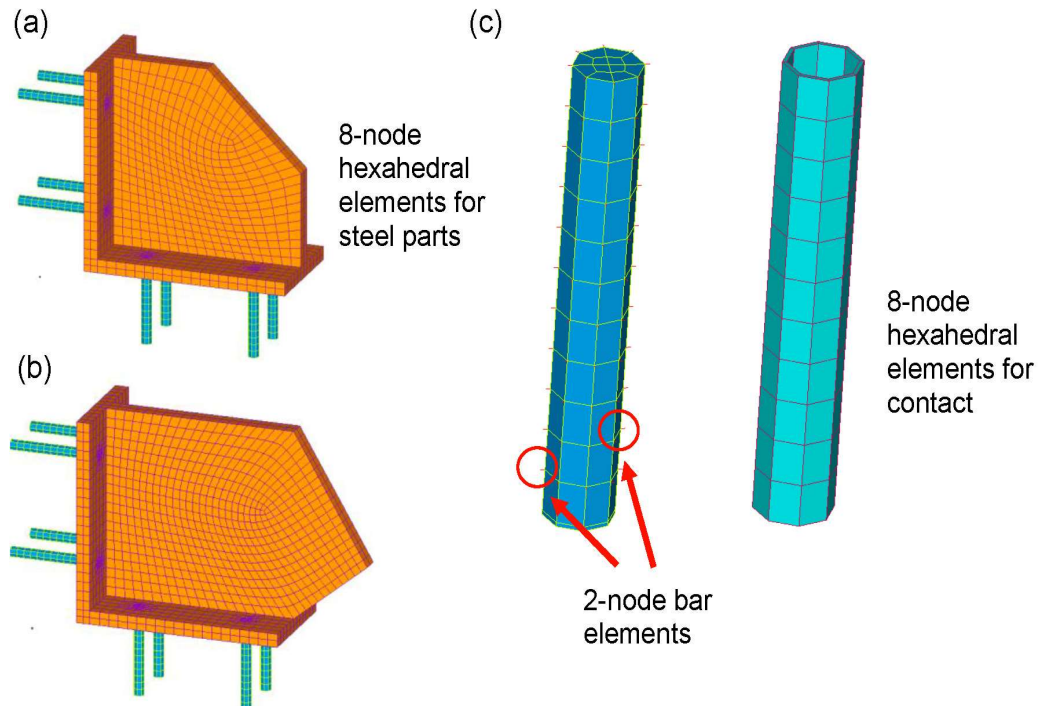
2-node bar elements

Figure 14.5. Discretization of corner configuration in case of (a) 45° load angle, (b) 30° load angle, and (c) discretization of contact elements and anchor rod with 2-node bar elements for bond.

14.3 Validation of the numerical modelling approach

In this section, the numerical modelling approach is validated against the experimental results obtained in test series BGC-80 and BGC-110 (see Chapter 13). For this purpose, the results obtained in the numerical analysis are compared to the experimental results in terms of the load-displacement behavior and the observed crack pattern.

Before proceeding with the comparison of the load-displacement curves, one should note that the displacement behavior observed in the experiments was considerably more pronounced compared to the displacement behavior in the numerical analysis. On average, the displacement measured at first peak was around four times larger. Similar applies to the displacement at ultimate load. These differences can be explained in part by the different points at which the displacements were measured. While in the experiments the total displacement of the connection was measured on the fixture which was connected to the gusset plate by bolts, in the numerical analysis

the total displacement was measured directly on the upper surface of the gusset plate. However, since the play of the bolted connection was as small as practically possible, the difference cannot solely be explained by the different points of measurement. In general, the stiffness observed in numerical simulations using MASA is notably higher than the stiffness observed in the experimental counterpart. As a result of the difference with respect to the actual displacement, further on it is deemed less meaningful to compare the displacement behavior directly. Instead, the relative displacement behavior is compared to see whether the progression of the load-displacement curves corresponds qualitatively. For this purpose, the displacement relative to the displacement at first peak, s/s_{first}, is compared.

Figure 14.6 shows the experimental and the numerical load-displacement behavior for an embedment depth of 80 mm (blue curves) and 110 mm (red curves), respectively. As discussed, the x-axis refers to the relative displacement, while the y-axis refers to the actual load of the connection. In large parts, the numerical curve follows the curves obtained in the experiments and thus reflects the actual behavior of the connection sufficiently well. With regards to the load at first peak and the ultimate load, the numerical results match well with the experimental results. For an embedment depth of 80 mm, the numerically obtained loads are around 7% higher than the loads obtained in the experiments. For an embedment depth of 110 mm, the loads at first peak are around 5% higher in the numerical analysis, while at ultimate load the results are almost identical.
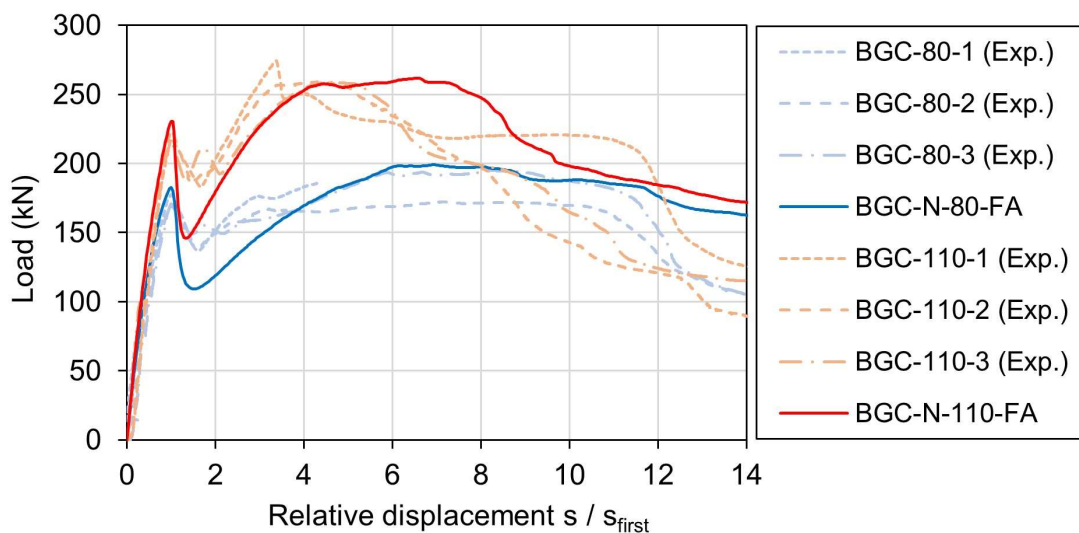
Figure 14.6. Comparison of the load-displacement behavior obtained from the numerical analysis and the experiments.

Figure 14.7 shows a comparison between the crack pattern obtained in the experiments and the numerical analysis. In the simulation, the crack pattern is depicted in terms of principle tensile strain where red elements represent a crack width larger than 0.1 mm. From the comparison, it can be seen that the numerical and experimental

crack patterns are in a good agreement. In general, the comparison between the numerical and experimental results showed that the applied modelling approach reflects the behavior that was observed in the experiments sufficiently accurate. However, in terms of stiffness and displacements, only a qualitative statement can be drawn from the numerical analysis.
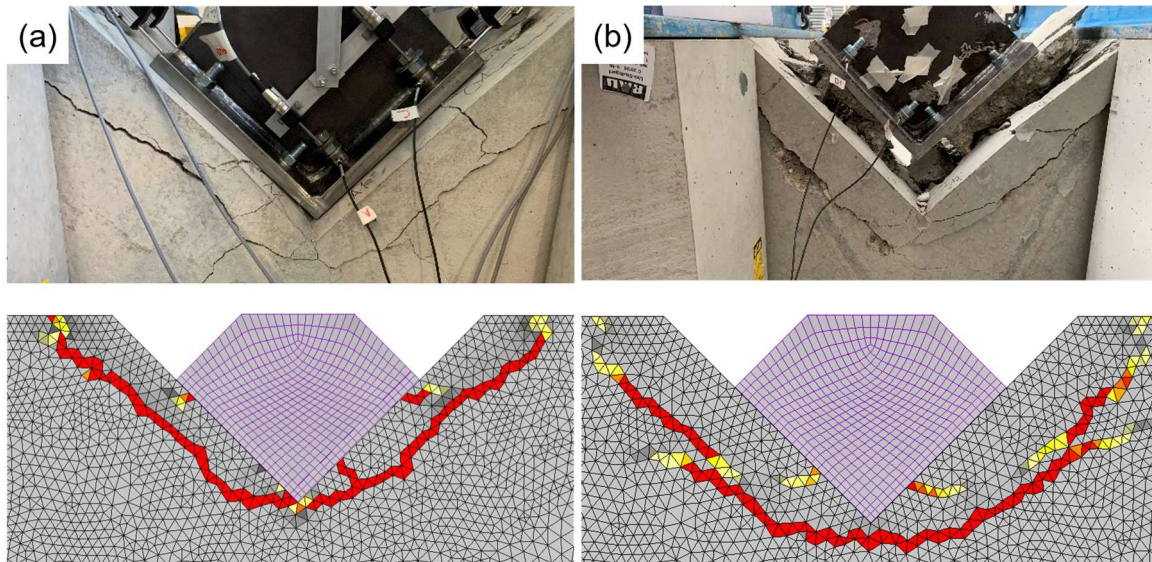
Figure 14.7. Comparison of the crack patterns obtained from the numerical analysis and the experiments (a) configuration with h_{ef} = 80 mm and (b) configuration with h_{ef} = 110 mm.

14.4 Numerical results and discussion

14.4.1 Influence of the embedment depth on the load-displacement behavior of the bracket configuration

The load-displacement curves of the simulated corner configurations with varying embedment depth are presented in Figure 14.8. Note that the digit included in the designation indicates the embedment depth of the anchors in the respective simulation. The x-axis refers to the displacement applied on the upper surface of the gusset plate as indicated in Figure 14.4 (a). The y-axis refers to total load on the connection calculated from the sum of forces of the loaded nodes in the direction of loading.

In accordance with the experimental results, the load-displacement curves are characterized by two distinct peaks. Initially, up to a load of around 50% of the load at the first peak, the behavior is rather similar regardless of the embedment depth of the anchors. With increasing embedment depth, the load at first peak increases. After the first peak has been reached, the load drops to a local minimum. Thereupon, the connection is able to regain its strength, whereby the behavior in this second phase,

up to the ultimate load, becomes markedly stiffer with increasing embedment depth. So far, it can be concluded that also for larger or smaller embedment depths, the overall load-displacement behavior of the bracket configuration appears to be consistent with the behavior observed in the experiments. What is interesting to see is that at smaller embedment depths, stiffness increase with increasing embedment depth appears to be less pronounced than for larger embedment depths. In the simulations BGC-N-60-FA and BGC-N-80-FA, the progression of the load-displacement curves in the second phase is rather similar, whereas it becomes increasingly steeper in simulations BGC-N-110-FA and BGC-N-160-FA. This can also be seen from the evaluation of the stiffness in the ascending branch of the second phase, where the connection regains its strength. The detailed extract of the load-displacement curve in Figure 14.8 provides the corresponding stiffness for all embedment depths relative to the stiffness at an embedment depth of 60 mm. It is apparent that increasing the embedment depth from 60 mm to 80 mm has only a small impact on the stiffness, whereas a notable increase is observed for larger embedment depths. Accordingly, the behavior in the descending branch becomes more brittle with increasing embedment depth of the anchors.
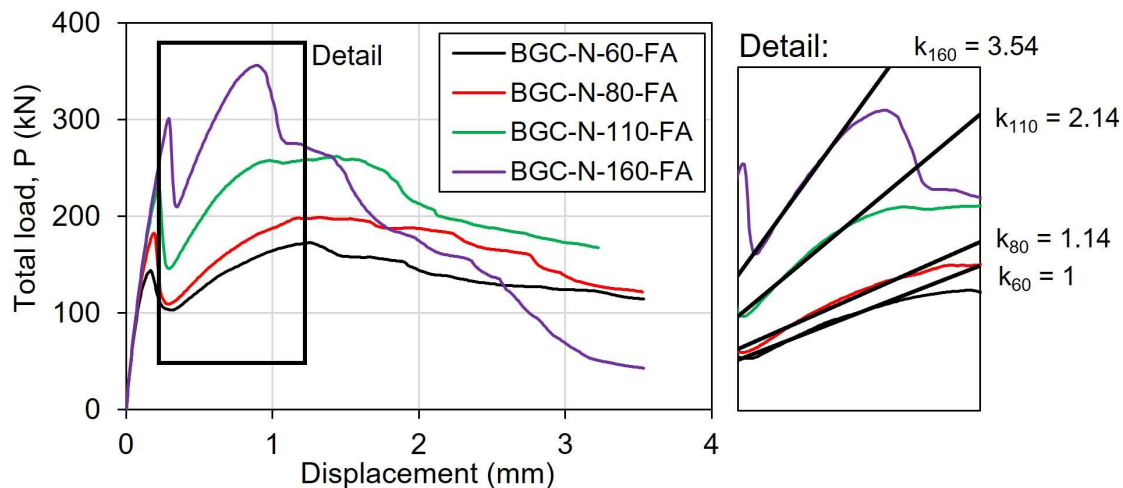
Figure 14.8. Load-displacement curves obtained from the numerical analysis of the corner configuration using anchors with an embedment depth of 60 mm, 80 mm, 110 mm, and 160 mm.

Similar observations can be made regarding the loads. While the load at first peak increases rather consistently with increasing embedment depth, the ultimate load exhibits a significant increase when increasing the embedment depth from 80 mm to 110 mm. However, the ultimate load changes only moderately when increasing the embedment depth from 60 mm to 80 mm. Assuming that the anchors exhibit a loss of tensile capacity when reaching the first peak (characterized by the load drop and cracking on the side surface of the concrete specimen), the capacity of the entire connection in the second phase would mainly depend on the shear capacity of the anchors. As shown in Grosser (2012), the shear capacity of anchor groups that are

installed in narrow concrete members and loaded parallel to the edges, is however not notably influenced by the embedment depth per se. It is therefore likely that the anchors are able to retain a certain residual tensile capacity after the first peak. Thereby it appears that the residual tensile capacity is to some extend influenced by the embedment depth of the anchors. To understand whether the load-bearing mechanisms differ depending on the embedment depth, the following section examines the principal compressive stresses within the concrete in more detail.

14.4.2 Evaluation of principle compressive stresses in the concrete

Figure 14.9 shows the evaluation of the principal compressive stresses in the concrete section at first peak (left column) and at ultimate load (right column) for the corner configuration with an embedment depth of 80 mm (first row), 110 mm (second row), and 160 mm (third row). At first peak, three points are striking about the stress distribution, which are marked by the numbers in Figure 14.9 (a). At the first point, bearing stresses arise in front of the anchors. These rather high stresses arise from the bearing of the anchors against the surface of concrete due to the shear load component (Eligehausen et al., 2006). At the second point, high circumferential stresses are apparent at the embedded ends of the anchors which arise from the tension load component. At point three, the initial formation of compression struts in the concrete between the embedded ends of the anchors and the concrete corner can be seen. The comparison of stresses at first peak clearly shows that up to this point, the load bearing mechanism of the bracket configuration is rather uniform for varying embedment depths. The observation of a uniform behavior up to the first peak is consistent with findings of the experimental evaluation.
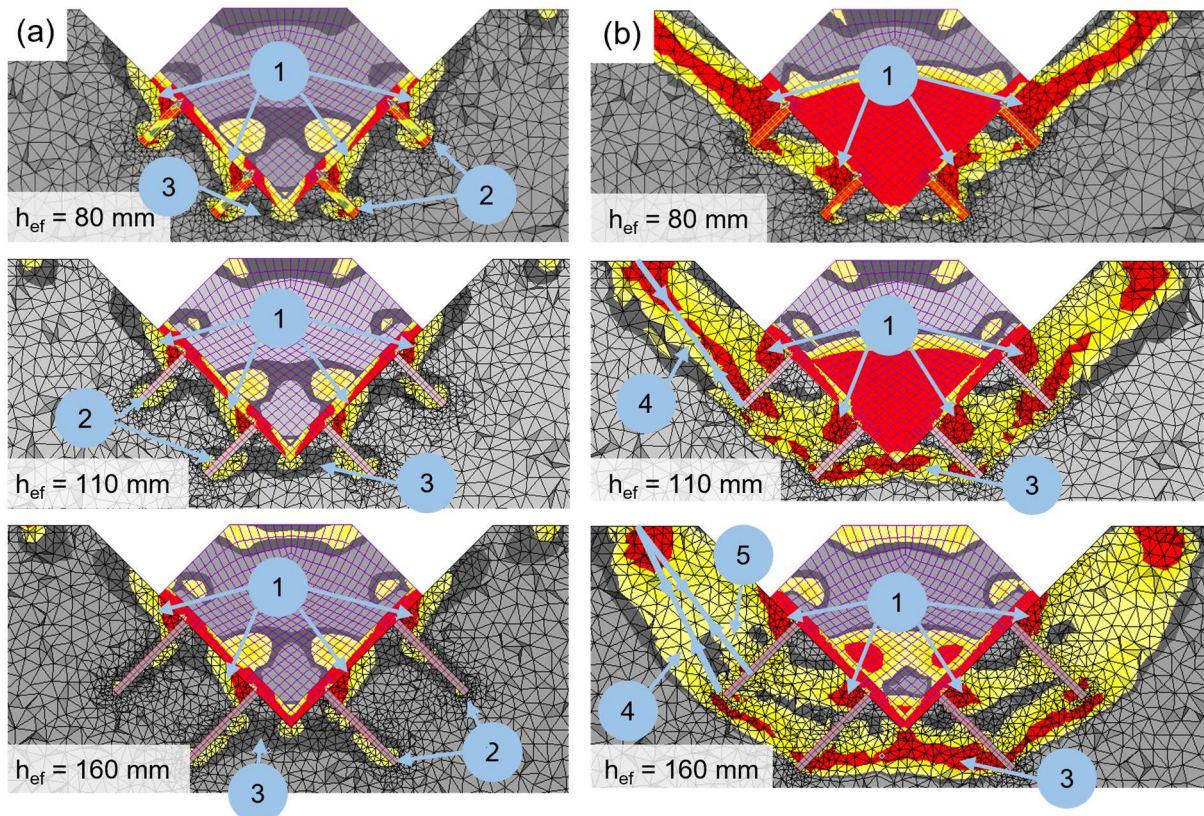
Figure 14.9. Principal compressive stresses corresponding to the point when (a: left column) the first peak and (b: right column) the ultimate load is reached.

On the other hand, clear differences are observed for the stress distribution at ultimate load shown in Figure 14.9 (b). For an embedment depth of 80 mm, the behavior of the corner configuration is dominated by the bearing stresses resulting from the shear load on the anchorage. A compression strut has formed from the front anchors towards the supports, which appears to be a superposition of the bearing stresses at the surface of the concrete specimen and the compression strut originating from the embedded ends of the front anchors. Presumably, the front anchors are able to withstand some tension load at ultimate load. Conversely, no compression strut is apparent between the embedded ends of the back anchors and the concrete corner. Neither is it between the back and front anchors. The absence of compression struts indicates that the back anchors have lost their capacity to bear tension loads.

The configuration using anchors with an embedment depth of 110 mm shows compression struts clearly originating from the embedded ends of the anchors. Besides the struts which have formed between the back anchors and the front anchors, compression struts have formed towards the supports (point four). Also, the strut between the back anchors and the concrete corner remained stable (point three). The presence of the stable compression struts suggests that all anchors maintain a certain residual tensile capacity when the ultimate load is reached.

A similar behavior is observed in case of 160 mm embedment depth of the anchors. Initially, the stress development equals the one for 110 mm embedment depth. Thus, primary compression struts form between the tip of the embedded end of the anchors and the supports (point four). With increasing load, secondary compression struts at point five form between the front anchors and the supports. The secondary strut further stabilizes the anchor behavior resulting in an increased global capacity. The formation of this secondary struts, however, is likely a result of the load transfer mechanism of bonded anchors and thus not accountable in case of other types of anchors.

The evaluation of the principal compressive stresses for various embedment depths offers an explanation for the global load-displacement behavior observed in the previous section. The stabilizing compression struts which emerged in case of larger embedment depths may cause the anchors to maintain a certain residual tensile capacity, which would contribute to the increased stiffness and capacity of the corner configuration. To investigate this hypothesis, the anchor forces will be evaluated in the next section. In addition, the evaluation of the anchor forces will be used to show how the observed behavior affects the force distribution and the behavior of the individual anchors.

14.4.3 Evaluation of anchor forces

In the numerical model, the forces are transferred from the anchors to the concrete by means of 2-node bar elements which are able to transfer compression and shear forces. Accordingly, the total axial and shear forces in one anchor can be calculated as the sum of forces on the nodes which connect the 2-node bar elements to the solid elements that form the anchor. In this way, the axial and shear forces of the individual anchors of a bracket configuration were determined. In order to verify that the applied procedure provides reliable results, it was checked whether the calculated anchor forces are in equilibrium with the load which was actually applied on the connection. It was found that up to the first peak, the forces acting on the connection are in equilibrium in all simulations. Thus, the applied approach can be deemed valid up to this point. In the second phase, the forces in the anchors are slightly higher compared to the actually applied load. This effect is caused by prying action of the baseplate after the loss of tensile capacity of the anchors upon first peak. It was found that this effect is particularly pronounced in the simulation with an embedment depth equal or smaller than 80 mm. A detailed discussion on this topic is found in Subsection 14.4.5. In the other simulations it was found that this effect of prying action is less pronounced (3% deviation) since all anchors are able to retain a certain residual tension capacity in the second phase (h_{ef} = 110 mm; h_{ef} = 160 mm).

The designation of the individual anchors follows the designation used in the experiments (see Figure 13.6). Thus, anchor A and B refer to the anchors which are located closest to the concrete corner and anchor C and D refer to the anchors which are located away from the corner. Anchor A and B are also referred to as back anchors

and anchor C and D are referred to as front anchors. The digits indicate whether an anchor belongs to the first or second group.

14.4.3.1 Distribution of forces among the groups which form the bracket

Before starting to evaluate the individual anchors of the corner configuration with respect to their tension and shear behavior, the first step is to look at how the forces are distributed among the two groups which form the bracket. For this purpose, the tension and shear forces of the anchors were summed up for each group, respectively. In other words, it is assumed that the sum of the tensile forces of the anchors which form a group represents the total tensile load acting on that group. Same applies for the shear load component. Figure 14.10 presents the tension and shear loads acting on the two perpendicular groups for a configuration with an embedment depth of 110 mm. The blue curves show the results for the first group and the red curves show the results for the second group. The loads are shown as a function of the displacement steps used in numerical analysis. The comparison between the two groups shows that the total load of the connection is evenly distributed to both groups. The behavior starts to diverge only after the bracket configuration has reached its ultimate load. However, it appears that only the shear component is concerned, while the tension load on both groups remains almost equal throughout the analysis.

In the experiments it was observed that the shear displacement of both groups diverges after reaching the first peak, indicating an uneven loading. The differences between the experimental and numerical results are likely to be related to irregularities in the experiments arising from installation differences (actual embedment depth of the anchors), unevenness of the concrete surface, initial misalignment of the connection, or the location of aggregates in the anchorage zone. Since such irregularities are not considered in the numerical models, the probability of a symmetric behavior of the connection is increased. This is also evident from the simultaneous start of cracking in the anchorage zones of both groups and a rather uniform crack propagation. The symmetric behavior of the connection might also be a major factor for the slightly higher loads obtained in the numerical analysis.

The equal distribution of forces among the two anchor groups that was observed for an embedment depth of 110 mm could be seen in all simulations. Moreover, it was found that the anchors of the two groups, which form the connection, exhibited a symmetrical behavior. Therefore, the following evaluation of individual anchors is performed only on the anchors of one group.

(a) Tension load   (b) Shear load
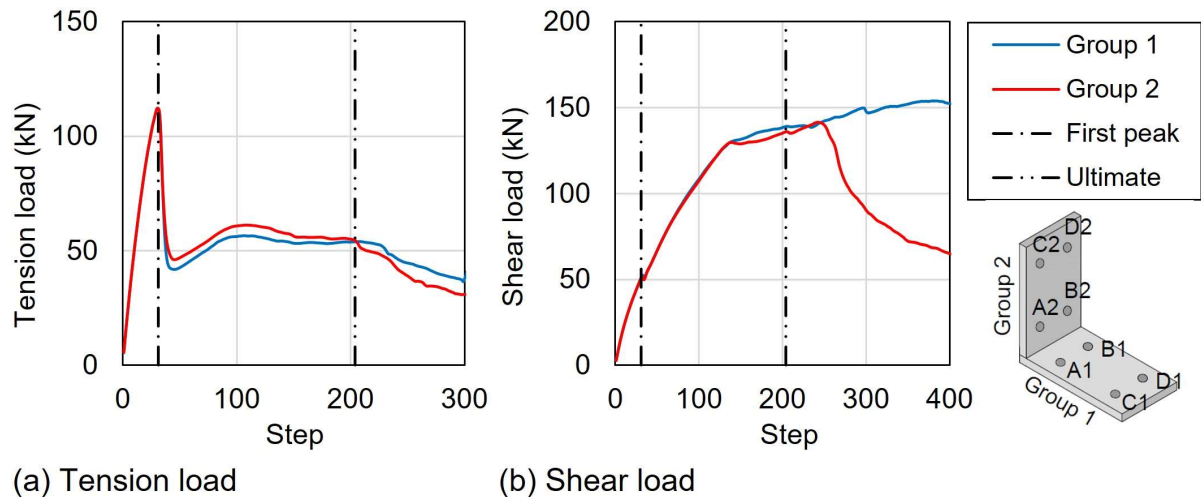
Figure 14.10. (a) Tension loads and (b) shear loads acting on the groups of the anchor bracket for a configuration with h_{ef} = 110 mm.

14.4.3.2 BGC-N-60-FA – Anchor forces

Figure 14.11 shows the distribution of forces among the individual anchors of one group obtained from the numerical simulation of the fully attached bracket configuration using anchors with an embedment depth of 60 mm. The left graph shows the axial forces taken up by the anchors, and the right graph shows the shear forces taken up by the anchors. Both are plotted as a function of the displacement steps. The dashed/dotted lines mark the points where the load-displacement curve of the complete connection reaches the first peak load and the ultimate load, respectively. In the beginning of the analysis, the total load acting on the bracket configuration is transferred via both axial and shear forces in the anchors. Thereby, at first peak, the load taken up in tension corresponds on average to around 1.5 times the load taken up in shear. When the load-displacement curve of the complete connection reaches the first peak, the anchors reach their tension capacity, and the axial forces drop to zero. Henceforth, the applied load on the bracket configuration is solely resisted by the anchors through shear.

It can be seen from the graphs that both the tension and shear forces are rather evenly distributed among the four anchors. In the beginning of load application, the axial forces of the anchors are almost identical. Only at first peak, the front anchors, C and D, show slightly higher forces compared to the back anchors. In general, these results match the observed axial displacements in the experiments, which also showed a uniform progression. Similarly, the shear forces progress rather uniformly almost up to the point where the connection reaches its ultimate load. Here, the shear forces on the back anchors are smaller compared to the forces on the front anchors, which are able to maintain a certain capacity before finally losing the shear capacity.

Figure 14.11. Distribution of forces among the anchors obtained from the numerical simulation of a bracket configuration using anchors with an embedment depth of 60 mm. (a) Anchor axial force and (b) anchor shear force as a function of the displacement steps.

14.4.3.3   BGC-N-80-FA – Anchor forces

Figure 14.12 shows the distribution of forces among the individual anchors associated with one of the groups that form the bracket. The results were obtained from the numerical simulation using anchors with an embedment depth of 80 mm. The left and right graph show the axial and shear forces taken up by the anchors, respectively. Both are plotted as a function of the displacement steps used in the analysis. The dashed/dotted lines mark the points where the complete connection reaches the first peak load and the ultimate load, respectively.

Figure 14.12. Distribution of forces among the anchors obtained from the numerical simulation of a bracket configuration using anchors with an embedment depth of 80 mm. (a) Anchor axial force and (b) anchor shear force as a function of the displacement steps.

Up to the first peak, the applied load on the connection is taken up mainly by tension with the tension forces in the anchors being almost twice of the shear forces in the anchors. As seen in the previous case as well, the loads are equally distributed among the anchors. Thereafter, the anchors rapidly lose their ability to bear axial forces. In contrast to the previous results for an embedment depth of 60 mm, however, the front anchors C and D retain a residual tensile capacity of around 15% - 20% of the maximum tensile capacity. This residual tensile capacity is maintained until the ultimate load of the bracket configuration is reached. The ability of the front anchors to retain a certain tensile resistance is presumably the result of the observed compression struts (see Figure 14.9) which remain stable until the ultimate load of the connection is reached. Moreover, the absence of compression struts for the back anchors matches the observed loss of tension capacity of the same. As already seen in case of h_{ef} = 60 mm, the behavior of the connection in the second phase is dominated by the shear behavior of the anchors, which show a uniform progression almost up to the ultimate load of the connection. When the connection reaches its ultimate load, the shear forces of the individual anchors are, on average, around 12% larger compared to those obtained at an embedment depth of 60 mm.

14.4.3.4 BGC-N-110-FA – Anchor forces

Figure 14.13 shows the distribution of forces among the individual anchors associated with one of the groups that form the bracket. The results were obtained from the numerical simulation using anchors with an embedment depth of 110 mm. The left and right graph show the axial and shear forces taken up by the anchors, respectively. Both are plotted as a function of the displacement steps. The dashed/dotted lines mark the points where the complete connection reaches the first peak load and the ultimate load, respectively.
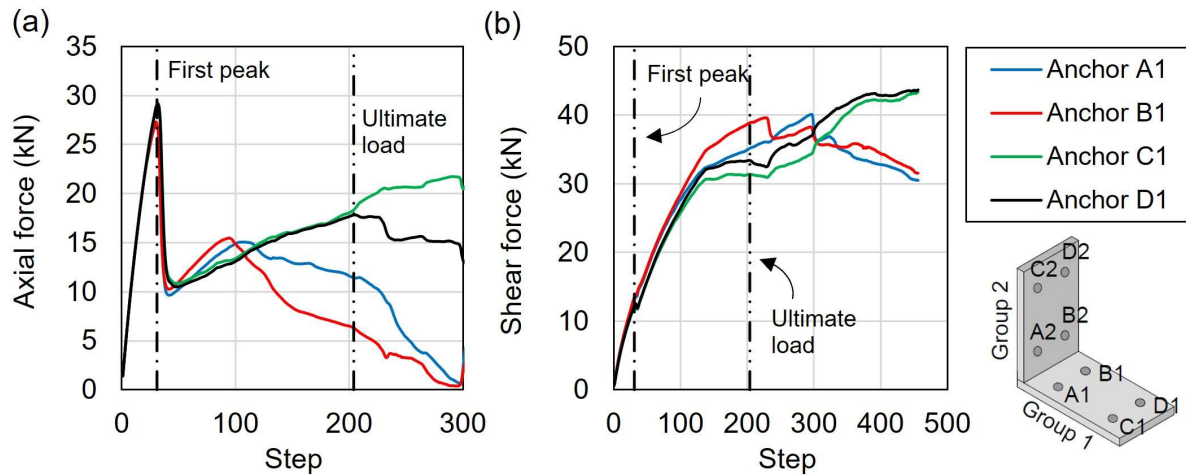
Figure 14.13. Distribution of forces among the anchors obtained from the numerical simulation of a bracket configuration using anchors with an embedment depth of 110 mm. (a) Anchor axial force and (b) anchor shear force as a function of the displacement steps.

The overall behavior is in general similar to the behavior observed so far. Due to increased embedment depth, the tension component in the anchors is significantly larger than their corresponding shear component up to the first peak. After the sudden loss of tensile capacity, the load is mainly resisted though shear. However, the anchors are able to maintain a significant residual tensile capacity after the initial drop of load. In Figure 14.13 (a) it can be seen that all anchors are able to resist tension loads beyond the point where the ultimate load of the connection is reached. On an average the residual tensile capacity at the point where the connection reaches its ultimate load is around 45% of the maximum tensile capacity. This residual capacity can be related to the observed compression struts (see Figure 14.9 (b)) which remain stable up to the ultimate load. These struts allow the anchors to resist tension forces. Moreover, it appears that the ability of the anchors to maintain a high amount of tensile capacity before final failure is the main reason for the marked increase of the total capacity of the connection in comparison to the same bracket configuration with anchors of smaller embedment depths. This becomes evident by comparing the average shear forces in the anchors at the point when the connection reaches the ultimate load. While for an embedment depth of 60 mm and 110 mm, the forces at this point are almost equal, the shear forces for h_{ef} = 80 mm were even slightly larger.

14.4.3.5 BGC-N-160-FA – Anchor forces

Figure 14.14 shows the axial and shear forces of individual anchors of one group for each step of the numerical analysis in simulation BGC-N-160-FA. The left and right graph show the axial and shear forces of the anchors, respectively. The dashed/dotted lines mark the points where the complete connection reaches the first peak load and the ultimate load, respectively.
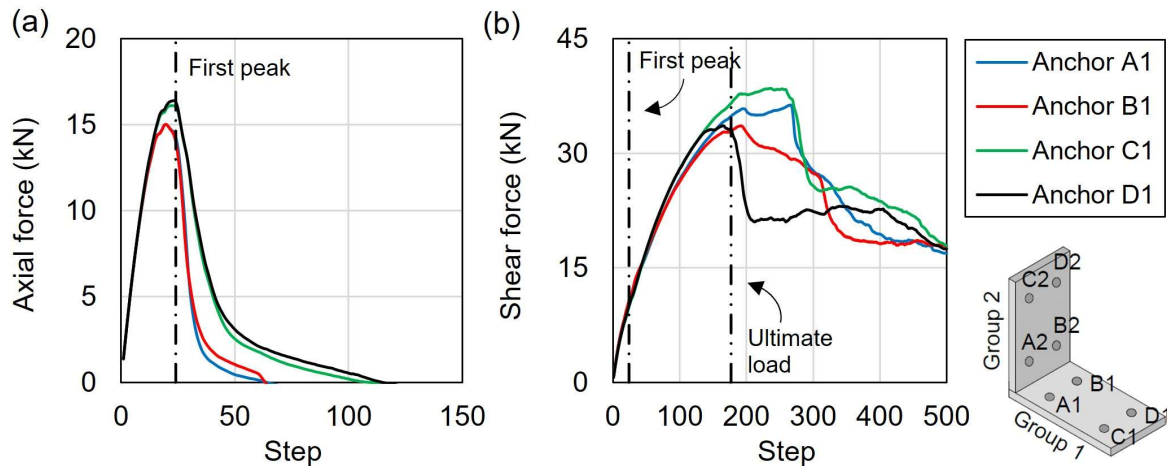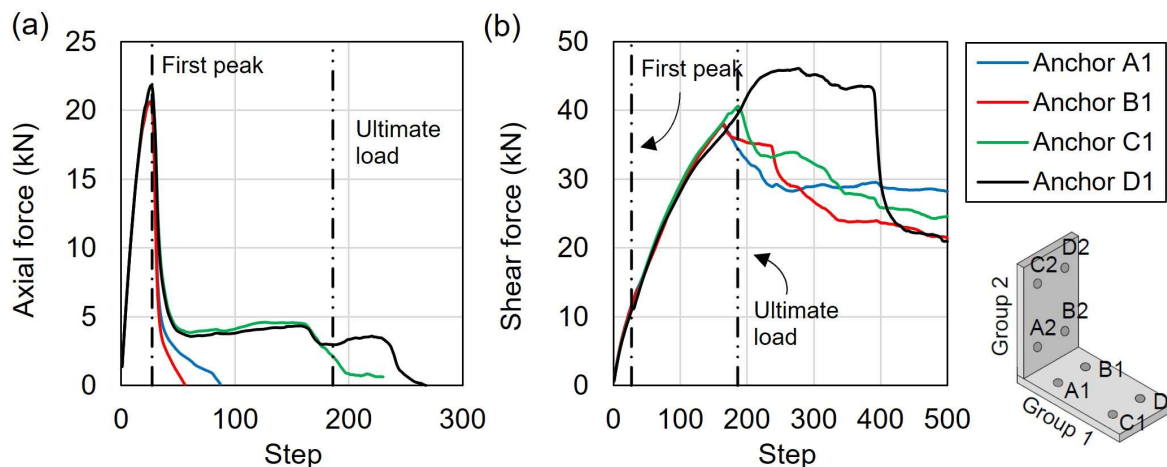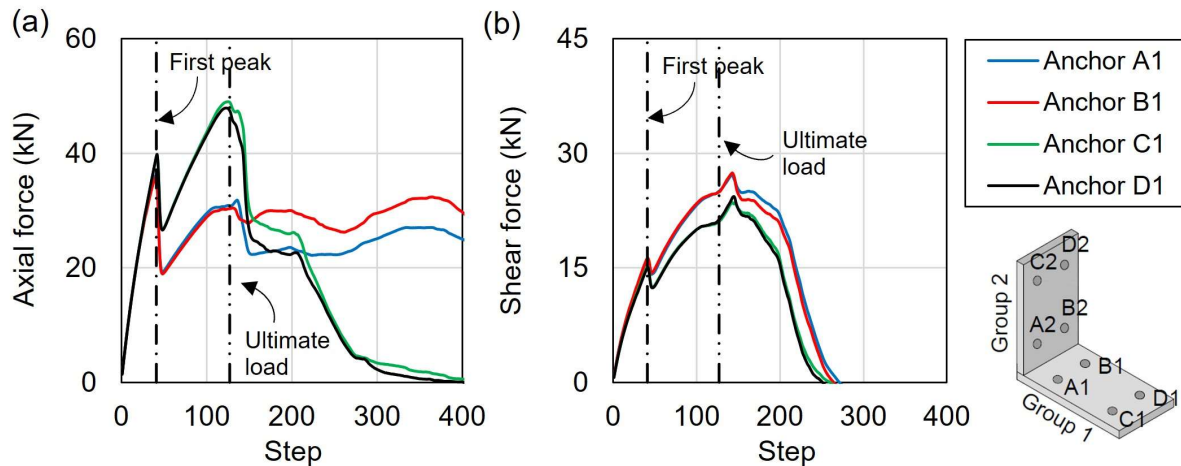
Figure 14.14. Distribution of forces among the anchors obtained from the numerical simulation of a bracket configuration using anchors with an embedment depth of 160 mm. (a) Anchor axial force and (b) anchor shear force as a function of the displacement steps.

For an embedment depth of 160 mm, the behavior of the individual anchors differs from the behavior observed so far. This applies in particular to the second phase after the first peak of the connection has been reached. Up to this point, in accordance with the behavior observed for smaller embedment depths, the total load on the connection is primarily resisted by the anchors through tension. At first peak, the shear component is around 40% - 50% of the tension component. Similar to the previously discussed simulations, the tension forces are rather evenly distributed among the anchors. However, it was observed that the front anchors take up slightly higher loads than the back anchors.

In the second phase, the anchors are still able to carry further tensile forces despite the previous loss of tensile load-bearing capacity. The two front anchors even show a significant increase in tensile capacity. The behavior of the anchors is attributable to the secondary compression struts that form after the first peak has been reached (see Figure 14.9). At the same time, the shear forces on the anchors are notably reduced in comparison to the simulations discussed earlier. Thus, the behavior in the second phase has shifted from a shear dominant to a tension dominant behavior.

14.4.3.6 Indicative conclusion

The initial behavior of the connection and the distribution of forces among the anchors for the simulated embedment depths is rather similar in the first phase of the load-displacement curve. However, variations of the behavior were observed in the second phase. This is mainly attributable to the load transfer mechanisms for the tension and shear forces after the anchors have reached their ultimate tensile capacity at the end of the first phase. At an embedment depth of 80 mm, there is still a partial superposition of the compression strut originating from the embedded end of the anchors, and the

bearing stresses at the surface of the concrete specimen. With increasing embedment depth, these two mechanisms are increasingly independent of each other. However, the behavior observed for an embedment depth of 160 mm is mainly due to the transfer mechanism of bonded anchors, which transfer the applied tensile forces along the entire bond length, thus allowing a secondary compression strut to form.

14.4.4 Influence of embedment depth on the anchor force distribution at first peak

The load which is applied on the bracket configuration is transferred by the anchors through a tension and a shear component. The results have shown so far that these components are of different magnitude, depending on the anchor embedment depth. In this subsection, the contributions of the tension and shear components to the load transfer of the two perpendicular groups are investigated in more detail. For this purpose, it is again assumed that the tension and shear load acting on one group corresponds to the sum of forces in the associated anchors. The objective is to determine how the ratio between tension and shear components changes for different embedment depths. The investigation will be carried out for the behavior at first peak, since the experimental and numerical results have shown so far that the bracket configuration exhibits a consistent and reliable behavior up to this point. This particularly includes the way in which the loads are resisted by the individual anchors. Thereafter, the behavior becomes more complex, and the load transfer mechanisms of the anchors can differ considerably as the embedment depth increases.

Considering the sum of tension forces on one group, $N_{sum,i}$, and the sum of shear forces, $V_{sum,i}$, the resulting load, P_i that is acting on one group can be calculated using vector addition. The corresponding internal load angle is considered for the evaluation of the ratio between the tension and shear component. The internal load angle is calculated according to Equation (14.1). The results are presented in Table 14.2.

$$\alpha_i = \tan^{-1}\left(\frac{N_{sum,i}}{V_{sum,i}}\right). \tag{14.1}$$

From the data it can be seen that the ratio between the tension component and the shear component slightly increases with increasing embedment depth (increasing load angle). Thus, the contribution of the tension component increases with increasing embedment depth. This finding is particularly evident for smaller embedment depths, which can be seen from the comparison between the results obtained from BGC-N-60-FA and BGC-N-80-FA. However, when the embedment depth is further increased, it seems that the ratio between the tension and shear components converges, and the load angle changes only moderately.

In general, the difference between the tension and shear component can be explained by the difference between the axial stiffness and the shear stiffness of bonded anchors.

As mentioned above, the shear stiffness of bonded anchors is considerably lower compared to the axial stiffness. As a result, the tension component of the anchors attracts higher forces. With increasing embedment depth of the anchors, the shear stiffness of bonded anchors basically remains constant as shown in Grosser (2012). At the same time, the failure mode of a tension loaded anchor group, with constant anchor spacing and anchor diameter, shifts from a predominantly concrete cone failure mode to a combined pull-out and concrete cone failure mode with increasing embedment depth (Lehr, 2003). A similar behavior has been observed in the evaluation of the principal compressive stresses, where a secondary compressive strut developed in the second phase, which was located closer to the concrete surface. This secondary compressive strut indicates the formation of a shallow breakout body. Presumably due to the concrete corner, which prevented the shallow breakout failure, the struts could stabilize, resulting in the increased capacity of the connection. At the same time, the observed change of failure mode of the tension component might explain why the axial stiffness does not vary as much for larger embedment depths as it does for smaller embedment depths.

Note that the values of the load angle reported in Table 14.2 are valid only for initial load transfer until approximately 80% of first peak.

Table 14.2. Evaluation of tension and shear load component on the groups at first peak.

ID		$N_{sum,i}$ (kN)	$V_{sum,i}$ (kN)	P_i (kN)	α_i
BGC-N-60-FA	Group 1	60.7	41.1	73.3	56°
	Group 2	61.0	41.1	73.5	56°
BGC-N-80-FA	Group 1	84.2	45.0	95.4	62°
	Group 2	84.6	44.7	95.7	62°
BGC-N-110-FA	Group 1	112.1	51.1	123.2	66°
	Group 2	112.1	50.6	122.9	66°
BGC-N-160-FA	Group 1	149.7	62.3	162.2	67°
	Group 2	150.9	63.1	163.6	67°

14.4.5 Fully attached vs. partly attached connection

To investigate the mere influence of the concrete corner on the behavior of the connection, simulations were performed where the connection element was only partly attached to the concrete specimen (Figure 14.2). Thereby, one simulation was performed where the connection element was placed in the corner of the concrete specimen (PA) and a second one where the connection element was solely attached to a narrow concrete member (NM). The behavior of the fully attached connection is used as a reference. The corresponding results in terms of the load-displacement

curves are provided in Figure 14.15 for an embedment depth of 80 mm. Table 14.1 provides the loads obtained at first peak and the ultimate loads.

When the connection element is placed in the corner of the specimen and only partly attached to it, it is evident that the behavior differs markedly from the behavior of the fully attached connection. Nonetheless, it can be seen that also the PA-simulation features a distinct first peak after which the connection is able to regain its strength. At first peak, the load that can be withstood by the connection reduces to around 50% of the first peak capacity for the corresponding fully attached (FA) connection. Equally important, the secant stiffness of the connection reduces by around 50%. Also, the second phase shows differences between the fully and partly attached connection. Although not as strongly with regard to the loads, the behavior differs more clearly with regard to the displacements. From Figure 14.15 it can be seen that the displacement behavior is more pronounced in case of the partly attached connection. At ultimate load, the secant stiffness is around 50% of the stiffness obtained from the fully attached connection. With respect to the ultimate loads, the partly attached connection is able to withstand around 80% of the ultimate load obtained from the fully attached connection. Thus, the difference between the ultimate load values is notably smaller compared to the difference at first peak. This observation can be related to relatively high prying forces that develop in the anchors of the FA-simulation and which increase the forces in the anchors. In turn, this effect has a negative influence on the total load that can be resisted by the connection. The prying action arises as in the second phase the tension component is solely resisted by the front anchors of the two perpendicular anchor groups. In case of the partly attached connection, the prying action is not as pronounced since the connection element is only attached to one concrete member. Since the additional prying forces in the anchors are lower, the connection is in turn able to resist higher loads. It is worth mentioning that the prying forces in the anchors are also the reason for why the sum of anchor forces at ultimate load are not in equilibrium with the load that is applied on the connection.
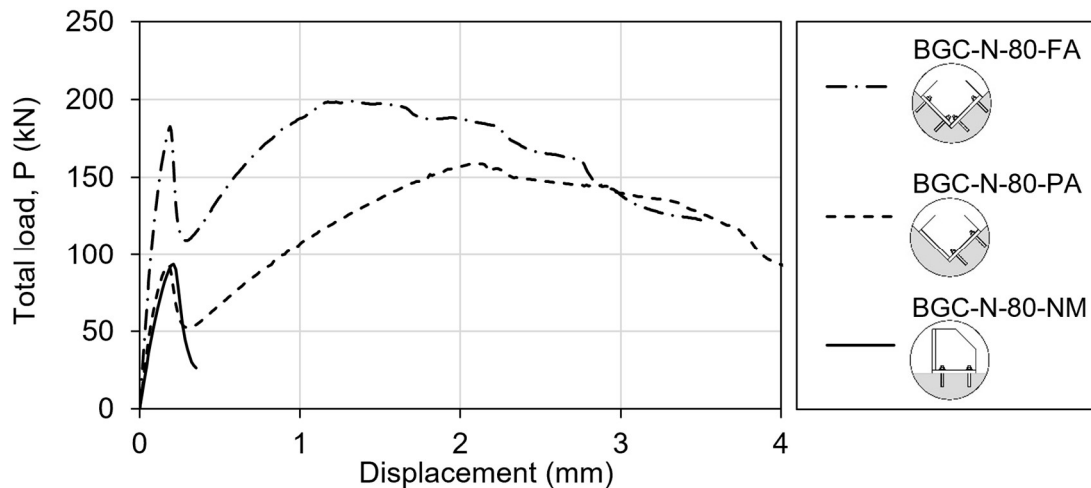
Figure 14.15. Load-displacement curves obtained from the numerical analysis of the corner configuration with varying level of attachment (h_{ef} = 80 mm).

When the connection is solely attached to a single narrow concrete member (no concrete corner, BGC-N-80-NM), the connection fails after reaching the tensile capacity of the anchors. The load-displacement curve is characterized by a single peak. Nonetheless, the obtained ultimate load matches with the load at first peak obtained from the simulation with the partly attached connection placed in the corner of the concrete member.

The numerical results allow three conclusions. First, it has been shown that up to the first peak, the behavior of the complete connection can be composed of the load-displacement behavior of two independent groups of anchors. This can be concluded from the fact that both the load at first peak and the corresponding secant stiffness are reduced by around 50% when only one of the groups is attached. Second, the comparison between the ultimate load in the NM-simulation and the load at first peak obtained from the PA-simulation has shown, that the mere presence of the concrete corner has basically no influence on the capacity of the connection at first peak. Third, the inability to regain strength after the anchors reach their tension capacity in the NM-simulation suggests that the presence of the concrete corner does prevent the breakout of the anchors after they have lost their tensile capacity. This allows the connection to utilize the shear capacity of the anchors as the displacements increase, which ultimately allows the connection to regain its strength.

14.4.6 Behavior under 30° applied load angle

Figure 14.16 shows the load-displacement curve obtained from the numerical analysis of the connection for an applied load angle of 30° (green line). For reference, the load-displacement curve for an applied load angle of 45° (BGC-N-110-FA) has also been reproduced (black line). The x-axis refers to the displacement applied on the upper surface of the gusset plate as indicated in Figure 14.4 (a). The y-axis refers to total load on the connection calculated from the sum of forces of the loaded nodes in the

direction of loading. It can be seen that the overall behavior for an applied load angle of 30° is not significantly different from the behavior for an applied load angle of 45°. Both the loads at first peak and the ultimate loads decrease only marginally. So does the corresponding secant stiffness.

Figure 14.16. Load-displacement curves obtained from the numerical analysis of the corner configuration with varying load angles (h_{ef} = 110 mm).

A more distinct difference can be observed with respect to the distribution of forces among the two perpendicular anchor groups and with respect to the tension and shear force components in the anchors that form those groups. In order to evaluate the force distribution among the anchor groups, again the sum of anchor forces will be compared for both groups, respectively. In this context, the sum of anchor forces of one group will be referred to as the load acting on this group. For improved clarity, the tension and shear loads acting on the groups will be shown separately in Figure 14.17 (a) and (b), respectively. The loads are plotted as a function of the displacement steps. Note that at first peak, the anchor forces are in equilibrium with the load applied on the connection, while at ultimate load the deviation is around 3%. Thus, it can be assumed that the sum of anchor forces reasonably well represents the loads acting on the two groups throughout the analysis.

In contrast to the behavior for an applied load angle of 45°, the behavior of the two groups differs markedly in terms of load distribution and the way the forces are resisted by the anchors through tension and shear. The first peak in the load-displacement curve of the overall connection is reached when the anchors of the second group reach their ultimate tensile capacity. At this point, the second group predominantly resists the load through tension, while the first group resists the load rather evenly through tension and shear. Thereafter, the tension load on the second group drops drastically, whereby the group is able to maintain a residual tensile capacity. Nonetheless, after the loss of tensile capacity, the second group resists the loads predominantly through shear. In principle the behavior of the second group is comparable to the behavior observed for

an applied load angle of 45°. The anchors of the first group reach their ultimate tensile capacity shortly after the first peak has been reached. Thereby, the ultimate tensile capacity of the first group is lower than the capacity of the second group. This can be related to the relatively high shear loads that are simultaneously resisted by the anchors. From this point onwards, the anchors resist the load predominantly through shear. At the same time, a residual tensile capacity can be maintained by the anchors of the first group up to point where the ultimate load of the connection is reached. This residual tensile capacity is almost equal in magnitude to the one of the second group.

(a) Tension load   (b) Shear load
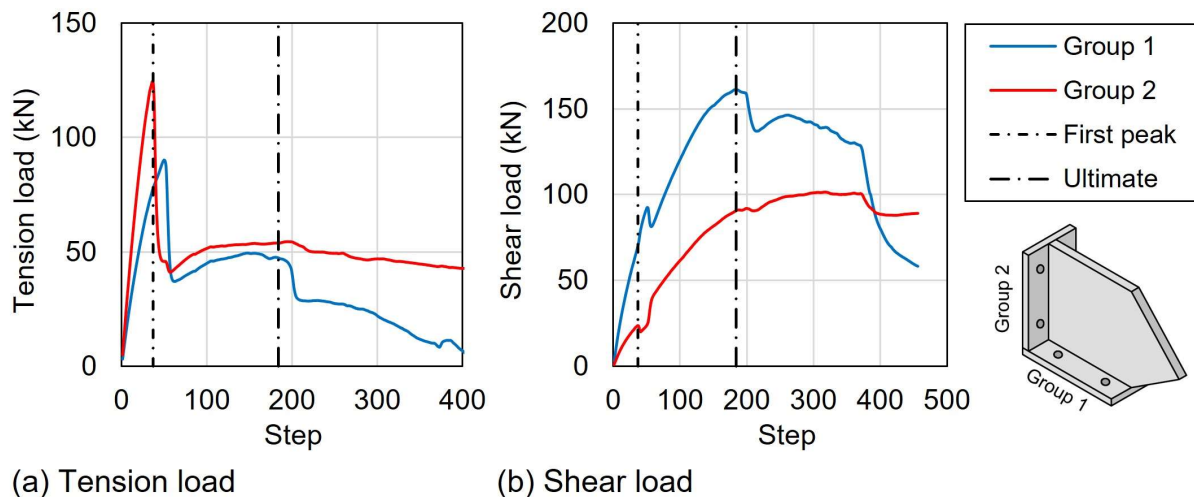
Figure 14.17. (a) Tension loads and (b) shear loads acting on the groups forming the anchor bracket. The results were determined for a configuration with h_{ef} = 110 mm.

In accordance with Section 14.4.4, the ratio between the tension and shear load component within the two groups can be expressed in terms of the internal load angles of the resulting internal forces. In contrast to the symmetrical configurations, where at first peak the load angles α_i of both groups where equal, in simulation BGC-N-110-30°, the angles of the two groups differ notably. At first peak, α_1 was obtained as 48° for the first group, and α_2 was obtained as 79° for the second group. The difference between the two groups is likely to be related to the difference in the displacement demand on both groups.

In conclusion, the variation of the applied load angle had only a minor effect on the general load-displacement behavior of the connection. This is an important finding since such a connection used for steel bracing may have different applied load angle based on the bay width and floor height in the structure. The distribution of forces, on the other hand, changed noticeably. Due to the variation of the applied load angle, which created an asymmetry, the loads were no longer equally supported by both groups. Since the load is applied in a displacement-controlled manner, an applied load angle of 45° results in equal displacement for both groups. However, in the case of an applied load angle of 30° as applied in simulation BGC-N-110-30°, the horizontal

component of the applied displacement is higher than the vertical component. As a result, the anchors in the second group are initially loaded predominantly in tension, while at the same time, the shear component of the anchors in the first group increases considerably compared to the previously discussed simulations. After the anchors in both groups have reached their maximum tensile capacity, the total load on the connection is resisted by the anchors mainly through shear. In accordance with the previous simulations, however, a residual tensile capacity can be observed after the preceding drop in load.

14.4.7 Influence of cyclic loading on the load-displacement behavior

Since one of the major intended uses of the investigated bracket configurations is the attachment of steel bracing for seismic retrofitting, the actual demands on the connection element will be cyclic in nature. The experimental results on single anchors (Chapter 5) and anchor groups (Chapter 8) have shown that cyclic loading has basically no influence on the load-displacement behavior of the anchors and anchor groups. In order to determine whether this also applies to this type of spatial bracket configuration, an additional simulation is performed. The configuration used is the same that was applied in simulation BGC-N-110-FA. Note that the intention of the simulation is to obtain a preliminary estimate of the influence of cyclic loading on the load-displacement behavior. In particular the question is addressed whether the damage caused by cyclic loading changes the progression of the load-displacement curve with respect to the observed first peak. For this purpose, five cycles at different displacement levels are applied, whereby the displacement amplitudes are smaller than the displacement corresponding to the first peak in the monotonic simulation with the same configuration. The applied displacement amplitudes were 0.025 mm, 0.055 mm, 0.085 mm, 0.11 mm, and 0.125 mm in the first, second, third, fourth, and fifth cycle respectively. The maximum load obtained in the cyclic phase corresponds to around 75% of the ultimate load in the monotonic simulation, which represents the characteristic resistance of the connection. After reaching the displacement amplitude in each cycle, the connection was unloaded to a displacement slightly above zero. The obtained load-displacement curve is shown in Figure 14.18. It can be seen that the shape of the load-displacement curve matches the behavior observed in the monotonic simulations. The load obtained at first peak and the ultimate load of the connection even increased in comparison to the monotonic simulation. In principle, these findings are in accordance with the experimental findings in this work and in the literature. The numerical results suggest that cyclic loading up to the characteristic resistance of the connection has basically no impact on the overall load-displacement behavior of the connection. However, due to the limitation of the study, these findings should be treated with caution. Further detailed numerical and experimental studies on cyclic behavior of bracket configurations are highly recommended but are out of scope of this work.
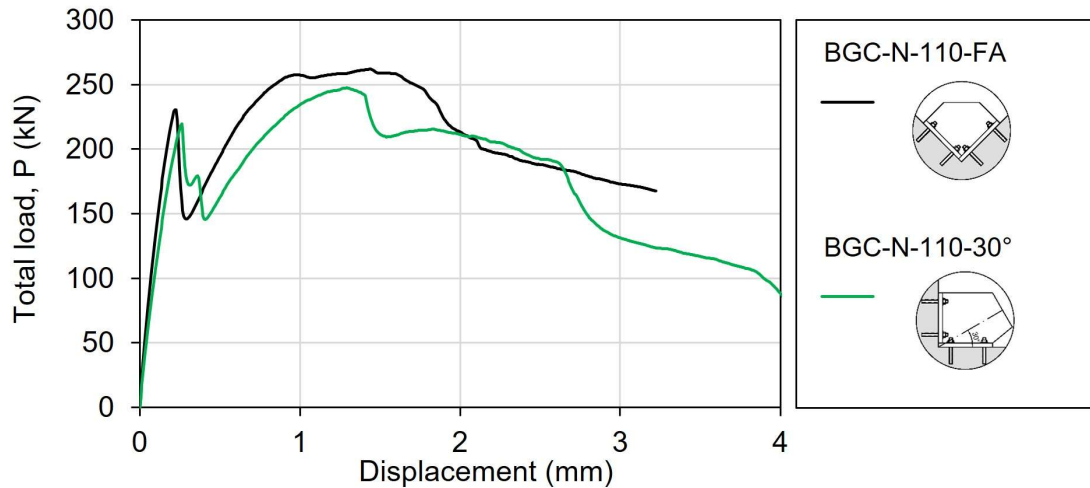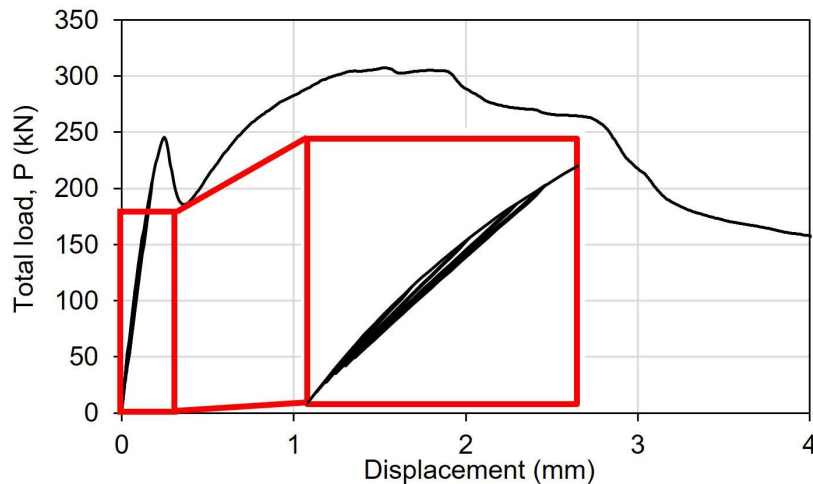
Figure 14.18. Load-displacement curve obtained from the numerical analysis of the corner configuration subjected to cyclic loading (h_{ef} = 110 mm).

14.5 Summary

In this chapter, numerical simulations were performed to gain a better understanding of the behavior of bracket configurations. The purpose of the numerical study was to investigate the distribution and redistribution of forces among the individual anchors, the influence of the corner on the capacity and displacement behavior, and the influence of varying embedment depths. The main focus of the investigation was to supplement the information gained from the experimental part. Thus, the geometry of the bracket-to-gusset plate connection were adopted from the experiments and the connection was monotonically loaded at an angle of 45°. The following conclusions can be drawn from the numerical results:

1. Under perfectly symmetric boundary conditions, it can be assumed that the loads are distributed equally among both groups, meaning that both groups participate equally in the load transfer. In particular up to the first peak, both the axial and the shear forces were essentially equal in all anchors. However, as the experiments have shown, such symmetry cannot be assumed in the second phase of the load-displacement curve after reaching the first peak. Nonetheless, the numerical results support the assumption of an equal behavior until the first peak is reached. Therefore, up to the first peak, the behavior of the complete connection can be composed of the load-displacement behavior of two independent groups of anchors.

2. For all simulated embedment depths, basically the same load transfer mechanism was observed in the initial phase, up to the first peak in the load-displacement curve of the connection. In this phase, the total load is largely resisted by the anchors through tension.

3. The drop of load after the first peak has been reached, which characterizes the load-displacement behavior of the bracket configuration, is due to the loss of tensile capacity of the anchors.

4. In the second phase, the anchors are able to utilize the shear capacity with increasing displacement of the connection. This is made possible by the presence of the concrete corner, which prevents the breakout of the anchors after they have reached the maximum tensile capacity.

5. The behavior in the second phase depends largely on the embedment depth of the anchors. For an embedment depth larger than 80 mm it was observed that all anchors of the connection are able to maintain a certain residual tensile capacity after their ultimate capacity has been reached. The observed residual capacity is likely to be related to stable compression struts, which allow the anchors to continue to transfer tension forces.

Two additional simulations were performed to allow an initial insight on the behavior of the spatial anchor configuration (i) for a different load angle and (ii) when subjected to cyclic loading. In spite of its limitations, the studies suggest following conclusions:

6. The numerical results for a load angle of 30° indicate that the overall load-displacement behavior of the connection does not change significantly. However, the distribution of forces among the anchors will change.

7. In accordance with the experimental findings for single anchors and anchor groups, cyclic loading up to the characteristic resistance of the connection obtained from the monotonic simulation appears to have no negative effect on the load-displacement behavior.

15 Analytical calculation approach for anchorages in spatial corner configurations

The scope of current standards and guidelines for the design of anchorages, such as EN 1992-4, is limited to two-dimensional (planar) anchor configurations. Spatial anchor configurations as investigated in this work are not covered by current standards. In order to allow the design of such connections, an analytical calculation approach for corner configurations is developed in this chapter, which is based on the experimental and numerical investigations. Thereby, the proposed concept follows the design approach given in EN 1992-4. First, the basic assumptions and the calculation approach are outlined, which were conceptualized based on the experimental and numerical investigations on symmetrical corner configurations loaded at an angle of 45°. The proposed calculation approach is then validated against the experimental data in this work. Subsequently, a generalized calculation approach is introduced which extends the initial concept to corner configurations with varying load angles or configurations where other types of post-installed anchors are used.

15.1 Assumptions behind the calculation approach

The major intended purpose of the calculation approach is the fastening of steel braces to an existing RC structure. Thereby, the anchors are only supposed to take up the load when the steel brace is under tension. Whereas, when the steel brace is under compression, the forces are directly transferred to the concrete structure by means of bearing pressure between the steel bracket and the concrete surface. Thus, the anchors are solely loaded in tension and shear. The experimental and numerical results indicate a reliable and rather constant behavior up to the first peak of the load-displacement curve of the connection. Thereupon, the failure mechanisms and the behavior become more complex and can vary rather strongly depending on the embedment depth of the anchors and potentially the type of anchor which is used to form the connection. Thus, the analytical calculation approach is focused on the behavior up to the first peak. For the development of an analytical calculation approach additional assumptions were made, which are presented in the following. A graphical representation of these assumptions is shown in Figure 15.1. Note that these assumptions were derived from the experimental and numerical investigations on symmetrical corner configurations which are loaded at an angle of 45°. In this context, the validity of the assumptions is initially limited to such connections.
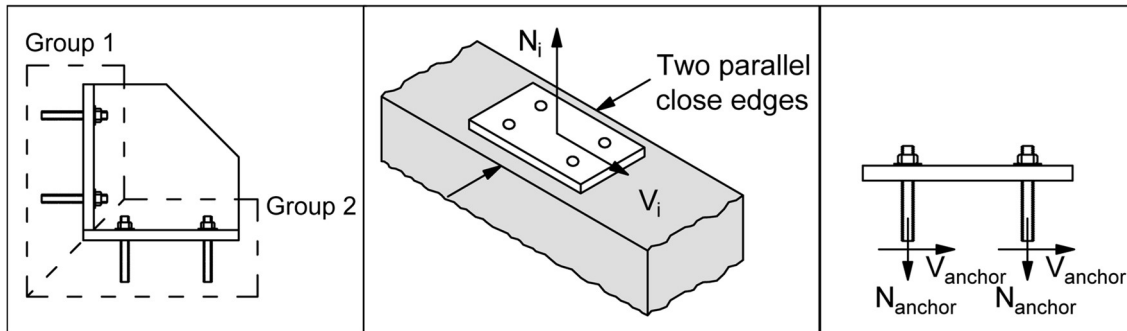
Figure 15.1. Graphical representation of the assumption made for the analytical calculation approach for corner configurations.

Assumption 1: The corner configuration can be treated as two independent perpendicular anchor groups, to which the total load on the connection is evenly distributed.

Justification for the assumption: The experimental and numerical results have shown that the total load is equally resisted by the two perpendicular anchor groups that form the connection. In the experiments it was shown that up to the first peak, the shear displacement of both groups was almost identical, indicating that both groups take up equal shear loads. Moreover, the evaluation of stresses in the gusset plate indicated an equal distribution of tension loads on both groups. The experimental findings are supported by the numerical results which showed that the sum of tension and shear forces in the anchors are equal in both groups.

Assumption 2: The capacity (resistance) of the two groups can be assessed individually. Thereby, the concrete corner and a mutual influence of the perpendicular anchor groups can be conservatively neglected.

Justification for the assumption: The numerical investigations on the partly attached connection have shown that at first peak, the behavior of the fully attached connection is basically composed of twice the behavior of the connection when only one anchor group is attached to the corner. Moreover, it was shown that when the connection is solely installed in a narrow concrete member (without the presence of a corner), the overall load-displacement behavior matches the behavior up to the first peak of the partly attached connection placed in the corner. These findings suggest that at first peak, the capacity of one group can be determined by considering only two parallel close edges and neglecting the presence of the concrete corner and the perpendicular anchor group.

Assumption 3: In one group, both the tension and shear loads are equally distributed among the anchors. Thus, the anchors equally participate in the load transfer meaning no eccentricity of loading is to be considered. Note that this assumption is valid for bonded anchors. Since the behavior of other types of anchors can vary from the

behavior of bonded anchors this assumption might not be valid for other types of anchors.

Justification for the assumption: The evaluation of the axial displacement of the anchors in the experiments showed an even progression over the duration of the experiments, indicating an even distribution of tension load among the anchors of a group. Moreover, due to the push through installation of the bonded anchors, the gap between steel plate and anchor is filled with mortar, which is why it can be assumed that the shear forces are equally distributed among the anchors. The conclusions drawn from the experimental results are supported by the evaluation of the individual anchor forces in the numerical analysis, which has shown that both the axial and shear forces in the anchors are almost identical up to the first peak.

Note that this assumption is limited to 2 x 2 anchor groups. In case of tension loaded anchor groups comprising of more than four anchors, such as 3 x 2 anchor groups, the distribution of forces among the anchors can be strongly influenced by the baseplate stiffness (Bokor, 2021). In this case, a sufficiently stiff baseplate should be ensured as stipulated by EN 1992-4. Nonetheless, the assumption of centric loading can be considered in these cases as well.

15.2 Description of the analytical calculation approach

The calculation approach follows a step by step procedure to determine the capacity of a corner configuration. As discussed above, it is assumed that both anchor groups which form the corner configuration are taking up equal loads. Therefore, in the first step, the tension and shear loads are determined that can be simultaneously resisted by one anchor group. For this purpose, the interaction equation for concrete related failure modes according to EN 1992-4 is considered:

$$\left(\frac{N_i}{N_R}\right)^{1.5} + \left(\frac{V_i}{V_R}\right)^{1.5} \leq 1. \tag{15.1}$$

Here, N_i and V_i are the tension and shear load component of one anchor group, respectively. N_R and V_R are the tension and shear capacity of an anchor group. The tension and shear capacity of an anchor group can be determined according to the CCD method, or by applying a displacement-based approach such as the spring modelling approach (Bokor, 2021). The latter case generally results in more accurate predictions of the tension capacity of anchor groups in narrow concrete members as shown in Chapter 11. For the calculation of the capacities, two parallel edges and centric loading are considered.

Note that due to the vicinity of two edges, often concrete related failure modes such as concrete cone failure and concrete edge failure are governing the tension and shear

capacity, respectively. Using the resulting internal load P_i, the internal tension and shear load components, N_i and V_i, can be expressed as follows:

$$N_i = P_i \cdot \sin \alpha, \tag{15.2}$$

$$V_i = P_i \cdot \cos \alpha. \tag{15.3}$$

Where α is the angle of the internal resulting force of the group. Substituting Equation (15.2) and (15.3) into Equation (15.1), the equation can be solved for P_i:

$$P_i = \sqrt[1.5]{1 / \left(\left(\frac{\sin \alpha}{N_R} \right)^{1.5} + \left(\frac{\cos \alpha}{V_R} \right)^{1.5} \right)}. \tag{15.4}$$

The resulting load P_i is the maximum load that can be resisted by one anchor group according to the design approach in EN 1992-4. Once P_i is calculated, the tension and shear load components can be determined using Equation (15.2) and (15.3). In other words, N_i and V_i represent the maximum tension and shear loads that can simultaneously be resisted by one group.

In the second step, the capacity of the corner configuration, P_{tot}, is calculated by assuming equilibrium of forces on the connection as indicated in Figure 13.17:

$$P_{tot} = \sqrt{(N_1 + V_2)^2 + (N_2 + V_1)^2}. \tag{15.5}$$

Due to the symmetry of the connection and the observation that the loads are evenly distributed to both groups, the tension load component of the first group is equal to the tension component of the second group, $N_1 = N_2 = N_i$. Accordingly, the shear component of the first group is equal to the shear component of the second group, $V_1 = V_2 = V_i$. Thus, in this case P_{tot} can be calculated as:

$$P_{tot} = \sqrt{2} \cdot (N_i + V_i). \tag{15.6}$$

In summary, first the tension and shear capacity of the anchor groups are calculated considering the anchor spacing and edge distance according to the given geometry of the corner configuration. Thereby, the vicinity to the concrete corner and the second perpendicular anchor group is neglected.

As the anchor groups are loaded in shear parallel to the edge, the shear failure load shall be taken as the smaller of the pry-out failure load or concrete edge failure load for loading parallel to the edge. To calculate the concrete edge failure load parallel to the edge for anchor groups with two parallel close edges, it is assumed that the shear load acting parallel to the edges is equally distributed to all anchors of the group. The

concrete edge failure load is calculated separately for each side of the narrow concrete member for a shear load acting parallel to the edge. Thereby, (on each side) only the anchors closest to the edge are effective. The concrete edge breakout capacity of the anchor group is taken as two times the breakout capacity of the anchors closest to the edge (Grosser, 2012). See also Figure 16.2 in Section 16.1.3.

Since generally tension and shear loads will act simultaneously on the anchor groups, the interaction equation provided in EN 1992-4 can be used to determine the tension and shear load components on the anchor groups based on the maximum capacity of the groups. Note that the interaction equation considers steel and concrete failure modes separately. Therefore, if steel failure is the dominant failure mode, the exponents in Equation (15.1) and (15.4) must be altered to k = 2. Finally, the total resistance of the corner configuration can be calculated by equilibrium of forces on the connection. If the total load on the connection is applied at an angle of 45°, it can be assumed that the forces are equally distributed among the two groups, resulting in equal tension and shear loads on both groups.

15.3 Application of the calculation approach to the corner configurations tested in this work and comparison with the experimental results

In all tests, the geometry of the investigated corner configurations in Chapter 13 was the same, while only the embedment depth of the anchors was varied. Two embedment depths were applied, namely h_{ef} = 80 mm and h_{ef} = 110 mm. In total, eight anchors were used to fasten the complete connection element to the concrete specimen, thus both groups of the connection comprised four anchors. In both groups, the spacing of the anchors was 80 mm in the direction perpendicular to the edges and 160 mm in the direction parallel to the edges. The distance to the edge was 80 mm on both sides of the anchor groups. For the calculation of the tension and shear capacities, the same geometrical conditions are adopted. The material properties, such as the mean concrete compressive strength are taken from the experiments as well. A detailed description of the configurations and material properties is given in Chapter 13.

For the described anchor groups, the mean tension and shear capacities for the relevant failure modes, which were calculated according to the CCD method, are given in Table 15.1. Note that the concrete is assumed to be uncracked. In accordance with the experimental and numerical findings, the design of the connection is governed by concrete related failure modes. In tension, concrete cone failure yields the lowest capacity for both embedment depths. In shear, the capacity is governed by the concrete edge failure mode for loading parallel to the edge. Therefore, for an embedment depth of 80 mm, the calculated tension and shear capacity are $N_{R,CCD}(80\,mm)$ = 78.5 kN and $V_{R,CCD}(80\,mm)$ = 138.0 kN, respectively. For an

embedment depth of 110 mm, the calculated tension and shear capacity are $N_{R,CCD}(110\ mm)$ = 77.1 kN and $V_{R,CCD}(110\ mm)$ = 148.2 kN, respectively.

Table 15.1. Calculated tension and shear capacities for 2 x 2 anchor group according to the CCD method for the relevant failure modes.

Load component	Failure mode	Calculated mean capacity (kN)	
		h_{ef} = 80 mm	h_{ef} = 110 mm
Tension	Steel failure	552.6	552.6
	Concrete cone failure	78.5	77.1
	Combined failure	136.3	114.1
	Splitting failure	225.8	342.8
Shear	Steel failure	278.8	278.8
	Concrete edge failure	138.0	148.2
	Pry-out failure	157.0	154.1

Once the capacities are determined, the tension and shear load components can be calculated using Equation (15.2) - (15.4). For this purpose, it is required to know the angle of the internal resulting force, α. The conventional solution would be to assume that the internal load angle corresponds to the angle of the applied load on the connection. Thus, α = 45°. In consequence, the tension and shear load component of the groups are of equal magnitude. However, the evaluation of stresses in the gusset plate suggests that the tension load that is resisted by the anchors of a group is larger than the shear load that is resisted by the anchors. In the numerical analysis it could be shown that indeed the capacity of the connection at first peak is governed by the tension resistance of the anchors. For the tested corner configurations, an internal load angle of α = 65° may be assumed to calculate the capacity of the individual groups. Following the proposed calculation approach, the total capacity of the configurations was calculated for both load angles. The results are summarized in Table 15.2. As can be seen, using the conventional solution, the calculated capacities are actually closer to the experimental results than when the capacity is calculated using the load angle obtained in the experimental and numerical studies. This somewhat unexpected finding can be explained by the observation that the CCD method underestimates the actual resistance of tension loaded anchor groups installed in narrow members (two parallel close edges), which was shown in detail in Chapter 11. This provides an explanation for why the approach with an angle of 65° yields rather low capacities, since the angle considers the tension dominant behavior of the groups. In turn, by using an angle of 45°, the tension dominant behavior is suppressed, and the shear component is actually overestimated. The overestimation of the shear component thus compensates for the conservatively calculated tension capacity, while at the same

time, the low tension capacity prevents the calculated capacity of the connection from being overestimated.

Table 15.2. Results of the analytical calculation approach for corner configurations using the CCD method to calculate the tension and shear capacity of the perpendicular anchor groups.

Test ID	α	P_{calc} (kN)	P_{calc} / $P_{exp,m}$
BGC-80	45°	175.0	1.01
BGC-110		176.2	0.80
BGC-80	65°	149.5	0.87
BGC-110		148.3	0.68

However, if a more realistic estimate of the tension capacity is provided, the overestimation of the shear component might result in an unsafe design when using the conventional solution. This is shown when the capacities of the corner configurations are calculated using the modification factor $\psi_{||,Approach2}$ (Chapter 11) to determine the tension capacity of the anchor groups. The results of the modified approach are provided in Table 15.3. It turns out that in these cases, not accounting for the actual performance of the anchors can result in a considerable overestimation of the capacity of the complete connection. At the same time, the realistic consideration of the tension and shear load components results in satisfactory estimates of the performance of the connection.

Consider a scenario where one of the groups is not installed in a beam but in a slab. In this case, it is not necessary to consider close edges and it can be assumed that the calculated capacities using the CCD method provide realistic estimates of the tension resistance. In this case, neglecting the way the anchors actually resist the applied loads through tension and shear may again result in an overestimation of the capacity of the connection.

These examples highlight the importance of considering the actual performance and displacement behavior of anchor connections. In particular when the connection is between two structural elements. This in turn means that if the internal load angle of the groups and thus the magnitude of the forces resisted through tension and shear does not correspond to the external load angle of the overall connection, the presented calculation approach, where an internal angle of 65° is assumed, cannot simply be applied to other connections with, for example, varying load angles or other types of anchors. Since the difference between the tension and shear load component is likely to be related to the difference between the tension and shear stiffness of the tested bonded anchors, a closer examination of the load distribution with respect to the stiffness of the anchors and the displacement behavior of the connection is provided

in the next section. Based on the theoretical considerations, a generalized analytical calculation approach is developed which is capable of directly considering the behavior of different types of anchors and corner configurations with varying load angles.

Table 15.3. Results of the analytical calculation approach for corner configurations using the modified approach according to Chapter 11 to calculate the tension capacity of the perpendicular anchor groups.

Test ID	α	P$_{calc}$ (kN)	P$_{calc}$ / P$_{exp,m}$
BGC-80		202.9	1.18
	45°		
BGC-110		219.7	1.00
BGC-80		181.1	1.05
	65°		
BGC-110		196.7	0.90

15.4 Generalized analytical calculation approach for corner configurations

An explanation for the observed differences between the tension and shear load components of the anchor groups can be found by considering the problem not from the perspective of forces that act on the connection but rather from the perspective of the applied displacement demand. For this reason, the following section first studies the displacement behavior of symmetric connections in which the load is applied at an angle of 45°. The findings that are derived from the study will then be applied to connections with arbitrary load angles.

15.4.1 Theoretical considerations for corner configurations with 45° load angle

The total applied displacement demand, s_P, can be split up into a horizontal (s_H) and a vertical (s_V) displacement component as shown in Figure 15.2. Since the displacement demand is applied at an angle of 45° it can be assumed that the magnitude of the horizontal and vertical displacement component is equal. The resulting displacement demand on the two groups is shown in Figure 15.2 (b) and (c). The displacement demand on the groups is resisted by the anchors through a tension and a shear component as discussed above. Thereby, the magnitude of the tension and shear load depends on the respective stiffness of the anchor group in tension and shear. Since the horizontal and vertical displacements are equal, the tension and shear load can be calculated as follows:

$$N_i = k_N \cdot s, \tag{15.7}$$

$$V_i = k_V \cdot s. \tag{15.8}$$

Where s is the displacement in both the horizontal and vertical direction, k_N is the tension stiffness of the anchor group, and k_V is the shear stiffness of the anchor group. Note that due to the fact that both anchor groups have the same geometry, it can be assumed that the stiffness values of both groups are the same. It can be seen that the ratio of the tension and shear force depends on the ratio between the tension stiffness and the shear stiffness:

$$\frac{N_i}{V_i} = \frac{k_N}{k_V}. \tag{15.9}$$

It becomes apparent that if the tension stiffness of the group is higher than the shear stiffness, the tension load will be larger than the shear load. The angle of the resulting load of the anchor group can therefore be determined as:

$$\alpha = \tan^{-1}\left(\frac{N_i}{V_i}\right) = \tan^{-1}\left(\frac{k_N}{k_V}\right). \tag{15.10}$$

Exemplarily, the angle α is determined for the corner configuration tested in test series BGC-110 (Chapter 13) and in the numerical analysis in simulation BGC-N-110-FA (Chapter 14). The configuration of the groups which form the bracket resembles the anchor group configuration tested in test series C-62 in narrow concrete members (tension loading, four anchors, equal anchor spacing, equal embedment depth and equal edge distance). Therefore, the stiffness k_N can be assumed as the mean initial stiffness of the anchor groups, which was around 200 kN/mm. According to Grosser (2012), the initial shear stiffness of a single M16 bonded anchor, which is installed close to the edge and loaded in shear in the direction parallel to the edge, can be assumed as 24 kN/mm. Since the gaps between the anchors and the steel plates were filled with mortar, the shear stiffness of the group, k_V, can be taken as four times the stiffness of a single anchor. Using Equation (15.10), the angle of the resulting load on the anchor groups is then calculated as $\alpha = 64°$. This value matches quite well with the experimental and numerical results.

Figure 15.2. Displacement demand on (a) complete connection, (b) first group, and (c) second group for corner configuration with 45° load angle.

The theoretical considerations emphasize the importance of the displacement behavior of anchors and anchor groups and support the experimental and numerical findings, which indicated that the way the forces are transferred from the bracing to the concrete largely depends on the stiffness of the anchors and the steel elements which form the connection. Provided the stiffness ratios are known, the above considerations can be used to extend the previous calculation approach, which is primarily based on experimental and numerical observations, to more general corner configurations with varying load angles or different types of anchors.

15.4.2 Theoretical considerations for corner configurations with 30° applied load angle

The variation of the angle of the applied load on the complete connection mainly causes an alteration of the distribution of forces among the two perpendicular anchor groups, and an alteration of the way the forces are resisted by the anchors within a group. Thus, the magnitude of the tension and shear component which resist the load on each group varies based on the angle of applied load. As shown in the numerical simulation BGC-N-110-30°, the tension load component of the first group differs from the tension component of the second group, $N_1 \neq N_2$. Accordingly, the shear component of the first group differs from the shear component of the second group, $V_1 \neq V_2$. In addition, the numerical analysis has shown that the ratio between the tension and shear component of the first group differs from the ratio observed for the second group. Also, the ratios differ from the one observed for both groups in the connection loaded at an angle of 45°.

As indicated in Figure 15.3, the horizontal component of the displacement is larger than the vertical component for the case where the load is applied at an angle of 30°. This in return means that also the displacement demands on both groups differ as indicated in Figure 15.3 (b) and (c). Consequently, the tension and shear load on the two groups can be calculated as follows:

$$N_1 = k_N \cdot s_H, \tag{15.11}$$

$$V_1 = k_V \cdot s_V, \tag{15.12}$$

$$N_2 = k_N \cdot s_V, \tag{15.13}$$

$$V_2 = k_V \cdot s_H. \tag{15.14}$$

Given that the displacement demands of the two groups differ, it is evident from Equation (15.11) - (15.14) that the respective ratio between shear and tension load will differ. With respect to Figure 15.3, the ratio for the first group can be expressed as:

$$\frac{N_1}{V_1} = \frac{k_N \cdot s_H}{k_V \cdot s_V} = \frac{k_N \cdot s_H}{k_V \cdot s_H \cdot \frac{\sin\theta}{\cos\theta}} = \frac{k_N}{k_V \cdot \frac{\sin\theta}{\cos\theta}}. \tag{15.15}$$

Similarly, the ratio of the second group is:

$$\frac{N_2}{V_2} = \frac{k_N \cdot s_V}{k_V \cdot s_H} = \frac{k_N \cdot s_V}{k_V \cdot s_V \cdot \frac{\cos\theta}{\sin\theta}} = \frac{k_N}{k_V \cdot \frac{co}{\sin\theta}}. \tag{15.16}$$

Once the ratio is known, the angle of the resulting load can be determined for both anchor groups, respectively. With the angle, the tension and shear component of the two groups can be calculated according to Section 15.2. Finally, the capacity of the complete connection can again be determined by equilibrium of forces using Equation (15.5). In this way, the capacity of a corner configuration can be determined for varying loading angles, provided that the stiffness of the two groups which form the bracket is known. Thereby, the calculation approach directly accounts for the varying displacement behavior of different types of anchors through the stiffness values.
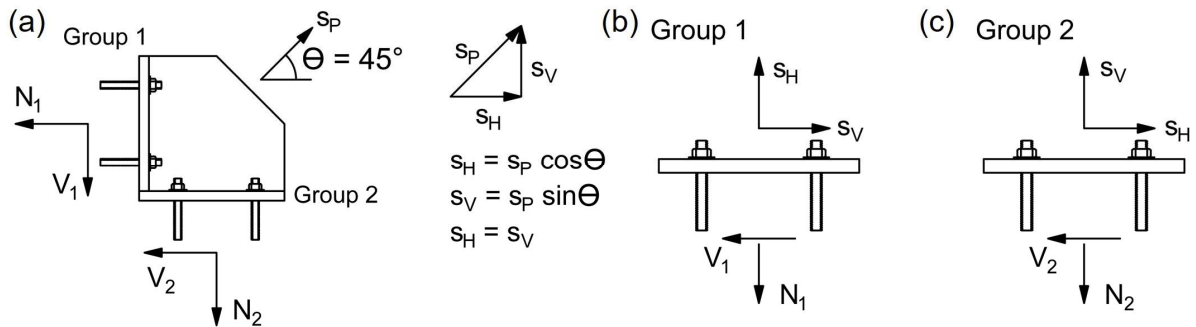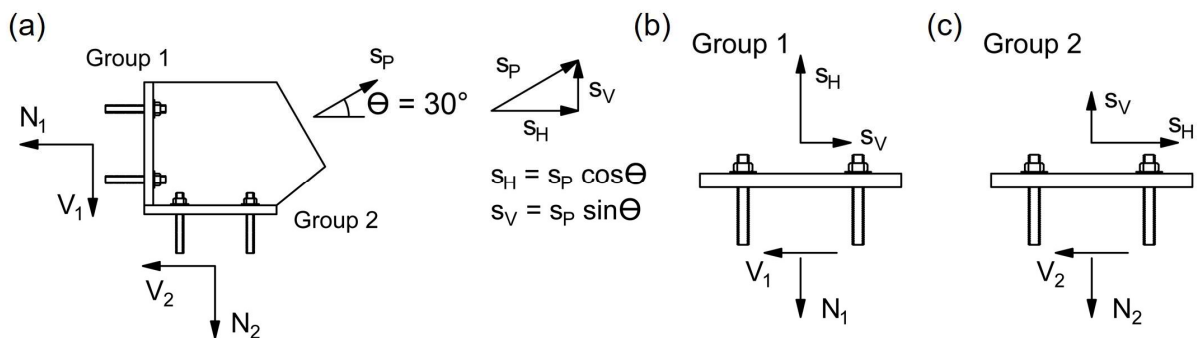

Figure 15.3. Displacement demand on (a) complete connection, (b) first group, and (c) second group for corner configuration with 30° load angle.

15.4.3 Example calculation for BGC-N-110-30°

In simulation BGC-N-110-30°, the dimensions of the steel bracket itself were the same as used for the corner configuration with a load angle of 45°. Since also the embedment depth of the anchors is equal, the stiffness values of the groups are the same as in Section 15.4.1, k_N = 200 kN/mm and k_V = 96 kN/mm. Also, the tension and shear capacity according to the CCD method are equal to the ones determined in Section 15.3 for an embedment depth of 110 mm. Hence, the calculated mean tension and shear capacity are $N_{Rm}(110\ mm)$ = 77.1 kN and $V_{Rm}(110\ mm)$ = 148.2 kN, respectively.

In the first step, the ratio between the tension and shear load of the anchor groups is determined. This is done for an applied load angle of θ = 30° according to Figure 15.3. The ratio for the first group is calculated according to Equation (15.5) as:

$$\frac{N_1}{V_1} = \frac{k_N}{k_V \cdot \frac{\sin\theta}{\cos}} = \frac{200}{96 \cdot \sin 30 / \cos 30} = 3.61$$

The ratio for the second group is calculated according to Equation (15.16) as:

$$\frac{N_2}{V_2} = \frac{k_N}{k_V \cdot \frac{\cos\theta}{\sin\theta}} = \frac{200}{96 \cdot \cos 30 / \sin 30} = 1.20$$

Using Equation (14.1), the corresponding angles of the resulting internal forces of the first and second group can then be calculated:

$$\alpha_1 = \tan^{-1}\left(\frac{N_1}{V_1}\right) = \tan^{-1}(3.61) = 75°$$

$$\alpha_2 = \tan^{-1}\left(\frac{N_2}{V_2}\right) = \tan^{-1}(1.20) = 50°$$

The calculated internal load angles match well with the angles obtained in the numerical analysis at the point where the first peak is reached ($\alpha_{1,num}$ = 79° and $\alpha_{2,num}$ = 48°).

Following the concept in Section 15.2, the capacities of the two groups and the corresponding tension and shear components can be calculated. At first, the resulting load P_i (maximum load that can be resisted by one anchor group according to the design approach in EN 1992-4) is calculated for both anchor groups according to Equation (15.4):

$$P_1 = \sqrt[1.5]{1/\left(\left(\frac{\sin\alpha_1}{N_{Rm}}\right)^{1.5} + \left(\frac{\cos\alpha_1}{V_{Rm}}\right)^{1.5}\right)} = \sqrt[1.5]{1/\left(\left(\frac{\sin 75}{77.1}\right)^{1.5} + \left(\frac{\cos 75}{148.2}\right)^{1.5}\right)} = 77.2\ kN$$

$$P_2 = \sqrt[1.5]{1/\left(\left(\frac{\sin\alpha_2}{N_{Rm}}\right)^{1.5} + \left(\frac{\cos\alpha_2}{V_{Rm}}\right)^{1.5}\right)} = \sqrt[1.5]{1/\left(\left(\frac{\sin 50}{77.1}\right)^{1.5} + \left(\frac{\cos 50}{148.2}\right)^{1.5}\right)} = 85.0\ kN$$

Using the resulting internal load P_i, the internal tension and shear load components, N_i and V_i, for both groups can be calculated using Equation (15.2) and (15.3), respectively:

$$N_1 = P_1 \cdot \sin \alpha_1 = 77.2 \cdot \sin 75 = 74.6 \ kN$$

$$V_1 = P_1 \cdot \cos \alpha_1 = 77.2 \cdot \cos 75 = 20.0 \ kN$$

$$N_2 = P_2 \cdot \sin \alpha_2 = 85.0 \cdot \sin 50 = 65.1 \ kN$$

$$V_2 = P_2 \cdot \cos \alpha_2 = 85.0 \cdot \cos 50 = 54.6 \ kN$$

Finally, the capacity of the corner configuration, P_{tot}, is calculated by assuming equilibrium of forces on the connection using Equation (15.5):

$$P_{tot} = \sqrt{(N_1 + V_2)^2 + (N_2 + V_1)^2} = \sqrt{(74.6 + 54.6)^2 + (65.1 + 20.0)^2} = 154.7 \ kN$$

The calculated capacity of the connection is obtained as 154.7 kN. This corresponds to 70% of the load at first peak obtained in the numerical analysis. The accuracy accords with the one achieved for corner configurations with a load angle of 45° when the load distribution is realistically accounted for (Table 15.2).

Using the modified approach for calculating the tension resistance of anchor groups in narrow concrete members, the calculated capacity increases to 202.9 kN, which corresponds to 92% of the load at first peak obtained in the numerical analysis. The results show that if the behavior of the connection is realistically accounted for, the proposed approach is able to accurately predict the capacity of a corner configuration at first peak even for varying load angles.

15.4.4 Special design case: Slotted holes

Connections with slotted holes are a special case, since by design, the anchors are not intended to transfer the loads through shear. If slotted holes are provided to all anchors of the bracket in the longitudinal direction, both anchor groups would solely resist the applied loads through tension. Considering a symmetric connection where the load is applied at an angle of 45°, the capacity of the complete connection can be calculated by vector addition of the tension capacity of the anchor groups. This is due to the equal horizontal and vertical displacement demand on the connection. However, if the load is applied at an angle different from 45°, the horizontal and vertical displacement demand will differ as indicated in Figure 15.3. Thereby, one group will resist the horizontal displacement demand and the other group will resist the vertical displacement demand. Provided the groups have the same dimensions, thus both groups have the same tension stiffness and capacity, the capacity of the complete connection is reached when the group with the higher displacement demand reaches its ultimate load. At the same time, the second group has not yet reached its ultimate capacity, since the displacement demand is smaller than for the first group. With reference to Figure 15.3, the ratio of the load acting on the two groups can be defined as follows:

$$N_1 = N_2 \cdot \frac{\cos \theta}{\sin \theta}, \tag{15.17}$$

$$N_2 = N_1 \cdot \frac{\sin\theta}{\cos\theta}. \tag{15.18}$$

Assuming the displacement demand on the first group is higher, the capacity of the connection can be calculated based on the tension capacity of the two groups, N_R, as:

$$P_{tot} = N_R \sqrt{1 + \left(\frac{\sin\theta}{\cos\theta}\right)^2}. \tag{15.19}$$

15.4.5 Closing remarks

The above introduced calculation approach accounts for the potential difference between the tension and shear stiffness of an anchor group by differentiating between the load angle of the externally applied load on the connection and the angle of the resulting load from the internal forces of one group. This results in a more complex and elaborate calculation approach compared to the conventional code-based approach. However, the conventional approach bears the potential risk of overestimating the actual load that a corner configuration can resist. In case of bonded anchors for example, the conventional approach overestimates the magnitude of load that is resisted by the anchors in shear, in turn increasing the calculated capacity of the connection. In contrast, the proposed analytical calculation approach accounts for the actual performance of the connection in a more realistic manner by considering the distribution of forces among the anchors.

The application of the proposed calculation approach requires the tension and shear stiffness of the anchor groups. Thereby, the stiffness values of the two groups which form the bracket should be equal. One way to obtain the stiffness values of the anchor groups without extensive experimental investigations is to use the nonlinear spring modelling approach by Bokor (2021). The tension and shear capacities which are also obtained from the analysis can then directly be used to design the corner configuration.

The proposed calculation approach is only applicable for corner configurations where the steel brace is attached at an angle between 30° and 60°. This range covers the common dimensions of RC frame structures. Angles beyond this range were not investigated in this work and may exhibit a deviating structural behavior.

15.5 Summary

Based on the experimental and numerical investigations in Chapter 13 and 14, an analytical calculation approach for corner configurations has been developed in this chapter. The basic assumptions and the calculation approach were first outlined for symmetrical corner configurations where the load is applied at an angle of 45° with respect to the anchor groups forming the bracket. Based on theoretical considerations

regarding the displacement behavior of the connection and the evaluation of the tension and shear stiffness of the anchor groups, the proposed calculation approach was then extended to corner configurations with varying load angles. Due to the consideration of the tension and shear stiffness of the anchor groups, the proposed calculation approach directly accounts for the use of different types of post-installed anchors.

The proposed calculation approach is able to provide information on the capacity of a corner configuration when both groups have the same tension and shear stiffness. However, it is not able to provide information on the displacement behavior of the complete connection. Thus, it cannot directly be applied in a performance based approach. The possible use of arbitrary configurations and the analysis of the displacement behavior is enabled through displacement-based calculations, which will be discussed in the next chapter.

16

Nonlinear spring modelling approach for spatial anchorages in corner configurations

In this chapter, the nonlinear spring modelling approach (Bokor, 2021) is applied to simulate and assess the behavior of spatial anchorages in corner configurations. The spring characteristics, which are required to model the anchor behavior, were determined for concrete cone failure and concrete edge failure to model the anchor behavior in tension and shear, respectively. In Section 16.1 the modelling approach is described, including the definition of the anchor spring characteristics for the tension and shear component, and the modifications made to consider the behavior of the anchors observed in the experimental and numerical investigations. In Section 16.2, the modelling approach is validated against the experimental results. Section 16.3 brings together the findings of this work by providing a case study to illustrate how such an anchorage for corner configuration can be designed and implemented in the context of a performance based approach for the strengthening of RC frame structures by means of steel bracing.

16.1 Concept

16.1.1 Basic modelling approach

Modelling spatial anchorages in corner configurations basically follows the approach described in Section 3.2.4, whereby the basic components of the nonlinear spring model are essentially the same as presented in Bokor (2021) for tension and shear loaded anchor groups. A schematic depiction of the complete model and the basic elements is given in Figure 16.1.

To model the gusset plate and the anchor bracket, 2D finite shell or 3D finite solid elements can be used. By doing so, the deformations of the steel elements that occur due to elongation and deflection are directly included in the analysis of the load-displacement behavior of the complete connection. Moreover, this approach allows the assessment of stresses in the gusset plate and the anchor bracket at all loading stages. The direct transmission of compression forces from the anchor bracket to the concrete is simulated by means of compression-only springs. The behavior of the anchors is considered individually for the two loading directions. The behavior in the axial loading direction is modelled by means of tension-only springs. The anchor behavior in the direction perpendicular to the axis of the anchors is simulated by means of shear

springs. For the case at hand, the shear load is acting in the direction parallel to the edges. Here, bi-directional shear springs for concrete edge failure are defined.

The investigations so far have shown that the overall load-displacement behavior of the bracket-to-gusset plate connection depends on the distribution and redistribution of tension and shear forces on the anchors and hence on the stiffness and nonlinear behavior of the anchors in tension and shear. If the complete load-displacement behavior of the connection is to be accurately determined by a model, it is necessary to perform a nonlinear static analysis in displacement control (Bokor, 2021).

As indicated in Figure 16.1, the total load on the connection is applied on the inclined surface of the gusset plate. With respect to the connection investigated in the experiments, the load angle was 45°. In the finite element software SAP2000, which was used to perform the analysis, the inclined loading case was simulated by applying the load equally in two directions (vertical and horizontal component). Consequently, in the case of a load angle of 45°, the magnitude of the load was equal in both directions. For load angles different from 45°, the magnitude of the load components in the two directions has to be adjusted accordingly. The nonlinear static analysis is performed in displacement control but not with displacement based loading. The analysis is performed by incrementing the displacement at the monitored node in small steps until the target displacement is reached. At each step, an iterative analysis is carried out to solve the nonlinear equations and ensure that the required load ratio is maintained. Note that although the displacements are incremented in nonlinear static analysis, at each step the ratio of applied forces is maintained constant. Therefore, if the analysis requires, the displacements are iteratively adjusted by the program to maintain the load angle of 45 degrees.
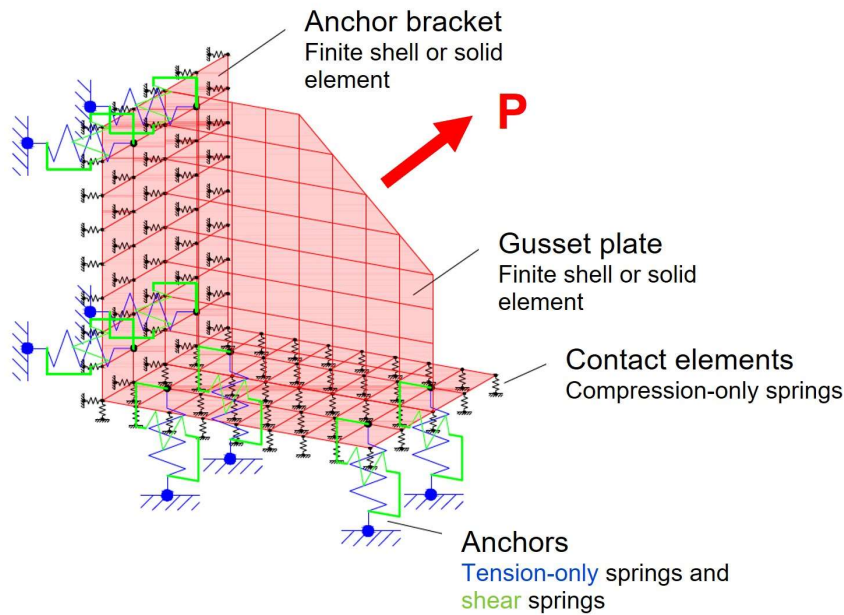
Figure 16.1. Schematic depiction of the spring model for corner configurations and its basic components.

16.1.2 Spring characteristics of the anchors for concrete cone failure

16.1.2.1 Characteristics of the load-displacement curve for single anchor spring

In order to idealize the load-displacement behavior of single anchors, the hexa-linear format introduced in Chapter 6 is applied. The characteristic points which define the idealized curve can either be determined from single anchor reference tests to best fit the experimental curves. Or if no reference tests are available, the characteristic points can be defined according to Table 6.1 for anchors failing due to concrete cone failure. In the latter case, the ultimate load of the anchors, the secant stiffness at ultimate load and the initial stiffness at 50% of the ultimate load in the ascending branch of the load-displacement curve have to be known.

16.1.2.2 Residual tensile strength of the anchors

The hexa-linear format accounts for the ability of the anchors to retain some residual strength after the formation of a concrete cone due to ability of concrete to transmit forces across cracks.

The numerical investigation on the individual anchor forces (Section 14.4.3) has shown that in case of larger embedment depths, the anchors exhibit a more pronounced residual tensile capacity which allows the anchors to continuously transfer forces through tension even after the ultimate tension load has been reached. This beneficial effect arises as the compression strut in the corner of the concrete specimen stabilizes after the tension capacity of the anchors has been reached, and, in particular, allows

the front anchors to retain some of their strength with increasing displacements. For the investigated bonded anchors, it appears that the residual tension load that can be resisted by the anchors increases with increasing embedment depth. However, further studies are required to verify the degree of residual capacity of the anchors for different embedment depths. Moreover, other parameters such as the diameter of the anchors, the relative distance to the corner and the relative distance to the parallel edges should be investigated to provide a valid conclusion. Aware of the limited data, a tentative relationship between the residual tensile capacity and the embedment depth can nonetheless be derived from the experimental and numerical results of this work. The results suggest that the residual tensile capacity increases from around 20% of the ultimate load at an embedment depth of 80 mm to 80% of the ultimate load at an embedment depth of 160 mm. In between, a linear progression may be assumed. This residual tensile strength observed in the numerical studies persisted roughly until the point where the ultimate load of the connection is reached.

Note that the realistic consideration of the residual tensile capacity is mainly intended for research purpose. For design purpose, the value of 20% of the ultimate tension load of the individual anchors should be taken. In this way, the design approach is harmonized, resulting in reasonably conservative results for larger embedment depths.

16.1.2.3 Definition of spring characteristics for individual anchors of the connection

Based on the spring characteristics of unrestricted single anchors, Bokor (2021) determines the spring characteristics of individual anchors within a group by means of the tributary area approach (see Chapter 3). In this way, the vicinity of close edges and the spacing of the anchors is accounted for.

When the connection element is installed in the beam and column forming the joint corner, besides the anchor spacing, two parallel close edges have to be considered to determine the tributary area of the individual anchors. Similar to the analytical calculation approach, however, the presence of the joint corner and the perpendicular anchor group are neglected. Taking the corner configuration investigated in the experimental part as an example, the spring characteristics of all eight anchors which form the connection are identical.

16.1.3 Spring characteristics of the anchors for concrete edge failure in narrow concrete members

16.1.3.1 Characteristics of the load-displacement curve for single anchor spring

In accordance with the idealized behavior for tension loaded anchors failing due to concrete cone failure mode, a hexa-linear format is applied for shear loaded anchors. In case of the investigated corner configurations, the anchors are installed close to the edge and the shear load is acting in the direction parallel to the edge. Therefore, the

characteristic points can either be determined to best fit the load-displacement curves obtained from single anchor reference tests, where the anchors are placed close to one edge and where the shear load is applied in the direction parallel to the edge. Or, if no reference tests are available, the characteristic points can be defined according to Table 6.1. The definition of the characteristic points in Table 6.1 is based on Bokor (2021) and principally follows the one for tension loaded single anchors failing due to concrete cone failure. Only the displacement of point F was changed to $1.5s_E$.

Note that if the ultimate load, V_u, is calculated according to the CCD method, the factor $\psi_{\alpha,V} = 2$ should be considered to account for the fact that the shear load is acting parallel to the close edge (EN 1992-4).

Table 16.1. Characteristic points of the idealized load-displacement curve for concrete edge failure of single anchors.

Point	Load (V_A – V_G)	Displacement (s_A – s_G)	Secant stiffness (k_1 – k_5)
A	0	$s_A = 0$	0
B	$0.8V_u$	$s_B = 0.8V_u / k_{50\%Vu}$	$k_1 = k_{50\%Vu}$
C	V_u	$s_C = V_u / k_{Vu}$	$k_2 = k_{Vu}$
D	V_u	$s_D = 1.25V_u / k_{Vu}$	$k_3 = 0.8k_{Vu}$
E	$0.2V_u$	$s_E = 2V_u / k_{Vu}$	$k_4 = 0.1k_{Vu}$
F	$0.2V_u$	$s_F = 1.5s_E$	$k_5 = 0.67k_4$
G	0	$s_G = s_F$	0

16.1.3.2 Definition of spring characteristics for individual anchors of the connection

The spring characteristics of the individual anchors of the connection are determined based on the tributary area approach presented in Bokor (2021). Again, the vicinity to the concrete corner and the perpendicular anchor group is neglected.

In case of shear loaded anchor groups installed in narrow concrete members, where the load is applied in the direction parallel to the edges, concrete edge failure is apparent on both sides of the narrow concrete member as shown in experiments conducted by Grosser (2012). It is assumed that the shear load acting parallel to the edges is equally distributed to all anchors of the group. Accordingly, the concrete edge failure load is calculated separately for each side of the narrow concrete member for a shear load acting parallel to the edge as explained in Chapter 15. This means that on each side, the anchors closest to the edge are effective. In the example given in Figure 16.2, a 2 x 2 anchor group installed in a narrow concrete member is loaded in shear in the direction parallel to the edges. In this example all anchors are effective. Anchors A and C on one side and anchors B and D on the other side. Accordingly, the tributary areas are determined for the anchors that are closest to the edge on the respective side. Figure 16.2 exemplarily shows how the tributary areas are determined for the

individual anchors in a 2 x 2 anchor group. Since only one anchor row is considered at a time, the tributary area approach, and the tributary volume approach (Bokor, 2021) lead to same results.
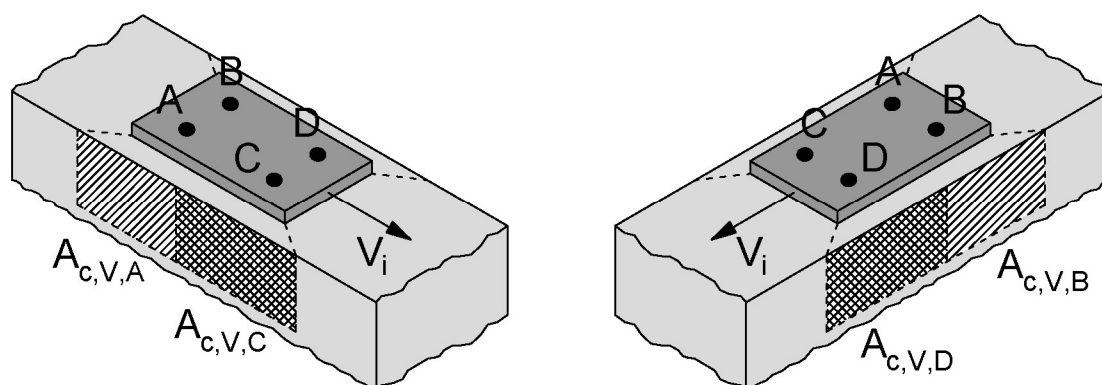
Figure 16.2. Segmentation into tributary areas for a 2 x 2 anchor group installed in a narrow concrete member and loaded in shear in the direction parallel to the edges.

16.2 Validation against experimental results

In this section, the nonlinear spring modelling approach for spatial anchorages in corner configurations is validated against the experimental results from this work, which were presented in Chapter 13. It should be noted that the experimentally obtained load-displacement curves, which are used to compare the simulated behavior of the corner configurations, are again shown in this chapter to facilitate the comparison.

16.2.1 Test series BGC-80

Since no single anchor reference tests have been performed in the experimental program, the spring characteristics for concrete cone failure of a single anchor are determined using the calculated mean capacity for concrete cone failure of a single anchor according to the CCD method. Thus, for an embedment depth of 80 mm and a mean cylinder concrete compressive strength of 25.0 N/mm², the mean ultimate load of a single anchor is determined as 52.3 kN. The required stiffness values $k_{50\%Nu}$ and k_{Nu} are taken from the results of the single anchor tests in Chapter 9 as 311.4 kN/mm and 69.7 kN/mm, respectively. Table 16.2 summarizes the corresponding spring characteristics of a single anchor for concrete cone failure.

Table 16.2. Spring model characteristics for concrete cone failure of a single anchor and individual anchors of the corner configuration in test series BGC-80.

	Load $N_{Rm,c,A-G}$ (kN)	Secant stiffness k_{1-5} (kN/mm)	Displacement, s_{A-G} (mm)
Single anchor			
A	0.0	0.0	0.000
B	41.8	311.4	0.134
C	52.3	69.7	0.750
D	52.3	55.8	0.938
E	10.5	7.0	1.501
F	10.5	5.3	1.996
G	0.0	0.0	1.996
Individual anchors of the corner configuration			
A	0.0	0.0	0.000
B	17.5	311.4	0.056
C	21.8	69.7	0.313
D	21.8	55.8	0.391
E	4.4	7.0	0.626
F	4.4	5.3	0.833
G	0.0	0.0	0.833

The spring model characteristics of the individual anchors in a group are determined on basis of the tributary area approach (Bokor, 2021). Similar to the analytical calculation approach, the two perpendicular anchor groups which form the bracket are considered independently. Thus, for the calculation of the tributary areas, a 2 x 2 group with two close edges is considered, which means that the individual areas of the anchors are equal. Since the two groups that form the bracket have the same geometry, all the anchors in the connection have the same tributary area and therefore the same spring characteristics. The spring characteristics of the individual anchors of the corner configuration in test series BGC-80 for concrete cone failure are provided in Table 16.2.

In a similar way, the spring characteristics for concrete edge failure are determined. Using the CCD method, the mean ultimate load for concrete edge failure of a single anchor loaded parallel to the edge is calculated as 41.4 kN. According to Grosser (2012), the initial stiffness $k_{50\%Vu}$ of M16 single bonded anchors loaded in the direction parallel to the edge can be assumed as 24.0 kN/mm. The secant stiffness corresponding to the ultimate shear load of a single anchor is assumed as 9 kN/mm. Following the tributary area approach, the capacities of the individual anchors can be determined. Equivalent to the tension spring characteristics, the shear spring characteristics are equal for all individual anchors of the connection. Table 16.3

summarizes the corresponding spring characteristics of a single anchor and the individual anchors of the corner configuration for concrete edge failure.

Table 16.3. Spring model characteristics for concrete edge failure of a single anchor and individual anchors of the corner configuration in test series BGC-80.

	Load $V_{Rm,c,A-G}$ (kN)	Secant stiffness k_{1-5} (kN/mm)	Displacement, s_{A-G} (mm)
Single anchor			
A	0.0	0.0	0.000
B	33.1	24.0	1.379
C	41.4	9.0	4.600
D	41.4	7.2	5.750
E	8.3	0.9	9.222
F	8.3	0.6	13.833
G	0.0	0.0	13.833
Individual anchors of the corner configuration			
A	0.0	0.0	0.000
B	27.6	24.0	1.150
C	34.5	9.0	3.833
D	34.5	7.2	4.792
E	6.9	0.9	7.667
F	6.9	0.6	11.505
G	0.0	0.0	11.505

The gusset plate and the anchor bracket were modelled using shell elements, where Young's Modulus for steel was considered as E_s = 200000 N/mm². The loads were directly applied onto the nodes of the gusset plate. Thereby, the load was applied in displacement-control by incrementally increasing the displacement, while maintaining the force ratio in two directions. The analysis was performed using the finite element software SAP2000.

Figure 16.3 shows the load-displacement curves obtained through the spring modelling approach compared to the respective curves obtained in the experiments. It can be seen that the overall progression of the curve obtained from the simulation matches well with the experimental curves. In the beginning the simulation is somewhat stiffer compared to the experimental curves. However, it should be noted that the bolted connection which was used in the experiments was not simulated in the analysis. After the first peak has been reached, the nonlinear spring modelling approach is able to accurately capture the drop of load and the subsequent regaining of strength up to the ultimate load of the connection. Thereby, the simulated curve shows a more severe drop of load. With respect to the obtained loads, the results of the analysis match well with the experimental results. In the nonlinear spring modelling approach, the obtained

loads are, however, slightly higher than the mean loads obtained in the experiments. At first peak, the calculated load is around 3% larger and the ultimate load is around 6% larger. On the whole, the comparison shows a satisfying agreement between the modelled and the experimental load-displacement behavior.
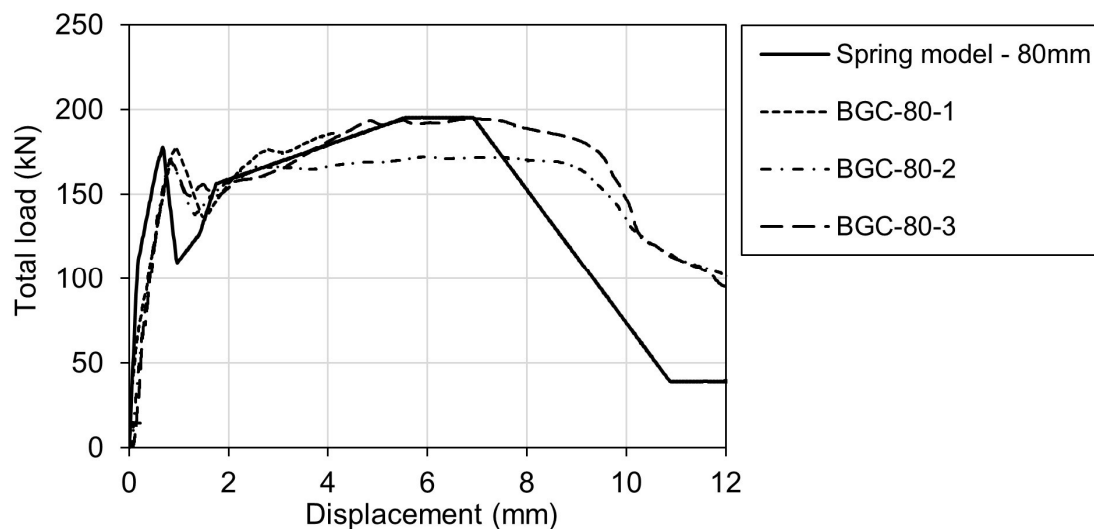
Figure 16.3. Comparison between spring modelling approach and experimentally obtained load-displacement curves for test series BGC-80.

16.2.2 Test series BGC-110

Again, the mean ultimate load of a single anchor for concrete cone failure is calculated according to the CCD method. For an embedment depth of 110 mm and a mean cylinder concrete compressive strength of 25.0 N/mm², the mean ultimate load of a single bonded anchor is calculated as 84.4 kN. In order to define the spring characteristics of a single anchor, the required stiffness values are taken from the experimental results in Chapter 9. For single bonded anchors with an embedment depth of 110 mm, the initial stiffness is considered as $k_{50\%Nu}$ = 274.3 kN/mm and the secant stiffness at ultimate load as k_{Nu} = 79.0 kN/mm. Using the tributary area approach, the tension spring characteristics of the individual anchors are determined. A summary of the respective tension spring characteristics for a single anchor and for the individual anchors of the corner configuration in test series BGC-110 is provided in Table 16.4.

As discussed above, the tension load that the bonded anchors in a corner configuration can resist after the ultimate load has been reached appears to increase with increasing embedment depth. To account for this effect, the load corresponding to point E and F is considered as 40% of the ultimate load instead of 20%. The residual strength is maintained approximately up to the point where the complete connection reaches its ultimate load. In the spring modelling approach this observation is considered by extending the length of the residual branch up to the point where the corresponding ultimate shear load of the anchors is reached (see Table 16.5). For this purpose, the

displacement of point F and G are modified with respect to the displacement corresponding to the ultimate shear load of the anchors.

Table 16.4. Spring model characteristics for concrete cone failure of a single anchor and individual anchors of the corner configuration in test series BGC-110.

	Load $N_{Rm,c,A\text{-}G}$ (kN)	Secant stiffness $k_{1\text{-}5}$ (kN/mm)	Displacement, $s_{A\text{-}G}$ (mm)
Single anchor			
A	0.0	0.0	0.000
B	67.5	274.3	0.246
C	84.4	79.0	1.068
D	84.4	63.2	1.335
E	33.8	15.8	2.137
F	33.8	10.6	3.171
G	0.0	0.0	3.171
Individual anchors of the corner configuration			
A	0.0	0.0	0.000
B	18.2	274.3	0.066
C	22.8	79.0	0.288
D	22.8	63.2	0.361
E	9.12	15.8	0.577
F	9.12	3.4	2.646
G	0.0	0.0	2.646

According to the CCD method, the mean ultimate load for concrete edge failure of a single anchor loaded parallel to the edge is calculated as 44.4 kN. The initial stiffness $k_{50\%Vu}$ is taken as 24.0 kN/mm. Note that the same stiffness value was considered for an embedment depth of 80 mm, since the initial shear stiffness is not significantly influenced by the embedment depth of the anchors (Grosser, 2012; Bokor, 2021). The secant stiffness corresponding to the ultimate shear load of a single anchor is assumed as 14 kN/mm. The capacities of the individual anchors were determined following the tributary area approach. A summary of the shear spring characteristics for a single anchor and the individual anchors of the corner configuration in test series BGC-110 is given in Table 16.5.

The gusset plate and the anchor bracket were modelled using shell elements with Young's Modulus for steel, E_s = 200000 N/mm². The loads were directly applied onto the nodes. Thereby, the load was applied in displacement-control by incrementally increasing the displacement, while maintaining the load ratio in two directions. The analysis was performed using the finite element software SAP2000.

Table 16.5. Spring model characteristics for concrete edge failure of a single anchor and individual anchors of the corner configuration in test series BGC-110.

	Load $V_{Rm,c,A-G}$ (kN)	Secant stiffness k_{1-5} (kN/mm)	Displacement, s_{A-G} (mm)
Single anchor			
A	0.0	0.0	0.000
B	35.5	24.0	1.479
C	44.4	14.0	3.171
D	44.4	11.2	3.964
E	8.9	1.4	6.343
F	8.9	0.9	9.515
G	0.0	0.0	9.515
Individual anchors of the corner configuration			
A	0.0	0.0	0.000
B	29.6	24.0	1.235
C	37.1	14.0	2.646
D	37.1	11.2	3.308
E	7.4	1.4	5.293
F	7.4	0.9	7.940
G	0.0	0.0	7.940

The comparison between the experimental results and the results obtained from the analysis are shown in Figure 16.4 in terms of the load-displacement curves. In principle, the load-displacement curve obtained from the numerical analysis follows the experimental curves. As can be seen, the ultimate loads are in a good agreement. Thereby, the ultimate load obtained from the analysis is around 4% higher compared to the mean ultimate load obtained from the experiments. The good agreement demonstrates that the approach followed to account for the residual tensile capacity of the anchors, adequately represents the real behavior. At first peak however, the calculated load is markedly lower compared to the experiments. In comparison to the experimental results, the analysis underestimates the load at first peak by around 18%. The underestimation of the actual capacity at first peak is likely to be related to the design approach for tension loaded anchor groups installed in narrow concrete members. It has been shown in Chapter 11 that with decreasing relative edge distance, the conservatism of the CCD method increases. While the nonlinear spring modelling approach already neglects the reduction factor $\psi_{s,N}$, the reduction of the individual anchor capacities due to the tributary area approach still appears to be rather high in case of two parallel close edges. Analogous to the findings regarding the CCD method, it can be assumed that the actual capacity of the individual anchors is underestimated to a greater extent as the relative distance decreases. This is indicated by the good agreement of the results at an embedment depth of 80 mm.

Figure 16.4. Comparison between spring modelling approach and experimentally obtained load-displacement curves for test series BGC-110.

To overcome this issue, the modification factor $\psi_{\|,Approach2}$ (Equation (11.2)), which was proposed in Chapter 11 can be applied to increase the capacity of the individual anchors. Since the factor was developed to modify the CCD method in case of two parallel close edges, it cannot readily be applied as it accounts for a reduction due to the factor $\psi_{s,N}$. It is therefore necessary to first adapt the proposed modification factor by multiplication with said reduction factor. Application of the factor for an embedment depth of h_{ef} = 110 mm and a distance of the anchors to the parallel edges of c_2 = 80 mm results in a 17% increase in tension load capacity. Figure 16.5 shows the load-displacement curve obtained through the modified spring modelling approach compared to the respective experimental curves. It can be seen that adjusting the tension spring characteristics according to the modification factor results in an increased load of the connection at first peak. In this way, the calculated load at first peak can be increased from 179.3 kN to 209.6 kN, which corresponds to 95% of the experimental mean load at first peak. At the same time, the analysis of the spring model predicts the remaining load-displacement behavior of the connection in accordance with that observed with the unmodified approach. Thus, the modification of the tension spring characteristics mainly alters the behavior in the first phase up to the first peak. This observation is in accordance with the experimental and numerical findings and shows the capability of the nonlinear spring modelling approach to accurately predict the behavior of such a spatial corner configuration.
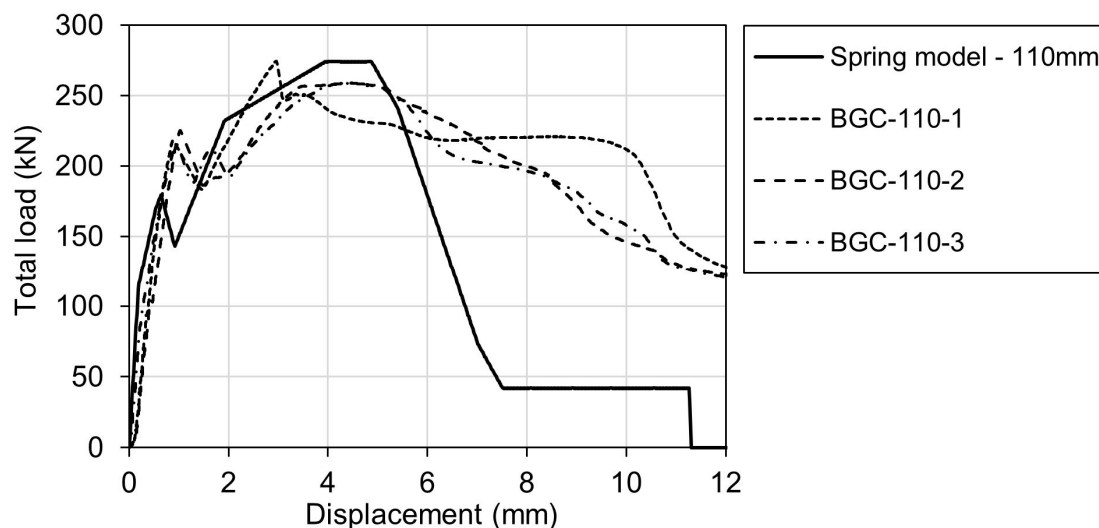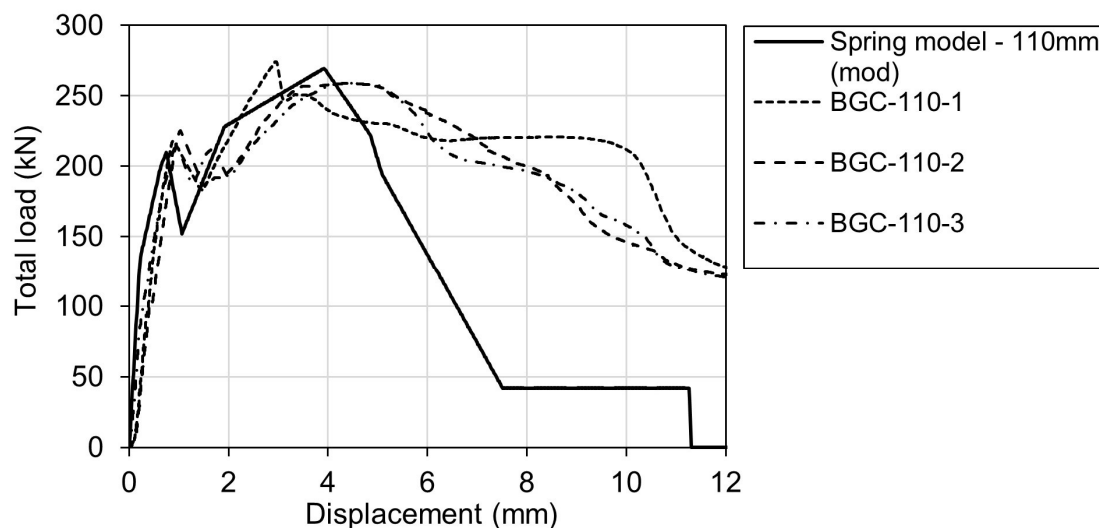
Figure 16.5. Comparison between modified spring modelling approach and experimentally obtained load-displacement curves for test series BGC-110.

16.3 Case study

The aim of this work has been the development of a suitable design approach for spatial anchorages in corner configurations for the purpose of directly connecting steel braces to RC frame structures. In this context both an analytical calculation approach and a displacement-based calculation solution on basis of the nonlinear spring modelling approach (Bokor, 2021) have been presented. The analytical calculation approach solely provides information on the capacity of the complete connection. It is mainly intended to design the anchorage in such a way that yielding of the steel bracing is ensured. In other words, the capacity of the connection between steel bracing and RC frame must be high enough to ensure the intended design purpose of the retrofit solution. The displacement-based calculation solution provides information on the complete load-displacement behavior of the connection. The obtained information can be used to implement the actual behavior of the connection in a performance based design solution to assess the overall behavior of the retrofitted structure.

The proposed calculation approaches have been validated against experimental and numerical results. In this section, they are exemplarily applied to demonstrate how the design of such a direct fastening solution with post-installed anchors can be carried out. For this purpose, a simple four-story RC frame structure is assessed in the context of pushover analysis. The details of the RC frame are presented below. In the following, the term "original structure" refers to the structure without retrofitting.

16.3.1 Description of the original structure

The original structure is a moment resisting RC frame structure with one bay and four stories. The structure has a total height of 10.7 m and a bay width of 3.85 m. The

corresponding line diagram is shown in Figure 16.6 (a). Each story has a height of 2.675 m. The finite element software SAP2000 was used to model the structure. The beams and columns were modelled using frame elements. In order to account for the nonlinearity of the structural members, rotational springs were modelled at the ends of the beams and columns at the location of the critical sections. These rotational springs are defined based on the moment-rotation behavior of the members following the recommendations by Sharma (2013). In all stories the respective section properties of the beams and columns were identical. The beams have a total depth of 350 mm and a width of 250 mm. The columns have a square shape with a side length of 250 mm. The longitudinal reinforcement of the beams and columns are the same. Both the upper and lower reinforcement layer comprise three bars with diameter 16 mm. The longitudinal reinforcement is enclosed by stirrups with a diameter of 8 mm. In the beams, the stirrups have a spacing of 150 mm and in the columns the spacing is 200 mm. Figure 16.6 (b) and (c) depicts the section properties for beams and columns, respectively.
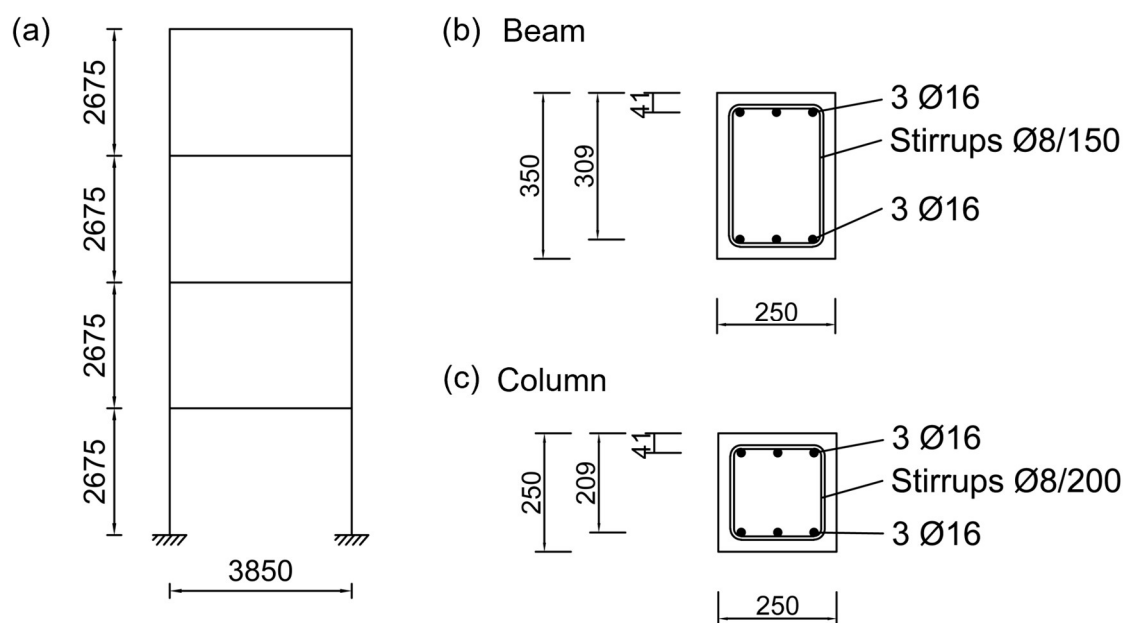
Figure 16.6. Description of the original structure. (a) Line diagram, (b) beam section properties, and (c) column section properties. (Note: All dimensions are in mm).

The RC members are made of normal strength concrete C25/30 with a cylinder concrete compressive strength of f_{ck} = 25 N/mm². Young's modulus of concrete is considered as 23650 N/mm² and Poisson's ratio of concrete as 0.2. Grade B500B reinforcement steel was used with a yield strength of f_{yk} = 500 N/mm². Young's modulus of steel is considered as 200000 N/mm² and Poisson's ratio of steel as 0.33.

For the pushover analysis, the distribution of the horizontal load along the height of the structure follows a prescribed modal pattern according to EN 1998-1 which is based

on the mass of the story and the corresponding height. The weight density of the RC members is herein considered as 25 kN/m³. With respect to Figure 16.6, the horizontal loads were applied on the joint node between the left columns and the beams. Apart from the horizontal loads, only the self-weight of the structure was considered.

16.3.2 Assessment of as-build structure

Figure 16.7 shows the base shear vs. roof displacement diagram for the original structure. The original structure has an ultimate strength of around of 93.8 kN, which is marked as point B in Figure 16.7. At this point, the roof displacement is 210 mm, which corresponds to a drift ratio of around 2%. The curve in Figure 16.7 indicates a rather brittle failure soon after the ultimate strength of the structure has been reached.
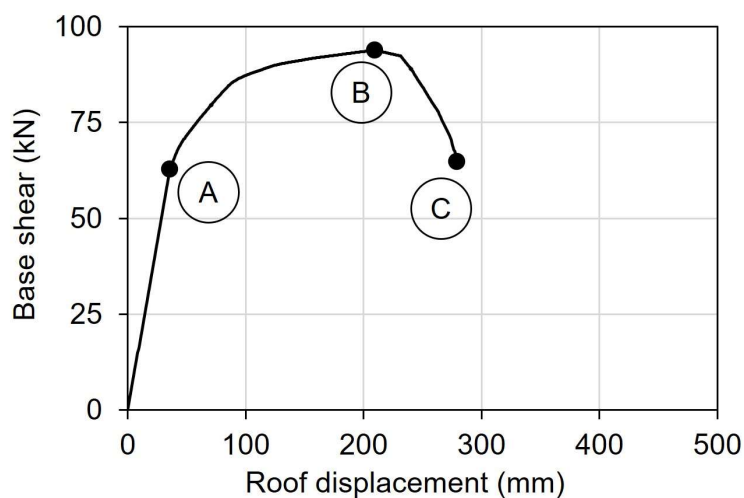
Figure 16.7. Base shear vs. roof displacement obtained from the analysis of the original structure.

To investigate the failure mechanism of the structure and the development of damage in the structural members, Figure 16.8 shows the damage at three different steps during the pushover analysis. The respective steps are marked as point A, B, and C on the load-displacement curve in Figure 16.7. Magenta dots indicate minor to moderate damage. In case of the beams and columns, this means that the tension reinforcement has started to yield. Orange dots indicate severe damage and red dots indicate complete damage of a member.

At point A, the structure goes into the nonlinear range. At this point, minor damage is apparent at the bottom end of the left column in the first story and at both ends of the first story beam. At point B the ultimate strength of the structure is reached. At this point, the bottom end of the left column in the first story is completely damaged. Severe damage is also apparent at the bottom end of the right column in the first story, at the right end of the first story beam and at the upper end of the left column in the second story. Minor to moderate damage is evident in the beams and columns of the second

and third floor. The structure finally fails when a soft story mechanism develops in the first story as shown in Figure 16.8 (c).
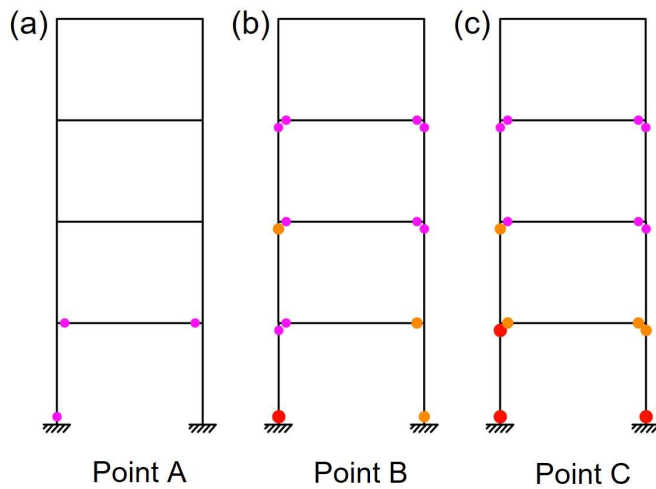
Figure 16.8. Depiction of damage in the structure with increasing roof displacement. (a) Point A, (b) point B, and (c) point C.

16.3.3 Design of the corner configuration

To overcome the brittle failure mechanism of the original structure and increase its strength against horizontal loads, the structure is retrofitted by means of diagonal steel bracing, where steel braces are installed in all stories. Thereby, the braces shall be directly connected to the original structure by means of post-installed anchors. Details of the retrofitted structure are provided in Figure 16.9.
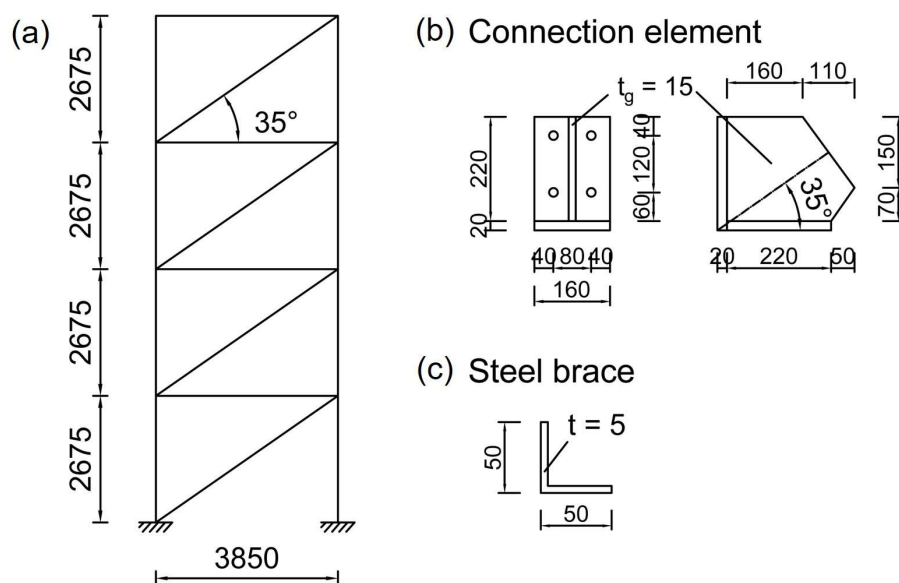
Figure 16.9. Description of the retrofitted structure. (a) Line diagram, (b) dimensions of the bracket-to-gusset plate connection element, and (c) section of the steel brace. (Note: All dimensions are in mm).

The steel braces have an L 50x50x5 section and are made of S235JR steel with a yield strength of f_{yk} = 235 N/mm² and an ultimate strength of f_{uk} = 360 N/mm². Young's modulus is considered as 200000 N/mm². With regard to the beams, the bracing has an inclination of 35°. The steel braces are intended to dissipate energy through yielding. Therefore, to ensure the effectivity of the strengthening solution, the connection has to be designed in such a way that the attached steel brace yields before the connection suffers severe damage. In this context, according to EN 1998-1, the connection is designed for a maximum load of:

$$P_{max} = 1.1 \cdot \gamma_{ov} \cdot f_{yk} \cdot A_S. \tag{16.1}$$

Where γ_{ov} = 1.25 is the overstrength factor according to EN 1998-1 and A_S is the cross-sectional area of the brace. In this example, the maximum load which is considered for the design of the connection is calculated as P_{max} = 154 kN.

16.3.3.1 Design of the connection

Figure 16.9 (b) shows the dimensions of the bracket-to-gusset plate connection used to attach the steel braces to the original frame structure. The gusset plate is welded to the anchor bracket, whereby the weld size is considered as a_w = 5 mm. Similar to the design approach in Chapter 13, the design of the gusset plate and anchor bracket is performed on basis of the principles in steel construction discussed in Chapter 2. The associated design checks include the welds at the gusset interfaces, yield strength at the Whitmore section, von Mises yield criteria at the interfaces, tensile rupture at the

interfaces and shear rupture at the interfaces. Also, yielding of the anchor bracket is checked. The obtained design-to-capacity ratios are summarized in Table 16.6.

Table 16.6. Overview of the demand-to-capacity ratios of the connection element in the case study.

Description of design checks	DCR
Weld at gusset-to-beam interface	0.19
Weld at gusset-to-column interface	0.14
Yield strength at Whitmore section	0.53
von Mises yield criteria at gusset-to-beam interface	0.28
von Mises yield criteria at gusset-to-column interface	0.12
Tensile rupture at gusset-to-beam interface	0.04
Tensile rupture at gusset-to-column interface	0.04
Shear rupture at gusset-to-beam interface	0.13
Shear rupture at gusset-to-column interface	0.05
Anchor bracket	0.86

16.3.3.2   Design of anchorage following the analytical approach

To fasten the connection element to the RC structure, bonded anchors of size M16 with an embedment depth of 150 mm are chosen. In total, eight anchors are used, four anchors in each of the perpendicular anchor groups of the bracket. Spacing of the anchors and the distance to the two parallel edges are given in Figure 16.9 (b). The design of the anchorage follows the concept described in Chapter 15.

First, the anchor groups are simulated using the spring modelling approach to determine the respective tension and shear capacity and the stiffness values. Since both groups have the same dimensions and anchor configuration, the required parameters are the same for both groups. Therefore, two simulations are performed, one where the group is loaded centrically in tension and one where the group is loaded in shear. For the tension loaded anchor groups, the characteristic maximum capacity is determined as 71.2 kN. The initial tension stiffness of the group as 360 kN/mm and the secant tension stiffness at ultimate load as 175 kN/mm. The characteristic ultimate shear load of the anchor groups is determined as 114.5 kN. The initial shear stiffness is calculated as 90 kN/mm and the secant shear stiffness at ultimate load as 53 kN/mm.

Following the approach presented in Chapter 15, the individual tension and shear load components of the groups are calculated as N_1 = 69.5 kN, V_1 = 12.2 kN, N_2 = 66.6 kN, and V_2 = 23.8 kN. Note that the designation of the load components and the assignment to the groups is based on Figure 15.3. By equilibrium of forces the capacity of the complete connection is calculated as 122.2 kN. The calculated resistance of the chosen anchor system following the analytical approach, is smaller than the anticipated

maximum load P_{max} = 154 kN. To achieve the required resistance, the anchorage would have to be redesigned. A reasonable approach would be to supplement the anchorage with additional anchors and to choose a larger spacing between the anchors in the direction parallel to the edges.

Alternatively, the complete connection can be assessed using nonlinear analysis. Directly considering the nonlinear behavior of the anchors and the connection allows a better evaluation of the actual behavior of the complete connection and also its resistance. For this purpose, the nonlinear behavior of the corner configuration will be evaluated using the nonlinear spring modelling approach.

It is worth mentioning that in this case study, the analytical calculation approach is rather intended for preliminary design. Therefore, the safety factors stipulated by the codes were omitted here. More importantly, as noted by Sharma (2013), in the context of the performance based analysis of the retrofitted structure, the nonlinearity of the connection and the anchors are directly accounted for, rendering the safety factors irrelevant.

16.3.3.3 Assessment of the connection using the nonlinear spring modelling approach

The complete connection is evaluated using the nonlinear spring modelling approach following the concept presented in Section 16.1. Note that the evaluation is performed at the mean level. The analysis was performed using the finite element software SAP2000. Figure 16.10 presents the load-displacement curve obtained from the analysis. It can be seen that the ultimate load obtained from the spring model analysis is notably higher compared to the ultimate load calculated from the analytical calculation approach (164 kN at the mean level). Using the nonlinear spring modelling approach, the ultimate load is calculated as 258.4 kN, which is almost 60% higher in comparison. This is due to the fact that the analytical approach (intentionally) solely considers the initial behavior up to the point where the first loss of tension (or shear) capacity appears. Any redistribution of forces thereafter is not considered in the analytical calculation approach. However, as can be seen, the ultimate load obtained from the analytical approach matches well with the point where connection enters the nonlinear range of the load-displacement curve (point B). Up to this point, the behavior of the connection is quite stiff. Subsequently, any further increase in load is associated with a considerable increase in displacement.

From the evaluation of the connection at mean level, the characteristic resistance of the connection may be determined as 75% of the mean ultimate load, assuming a coefficient of variation of 15%. This results in a characteristic resistance of 193.8 kN, which is higher than the anticipated maximum load P_{max} = 154 kN.
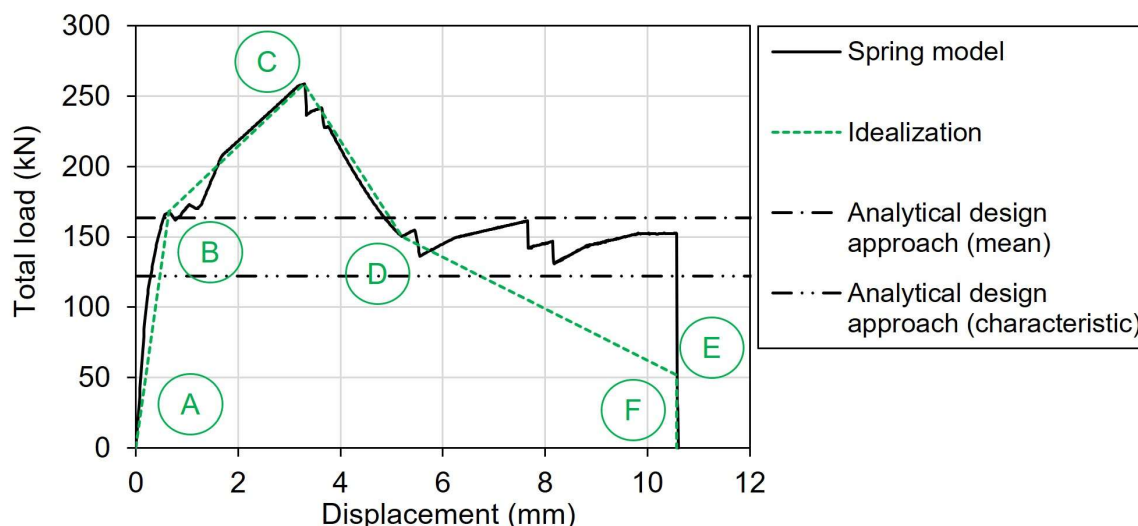
Figure 16.10. Load-displacement curve obtained from the analysis of the connection element using the nonlinear spring modelling approach.

To account for the nonlinear behavior of the connection in the analysis of the structure, the behavior is simulated by a single spring. The corresponding spring characteristics are determined in such a way that the idealized curve best fits the load-displacement curve obtained from the spring model. Thereby, the curve is idealized by six points, which are given in Table 16.7. From Figure 16.10 it can be seen that the idealized curve matches the original curve. However, the post-peak behavior has been adjusted such that the load of point E corresponds to 20% of the ultimate load.

Table 16.7. Spring characteristics of complete connection.

	Load P_{A-F} (kN)	Secant stiffness k_{1-5} (kN/mm)	Displacement, s_{A-F} (mm)
A	0.0	0.0	0.00
B	167.9	258.3	0.65
C	258.5	78.6	3.29
D	150.2	28.9	5.20
E	51.6	4.9	10.58
F	0.0	0.0	10.58

16.3.4 Assessment of retrofitted structure

Figure 16.11 presents the base shear vs. roof displacement diagram obtained from the analysis of the retrofitted structure. To enable a better comparison between the original and the retrofitted structure, the curve of the unbraced frame has been reproduced in the same graph. As can be seen, steel bracing of the frame structure results in both a significant increase in strength and stiffness of the entire structure. The base shear that can be resisted by the retrofitted structure is more than twice the resistance of the original structure. Moreover, due to the yielding of the steel braces, the complete

367

structure exhibits a more pronounced displacement behavior. At point E, where the steel brace in the first story fails and where the simulation was stopped, the drift ratio is almost 5%.
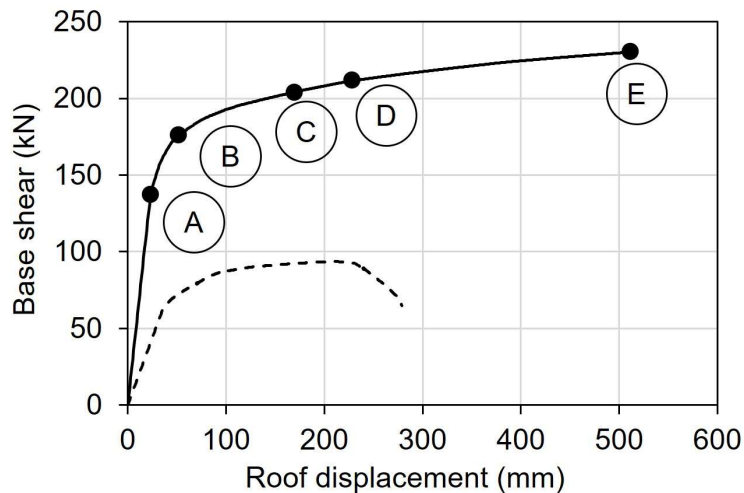
Figure 16.11. Base shear vs. roof displacement obtained from the analysis of the retrofitted structure in comparison to the performance of the original structure.

Figure 16.12 shows the damage at five different steps during the pushover analysis. The respective steps are marked as point A, B, C, D and E on the curve in Figure 16.11. Point A marks the end of the elastic range. At this step the steel braces in the first and second step start yielding. No damage has yet occurred in the RC members. Point B marks the point where also the steel brace in the third story begins to yield. Minor damage occurred mainly in the RC members in the first story at the beam and column ends. At point C, the bottom end of the left column in the first story collapses. Moderate to severe damage is apparent in the RC members. At point D, the bottom end of the right column in the first story and the upper end of the left column in the first story collapse. However, the structure is still able to maintain its load-bearing capacity and even withstand increasing loads on the structure as the steel braces remain intact. At point E, the first story brace fails. Note that at this point, the connections in the first story are already in the nonlinear range. Finally, when the steel brace in the first story fails, a soft story mechanism develops which results in the final failure of the entire structure.

The assessment of the retrofitted structure shows that the applied design approach for the connection has proven successful. The connections remain essentially in the elastic range beyond the point where the steel braces started to yield. Thereafter, the connections remained intact even at larger displacements of the entire structure. With increasing displacement demand on the structure, also the displacement demand on the connections increased, eventually resulting in the nonlinearity observed in the first story connections. Utilization of the nonlinear behavior of the connections allowed the steel braces to continue to dissipate energy through yielding even after the elastic limit

of the connections has been reached. At the same time, this observation highlights that in case of large displacement demands, it is of paramount importance to consider and assess the load-displacement behavior of connection elements, since an elastic design alone may be insufficient.
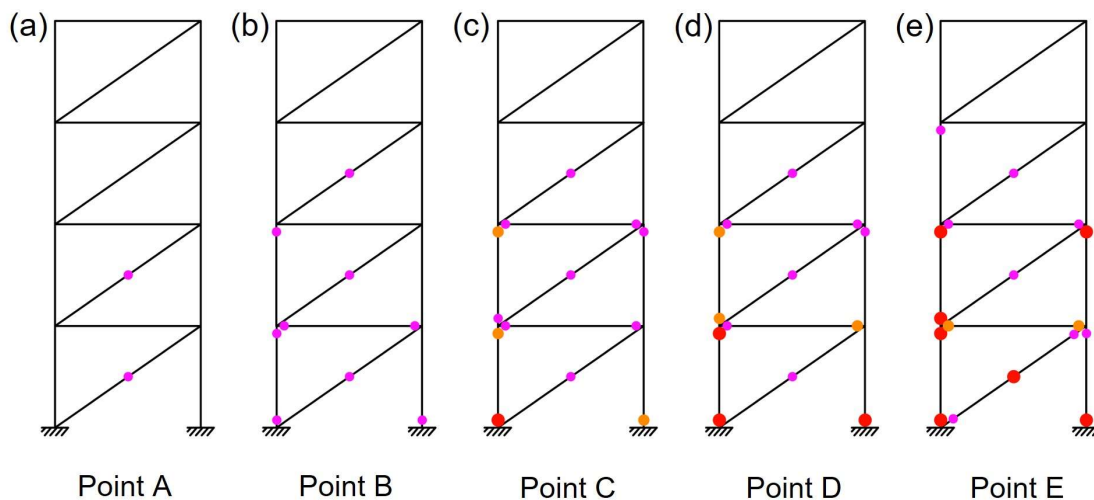
Figure 16.12. Depiction of damage in the retrofitted structure with increasing roof displacement. (a) Point A, (b) point B, (c) point C, (d) point D, and (e) point E.

16.4 Summary

In this chapter, the possible use of the nonlinear spring modelling approach (Bokor, 2021) to analyze spatial anchorages in corner configurations has been demonstrated. Thereby, the tension spring characteristics of the anchors were determined for concrete cone failure, while the shear spring characteristics were determined for concrete edge failure. Based on the experimental and numerical results in this work, the spring characteristics were partly modified according to the observed behavior of the anchors. A comparison between the load-displacement behavior observed in the experiments and the simulated load-displacement behavior has successfully demonstrated the suitability of the modelling approach.

By directly considering the nonlinear behavior of the anchors and the stiffness of the steel elements such as anchor bracket and gusset plate, it is possible to assess arbitrary spatial corner configurations through a nonlinear static analysis. The presented design approach allows a reliable evaluation of the load-displacement behavior without the need for elaborate experimental investigations.

The potential applicability of the proposed analytical design concept and the spring model concept was finally demonstrated in a case study. It was shown how the analytical approach can be used for pre-dimensioning of the anchorage and how the

displacement-based design approach can be included in a performance based analysis of the complete structure.

17 Summary and open questions

The goal of this work has been to investigate a low-invasive retrofit solution using post-installed anchors to form a direct connection between steel bracing and existing RC frame structure for seismic strengthening. For this purpose, both experimental and numerical investigations were carried out. The problem is defined in three levels. First, is the "anchor level", which deals with the questions of what type of anchor is suitable for this kind of connection, how to determine the suitability of the anchors, and how to assess and describe the hysteretic and displacement behavior of the anchors. Next, is the "anchor group level". On the one hand, it was investigated how anchor groups behave under cyclic loading and to what extent the findings obtained from the single anchor cyclic tests can be related to the cyclic behavior of anchor groups. On the other hand, it was investigated how tension loaded anchor groups behave when installed in narrow concrete members (two parallel close edges). Finally, the "subassembly level" is investigated, which deals with the behavior of the complete connection between steel brace and RC frame for the case where the connection is located in the corner of the frame. The findings obtained from the three levels, as well as open questions and suggestions for future research, are summarized below.

17.1 Single anchor level

An experimental program was conducted to investigate the cyclic behavior of post-installed anchors subjected to pulsating tension load. For this purpose, a new displacement-controlled loading protocol was proposed, which allows to assess the cyclic behavior of anchors in the post-peak range of the load-displacement curve. The results of tests using new protocol were compared to the results using current testing protocol for the qualification of anchors against seismic actions, namely the force-controlled protocol C2.3 according to EOTA TR 049. With regard to the overall behavior in terms of load, displacements, secant stiffness values and failure modes, the two cyclic protocols basically provide the same information. However, due to the structure of the new protocol, it captures the hysteretic behavior of the anchors in a broader range of the load-displacement curve, also covering the post-peak range. The new displacement-controlled testing approach allows the investigation of additional parameters, such as the strength degradation, unloading and reloading stiffness, or the residual displacements of an anchor when unloaded to almost zero displacement. Thereby, the new protocol enables the assessment of these parameters in almost the complete range of the load-displacement curve.

Five different types of anchors were investigated in the experimental program, namely undercut anchors, expansion anchors, bonded anchors, concrete screws, and bonded expansion anchors. The experimental results clearly showed that the displacement and the hysteretic behavior of the anchor systems varies significantly. Since the performance of a structure during an earthquake is defined in terms of deformation, it seems advisable to give more consideration to the varying behavior of different types of anchors and to assess and design them not solely based on their load-bearing capacity.

Based on the experimental investigation, a modelling approach, and hysteretic rules for the simulation of the cyclic behavior of tension loaded anchors were developed. The model is able to simulate the unloading and reloading behavior of various types of anchors, considering softening effects in the unloading and reloading branches, strength degradation in subsequent cycles, and the residual displacements of anchors after unloading.

The main quality of the hysteretic model is the unloading and reloading behavior of the anchors. It can be defined by the unloading and reloading stiffness at a certain point on the envelope curve. The experiments on the hysteretic behavior of single anchors have revealed that the unloading and reloading behavior of the anchors change with increasing displacement of the same. Thereby, different types of anchors exhibit a different hysteretic behavior. In order to consider the variations in anchor behavior, while maintaining a simple and consistent approach for modeling, a tri-linear format was proposed to idealize the unloading and reloading stiffness with increasing relative displacement. The comparison with the experimental results in this work has shown that the adopted simplification of the unloading and reloading behavior reproduces the real behavior of the tested anchors with a sufficient level of accuracy.

The actual hysteretic model is defined by a set of rules, which describe the anchor behavior during unloading and reloading. Three different levels of accuracy were presented which represent the development steps of the model. At each step, additional features, such as strength degradation in subsequent cycles, were added, resulting in an increasingly accurate representation of the actual anchor behavior. The difference between these levels was presented in detail using the experimental results from this work as reference examples. A comparison between the experimental results from this work and from the literature has shown that the proposed model is able to quite accurately simulate the anchor behavior subjected to different types of loading schemes.

In this work, the focus of the experimental investigation was on the hysteretic behavior of tension loaded anchors. Consequently, the proposed displacement-controlled testing approach and the hysteretic model for anchors solely cover the behavior of anchors under tension loads. However, to assess anchor behavior under seismic actions, it is equally important to consider the behavior under alternating shear loads.

The concept of the presented displacement-controlled test protocol for pulsating tension load can in principle be adapted to alternating shear load as well. The test protocol would simply have to be adjusted accordingly. Figure 17.1 exemplarily illustrates how the adjusted cyclic loading protocol can be set up. Here, the definition of the displacement amplitudes basically follows the rules presented in Chapter 5. However, further experimental investigations are needed to verify the applicability of the amplitudes for alternating shear loads. The information gained from the displacement-controlled tests for alternating shear load may then be used to extend the hysteretic rules to shear loading as well.

Displacement amplitude

$s_{1,V} = \pm 0.1 s_{u,V}$
$s_{2,V} = \pm 0.2 s_{u,V}$
$s_{3,V} = \pm 0.3 s_{u,V}$
$s_{4,V} = \pm 0.5 s_{u,V}$
$s_{5,V} = \pm 0.7 s_{u,V}$
$s_{6,V} = \pm s_{u,V}$
$s_{7,V} = \pm(2s_{u,V}/3 + s_{max,V}/3)$
$s_{8,V} = \pm(s_{u,V}/3 + 2s_{max,V}/3)$
$s_{9,V} = \pm s_{max,V}$
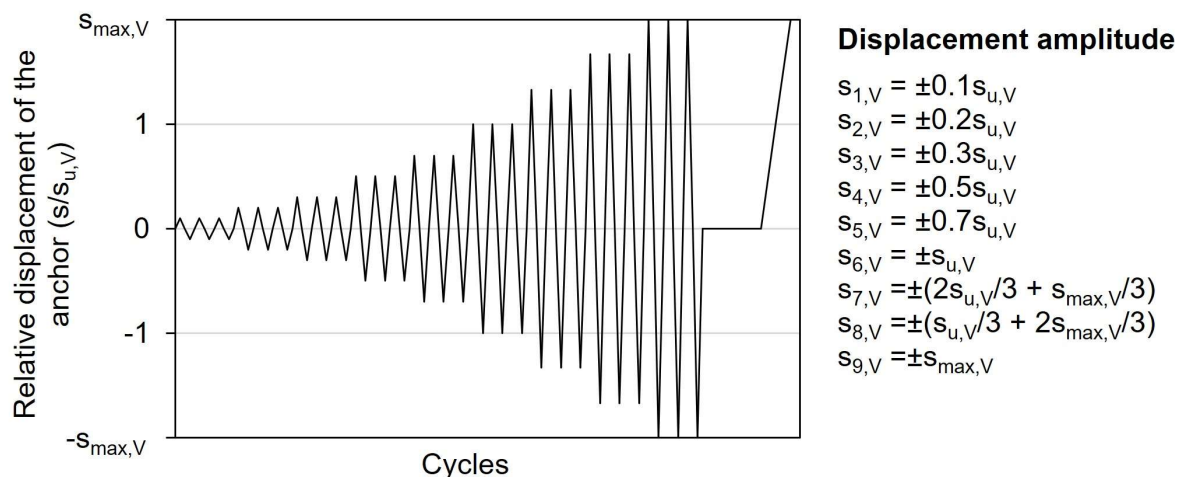
Figure 17.1. Proposed schematic test procedure for displacement-controlled protocol for alternating shear load.

Besides the cyclic behavior of anchors subjected to tension and shear loads, the influence of cracks and crack cycling is often pivotal for the qualification of anchors in current testing schemes (Eligehausen and Sharma, 2011; Muciaccia, 2017; Muciaccia and Marchisella, 2017). Conservatively, the load- and crack- cycling can be carried out in-phase, with the tension load increasing and reducing in phase with opening and closing of the cracks. Accordingly, a model is required to describe the displacement behavior of anchors during cyclic crack opening and closing. One possible solution was developed by the author within the BMWi research project no. 1501598: Influence from displacements of post-installed anchors on the safety of piping systems at earthquake loading. A detailed description can be found in MPA Report No. 8488 000 000 (2021).

A remaining issue is the development and harmonization of the individual models for pulsating tension load, alternating shear load and cyclic crack opening and closing, and the implementation of the hysteretic rules in a finite element software for possible use in the framework of the spring modeling approach.

17.2 Anchor group level

An experimental program has been conducted to investigate the behavior of anchor groups subjected to displacement-controlled pulsating tension load. The program comprised anchor groups with various anchor configurations, whereby the groups were loaded both monotonically in tension and according to the displacement-controlled protocol for pulsating tension load presented in Chapter 5. Thus, allowing a comparison between the monotonic and cyclic behavior of anchor groups. Besides the overall behavior and the influence of cyclic loading thereon, the focus was on the displacement and hysteretic behavior of the individual anchors within the group.

Analogous to the behavior of single anchors, the experimental results indicate that the overall behavior of anchor groups under displacement-controlled pulsating tension load in-principle, follows the behavior under monotonic loading. The envelope curves for anchor groups subjected to pulsating tension load are rather similar to the corresponding monotonic curves. The mean ultimate loads and secant stiffness values obtained from the cyclic tests agreed well with the results of the monotonic tests. Tests on anchor groups with varying anchor spacing but equal number of anchors in the group has shown that the stiffness or flexibility of the baseplate has a significant influence on the displacement behavior of the tested anchor groups and the distribution of forces among the anchors. Thereby, increasing the anchor spacing in the experiments resulted in a marked reduction of the overall stiffness of the anchor groups.

Besides the overall behavior of anchor groups, the individual behavior of the anchors within a group is particularly interesting. With respect to the unloading and reloading behavior of the tested bonded anchors it was found that in the initial loading phase, the behavior is very stiff. With increasing displacement of the anchors, however, both unloading and reloading stiffness degrade rather strong. Thereby, the behavior of individual anchors in a group and the behavior of single anchors principally matches well. This means that in case of the tested bonded anchors, regardless of whether they were arranged in an anchor group or tested alone, the unloading and reloading stiffness at the same displacement level is rather similar.

Based on the experimental results and the hysteretic model for single anchors, a simplified modelling approach was presented for the simulation of the hysteretic behavior of multiple anchor groups. The basis of this approach is the overall load-displacement behavior of the anchor group in terms of the envelope curve, and the hysteretic rules for single anchors. Interaction of the individual anchors is considered assuming that the anchors act like springs which are connected in parallel. Flexibility of the baseplate is considered assuming that the anchors and the baseplate are connected in series, whereby the baseplate remains elastic. This simplified approach comes, however, with certain limitations such as being restricted to anchor groups, where all anchors have the same displacement demand. Limitations on the usability

can be evaded when the hysteretic behavior of the individual anchors is directly accounted for in a step-by-step FE analysis.

A vast experimental and numerical campaign has been conducted to investigate the behavior of tension loaded anchor groups installed in narrow concrete members, such as beams or columns. Thus, the anchor groups are placed in the vicinity of two parallel edges, which has a negative effect on the breakout behavior of the tension loaded anchor groups due to the limited availability of concrete to resist the tension load. The main emphasis of the investigations was on the failure mechanism, the capacity of the anchor groups, and their displacement behavior. It was found that the breakout behavior of anchor groups with an edge distance smaller than the critical edge distance is governed by horizontal cracks starting from the embedded ends of the anchors towards the free edges. Thereby, the failure happens abruptly and is brittle in nature. However, basically no cracking was observed on the concrete surface before the failure of the anchor groups. In case of anchor groups with equal edge distance on both sides, it was observed that for the same projected area the tested configurations basically yielded the same ultimate capacities. Thereby, the relative distance to the edges seemed to have no significant influence, indicating that only considering the projected area for the design of anchor groups in narrow members would suffice for a practical and safe design. However, this is only the case for anchor groups where the distance to the parallel edges is equal on both sides. In case of geometric asymmetry or asymmetry of loading in the direction perpendicular to the edges an additional reduction of the capacity was indeed observed in the numerical investigations. Further experimental investigations are recommended to study the behavior of anchor groups in narrow members where the edge distance on one side differs from the edge distance on the other side (geometrical asymmetry).

Based on the results, it was shown that the current analytical design approach for the concrete cone breakout failure of anchor groups (CCD method) is quite conservative when it comes to anchor groups installed in narrow concrete members. In this context, four approaches were presented and evaluated which are aimed at modifying the current design approach. The first approach was introduced by Anderson et al. (2017) and considers a modification factor which increases the calculated capacities according to the CCD method. This factor is a function of the ratio s_2/c_2. However, experimental findings in this work suggest that this parameter is less meaningful, especially for larger ratios between s_2 and c_2, in which case the proposed factor may even lead to unreliable or unsafe predictions. The second approach considers a modification factor based on the relative edge distance, c_2/h_{ef}. The experimental results showed that for the tested anchor configurations, the conservatism of the current design approach increases with decreasing relative edge distance. This observation is likely to be related to the reduction factor $\psi_{s,N}$, which considers the disturbance of the rotationally symmetric stress condition in the concrete due to close edges (Eligehausen et al., 2006), and which is a function of the edge distance. The

comparison with the experimental data showed a good agreement between the proposed modification factor and the results obtained from the tested anchor groups. Based on the latter approach, the third solution is to omit the reduction factor $\psi_{s,N}$. This is the simplest option and avoids the need to introduce another factor to the CCD method. At the same time, it retains a certain conservatism. The fourth approach is similar to the existing design approach for concrete edge failure of shear laded anchors according to EN 1992-4, where the factor $\psi_{h,V}$ considers that the resistance in case of concrete edge failure does not reduce as strongly with decreasing thickness of the concrete member as determined by the ratio $A_{c,V}/A_{c,V}^0$. Hence, based on the assumption that in case of anchors installed in narrow concrete members, the resistance does not reduce as strongly with decreasing width of the concrete member as it is assumed by the ratio $A_{c,N}/A_{c,N}^0$, the modification factor $\psi_{w,N}$ is proposed. The comparison with the experimental data showed the suitability of the proposed modification factor for the investigated cases. The fourth approach is more conservative than the second approach and less conservative than the third approach. It should be noted, though, that the discussed modification approaches are based on the available experimental data, where anchor groups are loaded centrically in tension and have equal edge distance to both parallel edges and are therefore only applicable to these cases.

Additional modification factors are, however, a rather unsatisfying solution for the given problem, as the existing design approach becomes even more complex. Also, omitting the reduction factor $\psi_{s,N}$ is only partially solving the problem while it is not applicable to geometric imperfections either. A desirable analytical design approach should directly include cases with any number of close edges (also only one close edge) and where the edge distances to the parallel edges can be of different values. Basically, a holistic solution that can be applied when an anchor group is designed in the vicinity of one or more edges, without the need for modification or reduction factors. It is evident that the behavior of anchor groups close to the edges is an exciting topic with a number of open questions that offer ample research potential in the future. In particular with regard to the development of such a holistic design solution.

17.3 Subassembly level

The connection between steel bracing and RC frame structure was investigated in an experimental program focusing on the geometrical aspects of a spatial anchor configuration in corner applications. Here, bonded anchors were used to fasten the connection element to the concrete specimen. The feasibility of a direct connection using post-installed anchors is highlighted by the substantial loads that could be resisted by the connection, even for rather small embedment depths. Moreover, in terms of loads, the test results showed only little variation. With respect to the load-displacement behavior of the tested connections, two distinct peaks were observed.

Up to the first peak, the connections showed a reliable and consistent behavior. Thereupon, the behavior becomes more erratic and appears to depend largely on whether the connection is able to redistribute the forces among the anchors. The numerical investigation of the connections has shown that up the first peak, the behavior of the complete connection is dominated by the tension behavior of the bonded anchors. The drop of load after the first peak has been reached, which characterizes the load-displacement behavior of the corner configuration, is due to the loss of tensile capacity of the anchors. In the second phase, the anchors are able to utilize the shear capacity with increasing displacement of the connection. This is made possible by the presence of the concrete corner, which prevents the breakout of the anchors after they have reached the maximum tensile capacity. The behavior in the second phase, up to the ultimate load of the connection, is largely dominated by the shear behavior of the anchors and the ability to maintain a certain level of tensile capacity even at large displacements. Latter ability depends on the embedment depth of the anchors and appears to be a result of the load transfer mechanism associated with bonded anchors.

The results obtained from the experimental and numerical investigations have shown that an analytical calculation approach cannot be developed based on forces alone. Therefore, a calculation approach that includes the tension and shear stiffness was conceptualized and successfully validated against the experimental and numerical results. With respect to the tested bonded anchors, the concept addresses the resistance of the connection at first peak. The load-displacement behavior observed in this work is caused by the large difference between the tension stiffness and the shear stiffness of bonded anchors. For other types of anchors, the load-displacement behavior may be different. The presented analytical calculation approach already covers this by directly considering the stiffness values of the anchor groups forming the bracket. Nevertheless, further experimental investigations with different types of anchors are necessary to validate the concept and to modify it if required.

Displacement-based approaches offer a more suitable alternative to analytical design methods. For example, the nonlinear spring modelling approach (Bokor et al., 2019b; Bokor, 2021) directly considers the individual behavior of the anchors, as well as the stiffness of the steel elements, such as the anchor bracket and the gusset plate. In this way, arbitrary connections can be designed. At the same time, the entire load-displacement behavior of a connection is obtained. Thus, if the nonlinear behavior of the connections is to be considered in the context of a performance based analysis of the overall structure, the corresponding spring characteristics can be derived directly from the results of the nonlinear spring model. The feasibility of such a design solution has been demonstrated in the context of a case study.

With respect to corner configurations for seismic bracing of RC frame structure, not all aspects could be answered within the scope of this work and other open questions have been identified. In particular:

1. As mentioned above, using other types of anchors than used in this work will have an influence on the load-displacement behavior. Therefore, the connection can be investigated using other types of post-installed anchors to identify how exactly the behavior varies.

2. So far, the behavior of the connection was mainly studied for monotonic loading. Although the cyclic behavior appears to have no effect, as indicated by the preliminary numerical study, further evidence is needed.

3. The numerical investigation on the individual anchor forces has shown that in case of larger embedment depths, the anchors exhibit a more pronounced residual tensile capacity which allows the anchors to continuously transfer forces through tension even after the ultimate tension load has been reached. For the investigated bonded anchors, it appears that the residual tension load that can be resisted by the anchors increases with increasing embedment depth. However, further studies are required to verify the degree of residual capacity of the anchors for different embedment depths. Moreover, other parameters such as the diameter of the anchors, the relative distance to the corner and the relative distance to the parallel edges should be investigated to provide a valid conclusion.

4. In real RC frame structures, one of the groups which form the anchor bracket might be installed in a slab, while the second group is still installed in a narrow member. Further research is required to consider the potential effects of such configurations in the design of the connection.

5. Besides the geometrical influences on the connection arising from the corner itself, structural effects resulting from the bending of the RC members must be considered. Therefore, experimental, and numerical investigations on full-size RC frame structures with and without strengthening under cyclic loading are required to validate the expected performance and further investigate the behavior of the connection.

References

ACI 318-14. Building Code Requirements for Structural Concrete and Commentary. American Concrete Institute: Farmington Hills, Michigan, USA, 2014.

ACI 355.2. Qualification of post-installed mechanical anchors in concrete (355.2-07) and commentary. American Concrete Institute: Farmington Hills, Michigan, USA, 2007.

ACI 355.4. Acceptance criteria for qualification of post-installed adhesive anchors in concrete (ACI 355.4-11) and commentary. American Concrete Institute: Farmington Hills, Michigan, USA, 2007.

ACI 374.1-05(19). Acceptance Criteria for Moment Frames Based on Structural Testing and Commentary. American Concrete Institute: Farmington Hills, Michigan, 2005 (reapproved 2019).

ACI 374.2R-13. Guide for Testing Reinforced Concrete Structural Elements under Slowly Applied Simulated Seismic Loads. American Concrete Institute: Farmington Hills, Michigan, USA, 2013.

AISC. Steel construction manual (13th edition). American Institute of Steel Construction: Chicago, Illinois, USA, 2011.

Anderson, N.S., Koray Tureyen, A., Meinheit, D.F. (2017). Tension Tests of Headed Stud Anchorages in Narrow / Thin Edge Members. Proceedings of the 3rd International Symposium on Connections between Steel and Concrete, Stuttgart, Germany, 27 – 29 September 2017, 272–282.

ASCE 7. Minimum Design Loads and Associated Criteria for Buildings and Other Structures (ASCE/SEI 7-16). American Society of Civil Engineers: Reston, Virginia, USA, 2017.

ASCE/SEI 41-17. Seismic evaluation and retrofit of existing buildings. American Society of Civil Engineers: Reston, Virginia, USA, 2017.

ATC 3-06. Tentative provisions for the development of seismic regulations for buildings. National Bureau of Standards: Washington, D.C., USA, 1978.

ATC-40. Seismic evaluation and retrofit of concrete buildings. Report No. SSC 96-01, Volume 1, Applied Technology Council: Redwood City, California, USA, 1996.

Badoux, M., Jirsa, J.O. (1990). Steel bracing of RC frames for seismic retrofitting. Journal of Structural Engineering (ASCE), 116(1):55–74.

Bažant, Z.P. (1984). Size Effect in Blunt Fracture: Concrete, Rock, Metal. Journal of Engineering Mechanics, ASCE, 110(4):518-535.

Bažant, Z.P., Oh, B.H. (1983). Crack band theory for fracture of concrete. Materials and Structures, 16(3):155–177.

Black, R.G., Wenger, W.A., Popov, E.P. (1980). Inelastic Buckling of Steel Struts Under Cyclic Load Reversals. Report No. UCB/EERC-8Q/40, Earthquake Engineering Research Center, College of Engineering, University of California, Berkley, California, October 1980.

Bokor, B. (2021). Nonlinear spring modelling for evaluation of anchor groups. Ph.D. Thesis, University of Stuttgart, Germany.

Bokor, B., Sharma, A., Hofmann, J. (2017). On the limitations of the current provisions of PREN 1992-4 for design of anchor groups subjected to tension loads. Proceedings of 3rd International Symposium on Connections between Steel and Concrete, Stuttgart, Germany, 27-29 September 2017, 118–129.

Bokor, B., Sharma, A., Hofmann, J. (2018). Experimental investigations on tension loaded anchor groups of arbitrary configurations. Proceedings of the 2018 fib Congress, Melbourne, Australia, 7-11 October 2018, 1046–1063.

Bokor, B., Sharma, A., Hofmann, J. (2019a). Experimental investigations on concrete cone failure of rectangular and nonrectangular anchor groups. Engineering Structures, 188:202–217.

Bokor, B., Sharma, A., Hofmann, J. (2019b). Spring modelling approach for evaluation and design of tension loaded anchor groups in case of concrete cone failure. Engineering Structures, 197:109414.

Bujňák, J., Farbák, M. (2018). Tests of Short Headed Bars with Anchor Reinforcement Used in Beam-to-Column Joints. ACI Structural Journal, 115(1):203–210.

Bush, T.D., Jones, E.A., Jirsa, J.O. (1991). Behavior of RC Frame Strengthened Using Structural Steel Bracing. Journal of Structural Engineering, 117(4):1115–1126.

Delhomme, F., Debicki, G., Chaib, Z. (2010). Experimental behavior of anchor bolts under pullout and relaxation tests. Construction and Building Materials, 24:266–274.

Della Corte, G., D'Aniello, M., Landolfo, R., Mazzolani, F.M. (2011). Review of Steel Buckling-Restrained Braces. Steel Construction, 4(2):85–93.

Desramaut, N., Modaressi, H., Le Cozannet, G. (2013). Earthquake Damage. In: Bobrowsky P.T. (eds) Encyclopedia of Natural Hazards. Encyclopedia of Earth Sciences Series. Dordrecht: Springer, Netherlands. https://doi.org/10.1007/978-1-4020-4399-4_105.

Di Nunzio, G. (2020). Pull-Out of Cast-In-Place Fasteners – Influence of the Bearing Pressure and Structural Interaction with the Concrete Member. Ph.D. Thesis, Politecnico Di Milano, Italy.

DIBt (2010). Guideline for Fastenings with Anchors in Nuclear Power Plants and Nuclear Facilities. Deutsches Institut für Bautechnik (DIBt): Berlin, Germany, 2010.

DIN EN 1992-4/NA. National annex – Nationally determined parameters – Eurocode 2: Design of concrete structures – Part 4: Design of fastenings for use in concrete. German version DIN EN 1992-4/NA: 2019-04, DIN Deutsches Institut für Normung e. V.: Berlin, Germany.

DIN EN 1998-1/NA. National Annex – Nationally determined parameters – Eurocode 8: Design of structures for earthquake resistance – Part 1: General rules, seismic actions and rules for buildings. DIN Deutsches Institut für Normung e. V.: Berlin, Germany, 2011.

DIN EN 206. Concrete – Specification, performance, production and conformity. German version EN 206:2013+A2:2021, European Committee for Standardization: Brussels, Belgium, 2021.

Dwenger, F. (2019). Einfluss des Tragverhaltens von Dübelbefestigungen auf die Bauwerk-Komponenten-Wechselwirkung bei Erdbebenbeanspruchung. Ph.D. Thesis, University of Stuttgart, Germany.

EAD 330087-01-0601. European Assessment Document – EAD 330087-01-0601 Systems for post-installed rebar connections with mortar. European Organisation for Technical Assessment (EOTA): Brussels, Belgium, 2020.

EAD 330232. EAD 330232-00-0601 Mechanical fasteners for use in concrete. European Organisation for Technical Assessment (EOTA): Brussels, Belgium, 2016.

EAD 330499. EAD 330499-00-0601 Bonded fasteners for use in concrete. European Organisation for Technical Assessment (EOTA): Brussels, Belgium, 2017.

Eligehausen, R., Fuchs, W., Mayer, B. (1987). Tragverhalten von Dübelbefestigungen bei Zugbeanspruchung, Teil 1. Betonwerk + Fertigteil-Technik, Heft 12:826–832.

Eligehausen, R., Sawade, G. (1989). A Fracture Mechanics based Description of the Pull-Out Behaviour of headed Studs embedded in Concrete. Fracture Mechanics of Concrete Structures, From Theory to Applications. Editors: Elfgren, L., Chapman and Hall, London, New York, 1989, 281–299.

Eligehausen, R., Ožbolt, J. (1990). Size effect in anchorage behavior. Proceedings of ECF8 Fracture Behavior and Design of Materials and Structures, Turin, Italy, October 1990.

Eligehausen, R., Fuchs, W., Ick, U., Mallée, R., Reuter, M., Schimmelpfennig, K., Schmal, B. (1992). Tragverhalten von Kopfbolzenverankerungen bei zentrischer Zugbeanspruchung. Bauingenieur, 67:183–196.

Eligehausen, R., Mallee, R., Silva, J.F. (2006). Anchorage in concrete construction. Berlin: Ernst & Sohn, Germany.

Eligehausen, R., Grosser, P. (2007). Experimentelle und numerische Untersuchungen zur Bemessung von Befestigungen am Bauteilrand unter Querlasten (Experimental and numerical investigations on anchorages close to the edge under shear loading). IWB-Report No. EL 72/13-2. University of Stuttgart, Germany.

Eligehausen, R., Sharma, A. (2011). Seismic safety of anchorages in concrete structures of nuclear power plants. Proceedings of the Post-SMiRT Conference Seminar on Advances in Seismic Design of Structures, Systems and Components of Nuclear Facilities, Mumbai, India, 14 – 15 November 2011, 209-228.

EN 1992-1-1. Eurocode 2: Design of concrete structures – Part 1-1: General rules and rules four buildings. European Committee for Standardization: Brussels, Belgium, 2010.

EN 1992-4. Eurocode 2: Design of concrete structures – Part 4: Design of fastenings for use in concrete. English version EN 1992-4:2018 (E), European Committee for Standardization: Brussels, Belgium, 2018.

EN 1993-1-8. Eurocode 3: Design of steel structures – Part 1-8: Design of joints. German version EN 1993-1-8:2005 + AC:2009, European Committee for Standardization: Brussels, Belgium, 2009.

EN 1998-1. Eurocode 8: Design of structures for earthquake resistance – Part 1: General rules, seismic actions and rules for buildings. German version EN 1998-1:2004 + AC:2009, European Committee for Standardization: Brussels, Belgium, 2010.

EOTA TR 048. Technical Report 048:2016-08 Details of tests for post-installed fasteners in concrete. European Organisation for Technical Assessment (EOTA): Brussels, Belgium, 2016.

EOTA TR 049. Technical Report 049:2016-08 Post-installed fasteners in concrete under seismic action. European Organisation for Technical Assessment (EOTA): Brussels, Belgium, 2016.

ETA-05/0069. European Technical Assessment ETA-05/0069 for fischer Bolt Anchor FAZ II. Deutsches Institut für Bautechnik: Berlin, Germany, 2017.

ETA-15/0352. European Technical Assessment ETA-15/0352 for fischer concrete screw ULTRACUT FBS II. Deutsches Institut für Bautechnik: Berlin, Germany, 2018.

ETA-16/0637. European Technical Assessment ETA-16/0637 for fischer Highbond-Anchor FHB II Inject. Deutsches Institut für Bautechnik: Berlin, Germany, 2017.

ETA-17/0979. European Technical Assessment ETA-17/0979 for fischer injection system FIS EM Plus. Deutsches Institut für Bautechnik: Berlin, Germany, 2018.

ETA-98/0004. European Technical Assessment ETA-98/0004 for fischer-Zykon-Anchor FZA. Deutsches Institut für Bautechnik: Berlin, Germany, 2016.

Fajfar, P. (2018). Analysis in seismic provisions for buildings: past, present and future. Bulletin of Earthquake Engineering, 16:2567–2608.

FEMA 356. Prestandard and commentary for the seismic rehabilitation of buildings. Federal Emergency Management Agency (FEMA): Washington, D.C., USA, 2000.

FEMA 440. Improvement of Nonlinear Static Seismic Analysis Procedures. Federal Emergency Management Agency (FEMA): Washington, D.C., USA, 2005.

fib Bulletin 58. Fédération Internationale du Béton (fib): Design of Anchorages in Concrete: Part I-V. International Federation for Structural Concrete (fib): Lausanne, Switzerland, 2011.

Fichtner, S. (2011). Untersuchungen zum Tragverhalten von Gruppenbefestigungen unter Berücksichtigung der Ankerplattendicke und einer Mörtelschicht. Ph.D. Thesis, University of Stuttgart, Germany.

Fingerloos, F., Marx, S., Schnell, J. (2015). Tragwerksplanung im Bestand – Bewertung bestehender Tragwerke. In: Bergmeister, K., Fingerloos, F., Wörner, J.-D. (Editors), Betonkalender 2015: Bauen im Bestand, Brücken, Kapitel II, Berlin: Ernst & Sohn, Germany.

Fuchs, W., Eligehausen, R., Breen, J.E. (1995). Concrete Capacity Design (CCD) approach for fastening to concrete. ACI Structural Journal, 92:73–94.

Genesio, G. (2012). Seismic Assessment of RC Exterior Beam-Column Joints and Retrofit with Haunches Using Post-Installed Anchors. Ph.D. Thesis, University of Stuttgart, Germany.

Ghobarah, A., Aziz, T.S. (2004). Seismic qualification of expansion anchors to Canadian nuclear standards. Nuclear Engineering and Design, 228:377–392.

Gkournelos, P.D., Triantafillou, T.C., Bournas, D.A. (2021). Seismic upgrading of existing reinforced concrete buildings: A state-of-the-art review. Engineering Structures, 240:112273.

Goel, S.C., Lee, H.S. (1990). Seismic strengthening of RC structures by ductile steel bracing system. Proceedings of Fourth U.S. National Conference on Earthquake Engineering, Palm Springs, California, 20-24 May 1990, 3:323-331.

Grosser, P.R. (2012). Load-bearing behavior and design of anchorages subjected to shear and torsion loading in uncracked concrete. Ph.D. Thesis, University of Stuttgart, Germany.

Guha-Sapir, D., Hargitt, D., Hoyois, P. (2004). Thirty Years of Natural Disasters 1974-2003: The Numbers. Louvain-la-Neuve: Presses Universitaires de Louvain, Belgium.

Hoehler, M.S. (2006). Behavior and Testing of Fastenings to Concrete for use in Seismic Applications. Ph.D. Thesis, University of Stuttgart, Germany.

Hofmann, J. (2005). Tragverhalten und Bemessung von Befestigungen unter beliebiger Querbelastung in ungerissenem Beton. Ph.D. Thesis, University of Stuttgart, Germany.

Hofmann, J., Mahadik, V., Sharma, A. (2015). Modelling structure-anchor-component interaction for nuclear safety related structures under seismic loads – Part 2: Development of numerical model. Proceedings of the 23rd Conference on Structural Mechanics in Reactor Technology (Transactions, SMiRT-23), Manchester, United Kingdom, 10-14 August 2015.

Housner, G.W. (1984) Historical view of earthquake engineering. Proceedings of the 8th world conference on earthquake engineering, San Francisco, CA, post-conference volume: 25–39.

Ishimura, M., Sadasue, K., Miyauchi, Y., Yokoyama, T., Fujii, T., Minami, K. (2012). Seismic Performance Evaluation for Retrofitting Steel Brace of Existing RC Building with Low-Strength Concrete. Proceedings of the 15th World Conference on Earthquake Engineering, Lisbon, Portugal, 24-28 September 2012, 3:2277-2286.

Kam, W.Y., Pampanin, S., Elwood, K. (2011). Seismic Performance of Reinforced Concrete Buildings in the 22 February Christchurch (Lyttelton) Earthquake. Bulletin of the New Zealand Society for Earthquake Engineering, 44(4):239-78.

Karihaloo, B.L. (1995) Fracture Mechanics & Structural Concrete. Harlow: Longman Scientific & Technical, Essex, England.

Kolbe, A.R., Hutson, R.A., Shannon, H., Trzcinski, E., Miles, B., Levitz, N., Puccio, M., James L., Noel J.R., Muggah, R. (2010). Mortality, crime and access to basic needs before and after the Haiti earthquake: A random survey of Port-au-Prince households. Medicine, Conflict and Survival, 26(4):281–297.

Kuhlmann, U., Ruopp, J., Hofmann, J., Sharma, A., Wald, F., Bečková, S., Schwarz, I., da Silva, L.S., Gervásio, H., Gentili, F., Krimpmann, M., van Kann, J., Dehan, V. (2014). Entwurf von Anschlüssen zwischen Stahl und Beton – Handbuch I. University of Stuttgart.

Laichinger, S., Bergmeister, K. (2014). Randnahe Mehrfachbefestigungen unter kombinierter Belastung – Experimentelle und theoretische Untersuchungen. Beton- und Stahlbetonbau, 109(5):334–343.

Lee, C.-H. (2002). Seismic Design of Rib-Reinforced Steel Moment Connections based on Equivalent Strut Model. Journal of Structural Engineering, 128(9):1121–1129.

Lee, S., Jung, W. (2021). Evaluation of Structural Performance of Post-Installed Anchors Embedded in Cracked Concrete in Power Plant Facilities. Applied Science, 11:3488.

Lehr, B. (2003). Tragverhalten von Verbunddübeln unter zentrischer Belastung im ungerissenen Beton – Gruppenbefestigungen und Befestigungen am Bauteilrand. Ph.D. Thesis, University of Stuttgart, Germany.

Lettow, S. (2007). Ein Verbundelement für nichtlineare Finite Elemente Analysen – Anwendung auf Übergreifungsstöße. Ph.D. Thesis, University of Stuttgart, Germany.

Li, G.-Q., Guo, X.-K., Sun, F.-F., Chen, C. (2013). Study of the Anchorage Connections for Buckling Restrained Braces Part 1: Experimental Investigation. Advances in Structural Engineering, 16(4):759–771.

Liel, A.B., Haselton, C.B., Deierlein, G.G. (2011). Seismic Collapse Safety of Reinforced Concrete Buildings. II: Comparative Assessment of Nonductile and Ductile Moment Frames. Journal of Structural Engineering, 137(4):492–502.

Lin, P.C., Tsai, K.C., Wu, A.C., Chuang, M.C. (2014). Seismic design and test of gusset connections for buckling-restrained braced frames. Earthquake Engineering & Structural Dynamics, 43:565-587.

Loch, M. (2014). Beitrag zur Bestimmung von charakteristischen Werkstofffestigkeiten in Bestandstragwerken aus Stahlbeton. Ph.D. Thesis, Technische Universität Kaiserslautern, Germany.

Mahadik, V., Sharma, A. (2014). Monotonic Tension, Cyclic Tension, Crack Cycling, Out-of-phase and In-phase Tension and Crack Cycling and Monotonic Shear Tests on Fischer FZA-18x80-M12/25 Undercut Anchors. IWB-Report No. AF 15/01-GRS/01. University of Stuttgart, Germany, not published.

Mahadik, V., Sharma, A., Hofmann, J. (2016). Spring Model for Fischer FZA-18x80-M12/25 and Hilti HAD-T-22-M12x125/30 Undercut Anchors. IWB-Report No. AF 16/01-GRS/03. University of Stuttgart, Germany, not published.

Maheri, M.R., Sahebi, A. (1997). Use of steel bracing in reinforced concrete frames. Engineering Structures, 19(12):1018–1024.

Maheri, M.R., Hadjipour, A. (2003). Experimental investigation and design of steel brace connection to RC frame. Engineering Structures, 25:1707–1714.

Maheri, M.R., Kousari, R., Razazan, M. (2003). Pushover tests on steel X-braced and knee-braced RC frames. Engineering Structures, 25:1697–1705.

Maheri, M.R., Ghaffarzadeh, H. (2006). Internal steel bracing for seismic design of RC buildings. Proceedings of the 8th International Conference on Steel & Space Structures, Kuala Lumpur, Malaysia, 2006.

Maheri, M.R., Ghaffarzadeh, H. (2008). Connection overstrength in steel-braced RC frames. Engineering Structures, 30:1938–1948.

Maheri, M.R., Yazdani, S. (2016). Design of steel brace connection to an RC frame using Uniform Force Method. Journal of Constructional Steel Research, 116:131-140.

Mahrenholtz, C., Lin, P.-C., Wu, A.-C., Tsai, K.-C., Hwang, S.-J., Lin, R.-Y., Bhayusukma M.Y. (2015). Retrofit of reinforced concrete frames with buckling-restrained braces. Earthquake Engineering & Structural Dynamics, 44:59–78.

Mahrenholtz, P. (2011). Anchor Ductility – Development of Ductility Parameters and Evaluation of Data Base. Report No. III/08-11/02, Institute of Construction Materials, University of Stuttgart, not published.

Mahrenholtz, P. (2013). Experimental Performance and Recommendations for Qualification of Post-installed Anchors for Seismic Applications. Ph.D. Thesis, University of Stuttgart, Germany.

Mahrenholtz, P., Eligehausen, R. (2010). Behavior of anchor groups installed in cracked concrete under simulated seismic actions. Proceedings of the Conference on Fracture Mechanics of Concrete Structures (FraMCoS-7), Seoul, South Korea, 23-28 May 2010, 816-822.

Mahrenholtz, P., Eligehausen, R. (2015). Post-installed concrete anchors in nuclear power plants: Performance and qualification. Nuclear Engineering and Design, 287:48-56.

Mahrenholtz, P., Eligehausen, R. (2016). Anchor Displacement Behavior during Simultaneous Load and Crack Cycling. ACI Materials Journal, 113(5):645-652.

Mahrenholtz, P., Eligehausen, R., Hutchinson, T.C., Hoehler, M.S. (2016). Behavior of Post-Installed Anchors Tested by Stepwise Increasing Cyclic Load Protocols. ACI Structural Journal, 113:997–1008.

Mahrenholtz, P., Wood, R.L., Eligehausen, R., Hutchinson, T.C., Hoehler, M.S. (2017). Development and validation of European guidelines for seismic qualification of post-installed anchors. Engineering Structures, 148:497–508.

MASA Manual. MASA: Finite element program for 3D nonlinear analysis of concrete and reinforced concrete structures. Manual for MASA by Ožbolt, J., Institute of Construction Materials, University of Stuttgart, Germany.

Massumi, A., Tasnimi, A.A. (2008). Strengthening of low ductile reinforced concrete frames using steel x-bracings with different details. Proceedings of the 14th World Conference on Earthquake Engineering, Beijing, China, 12-17 October 2008.

Mazzolani, F.M., Della Corte, G., D'Aniello, M. (2009). Experimental Analysis of Steel Dissipative Bracing Systems for Seismic Upgrading. Journal of Civil Engineering and Management, 15(1):7–19.

Moehle, J.P. (2000). State of Research on Seismic Retrofit of Concrete Building Structures in the US. Proceedings of US-Japan Symposium and Workshop on Seismic Retrofit of Concrete Structures – State of Research and Practice, 2000.

Mohyeddin, A., Gad, E.F., Lee, J. (2019). Failure modes and tensile strength of screw anchors in non-cracked concrete. Construction and Building Materials, 221:501–513.

MPA Report No. 8488 000 000 (2021). Einfluss von Dübelverschiebungen auf den Sicherheitsnachweis von Rohrleitungen für den Lastfall Erdbeben. Influence from displacement of post-installed anchors on the safety assessment of piping systems at earthquake loading. MPA-Report No. 8488 000 000. University of Stuttgart.

Muciaccia, G. (2017). Behavior of Post-Installed Fastening under Seismic Action. ACI Structural Journal, 114(1):75-86.

Muciaccia, G., Marchisella, A. (2017). A review of existing provisions for seismic qualification and design of post-installed fasteners. Proceedings of the 3rd International Symposium on Connections between Steel and Concrete, Stuttgart, Germany, 27-29 September 2017.

Muir, L.S. (2008). Design compact gussets with the uniform force method. Engineering Journal, 2008, 1st quarter, 13–19.

Nuti, C., Santini, S. (2008). Fastening technique in seismic areas: A critical review. In Tailor Made Concrete Structures, Proceedings of the International fib Symposium 2008, Amsterdam, Netherlands, 19-21 May 2008. Walraven, J.C., Stoelhorst, D., Eds., London: Taylor & Francis Group, GB, 2008, 899-905.

Ohishi, H., Takahashi, M., Yamazaki, Y. (1988). A Seismic Strengthening Design and Practice of an Existing Reinforced Concrete School Building in Shizuoka City. Proceedings of Ninth World Conference on Earthquake Engineering, Tokyo-Kyoto, Japan, 2-9 August 1988, 7:415–420.

Okelo, R. (1996). The influence of the scatter of the load displacement curves of individual anchors on the bearing capacity of a quadruple anchor group. Report No. 20/29-96/34, Institute of Construction Materials, University of Stuttgart.

Ožbolt, J. (1995). Maßstabseffekt und Duktilität von Beton- und Stahlbetonkonstruktionen. Habilitation Thesis, University of Stuttgart, Germany.

Ožbolt, J., Li, Y., Kožar, I. (2001). Microplane model for concrete with relaxed kinematic constraint. International Journal of Solids and Structures, 38(16):2683–2711.

Ožbolt, J. (2009). Microplane model. Lecture notes, Engineering Materials – Concrete COMMAS E7-2, University of Stuttgart, summer term 2009.

Ozcelik, R., Binici, B., Akipinar, U. (2013). Seismic retrofit of non-ductile reinforced concrete frames with chevron braces. Structures and Buildings, 166(SB7):326–341.

Palazzo, G., López-Almansa, F., Cahís, X., Crisafulli, F. (2009). A low-tech dissipative buckling restrained brace. Design, analysis, production and testing. Engineering Structures, 31:2152–2161.

Park, R., Paulay, T. (1975). Reinforced Concrete Structures. New York: John Wiley & Sons, USA.

Paulay, T., Priestley, M.J.N. (1992). Seismic Design of Reinforced Concrete and Masonry Buildings. New York: John Wiley & Sons, USA.

Piccinin, R., Cattaneo, S., Biolzi, L. (2013). Breakout capacity of headed anchors in confined concrete: experimental evidence. ACI Structural Journal, 110(3):469–479.

Pincheira, J.A., Jirsa, J.O. (1995). Seismic response of RC frames retrofitted with steel braces or walls. Journal of Structural Engineering (ASCE), 121(8):1225–1235.

Popo-Ola, S.O., Newman, J.B. (1995). Centric tensile tests of bonded anchors in non-cracked concrete. IWB-Report No. 20/3-95/17. London/Stuttgart, not published.

Qu, Z., Xie, J.Z., Wang, T. (2015). Experimental tests of reinforced concrete frame subassemblies with buckling restrained braces in double-K configuration. Proceedings of 6th International Conference on Advances in Experimental Structural Engineering, University of Illinois, Urbana-Champaign, USA, 1-2 August 2015.

Reddy, G.R., Muruva, H.P., Verma, A.K. (2019). Textbook of Seismic Design. Singapore: Springer, Singapore.

Reitherman, R.K. (2012). Earthquakes and Engineers: An International History. Reston, Virginia: American Society of Civil Engineers, USA.

Ricci, P., De Luca, F., Verderame, G.M. (2011). 6th April 2009 L'Aquila earthquake, Italy: reinforced concrete building performance. Bulletin of Earthquake Engineering, 9(1):203–211.

Riemann, H. (1985). Das "erweiterte K-Verfahren" für Befestigungsmittel, Bemessung an Beispielen von Kopfbolzenverankerungen. Betonwerk + Fertigteil-Technik, Heft 12:808–815.

Sadjadi, R., Kianoush, M.R., Talebi, S. (2007). Seismic performance of reinforced concrete moment resisting frames. Engineering Structures, 29:2365–2380.

SEAOC. Vision 2000, A framework for performance based earthquake engineering, vol. 1. Structural Engineers Association of California: Sacramento, California, UAS, 1995.

Sharma, A. (2013). Seismic Behavior and Retrofitting of RC Frame Structures with Emphasis on Beam-Column Joints – Experiments and Numerical Modeling. Ph.D. Thesis, University of Stuttgart, Germany.

Sharma, A. (2017). Performance Based Approach for Anchorage in Concrete Construction. Proceedings of the 3rd International Symposium on Connections between Steel and Concrete, Stuttgart, Germany, 27-29 September 2017.

Sharma, A. (2019). Urgent Need for a Performance-Based Approach for Seismic Assessment and Design of Fastenings Used in Structural Applications. Advancements in Civil Engineering & Technology, 3(1):ACET.000555.

Sharma, A. (2020). Performance-based seismic design and strengthening of RC structures. Lecture notes, Institute of Construction Materials, University of Stuttgart, summer term 2019/20.

Sharma, A., Mahadik, V., Hofmann, J. (2016). Influence of Tension Loading Protocol on Crack Cycling Tests on Undercut Anchors. ACI Structural Journal, 113(4):779-790.

Sharma, A., Eligehausen, R., Asmus, J., Bujnak, J. (2019). Anchorages with Supplementary Reinforcement Under Tension, Shear and Interaction Loads – Experimental Database. Proceedings of the fib Symposium, Krakow, Poland, 27-29 May 2019.

Silva, J.F. (2001). Test methods for seismic qualification of post-installed anchors. Proceedings of the International Symposium on Connections between Steel and Concrete, Stuttgart, Germany, 10–12 September 2001. RILEM Publications: Cachan, France, 2001, Vol. 1:551–563.

Stehle, E.J., Sharma, A. (2019a). Assessment of post-installed anchors for seismic strengthening of RC structures using steel bracing. Proceedings of the SECED 2019 Conference on Earthquake risk and engineering towards a resilient world, Greenwich, London, UK, 9-10 September 2019.

Stehle, E.J., Sharma, A. (2019b). A new assessment approach for post-installed anchors used in seismic applications. Proceedings of the 7th International Conference on Euro Asia Civil Engineering Forum, Stuttgart, Germany, 30 September – 2 October 2019.

Stehle, E.J., Sharma, A. (2020). A new displacement-based approach for pulsating tension load tests of post-installed anchors for the use in structural applications under seismic actions. Engineering Structures, 211:110431.

Stehle, E.J., Sharma, A. (2021a). Review of Testing and Qualification of Post-Installed Anchors under Seismic Actions for Structural Applications. Civil Engineering, 2:406-420.

Stehle, E.J., Sharma, A. (2021b). Concrete cone breakout behavior of anchor groups in uncracked concrete under displacement-controlled cyclic tension load. Engineering Structures, 246:113092.

Stehle, E.J., Sharma, A. (2021c). Fastening of a gusset plate to concrete by means of post-installed anchors – Numerical investigation. Proceedings of the 13th fib International PhD Symposium in Civil Engineering, Paris, France, 21-22 July 2021.

Stehle, E.J., Sharma, A. (2021d). Post-Installed Anchors in Corner Configuration – Numerical Investigation. Otto Graf Journal, 20:199-210.

Sugano, S. (1996). State-of-the-Art in Techniques for Rehabilitation of Buildings. Proceedings of the 11th World Conference on Earthquake Engineering, Acapulco, Mexico, 28-28 June 1996.

TahamouliRoudsari, M., Entezari, A., Hadidi, M.H., Gandomian, O. (2017). Experimental Assessment of Retrofitted RC Frames With Different Steel Braces. Structures, 11:206–217.

Thornton, W.A. (1984). Bracing connections for heavy construction. Engineering Journal (AISC), 21(3):139–148.

Tsai, K.-C., Hsiao, P.-C., Wang, K.-J., Weng, Y.-T., Lin, M.-L., Lin, K.-C., Chen, C.-H., Lai, J.-W., Lin, S.-L. (2008). Pseudo-dynamic tests of a full-scale CFT/BRB frame - Part I: Specimen design, experiment and analysis. Earthquake Engineering & Structural Dynamics, 37(7):1081–1098.

Tsai, K.-C., Hsiao, P.-C. (2008). Pseudo-dynamic tests of a full-scale CFT/BRB frame - Part II: Seismic performance of buckling-restrained braces and connections. Earthquake Engineering & Structural Dynamics, 37(7):1099–1115.

Usami, H., Azuchi, T., Kamiya, Y., Ban, H., Kenjo, H., Suzuki, U. (1988). Seismic strengthening of existing reinforced concrete buildings in Shizuoka prefecture, Japan. Proceedings of Ninth World Conference on Earthquake Engineering, Tokyo-Kyoto, Japan, 2-9 August 1988, 7:421–426.

Wallemacq, P., Below, R., McClean, D. (2018). Economic Losses, Poverty & Disasters 1998-2017. Technical Report, Centre for Research on Epidemiology of Disasters (CRED), Brussels, Belgium.

Watanabe, A., Hitomi, Y., Saeki, E., Wada, A., Fujimoto, M. (1988). Properties of Brace Encased in Buckling-Restraining Concrete and Steel Tube. Proceedings of the Ninth World Conference on Earthquake Engineering, Tokyo-Kyoto, Japan, 2-9 August 1988, 4:719–724.

Watanabe, F. (1997). Behavior of Reinforced Concrete Buildings during the Hyougoken-Nanbu Earthquake. Cement and Concrete Composites, 19(3):492–502.

Whitmore, R.E. (1952). Experimental investigation of stresses in gusset plates. University of Tennessee, Engineering Experiment Station, Bulletin No. 16.

Wu, A.-C., Lin, P.-C., Tsai, K.-C. (2014). High-mode buckling response of buckling-restrained brace core plates. Earthquake Engineering & Structural Dynamics, 43:375–393.

Yooprasertchai, E., Warnitchai, P. (2008). Seismic retrofitting of low-rise nonductile reinforced concrete buildings by buckling-restrained braces. Proceedings of the 14th World Conference on Earthquake Engineering, Beijing, China, 12-17 October 2008.

Youssef, M.A., Ghaffarzadeh, H., Nehdi, M. (2007). Seismic performance of RC frames with concentric internal steel bracing. Engineering structures, 29:1561–1568.

Zeng, D.W., Wang, C.Y., Jiang, G.Y., Guo, Y.J. (2013). Study of the Bearing Capacity of Closely Spaced-Small Edge Distance Chemical Anchors Group System. Advanced Materials Research, 838–841:611–617.

Zhao, G., Fuchs, W., Eligehausen, R. (1989). Einfluss der Bauteildicke auf das Tragverhalten von Dübelbefestigungen im ungerissenen Beton unter Querzugbeanspruchung. IWB-Report No. 10/12A-89/5, University of Stuttgart, Germany.

Zhao, G., Eligehausen, R. (1992). Vorschläge zur Modifikation des CC-Verfahrens (Proposals for modification of the CC method). IWB-Report No. 12/20-92/11, University of Stuttgart, Germany, not published.

Curriculum vitae

Personal data

Erik Johannes Stehle

Born on October 27, 1990

in Schwäbisch Gmünd

Education

10/2015 - 05/2018	Master of Science (M.Sc.) in Civil Engineering, University of Stuttgart, Germany
10/2011 - 07/2015	Bachelor of Engineering (B.Eng.) in Civil Engineering, Stuttgart University of Applied Sciences, Germany
09/2001 - 06/2010	German Abitur Parler-Gymnasium, Schwäbisch Gmünd, Germany

Experience

08/2022 - Present	Project Engineer IEA GmbH & Co. KG, Stuttgart, Germany
07/2018 - 06/2022	Research Associate Institute of Construction Materials, University of Stuttgart, Germany